UNIVERSIDAD COMPLUTENSE DE MADRID
FACULTAD DE CIENCIAS QUÍMICAS
Departamento de Química Orgánica I

TESIS DOCTORAL

Estrategias para el análisis por luminiscencia de micotoxinas de alternaria utilizando polímeros de impronta molecular como elementos de reconocimiento

Strategies for luminiscence analysis of alternaria mycotoxins using molecularly imprinted polymers as recognition elements

MEMORIA PARA OPTAR AL GRADO DE DOCTOR

PRESENTADA POR

Rahma Ahmed Gebril Abou Hany

Directores

Guillermo Orellana Moraleda, Ana

Belén Descalzo López

Madrid, 2018

UNIVERSIDAD COMPLUTENSE DE MADRID

FACULTAD DE CIENCIAS QUÍMICAS

Departamento de Química Orgánica I

ESTRATEGIAS PARA EL ANÁLISIS POR LUMINISCENCIA DE MICOTOXINAS DE ALTERNARIA UTILIZANDO POLÍMEROS DE IMPRONTA MOLECULAR COMO ELEMENTOS DE RECONOCIMIENTO

STRATEGIES FOR LUMINESCENCE ANALYSIS OF ALTERNARIA MYCOTOXINS USING MOLECULARLY IMPRINTED POLYMERS AS RECOGNITION ELEMENTS

Memoria para optar al Grado de Doctor presentada por:

Rahma Ahmed Gebril Abou-Hany

Directores:

Prof. Dr. Guillermo Orellana Moraleda
Prof. Dr. Ana Belén Descalzo López

Madrid, 2017

An open world begins with an open mind

I dedicate this work to

To the soul of my dad, he was always an inspiration to me in life. He taught me the importance of an education. I would never have been able to get as far as I have if not for his sage advice. I dedicate this thesis to you, Dad. I will miss you greatly.

And for sure my whole life; Ahmed and Cinderella.

The Ph.D. process takes persistence. This has been a long journey, one that I have not travelled alone. Throughout my life, I have been fortunate to have great teachers, and I would not be here today if it were not for them. I wish to take this opportunity to thank everyone who has supported me along the way.

Prof. Guillermo Orellana has been a wonderful advisor, and his insight has shaped this research. Thanks for his patient guidance, enthusiastic encouragement and useful critiques of this research work. Also, it's hard for me to be away from my country but with his kind help as a father for me and my family, everything started from the beginning to be easier for us. For both research and unrelated discussions, I also wish to extend my thanks to the person who enlightening me the first glance of research and giving me much inspiration, Prof. Ana Bélen Descalzo, who remains an outstanding mentor, advisor, and also helped me to enter the scientific world. I could not have imagined having better advisors and mentors for my Ph.D. studies like you, Guillermo and Ana.

I want to thank the past and present members of GSOLFA group with whom I have formed fruitful collaborations and friendships. Thank you to Prof. Dr. Mª Cruz Moreno Bondi, that you have allowed me to work in the Analytical Chemistry Dpmt. laboratories of the GSOLFA group. Special thanks to Dr. Javier L. Urraca Ruiz, Andra Dumitru, Alberto Rico Yuste and Lidia N. Gómez Arribas for their contribution to the analytical and chromatographic experiments in chapter II. Thanks also to Dr. José Molina for his colaboration in chapter IV.

My thanks for the help and advice I got from Prof. Fernando Navarro Villoslada, Prof. Ana Mª Gutiérrez Carreras, Prof. Mª Concepción Pérez Conde, and Dr. Irene Núñez González.

To Nuria Martín for being always available, for all the help and friendship (*muchas gracias Nuria por haber estado siempre disponible, por toda tu ayuda y amistad*). I would also like to extend my thanks to the technicians of the Organic Chemistry department for their help during my Thesis.

After an intensive period of four months abroad during my PhD, I would like to express my sincere gratitude to international collaborator Prof. Dr. Robert Pansu (Supramolecular and

Molecular Photophysics and Photochemistry (PPSM), École normale supérieure de Cachan, France) for providing me an opportunity to join his team as intern, and who gave access to the laboratory and research facilities.

This research has been made possible thanks to the funding from the Spanish Ministry of Science and Innovation (MICINN, now MINECO) and the EU Funds for Regional Development (FEDER) through grants CTQ2009-14565-C03-01 and CTQ2012-37573-C02-01 to support this project, as well as the associated FPI fellowship (BES-2010-037023), and Complutense University of Madrid (GR35/10-A) for financial support. Also, thanks to MINECO FPI Mobility Scholarship to obtain the European Doctor label in my PhD degree..

I also dedicate my work to my parents *Ahmed Abou-Hany* and *Nawal Hany* who have instilled in me the values required to pursue a higher education and the drive to succeed, as well as my brother Mohmoud (*Sherif*) who has also been a great cheerleader throughout my graduate studies. Last, but not least, I dedicate this dissertation to my beloved sister Randa, her husband Prof. Atta and my nephews and nieces, who have inspired me to have strong work ethics and, most importantly, to always be humble. To our friends Firas, Mais, Taym, Ghassan, Khaled, Alaa, Dalia, Ahmed, Yassmen, Shaimaa, Lana, Hazem, Sameh, Ayman and, finally, the great uncle Mohamed Zamrawy.

Ahmed, thank you for your fight with me. Thank you for sharing my dreams, and for being willing to live with me. By always being the spring that takes me ahead. For making EVERYTHING easier for me. By boosting me at times when I am bored. And for giving new meaning to my life, and my beautiful and sweet daughter Cinderella, as well as future children who have given me light and hope in my pursuit of a doctoral degree in Chemistry.

ÍNDEX

List of Figures, Tables and Schemes

Symbols and Abbreviations

Å	:	Angstrom
δ	:	NMR chemical Shift/ppm
ε	:	Molar Absorption Coefficient/dm^3 mol^{-1} cm^{-1}
λ	:	Wavelength /nm
τ	:	Luminescence Lifetime
Φf	:	Luminescence Quantum Yield
A	:	Absorbance
AA	:	Atomic Absorption
AC		Acryloyl Chloride
AP	:	1-Amino Pyrene
a.u	:	Arbitrary units
AACA	:	Allyl Acetoacetate
ABDV	:	2,2′-azobis(2,4-dimethyl)valeronitrile
AcOH	:	Acetic acid
ADI	:	Acceptable daily intake
AIBN	:	2,2′-azobis(2-methylpropionitrile)
AIBN	:	2,2’-Azobisisobutyronitrile
ALPP	:	1-allylpiperazine
AME	:	Alternariol methylether
AMP	:	Aminopyrene
AOH	:	Alternariol
APTES	:	(3-aminopropyl)triethoxysilane
aq.	:	Aqueous
Ar.	:	Argon Gas
B_i	:	Bi-Exponential
Bn	:	Benzyl
BP	:	Boiling point
br	:	Broad
Br-DMBA	:	2-bromo-4,5-dimethoxybenzoic acid
Br-MBA	:	2-bromo-5-methoxy benzoic acid
bw	:	Body weight
c	:	Concentration/mol dm^{-3}
calc.	:	Calculated
CAS	:	Chemical Abstract Service
CT	:	Charge Transfer
CI	:	Chemical ionisation
con	:	Concentrated
CPDB	:	2-cyano-2-propyl benzodithioate
d	:	Doublet
d	:	Day
DBTL	:	Dibutyltin dilaurate
DCM	:	Dichloromethane
dd	:	Doublet of doublets
de	:	Diastereoselectivity
DEAM	:	Diethyl allylmalonate
DEPT	:	Distortionless Enhancement by Polarization Transfer
dia	:	Diameter

DMF	:	*N*,*N*-Dimethylformamide
DMSO	:	Dimethylsulfoxide (used as solvent)
DNA	:	Deoxyribonucleic acid
DVB	:	Divinylbenzene
EA	:	Activation energy
EAMA	:	2-aminoethyl methacrylate hydrochloride
EDMA	:	ethylene glycol dimethacrylate
EDTA	:	Ethylenediaminetetraacetic acid
EFSA	:	European Food Safety Authority
EI	:	Electron Ionisation
ELISA	:	Enzyme-linked immunosorbent assay
eq	:	Equation
Equiv.	:	equivalent
ESI	:	Electrospray ionisation
Et_2O	:	Diethyl ether
Et_3N	:	triethylamine
EtOAc	:	Ethyl acetate
EtOH	:	Ethanol
EuCl3	:	Europium(III) chloride
FAO	:	Food and Agriculture Organisation (of the United Nations)
Fig.	:	Figure
FL	:	Fluorescence
FLD	:	Fluorescence detector/detection
FM	:	Functional Monomer
FP	:	Fluorescence Polarization
FT-IR	:	Fourier transform infrared spectroscopy
GC	:	Gas chromatography
GS	:	Ground State
h	:	Hour
HCl	:	Hydrochloric acid
HEMA	:	2-hydroxyethyl methacrylate
HEPES	:	2-[4-(2-hydroxyethyl)piperazin-l-yl]ethanesulfonic acid
HPLC	:	High Performance Liquid Chromatography
HPLC-FLD	:	High Performance Liquid Chromatography: Fluorescence Detection
Hz	:	Hertz
I	:	Luminescence Intensity
i.e.	:	id est
IA	:	Immunoaffinity
IC	:	Internal Conversion
IF	:	Imprinting Factor
IR	:	Infrared spectroscopy
ISC	:	Intersystem Crossing
IUPAC	:	International Union of Pure and Applied Chemistry
J	:	Coupling Constant
K	:	Retention Factor
K_D	:	Bi-Molecular Quenching Constant
KBr	:	Potassium Bromide
l	:	Optical Pathlength/cm

LD_{50}	:	Median lethal Dose
Lit.	:	Literature
LOD	:	Limit Of Detection
LOQ	:	Limit Of Quantification
M	:	Molar Concentration
m	:	Multiplet
m/z	:	Molecular Mass to Charge Ratio
MAA	:	Methacrylic Acid
MAM	:	Methacrylamide
ME	:	Matrix effect
MeCN	:	Acetonitrile (methyl cyanide)
MEHQ	:	Monomethyl ether of hydroquinone
MeOH	:	Methanol
min	:	Minute
MIP	:	Molecularly Imprinted Polymer
MISPE	:	Molecularly Imprinted Solid-Phase Extraction
ML	:	Maximum level
mo	:	Month
MPE1	:	Micro particles TeA MIP-Eu (Template: Monomer:Cross-linker) TeA:DEAM:EDMA
MPE2	:	Micro particles TeA MIP-Eu (Template: Monomer:Cross-linker) TeA:AACA:EDMA
MPE3	:	Micro particles TeA MIP-Eu (Template: Monomer:Cross-linker) *s*TeA:DEAM:EDMA
MS	:	Mass spectrometry
MS/MS	:	Tandem mass spectrometry
MSI	:	Minimum sample intake
MTAC	:	MethAcryloyl Chloride
NIP	:	Non-Imprinted Polymer
NMR	:	Nuclear Magnetic Resonance
NPE1	:	Micro particles TeA NIP-Eu (Monomer:Cross-linker) DEAM:EDMA
NPE2	:	Micro particles TeA NIP-Eu (Monomer:Cross-linker) AACA:EDMA
NPE3	:	Micro particles TeA NIP-Eu (Monomer:Cross-linker) DEAM:EDMA
p.a.	:	Pro Analysi
PA	:	N-pyren-1-ylacrylamide
PBS	:	Phosphate Buffered Saline
PCC-P	:	phosphate-free liquid lab detergent
PET	:	Photoinduced Electron Transfer
Ph	:	Phenyl
pK_a	:	Logarithmic Acid Dissociation Constant
pK_{ap}	:	Logarithmic Apparent Acid Dissociation Constant
Pk_a	:	Acid dissociation constant
PLC	:	Preparative Layer Chromatography
PMA	:	N-pyren-1-ylmethacrylamide
PMeA	:	N-(pyren-1-ylmethyl)acrylamide
PMeMA	:	N-(pyren-1-ylmethyl)methacrylamide
ppb	:	Part per billion
ppm	:	Part per million

Py	:	Pyridine
r	:	Fluorescence polarization anisotropy
*rac*TeA	:	Synthetic Tenuazonic Acid
RAFT	:	Reversible Addition-Fragmentation Chain-Transfer
rpm	:	Revolutions Per Minute
RSD	:	Relative Standard Deviation
RT	:	Room Temperature
S	:	Singlet
S_0	:	Singlet Ground State
S_1	:	First Excited State
S_2	:	Second Excited State
S_3	:	Third Excited State
Sec	:	Second
SCF	:	Scientific committee for food
SD	:	Absolute standard deviation
SEM	:	scanning electron microscope
SPE	:	Solid Phase Extraction
Spp.	:	Several Species
*s*TeA	:	Tenuazonic acid surrogate
t	:	Triplet
TBAF	:	Tetra Butyl Ammonium Fluoride
TBMA	:	Tert-Butyl Methacrylate
TeA	:	Natural Tenuazonic Acid
TEM	:	Transmission Electron Microscopy
TEOS	:	Tetraethoxysilane
TFA	:	Trifluoroacetic Acid
THF	:	Tetrahydrofuran
TLC	:	Thin Layer Chromatography
TMEN	:	N,N,N′,N′-Tetramethylethylenediamine
tR	:	Retention Time
UV	:	Ultraviolet
UV-vis	:	Ultraviolet- Visible Region
VBA	:	4-Vinylbenzoicacid
VPY	:	4- Vinylpyridine
WHO	:	World Health Organisation
wk	:	Week

Resumen

ESTRATEGIAS PARA EL ANÁLISIS POR LUMINISCENCIA DE MICOTOXINAS DE ALTERNARIA UTILIZANDO POLÍMEROS DE IMPRONTA MOLECULAR COMO ELEMENTOS DE RECONOCIMEINTO

Rahma Ahmed Gebril Abou-Hany

Universidad Complutense de Madrid, 2017

Directores: Prof. Guillermo Orellana Moraleda
Prof. Ana Belén Descalzo López

Resumen

La contaminación de alimentos por hongos no es únicamente un inconveniente en lo que respecta a su comercialización debido a que provoca su deterioro, –con las consecuentes pérdidas económicas–, sino que también representa una amenaza para la salud animal y humana. Algunos de los metabolitos secundarios producidos por dichos hongos presentan una toxicidad aguda o crónica. Estos metabolitos se conocen como micotoxinas, y normalmente son moléculas de pequeño a mediano tamaño que son bastante estables a las condiciones de cocinado o de congelado. Por esa razón, no son fáciles de eliminar de los alimentos una vez que se han producido. Se requieren por tanto controles de calidad que permitan evitar o minimizar la introducción de estas sustancias tóxicas en la cadena alimentaria. Las toxinas más comunes en productos de agricultura son producidas por las familias de hongos *Aspergillus*, *Penicillium*, *Fusarium* o *Alternaria*. La última familia, *Alternaria*, produce varias micotoxinas de diversos tipos estructurales, de las cuales, las cinco principales son: alternariol, alternariol monometil éter y altenueno como benzopironas; ácido tenuazónico, como ácido tetrámico, y altertoxina-I, que es un derivado de tipo perileno. Estas toxinas pueden encontrarse en cereales, granos, frutas y vegetales, y también en comida procesada como cerveza, vino o derivados de tomate. Estudios recientes han puesto de manifiesto que la mayoría de dichas sustancias son mutagénas, teratógenas y/o cancerígenas, por lo que las micotoxinas se han convertido en una preocupación para la salud pública. Se ha encontrado

que ambos, alternariol y alternariol monometil éter (que frecuentemente se encuentran juntos), son mutágenos. El alternariol también está implicado en el desarrollo de carcinoma de células escamosas, y se ha relacionado con cambios precancerosos en la mucosa de esófago de ratones. Se sabe que el contenido natural de alternariol y alternariol monometil éter en productos alimentarios procesados se encuentra en niveles de ng/mL y sub-ng/mL, respectivamente.

A nivel mundial, ya en 2003 al menos 99 países tenían normas regulando la presencia de micotoxinas en productos alimentarios. La mayoría de las micotoxinas reguladas son producidas por especies de *Aspergillus, Penicillium* y *Fusarium*. A pesar de que las especies de *Alternaria* son unos de los hongos mayoritarios presentes en frutas y vegetales, ningún país tiene aún normativa y límites para sus toxinas. En mayo de 2012, la Comisión Europea publicó una recomendación para el control de micotoxinas de *Alternaria*: alternariol (AOH) y alternariol monomethyl éter (AME) como "toxinas de *Alternaria* de posible relevancia toxicológica que deberían ser analizadas"; ácido tenuazónic (TeA), tentoxina (TEN), y altenueno (ALT) como "toxinas de *Alternaria* cuya presencia en alimentos es relevante y para las cuales el análisis es conveniente" y otras toxinas de *Alternaria* como las alterotoxinas (ATX) o *alternaria alternate f sp lycopersici* (toxina AAL), las cuales se considera que "también podrían ser analizadas, pero son, respecto a la información actualmente disponible, de menor relevancia". Con respecto a los métodos de análisis para la determinación de toxinas de *Alternaria* en una amplia variedad de matrices, se recomienda la cromatografía líquida (LC) con tratamiento previo por SPE (extracción en fase sólida) para su preconcentración.

Los métodos empleados actualmente para detectar y cuantificar micotoxinas se basan, en su mayoría, en la cromatografía acoplada a espectrometría de masas (HPLC, GC, LC/MS-MS, y GC/MS-MS). Desafortunadamente, a pesar de que estas técnicas son muy sensibles, son costosas en tiempo y dinero, y requieren personal de laboratorio especializado para su manejo. Por esta razón, se han desarrollado y comercializado otros métodos basados en principios inmunológicos para análisis rápidos. Estos métodos incluyen, entre otros, ELISA

(ensayo por inmunoadsorción ligado a enzimas), fluorescencia directa, polarización de fluorescencia y varios procedimientos basados en biosensores y tiras reactivas.

En lo que respecta al desarrollo de biosensores, una atractiva alternativa al uso de anticuerpos como elemento de reconocimeinto es el empleo de los denominados "**polímeros de impronta molecular"** (MIPs, del inglés "*molecularly imprinted polymers*") sintéticos como *receptores biomiméticos*. Estos polímeros se producen siguiendo un procedimiento de impronta en el que la molécula diana, que ha de ser reconocida posteriormente en la muestra, se usa como plantilla, generando en el polímero cavidades con una forma específica y propiedades químicas complementarias a la diana. Tras eliminar la plantilla después de la polimerización, estas cavidades pueden actuar como *"receptores"* selectivos a la misma. A pesar de que la afinidad de enlace no es tan elevada como en el caso de los receptores naturales, es suficiente para muchas aplicaciones. La ventaja principal frente a los anticuerpos es que los MIPs son más estables, baratos y fáciles de integrar en procesos industriales estándar de fabricación.

El principal objetivo de esta Tesis, ha sido el desarrollo de nuevas estrategias para el análisis de micotoxinas de *Alternaria* (AOH, AME y TeA) empleando técnicas de luminiscencia y MIPs como elementos de reconocimiento artificial. Los métodos de análisis basados en detección de luminiscencia son normalmente muy sensibles y selectivos, representando una buena alternativa a los métodos basados en separaciones cromatográficas para el análisis de muestras. Aquí se proponen diferentes estrategias para la detección de los analitos, en función de si el propio analitos es fluorescente (e.g. AOH y AME) o no lo es (e.g. TeA). En el primer caso, la detección directa de los analitos diana es posible, bien utilizando medidas de fluorescencia basadas en variaciones de la intensidad, o bien monitorizando variaciones en la anisotropía de fluorescencia en presencia del MIP. En ambos casos pueden emplearse medidas en el estado estacionario o resueltas en el tiempo. En el segundo caso, para la detección de TeA, fue necesaria la preparación de un MIP luminiscente que contiene quelatos luminiscentes de Eu(III). Finalmente, también se ha explorado la posibilidad de emplear monómeros

luminiscentes derivados de pireno para la fabricación de MIPs y su empleo para monitorizar la unión de AOH o AME en las cavidades mediante la desactivación (*quenching*) que provocan sobre la fluorescencia de algunos de los nuevos monómeros.

La preparación de MIPs empleando los propios AOH, AME y TeA naturales como plantilla no es factible ya que, además de tóxicos, son compuestos de elevado precio. Por esta razón, proponemos aquí rutas sintéticas directas que facilitan la preparación de las plantillas sucedáneas a escala de gramos. En el caso del TeA, se ha preparado el propio analito (racémico) en nuestros laboratorios siguiendo un nuevo protocolo que conduce a excelentes rendimientos de su sal sódica estable. En el caso de AOH y AME, se describe la síntesis de análogos en lugar de las propias micotoxinas, ya que la ruta sintética completa para estos dos compuestos es muy larga y costosa. Se losan obtenido cuatro análogos (S1 a S4) con buenos rendimientos y que han conducido a la preparación de MIPs con excelente reconocimiento del AOH.

Los MIPs selectivos para AOH y TeA se seleccionaron entre una biblioteca de MIPs preparados a pequeña escala mediante una síntesis combinatoria. Las mejores composiciones de polímero se utilizaron para preparar MIPs en forma de microesferas porosas gracias a un núcleo sacrificable de sílice, que se disuelve al final del proceso empleando NH_4HF_2. quela disolución del “molde” da lugar a mesoporos vacíos que proporcionan esferas MIP con cinéticas de tranferencia de masa mejorada con respecto a los materiales ”en bloque” (*bulk*).

Además de una completa caracterización espectroscópica de los sistemas sensores con MIPs propuestos, también se ha llevado a cabo en paralelo una caracterización basada en métodos cromatográficos (HPLC con detección fluorescente o por absorción) en colaboración con los miembros del Grupo GSOLFA Javier L. Urraca, Lidia N. Gómez Arribas y Alberto Rico Yuste. Por ejemplo, el análisis por HPLC de algunos de los adsorbentes MIPs preparados para AOH ha permitido la optimización de condiciones cromatográficas para la aplicación de los MIPs como fases estacionarias selectivas en SPE para AOH en vez de sensores.

La Tesis está organizada en cinco capítulos: “I- Introducción”, “II- Polímeros de impronta molecular para el reconocimiento de alternariol”, “III- Desarrollo de MIPs luminiscentes para la detección de ácido tenuazónico”, “IV- Monómeros acrilamida marcados con pireno” y por último, “V- Parte experimental”.

I- Introducción. La parte introductoria proporciona una descripción del concepto de micotoxinas, centrándose en las propiedades de los metabolitos de *Alternaria* AOH, AME y TeA, así como en los métodos analíticos disponibles para su determinación. Tras esto, se explica el concepto de MIP (composiciones típicas de los polímeros, estrategias de polimerización, principios de SPE en relación con adsorbentes MIP, etc.). También se da una idea general de tipos de sensores químicos existentes, centrándonos en aquéllos que utilizan una señal luminiscente, y en los ensayos basados en MIPs y detección de luminiscencia. Finalmente, se proporciona una pequeña descripción de las propiedades (foto)químicas de quelatos luminiscentes de Eu(III) con β-dicetonas y también de luminóforos derivados del pireno –empleados en esta Tesis como sondas luminiscentes de polaridad de microambiente y “etiquetas” de reconocimiento de analitos que desactivan la fluorescencia de los mismos.

II- Polímeros de impronta molecular para el reconocimiento de alternariol. En la primera parte de este capítulo, se describe el diseño, preparación y caracterización espectroscópica de cuatro análogos fluorescentes del AOH (S1 a S4). Los análogos cuentan con un número diferente de grupos fenol en varias posiciones y distinto grado de *O*-metilación en el esqueleto de dibenzo[b,d]piran-6-ona, mimetizando la estructura química de las micotoxinas naturales AOH y AME. Los análogos se han caracterizado mediante espectrofotometría de absorción UV-Vis y fluorimetría en estado estacionario y con resolución en el tiempo. También se han sintetizado otros dos compuestos análogos de alternariol (S5 y S6) que no son fluorescentes. A continuación se describe la preparación de una biblioteca completa de MIPs, para reconocimiento de AOH, a pequeña escala empleando mezclas de monómeros básicos, ácidos o neutros, con divinilbenceno o dimetacrilato de etileneglicol como entrecruzantes, en presencia de los cuatro análogos fluorescentes de las toxinas. Esta biblioteca de polímeros ha

permitido la selección de la composición óptima para la síntesis posterior de MIPs en forma de microesferas. Así se eligieron la *N*-(2-aminoetil)metacrilamida (EAMA), el dimetacrilato de etilenglicol (EDMA) y el análogo molecular S2, como monómero funcional, (FM), entrecruzante (CL) y plantilla (T) óptimos, respectivamente. Los polímeros preparados con una relación molar de 1:2:2:20 (S2:EAMA:MAM:EDMA, donde MAM = ácido metacrílico, empleado como monómero diluyente), son capaces de unir AOH en mezclas agua–acetonitrilo (80:20, v/v) con una constante de afinidad de 109 ± 10 mM^{-1} y un número total de sitios de unión de 35 ± 2 µmol g^{-1}, siendo el alternariol monometil éter la única especie competidora de cuantas fueron ensayadas. Además, valoraciones por ^{1}H-RMN demostraron una estequiometría 1:2 para el aducto S2–EAMA, revelaron los puntos exactos de la interacción y proporcionaron una constante de enlace de 1.5 × 10^{4} M^{-2}. Finalmente, se ha optimizado un método de extracción en fase sólida MIP (MISPE) para el aislamiento selectivo de la micotoxina en muestras acuosas empleando un lavado con 3 mL de agua–acetonitrilo (80:20,v/v) seguido de la determinación por HPLC con detección por fluorescencia. El método se ha aplicado, en combinación con extracción asistida por ultrasonidos, al análisis de AOH en muestras de tomate fortificadas con la micotoxina a cinco niveles de concentración (de 33 a 110 µg kg^{-1}), con recuperaciones en el rango del 81–103% (RSD, n = 6). Hasta donde sabemos, se describe aquí el primer material con impronta capaz de reconocer a nivel molecular el frecuente contaminante alimentario alternariol.

Además, aprovechando que los analitos AOH y AME son moléculas pequeñas y fluorescentes (λ_{abs}^{max} = 341 nm, λ_{em}^{max} = 390 nm, en MeCN) y sus análogos de síntesis preparados por nosotros poseen propiedades similares, consideramos la posibilidad de emplear medidas de anisotropía de fluorescencia para monitorizar su unión a los MIPs. El grado en el que la luz emitida está polarizada, cuando el fluoróforo se excita con luz polarizada, depende del tiempo de rotación browniana del mismo, el cuál cambia drásticamente cuando el analito libre (muy baja polarización) se une a una cavidad del polímero de impronta (fuerte aumento de la polarización). Aparte de la elevada sensibilidad que normalmente proporciona la detección de fluorescencia, otra ventaja de la técnica es que las medidas basadas en

polarización de fluorescencia pueden proporcionar información libre de artefactos acerca de la cantidad de analito unido al MIP a distintas concentraciones, ya que son medidas relativas. Por ejemplo, una fuerte interacción de S2 al polímero disminuye su rotación, lo que causa un aumento en el valor de la anisotropía de su fluorescencia hasta 0.27. De esta forma, hemos empleado cambios en la polarización de fluorescencia para determinar la cantidad de toxina o análogos moleculares enlazados al MIP. Esta parte del trabajo se llevó a cabo bajo denle colaboración con el Prof. Robert Pansu en la *École Normal Supérieure de Cachan* (France).

III- Desarrollo de MIPs luminiscentes para la detección de ácido tenuazónico (TeA). En el tercer capítulo, se describe en primer lugar la síntesis de la micotoxina TeA (racémica) en forma de sal sódica (NaTeA) con un rendimiento del 85% (además del precio prohibitivo de TeA para la síntesis de MIPs, los proveedores comerciales proporcionan la micotoxina en forma de complejo de Cu(II), inservible como plantilla para la síntesis de MIPs). Se describen también varios estudios de complejación de la sal de TeANa en disolución metanólica, mostrando la gran capacidad de este ligando tipo β-dicetona para la coordinación de cationes Cu(II) y Eu(III). Esto último, junto con el hecho de que la sal de TeA presenta un máximo de absorción a 276 nm (284 nm si el TeA está complejado con Eu(III)), nos condujo a la posibilidad de utilizar TeA como ligando antena para la sensibilización de la luminiscencia del Eu(III). Así, si dopamos un MIP con un complejo de Eu(III), la coordinación del TeA debería inducir un aumento de la luminiscencia típica del Eu(III) a 615 nm. Este incremento de emisón podría, por tanto, emplearse para detectar la presencia de la toxina diana. En efecto, cuando se copolimeriza un complejo de Eu(III)-DEAM (donde DEAM = malonato de dietilalilo, un derivado tipo β-dicetona que posee una unidad polimerizable) con EDMA, en presencia de NaTeA, se obtienen MIPs luminiscentes que pueden indicar selectivamente la presencia de TeA. Siguiendo una estrategia de síntesis combinatoria, se prepararon en formato bloque distintos polímeros dopados con Eu(III) (MIPs y NIPs), con diferentes relaciones molares de Eu(III)/DEAM. Alternativamente, se empleó también como monómero funcional (FM) otra β-dicetona distinta a DEAM (acetoacetato de alilo, AACA) para la síntesis de MIPs. Valoraciones por espectroscopía de luminiscencia demostraron que la mejor relación molar Eu(III)/FM era

1:3. De esta manera, quedan dos posiciones de coordinación disponibles en el Eu(III) para la coordinación del TeA. También se estudió la influencia sobre la respuesta óptica del contenido en agua de la disolución a analizar . El aumento de señal más intenso en presencia de TeA se obtuvo en acetonitrilo puro, resultado esperable ya que el agua es un conocido desactivador de la luminiscencia de los complejos de Eu(III). Así, se obtuvo un aumento de la intensidad de emisión de hasta 3 veces al añadir NaTeA a una suspensión del correspondiente MIP–Eu(III) en MeCN (muy superior a la respuesta obtenida en el mismo ensayo para el polímero sin impronta). Finalmente, se prepararon tres tipos de microesferas porosas MIP: MPE1, MPE2 and MPE3, empleando la composición optimizada de TeA-Eu(III)-FM con una relación molar de 1:1:3. Valoraciones por luminiscencia con suspensiones de micropartículas MIP en MeCN (0.67 mg mL^{-1}) proporcionaron límites de detección para el TeA de 5.2, 9.9 y 4.0 µM en el caso de MPE1, MPE2 y MPE3, respectivamente, permitiendo la determinación de 15, 30 y 14 µM de TeA en MeCN. Estudios de reactividad cruzada con otras micotoxinas (zearalenona y alternariol) o componentes frecuentes en las muestras de alimentos (glucosa y fructosa) pusieron de manifiesto la elevada selectividad de los nuevos materiales poliméricos preparados para el reconocimeinto de TeA. Únicamente los análogos moleculares de TeA que también poseen estructura de *β*-dicetona, como el análogo del TeA con leucina como precursor o el ácido ciclopiazónico, fueron capaces de producir un aumento en la luminiscencia de los MIPs para reconocimiento de TeA preparados.

IV- Monómeros acrilamida marcados con pireno. En el cuarto capítulo de la Tesis se describe la síntesis y caracterización espectroscópica de cuatro monómeros derivados de la acrilamida y metacrilamida, que contienen grupos *N*-pirenilo o *N*-pirenometil como marcadores fluorescentes. Dichos monómeros pretenden explotar las conocidas propiedades de este hidrocarburo como sonda molecular de la polaridad del microentorno alrededor de la misma para la futura investigación de la polaridad de los sitios de unión del analito en el MIP. Asimismo, servirán como monómeros de reconocimiento de alternariol y otros analitos de estructura aromática extensa, debido a su capacidad de formar aductos dador-aceptor con dichas especies (en el sitio de unión del MIP). La caracterización fotofísica de los monómeros

ha revelado que la fluorescencia del pireno se ve gravemente disminuida cuando el pireno se une directamente al átomo de nitrógeno del monómero acrilamida, haciendo que sean inservibles para el fin que se persigue. Por el contrario, si se separa el monómero de la entidad de pireno mediante un grupo metileno, el elevado rendimiento cuántico (cercano a la unidad) y tiempo de vida de fluorescencia (superior a los 300 ns en ausencia de oxígeno disuelto) se recuperan, siendo estos parámetros tan elevados o más que los que presenta el hidrocarburo no sustituido. Ello convierte a las pirenometilacrilamidas sintetizadas en excelentes sondas de polaridad de su entorno inmediato, incluso cuando estén ancladas covalentemente a la matriz polimérica. Además, hemos investigado las características de su emisión y la velocidad de desactivación dinámica de la fluorescencia de los monómeros con el O_2 disuelto, en diferentes disolventes (acetonitrilo, ciclohexano y diclorometano). Finalmente, se ha estudiado la fotoquímica de la *N*-(piren-1-ilmetil)metacrilamida con uno de los sucedáneos de alternariol sintetizados, en el interior de micelas de surfactante aniónico, con el fin de modelar la interacción que se producirá cuando el monómero fluorescente se incorpore, en un futuro, a las cavidades de unión de alternariol en un MIP para el reconocimiento de esta toxina.

V- Parte experimental. Finalmente, la sección experimental proporciona una descripción detallada de los reactivos e instrumentación empleados; los protocolos sintéticos seguidos para la preparación de las distintas plantillas y los monómeros fluorescentes de pireno (con datos de ^{1}H- y ^{13}C-RMN, FTIR, espectrometría de masas, análisis elemental, absorción Uv-vis y fluorescencia en estado estacionario y resuelta en el tiempo); los procedimientos de preparación de bibliotecas MIP y NIP; los protocolos de polimerización para la síntesis de microesferas mesoporosas de MIP; la optimización de las condiciones cromatográficas para la separación y pre-concentración de AOH empelando SPE y el detalle de los estudios de polarización de fluorescencia.

Las Conclusiones más relevantes del trabajo de Tesis se recogen al final del texto, junto con un Anexo que detalla la caracterización espectroscópica completa de todos los compuestos sintetizados en nuestro laboratorio.

Abstract

STRATEGIES FOR LUMINESCENCE ANALYSIS OF ALTERNARIA MYCOTOXINS USING MOLECULARLY IMPRINTED POLYMERS AS RECOGNITION ELEMENTS

Rahma Ahmed Gebril Abou-Hany

Universidad Complutense de Madrid, 2017

Supervisors: Prof. Guillermo Orellana Moraleda
Prof. Ana Belén Descalzo López

Abstract

Food contamination with fungi is not only an inconvenience for food marketing because it causes food decay, –with the consequent economic losses–, but it also brings about animal and human health hazards. Some of the secondary metabolites produced by fungi have acute or chronic toxicity. These metabolites are known as mycotoxins and are normally small to medium size molecules that are rather stable to storage or cooking conditions. For this reason, they are not easy to eliminate from food once they are produced. Food quality controls are required in order to avoid or minimize the introduction of these toxic substances in the food chain. The most common toxins in agricultural goods are produced by the *Aspergillus*, *Penicillium*, *Fusarium* or *Alternaria* fungi families. The latter family, *Alternaria*, produces a number of mycotoxins, belonging to different structural classes, the five major compounds of which are alternariol, alternariol methyl ether and altenuene, as benzopyrone derivatives; tenuazonic acid, which is a tetramic acid derivative, and altertoxin-I, a perylene derivative. These products can be found in cereals, grains, fruits and vegetables, and also in processed foods such as beer, wine or tomato produces. Recent studies have pointed out that most of these substances are mutagenic, teratogenic and/or carcinogenic so that mycotoxins have become a major concern for public health. Both alternariol and alternariol monomethyl ether, which are frequently found in combination, were found to be mutagenic. Alternariol is also involved in the development of squamous cell carcinoma and has been linked to precancerous changes associated with the oesophagal mucosa in mice. The natural occurrence of alternariol

and alternariol methyl ether in processed food products has been reported at ng/mL and sub-ng/mL levels, respectively.

On a worldwide basis, at least 99 countries had mycotoxin regulations for food and/or feed already in 2003. Most of these regulated mycotoxins are produced by *Aspergillus*, *Penicillium* and *Fusarium* species. Whereas *Alternaria* species are among the major fungi in fruits and vegetables, no country in the world has formal regulations and limits for any of the *Alternaria* toxins. In May 2012, the EU published a recommendation for monitoring *Alternaria* mycotoxins: alternariol (AOH) and alternariol monomethyl ether (AME) as "*Alternaria* toxins of possible toxicological relevance which should be analysed", tenuazonic acid (TeA), tentoxin (TEN), and altenuene (ALT) as "*Alternaria* toxins of which the occurrence in feed and/or food is of relevance and for which the analysis is appropriate". Other *Alternaria* toxins such as altertoxins (ATX) or *Alternaria alternate f sp lycopersici* toxins (AAL toxin) were considered as those that "can also be analyzed but are, based on the currently available information, of less relevance". With regard to the methods of analysis to be used, liquid chromatography (LC) with SPE clean-up is the most appropriate method of analysis for the determination of *Alternaria* toxins in a wide range of matrices.

Current methods used to detect and quantify mycotoxins are mostly chromatography coupled to mass spectrometry (HPLC, GC, LC/MS-MS and GC/MS-MS). Although these techniques are very sensitive, they are also time-consuming, expensive, and laborious, often necessitating specialized laboratory staff. Hence, a range of methods, mostly based on immunological principles, have also been developed and commercialised for rapid analysis. These methods include ELISA (Enzyme-Linked Immunosorbent Assay), direct fluorometry, fluorescence polarization assays and various biosensors and strip-based methods.

Regarding the development of biosensors, a good alternative to the use of antibodies as the recognition-binding element is the utilization of synthetic molecularly imprinted polymers (MIPs) as *biomimetic receptors*. MIPs are produced following a templating process in which the target molecule to be recognized in the sample (or a surrogate of it) is used as the template

during polymerization, providing a specific shape and chemical properties to the generated polymer cavities. The latter, after removal of the template, perform as *selective binding sites*. Despite the fact that the binding affinity is not as high as in the case of the natural receptors, it is sufficient for many applications. The advantage is that MIPs are more stable, cheaper and easier to integrate into standard industrial fabrication processes.

The main focus of this Thesis work has been the development of strategies for the analysis of selected *Alternaria* mycotoxins (AOH, AME and TeA) using luminescence techniques and MIPs as artificial recognition elements. Luminescence-based methods are generally very sensitive, selective and represent a good alternative to chromatography-based methods for sample analysis. Different strategies are proposed for the analyte detection, depending on whether the analyte itself is fluorescent (e.g. AOH and AME) or not (e.g. TeA). In the first case, direct detection of the target analytes is possible either using intensity-based fluorescence measurements or fluorescence anisotropy in the presence of the MIP. Both, steady state and time resolved measurements have been carried out. In the second case, for TeA sensing, a luminescently-labeled MIP (containing a luminescent Eu(III) chelate as the functional monomer) had to be synthesized. Finally, the possibility of using pyrene monomers as fluorescent probes for monitoring AOH or AME binding to the MIP cavities through the quenching they cause has also been explored.

Since AOH, AME and TeA are rather expensive and toxic compounds, the up-scaled preparation of MIPs with these templates is not feasible. For this reason, we propose here straightforward synthetic routes that facilitate preparation of surrogate templates in multigram scale. In the case of TeA, the racemic mixture of the analyte itself was prepared in our laboratories following a protocol that allowed obtaining the pure TeA as its sodium salt. In the case of AOH and AME, however, the synthesis of molecular analogues is proposed instead, since the reported full synthesis of both compounds is very demanding. Molecularly engineered surrogates S1 to S4 were obtained in good yields and allowed preparation of the corresponding MIPs showing excellent recognition of AOH.

Selective MIPs for AOH and TeA were optimized with a library of MIPs prepared in bulk format in small scale following a combinatorial approach. The best polymer compositions were used to prepare MIPs in the form of highly porous microspheres. The latter are prepared in the presence of a sacrificial silica core, which is dissolved with NH_4HF_2 after polymerization, yielding mesoporous MIPs that confer the spheres improved mass transfer kinetics with respect to the bulk materials.

Besides a complete spectroscopic characterization of the proposed sensing systems, a thorough characterization based on chromatographic methods (HPLC with fluorescence or absorption detection) has also been carried out in collaboration with the GSOLFA Group members Javier L. Urraca, Lidia N. Gómez-Arribas and Alberto Rico-Yuste. For example, the HPLC analysis of some of the prepared MIP adsorbents for AOH has allowed optimization of chromatographic conditions for applying these MIPs as selective stationary phases in solid phase extraction (SPE) of AOH instead of sensors.

This Thesis Dissertation is organized into five chapters, namely "I- Introduction", "II- Molecularly imprinted polymers for alternariol recognition", "III- Development of luminescent MIPs for tenuazonic acid detection", "IV- Pyrene-labeled acrylamide monomers" and, finally, "V- Experimental part".

I- Introduction. The Introduction section provides a description of fungi and mycotoxins, focusing on the properties of the *Alternaria* metabolites AOH, AME and TeA, as well as on the available analytical methods for their determination. Then, the concept of MIP is described (polymer composition, polymerization strategies, principles of SPE related to MIP adsorbents, etc.). A brief overview of existing types of chemical sensors is also given, focusing on those providing a luminescent signal and the use of luminescence-based assays with MIPs. Finally, a brief description of the chemical and photochemical properties of luminescent Eu(III) β-diketone chelates and pyrene fluorophores,–characterized in this Thesis as both microenvironment polarity probes and photochemically active functional monomers–, is provided in this chapter.

II- Molecularly imprinted polymers for alternariol recognition. In the first part of this chapter, the design, preparation and spectroscopic characterization of four fluorescent surrogates of AOH (S1 to S4) are described. The surrogates bear a different number of phenol groups in various positions and different degree of *O*-methylation on the dibenzo[b,d]pyran-6-one skeleton, mimicking the chemical structure of the natural AOH and AME mycotoxins. The surrogates have been spectroscopically characterized by UV-Vis absorption spectroscopy as well as steady-state and time-resolved fluorometry. Also, two other non-fluorescent surrogates of AOH (S5 and S6) were synthetized. Then, a comprehensive library of mixtures of basic, acidic or neutral monomers, with divinylbenzene or ethyleneglycol dimethacrylate as cross-linkers, were polymerized at a small scale in the presence of the four fluorescent molecular mimics of the toxin molecule. This polymer screening has allowed selection of the optimal composition for the synthesis of MIP microbeads. *N*-(2-aminoethyl)methacrylamide (EAMA), ethylene glycol dimethacrylate (EDMA) and the surrogate S2, were finally chosen as the optimal functional monomer (FM), cross-linker (CL) and template (T), respectively. The polymers prepared with a 1:2:2:20 S2/EAMA/MAM/EDMA mole ratio (MAM, methacrylic acid, was employed as diluent monomer) were able to bind AOH in water–acetonitrile (80:20, v/v) mixtures with an affinity constant of 109 ± 10 mM^{-1} and a total number of binding sites of 35 ± 2 µmol g^{-1}, being alternariol monomethylether the only competitor species of those assayed. Moreover, ^{1}H-NMR titrations have unveiled a 1:2 S2-to-EAMA stoichiometry, the exact interaction sites and a binding constant of 1.5×10^{4} M^{-2}. A molecularly imprinted solid phase extraction (MISPE) method has been optimized for selective isolation of the mycotoxin from aqueous samples upon a discriminating wash with water–acetonitrile (80:20, v/v) mixture followed by HPLC analysis with fluorescence detection. The method has been applied, in combination with ultrasound-assisted extraction, to the analysis of AOH in tomato samples fortified with the mycotoxin at five concentration levels (33–110 µg kg^{-1}), with recoveries in the 81–103% range (RSD, $n = 6$). To the best of our knowledge, we describe the first imprinted material capable of molecularly recognizing the widespread food contaminant AOH.

As the analytes, AOH and AME, are small fluorescent molecules (λ_{abs}^{max} = 341 nm and λ_{em}^{max} = 390 nm, in MeCN) and its surrogates have similar properties, we considered that fluorescence anisotropy measurements could be employed for monitoring their binding to the MIP. The extent of which the emitted light is polarized (when the fluorophore is excited with polarized light), depends on the Brownian rotation time that dramatically changes when the free analyte (very low polarization) binds to a polymer cavity (an increase of polarization). In addition to the high sensitivity usually provided by fluorescence-based methods, another advantage is that polarization-based measurements can provide artifact-free information on the number of guest species bound to the MIP at different concentrations. For instance, a tight binding of S2 to the MIP slows down its rotation raising dramatically its fluorescence anisotropy (up to 0.27). In this way, we have used the changes in the fluorescence polarization to directly determine the amount of toxin or surrogates bound to the MIP. This part of the work was performed in collaboration with Prof. Robert Pansu in the *École Normal Supérieure de Cachan* (France).

III- Development of luminescent MIPs for tenuazonic acid (TeA) detection. In the third chapter, synthesis of the (racemic) TeA mycotoxin (85% yield) in the form of sodium salt (NaTeA) is described in the first place (besides the prohibitive price of TeA for upscaled MIP synthesis, all commercial suppliers provide the mycotoxin in the form of Cu(II) complex, useless as template for any MIP synthesis). Several complexation studies were carried out with this salt in methanolic solution, showing the good capability of this *β*-diketone ligand to coordinate Cu(II) and Eu(III) cations. The latter feature, together with the fact that NaTeA has a maximum absorption at 276 nm (at 284 nm when complexed to Eu(III)), led us to consider the possibility of using TeA as an antenna ligand for Eu(III) luminescence sensitization. If a MIP is doped with a Eu(III) complex with aqua-labile ligands, coordination of TeA should induce an increase in Eu(III) typical luminescence at 615 nm. This luminescence increase could be used for detecting the presence of the target mycotoxin. Indeed, when copolymerizing a Eu(III)-DEAM complex (DEAM = diethylallylmalonate, a *β*-diketone derivative carrying a polymerizable unit) with EDMA in the presence of NaTeA, pro-luminescent MIPs are obtained

that can selectively indicate the presence of TeA. Following a combinatorial approach, different Eu(III)-doped polymers (MIPs and NIPs) were prepared in bulk format with several Eu(III)-DEAM ratios. Also, a different *β*-diketone monomer (allyl acetoacetate, AACA) was alternatively employed as functional monomer (FM). Luminescence titration experiments demonstrated that the best Eu(III)-to-FM ratio was 1:3. In this way, two coordination positions are available for TeA coordination to the Eu(III) core. The effect of water on the luminescence of the MIP was also tested. The best signal output was collected in neat MeCN (water is a well-known quencher of Eu(III) emission). A three-fold increase in the luminescence intensity could be obtained upon addition of TeA to a suspension of the Eu(III)-doped MIP in MeCN (much stronger that the signal increase for the non-imprinted material). Finally, three different types of porous MIP microspheres were prepared (MPE1, MPE2 and MPE3) using the optimized TeA/Eu(III)/FM mole ratio of 1:1:3. Luminescent titrations with suspensions of the MIP microparticles in MeCN (0.67 mg mL^{-1}) provided limits of detection for TeA of 5.2, 9.9 and 4.0 µM for MPE1, MPE2 and MPE3, respectively, enabling the determination of 15, 30 and 14 µM of TeA in MeCN. Cross-reactivity studies with other mycotoxins (zearalenone and alternariol) or some usual food matrix components (glucose and fructose) revealed the excellent selectivity of the novel MIP materials for TeA recognition. Only a molecular surrogate of TeA (with leucine as a precursor, *s*TeA) or cyclopiazonic acid (an analogous toxin, also with a *β*-diketone structure) caused an increase of the luminescence of the Eu(III)-doped MIPs prepared.

IV- Pyrene-labeled acrylamide monomers. The Dissertation fourth chapter describes the synthesis and spectroscopic characterization of four acrylamide/methacrylamide monomers containing *N*-(pyren-1-yl) or *N*-(pyren-1-methyl) moieties as fluorescent labels. These monomers have been designed to exploit the well-known properties of pyrene as a molecular probe of the polarity of its immediate environment to explore in the future the MIP binding sites of the analyte. Moreover, these monomers will serve to recognize alternariol and other analytes with extended aromatic structure due to their ability to form donor-acceptor adducts with such species (in the MIP binding sites). The photophysical characterization of the

pyrenyl(meth)acrylamide monomers has shown that the pyrene moiety fluorescence is dramatically decreased when directly attached to the (meth)acrylamide *N* atom, making them useless for the sought purpose. However, if the polymerization and the pyrene moieties are separated by a methylene group, the high fluorescence quantum yield (close to unity) and lifetime (above 300 ns in the absence of dissolved molecular oxygen) are as high as those of the unsubstituted hydrocarbon. These features make the synthesized pyrenyl(meth)acrylamides excellent polarity probes also usable when they will be (covalently) tethered to the polymer backbone. We have also investigated the photophysical and photochemical features of their quenching with the dissolved O_2 in various solvents (acetonitrile, cyclohexane and dichloromethane). Finally, we have preliminarily studied the photochemistry of *N*-(pyren-1-ylmethyl)methacrylamide (PMeMA) with one of the alternariol surrogates described in chapter II, using anionic surfactant micelles to mimic the MIP binding sites for the real toxin. An efficient fluorescence quenching has been observed, paving the way for the future development of highly fluorescent pyrenemethyl(meth)acrylamide-based MIPs for polycyclic aromatic analytes.

V- Experimental Part. The Experimental section provides a detailed description of the reagents and instrumentation used; the protocols followed for preparation of the different templates and the fluorescent pyrene monomers (with full ^{1}H- and ^{13}C-NMR, FTIR, mass spectrometry and elemental analysis data, as well as UV-vis absorption, steady-state fluorescence and time-resolved fluorescence features); the procedures to prepare the MIP and NIP (non-imprinted polymer) libraries; the polymerization protocols for synthesizing the mesoporous MIP microbeads; the optimization of chromatographic conditions for the application of MIPs to the separation and pre-concentration of AOH by SPE and the fluorescence polarization studies.

The most relevant Conclusions of the Thesis work are collected at the end of the Dissertation, together with an Annex that provides details on the full spectroscopic characterization of all the compounds synthesized in our laboratory.

I-Introduction

INDEX

I.1. Fungi and mycotoxins

Fungi are eukaryotic organisms omnipresent occurring as yeasts, mushrooms or moulds. Upon presence of a decomposed organic matter like dead plant material or deceased animals, they take a vital part in the natural recycling processes which sustain evolution. However, the desirable fungal biodegradation may turn into a problematic biodeterioration if raw materials or food are infected. The apparent reasons for this are changes in looks, taste, smell and consistency of the infected material. While these changes are usually easily recognised, a fungal infection may also be accompanied by a release of toxic compounds. Such contamination is not readily perceived and thus represents a significant non-obvious aspect of fungal biodeterioration. Besides the products of their life-sustaining primary metabolism, fungi biosynthesize and release a wide range of biologically active secondary metabolites. Some of these compounds are qualified as drugs, a famous example being the first antibiotic known to man, Penicillin, a secondary metabolite of *Penicillium chrysogenum* discovered by Alexander Fleming in 1928. Other metabolites, however, are unfortunately toxic and hence unsuited for medicinal or safe uses.

A toxin, in general, can be defined as a small molecule, peptide or protein that synthesized by a plant, an animal species, or a micro-organism, which is harmful or able to cause disease to another organism. Mycotoxins are toxic secondary metabolites with a relatively low molecular weight (≤

700 g mol^{-1}), which are produced by a few fungal species under the right conditions of humidity and temperature [1, 2].

Mycotoxins can be produced by fungi imperfect and ascomycota, including those fungal genera which were colloquially referred to as mould, while compounds produced by poisonous mushrooms are not covered by this definition. Mycotoxins are heat-stable molecules. Around 300–400 mycotoxins and their biological conversion products are known [3], belonging to approximately 300 fungal species [4, 5], displaying a significant structural and toxicological diversity. The possible structure elements are pyrones, anthraquinones, coumarins, macrocyclic lactones, steroids and cyclic polypeptides. Their pathogenic effects range from slight skin irritations to severe organ impairment or to the genesis of malignant tumours. The reasons for the production of mycotoxins by moulds are understood only to a limited extent. Some mycotoxins trigger cellular differentiation processes in the fungal thallus [6], thus fulfilling a hormone-like function. Pathogenic fungi are known to use phytotoxic mycotoxins to weaken plant hosts. Eventually, the antimicrobial or even antifungal activity of certain mycotoxins suggests a defence mechanism directed against competitors like bacteria or other fungal species [7]. In any case, the adverse impact on humans and mammals appears to be a merely collateral effect.

Mycotoxicoses are intoxications caused by mycotoxins. They are usually triggered by the consumption of contaminated feed or food [8]. Almost all recent outbreaks of human mycotoxicoses can be related to a lack of GAP (good agricultural practice) favouring the growth of moulds, e.g. the wet storage of harvested grains. For this reason, acute mycotoxicoses in humans are not of great concern to the Western industrialised world [8], where GAP is largely established. Here, the vast majority of fatalities related to foodborne disease are caused by bacterial pathogens [9]. Still, though seemingly contradictory, mycotoxins are recognised as a major concern in scientific, economic and political arenas [10, 11-13]. This is due to the high risk of subacute or chronic intoxications which is sustained by the ubiquitous occurrence of low mycotoxin quantities in foods as well as by the often severe carcinogenicity, mutagenicity or teratogenicity of the compounds [3]. Mycotoxins are considered the most potent natural carcinogen known [14] and have consequently motivated researchers as well as regulatory authorities to focus on the chronic effects caused by the repeated ingestion of low quantities of mycotoxins.

I.2. Alternariol and alternariol monomethyl ether

I.2.1. Biosynthesis

Alternaria is one of the fungi families which has the ability of producing several mycotoxins such as alternariol (3,7,9-trihydroxy-1-methyl-6H-dibenzo[b,d]pyran-6-one) (AOH) or alternariol monomethyl ether (3,7-dihydroxy-9-methoxy-1-methyl-6H-dibenzo[b,d]pyran-6-one) (AME) [15, 16]. AOH and its methylated form AME are polyketide mycotoxins which involve in their biosynthesis a polyketide synthase. Polyketide synthases are large multifunctional enzymes, which are coded by one gene that is usually located within a cluster of biosynthesis genes of the respective mycotoxin. Recently, Saha, *et al.* identified the pksJ gene as the gene responsible for the biosynthesis of AOH and AME [17, 18].

I.2.2. Chemical structure

Alternaria fungi toxins are very different from a structural point of view. As recently described by Lou, *et al*. [19], secondary metabolites from *Alternaria* reported so far belong to several groups, such as nitrogen-containing compounds (amide, cyclopeptides, and others), steroids, terpenoids, pyranones, quinones, phenolics, and other miscellaneous compounds. Regardless, those relevant from a toxicological point of view can be classified as: (1) dibenzo-α-pyrones which include AOH and AME, and (2) tetramic acid derivatives such as tenuazonic acid. AOH and AME carry three and two phenolic hydroxyl groups, respectively, which make them good candidates for the formation of hydrogen bonds. Their structures are depicted in Fig. 1.1. As most of the food-relevant mycotoxins, AOH and AME are stable at acidic pH, but they can be easily degraded by alkali through the hydrolysis of the lactone moiety followed by decarboxylation [16]. However, alkaline conditions are not common for food processing; thus, it can be argued that these mycotoxins are rather stable upon the most widely used food-related treatments [20].

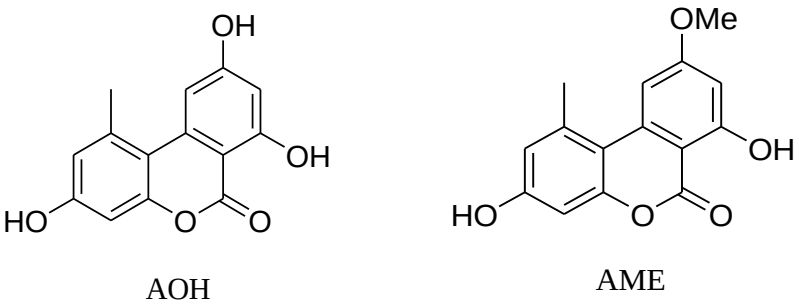

Figure 1.1: Chemical structure of the widest spread *Alternaria* species: alternariol (AOH) and alternariol monomethyl ether (AME).

I.2.3. Occurrence in food

Information on the natural occurrence of AOH or AME in food is still scarce; however, both mycotoxins have been detected in marketed products at concentrations in the 1 – 10^3 µg kg^{-1} range [21, 1]. High values have also been reported in sunflower seeds and food products including fruit juices, tomato derivatives, beer and wine [22]. The natural occurrence of AOH and AME has been reported in several cereal grains all over the world such as wheat, barley, and sorghum [23, 24]. Mycotoxins may also be found in beer and wine resulting from the use of contaminated barley, other cereals and grapes in their production. They can also enter the human food chain via meat or other animal products such as eggs, milk, and cheese. The fungi can grow at low temperatures, thus causing spoilage even during transport and storage. In the case of a plant, these molds can be found in soil, plants, food, feed and indoor air, and are among the main microorganisms responsible for pre- and post-harvest damage to agricultural products [21, 25-38].

I.2.4. Toxicological data

In 2011 the European Food Safety Authority (EFSA) reviewed information regarding the safety of *Alternaria* derived toxins in food and feed, such as alternariol and alternariol monomethyl ether [39, 40]. Alternariol and alternariol monomethyl ether are genotoxic for bacteria and mammalian cells in vitro. The biological activity of these compounds is described below [1, 41-48].

In plants. Phytotoxicity: *Alternaria* fungi include several species that are important plant pathogens, infecting all the aerial parts of plants and causing different plant diseases, e.g., early blight diseases of vegetables, brown spot of tangerines, or post-harvest black rot of fruit [49]. Also, they are widely

distributed on wheat, cotton, fruits, and vegetables as pathogen fungi. Therefore, they are responsible for significant financial losses in the food industry.

In human and animals. Among the numerous mycotoxins that commonly occur in foodstuffs, alternariol and alternariol monomethyl ether, draw scientific attention because of their toxigenic properties on animal and human health. The toxicological impact of *Alternaria* toxins on humans and livestock is still under study; some of the metabolites are powerful mycotoxins [50] with mutagenic [51] and teratogenic effects [52] and have been linked to certain types of cancer [53]. Current studies show that AOH can act as an endocrine disruptor by various modes of action. For example, AOH and AME can inhibit the ovarian steroid hormone progesterone (P4) secretion in cultured porcine granulosa cells. *Alternaria* toxin-contaminated food may, therefore, affect reproductive performance in mammalian species [47]. It has also been observed that AOH is a weak oestrogenic mycotoxin that also can interfere with the steroidogenesis pathway [54]. It was also recently reported that alternariol can act as a topoisomerase poison [55]. Moreover, the mold *Alternaria* is a recognised allergy-causing fungus [56]. On the other hand, some metabolites from species of *Alternaria* were used as antibacterial and antitumor substances [57, 58]. Some in vitro studies have demonstrated that both AOH and AME are mutagenic and clastogenic [59], with AOH showing higher genotoxicity than AME.

I.3. Tenuazonic acid

I.3.1 Biosynthesis

Tenuazonic acid (TeA), (3*Z*)(5*S*)-[(2*S*)-butan-2-yl]-3-(1-hydroxyethylidene)pyrrolidine-2,4-dione, is a natural "tetramic acid" (2,4-pyrrolidinedione) which is biosynthesized by moulds of the *Alternaria, Aspergillus, Pyricularia* genera as well as by soil fungi of the *phoma* genus. TeA was first isolated from *Alternaria tenuis* in 1957 [60], its structure elucidated in 1959 [61] and identified as a metabolite of *Alternaria* in 1963 [62]. The species *Alternaria alternata* is probably the most important TeA producer, as its pathogenic capacities enable it to attack over 100 potential plant hosts [63]. TeA itself contributes to the pathogenicity of *A. alternata* by acting as a phytotoxic agent [64] inhibiting the plant's photosystem II [65]. The biosynthesis of TeA is not entirely elucidated. However, it is assumed to proceed through *N*-acetoacetylation of the essential amino acid L-isoleucine by acetoacetyl-CoA (coenzyme A) and a subsequent ring formation [66, 67].

I.3.2. Chemical structure

TeA is a small, polar, non-volatile compound with an acid dissociation pK_a of 3.5 [68] comparable to that of formic acid (pK_a = 3.8). Its 1,3,5-triketone substructure enables TeA to efficiently chelate metal cations and allows for an extensive tautomerism involving keto/enol chemistry as well as bond rotation. In solution, TeA will hence be represented by a complex system of equilibrated structural species including different keto/enol tautomers, rotamers, protonated and deprotonated forms as well as various chelates, depending on the metal cation content of the solution [69, 70]. The structure of its most abundant tautomer is depicted in Fig. 1.2.

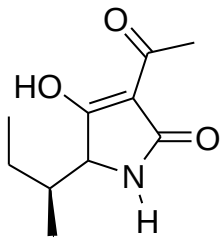

Figure 1.2: Chemical structure of *Tenuazonic acid* (**TeA**).

I.3.3. Occurrence in food

Tenuazonic acid is a prevalent *Alternaria* mycotoxin in processed tomato products, dried figs, sunflower seeds, wine, apples, beer, buckwheat flour, maize, mandarins, melons, oilseed rape, olives, peppers, rice or sorghum, and it can be found at high levels, up to a maximum of 1000 µg kg^{-1} [1, 32, 38, 71-73].

I.3.4. Toxicological data

Few data are available about acute toxicity of *Alternaria* major toxins in animal models, although these compounds have been identified for decades. The data on the different aspects of TeA toxicity can be considered insufficient. One of the main limitations to the design of extensive biological tests is the toxin amount required for these experiments. Due mainly to the production and purification costs, the use of high amounts of toxins for in vivo trials is still difficult; most of the acute toxicity tests have been thus performed using laboratory cultures [52, 57, 74, 75]. However, it is known that TeA is acutely toxic towards several mammalian species, *i.e.* mice, chickens, and dogs, with LD_{50} (median lethal doses) of 81 and 168 mg/kg bw (body weight) in female and male mice, respectively [1, 14]. It has been suggested that it is responsible for the lethality of crude alternaria extracts to mice and rats [76, 77]. It has also been associated with brown spot disease of tobacco [78] and with black spot of apple and pear trees [79]. The potential hazards of this compound are described in a recent review of alternaria metabolites [57]. In the case of mammalian species, the mechanism of toxicity probably involves the inhibition of peptide bond formation during ribosomal protein biosynthesis [80]. Certain subacute effects of TeA sodium salt inhibited the cytopathic effect of a broad spectrum of viruses. Also, it showed an antiviral effect against enteroviruses [81]. It has also been demonstrated in dogs, that feeding of 10 mg/kg bw resulted in haemorrhages in several organs [1]. In mice, feeding of 25 mg/kg bw TeA per day led to precancerous changes in esophageal mucosa, indicating a possible promotion of esophageal cancer by TeA Fig. 1.3 [82]. Other biological effects (antiviral, antibacterial, antifungal and antitumor) have been described as well [14, 52].

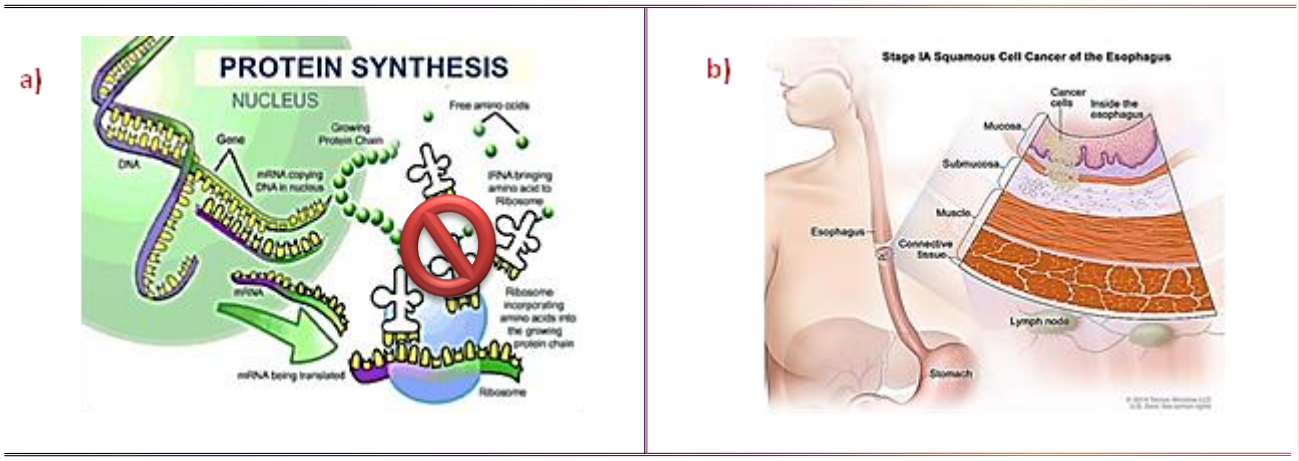

Figure 1.3: Some examples of the toxic effect of tenuazonic acid: **a)** Inhibition of peptide bond formation during ribosomal protein biosynthesis and, **b)** possible promotion of oesophagal cancer in mice [83, 84].

I.4. Current methods for detecting AOH, AME and TeA in food and feed samples

I.4.1. Detection of AOH and AME

Mycotoxin contamination is largely dependent on temperature and moisture conditions and may occur at various stages of production (e.g., in the field, during harvest, transport or storage) [85, 86]. Therefore, it is important to monitor their presence to prevent their introduction into the food chain. At present, no formal regulations or limits for any of the Alternaria toxins have been set in any country. However, sensitive and selective analytical methods are required to study their toxicity and detect their presence in different food matrices preventing mycotoxin contamination of derived commercial products [2, 5, 71-73, 82, 87-101].

Methods reported in the literature for AOH and AME analysis include gas chromatography, thin-layer chromatography or high-performance liquid chromatography with UV, fluorescence or mass spectrometry detection [1, 102-106]. Recently, two immunochemical methods (ELISA-type) have been set for determination of AOH in apple and tomato, with detection limits (IC_{20}) of 35 ± 6.9 pg mL^{-1} [107]. An indirect competitive assay in corn showed a sensitivity of 0.4 ng ml^{-1} for AOH [108].

I.4.2. Detection of tenuazonic acid mycotoxin

One of the first scientists who developed an analytical detection method for TeA was Pero and co-workers by using gas chromatography for the analysis of *Alternaria* metabolites [109]. Other methods of analysis involve an enzyme immunoassay [110], or methods relying on mass spectrometry such as i) a method that requires TeA derivatization with 2,4-dinitrophenylhydrazine (DNPH) for conversion of tenuazonic acid into a stable derivative that can be separated chromatographically [73] or, ii) a stable isotope dilution assay (SIDA) using [$^{13}C_6$,^{15}N] showing a limit of detection of 0.1 μg kg^{-1} and a limit of quantification of 0.3 μg kg^{-1} with a recovery close to 100% in the range of 3-300 μg kg^{-1} [90]. Tenuazonic acid has been determined in a series of food commodities [89, 90, 111]. The current methods based on liquid chromatography-tandem mass spectrometry (LC-MS/MS) can determine most of the mycotoxins simultaneously [112-114].

Still, it would be of interest the development of alternative analytical methods that could be more accessible, cheaper and easier to use, especially by non-trained personnel for the quick and sensitive detection of these widespread mycotoxins.

I.5. Molecularly imprinted polymers

Optical sensing methods that rely on the use of biomolecules (DNA, antibodies or enzymes) as recognition elements are very selective and sensitive [115, 116]. However, they have important drawbacks due to their high sensitivity to temperature changes, ionic strength, and pH of the medium. Also, there is the possibility of biomolecule contamination by traces on their active sites [117, 118]. *Synthetic* receptors that are capable of changing their optical characteristics in a predictable way in the presence of a substrate are likely to be less prone to suffer from these shortcomings and therefore could provide a promising alternative for developing sensors [119-121]. Molecularly imprinted polymers (MIPs) were introduced as a human-made alternative for the development of selective recognition elements.

The technique of molecular imprinting dates back to 1931 when the first “imprinted” polymer for benzene based on silica gel was serendipitously prepared by Polyakov [122]. MIPs have currently a broad range of applications from structural studies of ligand-receptor interactions to

selective binding matrices in detection, separation, and purification [123, 124]. The use of MIPs in the development of sensors is advantageous because they can be used to bind the targeted compound selectively while ignoring all others in a complex matrix [123, 125-133]. Modern MIPs are organic polymers which are synthesized in the presence of a template –our target analyte or, alternatively, a structurally related compound known as *surrogate*– in a way that, after polymerization, the template molecule is removed leaving behind binding sites which are complementary in shape, size and functional groups to the target analyte [134] Fig. 1.4. With the aim of keeping the *memory* of the imprinted cavities in different chemical environments, a highly cross-linked network must be prepared. One of the advantages of MIPs is that they can often be easily prepared in a one-pot synthesis. The cavities that have been created in such a way can selectively recognize and bind the target analyte, in a way that they resemble the selective binding pockets present in some proteins (notably antibodies). This makes the possibility of using MIPs as *biomimetic* recognition elements in the development of chemical sensors very interesting since the synthetic polymers are more stable and cheaper to produce than the corresponding biomolecules.

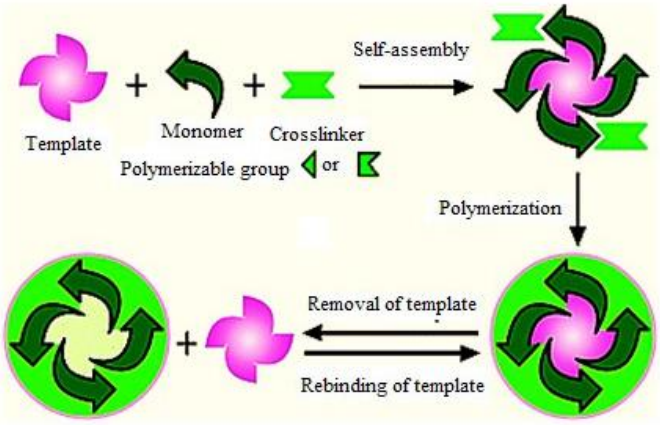

Figure 1.4: Synthetic scheme for the preparation of a molecularly imprinted polymer (MIP) [135].

I.5.1. Strategies for molecular imprinting of polymers

Since the pioneering work of Polyakov [136], several imprinting methods have been used for preparing MIPs for different purposes. Table 1.1 shows a summary of the main imprinting techniques described to date.

Table 1.1: Strategies for the preparation of MIPs.

Imprinting	Approach	Characteristics
Covalent [137, 138]	It requires the synthesis of a template derivative with polymerizable groups; the template is copolymerized with the matrix, thus linked by covalent bonds to the polymer. It normally yields better defined binding sites [139-141]	a) Need of template derivatization. b) Chemical cleavage of the covalently bound template molecule is required at the end (normally acid/base hydrolysis). c) Slow binding kinetics.
Non-covalent [142]	Based on physico-chemical interactions of the template molecule and the functional monomer: H-bonding, electrostatic interactions, van der Waals forces and/or hydrophobic interactions for organic analytes, or electrostatic interactions and/or coordinative bonds for inorganic templates.	a) Very simple. b) A wide variety of functional monomers can be used. c) Limited organic synthesis required. d) It has higher binding capacity than the covalent approach.
Semi-covalent [143]	Based on the use of sacrificial spacer methodology. This method can be viewed as a combination of covalent and non-covalent imprinting approaches. In fact, the template is covalently bonded to the polymer while the rebinding occurs through non-covalent interactions. This method is particularly of use with templates lacking binding sites.	

I.5.2. Polymer composition

Most MIPs described in the literature to date, have been prepared with the following basic approach: firstly, the template (T) and the functional monomer (FM) are co-dissolved in the appropriate solvent mixture (the solvent is normally called *porogen* in MIP literature, since it is the component providing a typical porosity to the resulting material) and then, a cross-linker (CL) is added to the polymerization mixture (sometimes also a "diluting co-monomer" (DM) is added for improving the T-FM interaction). Once the solution has been purged with an inert gas to avoid the presence of dissolved oxygen, a radical initiator (I) is added, and the polymerization is started either thermally or photochemically. For optimizing selectivity of a MIP, different T, FM, DM, CL, I and porogen can be tested, and also the T:FM:DM:CL:I molar ratio can be adjusted.

Template. Molecularly imprinted polymers have been developed for many classes of templates such as toxins, antibiotics, drugs, dyes, and metal ions [144-146]. These molecules normally have multiple sites for interaction with the functional monomers; therefore, they are likely to produce

highly specific and selective binding sites in the polymer. Thermodynamic studies indicate that non-rigid templates such as proteins, yield imprinted sites with very poor selectivity [147]. In contrast, rigid templates normally provide polymer binding sites with higher affinity and selectivity. Other studies show that a molar excess of functional monomer *vs.* template produces in most cases more favourable results [146].

Functional monomers. Commonly used functional monomers are listed in Fig. 1.5. The choice of monomer(s) type and optimisation of the ratio between monomer(s) and template are the most critical features for MIP performance including selectivity and binding capacity [148, 149]. An ideal situation in MIP technology is that a functional monomer should be able to form strong interactions with the template either through covalent or non-covalent bonding [150]. During MIP synthesis, especially when using the non-covalent imprinting approach, a large monomer-to- template ratio is used [151].

UV-vis, FTIR [152, 153], NMR [154-157] and computer simulation methods such as the density functional theory (DFT) [158, 159], as well as trial-and-error methods, have been used for the selection of a functional monomer that will produce the most stable monomer-template interactions. A more comprehensive review of the methods used for selection of appropriate functional monomers was published by Karim, *et al.* [160]. Other readings on the computer-aided selection of functional monomer and porogen can also be found in the following articles [161-168]. Molecular dynamics have been recommended as a fast and reliable method for searching for optimal imprinting conditions, including screening for functional monomers [152, 169-174].

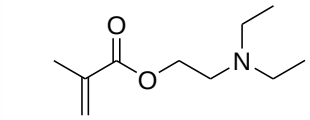
2-(diethylamino)ethylmethacrylate (DEM)

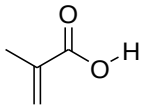
methacrylic acid (MAA)

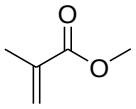
methylmethacrylate (MMA)

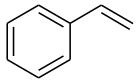
styrene

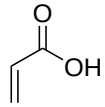
acrylic acid (AA)

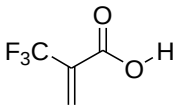
trifluoromethacrylic acid (TFMAA)

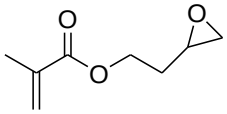
glycidylmethacrylate (GMA)

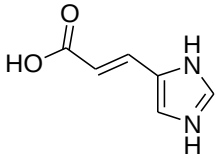
imidazole-4-acrylic acid

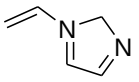
1-vinylimidazole

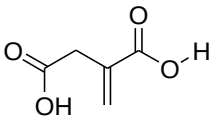
methylene succinic acid (IA)

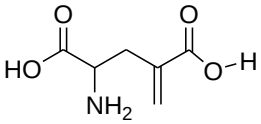
y-methylene-DL-glutamic acid

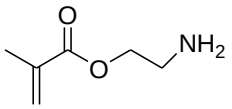
2-(Aminoethyl)methacrylate

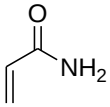
acrylamide (AAM)

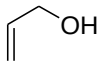
Allylalcohol

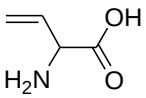
Vinylglycine

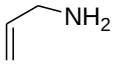
Allylamine

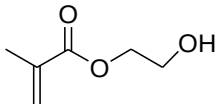
2-hydroxyethylmethacrylate (HEMA)

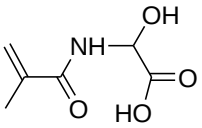
methacrylamidoglycolate

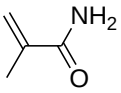
methacrylamide (MAM)

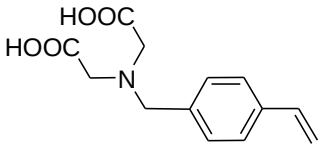
4-vinylbenzyl-iminodiacetic acid

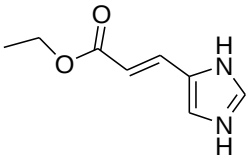
imidazole-4-acrylic acid ethyl ester

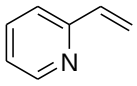
2- vinylpyridine (2-VPY)

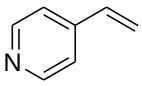
4- vinylpyridine (4-VPY)

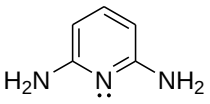
2,6-diaminepyridine

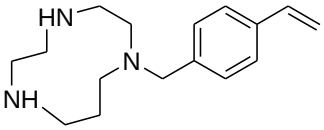
1-(4-vinylbenzyl)-1,4,7-triazocyclononane

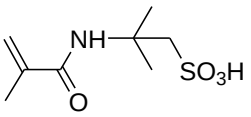
2-Acrylamide-2-methyl-1-propane sulphonic acid

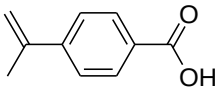
4-vinylbenzaldehyde (VBA)

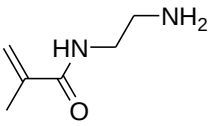
N-(2-aminoethyl) methacrylamide (EAMA)

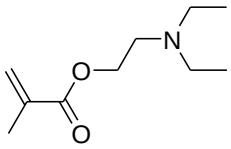
2-(Diethylamino)ethyl methacrylate (DAEM)

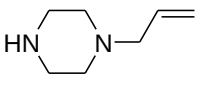
1-Allylpiperazine (1-ALPP)

Figure 1.5: Common functional monomers employed for MIP production.

Cross-linkers. A proper selection of the cross-linker is also of vital importance. Cross-linkers are responsible for the polymerization reaction yield, polymer morphology, stabilization of the binding sites, and mechanical and thermal stability of the polymer. Amongst the many cross-linkers used, ethylene glycol dimethacrylate (EDMA) and trimethylolpropane trimethacrylate (TRIM) are the most commonly utilized [175]. TRIM is more suitable when precipitation polymerization is used [176]. EDMA is mostly used in bulk polymerization and provides a lot of features and benefits to the obtained polymer: chemical resistance, flexibility, high crosslinking density and heat/solvent resistance [177]. Typically, a molar ratio of 4:1 or 5:1 of cross-linker to functional monomer is used. Using too much of the cross-linker can impede the binding of the analyte because it might be difficult to remove the template completely, resulting in polymers with low binding capacity. Also, the cross-linker should have fewer interactions with the template to prevent the formation of non-specific binding sites. Fig. 1.6 lists some of the most common cross-linkers.

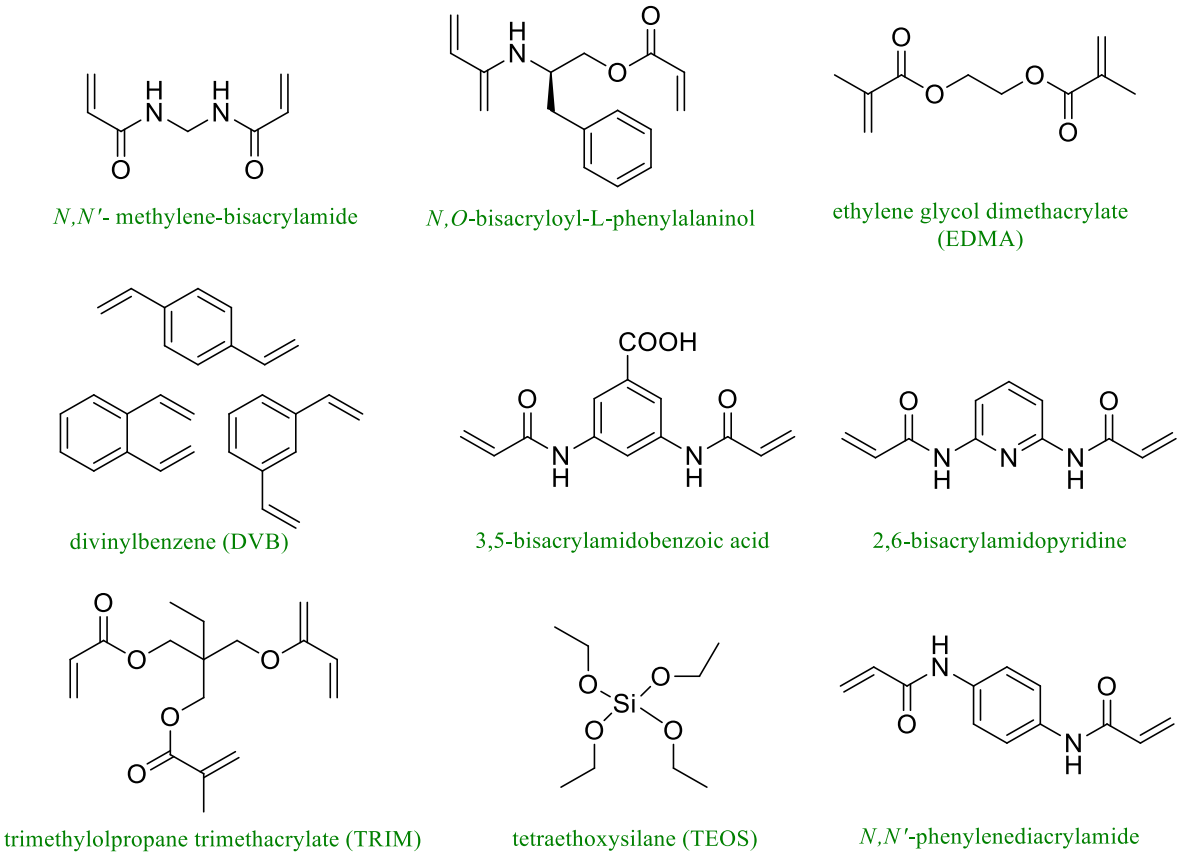

Figure 1.6: Examples of cross-linkers commonly employed for MIP synthesis.

Porogenic solvent. Of further importance is the role of the polymerization solvent. The choice of the porogenic solvent is critical in most molecular imprinting procedures. The porogen influences the morphology (inner surface area and average pore size) and accessibility of the binding sites [178]. For most functional monomers, the selective interaction with the analyte is achieved by H-bonding or ionic interactions, depending on the solvent and pH of the solution being percolated (in solid-phase extraction applications). A stable interaction between the functional monomers and the template will depend on the type of the solvent employed [179]; aprotic solvents favour H-bond interactions, while ionic interactions preferable occur in polar protic solvents (water:ethanol for example). Some common solvents used in MIP synthesis are acetone, acetonitrile, chloroform, dichloromethane, *N*,*N*-dimethylformamide, ethanol, methanol, tetrahydrofuran and toluene. Working in an aqueous medium, as required for pharmaceutical, clinical and environmental applications, make the task of MIP recognition very challenging, because water molecules compete with the template, making weaker or destroying noncovalent interactions with the functional monomer. Hydrophobic and ionic interactions, metal coordination and cyclodextrin complex formation are proving to be very promising to enhance template-functional monomer association in water.

Radical initiators. Literature reveals that the most commonly used method for preparing MIPs uses azo-derivatives as radical initiators [175]. One of the most widely used compound is the azo-*N*,*N*'-bis(isobutyronitrile) (AIBN) or related compounds. The polymerization reaction can be initiated thermally or by light. Normally, mild reaction conditions with temperatures under 80 ºC are used (or light if lower temperatures are selected). In MIP synthesis, the choice of initiator is equally important as other parameters as it can influence the morphology and binding capacity of the polymer. Therefore, to maximize the formation of the labile complex of template and monomer, the initiation conditions must be carefully chosen to minimize non-specific binding sites. Fig. 1.7 shows some of the available initiators that can be used as the radical source in free radical polymerization.

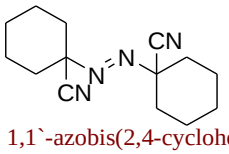

1,1`-azobis(2,4-cyclohexanecarbonitrile)

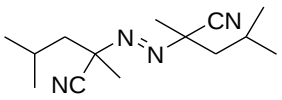

2,2`-azobis(2,4-dimethylvaleronitrile)

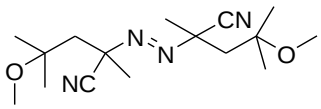

2,2`-azobis(2,4-dimethyl-4-methoxyvaleronitrile)

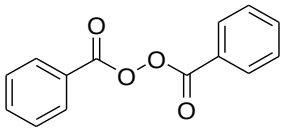

benzoyl peroxide

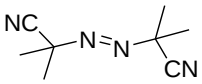

2,2'-Azobis(2-methylpropionitrile)

Figure 1.7: Radical initiators commonly employed for MIP synthesis.

Table 1.2: Different types of polymerization procedures for MIP synthesis.

Bulk polymerization	All components are dissolved in a small amount of solvent. A polymer monolith is formed who is grounded to obtain irregular micrometric particles. Drawbacks: i) destruction of the polymer binding cavity during the grinding process, ii) small surface to volume ratio of the particles obtained. Advantage: it is a simple method and no special equipment is needed.
Precipitation polymerization	It is an analogue to the bulk polymerization method, but using a higher dilution. The excess of solvent allows obtaining spherical particles in the range of 0.3-10 µm. Particle size depends on: i) stirring, ii) template was chosen and, iii) volume of solvent.
Grafting polymerization	Covalent attachment of the polymer to particles or a membrane that is used as the substrate. The initiator activates the substrate surface for polymer growth. Advantage: the use of an atom transfer radical polymerization (ATRP) initiator that generates two radicals during fragmentation. This method provides particle sizes of 15-20 nm or even 30 nm by increasing monomers concentration.
Core-shell polymerization	It is used for the preparation of structured composite particles consisting of at least two different components, a core and a shell.

I.5.3. Polymerization strategies for the synthesis of MIPs in different formats

Depending on the desired polymer particle size and shape, different polymerization techniques such as suspension, emulsion or seed polymerization techniques can be used. Table 1.2 summarizes the main characteristics of different polymerization techniques.

Optimization of MIP synthesis. Variables that can be optimised during polymer synthesis are the nature and amount of monomers, crosslinker, porogen, initiator and the method of initiating the polymerization (thermally or photochemically). For speeding up the optimization, *a combinatorial imprinting protocol* can be used. This approach relies on the systematic variation of the composition of the mixture used in the synthesis of MIP preparing only small amounts of polymers in a series of vials. The properties of each polymer are then evaluated, and the composition yielding a polymer with best recognition properties will be chosen for preparing a MIP on a larger scale.

I.5.4. Use of MIPs in solid phase extraction

Solid phase extraction (SPE) is a well-accepted sample preparation technique in the Analytical Chemistry community [180]. Since the 1980 decade, the use of SPE in Analytical Chemistry has greatly increased. SPE is a very common method for sample preconcentration and for clean-up protocols. This method is used to selectively extract, concentrate and purify target analytes prior to further analysis by chromatographic techniques, allowing a rapid sample preparation. It is a form of solid adsorption chromatography ranging from simple hydrophobic or hydrophilic partition chromatography to ion-exchange or affinity chromatography.

Principles. Sample preparation with SPE consists of four basic steps: i) cartridge conditioning, ii) sample loading, iii) washing off of the interferences and, iv) elution of the target analyte. The analyte is eluted as a clean extract before using a suitable analysis technique Fig. 1.8.

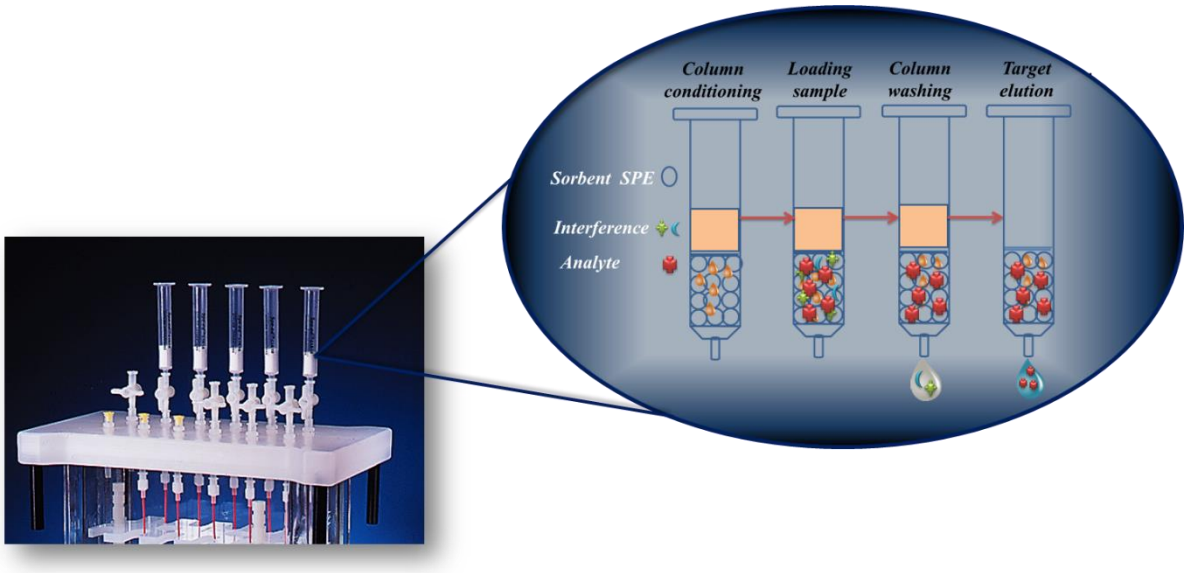

Figure 1.8: Basic steps in solid phase extraction SPE [181].

MISPE (Molecularly Imprinted Solid Phase Extraction). The application of MIPs as sorbents in SPE has been found to be very useful for selective extraction of a target analyte because MIPs offer higher selectivity than other conventional SPE sorbents. MIPs can efficiently reduce the influence of the matrix on the resulting chromatogram and high sample enrichment factors are achieved [182]. The first successful application of a MIP material as a sorbent in SPE (MISPE) was described by Sellergen in 1994. This author could successfully extract pentamidine –a drug used to treat pneumonia in AIDs patients– from human urine using a MISPE cartridge [183]. Since then, MISPE has been applied for sample pre-treatment in the fields of environmental and pharmaceutical analysis [184]. If this technique is used for selective extraction of the analyte from a complex matrix, the sensitivity of HPLC analysis is subsequently improved. Besides the offered selectivity, an additional advantage of using MIPs as a sorbent in SPE is that normally, the materials employed are very stable over a wide range of temperature, organic solvents and pH.

I.5.5. Challenges of molecularly imprinted polymers

Besides the many advantages of MIPs to be used in Analytical Chemistry as selective, cheap and stable recognition materials, still, some challenges should be faced in the design of new MIPs. Table

1.3 lists some of these handicaps and describes possible strategies that could be followed to overcome these problems.

Table 1.3. Current challenges in MIP technologies and possible solutions [185].

Problem	Possible solutions
Incompatibility with aqueous media	1. Two-step extraction 2. Polymerization in aqueous phase using hydrophilic monomers or non-hydrogen bond interactions (metal chelate or hydrophobic interactions) 3. Surface modification of MIPs: use of Restricted Access Materials-Molecularly Imprinted Polymers (RAM-MIP) with a hydrophilic external layer 4. Novel functional monomers
Bleeding of template molecules that gives false positive analysis	1. Molecular imprinting with an analogue or surrogate instead of the analyte itself [1] 2. Preparation of a nanostructured imprinted polymer 3. Preparation of a highly porous imprinted polymer
Heterogeneous binding sites	1. Semi-covalent imprinting or covalent imprinting 2. Selective chemical modification of low-affinity sites

I.6. Chemical sensors. Definition and classification

A sensor is something that receives information and transforms it into a form compatible with our perception, knowledge and understanding. In nature, our body is full of sensors that respond to light, heat, taste, and so forth [186, 187, 188]. Each sensor responds to an external stimulus by converting it into an electrical signal that is sent to the brain through the nerves. Examples of biological sensors are numerous. During the 20th century, the large development of industry has led to the large development of sensor technology. Nowadays, sensors have become an integral part of our daily life and are encountered in so many fields and used for such numerous applications, that it would be too long to describe all of them in this chapter. For example, sensors are used in the automotive industry, in environmental or food analysis, in clinical diagnostics, or for the detection of illicit drugs. Concerning these "artificial" sensors, they can be divided into two types: *physical* sensors and *chemical* sensors. Physical sensors provide information about a physical property of the system.

[1] If the analogue is not possible to obtain, an alternative could be using new template removal methods such as thermal annihilation, microwave-assisted extraction and desorption with supercritical fluids.

Chemical sensors respond to specific chemical substances (molecules or ions) by delivering a measurable physical or chemical signal. For chemical sensors, a *recognition element* is required to respond to the presence of the analyte. The recognition process can be of three types:

- Physical: no chemical reaction takes place. Typical measurements are based on the change of absorbance, refractive index, conductivity, temperature or mass.
- Chemical: a chemical or photochemical reaction involving the analyte and the recognition element induces the analytical signal.
- Biological ("biosensors"): a sub-class of the chemical sensors; here the chemical reaction occurs between the analyte and a biological recognition element, such as an enzyme, an antibody, a DNA strand or a cell.

This interpretation states that the receptor transforms the chemical information given by the presence of a specific analyte in the form of energy that can be measured by the transducer. Then the transducer transforms this energy into a useful, measurable signal that can be analysed by an observer.

The definition of the chemical sensor has been somewhat dynamic throughout the last thirty years, being updated as necessary and also with several literature examples of its misuse. In 1990, Wolfbeis defined "chemical sensors" as: "*small-sized devices comprising a recognition element, a transduction element, and a signal processor capable of continuously and reversibly reporting a chemical concentration*" [189, 190]. This interpretation states that if a device is to be considered as a chemical sensor, it is mandatory that it functions in a continuous and reversible way, eliminating from such group all test strips and disposable sensing schemes ("dosimeters"). One year later, in 1991, the International Union of Pure and Applied Chemistry (IUPAC) set a definition for a chemical sensor as "*a device that transforms chemical information, ranging from the concentration of a specific sample component to total composition analysis, into an analytically useful signal; the chemical information may originate from a chemical reaction of the analyte or a physical property of the system investigated*". Chemical sensors contain two basic functional units: a receptor and a transducer part. Some sensors may include a separator which is, for example, a polymer thin film [191]. A more restrictive definition of chemical sensors that was set in 2008 defines chemical sensors as "*miniaturized analytical devices that can deliver real-time and online information on the*

presence of specific compounds or ions in complex samples" [192]. Such statement is also known as the "Cambridge definition" and, although missing the term reversible, it states that a characteristics of good chemical sensors are the following: it must perform under online operation mode which implies it should work either reversibly, or be capable of (fast unattended) in situ regeneration [193]. This feature allows a unique specific response towards the measured analyte, high sensitivity, and fast response time. Moreover, it is cost effective and requires less human intervention.

In a recent publication, the authors show concern over the severe general misuse of the term chemical sensor in the last decade, justifying its use as the sole purpose of augmenting publication value [194]. The chemical sensing device may be described by three separate components: the sample which contains one or more analytes to be recognized by the molecular "detector", a transducer which accounts for the conversion of such recognition patterns into a measurable signal, and a signal processor to relate the signal to analyte concentration [192, 195]. Fig. 1.9 shows a real application of a chemical sensor for monitoring glucose levels in a blood sample. The working principle of the sensor is as follows: within the test strip, the blood is mixed with glucose oxidase, which reacts with the glucose in the blood sample to create gluconic acid. Another chemical within the test strip, ferricyanide, then reacts with the gluconic acid to create ferrocyanide. The electrode within the test strip then runs a current through the blood sample and the ferrocyanide influences this current in such a way that the concentration of blood glucose within the sample can be accurately measured within a fair margin of error.

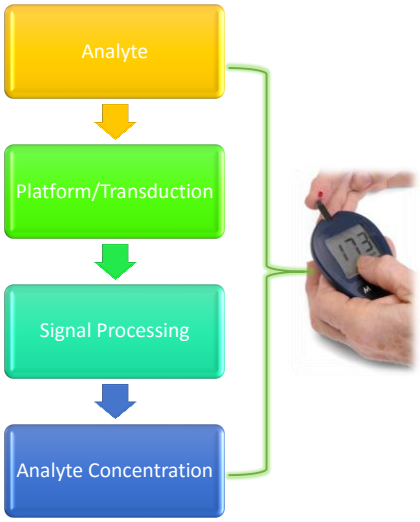

Figure 1.9 : Example of a chemical sensor used for monitoring glucose levels in a blood sample [196].

Chemical sensors can be divided into four main groups depending on the working principle of their transducers. Numerous literature reports describe the features of such groups, the two major ones being electrochemical and *optical*, but others are also identified such as electrical, mass sensitive, magnetic and thermometric sensors [189, 191, 197-200]. These groups can be divided into subgroups depending on the type of measurements. Table 1.4 summarizes a general way to classify sensors. There are, of course, other possible classifications, for example, depending on their applications or the analyte to be detected (pH sensors, metal ions sensors, gas sensors, etc.).

Table 1.4: General classification of chemical sensors, based on the classification made by IUPAC.

Type	Working principle of the transducer	Sensing mode	Measurement
Optical	Transforms changes in optical parameters resulting from the interaction between analyte - recognition element	Absorbance	In a transparent medium.
		Reflectance	In a non-transparent medium.
		Chemiluminescence	Light intensity emitted by a chemical reaction.
		Fluorescence	Positive emission caused by irradiation (includes also quenching).
		Refractive index	Result of a change in composition (includes surface plasmon resonance).
Electro-chemical	Transforms the effect of an electrochemical reaction between analyte - electrode into a measurable signal	Voltammetric	Electrical current.
		Potentiometric	Potential of the indicator electrode against a reference electrode.
Mass-sensitive	Transforms a mass change into a change in a property of the support	Piezoelectric	Frequency change of a quartz oscillating plate induced by mass adsorption of the analyte.
		Surface acoustic wave	Variation of the propagation velocity of an acoustic wave induced by mass adsorption of the analyte.
Calorime-tric	Heat effect induced by a chemical reaction or after adsorption of the analyte	Heat	Molar enthalpy changes in enzymatic reactions.

The next sections of this chapter will focus on the description of MIP based opto-chemical sensors, which are the purpose of this work.

I.7. Basic principles of fluorescence spectroscopy

Fluorescence, or more generally, luminescence is one of the most popular tools used for chemical sensing [191]. This is the result of immense developments on the optical platforms that improve their response regarding sensitivity, selectivity, stability, robustness, response time, etc. Compared to other traditional analytical methods, fluorescence spectroscopy is more sensitive, and can thus detect compounds in much lower concentrations. It is, additionally, a non-destructive technique that offers *multiparametric* information (spectral position, intensity, emission lifetime, light polarization) and can be used remotely with the employment of fiber optics.

Depending on the mode used for electronic excitation, the mechanism behind the luminescence change will be different [195, 201] Table 1.5.

Table 1.5: Different mechanisms of luminescence depending on the excitation mode.

Phenomenon	Excitation mode
Photoluminescence (fluorescence, phosphorescence)	Absorption of light (photons)
Radioluminescence	Ionising radiation (X-rays, α, β, γ)
Thermoluminescence	Heating after prior storage of energy
Chemiluminescence	Chemical process (e.g. oxidation)
Bioluminescence	Biochemical process

Luminescence describes the emission of ultraviolet, visible or infrared photons from an electronically excited species that decays through a radiative pathway to the ground state. There are several possibilities of returning to the ground state. Figs. 1.10 and 1.11 summarize the most important phenomena are occurring after electronic excitation of a molecule. Depending on the energy of the light, the molecule is excited to different electronic singlet states (S_1, S_2…). Relaxation

through emission of light though will normally occur from the lowest energy excited electronic state of a molecule S_1 (Kasha's rule) [202]. The excited molecule can return to the ground state via non-radiative processes: (i) internal conversion (IC, for example, by collision with the solvent), or (ii) intersystem crossing, ISC, towards the most stable triplet excited state (T_1). Emission of a photon from this triplet excited state is slower because the transition T_1 to S_0 is spin-forbidden. This slow emission of light is known as *phosphorescence* and normally occurs in the millisecond to the second or even minute's time range. On the other hand, if the radiative emission is spin allowed, that is, associated to a S_1 to S_0 transition, the term used is *fluorescence*, which is faster than phosphorescence and normally occurs within the 1 to 10 ns time range. Some compounds show an intermediate behaviour between fluorescence and phosphorescence. For example, some transition metal complexes show a metal to ligand charge transfer emission (MLCT) that decays radiatively in the microsecond time scale. These compounds are described as luminescent compounds. The heavy-atom effect (acceleration of the ISC rate) is responsible in these cases for the "mixed" singlet-triplet spin system, particularly known for rhodium(II), ruthenium(II), osmium(II) and iridium(II) complexes [203-213, 214-216].

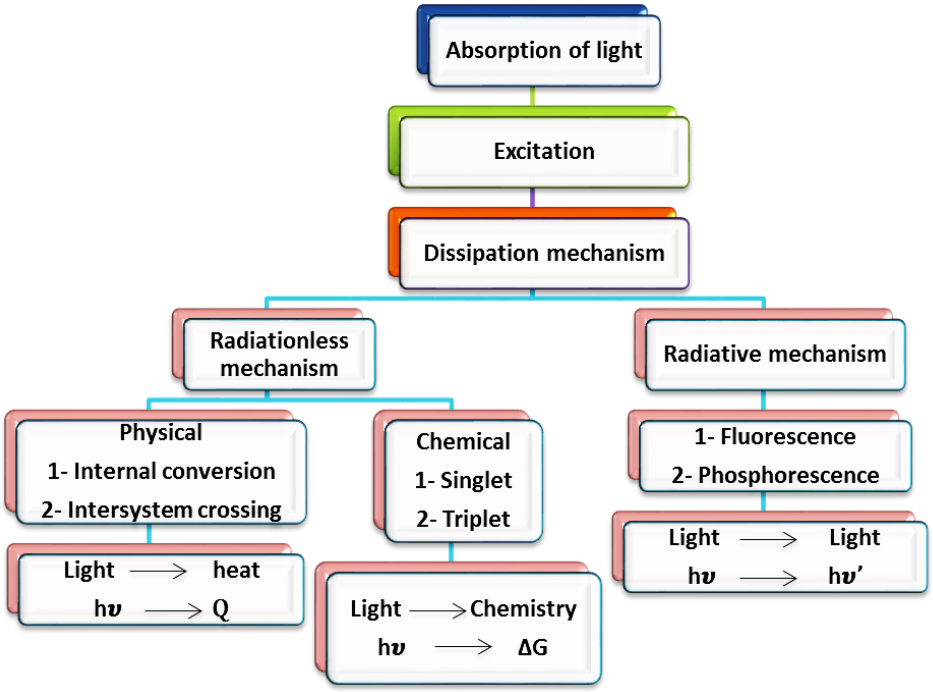

Figure 1.10: Deactivation processes that can take place after electronic excitation of a molecule.

As already mentioned, normally emission occurs from the lowest excited state, and thus at a specific wavelength, independent of the energy of the excitation light [217, 218]. Usually, there is a loss of energy (IC) before the light is emitted. Thus, the emitted light is red-shifted with respect to the absorbed light. This is known as the Stokes shift.

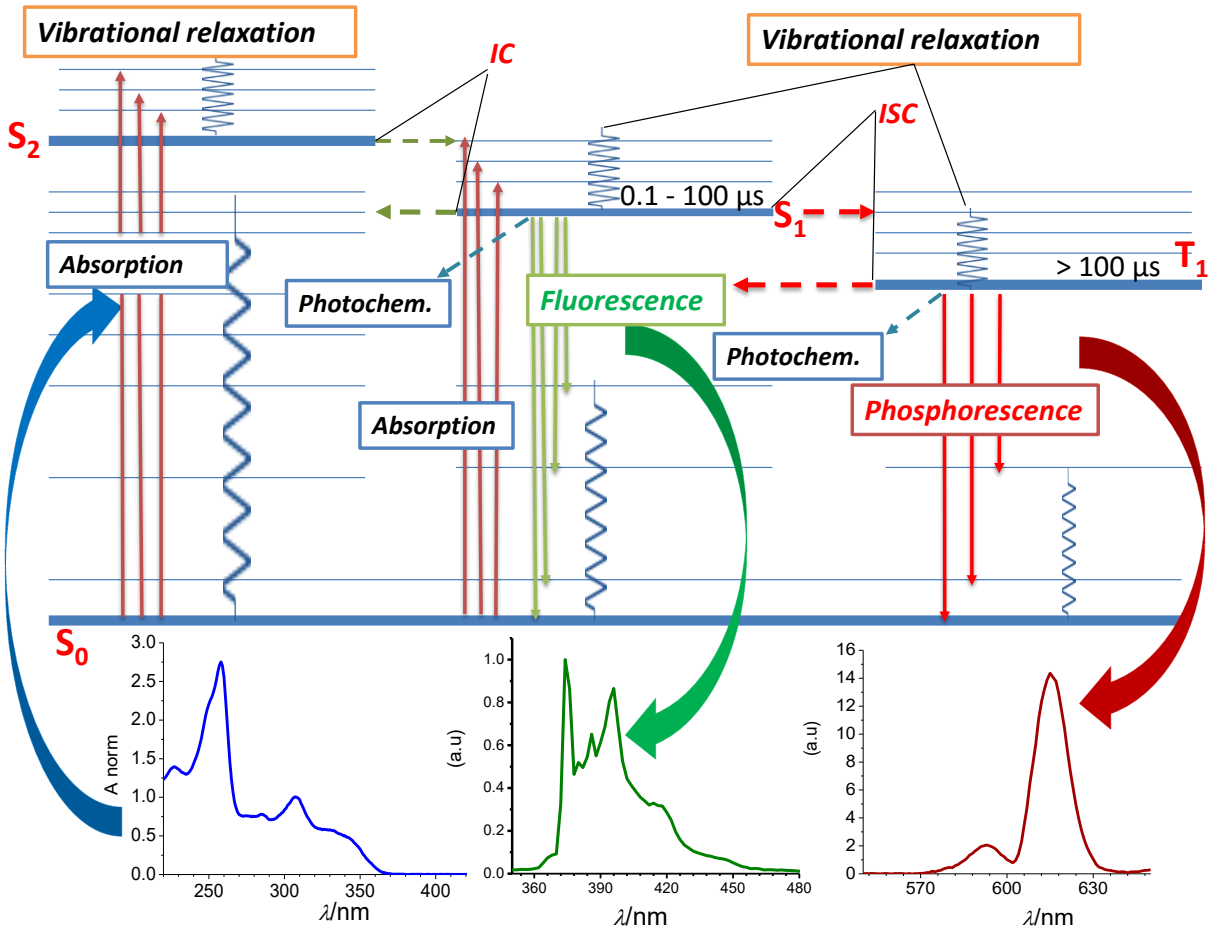

Figure 1.11: Energy level (*Jablonsky*) diagram for a molecule showing pathways for the deactivation of an excited state: ***IC*** is an internal conversion; and ***ISC*** is an intersystem crossing. The lowest vibrational energy level for each electronic state is indicated by a thicker line. The ground electronic state is shown in black, and three electronic excited states are shown; absorption process is shown in blue, the emission of fluorescence in green, and the emission of phosphorescence in red.

In principle, when measuring a single fluorescing molecule, the excitation and absorption spectra will be identical. Regarding the emission spectrum, it often has a single band with a Gaussian shape. However, sometimes there are "spikes" or "fingers" in the absorption and emission spectrum. This is due to the transitions to different vibrational levels. The shape of excitation and emission spectra is often described with the mirror image rule which states that the emission spectra ($S_1 \rightarrow S_0$ transition), is a mirror image of the excitation/absorbance spectrum ($S_0 \rightarrow S_1$ transition) [217, 218].

I.7.1. Luminescence and chemical sensing

Any fluorophore that suffers a change in its initial luminescence properties upon analyte addition, e.g. quenching or an increase of its emission ("turn-off" or "turn-on" sensing, respectively), emission wavelength shift or emission lifetime variations, is a potential fluorescent probe. Alternatively, it is also possible to directly determine the concentration of an analyte, if the target molecule itself has an intrinsic fluorescence.

The combination of fluorescence as detection technique with MIPs as the recognition element in a sensor device would be fascinating. This would allow the fast, selective and sensitive quantification of the mycotoxins of interest, in this thesis work, *i.e.* AOH and AME toxins –with intrinsic fluorescence–, and the non-fluorescent TeA food contaminant.

I.7.1.1. Type of sensors depending on the photochemical response

The relationship between a luminophore concentration (in solution) and the intensity of its emission is a linear one Eq. 1.1:

$$I_L = \phi_L I_0 \kappa \varepsilon_\lambda \; l \; c \qquad (1.1)$$

where ϕ_L is the luminescence quantum yield (the ratio of the emitted to absorbed photons per unit of time), I_0 the intensity of the excitation light, κ is an instrumental parameter, ε_λ is the luminophore absorption coefficient at the excitation wavelength ($dm^3\ mol^{-1}\ cm^{-1}$), l is the optical pathlength (cm) and c is the concentration of the luminophore (mol dm^{-3}).

When using a fluorescence emission signal for analysis of a sample, one must be careful with some drawbacks that can be encountered and can lead to false optical responses:

- Photobleaching of a dye can lead to a noticeable signal drift. To avoid this, a possibility is to use fluorescent probes that can respond via ratiometric measurements. Another option is to perform measurements based on the variation of emission lifetime values or variation of fluorescence anisotropy, instead of intensity-based measurements.
- Significant scattering when solid samples are measured in comparison to solution measurements. For minimizing scattering problems appropriate filtering of stray light can be performed, and also the problem is minimized when using luminophores with large Stokes shifts, that permit a good separation between excitation light and detected radiation. Luminescent molecules with large Stokes shifts are for example those displaying so called photoinduced intramolecular charge transfer (ICT) emission, due to the large difference in the dipolar moment of the excited state compared to that of the ground state.

One of the most widespread ways of detecting the presence of a target analyte in a sample is by *quenching* of the emission. It means, the luminescence of the corresponding luminophore is reduced or eliminated. This can normally be correlated with the concentration of the analyte. There are two different types of luminescence quenching:

i) Static quenching. When the luminophore and the quencher (the target analyte or a related species) are pre-associated before photoexcitation (they are forming a complex in the ground state). Normally molecular probes are designed with specific receptors that can bind a certain guest, and this binding induces a change in the intensity of luminescence of the probe (no change in the excited state lifetimes is observed). Different photochemical processes might be responsible for the latter, such as changes in a photoinduced ICT process, changes in a PET (photoinduced electron transfer), influence on an excited state proton transfer, etc.

ii) ***Dynamic quenching***. When the photochemical process is the result of a collision between the photoexcited indicator dye and the quencher species. In this case, both the intensity and the emission lifetime value are affected. Luminescent-based molecular oxygen sensors, for example, make use of the energy transfer after collisional quenching of a triplet excited state, which reduces both the intensity and lifetime of photoexcited coordination complexes due to dynamic quenching. A representative example is that using luminescent complexes of ruthenium(II) as probes [195].

I.7.2. Principles of fluorescence anisotropy

It should be reminded that light is an electromagnetic wave whose components are perpendicular to the direction of the light propagation. In the case of fluorescence anisotropy, we are only interested in the electrical field, where specific photoselection processes of excited fluorophores from the initial ensemble yield excited state fluorophores oriented in parallel to a specific axis. Fluorescence emission will be then partially or totally polarised as long as the fluorophore does not rotate faster than its emission lifetime. Measurements of the relative angle between the excitation and emission transition dipole moments determine both fluorescence polarization (*P*) and fluorescence anisotropy (*r*), as given by Eqs. 1.2 and 1.3:

$$P = \frac{I_{||} - I_{\perp}}{I_{||} + I_{\perp}} \tag{1.2}$$

$$r = \frac{I_{||} - I_{\perp}}{I_{||} + 2I_{\perp}} \tag{1.3}$$

Where, $I_{\parallel}$and $I_{\perp}$, are, respectively, the parallel and perpendicular components of the intensity of the emitted light of a fluorophore excited by a plane-polarized light.

Anisotropy and polarization are both expressions for the same phenomenon; the values can be easily interconverted. In most cases, the anisotropy expression is preferred because the associated mathematical equations are simpler. The relationship between *r* and *P* is given by Eq. 1.4:

$$r = \frac{2P}{(3 - P)} \tag{1.4}$$

According to the definition, the theoretical limit of *P* or *r* should be ± 1. Actually, this value is not reached because of the photoselected excitation of the fluorophores. Briefly, if a fluorophore sample is excited with polarized light, the molecules with their transition dipoles aligned parallel with the electric vector of the excitation light have the highest probability to absorb the light. This probability is proportional to $cos^2\theta$, where θ is the angle of the polarized excitation light and the transition dipole of the fluorophore. If θ = 0°, then the absorption is maximum; on the other hand, if θ = 90°, the probability of absorption will be minimum.

Therefore, any change in the direction of the transition moment during the lifetime of the excited state will cause the anisotropy to decrease. Consequently, it will induce a partial (or total) depolarization of fluorescence.

The causes of fluorescence depolarization are:

a. Non-parallel absorption and emission transition moments
b. Torsional vibrations (a shift along its axis of rotation)
c. Brownian motion (random movement of particles suspended in a fluid)
d. Transfer of the excitation energy to another molecule with a different orientation

The limits of the fluorescence polarization values can be the calculated by considering two extreme situations. First, if the angle θ between the excitation and emission transitions is 0° (which means that the excited fluorophore does not rotate during the excitation lifetime, for example in a frozen or very viscous medium), then the fluorescence anisotropy has a maximum value of 0.4. Second, if $\theta = 90°$, then $r = -0.2$ ($P = -0.33$). The limiting values for r are +0.4 and –0.2; details of the theoretical calculations can be found in the literature (e.g. [219]). If these limit values are exceeded, this could mean that a light scattering event occurred. Another source of error is related to the instrument itself because the varying anisotropy characteristics or efficiencies of monochromators at one given wavelength can affect the measurement of anisotropy. Thus, the anisotropy value must be corrected using a "*G*-factor", expressed as Eq. 1.5:

$$G = \frac{I_{\mathrm{HV}}}{I_{\mathrm{HH}}} \tag{1.5}$$

where, I_{HV} is the intensity with the excitation and emission polarizers oriented horizontally and vertically, respectively (based on the laboratory axes), and I_{HH} is the intensity when both, excitation and emission polarizers, are oriented horizontally. Thus the corrected anisotropy value can be expressed as Eq.1.6:

$$r = \frac{I_{\mathrm{VV}} - GI_{\mathrm{VH}}}{I_{\mathrm{VV}} + 2GI_{\mathrm{VH}}} \tag{1.6}$$

In general, several parameters influence the values of r, such as the molecular size of the fluorophore, its fluorescence lifetime or the viscosity of the solvent. Concerning the molecular size,

the bigger the fluorophore, the higher the anisotropy value, since the rotational rate decreases. Second, the shorter the lifetime, the less time the fluorophore has to rotate and the higher the polarization value will be. Finally, the more viscous the solvent the slower is the rotation of the fluorophore and the higher the anisotropy value. Importantly, fluorescence anisotropy values do not depend on fluorescence intensities or fluorophore concentrations.

Unlike bioanalytical binding assays where the fluorescence detection is based on intensity measurements of the free analyte in the supernatant after separation from the bound analyte, the analysis based on fluorescence polarization is a real-time method requiring no separation step of the bound and free fluorophores. It involves the use of a plane-polarized light to excite the fluorophore. In the case of a small free fluorophore, its tumbling rate is fast and thus the molecules become randomly oriented during the lifetime of the excited state before emitting the fluorescence light, resulting in depolarized emission. However, if the fluorophore is bound to a much larger receptor (an antibody or, in our case, a MIP receptor), the rate of tumbling motion of the complex will be comparable to the rate at which the fluorescence decays, resulting in polarized emission. Consequently, the interaction of a small fluorophore with a receptor, such as a MIP, can be monitored through the increase in fluorescence anisotropy [220, 221]. Also, interferences due to molecules present in the samples that influence the intensity of the excitation and/or fluorescence light are widely reduced in this method compared to simple intensity measurements.

A typical setup employed for fluorescence anisotropy measurements is shown in Fig.1.12.

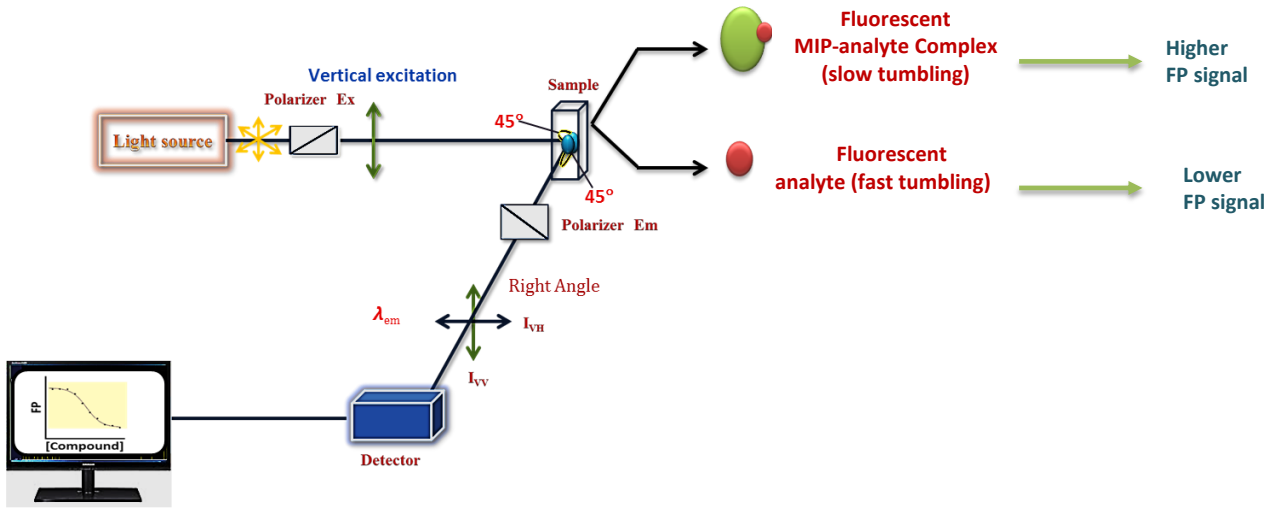

Figure 1.12: Experimental setup for measuring fluorescence polarization.

Applications of fluorescence polarization

Based on the above-described properties of fluorescence polarization (FP)-based measurements we can conclude that they can provide useful information on:

1. Molecular mobility
2. Size, shape and flexibility of molecules
3. Fluidity of a medium

Knopp and co-workers described for the first time a fluorescence polarization immunoassay for detection of environmental contaminants such as polycyclic aromatic hydrocarbons (PAHs) [222]. This authors synthesised fluorescein-labeled tracers based on different PAHs and used polarization and intensity measurements to develop a class-specific assay for small and large PAHs. After that, FP-based assays have become popular as a tool for monitoring small molecules such as abused drugs [223], therapeutic drugs [224], hormones (for example, testosterone [225]), pesticides such as 2,4-dicholorophenoxyacetic acid (2,4-D) [226], and food contaminants such as mycotoxins [227, 228]. Table 1.6 provides a brief information about the advantage that distinguishes FP over other analytical methods and its limitations.

Table 1.6: Advantages and limitations of fluorescence polarization-based techniques.

	Advantages	Limitations
Fluorescence Polarization	• Speediness (rapid reaction kinetics). Measurements usually take a few minutes or even seconds. • High specificity and sensitivity: the working range is generally in the ng mL^{-1} to µg mL^{-1} interval [221]. • Simple procedure: only addition of the tracer to the analyte solution is required, without separation or washing steps.	• The limit of detection is not always as low as that of ELISA technique. • FP is sensitive to light scattering and the presence of other fluorophores in the sample. • Non-specific binding of the analyte to other components present in the sample matrix can occur.

It should be emphasised that FP has the advantage to be easily automated in contrast to other methods using intensity-based tracers and thus, it is particularly suitable for simple and fast screening of small molecules for environmental control and food safety applications. Nowadays, FP is performed more often than ELISA for therapeutic drug and abused drug monitoring [221].

More recently, molecularly imprinted polymers have been used as recognition elements in fluorescence polarization assays. For instance, Hunt, *et al*. described the first pseudo-immunoassay using a MIP as an antibody mimic and the fluorescent probe 7-carboxymethoxy-4- methylcoumarin for the detection of the herbicide 2,4-D [229].

I.8. Fluorescence-based assays with MIPs

In the following sections, we will focus on examples of fluorescence-based assays that employ MIPs as the recognition element. For monitoring the binding event to the MIP, there are several possibilities: i) the analyte itself is fluorescent and it can be directly detected when bound to the polymer, ii) using a competitive assay with a fluorescently labelled analyte, in an analogous manner as that often used for fluorescence-based immunoassays, or iii) the polymer is fluorescent and binding of the analyte induces a change in its fluorescence.

I.8.1. MIPs for fluorescent analytes

If the analyte is fluorescent, the recognition event can be detected directly by measuring the fluorescence of the MIP-analyte complex after binding. The first MIP-based fluorescence sensor was developed by Mosbach and co-workers [230]. The device consisted of a layer of MIP held in front of a quartz window; a light guided with an optical fiber was used to excite the fluorescent analyte retained by the MIP. The emitted light was collected and guided through an optofiber bundle to the detector. The model analyte used here was the fluorescent amino acid derivative dansyl-L-phenylalanine (dansyl-L-Phe). The authors could follow the recognition process of dansyl-L-Phe since the emitted fluorescence signal was a function of the analyte concentration. Moreover, they could also demonstrate the specificity of the MIP using the opposite enantiomer dansyl-D-Phe. More recently, the same group found out that using double templating of PAHs the sensitivity of a MIP sensor could be increased. The authors used a mixture of naphthalene and pyrene (1:4, *w/w*) molecules for imprinting, and this resulted in an increase in the sensitivity of one order of magnitude for the detection of pyrene, with a limit of detection of 10 ng L^{-1} [231].

The major drawback of using fluorescent templates for the preparation of MIPs is that the final polymer usually exhibits residual fluorescence due to the entrapped template molecules that cannot

be washed out, even after a thorough process. To overcome this limitation, one possibility is to use a non-fluorescent analogue of the template [232].

I.8.2. Competitive assays using a luminescently labelled analyte

A representative example, in this case, is an approach followed by Descalzo, *et al.* [233]. In this work, the authors developed core-shell nanoparticles with a luminescent core and an imprinted shell for developing an assay based on FRET (Förster resonance energy transfer) signaling for the detection of the antibiotic enrofloxacin (ENR) [234]. For this analysis, a cyanine-labelled ENR was employed as tracer, providing a FRET signal when bound to the MIP layer. If the concentration of the free ENR analyte was increased, competition for the binding sites of the MIP resulted in displacement of the cyanine-ENR tracer in a way that the FRET signal between the luminescent core of the nanoparticles and the labelled analyte decreased. This signal change was used for ENR detection, with a LOD for the antibiotic of 2 μM.

I.8.3. Use of luminescent MIPs

An attractive approach for the design of fluorescence MIP-based sensors is to incorporate fluorescent probes in the MIP matrix, the fluorescence of which changes upon the target binding [235]. A first example was described by Turkewitsch and co-workers, who incorporated a fluorescent dye (trans-4-[*p*-*N*,*N*-dimethylamino)styryl]-*N*-vinylbenzylpyridinium chloride) as a functional monomer for the recognition of cyclic adenosine-3',5'-monophosphate (cAMP) [236]. Binding of cAMP to the MIP resulted in quenching of the MIP fluorescence. Time-resolved fluorescence spectroscopy was used to characterise the fluorescent cAMP-MIPs. Leung and co-workers, on the other hand, described for the first time a signalling MIP based on fluorescence enhancement upon binding of the analyte [237].

An example of a fluorescent MIP was developed in our laboratories by Pinheiro, *et al.* Here the authors describe the use of an ion-imprinted polymer (IIP) for the fluorescent detection of the Cu(II) cation. This IIP was prepared using a fluorescent functional monomer, 4-[(*E*)-2-(4'-methyl-2,2'-bipyridin-4-yl)vinyl]phenyl methacrylate that was spectroscopically characterized in methanolic solution in the absence and in the presence of Cd(II), Cu(II), Hg(II), Ni(II), Pb(II), and Zn(II) metal ions. The IIPs were prepared by radical polymerization using stoichiometric amounts of

the fluorescent monomer and the template metal cation Cu(II). The resulting cross-linked network did not show any leaching of the immobilised ligand allowing determination of Cu(II) in aqueous samples by fluorescence quenching measurements, with a detection limit of 0.04 μmol L^{-1} [238].

An interesting approach was described by the group of Murray, who used lanthanide luminescence combined with a MIP-based fiber optic sensor for measuring the hydrolysis product of the nerve agent Soman in water [239]. Detection of the nerve agent is based upon the changes that occur in the luminescence spectrum when the hydrolysis product pinacolyl methylphosphonate is coordinated to the Eu^{3+} cation in the MIP. MIPs containing coordinatively bound Eu ions were coated on the distal end of an optical fiber, and rebinding was characterised by the appearance of the narrow luminescence band in the 610 nm region, characteristic of Eu(III) emission, as a result of the coordination between the analyte and the copolymer. The influence of pH and thickness of polymer coating on the response time of the sensor was studied.

I.9. Lanthanide cations as luminescent probes

Regarding the last example, it is important to emphasise that the use of lanthanide(III) ions and more specifically Eu(III) cations, have some interesting features for sensing. The intricate optical properties of the trivalent lanthanide ions, hereafter called Ln(III), are fascinating and originate in the particular features of the electronic $4f_n$ configurations (where n = 0 to 14). As a corollary, inner-shell 4*f*-4*f* transitions, which span both the visible and near-infrared (NIR) ranges, are sharp and easily recognisable. Also, since these transitions are formally parity forbidden, the lifetimes of the excited states are long, which allows time-resolved detection (TRD) of their luminescence. Consequently, lanthanide luminescent probes are amongst the most sensitive luminescent probes known [240-242]. Complexation with Ln(III) has several advantages: i) their narrow excitation and emission spectra allow for sensitive and selective analyses; ii) the complexes possess long emission lifetimes and large Stokes shifts, and iii) they exhibit an intense luminescence when complexed by appropriate ligands; moreover, iv) they emit in the red/NIR region, avoiding the fluorescence background of the polymer matrix or sample components. The only drawback of *f-f* transitions is their weak oscillator strengths. This can be however solved by using so-called "*antenna* ligands" as sensitizers for improving the Ln(III) emission. An antenna ligand is an organic chromophore that coordinates the Ln(III) ion (diketones are employed frequently as chelating agents), can absorb the

excitation light and efficiently transfer it to the metal centre. Weissman demonstrated that excitation of lanthanide complexes into the ligand states results in metal-centered luminescence [243]. Part of the energy absorbed by the organic receptor(s) is transferred to Ln(III) excited states, and sharp emission bands originating from the metal ion are detected after rapid internal conversion to the emitting level Fig. 1.13. The sensitization process provides a large Stokes shift which is often far greater than those commonly shown by organic fluorophores, henceforth allowing an easy spectral discrimination of the emitted light.

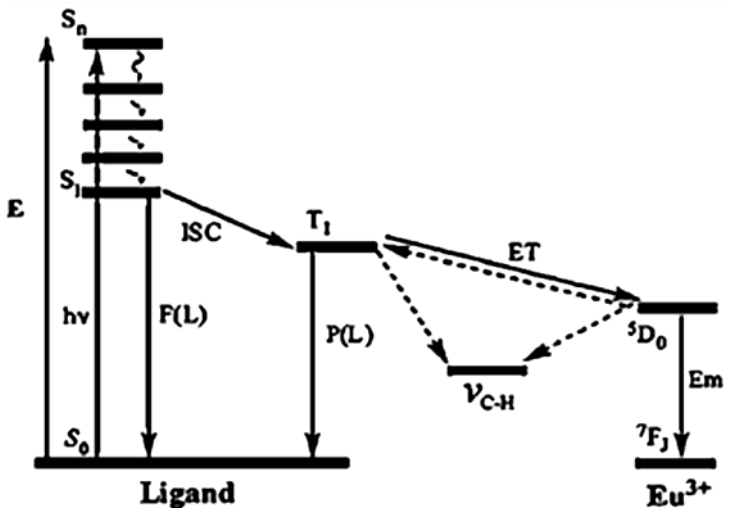

Figure 1.13: Representation of an energy transfer process from a sensitizer excited state (antenna ligand) to a lanthanide ion Eu(III). S_1 = first excited singlet state, T_1 = first triplet state, ET = Energy-transfer. Adapted from Bünzli [244].

I.10. Pyrene as luminescent probe

Pyrene Fig. 1.14 is an important and well-studied chromophore with a rather high fluorescence quantum yield and long emission lifetime (*e.g.* $\Phi_f = 0.6$ and $\tau = 450$ ns in oxygen-free cyclohexane at room temperature), with a violet-blue fluorescence [245, 246]. This fluorophore has been often used as a polarity probe because the relative intensities of the vibrational structure of pyrene fluorescence spectrum are sensitive to the polarity of the surrounding medium. Additionally, and due to its planar, π-conjugated structure, this molecule can easily form spectroscopically distinct, fluorescent excimers via π-π stacking, both in solution and in the solid-state, that can be used to

detect aggregation [247]. These excimers are formed when an excited pyrene forms a complex with another pyrene molecule in the ground state. This complex displays a range of photophysical properties that differ from those of the monomer [248]. In solution, at concentrations above ca. 10 μmol L^{-1} (in methanol), a broad, structureless emission band centred at 480 nm is observed, while the intensity of emission due to the monomer decreases with increasing concentration. π-π stacking interactions have played an important role in supramolecular chemistry [249-254], in particular, in the construction of complex supramolecules [255-260]. As a monomer in solution, pyrene displays an extended fluorescence lifetime. As a result of this long-lived fluorescence, the emission from pyrene is very sensitive to changes in the local environment, such as the addition of external substrates or changes in solvent polarity. Furthermore, it can participate in charge-transfer processes acting either as the electron-donor or as the electron-acceptor depending on the nature of the attached substituent.

All the above-mentioned properties of pyrene have led to its use in a wide variety of applications as a fluorescent *probe*. It can be for example used as an oxygen probe because molecular oxygen is an effective quencher of pyrene long-lived electronically excited state. Careful examination has shown that the fluorescent quantum yields and excited state lifetimes of pyrene derivatives decrease proportionately on aeration of the solutions [247].

I.10.1. Chemical properties of pyrene

Derivatives of pyrene that take advantage of the aforementioned properties are generally synthesised via electrophilic aromatic substitution of the pyrene moiety. Maximum contributions of the HOMO and LUMO can be found at the 1-, 3-, 6- and 8- positions Fig. 1.14; therefore, nearly all pyrene derivatives synthesised by electrophilic aromatic substitution are substituted at the 1-, 3-, 6- and/or 8- positions.

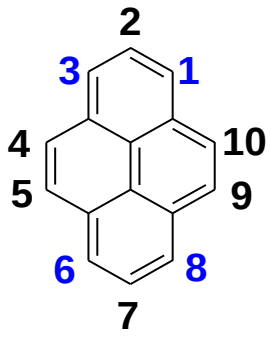

Figure 1.14: Chemical structure and carbon atom numbering of pyrene.

I.10.2. Pyrene in molecular imprinting technology

From the above-mentioned luminescent properties of pyrene, it can be expected that the incorporation of a pyrene derivative as a fluorescent probe in a MIP matrix could be an attractive approach for the detection of chemical species. For example, in the absence of other molecules, the emission of the pyrene monomer would be observed. If a specific target then binds to the MIP and is able to interact with the luminescent pyrene, it could affect to its vibronic structure, to its emission lifetime or to its luminescence intensity, changing the emission properties of the labelled MIP. The analyte could also form an exciplex (*excited state complex*) with the pyrene molecule, something that would deactivate the emission of the pyrene monomer band, and induce the formation of a new broad, red-shifted band.

Some examples of the literature have described the use of pyrene in MIP technology. In someplaces it is related with a direct derivatization of the MIP matrix with the pyrene luminophore; the incorporation of disulfonated pyrenedimethacrylamide into cross-linked poly(acrylate–acrylamide) films as a fluorosensor afforded membranes able to detect waterborne diquat and paraquat herbicides by selective charge-transfer interaction, was published by Chena, *et al.* [261]. Another example also in our group, has described a work where the pyrene probe has been used for labelling the non-fluorescent mycotoxin zearalenone (ZON). This luminescent tracer was applied for ZON determination via a displacement assay using a molecularly imprinted polymer for selective ZON binding –this MIP was prepared using a molecular surrogate of the mycotoxin as the

template–. Analysis of the mycotoxin was performed in an automated flow-through setup by following the displacement of the pyrene labelled ZON from the MIP matrix in the presence of the target mycotoxin. An increase in ZON concentration consequently induced a decrease in the fluorescence signal of the polymer [262]. Other examples in the literature describe the use of MIPs as selective sorbent materials for the extraction of polyaromatic hydrocarbons (PAHs) in environmental or tobacco samples. In these cases, the polymers are simply used for separation and preconcentration purposes [263, 264]. Also, a MISPE procedure was developed for adsorption of PAHs from tobacco smokes, with a good selectivity for benzo[a]pyrene recognition among other 16 PAHs [265].

Bibliography

1. Ostry, V., Alternaria mycotoxins: an overview of chemical characterization, producers, toxicity, analysis and occurrence in foodstuffs. *World Mycotoxin J.* **2008,** *1*, 175-188.
2. Turner, N. W.; Subrahmanyam, S.; Piletsky, S. A., Analytical methods for determination of mycotoxins: a review. *Anal. Chim. Acta.* **2009,** *632*, 168-180.
3. van Egmond, H. P., Natural toxins: risks, regulations and the analytical situation in Europe. *Anal. Bioanal. Chem.* **2004,** *378*, 1152-1160.
4. Hussein, H. S.; Brasel, J. M., Toxicity, metabolism, and impact of mycotoxins on humans and animals. *Toxicology* **2001,** *167*, 101-134.
5. Sulyok, M.; Krska, R.; Schuhmacher, R., A liquid chromatography/tandem mass spectrometric multi-mycotoxin method for the quantification of 87 analytes and its application to semiquantitative screening of moldy food samples. *Anal. Bioanal. Chem.* **2007,** *389*, 1501-1523.
6. Beppu, T., Secondary metabolites as chemical signals for cellular differentiation. *Gene* **1992,** *115*, 159-165.
7. Utermark, J.; Karlovsky, P.; Microbiology, A. a. E., Role of zearalenone lactonase in protection of Gliocladium roseum from fungitoxic effects of the mycotoxin zearalenone. *Appl Environ Microbiol.* **2007,** *73*, 637-642.
8. Peraica, M.; Radic, B.; Lucic, A.; Pavlovic, M., Toxic effect of mycotoxins in humans. *Bull. WHO* **1999,** *77*, 754-766.
9. Nyachuba, D. G., Foodborne illness: is it on the rise? *Nutr Rev.* **2010,** *68*, 257-269.
10. Köppen, R.; Koch, M.; Siegel, D.; Merkel, S.; Maul, R.; Nehls, I., Determination of mycotoxins in foods: Current state of analytical methods and limitations. *Appl Microbiol Biotechnol.* **2010,** *86*, 1595-1612.
11. van Egmond, H. P.; Schothorst, R. C.; Jonker, M. A., Regulations relating to mycotoxins in food. *Anal. Bioanal. Chem.* **2007,** *389*, 147-157.
12. Wu, F., Mycotoxin risk assessment for the purpose of setting international regulatory standards. *Environ. Sci. Technol.* **2004,** *38*, 4049-4055.
13. Wu, F., A tale of two commodities: How EU mycotoxin regulations have affected US tree nut industries. *World Mycotoxin J.* **2008,** *1*, 95-102.
14. Weidenbörner, M., Encyclopedia of food mycotoxins. In *Encyclopedia of food mycotoxins*, 1 ed. Springer-Verlag Berlin Heidelberg: Berlin, 2001; pp XII, 294.
15. Bottalico, A.; Logrieco, A., Toxicogenic alternaria species of economic importance. In *Mycotoxins in agriculture and food safety*, Sinha, K. K.; Bhatnagar, D., Eds. Marcel Dekker, Inc.: New York, 1998; pp 65-108.
16. Siegel, D.; Feist, M.; Proske, M.; Koch, m.; Nehls, I., Degradation of the alternaria mycotoxins alternariol, alternariol monomethyl ether, and altenuene upon bread baking. *J. Agric. Food Chem.* **2010,** *58*, 9622-9630.
17. Wojciechowska, E.; Weinert, C. H.; Egert, B.; Trierweiler, B.; Schmidt-Heydt, M.; Horneburg, B.; Graeff-Hönninger, S.; Kulling, S. E.; Geisen, R., Chlorogenic acid, a metabolite identified by untargeted metabolome analysis in resistant tomatoes, inhibits the colonization by Alternaria alternata by inhibiting alternariol biosynthesis. *Eur J Plant Pathol.* **2014,** *139*, 73-747.
18. Saha, D.; Fetzner, R.; Burkhardt, B.; Podlech, J.; Metzler, M.; Dang, H.; Lawrence, C.; Fischer, R., Identification of a polyketide synthase required for alternariol(AOH) and alternariol-9-methyl ether (AME) formation in Alternaria alternata. *PloS One* **2012,** *7*, e40564.
19. Lou, J.; Fu, L.; Peng, Y.; Zhou, L., Metabolites from alternaria fungi and their bioactivities. *Molecules* **2013,** *18*, 5891-5935.
20. Dall'Asta, C.; Cirlini, M.; Falavigna, C., Mycotoxins from alternaria: toxicological implications. In *Advances in molecular toxicology*, Elsevier Inc.2014; Vol. 8, pp 107-121.
21. Barkai-Golan, R.; Paster, N., *Mycotoxins in Fruits and Vegetables*. Elsevier Inc.: San Diego, CA, USA, 2008; p 395.

22. Marin, S.; Ramos, A. J.; Cano-Sancho, G.; Sanchis, V., Mycotoxins: occurrence, toxicology, and exposure assessment. *Food chem.* **2013,** *60*, 218-237.
23. Li, P.; Nijhawan, D.; Budihardjo, I.; Srinivasula, S. M.; Ahmad, M.; Alnemri, E. S.; Wang, X., Cytochrome c and dATP-dependent formation of Apaf-1/caspase-9 complex initiates an apoptotic protease cascade. *Cell* **1997,** *91*, 479-489.
24. Webley, D. J.; Jackson, K. L.; Mullins, J. D.; Hocking, A. D.; Pitt, J. I., Alternaria toxins in weather-damaged wheat and sorghum in the 1995-1996 Australian harvest. *Aust J Agr Res.* **1997,** *48*, 1249-1256.
25. Motta, S. D.; Valente Soares, L. M., Survey of Brazilian tomato products for alternariol, alternariol monomethyl ether, tenuazonic acid and cyclopiazonic acid. *Food Addit. Contam.* **2001,** *18*, 630-634.
26. Müller, M.; Waydbrink, V. D. G.; Peters, M.; Umann, K.; Seyfarth, W., Contamination of winter wheat with alternaria mycotoxins in the state of Brandenburg. *Mycotoxin Res.* **2002,** *18*, 217-220.
27. Magan, N.; Olsen, M., *Mycotoxins in food*. Woodhead Publishing2004; p 488.
28. Pose, G.; Ludemann, V.; Segura, J.; Pinto, F. V., Mycotoxin production by alternarla strains isolated from tomatoes affected by blackmold in Argentina *Mycotoxin Res.* **2004,** *20*, 80-86.
29. Terminiello, L.; Patriarca, A.; Pose, G.; Fernández, P. V., Occurrence of alternariol, alternariol monomethyl ether and tenuazonic acid in Argentinean tomato puree. *Mycotoxin Res.* **2006,** *22*, 236-240.
30. Abramson, D.; Delaquis, P.; Smith, D., Assessment of ochratoxin A and tenuazonic acid in Canadian ice-wines. *Mycotoxin Res.* **2007,** *23*, 147-151.
31. Patriarca, A.; Azcarate, M. P.; Terminiello, L.; Fernández, P. V., Mycotoxin production by Alternaria strains isolated from Argentinean wheat. *Int J Food Microbiol.* **2007,** *119*, 219-222.
32. Azcarate, M. P.; Patriarca, A.; Terminiello, L.; Fernández, P. V., Alternaria toxins in wheat during the 2004 to 2005 Argentinean harvest. *J Food Prot.* **2008,** *6*, 1262-1265.
33. Bräse, S.; Encinas, A.; Keck, J.; Nising, C. F., Chemistry and biology of mycotoxins and realted fungal metabolites. *Chem. Rev.* **2009,** *109*, 3903-3990.
34. Chun-sheng, W.; Liang, M.; Tao, J.; Li-yan, J.; Fang-fang, D.; Yu-hao, Z., A review on tenuazonic acid, a toxic produced by alternaria. *Shipin Kexue* **2014,** *35*, 295-301.
35. Massi, F. P.; Vieira, M. L.; Sartori, D.; Penha, R. E.; de Freitas Munhoz, C.; Ferreira, J. M.; Iamanaka, B. T.; Taniwaki, M. H.; Frisvad, J. C.; Fungaro, M. H., Brazil nuts are subject to infection with B and G aflatoxin-producing fungus, Aspergillus pseudonomius. *Int J Food Microbiol.* **2014,** *186*, 14-21.
36. Mikusova, P.; Sulyok, M.; Srobarova, A., Alternaria mycotoxins associated with grape berries in vitro and in situ. *Biologia* **2014,** *69*, 173-177.
37. Van de Perrea, E.; Deschuyffeleerb, N.; Jacxsensa, L.; Vekemana, F.; Van Der Hauwaertc, W.; Asamd, S.; Rychlikd, M.; Devlieghereb, F.; De Meulenaer, B., Screening of moulds and mycotoxins in tomatoes, bell peppers, onions, soft red fruits and derived tomato products. *Food Control* **2014,** *37*, 165-170.
38. Lopez, P.; Venema, D.; Rijk, T.; Kok, A.; Scholten, J. M.; Mol, H. G. J.; Nijs, M., Occurrence of alternaria toxins in food products in the Netherlands. *Food Control* **2016,** *60*, 196-204.
39. Gallo, A.; Giuberti, G.; Frisvad, J. C.; Bertuzzi, T.; Nielsen, K. F., Review on mycotoxin issues in ruminants: occurrence in forages, effects of mycotoxin ingestion on health status and animal performance and practical strategies to counteract their negative effects. *Toxins* **2015,** *7*, 3057-3111.
40. Authority, E. F. S., Scientific Opinion on the risks for animal and public health related to the presence of Alternaria toxins in feed and food. *EFSA J.* **2011,** *9*, 1-97.
41. Bradburn, N.; Coker, R. D.; Blunden, G.; Turner, C. H.; Crabb, T. A., 5-Epialtenuene and neoaltenuene, dibenzo-a-pyrones from Alternaria alternata cultured on rice. *Phytochemistry* **1994,** *35*, 665-669.
42. Horiuchi, M.; Maoka, T.; Iwase, N.; Ohnishi, K., Reinvestigation of structure of porritoxin, a phytotoxin of Alternaria porri. *J Nat Prod.* **2002,** *56*, 1204-1205.
43. Li, F.; Yoshizawa, T., Alternaria mycotoxins in weathered wheat from China. *J. Agric. Food Chem.* **2000,** *48*, 2920-2924.

44. Solfrizzo, M.; Vitti, C.; De Girolamo, A.; Visconti, A.; Logrieco, A.; P., F. F., Radicinols and radicinin phytotoxins produced by Alternaria radicina on carrots. *J. Agric. Food Chem.* **2004,** *52*, 3655-3660.
45. Stack, M. E.; Mazzola, E. P.; Page, S. W.; Pohland, A. E., Mutagenic perylenequinone metabolites of Alternaria alternate: altertoxins I, II, and III. *J Nat Prod.* **1986,** *49*, 866-871.
46. Stierle, A. C.; Caddlina, J. H.; Strobel, G. A., Phytotoxins from alternaria alternate, a pathogen of spotted knapweed. *J Nat Prod.* **1989,** *52*, 42-47.
47. Tiemann, U.; Tomek, W.; Schneider, F.; Müller, M.; Pöhland, R.; Vanselow, J., The mycotoxins alternariol and alternariol methyl ether negatively affect progesterone synthesis in porcine granulosa cells in vitro. *Toxicol Lett.* **2009,** *186*, 139-145.
48. Wollenhaupt, K.; Schneider, F.; Tiemann, U., Influence of alternariol (AOH) on regulator proteins of cap-dependent translation in porcine endometrial cells. *Toxicol Lett.* **2008,** *182*, 57-62.
49. Logrieco, A.; Moretti, A.; Solfrizzo, M., Alternaria toxins and plant diseases: an overview of origin, occurrence and risks. *World Mycotoxin J.* **2009,** *2*, 129-140.
50. Woody, M. A.; Chu, F. S., Toxicology of Alternaria mycotoxins. In *Alternaria biology, plant diseases and metabolites*, Chelkowsky, J.; Visconti, A., Eds. Elsevier: Amsterdam , Netherlands, 1992; pp 409-434.
51. Schrader, T. J.; Cherry, W.; Soper, K.; Langlois, I.; Vijay, H. M., Examination of Alternaria alternata mutagenicity and effects of nitrosylation using the ames salmonella test. *Teratogen Carcin Mut.* **2001,** *21*, 261-274.
52. Griffin, G. F.; Chu, F. S., Toxicity of the Alternaria metabolites alternariol, alternariol monomethyl ether, altenuene and tenuazonic acid in the chicken embryo assay. *Appl. Environ. Microbiol.* **1983,** *46*, 1420-1422.
53. Visconti, A.; Sibilia, A., Alternaria toxins. In *Mycotoxins in grain: compounds other than aflatoxin*, Miller, D.; Trenholm, H. L., Eds. Eagan Press1994; pp 315-336.
54. Frizzell, C.; Ndossi, D.; Kalayou, S.; Eriksen, G. S.; Verhaegen, S.; Sørlie, M.; Elliott, C. T.; Ropstad, E.; Connolly, L., An in vitro investigation of endocrine disrupting effects of the mycotoxin alternariol. *Toxicol Appl Pharmacol.* **2003,** *271*, 64-71.
55. Fehr, M.; Baechler, S.; Kropat, C.; Mielke, C.; Boege, F.; Pahlke, G.; Marko, D., Repair of DNA damage induced by the mycotoxin alternariol involves tyrosyl-DNA phosphodiesterase 1. *Mycotoxin Res.* **2010,** *26*, 247-256.
56. Kustrzeba-Wojcicka, I.; Siwak, E.; Terlecki, G.; Wolanczyk-Medrala, A.; Medrala, W., Alternaria alternata and its allergens: a comprehensive review. *Clin Rev Allergy Immunol.* **2014,** *47*, 354-365.
57. Pero, R. W.; Posner, H.; Blois, M.; Harvan, D.; Spalding, J. W., Toxicity of metabolites produced by the Alternaria. *Environ. Health Perspect.* **1973,** *4*, 87-94.
58. Xu, G. B.; Pu, X.; Bai, H. H.; Chen, X. Z.; Li, G. Y., A new alternariol glucoside from fungus Alternaria alternate cib-137. *Nat Prod Res.* **2015,** *29*, 848-852.
59. Brugger, E. M.; Wagner, J.; Schumacher, D. M.; Koch, K.; Podlech, J.; Metzler, M.; Lehmann, L., Mutagenicity of the mycotoxin alternariol in cultured mammalian cells. *Toxicol. Lett.* **2006,** *164*, 221-230.
60. Rosett, T.; Sankhala, R. H.; Stickings, C. E.; Taylor, M. E. U.; Thomas, R., Studies in the biochemistry of micro-organisms. 103. Metabolites of Alternaria tenuis Auct.: culture filtrate products. *Biochem. J.* **1957,** *67*, 390-400.
61. Stickings, C. E., Studies in the biochemistry of micro-organisms. 106. Metabolites of Alternaria tenuis auct.: the structure of tenuazonic acid. *Biochem. J.* **1959,** *72*, 332-340.
62. Von Ramm, C.; Lucas, G. B., Production of enzymes and antibiotic substances by Alternaria longipes. *Tobacco Sci.* **1963,** *7*, 81-84.
63. Thomma, B., Alternaria spp.: From general saprophyte to specific parasite. *Mol. Plant Pathol.* **2003,** *4*, 225-236.

64. Lebrun, M. H.; Nicolas, L.; Boutar , M.; Gaudemer , F.; Ranomenjanahary, S.; Gaudemer, A., Relationships between the structure and the phytotoxicity of the fungal toxin tenuazonic acid. *Phytochem.* **1988,** *27*, 77-84.
65. Chen, S. G.; Yin, C. Y.; Dai, X. B.; Qiang, S.; M., X. X., Action of tenuazonic acid, a natural phytotoxin, on photosystem II of spinach. *Environ. Exp. Bot.* **2008,** *62*, 279-289.
66. Gatenbeck, S.; Sierankiewicz, J., Biosynthesis of tenuazonic acid in Alternaria tenuis. *Acta Chem. Scan.* **1973,** *27*, 1825-1827.
67. Stickings, C. E.; Townsend, R. J., Studies in biochemistry of micro-organisms: 108. Metabolites of Alternaria tenuis auct.: The biosynthesis of tenuazonic acid. *Biochem. J.* **1961,** *78*, 412-418.
68. Shephard, G. S.; Thiel, P. G.; Sydenham, E. W.; Vleggaar, R.; Marasas, W. F. O., Reversed-phase high performance liquid chromatography of tenuazonic acid and related tetramic acids. *J. Chromatogr.* **1991,** *566*, 195-205.
69. Nolte, M. J.; Steyn, P. S.; Wessels, P. L., Structural investigations of 3-acylpyrrolidine-2,4-diones by nuclear magnetic-resonance spectroscopy and X-ray crystallography. *J. Chem. Soc., Perkin Trans. 1* **1980**, 1057-1065.
70. Dippenaar, A.; Holzapfel, C. W.; Boeyens, J. C. A., Crystal structure of copper bis(tenuazonate) monohydrate. *J. Chem. Crystallogr.* **1977,** *7*, 189-197.
71. Scott, P. M., Analysis of agricultural commodities and foods for Alternaria mycotoxins. *J. AOAC Int.* **2001,** *84*, 1809-1817.
72. Siegel, D.; Merkel, S.; Koch, M.; Nehls, I., Quantification of the Alternaria mycotoxin tenuazonic acid in beer. *Food Chem.* **2010,** *120*, 902-906.
73. Siegel, D.; Rasenko, T.; Koch, M.; Nehls, I., Determination of the Alternaria mycotoxin tenuazonic acid in cereals by high-performance liquid chromatography/electrospray ionization-multistage mass spectrometry after derivatization with 2,4-dinitrophenylhydrazine. *J. Chromatogr. A* **2009,** *1216*, 4582-4588.
74. Scott, P. M.; Stoltz, D. R., Mutagens produced by Alternaria alternata. *Mutat. Res.* **1980**, 33-40.
75. Sauer, D. B.; Seitz, L. M.; Burroughs, R.; Mohr, H. E.; West, J. L.; Milleret, R. J.; Anthony, H. D., Toxicity of Alternaria metabolites found in weathered sorghum grain at harvest. *J. Agric. Food Chem.* **1978,** *26*, 1380-1383.
76. Meronuck, R. A.; Steele, J. A.; Mirocha, C. J.; Christensen, C. M., Tenuazonic acid, a toxic produced by Alternaria alternata. *Appl. Microbiol.* **1972,** *23*, 613-617.
77. Smith, E. R.; Fredrickson, T. N.; Hadidian, Z., Toxic effects of the sodium and the N,N'-dibenzylethylenediamine salts of tenuazonic acid (NSC-525816 and NSC-82260). *Cancer Chemother. Rep.* **1968,** *52*, 579-585.
78. Mikami, Y.; Nishijima, Y.; Imura, H.; Suzuki, A.; Tamura, S., Chemical studies on brown-spot disease of tobacco plants. Part I. Tenuazonic acid as a vivotoxin of Alternaria longipes. *Agr. Biol. Chem.* **1971,** *35*, 611-618.
79. Kinoshita, T.; Renbutsu, Y.; Khan, I. D.; Komoto, K.; Nichimura, S., Distribution of tenuazonic acid production in the genus Atternaria and its pathological evaluation. *Ann. Phytopathol. Soc. Japan* **1972,** *38*, 397-404.
80. Carrasco, L.; Vazquez, D., Differences in eukaryotic ribosomes detected by the selective action of an antibiotic. *Biochimica et Biophysica Acta (BBA)* **1973,** *319*, 209-215.
81. Miller, F. A.; Rightsel, W. A.; Sloan, B. J.; Ehrlich, J.; French, J. C.; Bartz, Q. R.; Dixon, G. J., Antiviral activity of tenuazonic acid. *Nature* **1963,** *200*, 1338-1339.
82. Yekeler, H.; Bitmis, K.; Ozcelik, N.; Doymaz, M. Z.; Calta, M., Analysis of toxic effects of Alternaria toxins on esophagus of mice by light and electron microscopy. *Toxicol. Pathol.* **2001,** *29*, 492-497.
83. Grellmann, K. H.; Hentzschel, P., Mechanism of the photochemical cis .dblharw. trans isomerization of thioindigo and 6,6'-diethoxythioindigo in solution. *Chem. Phys. Lett.* **1978,** *53*, 545-550.

84. Richard, J. C.; Richard, H. C., Handbook of toxic fungal metabolites. Acadimic press: New York, 1981; p 32.
85. Miller, J. D., Fungi and mycotoxins in grain: Implications for stored product research. *J. Stored Prod. Res.* **1995,** *31*, 1-16.
86. (CAST), C. f. a. s. a. t. *Mycotoxins: risks in plant, animal, and human systems*: Ames, Iowa, USA, 2003; pp XVI, 199.
87. Ackkermann, Y.; Curtui, V.; Dietrich, R.; Gross, M.; Latif, H.; Martlbauer, E.; Usleber, E., Widespread occurrence of low levels of Alternariol in apple and tomato products, as determined by comparative immunochemical assessment using monoclonal and polyclonal antibodies. *J. Agric. Food Chem.* **2011,** *59*, 6360-6368.
88. Asam, S.; Konitzer, K.; Schieberle, P.; Rychlik, M., Stable isotope dilution assays of alternariol and alternariol monomethyl ether in beverages. *J. Agric. Food Chem.* **2009,** *57*, 5152-5160.
89. Asam, S.; Lichtenegger, M.; Liu, Y.; Rychlik, M., Content of the alternaria mycotoxin tenuazonic acid in food commodities determined by a stable isotope dilution assay. *Mycotoxin Res.* **2012,** *28*, 9-15.
90. Asam, S.; Liu, Y.; Konitzer, K.; Rychlik, M., Development of a stable Isotope dilution assay for tenuazonic Acid. *J. Agric. Food Chem.* **2011,** *59*, 2980-2987.
91. Da Motta, S.; Valente Soares, L. M., A method for the determination of two Alternaria toxins, alternariol and alternariol monomethyl ether, in tomato products. *Braz. J. Microbiol.* **2000,** *31*, 315-320.
92. Da Motta, S.; Valente Soares, L. M., Simultaneous determination of tenuazonic and cyclopiazonic acids in tomato products. *Food Chem.* **2000,** *71*, 111-116.
93. Fàbrega, A.; Agut, M.; Calvo, M. A., Optimization of the method of detection of metabolites produced by the Alternaria genus: Alternariol, alternariol monomethyl ether, altenuene, altertoxin I and tentoxin. *J. Food Sci.* **2002,** *67*, 802-806.
94. Fernández Pinto, V., Detection and determination of alternaria mycotoxins in fruits and vegetables. *Mycotox. Fruit. Veget.* **2008**, 271-278.
95. Gilbert, J.; Anklam, E., Validation of analytical methods for determining mycotoxins in foodstuffs. *Trends Anal. Chem.* **2002,** *21*, 468-486.
96. Jiang, T.; Hu, Y. Y.; Ma, L.; Zhang, Y.-H.; Wu, C.-S., Preparation of artificial antigens for tenuazonic acid. *Shipin Kexue* **2014,** *35*, 153-157.
97. Lau, B. P. Y.; Scott, P. M.; Lewis, D. A.; kanhere, S. R.; Cléroux, C.; Roscoe, V. A., Liquid chromatography-mass spectrometry and liquid chromatography-tandem mass spectrometry of the Alternaria mycotoxins alternariol and alternariol monomethyl ether in fruit juices and beverages. *J. chromatogr. A* **2003,** *998*, 119-131.
98. Solfrizzo, M.; De Girolamo, A.; Vitti, C.; Visconti, A.; Van Den Bulk, R., Liquid chromatographic determination of alternaria toxins in carrots. *J. AOAC Int.* **2004,** *87*, 101-106.
99. Walravens, J.; Mikula, H.; Rychlik, M.; Asam, S.; Ediage, E. N.; Di Mavungu, J. D.; Van Landschoot, A.; Vanhaecke, L.; De Saeger, S., Development and validation of an ultra-high-performance liquid chromatography tandem mass spectrometric method for the simultaneous determination of free and conjugated alternaria toxins in cereal-based foodstuffs. *J. Chromatogr. A* **2014,** *1372*, 91-101.
100. Wang, Y.-L.; Wang, F.; Wang, H.; Yang, J.-Y.; Xu, Z.-L.; Shen, Y.-D.; Xiao, Z.-L.; Lei, H.-T.; Sun, Y.-M., Spectroscopic studies of interaction between hapten and monoclonal antibody (McAb) against iso-tenuazonic acid. *Mod. Food Sci. Technol.* **2015,** *31*, 25-30.
101. Yang, J.; Zhang, Y.; Wang, H.; Sun, Y.; Lei, H.; Shen, Y.; Xu, Z.; Li, P. Chemiluminescent enzyme-linked immunosorbent assay kit of tenuazonic acid and application method thereof. 2014.
102. Lau, B. P.; Scott, P. M.; Lewis, D. A.; Kanhere, S. R.; Cléroux, C.; Roscoe, V. A., Liquid chromatography–mass spectrometry and liquid chromatography–tandem mass spectrometry of the Alternaria mycotoxins alternariol and alternariol monomethyl ether in fruit juices and beverages. *J. Chromatogr. A* **2003,** *998*, 119-131.

103. Prelle, A.; Spadaro, D.; Garibaldi, A.; Gullino, M. L., A new method for detection of five alternaria toxins in food matrices based on LC-APCI-MS. *Food chem.* **2013,** *140*, 161-167.
104. Scott, P. M.; Kanhere, S. R., Chromatographic method for alternariatoxins in apple juice. *Methods Mol. Biol.* **2001,** *157*, 225-234.
105. Scott, P. M.; Weber, D.; Kanhere, S. R., Gas chromatography-mass spectrometry of alternaria mycotoxins. *J. Chromatogr. A* **1997,** *765*, 255-263.
106. Yogendrarajah, P.; Jacxsens, L.; De Saeger, S.; De Meulenaer, B., Co-occurrence of multiple mycotoxins in dry chilli (Capsicum annum L.) samples from the markets of Sri Lanka and Belgium. *Food Control* **2014,** *46*, 26-34.
107. Ackermann, Y.; Curtui, V.; Dietrich, R.; Gross, M.; Latif, H.; Märtlbauer, E.; Usleber, E., Widespread occurrence of low levels of alternariol in apple and tomato products, as determined by comparative immunochemical assessment using monoclonal and polyclonal antibodies. *J. Agric. Food Chem.* **2011,** *59*, 6360-6368.
108. Burkin, A.; Kononenko, G. P., Enzyme immunassay of alternariol for the assessment of risk of agricultural products contamination. *Appl. Biochem. Microbiol.* **2011,** *47*, 72-76.
109. Harvan, D. J.; Pero, R. W., Gas chromatographic analysis of the alternaria metabolite, tenuazonic acid. *J. Chromatogr.* **1974,** *101*, 222-224.
110. Gross, M.; V., C.; Ackermann, Y.; Latif, H.; Usleber, E., Enzyme immunoassay for tenuazonic acid in apple and tomato products. *J. Agric. Food Chem.* **2011,** *59*, 12317-12322.
111. Asam, S.; Rychlik, M., Potential health hazards due to the occurrence of the mycotoxin tenuazonic acid in infant food. *Eur. Food Res. Technol.* **2013,** *236*, 491-497.
112. Ediage, E. N.; Di Mavungu, J. D.; Song, S.; Wu, A.; Peteghem, C. V.; De Saeger, S., A direct assessment of mycotoxin biomarkers in human urine samples by liquid chromatography tandem mass spectrometry. *Anal. Chim. Acta* **2012,** *741*, 58-69.
113. Warth, B.; Sulyok, M.; Fruhmann, P.; Mikula, H.; Berthiller, F.; Schuhmacher, R.; Hametner, C.; Abia, W. A.; Adam, G.; Frohlich, J.; Krska, R., Development and validation of a rapid multibiomarker liquid chromatography/tandem mass spectrometry method to assess human exposure to mycotoxins. *Rapid Commun Mass Spectrom.* **2012,** *26*, 1533-1540.
114. Solfrizzo, M.; Gambacorta, L.; Lattanzio, V. M. T.; Powers, S.; Visconti, A., Simultaneous LC-MS/MS determination of aflatoxin M1, ochratoxin A, deoxynivalenol, de-epoxydeoxynivalenol, α and β- zearalenols and fumonisin B1 in urine as a multi-biomarker method to assess exposure to mycotoxins. *Anal. Bioanal. Chem.* **2011,** *401*, 2831-2841.
115. Graf, G., Polymer scientists work to beef up biosensors. *Science* **1991,** *253*, 1097-1098.
116. Vadgama, P.; Crump, P. W., Biosensors: recent trends. A review. *Analyst* **1992,** *117*, 1657-1670.
117. Albery, W. J.; Boutelle, M. G.; Durrant, S. L. T.; Fillenz, M.; Hopkins, A. R.; Mangold, B. P., Sensitive enzyme electrodes. *Phil. Trans. R. Soc. Lond. A.* **1990,** *333*, 49-61.
118. Zhao, S. L.; Reichert, W. M. J., Protein adsorption using an evanescent chemical sensor with a fused optical fiber coupler. *Colloid. Interface. Sci.* **1990,** *140*, 294-297.
119. Marhold, S.; Koller, E.; Mayer, I.; Wolfbeis, O. S., A sensitive fluorometric assay for cationic surfactants. *Fresen. J. Anal. Chem.* **1990,** *336*, 111-113.
120. Seitz, W. R., Chemical sensors based on fiber optics. *Anal. Chem.* **1984,** *56*, 16A-34A.
121. Solsky, R. L., Ion-selective electrodes. *Anal. Chem.* **1990,** *62*, 21R-33R.
122. Alexander, C.; Andersson, H. S.; Andersson, L. I.; Ansell, R. J.; Kirsch, N.; Nicholls, I. A.; O'Mahony, J.; Whitcombe, M. J., Molecular imprinting science and technology: a survey of the literature for the years up to and including 2003. *J. Mol. Recognit.* **2003,** *19*.
123. Mosbach, K., Molecular imprinting. *Trends Biochem. Sci.* **1994,** *19*, 9-14.

124. Andersson, L. I.; Müller, R.; Vlatakis, G.; Mosbach, K., Mimics of the binding sites of opioid receptors obtained by molecular imprinting of enkephalin and morphine. *Proc. Natl. Acad. Sci. USA* **1995,** *92*, 4788-4792.
125. Vulfson, E. N.; Alexander, C.; Whitcombe, M. J., Assembling the molecular cast. *Chem. Br.* **1997,** *33*, 23-26.
126. Mosbach, K.; Ramström, O.; Bio/Technology 1996, 163. , The emerging technique of molecular imprinting and its future impact on biotechnology. *Nat. Biotechnol.* **1996,** *14*, 163-170.
127. Mosbach, K.; Haupt, K., Some new developments and challenges in non-covalent molecular imprinting technology. *J. Mol. Recognit.* **1998,** *11*, 62-68.
128. Ramström, O.; Ansell, R. J., Molecular imprinting technology: challenges and prospects for the future. *Chirality* **1998,** *10*, 195-209.
129. Shea, K. J., Molecular imprinting of synthetic network polymers: the de novo synthesis of macromolecular binding and catalytic sites. *Trends Polym. Sci.* **1994,** *2*, 166-173.
130. Steinke, J.; Sherrington, D. C.; Dunkin, I. R., Imprinting of synthetic polymers using molecular templates. *Adv. Poly. Sci.* **1995,** *123*, 81-125.
131. Vidyasankar, S.; Arnold, F. H., Molecular imprinting: selective materials for separations, sensors and catalysis. *Curr. Opinion Biotech.* **1995,** *6*, 218-224.
132. Wulff, G., Molecular imprinting in cross-linked materials with the aid of molecular templates-away towards artificial antibodies. *Angew. Chem. Int. Ed. Engl.* **1995,** *34*, 1812-1832.
133. Bartsch, R. A.; Maeda, M., *Molecular and Ionic Recognition with Imprinted Polymers*. ACS: Washington DC, 1998; Vol. 703.
134. Tamayo, F. G.; Turiel, E.; Martin-Esteban, A., Molecularly imprinted polymers for solid-phase extraction and solid-phase microextraction: recent developments and future trends. *J. Chromatogr. A* **2007,** *1152*, 32-40.
135. Shen, X.; Zhu, L.; Wang, N.; Yec, L.; Tang, H., Molecular imprinting for removing highly toxic organic pollutants. *Chem. Commun.* **2012,** *48*, 788-798.
136. Polyakov, M. V., *Zh. Fiz. Khim.* **1931,** *2*, 799-805.
137. Wulff, G.; Sarhan, A., Use of polymers with enzyme-analogous structures for resolution of racemates. *Angew. Chem. Int. Ed.* **1972,** *11*, 341-344.
138. Wulff, G., Enzyme-like catalysis by molecular imprinted polymers. *Chem. Rev.* **2002,** *102*, 1-27.
139. Kim, H.; Spivak, D. A., New insight into modeling non-covalently imprinted polymers. *J. Am. Chem. Soc.* **2003,** *125*, 11269-11275.
140. O'Mahony, J.; Molinelli, A.; Nolan, K.; Smyth, M. R.; Mizaikoff, B., Anatomy of a successful imprint: analysing the recognition mechanisms of a molecularly imprinted polymer for quercetin. *Biosens. Bioelectron.* **2006,** *21*, 1383-1392.
141. O'Mahony, J.; Wei, S.; Molinelli, A.; Mizaikoff, B., Imprinted polymeric materials. insight into the nature of prepolymerization complexes of quercetin imprinted polymers. *Anal. Chem.* **2006,** *78*, 6187-6190.
142. Arshady, R.; Mosbach, K., Synthesis of substrate-selective polymers by host-guest polymerization. *Makromol. Chem.* **1981,** *182*, 687-692.
143. Whitcombe, M. J.; Rodriguez, M. E.; Villar, P.; Vulfson, E. N., A new method for the introduction of recognition site functionality into polymers prepared by molecular imprinting - synthesis and characterization of polymeric receptors for cholesterol. *J. Am. Chem. Soc.* **1995,** *117*, 7105-7114.
144. Heng, L. Y.; Hall, E. A. H., Methacrylate-acrylate based polymers of low plasticiser content for potassium ion-selective membranes. *Anal. Chim. Acta* **1996,** *324*, 47-56.
145. Heng, L. Y.; Hall, E. A. H., Producing "self-plasticizing" ion-selective membranes. *Anal. Chem.* **2000,** *72*, 45-51.
146. Pringsheim, E.; Terpetschnig, E.; Piletsky, S. A.; Wolfbeis, O. S., A Polyaniline with near-infrared optical response to saccharides. *Adv. Mater.* **1999,** *11*, 865-868.

147. Moradian, A.; Mohr, G. J.; Linnhoff, M.; Fehlmann, M.; Spichiger-Keller, U. E., Continuous optical monitoring of aqueous amines in transflectance mode. *Sensor Actuat B-Chem* **2000,** *62*, 154-161.
148. Koohpaei, A. R.; Shahtaheri, S. J.; Ganjali, M. R.; Forushani, A. R.; Golbabaei, F., Application of multivariate analysis to the screening of molecularly imprinted polymers (MIPs) for ametryn. *Talanta* **2008,** *75*, 978-986.
149. Shamsipur, M.; Fasihi, J.; Khanchi, A.; Hassani, R.; Alizadeh, K.; Shamsipur, H., A stoichiometric imprinted chelating resin for selective recognition of copper(II) ions in aqueous media. *Anal. Chim. Acta.* **2007,** *599*, 294-301.
150. Wu, S.; Xu, Z.; Yuan, Q.; Tang, Y.; Zuo, X.; Lai, J., Recognition characteristics of molecularly imprinted microspheres for triazine herbicides using hydrogen-bond array strategy and their analytical applications for corn and soil samples. *J. Chromatogr. A* **2011,** *1218*, 1340-1346.
151. Zhang, H. T.; Song, T.; Zong, F. L.; Chen, T. C.; Pan, C. P., Synthesis and characterization of molecularly imprinted polymers for phenoxyacetic acids. *Int. J. Mol. Sci.* **2008,** *9*, 98-106.
152. Molinelli, A.; O'Mahony, J.; Nolan, K.; Smyth, M. R.; Jakusch, M.; Mizaikoff, B., Analyzing the mechanisms of selectivity in biomimetic self-assemblies via IR and NMR spectroscopy of prepolymerization solutions and molecular dynamics simulations. *Anal. Chem.* **2005,** *77*, 5196-5204.
153. Lv, Y.; Lin, Z.; Feng, W.; Tan, T., Evaluation of the polymerization and recognition mechanism for phenol imprinting SPE. *Chromatographia* **2007,** *66*, 339-347.
154. Courtois, J.; Fischer, G.; Schauff, S.; Albert, K.; Irgum, K., Interactions of bupivacaine with a molecularly imprinted polymer in a monolithic format studied by NMR. *Anal. Chem.* **2006,** *78*, 580-584.
155. Sun, H. W.; Qiao, F. X., Recognition mechanism of water-compatible molecularly imprinted solid-phase extraction and determination of nine quinolones in urine by high performance liquid chromatography. *J. Chromatogr. A* **2008,** *1212*, 1-9.
156. Malosse, L.; Palmas, P.; Buvat, P.; Ades, D.; Siove, A., Novel stoichiometric, noncovalent pinacolyl methylphosphonate imprinted polymers: a rational design by NMR spectroscopy. *Macromolecules* **2008,** *41*, 7834-7842.
157. Ansell, R. J.; Wang, D., Imprinted polymers for chiral resolution of (±)-ephedrine. part 3: NMR predictions and HPLC results with alternative functional monomers. *Analyst* **2009,** *134*, 564-576.
158. Becke, A. D., Density-functional thermochemistry. III. The role of exact exchange. *J. Chem. Phys.* **1993,** *98*, 5648-5652.
159. Frisch, M. J. e. a. *Gaussian Development Version*, Gaussian Inc.: Pittsburgh, PA, 2003.
160. Karim, K.; Breton, F.; Rouillon, R.; Piletska, E. V.; Guerreiro, A.; Chianella, I.; Piletsky, S. A., How to find effective functional monomers for effective molecularly imprinted polymers? *Adv. Drug Deliv. Rev.* **2005,** *57*, 1795-1808.
161. Piletsky, S. A.; Karim, K.; Piletska, E. V.; Day, C. J.; Freebairn, K. W.; Legge, C.; Turner, A. P. F., Recognition of ephedrine enantiomers by molecularly imprinted polymers designed using a computational approach. *Analyst* **2001,** *126*, 1826-1830.
162. Wu, L.; Sun, B.; Li, Y.; Chang, W., Study properties of molecular imprinting polymer using a computational approach. *Analyst* **2003,** *128*, 944-949.
163. Meng, Z.; Yamazaki, T.; Sode, K., A molecularly imprinted catalyst designed by a computational approach in catalysing a transesterification process. *Biosens. Bioelectron.* **2004,** *20*, 1068-1075.
164. Diñeiro, Y.; Menéndez, M. I.; Blanco-López, M. C.; Lobo-Castañón, M. J.; Miranda-Ordieres, A. J.; Tuñón-Blanco, P., Computational approach to the rational design of molecularly imprinted polymers for voltammetric sensing of homovanillic acid. *Anal. Chem.* **2005,** *77*, 6741-6746.
165. Diñeiro, Y.; Menéndez, M. I.; Blanco-López, M. C.; Lobo-Castañón, M. J.; Miranda-Ordieres, A. J.; Tuñón-Blanco, P., Computational predictions and experimental affinity distributions for a homovanillic acid molecularly imprinted polymer. *Biosens. Bioelectron.* **2006,** *22*, 364-371.

166. Farrington, K.; Regan, F., Investigation of the nature of MIP recognition: the development and characterization of a MIP for ibuprofen. *Biosens. Bioelectron.* **2007,** *22*, 1138-1146.
167. Azenha, M.; Kathirvel, P.; Nogueira, P.; Fernando-Silva, A., The requisite level of theory for the computational design of molecularly imprinted silica xerogels. *Biosens. Bioelectron.* **2008,** *23*, 1843-1849.
168. Yao, J.; Li, X.; Qin, W., Computational design and synthesis of molecular imprinted polymers with high selectivity for removal of aniline from contaminated water. *Anal. Chim. Acta* **2008,** *610*, 282-288.
169. Pavel, D.; Lagowski, J., Computationally designed monomers and polymers for molecular imprinting of theophylline and its derivatives. Part I. *Polymer* **2005,** *46*, 7258-7542.
170. Piletska, E. V.; Turner, N. W.; Turner, A. P. F.; Piletsky, S. A., Controlled release of the herbicide simazine from computationally designed molecularly imprinted polymers. *J. Control. Release* **2005,** *108*, 132-139.
171. Chianella, I.; Karim, K.; Piletska, E. V.; Preston, C.; Piletsky, S. A., Computational design and synthesis of molecularly imprinted polymers with high binding capacity for pharmaceutical applications-model case: adsorbent for abacavir. *Anal. Chim. Acta* **2006,** *559*, 73-78.
172. Pavel, D.; Lagowski, J.; Lepage, C. J., Computationally designed monomers for molecular imprinting of chemical warfare agents - Part V. *Polymer* **2006,** *47*, 8389-8399.
173. Breton, F.; Rouillon, R.; Piletska, E. V.; Karim, K.; Guerreiro, A.; Chianella, I.; Piletsky, S. A., Virtual imprinting as a tool to design efficient MIPs for photosynthesis-inhibiting herbicides. *Biosens. Bioelectron.* **2007,** *22*, 1948-1954.
174. Wei, S.; Jakusch, M.; Mizaikoff, B., Investigating the mechanisms of 17 b-estradiol imprinting by computational prediction and spectroscopic analysis. *Anal. Bioanal. Chem.* **2007,** *389*, 423-431.
175. Vasapollo, G.; Del Sole, R.; Mergola, L.; Rosaria Lazzoi, M.; Scardino, A.; Scorrano, S.; Mele, G., Molecularly imprinted polymers: present and future prospective. *Int. J. Mol. Sci.* **2011,** *12*, 5908-5945.
176. Yoshimatsu, K.; Reimhult, K.; Krozer, A.; Mosbach, K.; Sode, K.; Ye, L., Uniform molecularly imprinted microspheres and nanoparticles prepared by precipitation polymerization: the control of particle size suitable for different analytical applications. *Anal. Chim. Acta* **2007,** *584*, 112-121.
177. Sellergren, B., Polymer-and template-related factors influencing the efficiency in molecularly imprinted solid-phase extractions. *Trends Anal. Chem.* **1999,** *18*, 164-174.
178. Narayanaswamy, R. R., *Optical sensors : industrial environmental and diagnostic applications*. Springer: Berlin ; New York, 2004.
179. Mayes, A. G.; Whitcombe, M. J., Synthetic strategies for the generation of molecularly imprinted organic polymers, . *Adv. Drug Deliv. Rev.* **2005,** *57*, 1742-1778.
180. Fritz, J. S., *Analytical Solid-Phase Extraction*. WILEY-VCH: New York, 1999; p 224.
181. Saeger, S., *Determining mycotoxins and mycotoxigenic fungi in food and feed*. Woodhead Publishing Ltd.: Cambridge, UK; p 456.
182. He, C.; Long, Y.; Pan, J.; Li, K.; Liu, F., Application of molecularly imprinted polymers to solid-phase extraction of analytes from real samples. *J. Biochem. Biophys. Methods* **2007,** *70*, 133-150.
183. Sellergen, B., Direct drug determination by selective sample enrichment on an imprinted polymer. *Anal Chem* **1994,** *66*, 1578-1582.
184. Muldoon, M. T.; Stanker, L. H., Molecularly imprinted solid phase extraction of atrazine from beef liver extracts. *Anal. Chem.* **1997,** *69*, 803-808.
185. Chen, L.; Xua, S.; Li, J., Recent advances in molecular imprinting technology: current status. *Chem. Soc. Rev.* **2010,** *40*, 2922-2942.
186. Orellana, G.; Moreno-Bondi, M. C., *Frontiers in chemical sensors: novel principles and techniques*. Springer-Verlag: Berlin Germany, 2005; Vol. 3.
187. Orellana, G.; Moreno Bondi, M. C.; García-Fresnadillo, D.; Marazuela, M. D., The interplay of indicator, support and analyte in optical sensor layers. In *Frontiers in chemical sensors: novel principles and techniques*, Springer-Verlag2005; Vol. 3, pp 189-225.

188. Orellana, G., Fluorescence-based optical sensors. In *Optical Chemical Sensors*, Springer-Kluwer2006; Vol. 224, pp 99-116.
189. Wang, X. D.; Wolfbeis, O. S., Fiber-optic chemical sensors and biosensors (2008-2012). *Anal. Chem.* **2013,** *85*, 487-508.
190. Orellana, G.; Haigh, D., New trends in fiber-optic chemical and biological sensors. *Curr. Anal. Chem.* **2008,** *4*, 273-295.
191. Orellana, G.; Cano-Raya, C.; López-Gejo, J.; Santos, A. R., Online monitoring sensors. In *Treatise on water science*, Wilderer, P., Ed. Elsevier: Oxford, UK, 2011; Vol. 3, pp 221-262.
192. McDonagh, C.; Burke, C. S.; MacCraith, B. D., Optical chemical sensors. *Chem. Rev.* **2008,** *108*, 400-422.
193. Fu, F.; Wang, Q., Removal of heavy metal ions from wastewaters: a review. *J. Environ. Manage.* **2011,** *92*, 407-418.
194. Wolfbeis, O. S., Probes, sensors, and labels: why is real progress slow? *Angew. Chem. Int. Ed. Eng.* **2013,** *52*, 9864-9868.
195. López-Gejo, J.; Haigh, D.; Orellana, G., Relationship between the microscopic and macroscopic world in optical oxygen sensing: a luminescence lifetime microscopy study. *Langmuir* **2010,** *26*, 2144-2150.
196. McDonagh, C.; Burke, C. S.; MacCraith, B. D., Optical chemical sensors. *Chem Rev* **2008,** *108*, 400-22.
197. Wolfbeis, O. S., Chemical sensors-survey and trends. *Fresen. J. Anal. Chem.* **1990,** *337*, 522-527.
198. Orellana, G., Fluorescence-based sensors. In *Optical chemical sensors*, Baldini, F.; Chester, A. N.; Homola, J.; Martellucci, S., Eds. Springer Netherlands2006; Vol. 224, pp 99-116.
199. Joo, S.; Brown, R. B., Chemical sensors with integrated electronics. *Chem. Rev.* **2008,** *108*, 635-651.
200. Hulanicki, A.; Glab, S.; Ingman, F., Chemical sensors definitions and classification. *Pure Appl. Chem.* **1991,** *63*, 1247-1250.
201. Tormo, L.; Bustamante, N.; Colmenarejo, G.; Orellana, G., Can luminescent Ru(II) polypyridyl dyes measure pH? *Anal. Chem.* **2010,** *82*, 5195-5204.
202. Kasha, M., Characterization of electronic transitions in complex molecules. *Discuss. Faraday Soc.* **1950,** *9*, 14-19.
203. http://www.astisensor.com. (accessed on 04/2015)
204. http://www.nexsens.com. (accessed on 04/2015)
205. https://www.ysi.com. (accessed on 04/2015)
206. http://www.hach.com. (accessed on 04/2015)
207. http://www.swan.ch. (accessed on 04/2015)
208. http://www.nico2000.net. (accessed on 04/2015)
209. http://www.in-situ.com. (accessed on 04/2015)
210. http://www.s-can.at. (accessed on 04/2015)
211. http://www.horiba.com. (accessed on 04/2015)
212. http://www.hannainst.com. (accessed on 04/2015)
213. http://www.environnement-sa.com. (accessed on 04/2015)
214. Bedoya, M.; Diez, M. T.; Moreno-Bondi, M. C.; Orellana, G., Humidity sensing with a luminescent Ru (II) complex and phase-sensitive detection. *Sens. Actuat. B Chem.* **2006,** *113*, 573-581.
215. Dixon, E. N.; Snow, M. Z.; Bon, J. L.; Whitehurst, A. M.; DeGraff, B. A.; Trindle, C.; Demas, J. N., Environmental sensitivity of Ru(II) complexes: the role of the accessory ligands. *Inorg. Chem.* **2012,** *51*, 3355-3365.
216. Rowe, H. M.; Xu, W.; Demas, J. N.; DeGraff, B. A., Metal ion sensors based on a luminescent Ruthenium(II) complex: the role of polymer support in sensing properties. *Appl. Spectrosc.* **2002,** *56*, 167-173.
217. Lakowicz, J. R., *Principles of fluorescence spectroscopy*. Springer US2006; p XXVI, 954.

218. Valeur, B., *Molecular fluorescence: principles and applications*. Wiley-VCH: Weinheim, 2002.
219. Lakowicz, J. R., *Principles of Fluorescence Spectroscopy*. Springer: New York, USA, 2006; p 938.
220. Jameson, D. M.; Ross, J. A., Fluorescence polarization/anisotropy in diagnostics and imaging. *Chem. Rev.* **2010,** *110*, 2685-2708.
221. Smith, D. S.; Eremin, S. A., Fluorescence polarization immunoassays and related methods for simple, high-throughput screening of small molecules. *Anal Bioanal Chem.* **2008,** *391*, 1499-1507.
222. Goryacheva, I. Y.; Eremin, S. A.; Shutaleva, E. A.; Suchanek, M.; Niessner, R.; Knopp, D., Development of a fluorescence polarization immunoassay for polycyclic aromatic hydrocarbons. *Anal. Lett.* **2007,** *40*, 1445-1460.
223. Pérez-Bendito, D. P.; Gómez-Hens, A.; Gaikwad, A., Direct stopped-flow fluorescence polarization immunoassay of abused drugs and their metabolites in urine. *Clin. Chem.* **1994,** *40*, 1489-1493.
224. Tachi, T.; Hase, T.; Okamoto, Y.; Kaji, N.; Arima, T.; Matsumoto, H.; Kondo, M.; Tokeshi, M.; Hasegawa, Y.; Baba, Y., A clinical trial for therapeutic drug monitoring using microchip-based fluorescence polarization immunoassay. *Anal. Bioanal. Chem.* **2011,** *401*, 2301-2305.
225. Adamczyk, M.; Chen, Y. Y.; Johnson, D. D.; Reddy, R. E., A stereoselective synthesis of 1α-(3'-Carboxypropyl)-4-androsten-17β-ol-3-one: Preparation of immunoreagents for quantification of testosterone by fluorescence polarization immunoassay. *Tetrahedron* **1997,** *53*, 12855-12866.
226. Hatzidakis, G. I.; Tsatsakis, A. M.; Krambovitis, E. K.; Spyros, A.; Eremin, S. A., Use of L-lysine fluorescence derivatives as tracers to enhance the performance of polarization fluoroimmunoassays. a study using two herbicides as model antigens. *Anal. Chem.* **2002,** *74*, 2513-25121.
227. Chun, H. S.; Choi, E. H.; Chang, H. J.; Choi, S. W.; Eremin, S. A., A fluorescence polarization immunoassay for the detection of zearalenone in corn. *Anal. Chim. Acta* **2009,** *639*, 83-89.
228. Maragos, C., Fluorescence polarization immunoassay of mycotoxins: a review. *Toxins* **2009,** *1*, 196-207.
229. Hunt, C. E.; Ansell, R. J., Use of fluorescence shift and fluorescence anisotropy to evaluate the re-binding of template to (S)-propranolol imprinted polymers. *Analyst* **2006,** *131*, 678-683.
230. Kriz, D.; Ramstroem, O.; Svensson, A.; Mosbach, K., A biomimetic sensor based on a molecularly imprinted polymer as a recognition element combined with fiber-optic detection. *Anal. Chem.* **1995,** *67*, 2142-2144.
231. Lieberzeit, P. A.; Halikias, K.; Afzal, A.; Dickert, F. L., Polymers imprinted with PAH mixtures - Comparing fluorescence and QCM sensors. *Anal. Bioanal. Chem.* **2008,** *392*, 1405-1410.
232. Fuchs, Y.; Linares, A. V.; Mayes, A. G.; Haupt, K.; Soppera, O., Ultrathin selective molecularly imprinted polymer microdots obtained by evanescent wave photopolymerization. *Chem. Mat.* **2011,** *23*, 3645-3651.
233. Descalzo, A. B.; Somoza, C.; Moreno-Bondi, M. C.; Orellana, G., Luminescent core-shell imprinted nanoparticles engineered for targeted Forster resonance energy transfer-based sensing. *Anal Chem* **2013,** *85*, 5316-20.
234. Descalzo, A. B.; Somoza, C.; Moreno-Bondi, M. C.; Orellana, G., Luminescent core-shell imprinted nanoparticles engineered for targeted förster resonance energy transfer-based sensing. *Anal. Chem.* **2013,** *85*, 5316-5320.
235. Wan, W.; Wagner, S.; Rurack, K., Fluorescent monomers: "bricks" that make a molecularly imprinted polymer "bright". *Anal Bioanal Chem* **2016,** *408*, 1753-71.
236. Turkewitsch, P.; Wandelt, B.; Darling, G. D.; Powell, W. S., Fluorescent functional recognition sites through molecular imprinting. a polymer-based fluorescent chemosensor for aqueous cAMP. *Anal. Chem.* **1998,** *70*, 2025-2030.
237. Leung, M. K.-P.; Chow, C.-F.; Lam, M. H.-W., A sol–gel derived molecular imprinted luminescent PET sensing material for 2, 4-dichlorophenoxyacetic acid. *J. Mater. Chem.* **2001,** *11*, 2985-2991.

238. Pinheiro, S. C.; Descalzo, A. B.; Raimundo, I. M. J.; Orellana, G.; Moreno-Bondi, M. C., Fluorescent ion-imprinted polymers for selective Cu(II) optosensing. *Anal. Bional. Chem.* **2012,** *402*, 3253-3260.
239. Jenkins, A. L.; Uy, O. M.; Murray, G. M., Polymer-based lanthanide luminescent sensor for detection of the hydrolysis product of the nerve agent soman in water. *Anal. Chem.* **1999,** *71*, 373-378.
240. Yuan, J.; Wang, G., Lanthanide-based luminescence probes and time-resolved luminescence bioassays. *Trends Anal. Chem.* **2006,** *25*, 490-500.
241. Nishioka, T.; Fukui, K.; Matsumoto, K., lanthanide chelates as luminescent labels in biomedical analyses. In *Handbook on the physics and chemistry of rare earths*, Gschneidner, K. A.; Bünzli, J. C.; Pecharsky, V. K., Eds. Elsevier Science BV: Amsterdam, 2007; Vol. 37, pp 171–216.
242. Hovinen, J.; Guy, P. M., Bioconjugation with Stable Luminescent Lanthanide(III) Chelates Comprising Pyridine Subunits. *Bioconjugate Chem.* **2009,** *20*, 404-421.
243. Weissman, S. I., Intramolecular energy transfer the fluorescence of complexes of europium. *J. Chem. Phys.* **1942,** *10*, 214-217.
244. Bünzli, J. C. G., Lanthanide luminescent bioprobes (LLBs). *Chem. Lett.* **2009,** *38*, 104-109.
245. Crawford, A. G.; Dwyer, A. D.; Liu, Z.; Steffen, A.; Beeby, A.; Pålsson, L. O.; Tozer, D. J.; Marder, T. B., Experimental and theoretical studies of the photophysical properties of 2- and 2,7-functionalized pyrene derivatives. *J. Am. Chem. Soc.* **2011,** *133*, 13349-13362.
246. Birks, J. B., Photophysics of aromatic molecules. *Wiley-Interscience: London* **1970,** *74*, 1294-1295.
247. Yao, C.; Kraatz, H. B.; Steer, R. P., Photophysics of pyrene-labelled compounds of biophysical interest. *Photochem. Photobiol. Sci.* **2005,** *4*, 191-199.
248. Turro, N. J.; Ramamurthy, V.; Scaiano, J. C., *Principles of molecular photochemistry, an introduction.*; University Science Books: Sausalito, Calif., 2009.
249. Hunter, C. A.; Lawson, K. R.; Perkins, J.; Urch, C. J., Aromatic interactions. *J. Chem. Soc., Perkin Trans. 2* **2001**, 651-669.
250. Hunter, C. A.; Sanders, J. K. M., The nature of .pi.-.pi. interactions. *J. Am. Chem. Soc.* **1990,** *112*, 5525-5534.
251. Lehn, J. M., *Supramolecular Chemistry: Concepts and Perspectives*. 1995.
252. Rowan, S. J.; Cantrill, S. J.; Cousins, G. R.; Sanders, J. K.; Stoddart, J. F.; Angew. Chem., I. E., 41, 898–952., Dynamic covalent chemistry. *Angew. Chem., Int. Ed. Eng.* **2002,** *41*, 898-952.
253. Steed, J. W.; Atwood, J. L., *Supramolecular chemistry*. Wiley: Chichester2000.
254. Waters, M. L., Aromatic interactions in peptides: Impact on structure and function. *Biopolymers* **2004,** *76*, 435-445.
255. Amabilino, D. B.; Stoddart, J. F., Interlocked and intertwined structures and superstructures. *Chem. Rev.* **1995,** *95*, 2725-2828.
256. Bhosale, S. V.; Jani, C. H.; Langford, S. J., Chemistry of naphthalene diimides. *Chem. Soc. Rev.* **2008,** *37*, 331–342.
257. Colquhoun, H. M.; Stoddart, J. F.; Williams, D. J., Second-sphere coordination–a novel role for molecular receptors. *Angew. Chem. Int. Ed.* **1986,** *25*, 487-507.
258. Philp, D.; Stoddart, J. F., Self-assembly in natural and unnatural systems. *Angew. Chem. Int. Ed.* **1996,** *35*, 1154-1196.
259. Stoddart, J. F., Molecular machines. *Acc. Chem. Res.* **2001,** *34*, 410-411.
260. Stoddart, J. F.; Colquhoun, H. M., Big and little meccano. *Tetrahedron* **2008,** *64*, 8231-8263.
261. Chena, Z.; Álvarez-Pérez, M.; Navarro-Villoslada, F.; Moreno-Bondi, M. C.; Orellana, G., Fluorescent Sensing of "Quat" Herbicides with a Multifunctional Pyrene-Labeled Monomer and Molecular Imprinting. *Sens. Actuators, B* **2014,** *191*, 137– 142.
262. Navarro-Villoslada, F.; Urraca, J. L.; Moreno-Bondi, M. C.; Orellana, G., Zearalenone sensing with molecularly imprinted polymers and tailored fluorescent probes. *Sensor. Actuat. B* **2007,** *121*, 67-73.

263. Krupadam, R. J.; Bhagat, B.; Wate, S. R.; Bodhe, G. L.; Sellergren, B.; Anjaneyulu, Y., Fluorescence spectrophotometer analysis of polycyclic aromatic hydrocarbons in environmental samples based on solid phase extraction using molecularly imprinted polymer. *Environ. Sci. Technol.* **2009,** *43*, 2871-2877.
264. Stig, J.; Staffan, B.; Johan, B. A method for removing polycyclic aromatic hydrocarbons. 2013.
265. Ho, W. L.; Liu, Y. Y.; C., L. T., Development of molecular imprinted polymer for selective adsorption of benz[a]pyrene among airborne polycyclic aromatic hydrocarbon compounds. *Environ. Eng. Sci.* **2011,** *28*, 421-434.

II-Molecularly Imprinted Polymers for Alternariol Recognition

INDEX

General objectives

The aim of this Chapter is the development of a MIP selective for Alternariol (AOH) recognition. AOH is a mycotoxin of analytical interest because its effect in human health and because it is a wide-spread contamination in common food commodities. Since AOH itself is a toxic, expensive and difficult to synthetize molecule, here we will seek alternative molecules to be used as mimic template. For the MIP synthesis, polymerization conditions will be optimized by a combinatorial approach. The polymers and their interaction with AOH will be characterized by chromatographic and fluorescence spectroscopy techniques.

Specific objectives

1- *Selection of molecular mimics to be employed as cheap alternative to AOH or AME for the preparation of MIPs. Synthesis of the selected molecular surrogates and spectroscopic characterization.*

2- *Synthesis of bulk MIPs and NIPs following a combinatorial approach and using the selected molecular surrogates of AOH as the template. Different compositions of the polymerization mixture will be tested.*

3- *Characterization of the MIP/NIP library and their interaction with the mycotoxins by chromatographic methods. Selection of the optimal polymer composition for selective AOH recognition.*

4- *Synthesis of MIP porous microparticles with the selected polymer composition.*

5- *Application of MIP microparticles as stationary phase in solid phase extraction (SPE) for separation of AOH.*

6- *Study of AOH binding to molecularly imprinted polymers by fluorescence polarization of the intrinsic fluorescence of the AOH molecule (or a surrogate of it).*

II.1. Template selection and preparation

For the synthesis of molecularly imprinted polymers –even in a small laboratory scale–, important amounts (from several mg to multi-gram scale) of the molecular template are normally required. This makes the discovery of novel MIPs for certain compounds not affordable. If the compounds are toxic, expensive or require a multi-step demanding synthesis, alternatives might be seeking, the use of a molecular analogue which is easier to obtain or less dangerous to handle. This alternative molecule should be as similar as possible (structurally and chemically) to the target analyte. The use of *surrogate* molecules instead of the analyte itself has an additional advantage: gradual leaching of the remaining template traces will not contaminate the sample, preventing false positives as the surrogate has different physicochemical properties than those of the analyte (retention time in chromatography, optical absorption/emission spectra, or different molecular weight for mass spectral analysis).

In our case, both alternariol (AOH) and its monomethyl ether (AME) Fig. 2.1 are expensive toxic chemicals. Moreover, the total synthesis of AOH is a time-consuming procedure that involves seven synthetic steps [1]. For all these reasons, we considered preparation of the easy-to-obtain S1-S4 molecular surrogates of AOH and AME Fig. 2.2 [2] for the MIP synthesis. The structure of AOH and

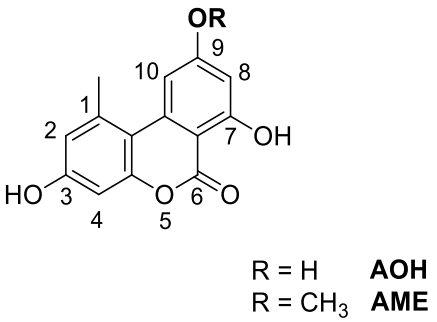

Figure 2.1: Molecular structure of AOH and AME.

AME points at their phenol groups, biphenyl ring system and the lactone moieties as the key features to provide interactions with the functional monomers [3]. Selective recognition by the surrogate-imprinted polymers might be based on hydrogen bonding or hydrophobic interactions. The acidity of the phenol group(s) might also lead to important electrostatic interactions in organic media if they are deprotonated by strongly basic functional monomers, as it has been demonstrated for other phenolic toxins such as zearalenone [4, 5]. The commercial availability of 2-bromo-(di)methoxybenzoic acids and resorcinol were the basis for the design and synthesis of *surrogates* S1 and S3 Fig. 2.2; subsequent demethylation should allow preparation of surrogates S2 and S4 in multi-gram amounts.

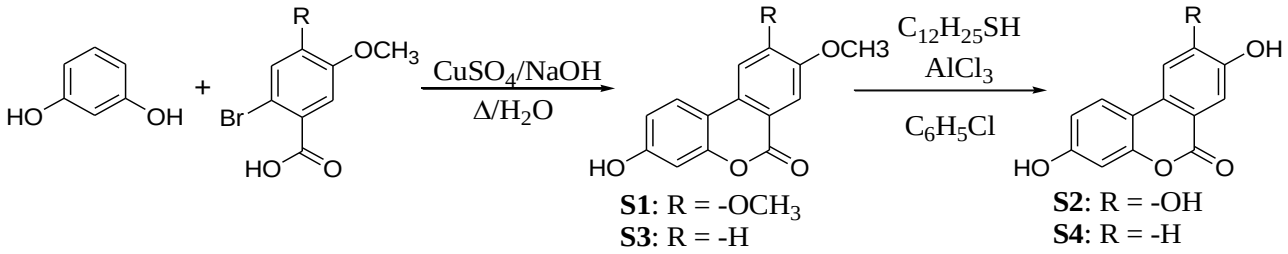

Figure 2.2: Synthesis of the **S1**-**S4** surrogates of AOH and AME.

Additionally, and for providing molecular analogues of AME and AOH that could minimize interference problems in fluorescence-based measurements, the non-rigid S5 and S6 surrogates Fig. 2.3 were also prepared as described by Kumar et al. [6]. These molecular analogues are *non-fluorescent* compounds that would be suitable for avoiding problems of MIP bleeding in case of a non-complete template removal during the washing step of the materials. The synthesis and characterization of surrogates S5 and S6 are also described in the Experimental part of this Thesis. However, and due to a lack of time, the preparation of MIPs with these templates could not be carried out yet.

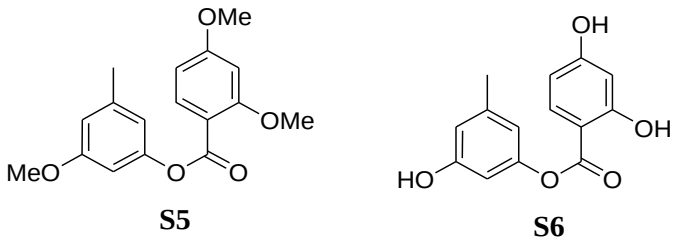

Figure 2.3: Chemical structure of the non-fluorescent surrogates **S5** and **S6**.

Alternatively, and with the aim of having a surrogate that could also be employed for covalent imprinting of the polymers, a *urethane* derivative of S4 was prepared by a straightforward reaction between the surrogate itself S4 and an isocyanate Fig. 2.4. If the isocyanate subunit carries out a polymerizable group such as a methacrylic group, the urethane derivative can be copolymerized with the other monomers, providing a *covalent* attachment of the template molecule (S4 in this case) on the MIP matrix. Removal of the template after polymerization, can be done by mild heating and washing with the proper solvent mixture. It has been previously demonstrated that urethane bonds formed between a phenol group and isocyanates are stable at room temperature, but can be broken by heating at T > 60 ºC [7, 8]. For the synthesis of the S7, a first trial was performed using dibutiltin dilaurate (DBTL), as a catalyst, both at room temperature and by heating at 45 ºC. None of these trials was successful either at room temperature or 45 ºC in anhydrous THF.

The actual procedure followed was adapted from the work of Pandey et al. [9], where pyridine is used for enhancing the reactivity Fig. 2.4.

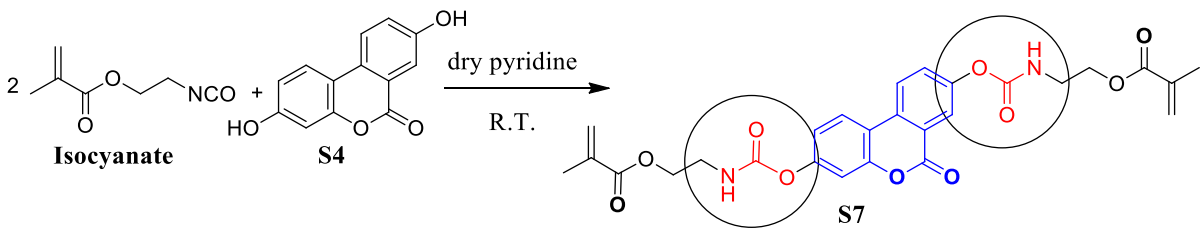

Figure 2.4: Synthesis of an AOH surrogate (**S7**) with urethane functionalities for covalent imprinting of polymers.

The S7 molecule obtained in this way displays absorption and emission maxima at 323 and 418 nm, respectively Fig. 2.5. The fact that the template presents two-point binding sites is expected to provide complementary cavities in the MIP with a high binding constant with S4 and a rapid kinetic uptake of the template molecule.

II.2. Optical properties of the surrogates

The structural resemblance between AOH, AME and the novel surrogates S1-S4 is supported by the similarity of their spectroscopic features. Fig. 2.5 and Table 2.1 show that surrogates S1 and S2 display almost identical band shape and maxima (absorption and emission at ca. 330 and 398 nm, respectively). The same observation holds for surrogates S3 and S4 (lowest energy absorption band at ca. 350 nm and emission at 421 nm for both compounds). All surrogates are significantly fluorescent, with quantum yields (Φ_f) between 0.18 and 0.26, and fast decay from the excited state (emission lifetimes, τ_f, ranging between 1.7 and 2.5 ns). While demethylation of the molecules (from S1 to S2 and S3 to S4) does not affect the position or shape of the absorption and emission spectra, it slightly affects the excited state decay by introducing additional non-radiative deactivation modes involving the O–H bond: for example, conversion of S1 to S2 decreases Φ_f from 0.25 to 0.18 and τ_f from 1.84 to 1.74 ns; similarly, demethylation of S3 to S4, changes Φ_f from 0.26 to 0.22 and τ_f from 2.54 to 2.40 ns).

A similar trend is also observed for AOH and AME: their absorption and emission spectra are superimposable. Remarkably, the fluorescence spectra of AOH and AME are different from those of S1-S4, the toxins showing an additional broad, red-shifted emission at *ca.* 470 nm in addition to the 390 nm band. We attribute this supplementary fluorescence to an excited state intramolecular proton transfer (ESIPT) species that occurs in the AOH and AME molecules and not in their surrogates due to the relative position of the –OH on C-7 of the aromatic skeleton and the C-6 carbonyl groups. Such dual emission has been described in the literature for related chemical structures (e.g. salicylic acid) and attributed to ESIPT [10, 11].

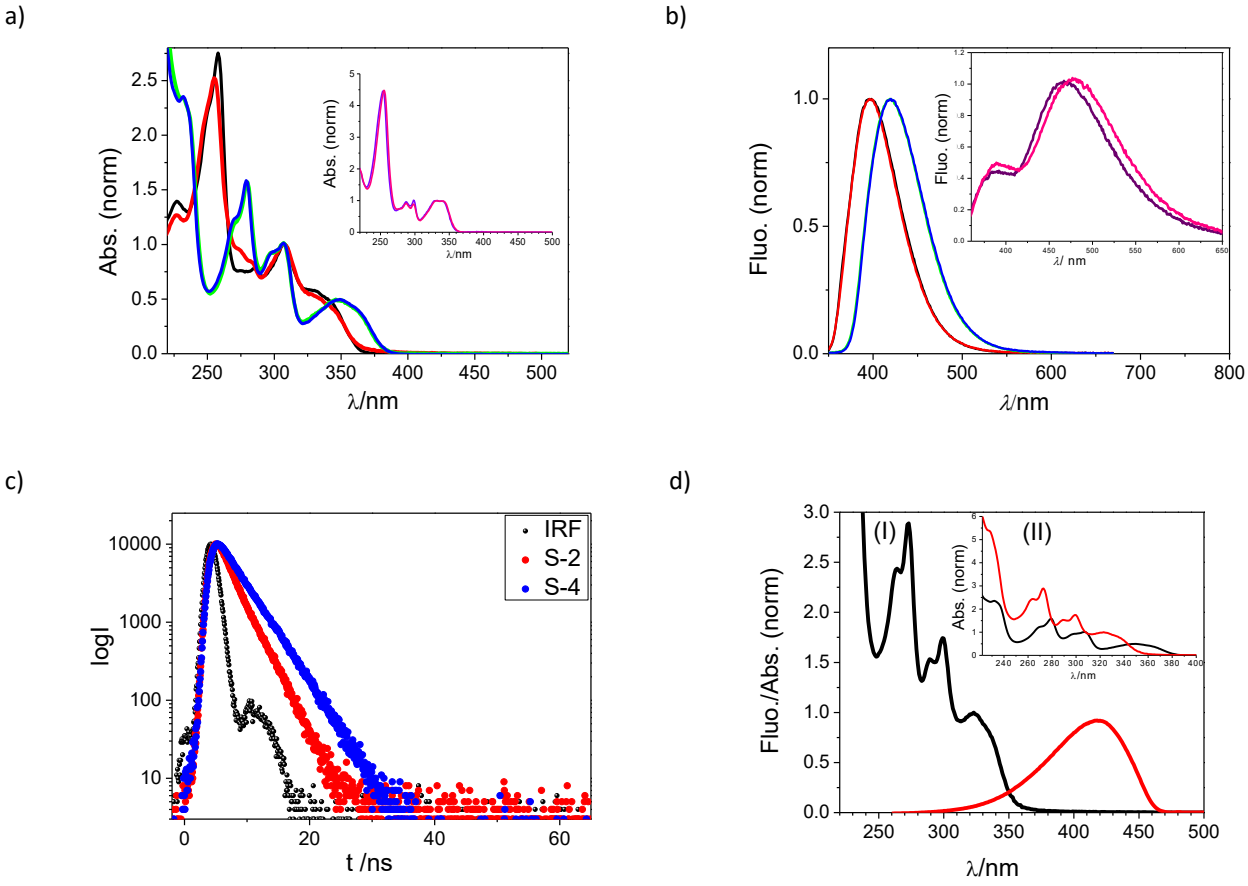

Figure 2.5: Normalized a) absorption and; b) fluorescence (λ_{exc} = 300 nm) spectra of surrogates S1 (black), S2 (red), S3 (green), S4 (blue), and target analytes AOH (purple) and AME (pink) in aerated MeCN; c) Fluorescence decays at 420 nm for S2 and S4 (λ_{exc} = 343 nm); d) Normalized spectra of S7 (I) (absorption (black) and fluorescence (red); λ_{ex} = 340 nm). (II) Absorption spectra of S4 (black) and S7 (red).

Table 2.1: Photophysical data for surrogates S1 - S4, AOH and AME in acetonitrile at 298 K under air.

	λ_{abs} [a]/nm ($\varepsilon/10^3$ M^{-1} cm^{-1})	λ_{em} [a]/nm	Φ_f [b]	τ_f/ns[c]
S1	258 (42.6 ± 1.2), 308 (15.5 ± 0.4), 330 (9.0 ± 0.3, sh)	398	0.25	1.84
S2	255 (24 ± 4), 308 (9.2 ± 1.3), 330 (4.5 ± 0.5, sh)	398	0.18	1.74
S3	280 (17.3 ± 0.5), 308 (11.1 ± 0.3), 346 (5.5 ± 0.2)	421	0.26	2.54
S4	279 (16.3 ± 1.2), 308 (10.2 ± 0.8), 350 (5.1 ± 0.3)	421	0.22	2.40
AOH	331, 341[d]	390, 461	0.062	< 1[e]
AME	331, 341[d]	390, 471	0.062	< 1[e]

[a] Uncertainties of the absorption and emission maxima are ±1 nm. [b] λ_{ex} = 340 nm; 9,10-diphenylanthracene in cyclohexane was used as standard (Φ_f = 0.90 ± 0.04) [12]; the uncertainty of the Φ_f value is 5%. [c] λ_{ex} = 343 nm, λ_{em} = 420 nm; the uncertainty of the τ_f values is 2%. [d] Molar absorption coefficients were not determined due to the cost of the natural toxin. [e] Regardless the emission wavelength, the measured fluorescence lifetime is below the instrument lowest limit (1 ns).

II.3. Ionisation state of surrogate S2 (pK_a calculation)

Typically, phenolic compounds (e.g. AOH, AME and their surrogates) are weakly acid but still, have recognisable acidic properties. For example, deprotonation of the –OH group causes a colour change (from colorless to pink) that can be used for indication of the end point of a pH titration of S2. Therefore, a convenient way to determine the ionisation constant of a species is by monitoring spectroscopic changes (UV-vis absorption or fluorescence) upon protonation or deprotonation.

Taking into account the ionization equilibrium and its constant K_a Eq. 2.1,

$$AOH \rightleftarrows H^+ + AO^-$$

$$K_a = \frac{[H^+][AO^-]}{[AOH]} \qquad (2.1)$$

and the conversion to the logarithm scale Eqs. 2.2 and 2.3,

$$-\log K_a = -\log[H^+] - \log\frac{[AO^-]}{[AOH]} \qquad (2.2)$$

$$pK_a = pH - \log\frac{[AO^-]}{[AOH]} \qquad (2.3)$$

it is possible to state that the AOH pK_a corresponds to the pH of an AOH solution when the logarithmic term equals zero (i.e., when [AO^-] equals [AOH]).

The determination of the p*K*a value of our surrogates is essential since the protonation state of the template will influence its binding with functional monomers carrying basic groups (for example, 2-aminoethyl methacrylate, EAMA, one of the monomers employed in this work) [13, 14]. Based on the theoretical p*K*a values estimated for the S2 template Fig. 2.6, we can conclude that interactions with the amino group of EAMA would take place preferentially with the two neighbour -OH groups of the template (both have very similar pK_a values: pK_{a1} = 7.5, and pK_{a2} = 8.9).

The experimental pK_a value was determined spectroscopically with both UV-visible absorption and fluorescence pH titrations as described in the following section [15].

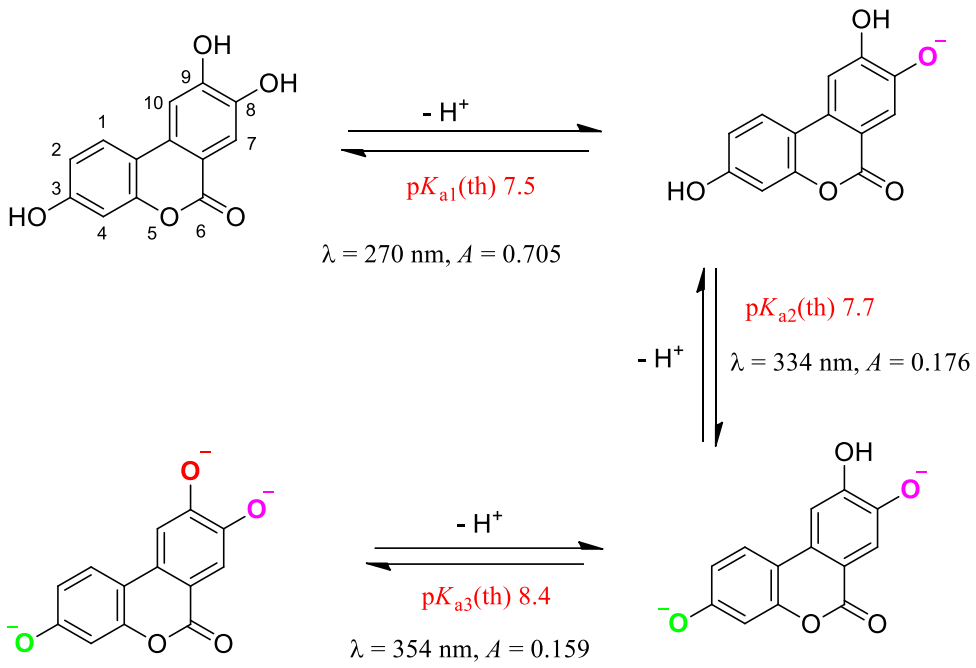

Figure 2.6: Theoretical pK_a values of the different microspecies of the template molecule S2 present in aqueous solution estimated with Marvin ChemSketch 6.3.1 (*ChemAxon*) software (*A* = experimental absorbance at the specified wavelength). According to this software, the macroscopic pK_a values should be found at 7.27, 7.97 and 11.28.

II.3.1. Protocol for pH titrations

The pH of the surrogate solutions was adjusted by adding small amounts of a concentrated solution of NaOH or HCl to a universal buffer solution (see V.2.2 section) under stirring. A styrofoam pad was placed under the solution, on top of the magnetic stirrer, to reduce any heat transfer to the beaker. The pH of the solution was monitored with a Fisher Scientific 625 pH meter. HCl or NaOH was added depending on the desired pH, to the universal buffer solution to obtain pH changes of approximately 0.5 pH units. At these incremental points, the actual pH values were recorded with the pH meter with a manufacturer's stated error of ±0.02 pH units.

Typical titration experiments run in the absorption and fluorescent modes as a function of the solution pH for surrogate S2 are shown in Fig. 2.7. As the solution pH is changed from pH 6.5 to pH 12.0, evolution of both the absorption and emission spectra is observed: the peak centred at 265 nm (λ_1) is shifted to 277 nm (λ_2) while the peak at 308 nm shifts to 322 nm (λ_3) and the peak at 341 nm shifts to 363 nm (λ_4). In the case of the fluorescence spectra, by raising the pH the peak centred at 415 nm

decreases its intensity while the band at 540 increases its intensity upon deprotonation. Further examination of the spectra revealed two wavelengths, noted by blue and red stars on Fig. 2.7.a, where the absorption is essentially independent of pH (isosbestic points). However, taking into account the complexity of the acid-base equilibria of S2 due to the expected proximity of the pK_a values of the –OH groups at C3 and C8 Fig. 2.6, the isosbestic points are not strictly defined. This can also be observed in the fluorescence spectra, where an *isoemissive point* shows up at approximately 467 nm, noted by a black star on Fig. 2.7.b.

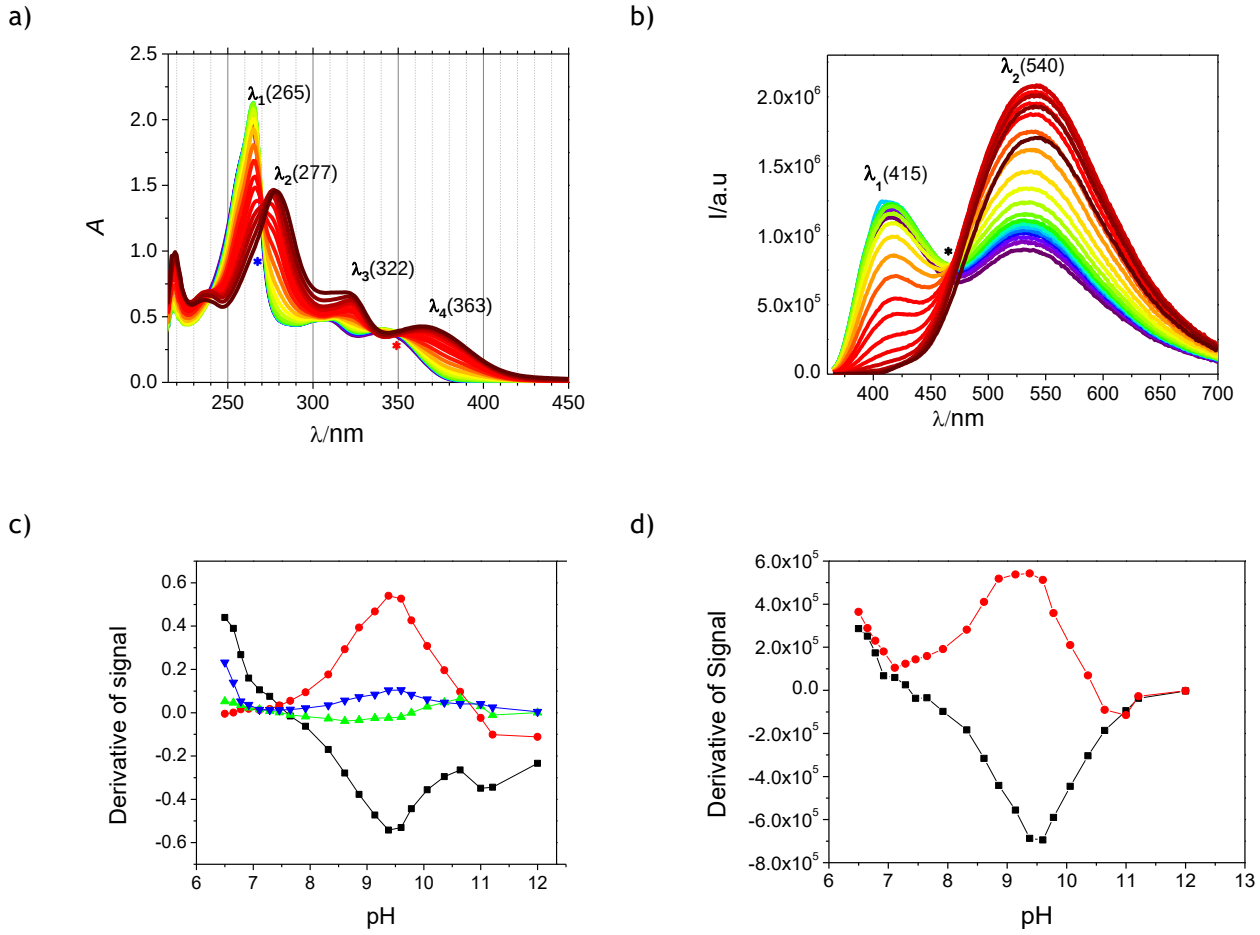

Figure 2.7: pH titrations of S2 (1×10^{-4} mol L^{-1}) in MeCN–universal buffer 0.04 mol L^{-1} (1:4, *v/v*), from acidic (pH 6.5) to basic (pH 12.0) medium at 25 °C. a) UV-vis absorption spectra, showing isosbestic points at 270 nm and 348 nm; b) fluorescence spectra, displaying an isoemissive point at 467 nm. First derivatives of the plots of the: c) absorption spectra at 265 nm, 277 nm, 322 nm and 363 nm as a function of pH; d) emission spectra at 415 nm and 540 nm as a function of pH.

A closer examination of the trends in the spectra is shown in Fig. 2.7 c-d (titration of S2 in MeCN-universal buffer 40 mM (1:4, *v/v*)): the first derivatives of the plots at each monitored wavelength as a function of the solution pH for the absorption and emission spectra should be maximum at the inflection point(s). In this way, an approximate pK_a value of 9.5 ± 0.1 has been determined corresponding, probably, to the deprotonation of the –OH group at C9.

The difference between the calculated (11.28) and the experimental pK_a values might be due to solvation effects in the acetonitrile/water solvent mixture, as well as to the effect of the neighbouring $-O^-$ group at C8 that increases by intramolecular hydrogen bonding the acidity of the least acidic group (the –OH at C9) beyond the calculated value.

II.4. MIPs for alternariol and alternariol monomethyl ether

A combinatorial screening approach has been followed to select the optimal template mimic, functional monomer and cross-linker formulation for the polymer synthesis. Selective rebinding of AOH to the MIP library elements vs. the non-imprinted (NIP) controls has been evaluated by HPLC, and the best composition was selected for preparation of microspherical particles using porous silica beads as sacrificial scaffolds for the polymerization [16].

II.4.1. Choice of the polymer

In order to be able, firstly, to assess which polymer composition might be more suitable for a selective recognition of the target analyte (AOH), a combinatorial MIP/NIP library was prepared (*Experimental section*, Table 5.1) by employing the four different templates, S1-S4, in combination with various functional monomers and cross-linkers. The library was prepared in small scale following a procedure that yields polymers in bulk format. The optimal composition will be afterwards selected for the preparation of the polymers in bead format.

The phenol groups of AOH and its surrogates suggest that all of them should effectively interact with functional monomers bearing sufficiently basic groups to undergo hydrogen bonding or an acid-base reaction with them. If the latter occurs, it will be followed immediately by ion pairing in organic solvents, yet this type of interaction in MIP technology is deemed to furnish less selectivity than

hydrogen bonding without deprotonation [5]. Taking into account this fact, a set of functional monomers (MAM, EAMA, 2-DAEM, 4-VIPY, TBMA) containing a basic nitrogen atom Fig. 2.8 was selected to manufacture the MIP/NIP library. Other common neutral monomer such as HEMA, or even carboxylic monomers (MAA, VBA), were also tested to explore other possible interaction modes with the surrogate templates. To allow full solubilization of monomer, cross-linker, surrogate and initiator, all the polymers were prepared in dimethyl sulfoxide, a hydrogen bond-preserving, moderately porogenic solvent [17]. Two cross-linkers, namely the fairly polar EDMA and the hydrophobic DVB, were chosen for the imprinting process to investigate the influence of the polymer matrix polarity on its affinity for AOH. The final composition of the library is described in (Chapter V, Table 5.1). Each MIP was prepared using the same template/functional monomer/crosslinker (T/FM/CL) mole ratio (1:32:160) [18]. In the absence of a template, an identical FM-to-CL ratio was employed for the NIP syntheses.

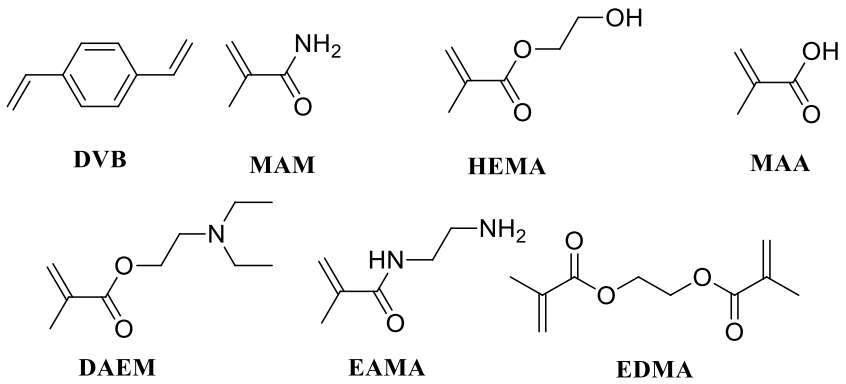

Figure 2.8: Chemical structures of the functional monomers and cross-linkers employed in for the combinatorial synthesis of MIPs and NIPs.

Once the templates were thoroughly extracted after polymerization, the MIP/NIP library was incubated for 24 h with solutions of AOH in either 100 mM pH 7.5 HEPES buffer or MeCN. The concentration of free analyte in the supernatants was used to calculate the amount of bound analyte per polymer (Q_{bound}, %) Tables 2.2 and 2.3. These results show that the combination of EAMA as functional monomer and EDMA as cross-linker renders the strongest binding of AOH in both solvents when surrogate S2 is used as the template molecule. Moreover, such combination provides the maximum difference between the corresponding MIP/NIP bindings. The moderate polarity of EDMA probably avoids the unspecific binding of the highly hydrophobic toxin. Therefore, the EAMA-EDMA mixture was chosen for a large-scale synthesis of MIP beads.

Table 2.2: Rebinding (%) of AOH after 24 h incubation of 20 mg of polymer with 7.5 mg L^{-1} of mycotoxin in 100 mM pH 7.5 HEPES buffer (*n* = 2).

HEPES	NIP	S2	S1	S3	S4	NIP	S2	S1	S3	S4
A (ALPP)	82	75	96	92	91	88	93	98	97	92
B (MAM)	69	92	94	90	95	78	94	98	99	97
C (HEMA)	77	93	93	93	93	75	94	98	98	98
D (MAA)	93	96	100	100	98	55	96	99	97	96
E (VBA)	78	96	92	98	97	65	95	93	93	87
F (DAEM)	98	100	100	99	98	81	96	98	98	88
G (VPY)	97	97	98	97	94	49	95	97	93	96
H (EAMA)	100	100	100	100	100	100	99	100	100	100
	EDMA					DVB				

Table 2.3: Rebinding (%) of AOH after 24 h incubation of 20 mg of polymer with 7.5 mg L^{-1} of mycotoxin in acetonitrile (*n* = 2).

MeCN	NIP	S2	S1	S3	S4	NIP	S2	S1	S3	S4
A (ALPP)	55	52	54	54	63	61	58	54	57	56
B (MAM)	50	54	56	54	56	56	56	57	61	57
C (HEMA)	45	54	54	54	53	57	57	58	55	55
D (MAA)	57	59	59	56	55	53	53	38	57	56
E (VBA)	47	56	53	52	53	55	53	60	56	62
F (DAEM)	26	59	62	61	64	67	89	52	65	62
G (VPY)	22	65	62	60	62	64	76	78	74	80
H (EAMA)	**71**	**90**	66	71	78	72	76	75	66	64
	EDMA					DVB				

II.4.2. ^{1}H-NMR experiments

After having found the molecular surrogate (S2) and functional monomer (EAMA) that provide a MIP with the best AOH recognition properties within the investigated polymer library, NMR titrations were carried out in order to determine the surrogate-monomer binding stoichiometry. This will provide the optimal template-to-functional monomer molar ratio before proceeding with the synthesis of the final polymer. Using a too low functional monomer-to-template ratio would decrease binding constants. On the other hand, too high ratios could lead to an unwanted increase of unspecific adsorption in the final MIP.

Monitoring changes in the chemical shift of key surrogate molecule protons *vs.* the mole fraction of EAMA will yield the desired information. The imprinted polymers prepared with EAMA functional monomer, template S2 and EDMA as cross-linker, showed the highest affinity for AOH. Therefore, the interaction of the EAMA with S2 was investigated by ^{1}H-NMR in MeCN-d_3/DMSO-d_6 (70:30 *v/v*). The template concentration was kept constant, while increasing amounts of EAMA were added to the mixture. Fig. 2.9 displays the ^{1}H-NMR spectra for the different titration steps. Protons H7 and H10 were those undergoing the largest chemical shift changes, with a maximum value of –0.48 (H7) and –0.32 (H10) ppm, pointing out to the preferential interaction of EAMA with the –OH group at C8 the most acidic one, Fig. 2.6. Therefore, their chemical shifts were monitored for obtaining the $\Delta\delta_{obs}$ values represented in the Job plot of Fig. 2.10. Nevertheless, the remaining aromatic H1, H2 and H4 protons also display (smaller) visible changes.

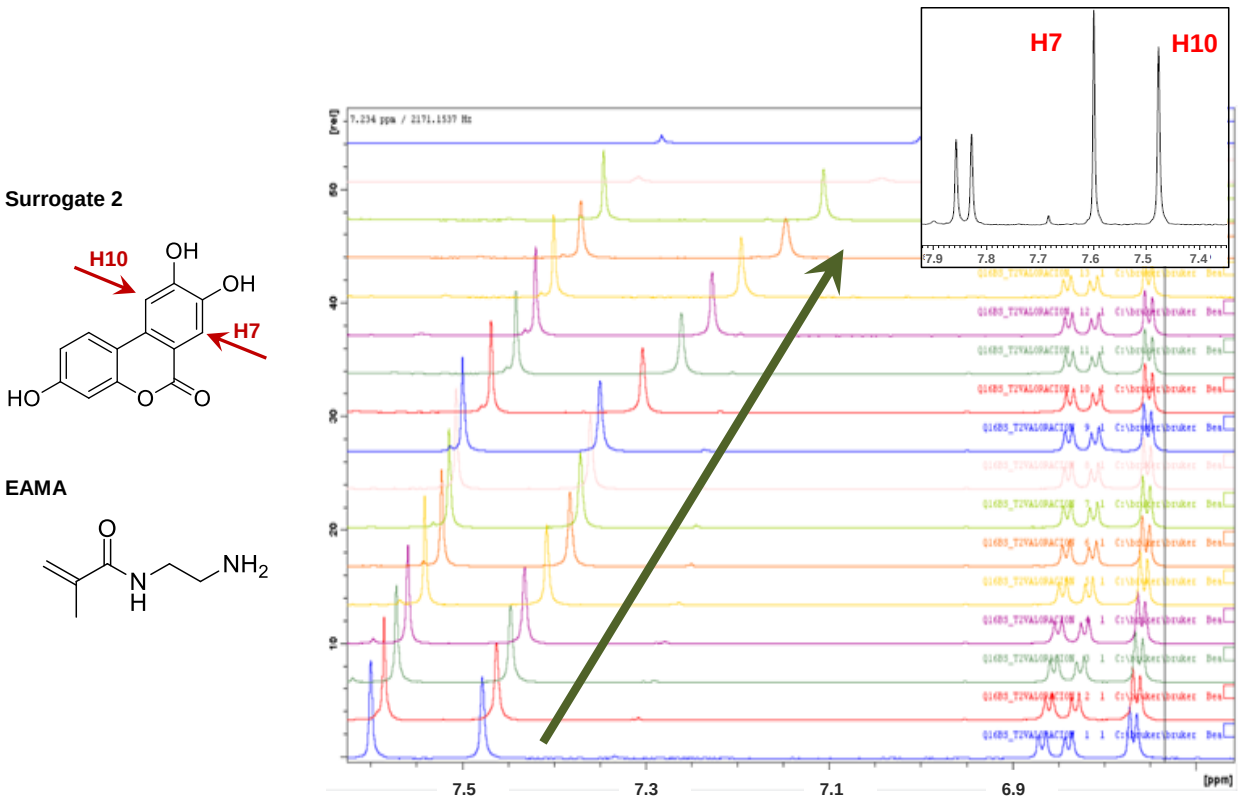

Figure 2.9: ^{1}H-NMR titration of surrogate **S2** with EAMA in MeCN-d_3/DMSO-d_6 (70:30, *v/v*).

The shielding of the aromatic protons of surrogate S2 in the presence of EAMA is compatible with a hydrogen donor-acceptor interaction (or deprotonation, when larger amounts of base are

added) between the template and the monomer molecules. The Job plot shown in Fig. 2.10 allows determination of the stoichiometry of the monomer-template interaction. The maximum in the Job plot is 0.67, which means that a 2:1 EAMA-to-S2 complex is formed. Then, a series of titration experiments was performed to determine precisely the association constants for a 2:1 complex from Eqs. 2.4 and 2.5 [19].

The difference between the chemical shift of the monitored S2 proton (H7 or H10) in the absence and in the presence of EAMA ($\Delta\delta_{obs}$), can be calculated from equations Eqs. 2.4 and 2.5:

$$\Delta\delta_{obs} = \frac{K_{11}\Delta\delta^0_{11} + 2K_{11}K_{21}[A]\Delta\delta^0_{21}}{\frac{1}{[T]} + K_{11} + 2K_{11}K_{21}[A]} \quad (2.4)$$

$$[A] = \frac{[A]_T + 2K_{11}K_{21}[T]_T[A]^2_T}{1 + K_{11}[T]_T + 4K_{11}K_{21}[T]_T[A]_T} \quad (2.5)$$

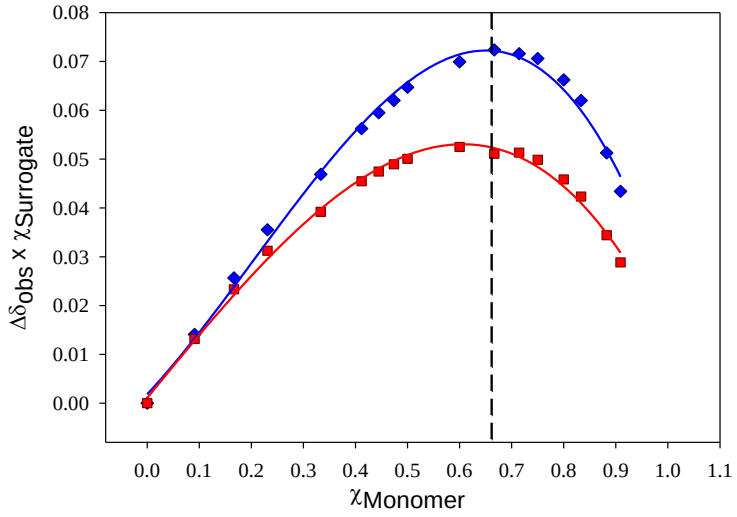

Figure 2.10: Changes in the chemical shifts of the H7 (**blue line**) and H10 protons (**red line**) of the template molecule (0.025 mol L^{-1}), according to the concentration of free EAMA in MeCN-d_3/DMSO-d_6 (70:30, *v/v*). The continuous line represents the best fit of the experimental Eq. 2.5 with the parameters of Table 2.4.

where $\Delta\delta^0_{11}$ and $\Delta\delta^0_{21}$ are the differences between the proton chemical shifts of the free, 1:1 or 2:1 complexed species, respectively, K_{11} and K_{21} are the corresponding association constants, while [A] and [T] are the concentrations of the free EAMA and S2, respectively. The approximate free EAMA concentration is a function of the total concentrations of template and amine ($[T]_T$ and $[A]_T$), K_{11}, and K_{21} for all the points in the experimental curves showed in Fig. 2.10, according to Eq. 2.5 [20].

The variables $\Delta\delta_{obs}$ and $[A]_T$ are measured experimentally, while $\Delta\delta^0_{11}$, $\Delta\delta^0_{21}$, K_{11} and K_{21} need to be estimated from the curve to fit Eq. 2.4. The value of the intermediate variable [A] must be iteratively calculated using Eq. 2.5 for all the points of the experimental curve.

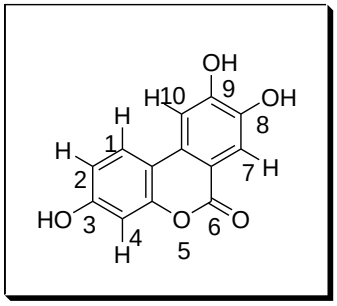

Figure 2.11: Chemical structure of surrogate S2.

Table 2.4: Association constants of **EAMA** and **S2** calculated from the ^{1}H-NMR data in MeCN-d_3/DMSO-d_6 (70:30, *v/v*).

	H7	H10
K_{11} /M^{-1}	$(2.6 \pm 0.1) \times 10^3$	$(2.4 \pm 0.1) \times 10^3$
K_{21} /M^{-1}	5.7 ± 0.2	6.3 ± 0.3

Non-linear least squares fitting renders binding constants of 2.6 and 2.4 x 10^3 M^{-1} for K_{11} (depending on the proton that is being monitored, H7 or H10) and 5.7 and 6.3 M^{-1} in the case of K_{21}. The strongest acidity of the phenol group on C_8 Fig. 2.6[1] suggests that it may be the preferred interaction site with the EAMA monomer. The larger chemical shift variation experimented by H7 is in agreement with such allocation. These binding constants are *ca.* one tenth of those determined by ^{1}H-NMR for the interaction between cyclododecyl 2,4-dihydroxybenzoate (a surrogate of the zearalenone toxin) and 1-allylpyperazine [5]. The stronger basicity of the latter compared to EAMA, together with the fact that the determination was carried out in MeCN-d_3 rather than DMSO-d_6, might account for these differences in spite of the common diphenol moiety present in both analytes.

II.4.3. Alternariol MIP in bulk format (BMP1/BNP1)

Initially, we proceeded to the synthesis of a MIP in a *bulk* form using the stoichiometric ratio template molecule (S2) to functional monomer (EAMA) determined from the ^{1}H NMR experiments. In this case, the polymer is prepared using MAM as diluent monomer, since its presence increases the

[1] The ACD/Labs 12.02 software predicts similar values to those of Marvin ChemSketch 6.3.1 (*ChemAxon*): pK_a = 7.5 ± 0.2 for –OH on C8, compared to 8.9 ± 0.2 and 12.3 ± 0.2 for the phenol groups on C3 and C9, respectively).

polarity of the polymer facilitating the selective recognition of analytes in *aqueous* media. The molar ratio employed was: template (S2)/functional monomer (EAMA)/diluent monomer (MAM)/crosslinker (EDMA) **1:2:2:20**. The reference name BMP1 was given. The corresponding BNP1 non-imprinted polymer was prepared using the same ratio, but omitting the template molecule.

The BMP1 and BNP1 materials obtained in this way were grounded and sieved and, finally, packaged in solid phase extraction (SPE) cartridges[2] (25 mg of MIP or NIP each) to optimise the conditions for selective extraction of the mycotoxin in the polymer. The method of solid phase extraction is commonly used in analytical chemistry as a technique for cleaning and pre-concentration of samples. It involves the selective retention of the analyte of interest in a solid phase, in our case the MIP, while contaminants in the matrix are eluted during sample loading or washing steps, or are retained in the polymer. The analyte is eluted from the column using a suitable solvent. In any SPE method, the charging, washing and elution steps are optimised in order to achieve a maximum recovery of the compounds of interest.

II.4.4. Optimisation of the cartridge washing solvent

For achieving maximum retention of AOH in the BMP1 and the minimum in the BNP1, a study varying the composition of the washing solution was performed. Fig. 2.12 shows the extraction recoveries obtained for both polymers by washing the cartridge with 0.5 mL of a MeCN-H_2O mixture with variable composition (100-0%, *v/v*). In all cases, 1 mL of a solution of AOH (2 mg L^{-1}) in HEPES buffer (0.1 M, pH 7.5) was loaded and, after washing the sample-loaded support, elution was carried out with 1 mL of MeOH-TFA (95:5, *v/v*) mixture.

[2] 1 mL polypropylene SPE cartridges; the cartridges were connected to a vacuum manifold.

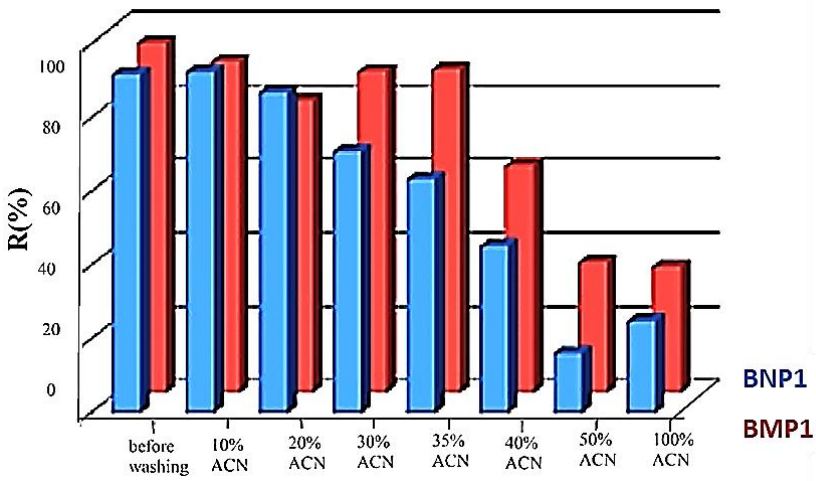

Figure 2.12: Recoveries of AOH obtained for **BMP1** and **BNP1** as a function of the composition of the washing solution (*n* = 3). Sample volume: 1 mL of AOH (2 mg L^{-1}) in HEPES (0.1 M, pH 7.5) buffer; flow rate 1 mL min^{-1}; washing with 0.5 mL of 0%, 15%, 20%, 30%, 35%, 40%, 50% and 100% H_2O-MeCN (*v/v*); elution: 1 mL MeOH-TFA (95:5, *v/v*).

As shown in Fig. 2.12, increasing the percentage of MeCN in the washing solution decreases the recovery of AOH, although recovery is always higher with the MIP than with the NIP above 20% MeCN demonstrating selective retention (recognition) in the cavities of the imprinted polymer. The largest differences are obtained when 30–35% MeCN-H_2O (*v/v*) is used. Increasing the concentration of MeCN in the washing solution, a very good solvent for AOH, decreases the affinity of the polymers for the AOH molecule, especially in the NIP which does not have any complementary cavities to the mycotoxin. By increasing the volume (0.5 to 1.0 mL) of the 30% MeCN-H_2O washing mixture Fig. 2.13, the recovery from the NIP is much lower than that from the MIP. However, if the washing volume is further increased to 2 mL, a smaller recovery of AOH from the MIP is observed, although it is still higher than that from the NIP in the same conditions Fig. 2.13, demonstrating the delicate balance between the AOH-polymer (MIP/NIP) interactions and the affinity of the analyte for the organic solvent.

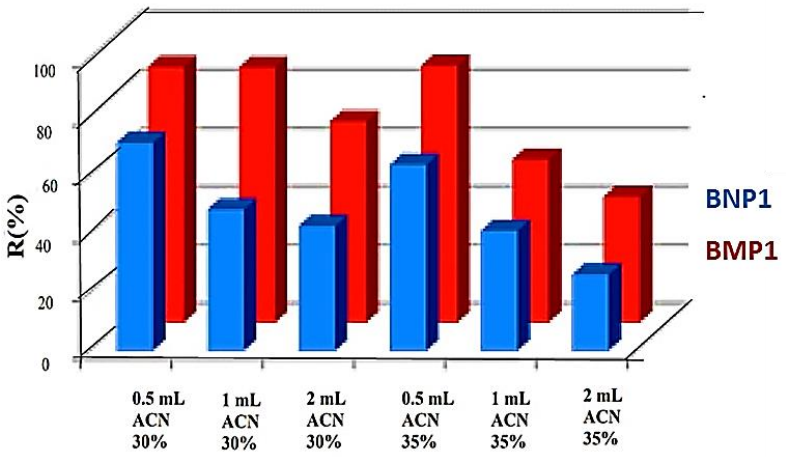

Figure 2.13: Recoveries of AOH obtained for **BMP1** and **BNP1** as a function of the volume and composition of the washing solution (n = 3). Sample volume: 1 mL of AOH (2 mg L^{-1}) in HEPES (0.1 M, pH 7.5) buffer; flow rate 1 mL min^{-1}; washing mixture: 30% or 35% MeCN-H_2O (*v/v*); elution: 1 mL MeOH-TFA (95:5, *v/v*).

II.4.5. Effect of the washing solution pH on the retention of AOH in BMP1 and BNP1

Considering that EAMA pK_a is 9.16, and the experimental pK_a value of S2 (9.5, see II.3.1), the effect of the pH of the washing solution on the recognition of AOH by the MIP (and the NIP) was studied in the 6.5–8.5 range using 0.05 M phosphate buffer (NaH_2PO_4/Na_2HPO_4), to promote also electrostatic interactions between doubly deprotonated AOH and the ammonium groups in the polymer backbone [21]. The recoveries obtained after the washing step are not significantly different for the three pH values investigated Fig. 2.14, probably due to the fact that even at pH 6.5 the formation of diprotonated AOH Fig. 2.7 has not occurred in a large extent.

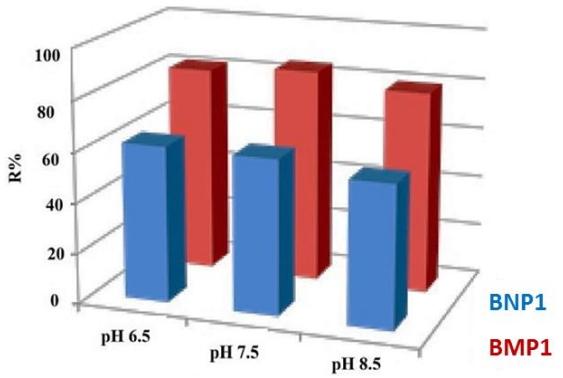

Figure 2.14: Recoveries of AOH obtained for **BMP1** and **BNP1** as a function of the pH of the washing solution (*n* = 3). Sample volume: 1 mL of AOH (2 mg L^{-1}) in 0.05 M phosphate buffer; flow rate 1 mL min^{-1}; washing mixture: 30% MeCN-H_2O (*v/v*); elution: 1 mL MeOH-TFA (95:5, *v/v*).

II.4.6. Breakthrough volume

The charaterization of a solid phase extraction (SPE) procedure requires evaluation of the cartridge capacity, i.e., the volume of sample, assumed to have a constant analyte concentration, that can be passed through the SPE cartridge before the concentration of the analyte at the outlet of the device reaches a certain fraction of the concentration of the analyte at the inlet. The determination of this parameter for the selected polymers BMP1 and BNP1 was carried out by percolating through the cartridges 1, 2, 5, 10 or 20 mL of a mixture HEPES (0.1 M pH 7.5)–MeCN (70:30, *v/v)* containing a fixed amount of AOH (200 µg L^{-1}) [22]. The results are shown in Fig. 2.15.

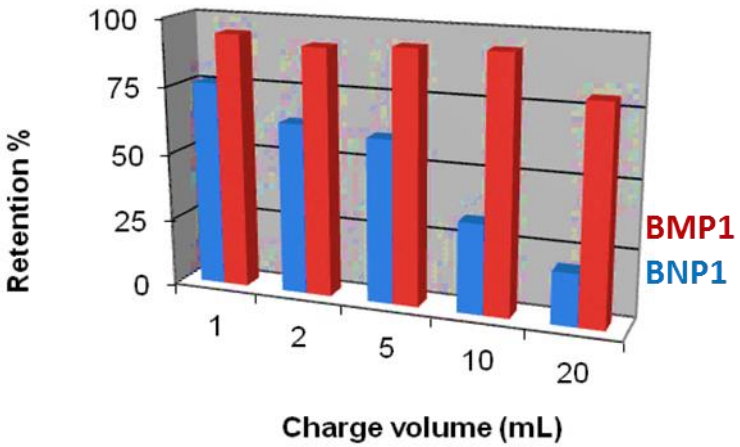

Figure 2.15: Retention of AOH in BMP1/BNP1 for different sample volumes. The concentration of AOH was 200 µg L^{-1} in HEPES (0.1 M, pH = 7.5)–MeCN (70:30, *v/v*) mixture; the cartridges were washed with 0.5 mL HEPES (0.1 M pH = 7.5)–MeCN (70:30, *v/v*) after passing the loading volume; elution with 1 mL MeOH-TFA (95:5, *v/v*).

From the onset at a charge volume of 1 mL, significant differences in the recovery of alternariol between BMP1 and BNP1 could be observed. As the loading volume increases, the retention in the MIP stays constant at near 100% up to 10 mL, whereas the NIP retention decreases continuously. This behaviour is due to the fact that the NIP has a lower binding capacity. The experimental data show a strong interaction between BMP1 and AOH, allowing the pre-concentration of the sample with excellent recovery. Volumes higher than 20 mL are not practical due to the smaller volumes of the extracts containing alternariol.

II.4.7. Alternariol MIP and NIP porous microbeads

The functional (EAMA) and cross-linker (EDMA) monomers that yielded MIPs with the best recognition of AOH were then used for preparing porous MIP beads. Two polymers were synthesized, one of them including MAM as a diluent monomer. The final MIP compositions were S2/EAMA/MAM/EDMA (molar ratio 1:2:2:20), coded MP-ME1, and S2/EAMA/EDMA (molar ratio 1:4:20), coded MP-ME2. Similar non-imprinted polymers were also prepared in the absence of template (NP-ME1 and (NP-ME2). The corresponding microspheres are obtained by polymerizing the monomer and template mixture in MeCN-DMSO (3:7, *v/v*) into the pores of commercial 40-75 µm diameter silica beads Fig. 2.16. The latter is dissolved with NH_4HF_2 after polymerization, leaving behind void channels in the resulting MIP bead structure [16]. These channels accelerate mass transfer kinetics of the target analyte to the recognition sites into the beads with respect to bulk MIPs. The highly porous MIP/NIP spheres obtained in this way are roughly the same size than the initial silica beads, see SEM picture on Fig. 2.16.

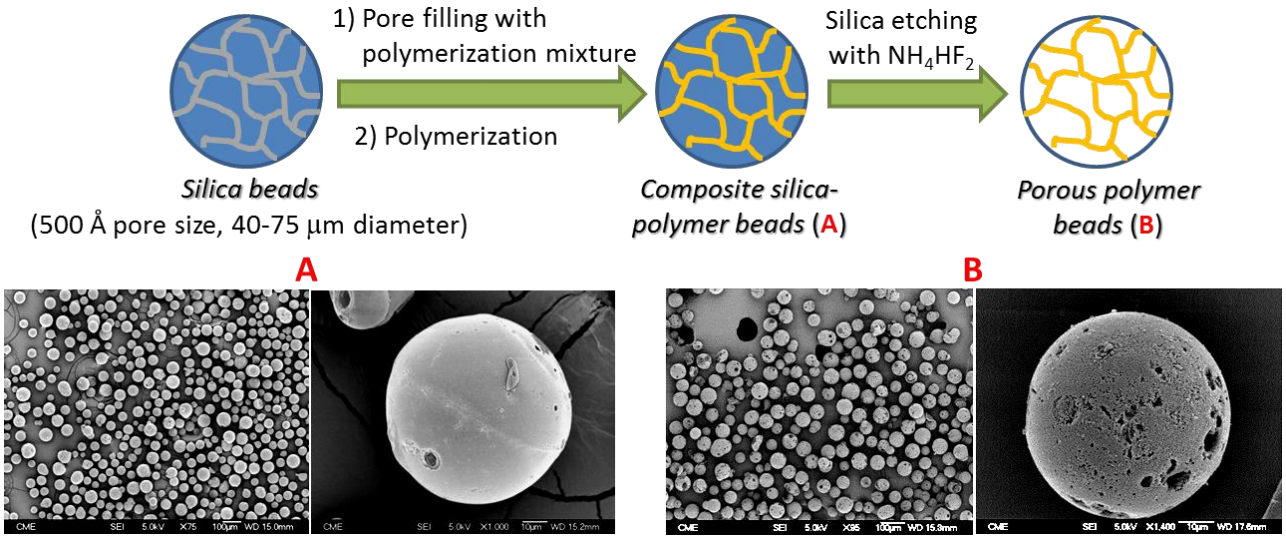

Figure 2.16: Scheme of the preparation of the MIP and NIP microspheres with a silica mold, and SEM images of the intermediate composite material (**A**) and the same beads after treatment with 3 M aqueous NH_4HF_2 (**B**), for the MP-ME1 beads.

After silica etching, both the MIP and the NIP maintain the spherical shape mold feature; however, a significant increase in the porosity of the material is obtained compared to the composite material. The results of the elemental analysis for MP-ME1 and the corresponding NIP (IP-ME1) are shown in Table 2.5. The C (*ca.* 55%), H (*ca.* 7%) and N (*ca.* 1.5%) content is very similar for the MIP and the NIP polymers, and the values approach the expected value of 61% C, 7% H and 1.3% N from the monomers mixture (the slightly lower values of C and N content could be due to the fact that still some silica remains in the microspheres after the treatment with NH_4HF_2 or that some water was retained into the polymer).

Table 2.5: Elemental analyses of the MP-ME1 and NP-ME1 polymers obtained in the form of spherical particles using silica gel as sacrificial molds for.

	% C	% H	% N
MP-ME1	54.68	6.64	1.58
NP-ME1	56.81	6.91	1.54
Theoretical value	60.59	7.29	1.28

To evaluate the performance of the EAMA-based polymers as MISPE sorbents, fixed amounts of the beads (20 mg) were packed in SPE cartridges, equilibrated with 5 mL of methanol and 10 mL

of phosphate buffer (100 mM, pH 8.5) and loaded with 1 mL solution of AOH (1 mg L^{-1}) in phosphate buffer (100 mM, pH 8.5). The cartridges were rinsed with 0 or 1 mL of water–MeCN mixture (80:20, *v/v*) and eluted with 1 mL 1% TFA in MeOH. As shown in Fig 2.17, no significant differences in the AOH recoveries were obtained with both MIPs in the absence of a washing step (n = 3; $R_{MP\text{-}ME1}$ = 97%, RSD 7%; and $R_{MP\text{-}ME2}$ = 102%, $RSD_{MP\text{-}ME2}$ 1%; $R_{NP\text{-}ME2}$ 103%, RSD 0.4%), in agreement with the results obtained in the library evaluation. However, the use of an equimolar mixture of EAMA and MAM as functional monomers resulted in NIPs with much lower non-specific binding ($R_{NP\text{-}ME1}$ = 5 %; RSD 1%) than those prepared with EAMA ($R_{NP\text{-}ME2}$ = 66%, RSD 6%) after a washing step with 1 mL water-MeCN (80:20, *v/v*). Therefore, the S2/EAMA/MAA/EDMA (**1:2:2:20**) molar composition was selected for further experiments (MP/NP-ME1).

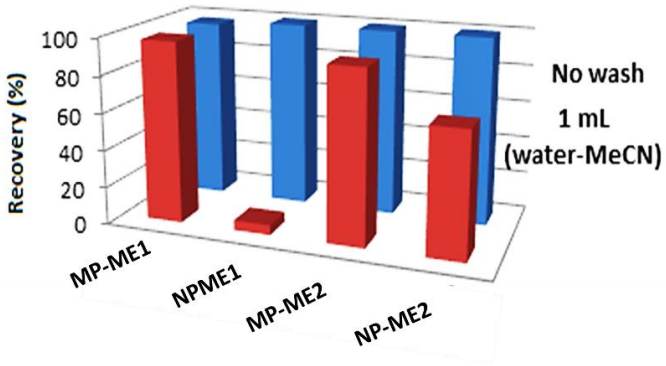

Figure 2.17: Alternariol extraction recoveries (%) obtained with the MP-ME/NP-ME bead cartridges as a function of the polymer composition, with and without a washing step. MP-ME1: **S2**/EAMA/MAM/EDMA (molar ratio 1:2:2:20); MP-ME2: **S2**/EAMA/EDMA (molar ratio 1:4:20). Loading: 1 mL of AOH (1 mg L^{-1}) in phosphate buffer (100 mM pH 8.5); washing: 1 mL of 80:20 water-MeCN (*v/v*); elution: 1 mL of 1% TFA in MeOH (RSD_{MIP} < 7%; RSD_{NIP} < 6%; n = 3).

II.4.8. Chromatographic evaluation of the polymer selectivity

In order to find out the selectivity of the imprinted material MP-ME1 for alternariol, this toxin and other compounds with a similar structure were analysed by HPLC using a home-packed MP-ME1 column. Because phenols are far less acidic in organic media [23], the retention capacity of the imprinted and non-imprinted polymers in pure acetonitrile is moderate because there is no ionic interaction between the non-ionized AOH and the (protonated) amine-containing polymer. However, a significant imprinting effect for the template S2 was observed when the mobile phase was an (80:20,

v/v) mixture of water–MeCN. Under these conditions, the retention time of AOH in the MIP rose 9-fold with respect to that measured in the NIP thanks to deprotonation of the phenolic toxin. This remarkable increase of the AOH retention time in the MIP vs. the NIP is actually larger than in the case of the S2 template itself (IF = 6.42), Table 2.6; therefore, such solvent composition was deemed optimal for the AOH recognition. Other solvent compositions provided less imprinting effect. The ability of the imprinted polymer to retain other related analytes with the optimal water-MeCN mobile phase are collected in Table 2.6. Retention factors (k) and the imprinting factor (IF) for each compound were calculated using Eqs. 2.6 and 2.7.

$$k = \frac{t_R - t_0}{t_0} \qquad (2.6)$$

$$\mathrm{IF} = \frac{K_{MIP}}{K_{NIP}} \qquad (2.7)$$

where, t_R is the retention time of the compound in the column and t_o is the retention time of an unrestrained compound, in our case methanol. A larger k means greater affinity for the stationary phase compound. The imprinting factor IF is the relation between retention factors of each analyte in the MIP and in the NIP columns and indicates the selectivity of the MIP for a given compound.

Table 2.6: Parameters of the binding of different phenolic compounds to the best imprinted polymer (MP-ME1) and to the corresponding non-imprinted polymer (NP-ME1): t_R: retention time; k: retention factor; *IF*: imprinting factor.[a]

	t_R/min (MP-ME1)	t_R/min (NP-ME1)	k_{MP-ME1}	k_{NP-ME1}	*IF*	log *P*
AOH	16.63	1.87	36.03	3.96	9.10	2.7 ± 0.8 [24]
S2	3.33	0.75	6.41	0.99	6.42	1.6 ± 1.1 [25]
AME	28.61	3.12	62.71	7.28	8.61	3.9 ± 0.4 [25]
S4	19.41	2.16	42.20	4.71	8.95	2.3 ± 0.8 [25]
Catechol	0.88	0.51	0.95	0.37	2.55	0.7 ± 0.6 [26]
Phenol	1.28	0.64	1.84	0.68	2.71	1.5 [27]
Resorcinol	0.78	0.49	0.73	0.29	2.59	0.8 [24]

[a] In water–MeCN (80:20, *v/v*); [phenol]: 200 mg L^{-1}. Void volume marker: methanol ($t_{0\ NIP}$ = 0.38 min, $t_{0\ MIP}$ = 0.45 min).

The imprinting factors (*IF*s) measured for AOH, AME and surrogate S4 were 9.10, 8.61 and 8.95, respectively, indicating a very high degree of molecular recognition of the MIP for these three species although it was prepared using surrogate S2 as a template. However, binding of AME and surrogate S4 to their respective MIP contains a significant contribution from their hydrophobicity. We must bear in mind that not only the shape and structure of the molecule influences the retention capacity of the polymer, but the polarity of the guest also plays a significant role if rebinding is carried

out in aqueous or predominantly aqueous media. The hydrophobicity of a compound is measured by its log *P* parameter (*P* is the *n*-octanol/water partition coefficient). AOH, AME and S4 exhibit a lower polarity than S2 (higher log *P* values), Table 2.6 and, therefore, their retention times both in the MIP and in the NIP Table 2.6 are longer than those measured in S2 due to their stronger hydrophobic interactions with the polymer material. Moreover, the relatively high imprinting factors obtained for catechol, resorcinol and phenol should not be considered *real* values due to the similar retention times of the analytes and the void marker in the imprinted and non-imprinted polymers.

II.4.9. Binding capacity of MP-ME1/NP-ME1

Efficient MIP materials should display, in addition to high affinity and selectivity, a substantial binding capacity for the analyte of interest. The latter requirement is particularly relevant in solid phase extraction (SPE) applications so that SPE can be performed with small amounts of the polymer, allowing reduction or suppression of non-selective adsorption of unrelated species that accompany the target in real samples. For evaluating the binding capacity of the MIP microspheres, polymer beads (20 mg) were incubated for 24 h with mechanical stirring with different concentrations of the AOH mycotoxin (from 2.58 mg L^{-1} to 258 mg L^{-1}). Then, the amount of free AOH present in the supernatant was evaluated by HPLC with fluorescence detection. For obtaining adsorption isotherms, the amount of bound AOH per unit mass (*B*) was represented as a function of the concentration of free AOH remaining in the solution (*F*) Fig. 2.18. For data analysis, the most widely applied binding model is the continuous distribution represented by the Freundlich isotherm Eq. 2.8.

$$B(F) = aF^{m} \qquad (2.8)$$

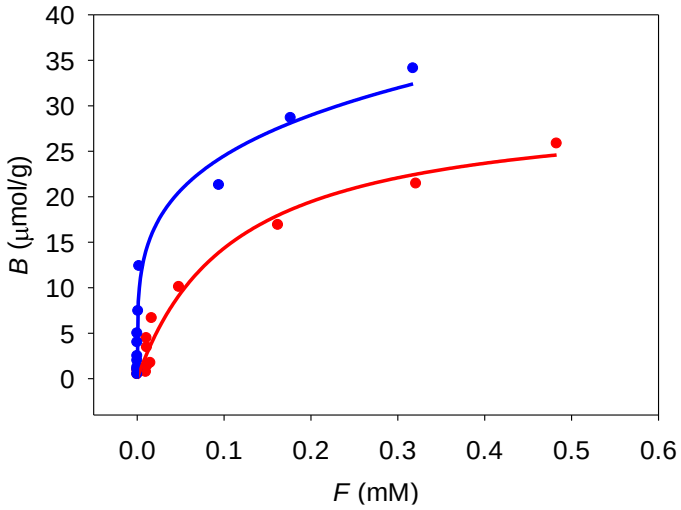

Figure 2.18: Equilibrium binding isotherms for the uptake of AOH by the selected MP-ME1 (**blue**) and its corresponding NP-ME1 (**red**) in water–MeCN (80:20, *v/v*). *F* and *B* represent the amount of free and bound AOH in the solution, respectively. The symbols represent experimental data (8 data per plot; $n = 2$), while the solid lines are their fits calculated by the Freundlich equation ($B = aF^m$).

The latter assumes that the number of guest molecules bound to the polymer (B) is a power function of the amount of the free ones (F). The two equation fitting parameters carry a physical meaning: a is proportional to the number of binding sites of the polymer (N_T) and their average affinity for the guest (K_0), while m provides a measure of the binding sites heterogeneity ("heterogeneity index"). The value of m varies from one to zero, decreasing with increasing heterogeneity of the binding sites. The apparent number of sites, N_{K1-K2}, and the apparent weighted average affinity, K_{K1-K2}, derived from *Rampey's equations* [27] Eqs. 2.9, 2.10 and 2.11 are summarised in Table 2.7.

$$N(K) = 2.303\mathrm{am}(1-\mathrm{m}^2)\mathrm{e}^{2.303\log K} \qquad (2.9)$$

These data will only be valid on a range of values of the affinity constant K (K_{min} and K_{max}) that can be calculated from the concentrations of free analyte (F_{min} and F_{max}) using Eqs. 2.12 and 2.13.

The binding parameters N_{K1-K2} and K_{K1-K2} can be measured for any set of K_1 and K_2 values that are within the boundaries K_{min} and K_{max}. The subscripts on N_{K1-K2} and K_{K1-K2} mean that these equations yield values that represent only a subset of the entire distribution from K_1 to K_2. These limits are set by the concentration range over which the experimental binding isotherm was measured (F_{min} to

F_{max}). For comparison purposes, it is important to calculate N_{K1-K2} and K_{K1-K2} over the same range of binding affinities (K_1 to K_2).

$$N_{K1-K2} = a(1 - m^2)(K_1^{-m} - K_2^{-m}) \quad (2.10)$$

$$K_{K1-K2} = \left(\frac{m}{m-1}\right)\left(\frac{K_1^{1-m} - K_2^{1-m}}{K_1^{-m} - K_2^{-m}}\right) \quad (2.11)$$

$$K_1 = K_{min} = {}^{1}/_{F_{max}} \quad (2.12)$$

$$K_2 = K_{max} = {}^{1}/_{F_{min}} \quad (2.13)$$

The curve displayed in Fig. 2.18 shows the higher affinity of the S2-imprinted polymer for AOH compared to that of the non-imprinted material. The differences in the adsorption isotherms shown in Fig. 2.18, indicate that the binding capacity of the MP-ME1 (N_{MP-ME1} = 35 µmol g^{-1}) is higher than that of the corresponding NP-ME1 (N_{NP-ME1} = 22 µmol g^{-1}). The same is true for the weighted average affinity in the measured 0.005–0.75 mM concentration range (K_{MP-ME1} = 109 mM^{-1}; K_{NP-ME1} = 50 mM^{-1}). No significant differences were observed in the heterogeneity index of the imprinted polymer (0.41±0.07), Table 2.7 and the corresponding NP-ME1 (0.49 ± 0.02).

Table 2.7: Equilibrium binding isotherm parameters for the uptake of AOH by the MP-ME1 and NP-ME1 in 50 mM 80:20 water–MeCN (*v/v*). The polymer binding capacity (*a*) and the binding site heterogeneity index (*m*) were obtained from the fit of the experimental data Fig. 2.18 to the corresponding Freundlich isotherm Eq. 2.8. The association constants (*K*) and specific binding capacities (*N*) were calculated from Eqs. 2.10 and 2.12.

	a (µmol g^{-1}(mM^{-1})m)	*m*	N_{K1-K2} (µmol g^{-1})	K_{K1-K2} (mM^{-1})	K_{range} (mM^{-1})
MP-ME1	75 ± 9	0.41 ± 0.07	35 ± 2	109 ± 10	31 – 2014
NP-ME1	46 ± 2	0.49 ± 0.02	22 ± 2	50 ± 4	23 – 1007

II.4.10. Optimization of the MISPE procedure for AOH extraction

Several factors were evaluated to establish the optimum conditions for the SPE procedure including the study of the composition and volume of the eluting solvent, the flow rate of the loading solution, the composition of the washing solvent and the breakthrough volume (maximum sample volume that can be pre-concentrated with quantitative recovery of analyte).

To select the composition of the elution solvent, 10 mL samples of AOH (200 μg L^{-1}) dissolved in phosphate buffer (100 mM, pH 8.5) were percolated through the cartridges (containing 20 mg of polymer) and eluted with 1% TFA in MeOH. Quantitative mycotoxin recoveries (R = 102%, RSD 5%, *n* = 3) were achieved using 1 mL of 1% TFA in MeOH (*v/v*), a solvent that was selected for further experiments.

Fig. 2.19 shows the effect of the loading solution flow rate on the recovery of AOH when 10 mL samples of AOH (200 μg L^{-1}) dissolved in phosphate buffer (100 mM, pH 8.5) were loaded into the MP-ME1 cartridge. Recoveries close to 100% were obtained at flow rates ≤ 0.93 mL min^{-1}. The use of higher rates led to a continuous decrease in the recovery values as the interaction time between the analytes, and the sorbent was decreased. Thus, a loading flow rate of 0.93 mL min^{-1} was selected as optimal for further experiments.

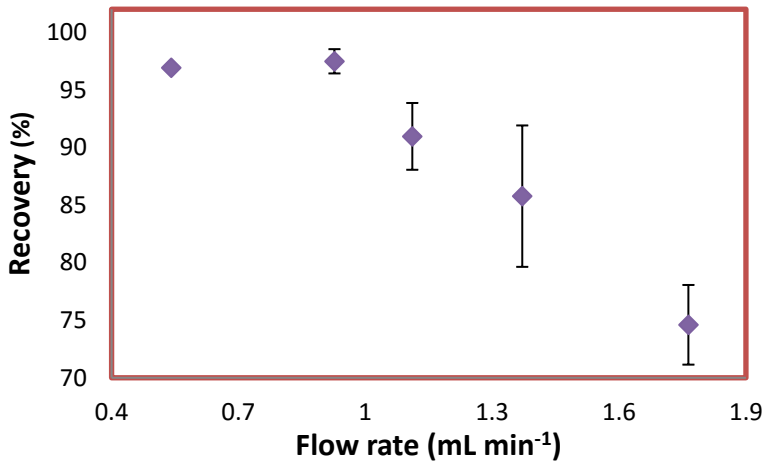

Figure 2.19: Recoveries obtained for different flow rates using a 10 mL solution of AOH (200 μg L^{-1}) in phosphate buffer (100 mM, pH 8.5) as percolation medium. The mycotoxin was eluted from the MP-ME1 cartridge with 1 mL solution of 1% TFA in MeOH (RSD < 7%, *n* = 3).

Several water-MeCN mixtures (100–50%, *v/v*) were evaluated as washing solvents for the MISPE procedure to minimise the non-specific interactions between the mycotoxin and the imprinted polymer. As shown in Fig. 2.20, the retention of AOH in the MP-ME1 and in the NP-ME1 was higher at lower MeCN concentrations in the washing solvent. The highest differences between the MP-ME1 and NP-ME1 were obtained using water-MeCN (80:20, *v/v*) mixture. Under these conditions, AOH

recoveries were 96% (RSD 2%, *n* = 3) for the MP-ME1 and lower than 1% in the NP-ME1. Therefore, this solvent composition was selected for the washing step.

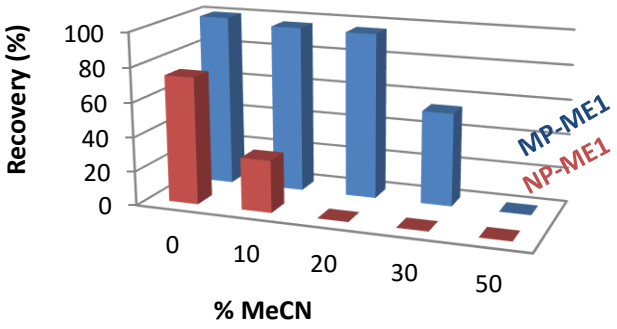

Figure 2.20: Extraction recoveries (%) of AOH from the MP-ME1 and the NP-ME1 after percolation of 1 mL of phosphate buffer (100 mM, pH 8.5) spiked with 0.2 μg of the mycotoxin, using a washing step with 1 mL of water-MeCN (0–50% MeCN, *v/v*) followed by elution with 1 mL of 1% TFA in MeOH (RSD_{MP-ME1} < 9; RSD_{NP-ME1} < 5; *n* = 3).

As shown in Fig. 2.21, an increase in the washing volume from 1 to 3 mL of the (80:20, *v/v*) water-MeCN mixture did not significantly affect the retention of AOH in the MP-ME1 with recoveries in the range of 96 – 102% (RSD < 5%, *n* = 3), while retention in the NP-ME1 was negligible. Finally, a volume of 3 mL of water-MeCN (80:20, *v/v*) was selected for the washing step. Larger volumes were not tested to avoid an increase in the analysis time.

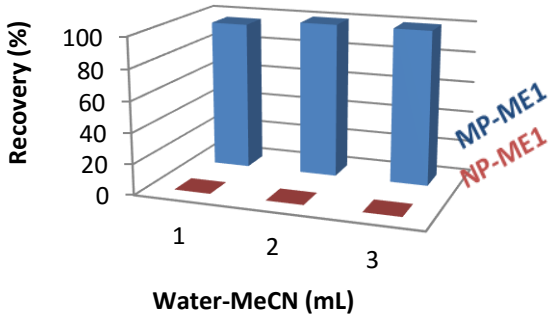

Figure 2.21: Extraction recoveries (%) obtained on the MP-ME1 and the NP-ME1 for AOH after percolation of 10 mL of phosphate buffer (100 mM, pH 8.5) spiked with 2 μg AOH using a washing step with 1, 2 or 3 mL of water-MeCN (80:20, *v/v*). The mycotoxin was eluted from the MP-ME1 cartridge with 1 mL solution of 1% TFA in MeOH (RSD_{MP-ME1} < 5%; RSD_{NP-ME1} < 1%; *n* = 3).

In order to evaluate the *breakthrough volume*, the cartridges were loaded with increasing volumes (1–50 mL) of AOH (200 μg L^{-1}) in phosphate buffer (100 mM pH 8.5) and rinsed with 3 mL of water-

MeCN (80:20, *v/v*); then, the analyte was eluted with 1 mL of 1% TFA in methanol and the eluates were analysed by HPLC-FLD. As shown in Table 2.8, an increase from 20 to 100 mg in the amount of polymer per cartridge led to larger breakthrough volumes, and recoveries higher than 91% were obtained for sample volumes up to 50 mL Recoveries in the NIP were below 10% in all cases.

Table 2.8: Extraction recoveries (%) obtained with the MP-ME1 cartridges (20 mg and 100 mg polymer) for AOH after loading increasing volumes of a 200 µg L^{-1} solution of AOH in phosphate buffer (100 mM pH 8.5), using a washing step with 3 mL of (80:20, *v/v*) water-MeCN. Samples were eluted with 1 mL of 1% TFA in MeOH and analysed by HPLC-FLD.

Volume, mL	20 mg polymer		100 mg polymer	
	Recovery (%)	RSD (%)	Recovery (%)	RSD (%)
1	100	7	100	0.6
5	99	2	94	1
10	93	3	98	13
25	87	2	96	3
50	84	1	91	5

II.4.11. MISPE application to the determination of AOH in tomato samples

Finally, a preliminary valuation of the performance of the MP-ME1 cartridges for AOH extraction in food samples was carried out by applying the optimised method to the determination of the mycotoxin in five fortified ground tomato samples (0–110 µg kg^{-1}, n = 6). After sonication in phosphate buffer (100 mM, pH 8.5), 15 mL of the extract were loaded into the cartridges, and the samples were pre-concentrated using the optimised MISPE method followed by HPLC-FLC analysis. The results are summarised in Table 2.9. Mean recoveries ranged from 81% to 103% with RSDs <4%. Fig. 2.22 shows the chromatogram of an AOH-spiked (33 µg L^{-1}) tomato extract before and after MISPE. The chromatogram from a blank extract after MISPE is also included in the plot showing the lack of interferences co-eluting with the analyte.

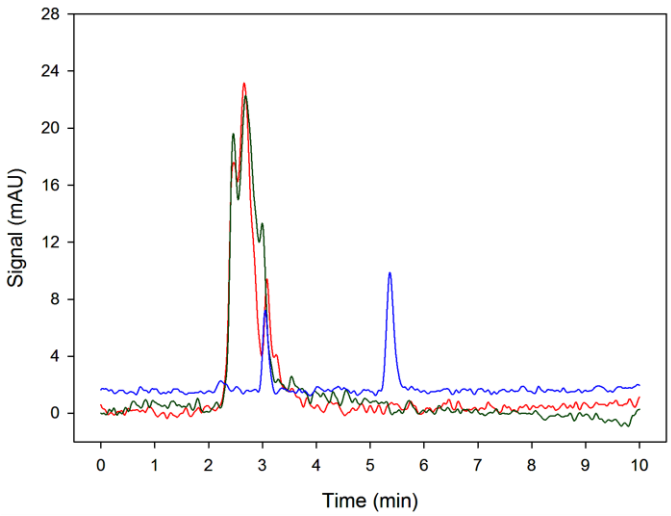

Figure 2.22: HPLC–FLD chromatograms of a non-fortified tomato extract after MISPE (**red**), a tomato extract spiked with 33 μg Kg^{-1} AOH without MISPE (**green**); and a tomato extract spiked with 33 μg Kg^{-1} AOH after MISPE (**blue**).

Table 2.9: Average recoveries (%) and relative standard deviations (RSDs, %, *n* = 6) obtained after ultrasound extraction followed by MISPE-HPLC-FLD of tomato samples fortified with AOH at five different concentration levels.

Spiking level (μg Kg^{-1})	Found level (μg Kg^{-1})	Recovery (%)	RSD (%)
33.0	26.9	81	4
50.0	51.7	103	4
66.0	65.2	99	2
75.0	74.3	99	1
110.0	111.9	102	2

These results demonstrate the usefulness of the synthesized MP-ME1 for the selective extraction of AOH from food samples.

II.5. Alternariol MIP core-shell nanoparticles

In order to provide MIP sorbent materials in different formats, we also explored the possibility of preparing MIP beads in nanometric core-shell format. To this end, silica cores (200-300 nm diameter) were employed as the support for growing a thin MIP layer (of only a few nanometers) on top of it by RAFT (reversible addition-fragmentation chain transfer) polymerization. RAFT is a quasi-living polymerization that leads to more homogeneous networks, more accessible sites, and hence higher

binding capacity [28,29]. This technique yields a thin polymer shell onto core particles if a surface-initiated polymerization is employed [30-32]. The very thin MIP layer grown in this way promises fast response times and should allow quantitative extraction of the template in a comparatively short time [33].

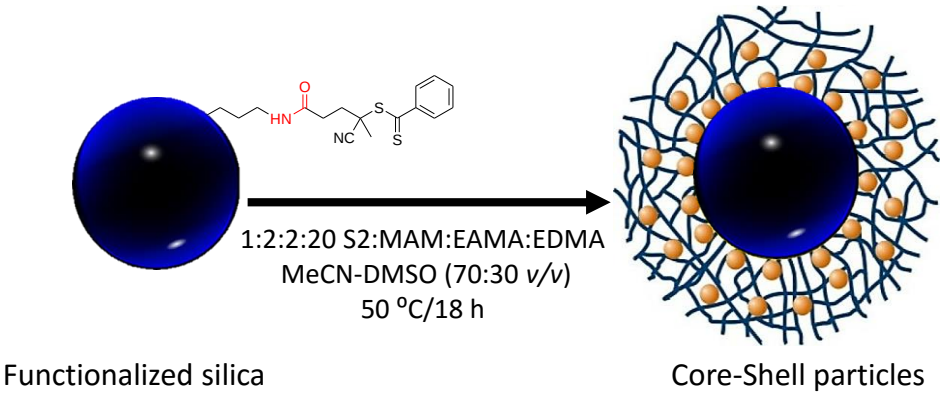

Figure 2.23: Schematic representation of the preparation of silica core-MIP shell nanoparticles for the alternariol surrogate S2 (MP-MER1).

Some 200-nm silica nanoparticles should provide a high surface for growing the MIP layer. The silica core was prepared following the Stöber method [34]. The polymerization mixture was the same as the one optimized in the previous part II.4: S2:MAA:EAMA:EDMA (1:2:2:20 mol ratio). In order to obtain a homogeneous polymer layer around SiO_2 core, the RAFT agent (CPDB, 2-cyano-2-propyl benzodithioate) was coupled to the activated SiO_2 surface with aminosilane, by following a procedure adapted from Wan et al. [29].

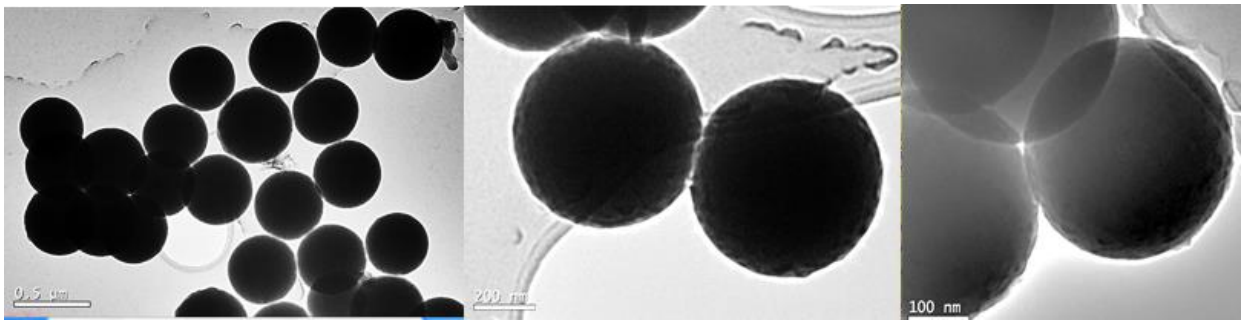

Figure 2.24: TEM pictures of silica-core nanoparticles (200-300 nm diameter) covered with a MP-ME1 layer grown by RAFT polymerization.

Fig. 2.24 shows TEM images of the MIP core-shell NPs (MP-CS) prepared in this way. The pictures show that indeed, a thin polymer layer of ca. 10 nm had grown over the silica core. Lack of time before the end of this work has prevented to carry out the characterization and application of the core-shell MIP nanoparticles, but it is being performed in our laboratories at the time of submission of this Thesis.

Monitoring AOH mycotoxin binding to molecularly imprinted polymers by fluorescence polarization

II.6. Evaluation of AOH binding to polymers using fluorescence anisotropy

Previously, we have described the preparation of MP-ME1 (S2:MAA:EAMA:EDMA 1:2:2:20) microparticles for selective binding of AOH, as well as their application to sample preconcentration by MISPE. However, the application of MIPs as recognition elements in the development of methods for fluorescence sensing is also of high interest. AME, AOH and the molecular surrogates that have been prepared in this work, are molecules with an *intrinsic fluorescence* that can be capitalized for direct detection of the analyte by fluorescence spectroscopy. Therefore, and with the aim of developing an innovative fluorescence-based method for mycotoxin detection based on MIP technology for fast and direct quantification of AOH in food samples, the following work was carried out. Here, it will be discussed how it is possible to benefit from fluorescence *anisotropy* measurements for evaluation of mycotoxin binding in the polymers. The results shown here were obtained during a short research stage under the supervision of *Prof. Robert Pansu*, in the *Supramolecular and Molecular Photophysics and Photochemistry Laboratory (PPSM)* of the École Normale Supérieure (ENS) de Cachan in France.

II.6.1. Characterization of S2 surrogate in the medium of interest and when bound to a polymer by steady-state fluorescence

Since the previous chromatographic studies for MISPE characterization had yielded that one of the best solvents for an efficient AOH-MIP interaction (where a good imprinting effect was obtained, with a good selectivity in binding towards other species) was the mixture H_2O-MeCN (7:3, *v/v*), this was the medium selected for the characterization of the polymers by fluorescence spectroscopy (and, particularly, for fluorescence anisotropy measurements). The polymers used here were the previously described MP-ME1 microparticles, with EAMA as the functional monomer and a (S2:MAA:EAMA:EDMA 1:2:2:20) molar composition, and a new type of microparticles, coded MP-MV, with the same molar composition but using 4-vinyl-pyridine (VPY) instead of EAMA as the functional monomer (S2:MAA:VPY:EDMA 1:2:2:20).

Since the medium chosen for characterization of the S2 to MIP binding was H_2O-MeCN (7:3, *v/v*), the emission of S2 was recorded in this solvent prior to the measurements in the presence of the

polymers Fig. 2.25. By comparing the results obtained in this solvent mixture with the previous ones obtained in neat MeCN (see section II.2), we can observe that the addition of H_2O induces a shift of the emission maximum for the free S2 surrogate from 397 nm in pure MeCN to 420 nm in the H_2O-MeCN (7:3, *v/v*) mixture. Also, a new broad, red-shifted band appears at ca. 560 nm with the solvent change. On the other hand, when S2 is added to a suspension of the MP-MV in the water-MeCN mixture, there is a blue shift of the emission from 425 to 400 nm. It can also be observed that the ratio between the band at 540 nm and that at 400 nm decreases compared to that of the free S2 in H_2O-MeCN (7:3, *v/v*). This seems to indicate that, when S2 binds to the polymer, the emission spectra is more similar to that in the absence of water (i.e. when neat MeCN is used), pointing out to the higher hydrophobicity of the analyte binding site into the MIP. The new emission band peaking at 560 nm might be due to the formation of an intramolecular charge transfer (ICT) excited state from the initially populated locally excited (LE) state, by stabilization from water solvation, and/or to (partial) deprotonation of the phenolic –OH group on C-8 of S2 (see II.3.1 above) in the presence of water.

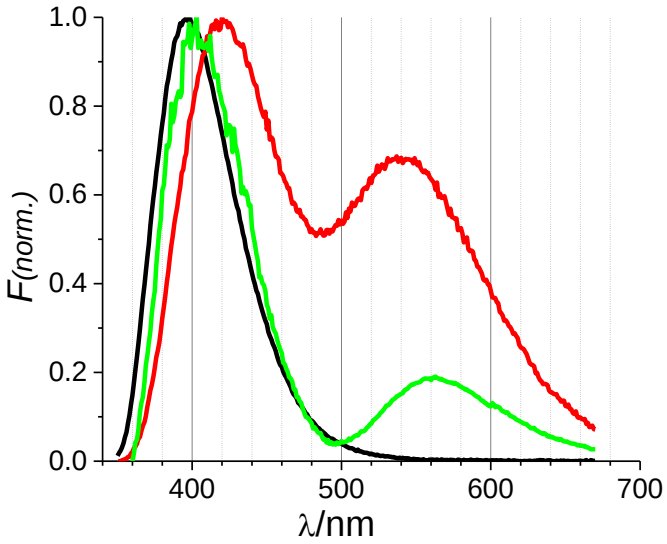

Figure 2.25: Normalized fluorescence spectra of 10 µM S2 in MeCN (**black**); 10 µM S2 in H_2O-MeCN (7:3, *v/v*) (**red**), and 10 µM S2 with 2 mg mL^{-1} MP-MV (**green**) where, 10 µM S2 with 2 mg. mL^{-1}, excitation wavelength 343 nm.

II.6.2. Fluorescence anisotropy measurements for investigation of the AOH/S2 binding to MP/NP-MV spherical microparticles

Our objective was to investigate whether it was possible to determine the concentration of the alternariol surrogate S2 by using MP-MV as the recognition element in combination with fluorescence anisotropy measurements, taking into account that the analyte itself is fluorescent and that the fluorescence anisotropy value should increase significantly when bound to a polymer.

For the (MP-MV)–S2 binding experiments, an excess of the surrogate S2 was normally incubated with the corresponding polymer for a period of time in the H_2O-MeCN (7:3, *v/v*) mixture. The amount of S2 that remained bound to the polymers was calculated by difference, determining the amount of free S2 by its fluorescence intensity after separation of the polymers by centrifugation.

II.6.2.1. Fluorescence binding assay of alternariol surrogate S2 to a MP-MV

For doing fluorescence anisotropy measurements, it is important to avoid scattering of the excitation light by the polymer particles. A good separation between the excitation and the emission peaks is preferred for that purpose [35]. For this, this is important that the fluorophores under study possess a large Stokes shift, which is the case for AOH and its surrogate S2 (excitation/emission wavelengths 343/420 nm).

Equilibrium binding tests[3] [36] were performed with suspensions of MP-MV polymers in H_2O-MeCN (7:3, *v/v*). To this end, a fixed amount of MIP[4] (2 mg mL^{-1}) was incubated for 24 h with different concentrations of S2, ranging from 0.1 µM to 1 mM at 21 °C. The studies were carried out at 21 ºC because, as shown in Fig. 2.26 a, for a fixed concentration of both MP/NP-MV and S2, it was found that this temperature gave both the best binding and the largest difference between MP-

[3] This work has been done by using *L-Tryptophan* 15 µM in H_2O - MeCN (7:3, *v/v*), $\lambda_{ex/em}$ = 295/430 nm as a fluorescence anisotropy standard, with an anisotropy value *r* = 0.022, P = 0.032.

[4] When dealing with MIPs prepared with a fluorescent template, interference from the fluorescence of some residual template trapped in the polymer is possible. Therefore, anisotropy measurements were also made on the MIP *before* the incubation with S2. Regardless the concentration of MIP tested (0.1 to 2 mg mL^{-1}), the same anisotropy value was obtained ($r \approx 0.23$) in H_2O-MeCN (7:3, *v/v*). This high anisotropy value indicates the presence of traces of trapped S2, which was impossible to remove during the thorough washing following the polymerization process. However, this residual template does not seem to have a significant effect on the binding measurements.

MV and NP-MV [37]. The fluorescence anisotropy of S2 was measured for suspensions of both MP-VP and NP-VP, yielding the curves shown in Fig. 2.26 b. This result is compatible with the fact that the more rapid the motion of the fluorophore, the more its fluorescence is depolarised (lower anisotropy value); therefore, in the absence of polymers, the measured *r* value is negligible. When S2 binds to the MP-MV, its tumbling rate is greatly reduced, resulting in a steep increase of the fluorescence anisotropy.

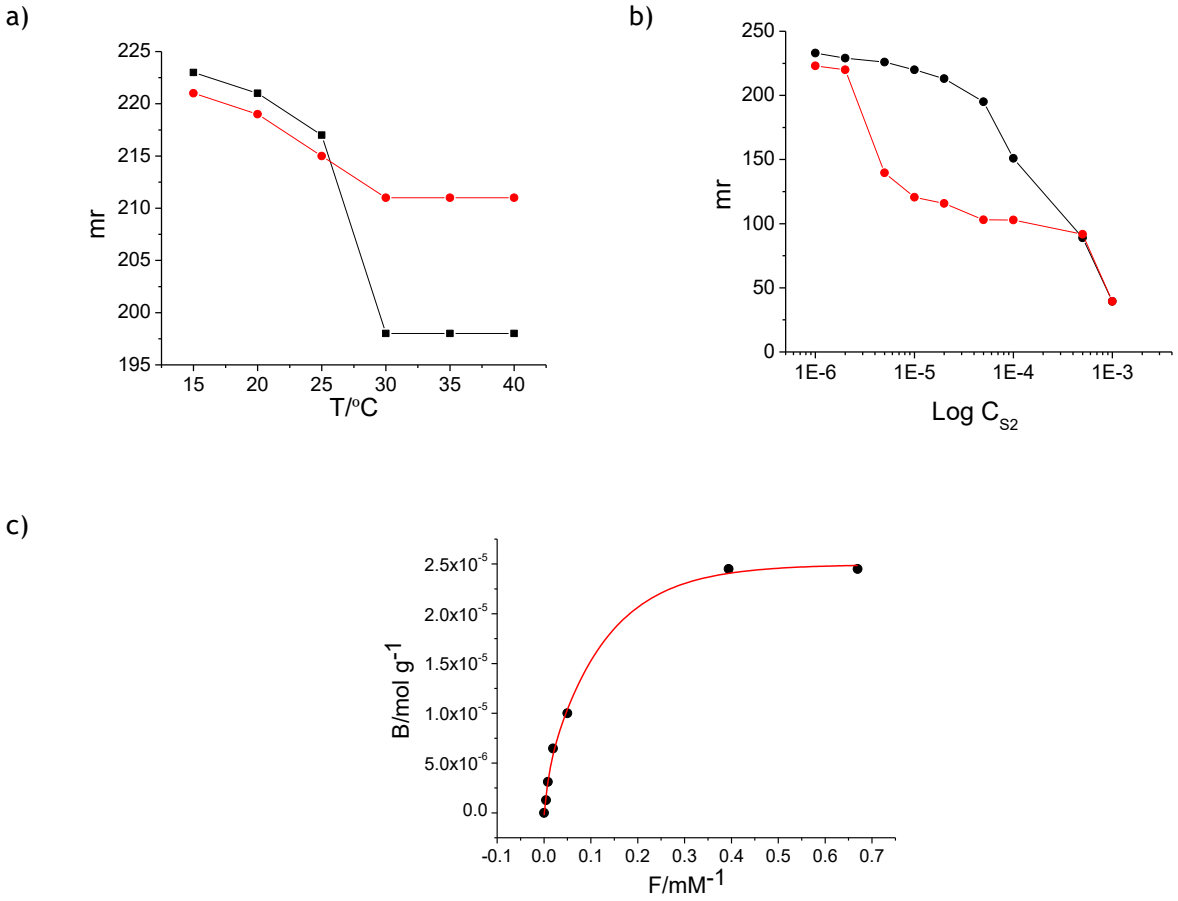

Figure 2.26: a) Value of the fluorescence anisotropy (in *mr* units) as a function of the temperature for suspensions of MP-MV (black) and NP-MV (red) incubated with S2 (c_{S2} = 50 µM). b) Fluorescence anisotropy for varying concentrations of S2 (0.1 µM to 0.7 mM) incubated with 2 mg mL^{-1} of MP-MV (black) or NP-MV (red) for 24 h. c) Equilibrium isotherm for the binding of S2 to MP-MV in H_2O-MeCN (7:3, *v/v*). *F* represents the concentration of the *free* S2 in solution, while *B* stands for the amount of polymer-bound S2. In all cases, the solvent was H_2O-MeCN (3:7, *v/v*).

For low concentrations of ligand (0.1–50 µM), the anisotropy value is high because all S2 molecules are bound to the MP-MV. For higher S2 concentrations, the anisotropy value decreases because of the amount of free S2 increases. Thus, it is possible to quantify the amount of S2 present in solution

for concentrations in the linear part of the binding isotherm, namely between (0.1 µM and 50 µM) Fig. 2.26 c. This titration gave an equilibrium binding constant of MP-MV to S2 of 25 µmol g^{-1}. In the case of the NP-MV, some non-specific binding to the polymer could be observed, probably due to the presence of the VP functional monomer.

II.6.2.2. Evaluation of MP-MV binding to AOH using fluorescence anisotropy

The binding of MP-MV to the analyte of interest, AOH, was also studied by fluorescence anisotropy. As shown in Fig. 2.27, both AOH and its surrogate S2 (c = 0.1 µM to 1 mM, at 21 °C) display a similar behaviour. These results show that the S2-imprinted polymer possesses almost the same affinity for AOH as for S2, and confirm that choosing the S2 surrogate as an alternative molecular template for the preparation of MIPs for AOH is a suitable (cheaper) option.

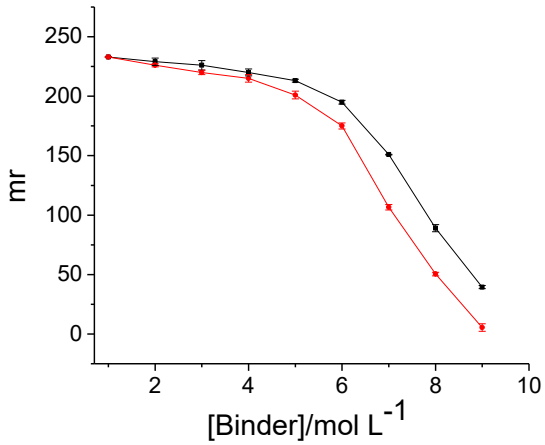

Figure 2.27 Variation of the fluorescence anisotropy values for suspensions of MP-MV (2 mg mL^{-1}) upon the addition of increasing amounts of S2 (black) or AOH (red) in H_2O-MeCN (7:3, *v/v*) mixtures at 21 °C. (n = 3, the error bars represent standard deviation).

II.6.2.3. Time-resolved fluorescence and anisotropy

Other aspect of the fluorescence anisotropy is the comparison between the fluorescence lifetime and the rotational relaxation time of the fluorophore. If the fluorescence lifetime is shorter than the rotational relaxation time, the fluorophore does not have the time to rotate during the relaxation time so even the free ligand will give a high anisotropy value. On the contrary, if the lifetime of the fluorophore in the excited state is longer than the rotational relaxation time, the free fluorophore can

rotate before emitting the photon, giving a small anisotropy value. In our case, it is important that the free ligand has a low anisotropy value in a fluid solution since we want to measure the difference of fluorescence anisotropy between the free ligand and the ligand bound to the MIP. A rule exists to estimate the rotational relaxation time of a molecule in a low viscosity solvent: its molecular mass (in g mol^{-1}) must be divided by 1000 to give the value of the rotational relaxation time of nanoseconds (ns). In this way, for AOH surrogate S2, with a molecular mass of 244.20, its rotational relaxation time can be estimated to be 0.24 ns [38].

The fluorescence lifetimes of free S2 and of a suspension of MP-MV incubated with S2 were measured in H_2O-MeCN (7:3, *v/v*). Fig. 2.28 shows the different fluorescence decay kinetics obtained for the free S2 and for the suspension of MP-MV incubated with S2. When S2 is bound to the polymer the emission lifetime is longer. Fluorescence lifetime values and the respective amplitudes of both samples are summarised in Table 2.10. In both cases, the results were fitted to a two-exponential function. Concerning the lifetimes of 0.54 ns and 2.21 ns found for free S2, we can notice that both components are higher than the estimated rotational relaxation time of S2 (0.24 ns). The last means that free S2 in solution will give a small anisotropy value (low is typically r = 0.006 [39]).

We can note that two lifetimes were found for the free S2 in H_2O-MeCN. This can be explained by the presence of two different excited state in the presence of water, the LE and the ICT (without or with deprotonation in the latter), as it was already observed in the fluorescence spectra of Fig. 2.25. Since these lifetime values are short, it should be easier to distinguish the free S2 from the polymer-bound S2 by fluorescence polarization. For the suspension of MP-MV incubated with S2, the fluorescence decay Fig. 2.28 was also fitted to a bi-exponential function, with a long 8.76 ns component and a shorter one of 0.77 ns. The longer fluorescence lifetime for the bound S2 compared to the free species might be explained by the enhanced rigidity of the fluorescent mycotoxin surrogate upon binding to the polymer cavities, that decrease the contribution of the non-radiative (namely, internal conversion) deactivation pathways.

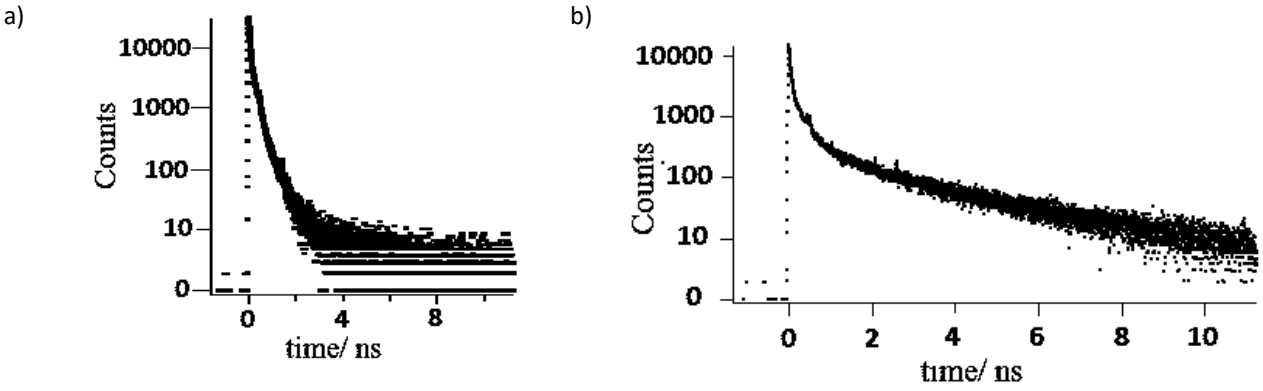

Figure 2.28: Fluorescence decay profile of a) a 50 µM solution of S2 in H_2O:MeCN (7:3, *v/v*); b) (7:3, *v/v*). $\lambda_{ex/em}$ 343/420 nm.

The fluorescence binding assay that was performed with 2 mg mL^{-1} MP-MV and 0.6 mM S2 resulted in around 25 µM bound S2 Fig. 2.29 binding isotherm. By comparison with the corresponding NP-MV microparticles, it was found that binding was stronger in the case of the imprinted beads.

Table 2.10: Fluorescence lifetimes and corresponding relative amplitudes obtained from least-square fitting of the fluorescence decays of 50 µM solution of S2 in H_2O:MeCN (7:3, *v/v*) (free) and (7:3, *v/v*) using a bi-exponential decay. The fluorescence anisotropy of the samples (*r*) is also given.

	τ_1 (ns)	Rel. Amp_1	τ_2 (ns)	Rel. Amp_2	χ^2	*r*
Free S2	0.54	13.36	2.21	86.64	1.130	0.006
MP-MV+S2	0.77	22.02	8.76	77.98	1.100	0.234

These results show that MP-MV microparticles have been obtained with a high affinity for AOH and S2 binding. This is consistent with our previous results and confirms the imprinting effect generated by the template S2. The use of fluorescence anisotropy measurements has confirmed that the fluorescent analytes bind tightly to the MIP cavities.

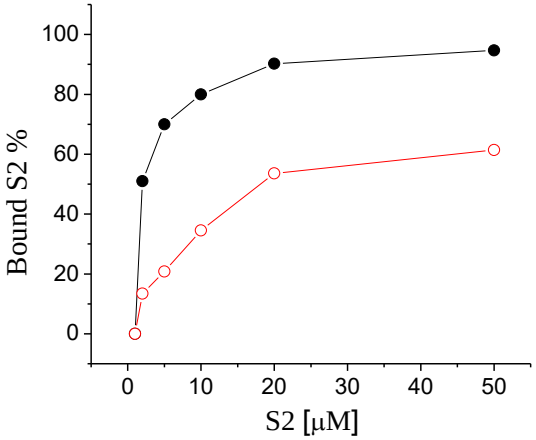

Figure 2.29: Binding of S2 to MP-MV (black) and NP-MV (red) microparticles in H_2O-MeCN (7:3, *v/v*) as a function of the S2 concentration.

Bibliography

1. Koch, K.; Podlech, J.; Pfeiffer, E.; Metzler, M., Total synthesis of alternariol. *J. Org. Chem.* **2005,** *70*, 3275-3276.

2. Orellana, G.; Moreno Bondi, M. C.; Descalzo Lopez, A. B.; Urraca, J. L.; Abou-Hany, R. A. G. Materials for selective recognition of alternaria mycotoxins (alternariol and alternariol monomethyl ether). 2013.

3. Moreno Bondi, M. C.; Urraca, J. L.; Carrasco, S.; Navarro-Villoslada, F.; Alvarez-Lorenzo, C.; Concheiro, A., Handbook of Molecularly Imprinted Polymers. Smithers Rapra Technology: UK, 2013; pp 23-86.

4. Urraca, J. L.; Marazuela, M. D.; Merino, E. R.; Orellana, G.; Moreno-Bondi, M. C., Molecularly imprinted polymers with a streamlined mimic for Zearalenone analysis. *J. Chromatogr. A* **2006,** *1116*, 127-134.

5. Urraca, J. L.; Carbajo, M. C.; Torralvo, M. J.; González-Vázquez, J.; Orellana, G.; Moreno-Bondi, M. C., Effect of the template and functional monomer on the textural properties of molecularly imprinted polymers. *Biosens. Bioelectron.* **2008,** *24*, 155-161.

6. Sunil, K. K. C.; Klaus, M., Depsides as non-redox inhibitors of leukotriene B4 biosynthesis and HaCaT cell growth. 1. Novel analogues of barbatic and diffractaic acid. *Eur. J. Med. Chem.* **1999,** *34*, 1035-1042.

7. Lee, K.; Ki, C. D.; Kim, H.; Chang, J. Y., Selectivity control by chemical modification of the recognition sites in two-point binding molecularly imprinted polymer. *Macromolecules* **2004,** *37*, 5544-5549.

8. Jung, B. M.; Kim, M. S.; Kima, W. J.; Chang, J. Y., Molecularly imprinted mesoporous silica particles showing a rapid kinetic binding. *Chem. Commun.* **2010,** *46*, 3699-3701.

9. Pandey, J.; Jha, A. K.; Hajela, K., Synthesis and biological activities of some new dibenzopyranones and dibenzopyrans: search for potential oestrogen receptor agonists and antagonists. *Bioorg. Med. Chem.* **2004,** *12*, 2239-2249.

10. Weller, A., Über die fluoreszenz der salizylsäure und verwandter verbindungen. *Naturwissenschaften* **1955,** *42*, 175-176.

11. Acuña, A. U.; Toribio, F.; Amat-Guerri, F.; Catalán, J., Excited state proton transfer: a new feature in the fluorescence of methyl 5-chlorosalicylate and methyl 5-methoxysalicylate. *J. Photochem.* **1985,** *30*, 339-352.

12. Rurack, K., Fluorescence quantum yields: methods of determination and standards. In *Standardization and Quality Assurance in Fluorescence Measurements. I*, Resch-Genger, U., Ed. Springer: Berlin/Heidelberg, 2008.

13. Schultz, T. W., The use of the ionization constant (pK_a) in selecting models of toxicity in phenols. *Ecotoxicol. Environ. Saf.* **1987,** *14*, 178-183.

14. Huntera, N. E.; Seybold, P. G., Theoretical estimation of the aqueous pK_as of thiols. *Mol. Phys.* **2014,** *112*, 340-348.

15. Foster, L. S.; Gruntfest, I. J., Demonstration experiments using universal indicators. *J. Chem. Educ.* **1937,** *14*, 274-276.

16. Titirici, M. M.; Hall, A. J.; Sellergren, B., Hierarchically imprinted stationary phase:mesoporous polymer beds containing surface-confind binding sites for adenine. *Chem. Mat.* **2002,** *14*, 21-23.

17. Sellergren, B., Molecularly imprinted polymers, man-made mimics of antibodies and their application in analytical chemistry. Elsevier Science: Amsterdam, 2000; Vol. 23.

18. Urraca, J. L.; Aureliano, C. S. A.; Schillinger, E.; Esselmann, H.; Wiltfang, J.; Sellergren, B., Polymeric complements to the Alzheimers disease biomarker ß-amyloid isoforms Aß1-40 and Aß1-42 for blood serum analysis under denaturing conditions. *J. Am. Chem. Soc.* **2011,** *133*, 9220-9223.

19. Fielding, L., Determination of association constants (K_a) from solution NMR data. *Tetrahedron* **2000,** *56*, 6151-6170.

20. Eliadou, K.; Yannakopoulou, K.; Rontoyianni, A.; Mavridis, I. M., NMR detection of simultaneous formation of [2]- and [3]pseudorotaxanes in aqueous solution between α-cyclodextrin and linear aliphatic α,ω-amino acids, an α,ω-diamine and an α,ω-diacid of similar length, and comparison with the solid-state structures. *J. Org. Chem.* **1999,** *64*, 6217-6226.

21. Hoshina, K.; Horiyama, S.; Matsunaga, H.; Haginaka, J., Simultaneous determination of non-steroidal anti-inflammatory drugs in river water samples by liquid chromatography–tandem mass spectrometry using molecularly imprinted polymers as a pretreatment column. *J. Pharm. Biomed. Anal.* **2011,** *55*, 916–922.

22. Delgado, T.; Gómez-Cordovés, C.; Scott, P. M., Determination of alternariol and alternariol methyl ether in apple juice using solid-phase extraction and high performance liquid chromatography. *J Chromatogr A.* **1996,** *731*, 109-114.

23. Kütt, A.; Leito, I.; Kaljurand, I.; Sooväli, L.; Vlasov, V. M.; Yagupolskii, L. M.; Koppel, I. A., A comprehensive self-consistent spectrophotometric acidity scale of neutral Brønsted acids in acetonitrile. *J. Org. Chem.* **2006,** *71*, 2829-2838.

24. Bukowska, B.; Michałowicz, J.; Krokosz, A.; Sicińska, P., Comparison of the effect of phenol and its derivatives on protein and free radical formation in human erythrocytes (in vitro). *Blood Cells, Molecules, and Diseases* **2007,** *39*, 238-244.

25. ACD/Labs *Calculated using advanced chemistry development*, 2014.

26. Li, J., Prediction of internal standards in reversed-phase liquid chromatography. *Chromatographia* **2004,** *60*, 63-71.

27. Rampey, A. M.; Umpleby, R. J.; Rushton, G. T.; Iseman, J. C.; Shah, R. N.; Shimizu, K. D., Characterization of the imprint effect and the influence of imprinting conditions on affinity, capacity, and heterogeneity in molecularly imprinted polymers using the freundlich isotherm-affinity distribution analysis. *Anal. Chem.* **2004,** *76*, 1123-1333.

28. Salian, V. D.; Vaughan, A. D.; Byrne, M. E., The role of living/controlled radical polymerization in the formation of improved imprinted polymers. *J. Mol. Recognit.* **2012,** *25*, 361-369.

29. Wan, W.; Biyikal, M.; Wagner, R.; Sellergen, B.; Rurack, K., Fluorescent sensory microparticles that "light-up" consisting of a silica core and a molecularly imprinted polymer (MIP) shell. *Angew. Chem. Int. Ed. Engl.* **2013,** *52*, 7023-7027.

30. Barbey, R.; Lavanant, L.; Paripovic, D.; Schüwer, N.; Sugnaux, C.; Tugulu, S.; Klok, H. A., Polymer brushes via surface-initiated controlled radical polymerization: synthesis, characterization, properties and applications. *Chem. Rev.* **2009,** *109*, 5437-5527.

31. Halhalli, M. R.; Aureliano, C. S. A.; Schillinger, E.; Sulitzky, C.; Titirici, M. M.; Sellergren, B., An improved grafting technique for producing imprinted thin film composite beads. *Polym. Chem.* **2012,** *3*, 1033-1042.

32. Halhalli, M. R.; Schillinger, E.; Aureliano, C. S. A.; Sellergren, B., Thin walled imprinted polymer beads featuring both uniform and accessible binding sites. *Chem. Mater.* **2012,** *24*, 2909−2919.

33. Tokonami, S.; Shiigi, H.; Nagaoka, T., Review: micro- and nanosized molecularly imprinted polymers for high-throughput analytical applications. *Anal. Chim. Acta.* **2009,** *641*, 7-13.

34. Stöber, W.; Fink, A.; Bohn, E., Controlled growth of monodisperse silica spheres in the micron size range. *J. Colloid. Interface. Sci.* **1968,** *26*, 62–69.

35. Hunt, C. E.; Ansell, R. J., Use of fluorescence shift and fluorescence anisotropy to evaluate the re-binding of template to (S)-propranolol imprinted polymers. *Analyst* **2006,** *131*, 678-683.

36. Thompson, R. B.; Gryczynski, I.; Malicka, J., Fluorescence polarization standards for high-throughput screening and imaging. *Biotechniques* **2002,** *32*, 32-42.

37. Weigert, F., Über einen neuen effekt der strahlung. *Z. Phy.* **1920,** *2*, 1-12.

38. Jameson, D. M.; Ross, J. A., Fluorescence polarization/anisotropy in diagnostics and imaging. *Chem. Rev.* **2010,** *110*, 2685-2708.

39. Smith, D. S.; Eremin, S. A., Fluorescence polarization immunoassays and related methods for simple, high-throughput screening of small molecules. *Anal Bioanal Chem.* **2008,** *391*, 1499-1507.

III-Development of luminescent MIPs for Tenuazonic Acid detection

ÍNDEX

General objectives

The first aim of the present study *is to synthesize surrogates of the mycotoxin tenuazonic acid (TeA) to be used as templates for the synthesis of luminescent MIPs selective for TeA quantification.*

The second main objectiv*e of this part is the development of molecularly imprinted polymers for TeA recognition which are functionalized with luminescent functions (Eu(III) chelates) able to coordinate TeA. TeA binding in the MIP is expected to induce a change in the luminescent properties of the Eu(III) chelate. The latter could be employed for monitoring the presence of the mycotoxin in a sample.*

Specific objectives

1- Organic synthesis and characterization of *a stable form of TeA and an analogue of it.*

2- Evaluation of the stability of the TeA–copper(II) complex, Cu(TeA)$_2$, *by spectrophotometric measurements.*

3- Preparation of Eu(III) ion-imprinted polymers *in bulk format using different diketones as chelating functional monomers and the synthetic TeA as the template. If the approach is successful, then:*

4- Synthesis of a Eu(III)-MIP library for choosing the best polymer composition for TeA recognition. *The optimized polymerization mixture will be employed for the preparation of speherical, highly porous, Eu-MIP microparticles.*

5- Analytical characterization of the selected MIPs and optimization of the TeA analysis procedure.

III.1. Synthesis of tenuazonic acid surrogate (*r*TeA)

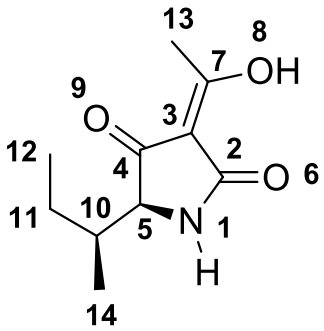

Figure 3.1: Chemical structure of Tenuazonic Acid (TeA).

Several methods have been described in the literature for the preparation of tenuazonic acid (TeA), or (*S*)-3-acetyl-5-(*S*)-*sec*-butyltetramic acid Fig. 3.1 [1-4]. The route involving a Dieckmann intramolecular cyclisation, –a base-catalyzed intramolecular reaction of diesters to give a β-ketoester after C-acetylation of *N*-acyl amino esters–, is generally favoured because of its swiftness yet it yields variable degrees of racemization at C5. Following this approach, some reported synthesis of tenuazonic acid sodium salt (as a mixture of the *R* and *S* enantiomers in the chiral C5), (Na^+ *(r)*TeA^-) involves *N*-acetoacetylation of the α–amino group of the methyl ester of L-isoleucine with diketene using *m*-xylene as the solvent [3,4]. This reaction provides the *N*-acetoacetylamino acid ethyl ester, which is then cyclized in the presence of a base, –sodium methoxide–, in methanol to yield the tenuazonic acid sodium salt [2]. In the present Thesis, Wang et al. [2] and Asam et al. [4] methods with modifications have been followed. For *N*-acetylation we used 2,2,6-trimethyl-4*H*-1,3-dioxin-4-one instead of diketene because it has been described to be a more convenient acetoacetylation agent than diketene itself [5, 6]. This compound is a diketene-acetone adduct that is stable at room temperature and releases diketene slowly during heating. This reagent allowed us to obtain the sodium salt of tenuazonic acid with a reaction yield

exceeding 75%. Due to the use of a strong base such as NaMeO under heating in the last cyclization step, the compound is obtained as a mixture of the 5*R* and 5*S* isomers (hereafter called Na^+ *r*TeA^-) [7]. The starting material was the methyl ester of the aminoacid L-isoleucine Fig. 3.2. For comparison purposes, a molecular surrogate of TeA (hereafter called *s*TeA) was also prepared starting from the methyl ester of the aminoacid L-leucine.

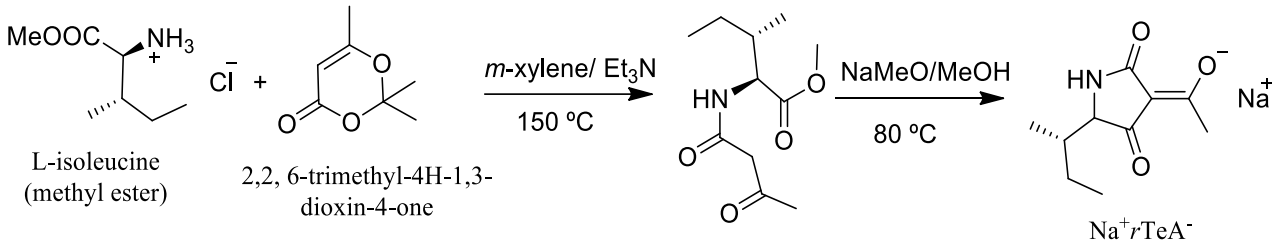

Figure 3.2: Synthesis of tenuazonic acid sodium salt surrogate Na^+*r*TeA^-.

The synthesised Na^+*r*TeA^- was preliminary characterized using UV-Vis spectroscopy and HPLC Table 3.1 and Fig. 3.3. The absorbance maxima of Na^+*r*TeA^- at 240 and 277 nm in methanol met those values published in the literature for the natural compound [8] (see part III.2). Elemental analysis, specific optical rotation at room temperature, ^{13}CNMR, ^{1}HNMR, FTIR and LC-MS measurements further confirmed the expected structure (see *Experimental Part and Annex II*).

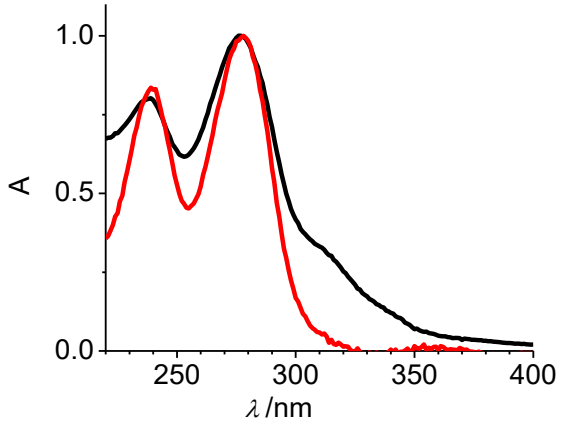

Figure 3.3: Normalized UV-vis absorption spectra of Na^+*r*TeA^- (**black**) and Na^+*(s)*TeA^- (**red**) in MeOH (*c* = 10 μM).

Table 3.1: HPLC data and UV-vis absorption for as synthetised Na^+rTeA^-, Na^+sTeA^- and a comercial $Cu(TeA)_2$ sample.

Sample	t_R/min	λ_{max}/nm
Na^+rTeA^-	11.2	277
Na^+sTeA^-	11.4	278
$Cu(TeA)_2$ (commercial)	10.6	284

III.2. Copper(II)–tenuazonic acid complex

The most common method for extracting TeA from food samples is by forming a chelate complex with Cu(II), $Cu(TeA)_2$. This is actually the only form in which most commercial suppliers provide TeA. The reason for this is that non-ionized free TeA is not a very stable compound. When forming the Cu(II) complex, however, stability is improved. Conversion of the free *r*TeA or the sodium salt Na^+rTeA^- to the Cu(II) chelate can be confirmed by spectrophotometry: a red shift from 277 to 289 nm is observed when $Na^+(r)TeA^-$ is converted to $Cu(TeA)_2$ in methanolic solution Fig. 3.4. The results obtained with the synthesised Na^+rTeA^- and upon formation of the copper complex, agree with those reported in the literature (λ_{abs} = 288 nm for $Cu(TeA)_2$, see Lebrun et al. [9], and 280 nm or 276 nm for the for the *rTeA* sodium salt or the free acid, respectively [10].

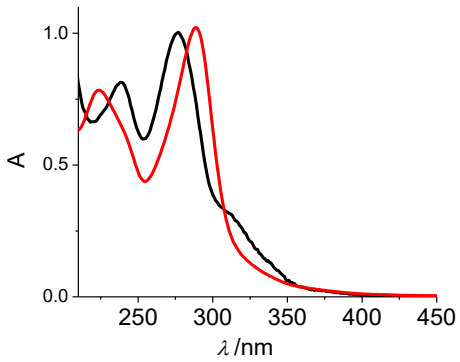

Figure 3.4: Normalized UV-vis absorption spectra of 10 μM Na^+rTeA^- (**black**) and $Cu(TeA)_2$ (**red**) in MeOH.

In order to evaluate how stable the $Cu(TeA)_2$ complex is in the presence of other multidentate ligands, a complexometric study using UV-vis absorption spectrophotometry was carried out. The

ligands shown in Fig. 3.5 can all be used for complexation of Cu(II). The stability of each complex is related to the basicity of the coordinating nitrogen atoms. The stability of the metal complex is also influenced by the relative increase of the entropy upon complex formation. With this study, we have found that by titration of either $Cu(BsOH)_2^{2+}$ [11], $Cu(TMEN)_2^{2+}$ or $Cu(bpy)_2^{2+}$ Fig. 3.5 in methanol with increasing amounts of *r*TeA at 25 °C, a substitution with Na^+rTeA^- happens at certain point to form the $Cu(TeA)_2$ complex with its characteristic absorption peak at 288 nm in methanolic solution Fig. 3.6. The absorption of $Cu(BSOH)_2^{2+}$ and $Cu(bpy)_2^{2+}$ shows a hypsochromic shift upon addition of Na^+rTeA^- while that of $Cu(TMEN)_2^{2+}$ displays a bathochromic shift. Bathochromic or hypsochromic shifts are attributed to an increase or decrease of the conjugation in the chromophoric system of the corresponding Cu(II) complexes due to the intraligand nature of the monitored transition.

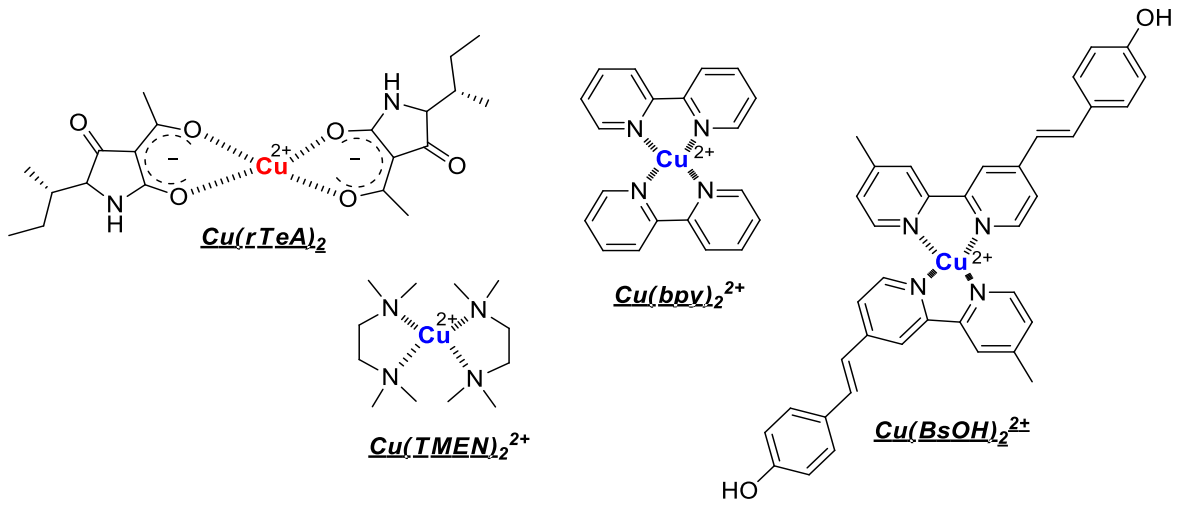

Figure 3.5: Structure of different Cu(II) bidentate chelates selected for evaluating the relative stability of the Cu(*r*TeA)$_2$ complex. TMEN: *N,N,N',N'*-tetramethylethylenediamine; BsOH: (4-[(*E*)-2-(4´-methyl-2,2´-bipyridin-4-yl)vinyl] phenol; bpy: 2,2'-bipyridine.

The conclusion of these titrations is that the Cu(*r*TeA)$_2$ complex shows a higher stability in comparison to those complexes formed with the bidentate neutral *N*-coordinated ligands in methanol. This indicates a higher affinity of the Cu(II) cation for the oxygen atoms of the negatively charged β-diketonate moiety of the tenuazonic acid.

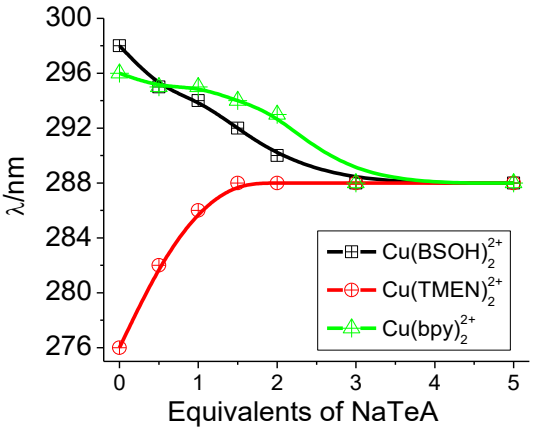

Figure 3.6: Variation of the absorption maxima of different methanolic solutions of the bidentate complexes of Cu(II) (c = 50 μM): $Cu(BSOH)_2^{2+}$ (**black**), $Cu(TMEN)_2^{2+}$ (**red**), and $Cu(bpy)_2^{2+}$ (**green**), upon the addition of 0, 0.5, 1.0, 1.5, 2.0, 3.0 and 5.0 equivalents of Na^+rTeA^- at 25 °C.

The high stability of this Cu(II)-TeA complex led us to discard the use of the commercially available $Cu(TeA)_2$ compound as the template for the preparation of MIPs.

III.3. Synthesis of a luminescent MIP for tenuazonic acid

With the aim of developing a sensitive and selective method for optical transducing of the presence of the TeA mycotoxin in food, and taking into account the ability of this compound for acting as a bidentate ligand for metal cations (see previous III.2 part), we considered the development of a sensing method based on the use of Eu(III) luminescent chelate complexes. As already described in the Introduction, Eu(III) or, in general, Ln(III) ions, present a narrow, well defined long-lived luminescence that arises from *f-f* orbital transitions. Since these transitions are formally forbidden, their corresponding excited states deactivate very slowly, and emission of photons from the excited state typically occurs in the phosphorescence time scale. Unfortunately, the "forbidden" character of the electronic transition also lowers the probability of absorption of a photon, resulting in the very weak absorption coefficient of the metal cation. The last handicap, however, can be easily overcome by a *sensitization* process, in which an organic chromophore which is coordinating the lanthanide cation, acts as an *antenna* ligand. This ligand must be able of effectively absorb UV-vis radiation and

transferring it to the ion centre. Frequently employed ligands for Eu(III) coordination are bidentate β-diketonates [12].

Some examples in the literature describe the use of luminescent MIPs for sensing applications based on the principle of using an antenna ligand for sensitization of the Eu(III) luminescence. In a first example, the authors use functional monomers who are able to coordinate and photosensitize the Eu(III) ion centre. The Eu(III) chelate is then copolymerized with a cross-linker in the presence of the analyte. Coordination of the analyte induces a change in the Eu(III) sensitized luminescence, which is employed for the detection of dangerous species, such as the soman nerve agent, an organophosphor derivative [13,14,15,16]. Another example involving the use of MIPs and a sensitization process of the Eu(III) luminescence has been described by our research group [17]. In this case, the functional monomers have no chromophoric groups, and the analyte itself (enrofloxacin, a β-diketonate antibiotic) is acting as the chromophore in the sensitization process. The Eu(III) ion is only added after formation of the MIP, as a developing reagent whose luminescence increases when enrofloxacin is present in the cavities of MIP nanofilaments. A recent example described in the literature involves also the use of non-chromophoric functional monomers for Eu(III) chelation. The analyte,–a chlorinated herbicide, picloram– is the antenna ligand who can bind Eu(III) and sensitize Eu(III) luminescence [18]. The addition of the analyte induces an increase in the emission of the Eu(III) ion, that is employed for its detection.

In our work, we have followed a similar approach to that described in the last example. We will take advantage of the fact that our target analyte, *r*TeA, has a β-diketone moiety, which is able to form stable metal complexes absorbing the light close to 300 nm, as shown in Figs. 3.4 and 3.6. If the metal used for chelation is Eu(III), the luminescence of the Eu(III)/MIP-based sensor system should increase upon *r*TeA binding, as schematically shown in Fig. 3.7.

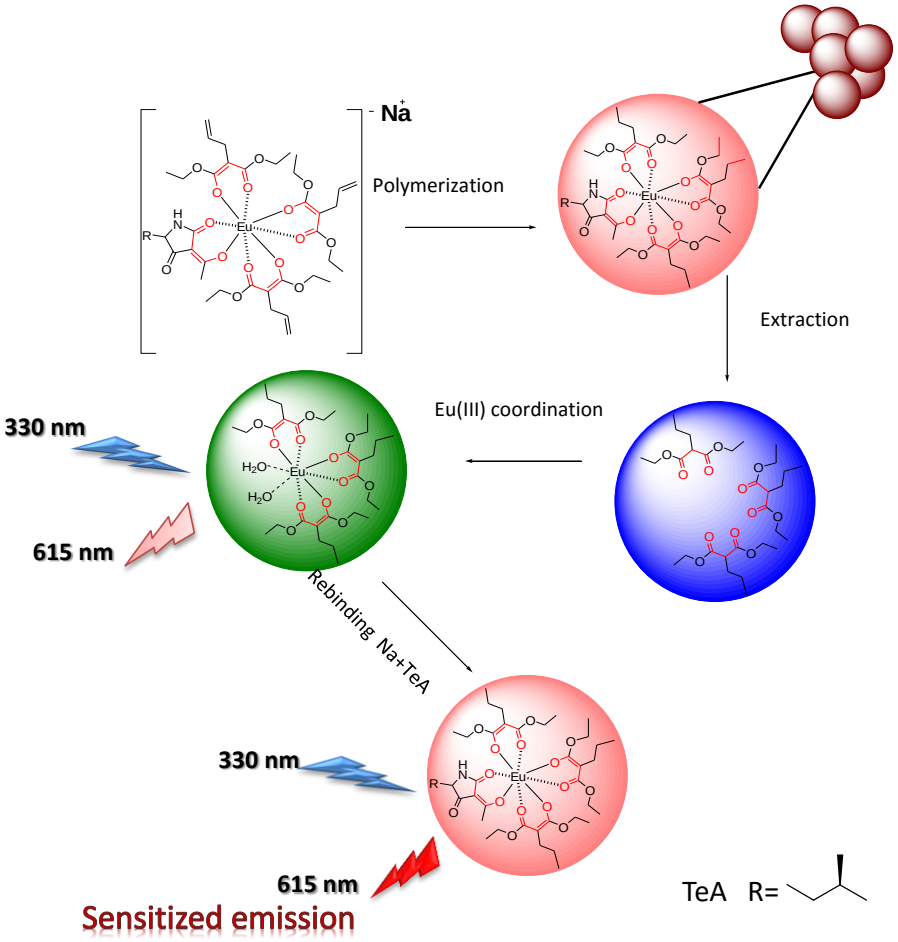

Figure 3.7: Schematic description of the preparation of an Eu(III)-loaded MIP with selective cavities created for *r*TeA recognition. Upon *r*TeA rebinding, the luminescence intensity of the Eu(III) chelate at 615 nm should increase.

The functional monomer that we have selected here for Eu(III) coordination is DEAM (diethyl allylmalonate). DEAM has a β-diketone structure, with a good coordinating ability to metal ions [19]. By adding this bidentate ligand in a 3:1 DEAM:Eu(III) molar ratio, two coordination positions should still be available in the metal centre for *r*TeA binding (the usual coordination number for Eu(III) is eight). The idea is preparing a pre-polymerization mixture containing DEAM: *r*TeA:Eu(III) in a 3:1:1 molar ratio. After addition of a cross-linker and a radical initiator, we should obtain a polymer capable (after *r*TeA extraction) of re-binding the natural TeA mycotoxin. As represented in Fig. 3.7, coordination of the TeA chromophore should influence Eu(III) luminescence at 615 nm, thus generating an optical signal that can be employed for *r*TeA detection.

III.3.1. UV/vis studies of the functional monomer-template interaction

Before proceeding with the preparation of the Eu(III)-MIP, we considered the need to carry out a previous characterization of the interaction between *r*TeA, the functional monomer DEAM and the Eu(III) cation in the solvent mixture where the polymerization will be performed (2 M $NaOH_{aq}$:EtOH 1:20 *v/v*). To this end, a spectrophotometric titration using a 50 μM stock solution of $EuCl_3$ was carried out.

Firstly, the titration was performed by adding 0 to 5 equivalents of *r*TeA to a Eu:DEAM (1:4) complex ("1 equivalent" means 1 mol of *r*TeA per mol of Eu(III)). Upon addition of *r*TeA to Eu(III):DEAM 1:4 complex, a red shift in the absorption from 277 to 284 nm is observed Fig. 3.8 a, what might be indicative of substitution of some of the DEAM molecules in the complex by *r*TeA molecules. It was also observed that when the solution is excited at 330 nm, the intensity of the characteristic Eu(III) emission at 615 nm increases linearly upon increasing the *r*TeA concentration. This is indicative of an efficient energy transfer between the excited state of the TeA to the ground state of the lanthanide ion and therefore, of complex formation. For further confirmation of the stability of the *r*TeA -Eu(III) complex, in a different experiment, DEAM was added to a mixture of *r*TeA:Eu(III) 4:1 in (2 M $NaOH_{aq}$):EtOH 1:20 *v/v*. In this case, absorption remained constant Fig. 3.8 c, what indicates that DEAM is not displacing the *r*TeA molecules from the Eu(III) complex. This would point out that binding between *r*TeA and Eu(III) is stronger than the complex between DEAM and Eu(III), and *r*TeA is able to displace the DEAM ligands from the complex.

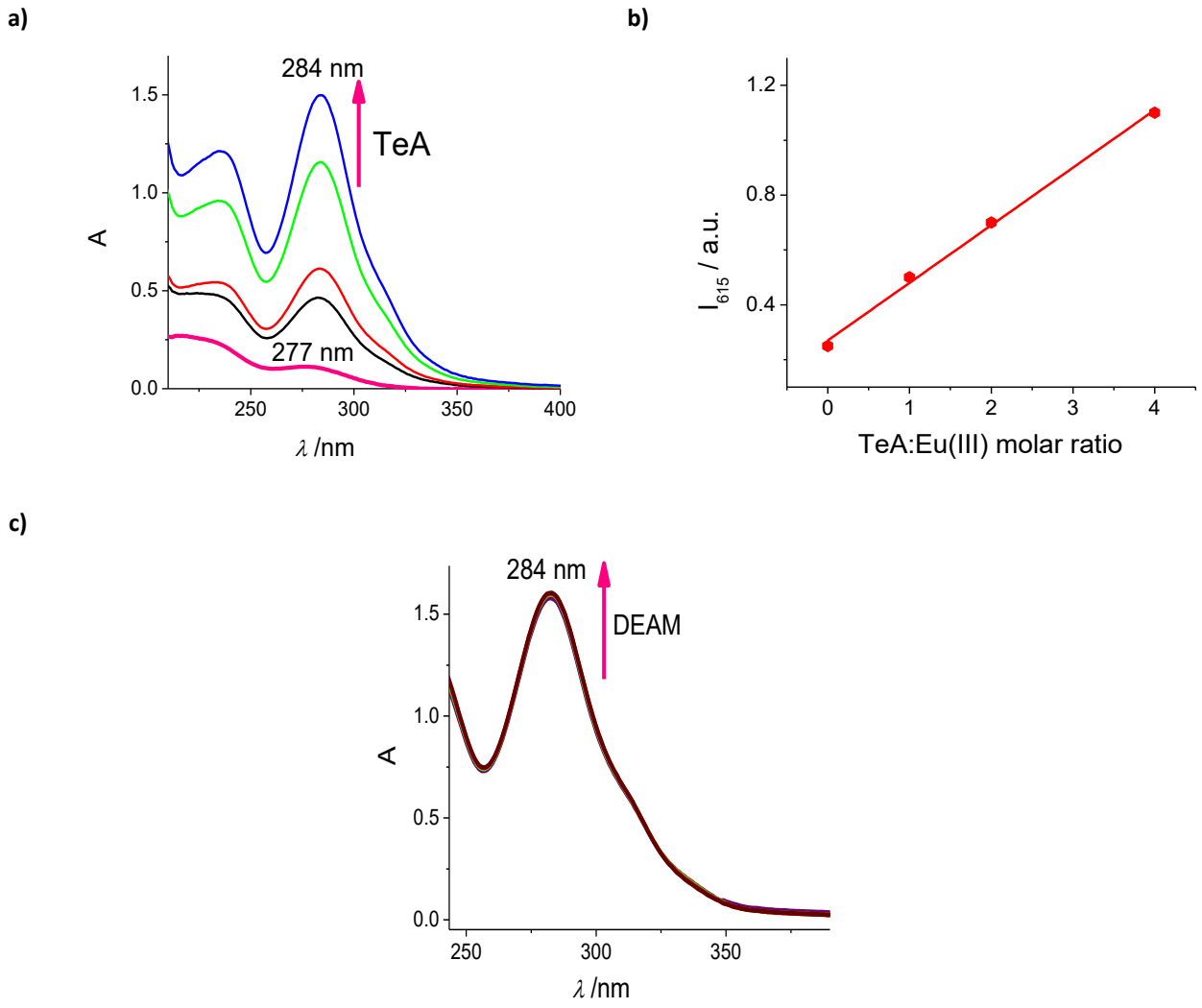

Figure 3.8: **a)** UV-vis absorption titration in 2 M NaOH(aq):EtOH 1:20 *v*/*v* of a 4:1 mixture of DEAM:Eu(III) (c_{DEAM} = 20 μM, $c_{Eu(III)}$ = 5 μM) by increasing the amount of the *r*TeA template (pink: only DEAM:Eu(III) 4:1; blue: after the addition of 5 equivalents of *r*TeA); **b)** increase in the emission intensity at 615 nm in a DEAM:Eu(III) 4:1 mixture upon increasing *r*TeA concentration λ_{exc} = 330 nm); **c)** absorption spectra of a *r*TeA:Eu(III) 4:1 mixture and upon increase of the amount of the DEAM monomer.

For the MIP preparation, a 1:1:3, Eu(III):*r*TeA:DEAM molar ratio was regarded to be optimal. In this way, 6 coordination sites would be occupied by the DEAM bidentate ligand, and two coordination sites would be free for *r*TeA binding. Taking into account that the *r*TeA complex seems to be more stable than the DEAM–Eu(III) complex, for the polymerization procedure we should first ensure the formation of the DEAM:Eu(III) complex in a 3:1 ratio (probably with two water molecules

to satisfy the coordination sphere) and, once it is formed, proceed with the addition of 1 equivalent of the template molecule (*r*TeA). Absorption and emission spectra were determined for this mixture and are shown in Fig. 3.9. The large Stokes shift (up to 286 nm) and the narrow emission band at 616 nm in the red region of the spectrum are important advantages of the luminescent system chosen here.

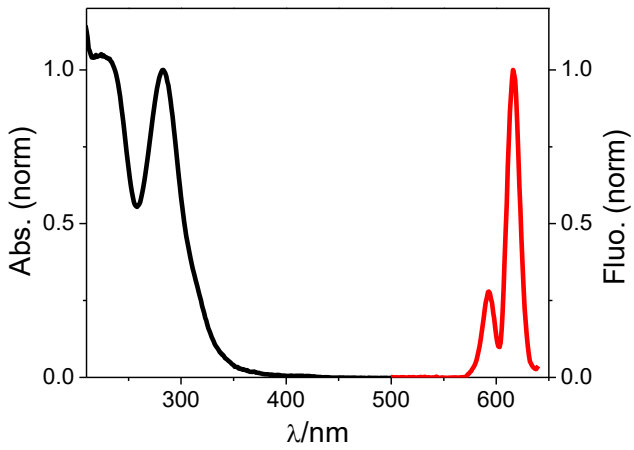

Figure 3.9: Normalized absorption (**black**) and emission (red) of a Eu(III): *r*TeA:DEAM 1:1:3 mixture in (2 M NaOHaq):EtOH 1:20 *v/v*; λ_{exc} = 330 nm.

III.3.2. Influence of the addition of water on the Eu(III)-*r*TeA binding

It is well known that water molecules can coordinate the Eu(III) cation. This fact can have two consequences:

- The hydration state can influence the binding process with *r*TeA. An increase of water in a solvent mixture can affect the dissociation constant of binding groups [20].
- Water can induce a quenching of the luminescence of a Eu(III) chelate [21].

Therefore, a photoluminescence study was performed in solutions containing 1 mol of $EuCl_3$ per 5 mol of Na^+rTeA^- ($c_{Eu(III)}$ = 50 μM) in water–MeCN mixtures by increasing the amount of water from 0 to 100%. It can be observed in Fig. 3.10 that, indeed, the increase in the water ratio causes a decrease in the luminescence signal at 615 nm. It is evident, from Fig. 3.10, that the best Eu(III) emission signal is obtained in neat acetonitrile, indicating either a quenching process due to the

presence of water, or a weaker association constant of the *r*TeA -Eu(III) complex when the water concentration is increased.

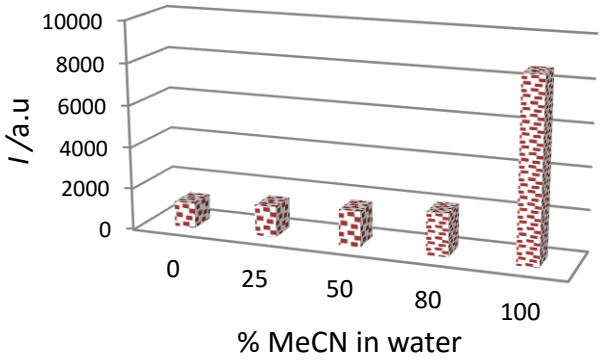

Figure 3.10: Effect of the water content in H_2O:MeCN solvent mixtures on the emission properties (λ_{em} = 615 nm) of a *r*TeA–Eu(III) complex (molar ratio *r*TeA:$EuCl_3$ 5:1, c_{EuCl3} = 50 μM) at 25 °C.

III.3.3. Luminescent MIP for tenuazonic acid in bulk format

III.3.3.1. Synthesis of Eu(III):DEAM:*r*TeA MIPs in bulk format (BMP-Eu)

For the synthesis of the luminescent MIPs, we firstly proceeded to the coordination of the DEAM β-diketone ligands to the Eu(III) cation in a 3:1 molar ratio, as concluded in the previous section. For the formation of the chelate, deprotonation of the diketone ligands is necessary, in order to form the diketonate anions that form a strong Eu(III) complex. For this, $EuCl_3$ and DEAM were dissolved in alkaline aqueous ethanol. Since, normally, the coordination number of a trivalent europium ion is eight, still two positions are available for *r*TeA binding. Therefore, 1 equivalent of the bidentated template ligand was added afterwards to the alkaline ethanolic mixture.

Once the complex was formed, copolymerization of its allylic groups with the crosslinker EDMA (ethylenglycol methacrylate) was carried out using ABDV (2,2'-azobis(2,4-dimethyl)valeronitrile) as initiator. ABDV was chosen because it has a good reactivity at 50 °C (10 h half-life at 30 °C) and is a good initiator for methacrylates and acrylates [22]. We used a considerably large amount of

initiator to obtain a highly crosslinked, insoluble polymer (BMP-Eu). For comparison purposes, the corresponding non-imprinted polymer (BNP-Eu) was also prepared in the same way, but excluding the addition of the template molecule Na^{+}*r*TeA^{-}.

III.3.3.2. Template removal studies

After polymerization, the corresponding bulk MIP-Eu and NIP-Eu were crushed, grounded and sieved to the desirable particle size. The particles were thoroughly washed with methanol and then acetone to remove unreacted monomers and weakly retained template. This procedure was carried out by stirring the polymer particles in the mentioned solvents followed by sedimentation for removing finer particles. Then the solids were filtered, dried at 70 °C and the particles were finally placed in a Soxhlet extractor to remove the template using HCl-EtOH 1:9 *v/v*.

After the Soxhlet extraction, the polymer particles were suspended in water for neutralising the remaining HCl. After filtration, the particles were dried in an oven overnight. Since during the procedure for template removal, part of the Eu(III) ions are extracted as well, the metal cation had to be re-introduced in the polymer matrix by preparing a suspension of the extracted polymer (200 mg) in ethanol and adding 12.5 mmol of $EuCl_3$ dissolved in 0.66 mL of a (2 M $NaOH_{aq}$):EtOH 1:20 *v/v* solution. Fig. 3.11 shows the intensity changes on the characteristic Eu(III) emission of three different suspensions of BMP-Eu: i) as-synthesised, ii) after the *r*TeA template removal and, iii) after reincorporation of Eu(III) to the polymer cavities. Non-imprinted Eu(III) polymers (BNP-Eu) were also subjected to the same washing and re-incubation procedures in order to ensure comparability of the results.

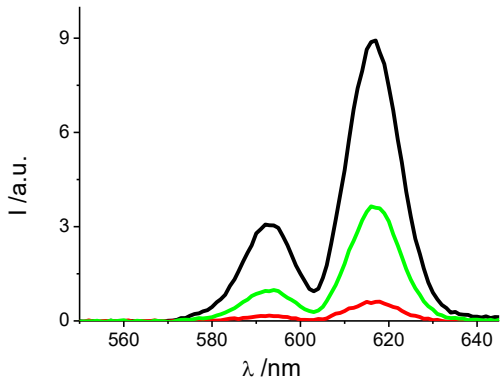

Figure 3.11: Emission spectra of BMP-Eu suspensions (λ_{ex} = 330 nm) in H_2O-MeOH 1:1 *v*/*v* (*c* = 1 mg solid/mL). **Black**: as-synthesized polymer; **red**: after removal of the Eu(III)–*r*TeA complex, and **green**: after reincorporation of the Eu(III).

The influence of the water content on different water–acetonitrile mixtures on the binding of *r*TeA in the synthesised polymer was evaluated by incubating a 10 µM *r*TeA solution for 1 h in 2 mL of the solvent mixture. Fig. 3.12 shows the luminescence intensity of the polymer suspensions as a function of the water content (in % *v*/*v*). As expected, the maximum luminescence signal in the MIP was obtained for a suspension in 100% MeCN, indicating either a stronger complex formation with *r*TeA or a weaker quenching of its luminescence in the absence of water. In the case of the NIP, the strongest luminescent signal is obtained in neat water, what might indicate a higher nonspecific binding to the non-imprinted material.

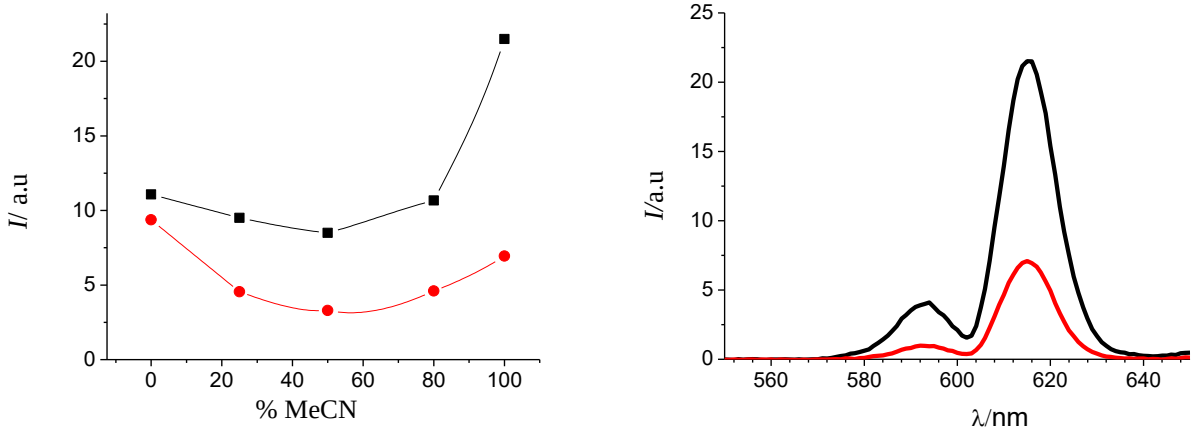

Figure 3.12: Effect of the water content on the rebinding process of *r*TeA (*c* = 10 µM) to a suspension of BMP-Eu (black) or BNP-Eu (red) ($c_{suspension}$ = 1 mg mL^{-1}). Left: Luminescence intensity for different H_2O-MeCN ratios; right: luminescence spectra in neat MeCN. Contact time 1 h at 25 °C.

III.3.3.3. Kinetics of *r*TeA rebinding to the MIP

The effect of the incubation time on the re-binding process of *r*TeA to the BMP-Eu and BNP-Eu particles was monitored by measuring the luminescence of the corresponding suspensions. The results are shown in Fig. 3.13. It can be observed that, after 45 min of incubation with a *r*TeA solution, the BNP-Eu reaches signal saturation (meaning longer contact times with the template solution did not provide further binding of the template), while the MIP needed an slightly longer contact time (60 min) for reaching saturation. For this reason, 60 min was chosen as an optimum incubation time for both polymers, Eu-MIP and Eu-NIP, for proceeding with further experiments.

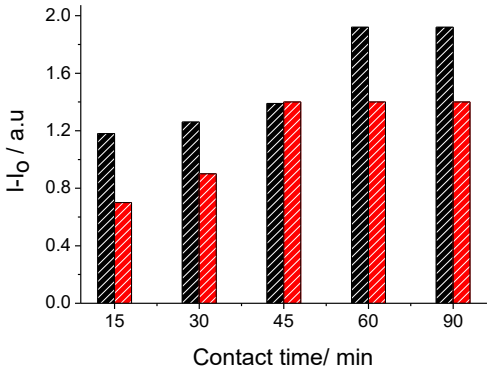

Figure 3.13: Variation of polymer luminescence as a function of the incubation time with *rTeA* (*c* = 40 μM): BMP-Eu (**black**) and BNP-Eu (**red**). The concentration of the polymers was 0.67 mg mL^{-1} in a water-MeCN 1:1 v/v mixture.

III.3.4. Choice of the polymer. Preparation of BMEu1 to BMEu12 library

In order to optimize the composition of the polymerization mixture that should lead to the MIP with the best recognition properties for the target analyte, *r*TeA, a combinatorial synthesis approach was followed. A library of different MIPs (and the corresponding NIPs) was prepared by using two different β-diketone functional monomers, namely diethyl allylmalonate (DEAM) and allyl acetoacetate (AACA) Fig. 3.14, combined in different molar ratios with Eu(III), Na^{+}*r*TeA^{-} as the template, and EDMA as cross-linker. For the polymerization, two different initiators, AIBN (2,2'-azobis(2-methylpropionitrile)) and ABDV (2,2`-azobis(2,4-dimethylvaleronitrile)) were tested. In all cases, the polymerization was performed at 65 °C in basic aqueous ethanol. The final composition of the library is described in the Experimental section, Table 5.2. Each MIP was prepared using different T/Eu/FM/CL molar ratios, with a fixed Eu(III)/CL ratio of 1:15. The T/FM ratio was varied as shown on Table 3.2, where 3:1, 2:2 and 1:3 T/FM compositions were tested [23]. For comparison purposes, different NIPs were also prepared (BNPEu1 to BNPEu12), which were synthesised with the same Eu/FM/CL ratio than the corresponding MIPs, but in the absence of the *r*TeA template.

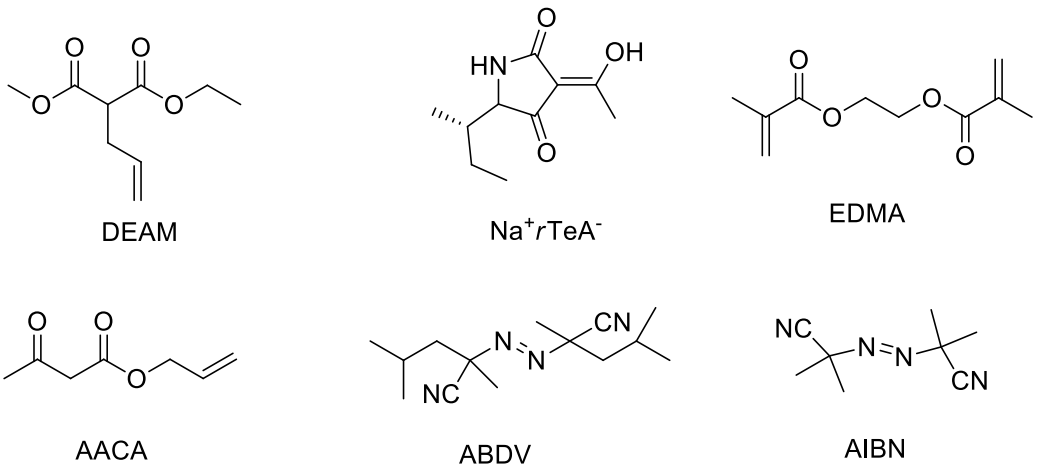

Figure 3.14: Chemical structures of the chemicals used for preparation of the BMP-Eu library: DEAM and AACA are the functional monomers, $Na^{+}rTeA^{-}$ is the template, EDMA is the cross-linker and ABDV or AIBN are the radical initiators.

As previously described, once the polymerization was finished, the template molecules together with the Eu(III) ions were extracted using a mixture of HCl and EtOH in a Soxhlet apparatus. Then, the BMPEu/BNPEu library was re-incubated with $EuCl_3$ in basic aqueous ethanol.

Table 3.2. Relative increase of the luminescence intensity, $(I-I_0)/I_0$, of different polymer suspensions after incubation with 12 ppm of the target analyte *r*TeA in MeCN. For all polymers, the Eu(III):CL molar ratio was fixed to 1:15. The *r*TeA to FM molar ratio was varied as shown on the table.

T:FM Molar ratio		I_{615} (BMPEuX)	I_{615} (BNPEuX)	I_{615} (BMPEuX)	I_{615} (BNPEuX)
rTeA:DEAM	3:1	10.96 (**BMPEu1**)	4.32 (**BNPEu1**)	5.03 (**BMPEu7**)	26.11 (**BNPEu7**)
	2:2	11.07 (**BMPEu2**)	8.79 (**BNPEu2**)	7.08 (**BMPEu8**)	9.54 (**BNPEu8**)
	1:3	12.48 (**BMPEu3**)	5.81 (**BNPEu3**)	7.42 (**BMPEu9**)	3.48 (**BNPEu9**)
rTeA:AACA	3:1	12.57 (**BMPEu4**)	6.86 (**BNPEu4**)	6.93 (**BMPEu10**)	7.89 (**BNPEu10**)
	2:2	8.44 (**BMPEu5**)	8.91 (**BNPEu5**)	5.34 (**BMPEu11**)	4.79 (**BNPEu11**)
	1:3	10.50 (**BMPEu6**)	8.14 (**BNPEu6**)	6.81 (**BMPEu12**)	3.59 (**BNPEu12**)
		ABDV (65 °C)		AIBN (65 °C)	

The recognition ability of the BMP-Eu/BNP-Eu library was investigated by using luminescence spectroscopy measurements after 24 h of incubation with solutions of $Na^{+}rTeA^{-}$ in MeCN (c = 12

ppm). Table 3.2 shows that 1:3 was the best molar ratio of *r*TeA:FM for the different functional monomers and initiators (except in the case of the polymers prepared with AACA as functional monomer and ABDV as radical initiator. In this case, the *r*TeA:AACA molar ratio that provides the largest difference between the MIP and NIP is 3:1 instead of 1:3). This ratio renders the strongest binding of *r*TeA with BMPEu in MeCN. Moreover, such combination provides the maximum difference between the binding with the corresponding MIP and NIP pair. Based on these results, the *r*TeA:Eu:DEAM:EDMA and *r*TeA:Eu:AACA:EDMA 1:1:3:15 composition was chosen for a large-scale synthesis of MIP porous microbeads.

In this case, the influence of the water content in MeCN on the *r*TeA binding to the polymers was also studied for two types of polymers: Eu:*r*TeA:DEAM:EDMA (**BMPEu3**) and Eu: *r*TeA:AACA:EDMA (**BMPEu6**), both prepared with the Eu:*r*TeA:FM:CL molar ratio of 1:1:3:15. In Table 3.3 we can see that the results already obtained in section III.3.3.2 for a different Eu(III) polymer prepared in bulk format are confirmed: the strongest emission signal at 615 nm and, also, the strongest difference of emission intensity between a MIP and the corresponding NIP, is obtained if neat MeCN is used as the solvent.

The optimised TeA-Eu(III)-MIP composition as described in section III.3.4 was chosen for the preparation of MIPs on a larger scale and in a more convenient format for a better (faster and with higher yield) mass transfer of guest into the polymers. The format chosen was porous microbeads. These MIP beads can be prepared using micrometric porous silica spheres as a sacrificial template as described in the previous Chapter II (section II.4.6). The final MIP microspheres are obtained by polymerizing the corresponding mixture of functional monomer-template complex and cross-linker in basic aqueous ethanol into the pores of commercial 40-75 µm diameter silica beads. The silica matrix is then dissolved with NH_4HF_2, leaving behind void channels in the resulting MIP bead structure [24]. These channels increase the porosity of the materials, and therefore, accelerate the kinetics of analyte exchange (washing or rebinding) with the recognition sites with respect to bulk MIPs.

Table 3.3: Luminescence intensity at 615 nm for suspensions of Eu-MAE, Eu-MDE and the corresponding NIPs, Eu-NAE and Eu-NDE, polymers after 1 h incubation with 12 ppm of *r*TeA in different H_2O:MeCN solvent mixtures.

MeCN%	BMPEu3	BNPEu3	BMPEu6	BNPEu6
0%	33524	18380	44347	37796
25%	47725	26182	57048	40692
50%	32886	24566	66885	106460
80%	51884	32877	47179	46269
100%	**55756**	**16456**	**96534**	**56606**

III.3.5. Tenuazonic acid luminescent MIPs in porous microbeads format

Three types of MIP spheres were prepared: MPE1 (with a *r*TeA Eu(III):DEAM:EDMA (1:1:3:15) molar composition), MPE2 (*r*TeA:Eu(III):AACA:EDMA (1:1:3:15)) and MPE3, who has the same composition as ME1, but is prepared in the presence of the *s*TeA surrogate instead of the *r*TeA as molecular template. In the next sections, the characterization of each kind of microparticles is described.

III.3.5.1. Characterization of the porous microbeads MPE1, MPE2 and MPE3

The morphology of the porous microbeads MPE1, MPE2 and MPE3 was characterised by confocal optical microscopy and also by scanning electron microscopy (SEM). The results are shown in Fig. 3.15. The images revealed that MPE1, MPE2 and MPE3 particles have a spherical form that is kept even after silica etching. On Fig. 3.15 II we can observe how etching of the silica template with the 3.6 M ammonium fluoride aqueous solution generates spheres with a high porosity. This porous structure should help for analyte transport in the analytical assays.

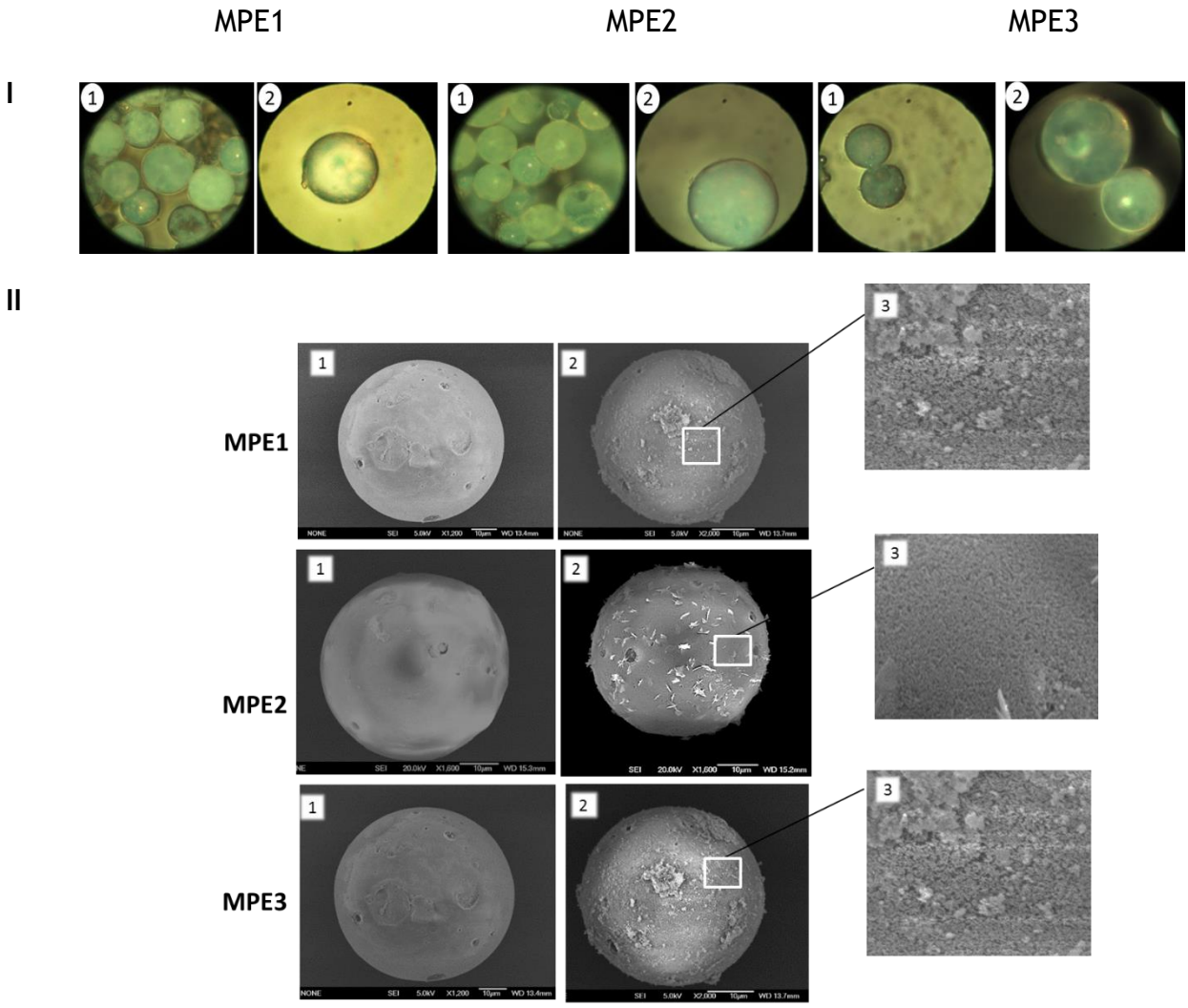

Figure 3.15: I) Bright field confocal optical microscopy images of MPE microspheres under 20X (1) and 40X (2) objectives ; **II)** SEM images for MPE1, MPE2 and MPE3 spherical particles before (1) and after (2) silica etching (10 µm scale bar); (3) shows a zoom of the corresponding images in (2).

Once the polymers were prepared, the Eu(III) and *r*TeA template were removed by shaking the polymer in HCl-EtOH 1:9, *v/v*. The process was repeated with fresh HCl-EtOH 1:9, *v/v* in 1 h intervals until satisfactory removal of the Eu(III):*r*TeA complex. Complete template removal was confirmed by measuring the luminescence intensity of the corresponding supernatant after washing as shown in Fig. 3.16. The MPE1, MPE2 and MPE3 particles were then collected separately and washed several times with Milli-Q water until neutral pH. Finally, the particles were dried at 70 °C overnight and

hence were ready for use. Eu(III) ions were reintroduced into the polymer matrix by adding $EuCl_3$ in basic aqueous ethanol. The corresponding non-imprinted particles, NPE1, NPE2 and NPE3 were treated likewise for comparison purposes.

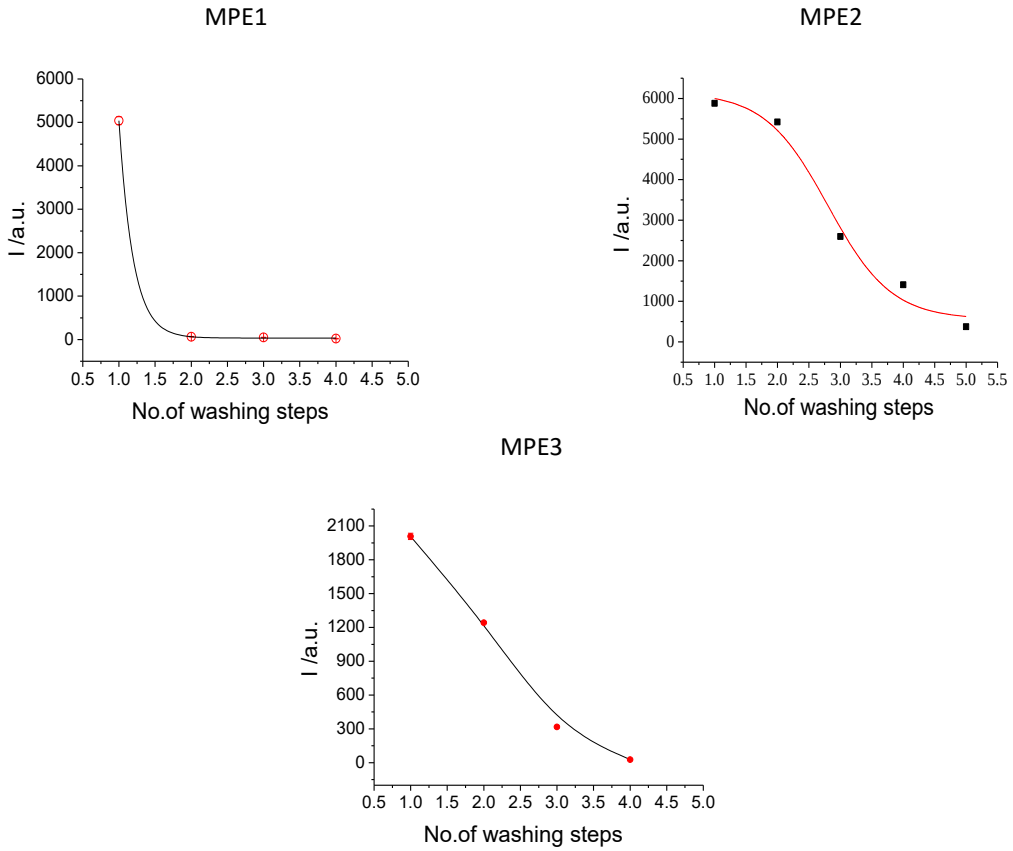

Figure 3.16: Decrease in the luminescence intensity from the supernatants as a function of the number of washings for template extraction for the MPE polymers.

III.3.5.2. Influence of the water concentration on the MPE1, MPE2 and MPE3 response

Rebinding studies with *r*TeA and MPE1, MPE2 and MPE3 were performed using H_2O/MeCN mixtures by increasing the amount of MeCN as follows: 5, 25, 50, 80 and 100% MeCN (*v/v*). Equal amounts of *r*TeA (c = 50 µM) were added to the polymer (MPE and NPE) suspensions (c = 0.67 mg/mL). The results were similar to those previously obtained for the bulk polymers in section III.3.3.2): a stronger increase in the luminescence signal at 615 nm upon addition of *r*TeA in 100% MeCN than that for the water mixtures Fig. 3.17.

These results were confirmed by determining the percentage of bound analyte for two of the polymers, MPE2 and MPE3, using HPLC analysis in different H_2O:MeCN mixtures, as shown in Table 3.4. In neat MeCN, the *r*TeA mycotoxin was more strongly bound in both cases.

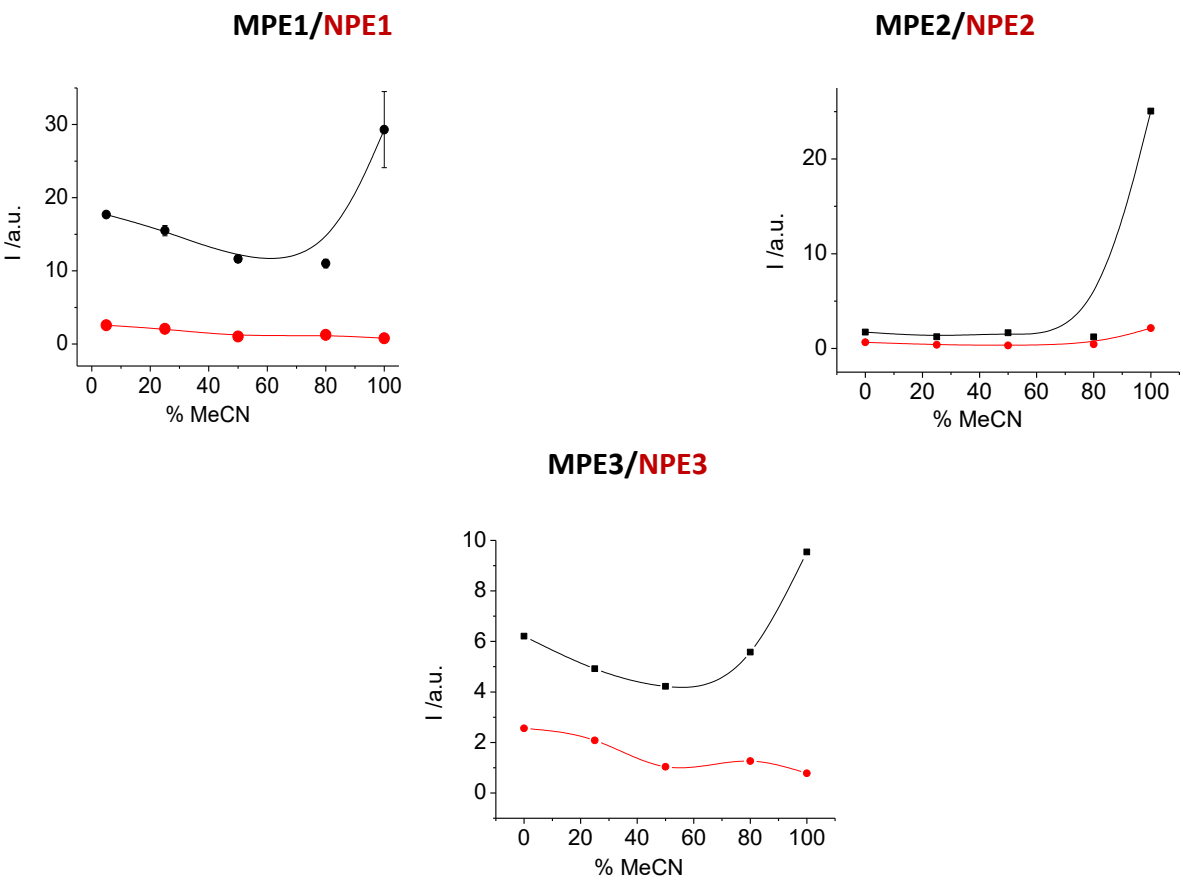

Figure 3.17: Intensity of the luminescence signal at 615 nm (λ_{ex} = 330 nm) for suspensions of MPE (**black**) and NPE (**red**) ($c_{suspension}$ = 0.67 mg/mL) after the addition of 50 µM *rTeA* upon increasing %MeCN in water-MeCN mixtures (incubation time 1 h at 25 °C, *n* = 3).

Table 3.4: Percentage of bound $Na^{+}rTeA^{-}$ in MPE2 and MPE3 polymer suspensions using different H_2O-MeCN solvent mixtures for incubation. Analysis performed by HPLC for determining the percentage of non-bound analyte found in the supernatant after incubation (n = 3).

% MeCN	% *r*TeA in supernatant for MPE2 (S.D.)	% *r*TeA bound in MPE2	% *r*TeA in supernatant for MPE3 (S.D.)	% *r*TeA bound in MPE3
0	82 (1)	18	79 (2)	21
25	83 (2)	17	80 (1)	20
50	84 (5)	16	87 (1)	13
80	92 (1)	8	89 (4)	11
100	58 (1)	42	9 (1)	91

III.3.5.3. Kinetic study of the *r*TeA rebinding to MPE1, MPE2 and MPE3 polymers

In order to determine the minimum incubation time of the mycotoxin *r*TeA and a suspension of MPE1, MPE2 and MPE3 polymers necessary for having a stable and reproducible emission signal at 615 nm, a calibration was made. The results are shown in Fig. 3.18. A suspension of the MPE polymers in MeCN (c = 0.67 mg/mL) was incubated with a solution of 10 µM *r*TeA. Emission of the suspensions was then recorded at 615 at different time intervals. The same experiment was conducted in parallel with the corresponding non-imprinted polymers.

From Fig. 3.18 we can conclude three things: i) the optical response of the MIPs is stronger than that obtained with the corresponding NIPs, indicating a higher loading of Eu(III) centers in the MIP and a more accesible binding sites for *r*TeA in the case of the imprinted spheres; ii) signal saturation is reached after 60 min of stirring for MPE1 (in the case of NPE1 saturation is reached after 15 min). Therefore, 60 min was chosen as the optimum incubation time for further experiments; iii) MPE2 and MPE3 reached saturation after 15 min.

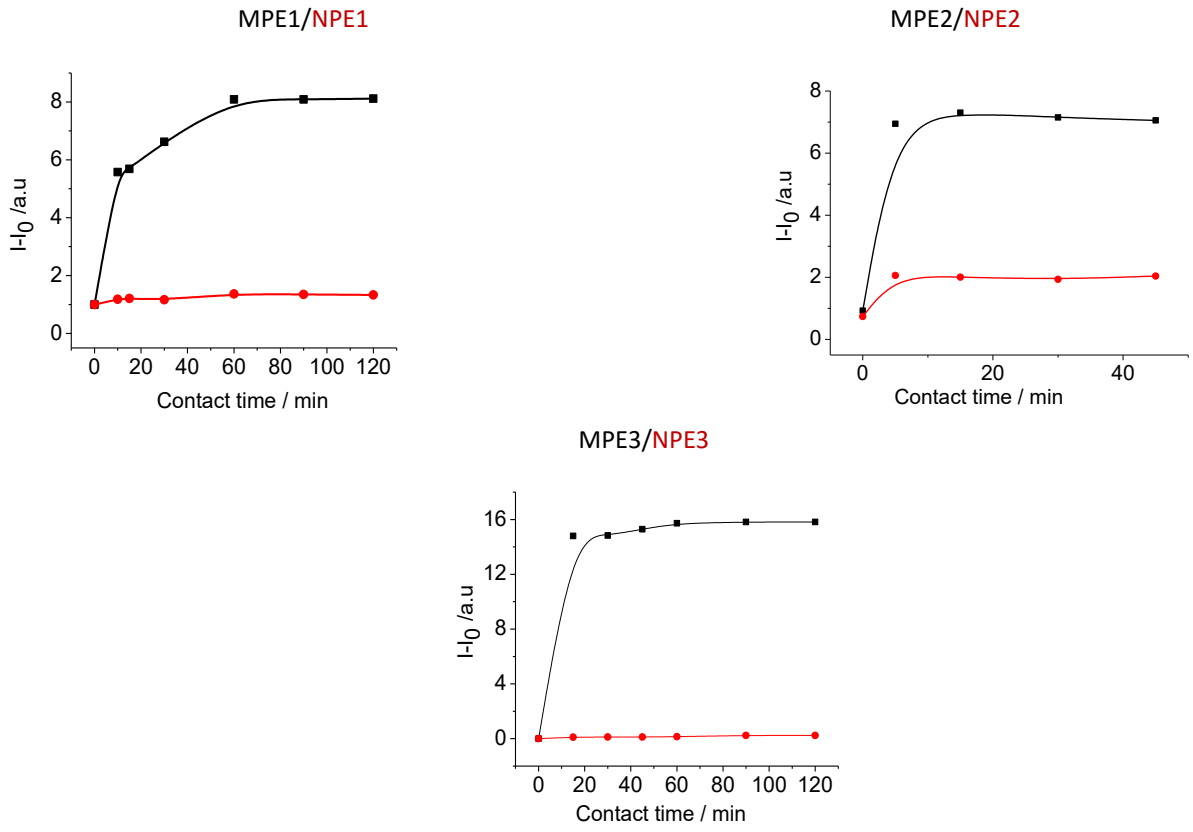

Figure 3.18: Intensity of the luminescence signal at 615 nm (λ_{ex} = 330 nm) for suspensions of MPE (**black**) and NPE (**red**) ($c_{suspension}$ = 0.67 mg mL^{-1}) after the addition of 10 µM *r*TeA at different incubation times with *r*TeA.

III.3.5.4. Analytical performance of the imprinted luminescent microspheres. Determination of LODs and LOQs for tenuazonic acid detection with MPE1/NPE1, MPE2/NPE2 and MPE3/NPE3

The analytical characterization of the MPE1, MPE2 and MPE3 polymers in the presence of *r*TeA was performed by photoluminescence spectroscopy and HPLC analysis.

a) *Spectroscopic studies*. Rebinding studies were carried out by adding 3 mL of Na^{+}*r*TeA^{-} solutions in MeCN of various concentrations (from 0.001 to 1 mM) to 2 mg of the corresponding polymer (MPE or, for comparative purposes, NPE). The suspensions were incubated for 1 h with shaking at 25 °C. The corresponding emission was recorded upon excitation at 330 nm. In Fig. 3.19 it can be observed the characteristic and narrow emission

peaks of the Eu(III) ions at 594 and 615 nm, corresponding to the $^5D_0$-$^7F_1$ and $^5D_0$-$^7F_2$ transitions, respectively. The intensities of these peaks increase when increasing the *r*TeA concentration.

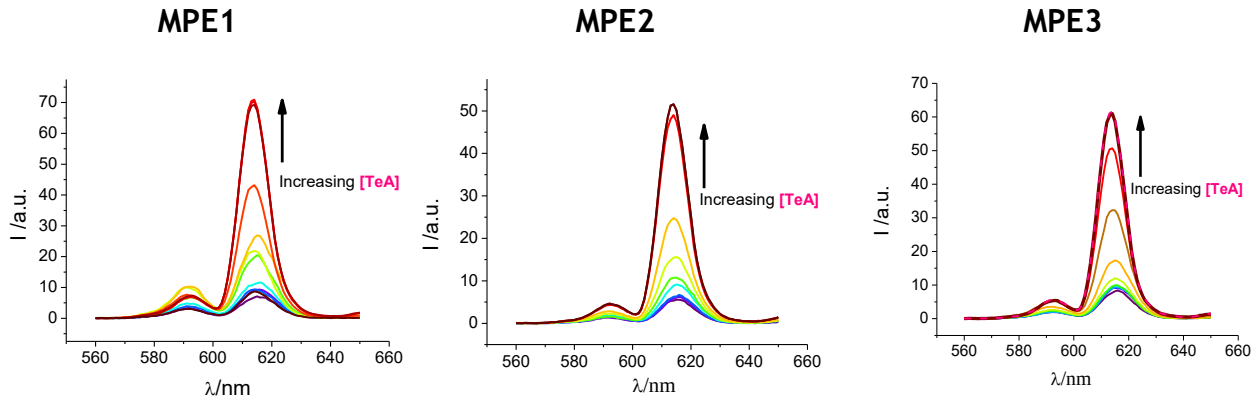

Figure 3.19: Increase on the Eu(III) luminescence signal at 615 nm upon addition of *r*TeA (0.001 - 1 mM) to a suspension of MPE1, MPE2 or MPE3 (c = 0.67 mg mL^{-1}) in MeCN at 25 °C (λ_{exc} = 330 nm). The suspension was equilibrated with the *r*TeA solution for 60 min before recording the emission.

In Fig. 3.20, the variation of the luminescence intensity of MPE1-I (I-I$_0$/I$_0$, where I$_0$ is the intensity in the absence of *r*TeA) is represented *vs*. the *r*TeA concentration. It can be observed that the emission of MPE1 (Eu:*r*TeA:DEAM:EDMA, 1:1:3:15) is more sensitive to the presence of *r*TeA than that of NPE1. In the case of MPE1, the ΔI/I$_0$ ratio increases sharply with the increase in the *r*TeA concentration up to 0.5 mM and then more slowly thereafter. In Fig. 3.20 MPE2-I, the MPE2 polymer (Eu:*r*TeA:AACA:EDMA, 1:1:3:15) shows a sharp increase of the ΔI/I$_0$ ratio with the increase in the *r*TeA concentration up to 0.2 mM and then the signal reaches saturation. The enhancement of the emission intensity of MPE1 and MPE2 is more than four times that of NPE1 and NPE2, respectively. In the case of MPE3 (Eu:sTeA:DEAM:EDMA, 1:1:3:15) saturation in the ΔI/I$_0$ signal is reached at a *r*TeA concentration of 0.3 mM. The enhancement of the emission signal in the case of NEP3 is about the half of that of MEP3. From these results, we can conclude that: i) MPEs have more binding sites due to imprinting effect and, therefore, a stronger signal enhancement upon *r*TeA binding than the corresponding NIPs (there are more Eu(III) centers available for *r*TeA coordination); ii) the saturation of binding sites (signal saturation) is reached at 0.5 mM of *r*TeA for the polymer prepared with

DEAM as functional monomer and *r*TeA as the template (MPE1) while, in the case of MPE2 and MPE3, saturation of binding sites occurs at lower MIP concentrations (*ca.* 0.2 mM), indicating a lower binding capacity when preparing a MIP with AACA as the functional monomer (MPE2) or when using the surrogate *s*TeA as the template (MPE3).

The plots corresponding to the linear part are shown for all polymers in Fig. 3.20 II. Dynamic ranges, LODs and LOQs were determined with the OriginPro8 software for statistic analysis using Eqs. 3.1 and 3.2, and the results are displayed on Table 3.5. The goodness of the linear fittings was confirmed by a r^2 value ≥ 0.90 in all cases.

$$\mathrm{LOD} = 3.3 \times \mathrm{SD}\frac{(\mathrm{x})}{slope\ (S)} \tag{3.1}$$

$$\mathrm{LOQ} = 10 \times \mathrm{SD}\frac{(\mathrm{x})}{slope\ (S)} \tag{3.2}$$

Table 3.5: LODs, LOQs and dynamic ranges for calibrations with *r*TeA performed by luminescence spectroscopy, with 2 mg of the polymer supensions (MPE1, MPE2 and MP3) with increasing amounts of Na^{+}*r*TeA^{-} in 3 mL of MeCN.

Polymer	LOD/μM	LOQ/μM	Dynamic range/μM
MPE1	5.2	15.0	2.0 – 80.0
MPE2	9.9	29.9	5.0 – 80.0
MPE3	4.0	14.0	8.0 – 200.0

I

II

MPE1

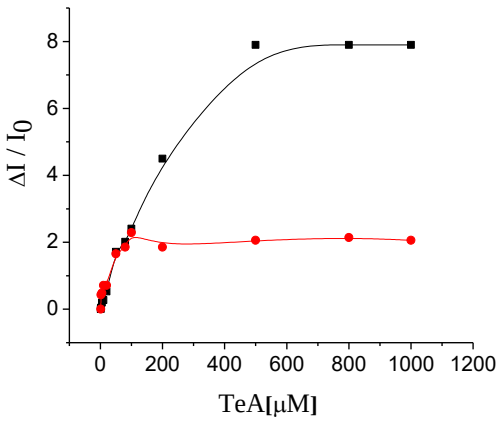

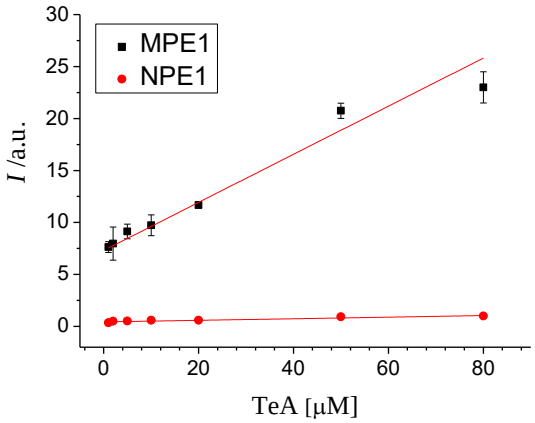

MPE2

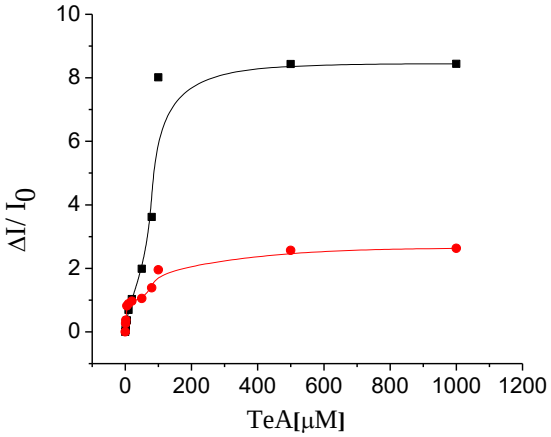

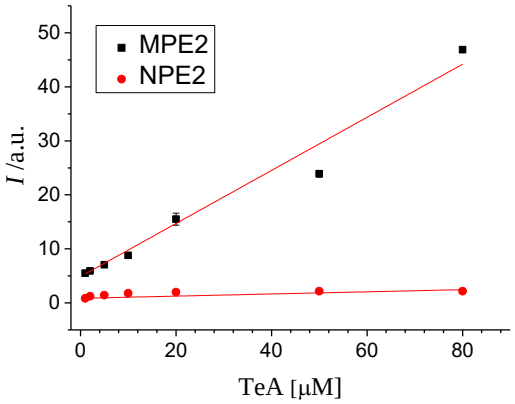

MPE3

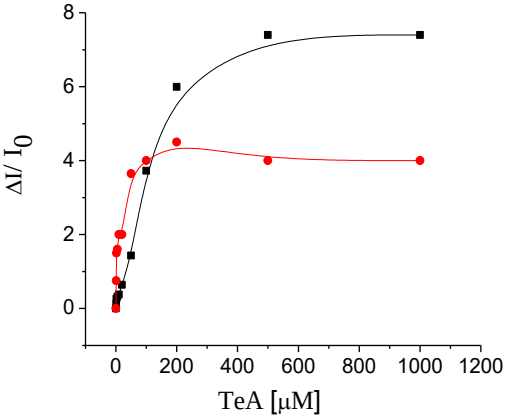

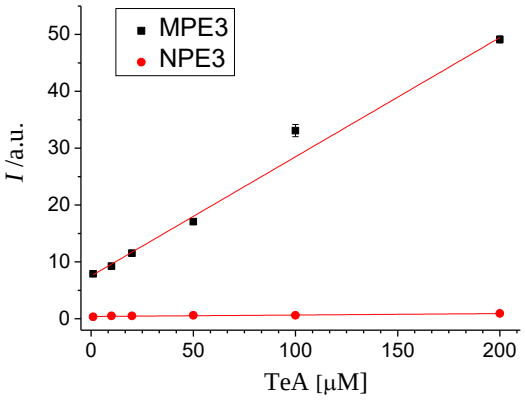

Figure 3.20: I) Dependence of luminescence intensity of suspensions of MPEs (**black**) and NPEs (**red**) suspensions in MeCN upon increasing *r*TeA concentration. ΔI: $I-I_0$, and I_0: emission intensity in the absence of *r*TeA; **II)** Linear fit of the corresponding linear regions of the former plots (calibration curves): MPE (**black**) and NPE (**red**) (λ_{ex} = 330 nm, 1 h incubation time, 25 °C, n = 3).

b) *HPLC studies*. Binding of *r*TeA to the polymers was also evaluated by liquid chromatography. Fig. 3.21 shows the percentage of bound *r*TeA for suspensions of the three different polymers, MPE1, MPE2 and MPE3 (c = 0.67 mg mL^{-1}), after incubation with increasing amounts of TeA (from 0.001 to 1 mM) in MeCN at 25 °C during 1 h. After analyzing the amount of free *r*TeA present in the supernatant after incubation, the percentage of bound *r*TeA was calculated by subtraction, taking into account the known initial amount of added *r*TeA in the sample. In Fig. 3.21 we can observe that, at low concentrations of *r*TeA, all the analyte remains adsorbed into the MPE polymers. When increasing the concentration to 0.5 mM, 0.08 or 0.10 mM for MPE1, MPE2 and MPE3, respectively, only *ca.* 50% of the analyte remains bound to the polymer, indicating that saturation of the cavities has been reached. These results are in agreement with those obtained with the previous spectroscopic studies, where MPE1 showed the highest binding capacity, with saturation at 0.5 mM of *r*TeA.

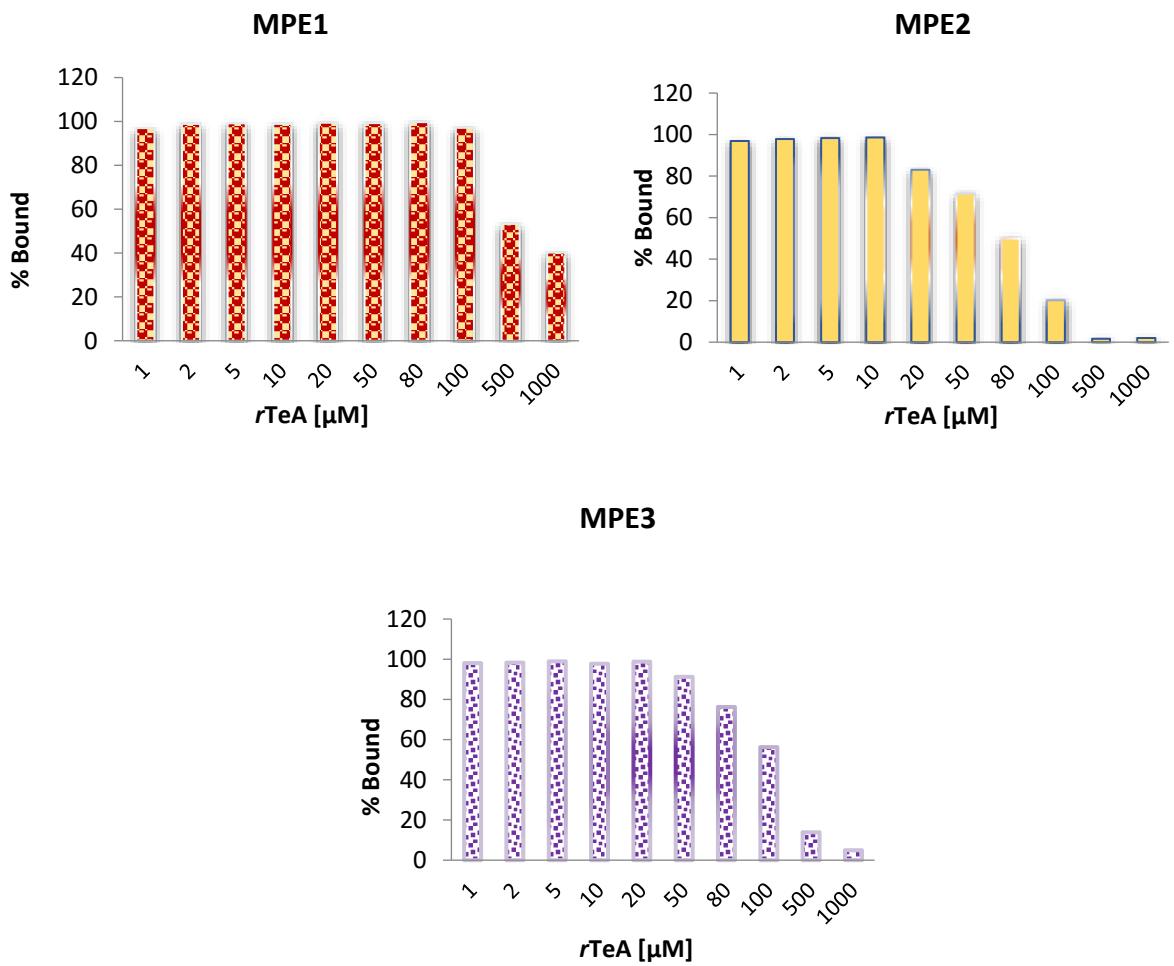

Figure 3.21: Amount of bound *r*TeA to the MPE polymers *vs.* the concentration of *r*TeA in MeCN solution. The amount of MPE particles was 2 mg; the volume of solvent was 3 mL; contact time 1 h at 25 °C.

III.3.5.5. Cross-reactivity studies with MPE1, MPE2 and MPE3

In order to asses the *selectivity* of the response towards *r*TeA of the three different type of MIP microparticles, MPE1, MPE2 and MPE3, equilibrium binding tests were performed by fluorescence spectroscopy in MeCN with two related β-diketone structures: cyclopiazonic acid (Cyclo) and the surrogate *s*TeA. Also, four other compounds that do not possess the *β*-diketone structure but can normally be found together with *r*TeA in food samples were tested, namely alternariol (AOH) and zearalenone (ZON), who are also mycotoxins produced by the *Alternaria* fungi, and glucose and fructose, two ubiquitous saccharides. The chemical structure of the investigated compounds is depicted in Fig. 3.22.

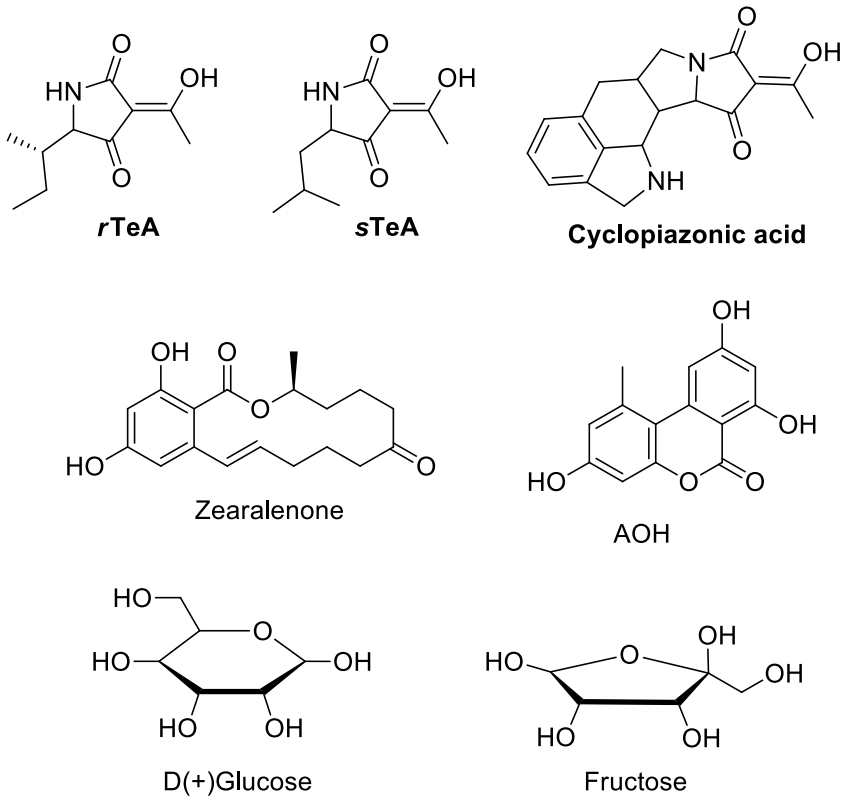

Figure 3.22: Chemical structures of the investigated competitors for TeA recognition.

In order to previously evaluate the potential optical response when bound to the Eu(III)-loaded polymers, the absorption spectrum of cyclopiazonic acid was recorded. Fig. 3.23 shows the similar UV-Vis absorption pattern of the three different β-diketones investigated, *r*TeA, sTeA and cyclopiazonic acid. For AOH, its absorption spectrum is provided in Chapter II (λ_{abs} = 331 and 341 nm) while zearalenone has absorption maxima at 274 and 314 nm [25].

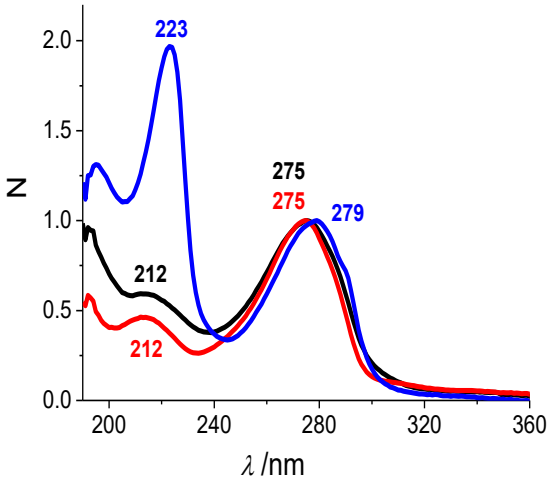

Figure 3.23: Normalized absorption spectra of 0.1 mM *r*TeA (**black**), *s*TeA (**red**) and cyclopiazonic acid (**blue**) in MeCN, with the absorption maxima (in nm) displayed for each species.

In Fig. 3.24 I, the effect of the addition of the different competitors at a c = 50 µM in MeCN on the luminescence signals of the Eu(III) complex is shown for the three different types of MIP microparticles, MPE1, MPE2 and MPE3. The emission was recorded for suspensions of the polymers in MeCN after 1 h incubation with the corresponding molecule, *r*TeA, sTeA, Cyclo, ZON, AOH, glucose or fructose. In all cases, the strongest signal is obtained when the β-diketones *r*TeA, *s*TeA and Cyclo are added, especially in the case of Cyclo. The latter could be due to the higher lipophylic character of this molecule that could improve the binding to the hydrophobic MIP structure. Fig. 3.24 II displays a comparison of the effect of the addition of the competitors on the Eu(III) luminescence signal for the MPE and NPE pairs. In all cases, the response (difference between the emission intensity after analyte addition and the emission of the polymer before the incubation) is stronger for the MIP than for the corresponding NIP. These results confirm that imprinting with the TeA template molecules in the case of MIPs has created highly porous materials with cavities that facilitate analyte diffusion and make more accessible the coordination sphere of the Eu(III) centers. Regarding phenolic or saccharide competitors, no effect on the luminescence was observed. These results suggest that the molecular recognition process is only based on the interactions taking place between the β-diketonate structure and the Eu(III) complex.

I

II

MPE 1

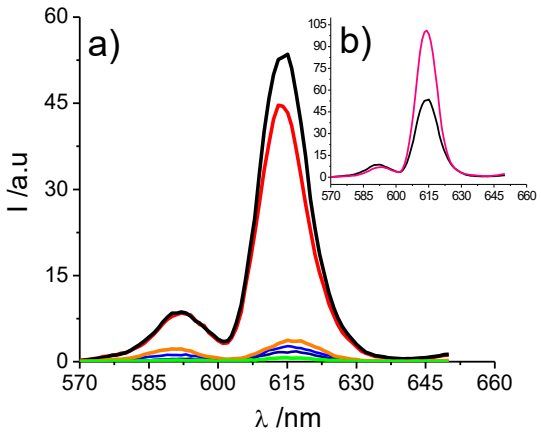

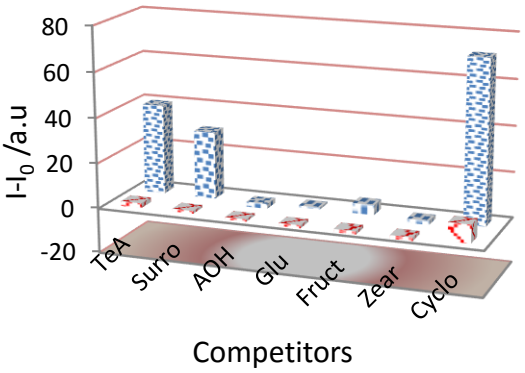

MPE 2

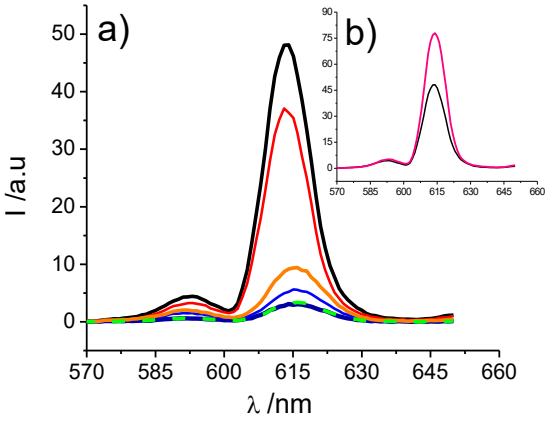

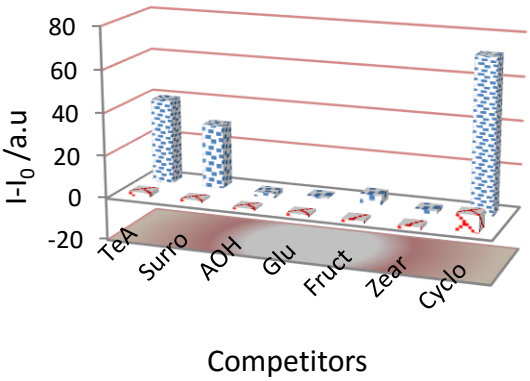

MPE 3

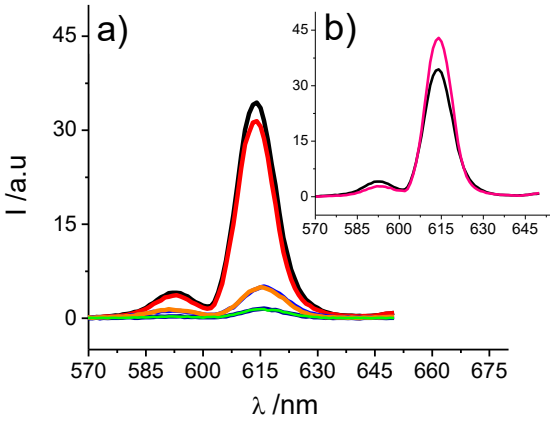

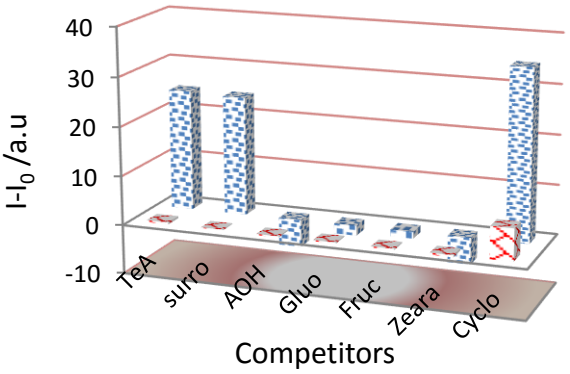

Figure 3.24: I) a) Luminescence spectra of MPE1, MPE2 and MPE3 suspensions in MeCN (*c* = 0.67 mg/mL) and upon the addition of different analytes (*c* = 50 µM): *r*TeA (**black**), *s*TeA (**red**), AOH (**blue**), glucose (**cyan**), fructose (**orange**) and zearalenone (**green**); b) comparison between the Cyclo (**pink**) and TeA (**black**) addition; II) Luminescence intensity at 615 nm after the addition of competitors MPE (**blue bars**) and NPE (**red bars**) (I_0: intensity in absence of competitor).

In order to evaluate the analytical performance of the imprinted microspheres, the polymers MPE2 and NPE2 (as control) were incubated with increasing amounts of Na^+*r*TeA^- in MeCN. Fig. 3.25 shows a titration based on luminescence measurements in the wells of a microplate with a microplate reader. The microtiter plate employed here has a standard configuration of 96 wells, but these wells incorporate, individually, a filter at the bottom that allows removal of the solvent by suction once the incubation period with the analyte is finished. The latter allows direct detection of the luminescence of the *dry polymers* on the plate without the need of an intermediate transfer step after incubation, eliminating losses of polymer mass and, consequently, minimizing the error in the measurements. Fig. 3.25 shows the luminescence intensity recorded at 615 nm with an acquisition delay of 30 µs with respect to the excitation pulse. This time delay was optimized for obtaining the best sensitivity in the measurement: a compromise was reached between i) the minimum gating for eliminating the background signal (especially problematic when directly measuring over dry, irregular powders with large particle size) and, ii) the minimum time elapsed between excitation and detection for maximizing the Eu(III) luminescence signal.

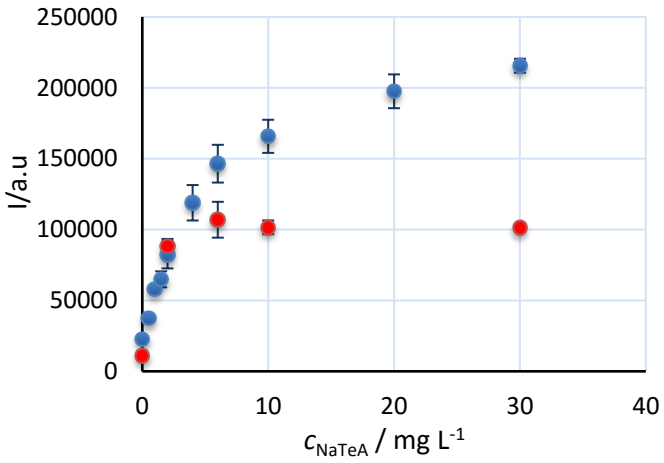

Figure 3.25: Change on emission intensity for MPE2 (**blue**) and NPE2 (**red**) powders after 1 h incubation with increasing amounts of Na^{+}*r*TeA^{-} in MeCN. After incubation, the solvent was filtered out and the emission was collected *directly* in each well containing the dry solid material.

In Fig. 3.25 it can be observed that at low *r*TeA concentrations (< 6 mg mL^{-1}), the response of MIP and NIP is similar. However, at higher concentrations of analyte, the emission signal of NPE2 does not show any further change while, in the case of the MIP, the emission intensity continues increasing up to a concentration of at least, 20 mg mL^{-1} indicating that the MIP has a higher binding capacity for *r*TeA than the NIP.

Bibliography

1. Carroll, M. F.; Bader, A. R., The reactions of diketene with ketones. *J. Am. Chem. Soc.* **1953,** *75*, 5400-5402.

2. Wang, X.; Si, T.; Li, Q.; Zhu, Z.; Zhu, X.; Qiang, S.; Yang, C., Synthesis, characterization and biological activity of novel (5RS,6S)-5-sec-butyl-3-(1-substitutedamino)ethylidene -1H-pyrrolidine-2,4-diones (10-4679HP). *ARKIVOC.* **2010,** *ii*, 31-48.

3. Inoue, S.; Kumagai, T.; Tamezawa, H.; Aota, H.; Matsumoto, A.; Yokoyama, K.; Matoba, Y.; Shibano, M., Pursuit of reinitiation efficiency of resonance-stabilized monomeric allyl radical generated via "degradative monomer chain transfer" in allyl polymerization. *J. Polym. Sci. A: Polym. Chem.* **2011,** *49*, 156-163.

4. Asam, S.; Liu, Y.; Konitzer, K.; Rychlik, M., Development of a Stable Isotope Dilution Assay for Tenuazonic Acid. *J. Agric. Food Chem.* **2011,** *59*, 2980–2987.

5. Clemens, R. J.; Hyatt, J. A., Acetoacetylation with 2,2,6-trimethyl-4H-1,3-dioxin-4-one: a convenient alternative to diketene. *J. Org. Chem.* **1985,** *50*, 2431-2435.

6. Sato, M.; Ogasawara, H.; Kato, K.; Sakai, M.; Kato, T., Reaction of diketene-acetone adduct with enamines, ketene acetals, vinyl ethers, and β-diketones. *Chem. Pharm. Bull.* **1983,** *31*, 4300-4305.

7. Poncet, J.; Jouin, P.; Castro, B.; Nicolas, L.; Boutar, M.; Gaudemer, A., Tetramic acid chemistry. Part 1. Reinvestigation of racemization during the synthesis of tetramic acids via Dieckmann cyclization. *J. Chem. Soc., Perkin Trans 1* **1990,** *3*, 611–616.

8. Shephard, G. S.; Thiel, P. G.; Sydenham, E. W.; Vleggaar, R.; Marasas, W. F. O., Reversed-phase high performance liquid chromatography of tenuazonic acid and related tetramic acids. *J. Chromatogr. B Biomed. Sci. App.* **1991,** *566*, 195-205.

9. Lebrun, M. H.; Duvert, P.; Gaudemer, F.; Gaudemer, A.; Deballon, C.; Boucly, P., Complexation of the fungal metabolite tenuazonic acid with copper (II), iron (III), nickel (II), and magnesium (II) ions. *J. Inorg. Biochem.* **1985,** *24*, 167-81.

10. Harris, S. A.; Fisher, L. V.; Folkers, K., The synthesis of tenuazonic and congeneric tetramie acids. *J. Med. Chem.* **1965,** *8*, 478-82.

11. Pinheiro, S. C.; Raimundo, I. J.; Moreno-Bondi, M. C.; Orellana, G., Simultaneous determination of copper, mercury and zinc in water with a tailored fluorescent bipyridine ligand entrapped in silica sol-gel. *Anal. Bioanal. Chem.* **2010,** *398*, 3127-3138.

12. Bunzli, J. C.; Piguet, C., Taking advantage of luminescent lanthanide ions. *Chem. Soc. Rev.* **2005,** *34*, 1048-77.

13. Jenkins, A. L.; Uy, O. M.; Murray, G. M., Polymer-based lanthanide luminescent sensor for detection of the hydrolysis product of the nerve agent Soman in water. *Anal. Chem.* **1999,** *71*, 373-8.

14. Jenkins, A. L.; Bae, S. Y., Molecularly imprinted polymers for chemical agent detection in multiple water matrices. *Anal. Chim. Acta.* **2005,** *542*, 32-37.

15. Southard, G. E.; Van Houten, K. A.; Murray, G. M., Soluble and processable phosphonate sensing star molecularly imprinted polymers. *Macromolecules* **2007,** *40*, 1395-1400.

16. Southard, G. E.; Van Houten, K. A.; Ott, E. W., Jr.; Murray, G. M., Luminescent sensing of organophosphates using europium(III) containing imprinted polymers prepared by RAFT polymerization. *Anal. Chim. Acta.* **2007,** *581*, 202-7.

17. Zdunek, J.; Benito-Pena, E.; Linares, A.; Falcimaigne-Cordin, A.; Orellana, G.; Haupt, K.; Moreno-Bondi, M. C., Surface-imprinted nanofilaments for europium-amplified luminescent detection of fluoroquinolone antibiotics. *Chem. Eur. J.* **2013,** *19*, 10209-16.

18. Kim, H.; Kim, Y.; Chang, J. Y., Preparation of a molecularly imprinted polymer containing Europium(III) ions for luminescent sensing. *J. Polym. Sci. A, Polym. Chem.* **2012,** *50*, 4990-4994.

19. Gao, L.; Guan, M.; Wang, K.; Jin, L.; Huang, C., A comparative study of the optical and electroluminescent properties of EuIII complexes with TTA and 2-(2′-Pyridyl)azoles: the crystal structure of [Eu(TTA)3(PBO)]. *Eur. J. Inorg. Chem.* **2006,** *2006*, 3731–3737.

20. Sucha, L.; Kotrly, S., *Solution equilibria in analytical chemistry*. Van Nostrand Reinhold: New York, 1972.

21. Bunzli, J. C., Lanthanide luminescence for biomedical analyses and imaging. *Chem. Rev.* **2010,** *110*, 2729-55.

22. Szablan, Z.; Junkers, T.; Koo , S. P. S.; Lovestead, T. M.; Davis, T. P.; Stenzel, M. H.; Barner-Kowollik, C., Mapping photolysis product radical reactivities via soft ionization mass spectrometry in acrylate, methacrylate, and itaconate systems. *Macromolecules* **2007,** *40*, 6820-6833.

23. Kim, H.; Y., K.; Chang, J. Y., Preparation of a molecularly imprinted polymer containing europium(III) ions for luminescent sensing. *J. Polym. Sci. A: Polym. Chem.* **2012,** *50*, 4990-4994.

24. Titirici, M. M.; Hall, A. J.; Sellergren, B., Hierarchically imprinted stationary phase:mesoporous polymer beds containing surface-confind binding sites for adenine. *Chem. Mat.* **2002,** *14*, 21-23.

25. Pfeiffer, E.; Hildebrand, A. A.; Becker, C.; Schnattinger, C.; Baumann, S.; Rapp, A.; Goesmann, H.; Syldatk, C.; Metzler, M., Identification of an aliphatic epoxide and the corresponding dihydrodiol as novel congeners of zearalenone in cultures of Fusarium graminearum. *J. Agric. Food Chem.* **2010,** *58*, 12055-62.

IV- Pyrene-Labeled Acrylamide Monomers as Fluorescent Probes

INDEX

IV- PYRENE-LABELED ACRYLAMIDE MONOMERS AS FLUORESCENT PROBES

General Objectives

1) *To prepare the acrylamide monomers N-pyren-1-ylacrylamide (PA), N-pyren-1-ylmethacrylamide (PMA), N-(pyren-1-ylmethyl)acrylamide (PMeA) and N-(pyren-1-ylmethyl)methacrylamide (PMeMA).*
2) *To characterize the electronic absorption and emission properties of the monomers, the latter including both steady-state (i.e. spectral) and time-resolved (i.e. fluorescence lifetime) data.*
3) *To determine the feasibility of the photochemical quenching of the monomers by the alternariol toxin in a confined space.*

IV.1. Introduction

As it has been detailed in (*section I.10)*, polycyclic aromatic hydrocarbons, particularly **pyrene** and its derivatives, have served as fluorescence probes in a vast number of different applications due to the sensitivity of their emission to the immediate environment around them [1-3]. For instance, several *solvent polarity scales* have been developed on the basis of the photophysical properties of dissolved (polycyclic) aromatic hydrocarbon molecules and, particularly, unsubstituted pyrene [4]. This application is possible due to the fact that many of such molecules are strongly fluorescent (Φ_{em} > 0.5) and their emission spectrum shows vibronic fine structure bands, the relative intensity of which is dependent on the solvent polarity and molecular structure. The same effect has been employed to study the surface microenvironment of chromatographic stationary phases, surfactant micellization/adsorption, polymer-surfactant interactions, microemulsions, zeolite materials and other organised media. Pyrene *excimer* formation has also been used to characterize macromolecules and their supramolecular assemblies. Therefore,

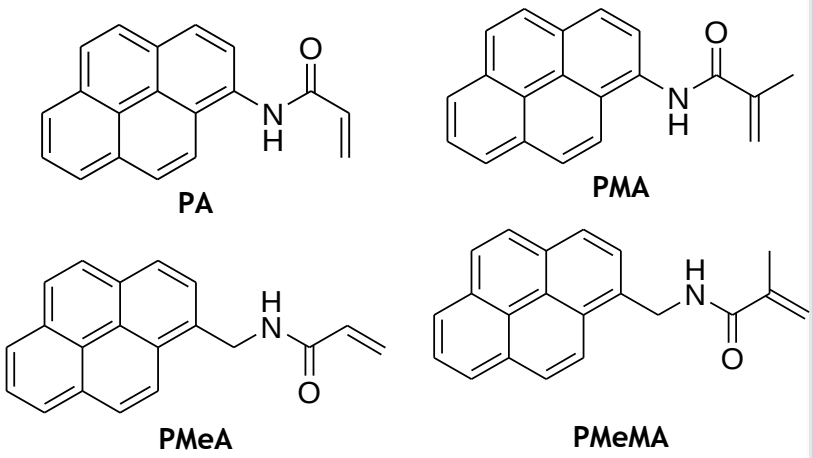

Figure 4.1: Pyrene-labeled acrylamide monomers

pyrene derivatives seem to be apt systems both to investigate the *microstructure* of the binding sites of molecularly imprinted polymers and to develop MIPs to *recognize alternariol* and related polycyclic aromatic toxins by way of donor-acceptor π-π* interactions. The latter has recently been demonstrated by our Group for the first time with the synthesis of a MIP containing disulfonated dihydroxypyrenedimethacrylamide as functional monomer to selectively recognize Diquat (6,7-dihydrodipyrido[1,2-*a*:2',1'-*c*]pyrazinediium) and Paraquat (1,1'-dimethyl-4,4'-bipyridinium) in aqueous samples thanks to the strong monomer (donor)-herbicide (acceptor) and electrostatic interactions in the binding sites [5]. As a part of our ongoing effort to develop analyte-sensitive fluorescent monomers, we set out to explore the possibility of using pyrene-labeled acrylamides to provide signaling features to functional monomers for MIP synthesis. This chapter focuses on the **synthesis** of four (meth)acrylamides Fig. 4.1 containing a fluorescent *pyrenyl* probe, and a thorough **characterization** of their spectroscopic and photophysical properties as a function of the surrounding media. Unfortunately, subsequent synthesis of the corresponding MIPs for alternariol recognition has not been possible within the time frame of this Thesis but will be carried out in our Group shortly. Nevertheless, this section also describes the preliminary testing of their interaction with the Alternariol toxin in a confined space to mimic the interactions taking place with the binding cavities of the MIP.

IV.2. Synthesis of pyrene-labeled acrylamide monomers

While none of the target monomers is new, their synthesis and characterization are ill-described in the literature because most of the information about them appears only in Asian patents, or within papers mainly focused on the corresponding polymers.

The preparation of *N*-pyren-1-ylacrylamide (PA) monomer is barely reported in just two references [6, 7] and neither structural confirmation by spectroscopic data is provided, nor its electronic absorption or emission features are described therein. Similarly, the *N*-pyren-1-ylmethacrylamide (PMA) monomer appears in just two patent documents and a journal reference [8, 9, 10]. Its preparation is reported in 39% yield, and only supporting ^{1}H-NMR and uv-vis absorption data are provided [10]. Surprisingly enough, the latter reference even states that "no fluorescence is observed from the PMA monomer"!

Syntheses of pyrenemethylacrylamide monomers are slightly often reported in the literature. *N*-(Pyren-1-ylmethyl)acrylamide (PMeA) has been found in five references [11-15], but just two

different procedures for its preparation and structural confirmation by spectroscopic methods are reported [14, 15]. Finally, *N*-(pyren-1-ylmethyl)methacrylamide (PMeMA) appears in 5 references, being patents three of them [9, 16-19]. Only the last one describes its synthesis in 64% yield and ^{1}H-NMR characterization together with its microanalytical data.

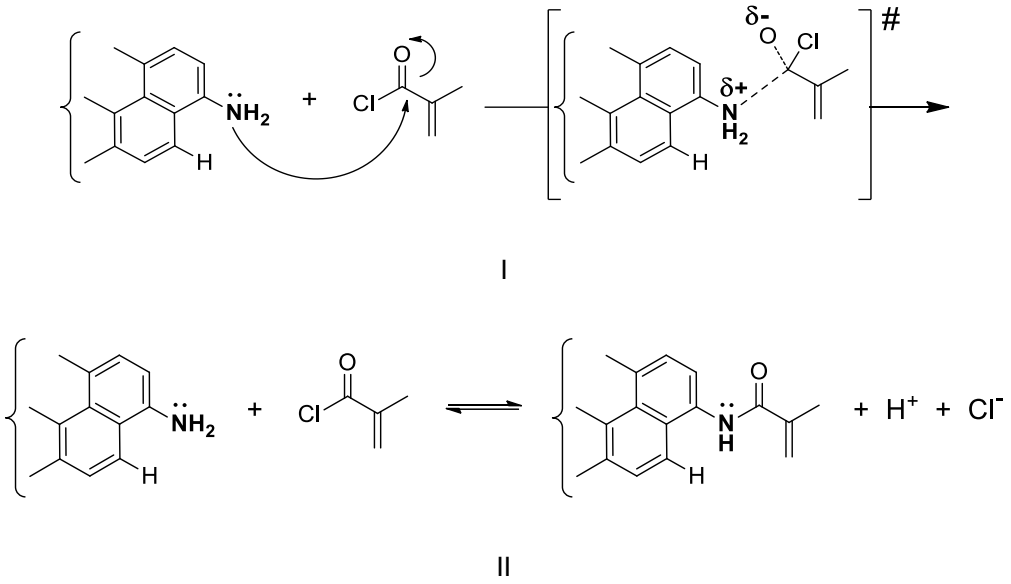

Figure 4.2: Scheme of the rate-limiting step (if irreversible, I) or the nucleophilic attack equilibrium (if reversible, II) in the acylation of 1-aminopyrene with methacryloyl chloride.

In our hands, pyrenylacrylamides PA and PMA have been successfully prepared in ≥60% yield from commercial 1-aminopyrene and the corresponding acyl chlorides (*5.4.1 and 5.4.2*). The use of a more polar solvent medium (acetonitrile–water 95:5 and 98:2 v/v, respectively, optimum ratios after many trials with different amounts) instead of THF (PA [7]) or CH_2Cl_2 (PMA [10]) was strongly beneficial to the reaction chemical yield thanks to acceleration of its rate-determining step (the nucleophilic attack of the sterically-hindered poorly-nucleophilic 1-aminopyrene on the acyl chloride) by preferential solvation of the transition state Fig. 4.2 I, or a shift of the chemical equilibrium towards the products due to more efficient solvation of the latter, if equilibrium is established Fig. 4.2 II.

The chemical yield of the synthesis of pyrenylmethylacrylamides PMeA and PMeMA in toluene (*5.4.3 and 5.4.4*) was always higher than 85% thanks to the higher nucleophilic character and far less steric hindrance of the corresponding pyrenylmethylamine. The purity of all products after recrystallization or column chromatography was assessed from the single spot in TLC and the unique molecular ion observed in ESI-MS.

IV.3. Structural confirmation by spectroscopic data

The **IR spectra** in the solid state (ATR) of the *N*-aryl and *N*-alkyl (meth)acrylamides (*see Annex*) display the characteristic N–H stretching broad band at 3420–3450 cm^{-1}, in addition to the strong amide I (C=O stretching) band at 1651–1661 cm^{-1}. The *N*-pyrenylmethylamides display this absorption at lower wavenumbers (lower energy) than that of the *N*-pyrenylamides due to the important conjugation of the unshared electron pair on the N atom with the aromatic ring that increases the force constant of the C=O bond. The also strong amide II (N–H bending and N–C stretching combination of the C–N–H moiety) band is observed at 1516–1535 cm^{-1} but, in this case, the conjugation of the unshared electron pair on the N atom leads to *N*-pyrenylmethylamides displaying higher frequencies than those of the *N*-pyrenylamides due to the different nature of the absorption. Between the amide, I and amide II bands, the strong C=C stretching band of the acrylamide group is clearly observed at 1608–1630 cm^{-1}, the *N*-pyrenylamides displaying higher wavenumbers as observed for the amide I absorption.

Their **^{1}H-NMR spectra** in DMSO-d_6 (see Annex) show the characteristic N**H** proton at ca. 10.5 and ca. 8.7 ppm for the *N*-pyrenyl- and *N*-pyrenylmethylamides, respectively, due to the slow exchange in this solvent. The signal of the latter amides appears as a triplet due to vicinal coupling with the neighboring methylene group. The coupling is also visible in the corresponding –C**H**$_2$– signal at ca. 5.1 ppm. Interestingly, the restricted rotation around the N–C bond of the amide group is only noticeable in the latter signal of the *N*-pyrenylmethylacrylamide but not in its methacrylamide analogue. The methacrylamides display the characteristic –C**H**$_3$ group at ca. 2 ppm, but its allylic coupling with the alkylidene protons is not resolved. The latter are found at ca. 5.5 and 6 ppm as somewhat broadened singlets due to the unresolved allylic coupling. The neat AMX spin system of the acrylamides is found at ca. 5.9, 6.4 and 6.8 ppm for the *N*-pyrenylacrylamide but at 5.67, 6.22 and 6.35 ppm for the *N*-pyrenylmethylacrylamide, a consequence of the higher electron-withdrawing character of the *N*-arylamide group due to the efficient conjugation of the unshared electron pair on

the N atom with the 1-pyrenyl moiety. The most deshielded proton of the AMX systems is always the *geminal* one with respect to the amide group, while the most shielded proton is that in *cis* position with respect to the geminal, as follows from the clear difference between the *cis* and *trans* ^{3}J coupling of the acrylamide protons (10 and 17 Hz, respectively). Assignment of the protons of the 1-monosubstituted pyrene has not been attempted.

Their **^{13}C-NMR spectra** in DMSO-d_6 (see Annex) are dominated by the characteristic amide **C**=O carbon atom at ca. 164 ppm for the acrylamides and at ca. 168 ppm for the methacrylamides due to the well-documented deshielding α-effect of the methyl group on the alkene carbon shift (a more important effect on the chemical shift of the N–**C**=O than the differential conjugation of the unshared electron pair on the N atom with the aromatic ring). No attempt has been made to unveil the alkene signals "buried" among those from the pyrene carbon atoms, except those from the terminal alkylidene carbon atom of methacrylamides PMeA and PMeMA, readily identified at ca. 120 ppm.

The electrospray ionization **mass spectra** (MS) of the pyrenyl(meth)acrylamides in methanol solution (see Annex) clearly show in all cases the adduct of the intact molecule with a Na^+ atom (the [**M**+Na^+] ion) from the glass container. Interestingly, all MS spectra also display a small abundance peak of the corresponding [$\mathbf{M}_2$+Na^+] ion, due to the formation of relatively long-lived pyrene dimers sandwiching a sodium ion at the significant low pressure within the mass spectrometer (ca. 10^{-5} Torr). These rather stable Na(**A**)$^+$ and Na(**A**)$_2^+$ complexes have recently been rationalized by computational studies for benzene with Na^+, Fe^{2+} and Mg^{2+} ions [20] and experimentally verified for all the alkaline ions by collision-induced dissociation with Xe in a guided ion beam mass spectrometer [21].

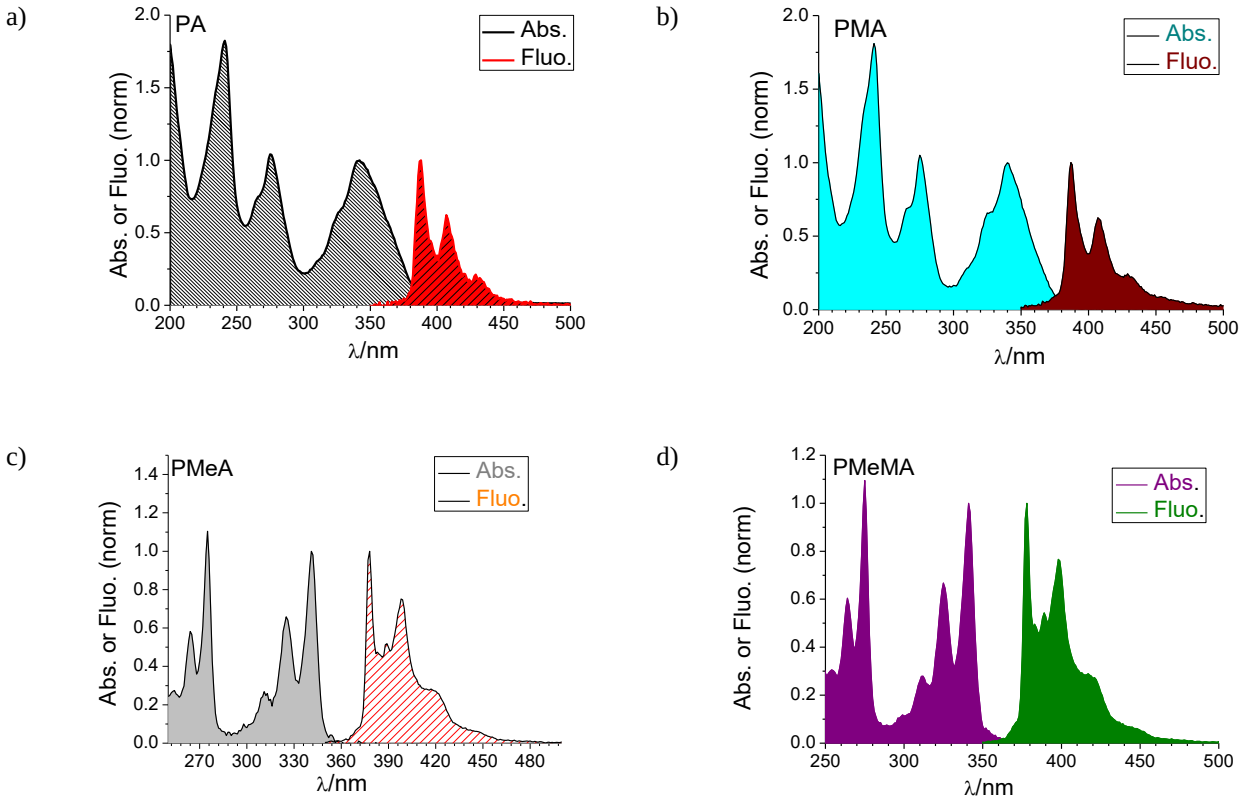

Figure 4.3: Normalized absorption and emission spectra of a) PA; b) PMA; c) PMeA; d) PMeMA (3 µM) in MeCN at (25 ± 1) °C; λ_{ex} = 340 nm; slits 4/4 nm for a and b; 1/1 nm for c and d.

IV.4. UV-vis absorption and fluorescence properties of the pyrenyl(meth)acrylamide monomers

The fluorescent-labelled monomers were characterized by *absorption* and *emission* spectroscopy in order to demonstrate their fit-to-purpose features see Fig. 4.3 and Table 4.1. Their absorption spectra have been recorded at room temperature in acetonitrile and show the typical strong β (also called E_1 or "A") and p (E_2, K or "B") bands of benzene and most monocyclic and polycyclic aromatic hydrocarbons (PAHs) such as pyrene in the uv Fig. 4.4 [22, 23]. These bands show clear vibronic structure even in polar solvents, except if the substituent is strongly conjugated with the aromatic hydrocarbon or if solubility leads to aggregation in solution (see below). The lowest energy α (or "C") weak absorption band of benzene and PAHs ($\varepsilon_{max} \leq 200\ M^{-1}\ cm^{-1}$) is severely forbidden in pyrene due to symmetry reasons and cannot be observed readily because it is buried into the low-energy tail of the much stronger $S_0 \rightarrow S_2$ band. If the solvent absorption permits, pyrene and the

substituted pyrenes also display and additional band (β') at ca. 240 nm, which is the strongest one of the absorption spectrum. [24].

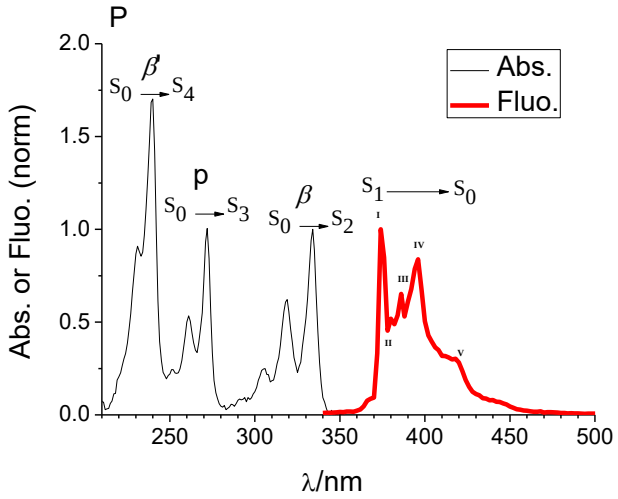

Figure 4.4: Normalized UV/vis-absorption (black) and emission (red) spectra of pyrene in MeCN at (25 ± 1) °C.

The fluorescence spectra of the monomers Fig. 4.3 and Table 4.1 also display vibrational structure, as it is the case for pyrene Fig. 4.4 [25]. The highest intensity band (or "I" band) of the emission spectrum of pyrene in acetonitrile corresponds actually to the $S_1^{(v=0)} \rightarrow S_0^{(v=0)}$ transition and is extremely sensitive to the solvent *polarity* (see below) because it corresponds to a forbidden transition, the intensity of which is enhanced in polar solvents because of the reduction in the symmetry of the pyrene molecule due to the solvent-pyrene interactions [26].

Table 4.1: UV absorption and fluorescence parameters of the pyrenylacrylamide monomers in MeCN; λ_{ex}= 340 nm, at (25 ± 1) °C.

	λ_{abs}^{max}/nm (ε_{max}/ $M^{-1}cm^{-1}$)		λ_{em}^{max}/nm
	p-band	*β*-band	
PA	342 (48.7×10^3)	275 (49.0×10^3)	389
PMA	342 (–)[a]	275 (–)[a]	389
PMeA	341 (37.0×10^3)	275 (38.8×10^3)	378
PMeMA	341 (58.0×10^3)	275 (61.7×10^3)	378

[a] Not determined due to the scarce solubility in this solvent.
[b] Uncertainty: λ ± 1 nm; ε ± 2%.

With regard to their uv-vis absorption and emission spectral features, pyrene derivatives can be classified into two major groups. The first one includes the *pyrene-like* derivatives (exemplified by 1-methylpyrene), where the substituent weakly perturbs the symmetry of the π-electron cloud, and which exhibit roughly the spectroscopic properties of pyrene itself. The second group includes derivatives such as 1-amino-pyrene and 1-pyrenecarboxaldehyde, which have a fundamentally different spectral behavior due to the important inductive and resonance effects caused by those substituents [27]. The investigated *N*-pyrenylmethylacrylamides PMeA and PMeMA of our work belong to the former group, as their absorption and emission features closely match those of pyrene Fig. 4.3 and 4.4, with a small (< 10 nm) bathochromic shift due to the weak electron-releasing effect of the 1-methylene substituent on the pyrene by hyperconjugation with the aromatic π electron cloud. However, the investigated *N*-pyrenylacrylamides PA and PMA belong to the second group, as their absorption and fluorescence bands are significantly distorted with respect to those of the unsubstituted pyrene due to the combination of the (weak) electron-withdrawing inductive and (strong) electron-releasing mesomeric effects of the aminocarbonyl substituent. The important aggregation of these monomers in solution due to their low solubility in the three investigated solvents (acetonitrile, dichloromethane and cyclohexane, see section 4.5), together with the perturbation of the symmetry of the π-electron cloud of pyrene, leads to significant broadening of both the absorption and the emission bands, with partial loss of their fine structure and a red shift of their position.[1] Fig. 4.5 depicts the frontier molecular orbitals (in vacuo) of pyrene, PA and PMeA. The calculations show perturbation of the HOMO in PA due to its amide nitrogen atom (further enhanced by the solvent-solute interactions) but the very close resemblance of the pyrene and PMeA orbitals, both of which determine the observed electronic absorption features of the investigated 1-substituted pyrenes.

The molar absorption coefficients (ε) of the $S_0 \rightarrow S_2$ and $S_0 \rightarrow S_3$ transitions Table 4.1 of PA and PMA in acetonitrile are smaller than those of pyrene and PMeMA as a consequence of the n-π* contribution to those (forbidden) transitions in PA and PMA, compared to their pure π-π* character in PMeA and PMeMA Fig. 4.5.

[1] Moreover, the very low fluorescence quantum yield of PA and PMA (see below) requires the use of wider slits in the emission monochromator that additionally contribute to the loss of resolution.

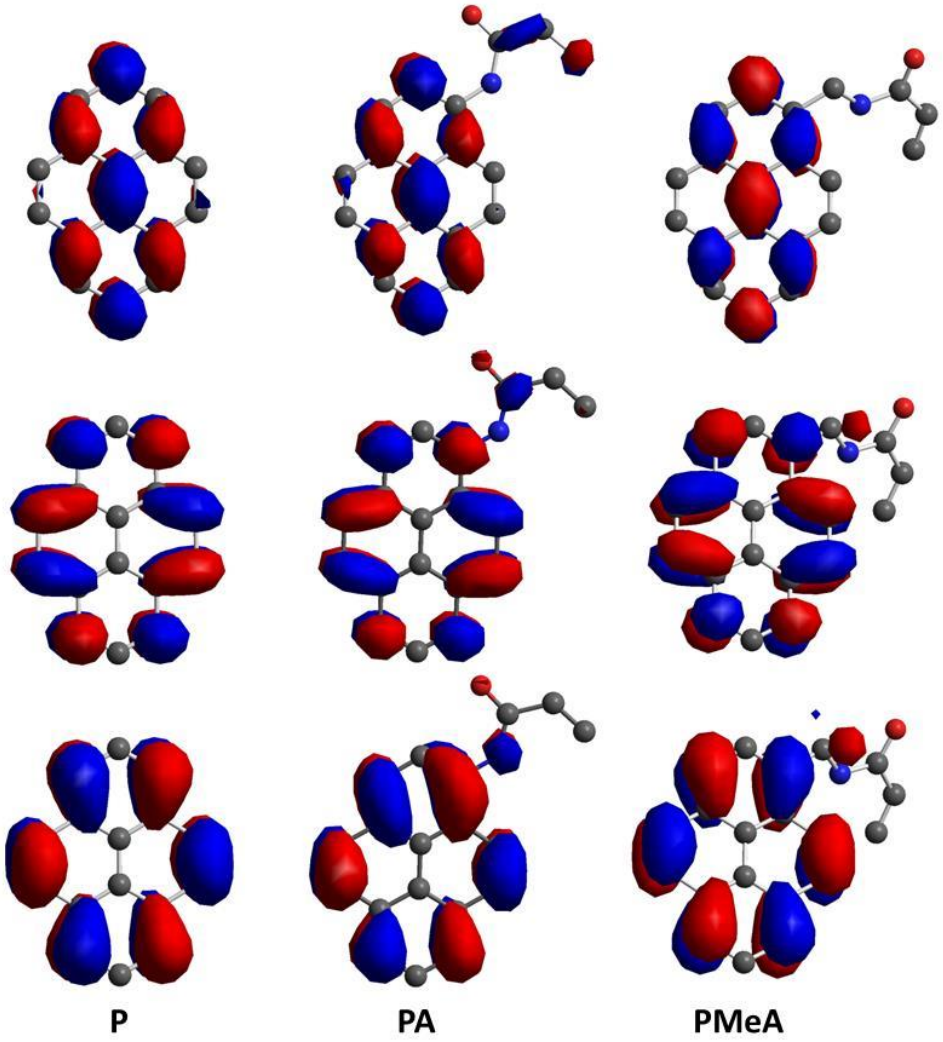

Figure 4.5: Contour plots of the HOMO (bottom), LUMO (center) and LUMO+1 (top) molecular orbitals of pyrene (**P**), *N*-pyren-1-ylacrylamide (**PA**) and *N*-(pyren-1-ylmethyl)acrylamide (**PMeA**). The 3-D structures of these compounds have been modeled in vacuo by energy minimization (MOPAC, AM1 force field) using Chem3D Ultra 7.0 (CambridgeSoft, MA) software, and the energies of the molecular orbitals and their surfaces have been calculated with the same software.

Taking into account the almost identical position of the absorption maxima of the four investigated pyrenyl(meth)acrylamides, the larger (apparent)[2] Stokes shift displayed by the emission of PA and PMA (46 nm), Fig. 4.3 and Table 4.1, compared to those observed for PMeA and PMeMA (37 nm) and pyrene itself 40 nm, Fig. 4.3, is a consequence of the substantially greater stabilization of the S_1

[2] We call it "apparent" because we are measuring the separation between the $S_0 \rightarrow S_2$ absorption and the $S_1 \rightarrow S_0$ emission bands as the $S_0 \rightarrow S_1$ transition cannot be observed in the spectra (see text above).

excited state of the *N*-pyrenylacrylamides by the polar solvent (acetonitrile). This result demonstrates the efficient delocalization of the unshared electron pair on the nitrogen atom of the amide group in the emissive excited state of the pyrene moiety, in contrast to the pyrenylmethylacrylamides where the insertion of the methylene group between the pyrene and amide moieties prevents the electron delocalization and, therefore, the polarity of the emissive state of the probe is considerably lower and so is stabilization by the acetonitrile.

The fluorescence **quantum yield** (Φ_F) and **lifetime** (τ) of the four pyrene-labelled monomers were measured in acetonitrile due to their higher solubility in this solvent, compared to that in hydrocarbons or chlorinated hydrocarbons, both under air and in argon-saturated solution, taking into account the high sensitivity to molecular oxygen of the excited state of pyrene [28]. The results are collected in Tables 4.2 and 4.3.

Table 4.2: Fluorescence quantum yields (Φ_F) of pyrene (**P**) and the pyrenyl-acrylamide monomers at 293 K in argon-saturated organic solvents; λ_{ex} = 343 nm; PMeA and PMeMA with 2/2 nm slits; PA and PMA with 1/1 nm slits; T = (25 ± 1) °C.[a]

	Φ_F									
	P		PA		PMA		PMeA		PMeMA	
	AIR	Ar	AIR	Ar	AIR	Ar	AIR	Ar	AIR	Ar
MeCN	–	0.62[b]	0.003	0.004	0.016	0.028	0.061	0.90	0.066	0.95
DCM	–	0.38[b]	0.007	0.009	0.016	0.020	0.135	0.63	0.136	0.66
CH	0.29[c]	0.65[c]	0.004	0.006	0.007	0.010	0.054	0.77	0.065	0.88

[a] λ_{ex} = 340 nm; quinine sulfate in 0.5 M H_2SO_4 was used as the standard (Φ_f = 0.510; *n* = 1.336), except for pyrene (see literature references); uncertainty of the measurements: ± 10%.
[b] [29, 30].
[c] [31].

The *N*-pyrenylmethylacrylamides PMeA and PMeMA are more fluorescent than the unsubstituted pyrene (Φ_F = 0.62 ± 0.07) [28], and significantly brighter (up to 45-fold) than their corresponding *N*-pyrenyl-acrylamides [32].[3] A possible explanation for this result might lie on the mixing of the n-π* and π-π* transitions for the lowest excited state of the latter compared to the pure π-π* nature of the same excited state of pyrene and alkyl-substituted pyrenes. Therefore, if a methylene group is

[3] Surprisingly enough [18], reports the fluorescence quantum yield of *N*-pyren-1-ylpropionamide (PPA) to be 0.35, almost identical to those of pyrene and alkylpyrenes. This result strongly disagrees with our observation of the much weaker emission of PA and PAA, and the literature report describing the lack of fluorescence of PMA [10]. The only explanation might be contamination of their product with pyrene, yet the fluorescence lifetime of PPA reported by those authors (10.8 ns, 84%) is in agreement with our measurements of PA and PMA (see below).

introduced between the nitrogen atom and the pyrene moiety, the emission quantum yields come back to the "normal" high values of pyrene. Some perturbation of the symmetry of the π-electron cloud of pyrene in the excited state of the pyrenylmethylacrylamides (*see also section 4.5*) would account for their higher fluorescence compared to the unsubstituted pyrene. In any case, the very high emission quantum yields of PMeA and PMeMA makes these monomers extremely suitable for fluorescent MIPs development provided we are able to place them exclusively in the analyte-binding cavities and undergo a quenching interaction with the bound analyte [33].

The fluorescence quantum yield of pyrene is extremely sensitive to the presence of O_2. Actually, embedded in gas-permeable polymer thin films (e.g. polydimethylsiloxane), it was one of the first indicator dyes used for fabrication of optical O_2 sensors due to its much longer excited state lifetime than typical fluorophores (see below) [34], most often as pyrenebutyric acid for solubility reasons. Table 4.2 collects the emission quantum yields of the synthesized pyrene-labelled monomers in argon-saturated and in air-equilibrated solutions in acetonitrile. Due to the very special electronic configuration of triplet ground state molecular oxygen ($^3O_2$), energy transfer quenching of *both* excited singlet and triplet states is spin-allowed, in contrast to many competing deactivation processes [35]. Moreover, the very small size of the O_2 molecule allows for particularly rapid diffusion in solution making quenching of excited states by this gas a highly competitive process in air-equilibrated solution, with a quenching rate constant close to or at the diffusion limit (2.7×10^{10} to 4.3×10^{10} $M^{-1}s^{-1}$ in acetonitrile) [36]. In the case of quenching of S_1 states by $^3O_2$, an enhanced intersystem crossing (ISC) pathway to T_1 (or, sometimes, T_2) may occur, together with enhanced internal conversion (IC) processes to the aromatic hydrocarbon ground state (S_0). Both quenching types lead to either of the three lowest states of the O_2 molecule, namely, its ground state ($^3\Sigma_g^-$) or its $^1\Delta_g$ or $^1\Sigma_g^+$ excited states. The quenching by $^3O_2$ has been considered to occur through *exciplex* formation in the encounter complex $^3(^1P^*,^3O_2)$.

The enhanced ISC deactivation routes have been shown to predominate in most cases and, particularly, the formation of the T_1 state of the aromatic hydrocarbon and ground-state $O_2(^3\Sigma_g^-)$ has been shown to be the dominant one [35]. However, the unity efficiency of T_1 state generation in the fluorescence quenching by O_2 in non-polar solvents decreases with increasing solvent polarity for polycyclic aromatic hydrocarbons and amounts to only 0.6 for pyrene in acetonitrile, pointing out

that the interaction between S_1 and ground-state O_2 leading to the T_1 of the hydrocarbon, is charge-transfer in nature in polar solvents [37].

Taking into account the dissolved O_2 concentration in acetonitrile (1.9 mM at 1.013 bar atmospheric pressure) [38] and the fluorescence lifetime of the corresponding pyrene-labelled monomers in argon-saturated solution Table 4.3, and assuming the collisional quenching mentioned above, the Stern-Volmer equation Eq. 4.1 [39] provides O_2 quenching constants of 2.9×10^{10} and 3.0×10^{10} $M^{-1}s^{-1}$ for PMeA and PMeMA at 960 ± 10 mbar, respectively, in agreement with the literature values for aromatic hydrocarbons in this solvent (see above) [40].

$$\frac{\Phi_{F0}}{\Phi_F} = 1 + k_q \tau_0 [O_2] \qquad (4.1)$$

The much smaller emission quantum yields of PA and PMA, both in aerated and argon-saturated acetonitrile Table 4.2, prevent an accurate calculation of the O_2 quenching rate constants but their values lie also at or very near the diffusion limit taking into account their fluorescence lifetimes Table 4.3.

The **fluorescence lifetimes** of all four pyrene-substituted monomers have been measured at a micromolar concentration in acetonitrile, both in air-equilibrated and O_2-free solutions Table 4.3. In spite of choosing this solvent, the solubility of PA is not complete and its decay had to be fitted to a double-exponential function with a ca. 4% contribution of a longer-living excited species both in the air- and Ar-saturated solution. We attribute the latter to ground-state PA aggregates which undergo O_2 quenching at a ca. four times slower pace than the non-aggregated species due to partial self-protection from the quencher [32].[4]

[4] The observation of a biexponential fluorescence decay in *N*-pyren-1-ylpropionamide (PPA) and pyrenemethylacrylamides has been attributed by Yao et al. to the existence of the *stereoisomers* in solution, with lifetimes from 0.5 to 20 min, due to the significant double bond character of the **N–C** bond of amides. [18] However, we strongly disagree with this explanation on the following grounds: (i) if it is caused by the s-*Z*/s-*E* equilibrium of amides, it should disappear if the *N*-amide group is "disconnected" from pyrene by a methylene group, because then the excited state is exclusively localized on the pyrene moiety Fig. 4.4, yet we also observe biexponential decay for the pyrenemethylamides PMeA in dichloromethane, the same solvent used by Yao et al.; (ii) we have not observed biexponential decay for PMA in acetonitrile, the best solvent of all those investigated, but we did observe such fluorescence decay for PA Table 4.3. Therefore, we must attribute the non-exponential fluorescence decay to the presence of pyrene aggregates in solution, which are subject to different influence of the solvent than the isolated molecules in solution (*see section IV.5*).

Table 4.3: Fluorescence lifetime (τ) of the pyrenyl-acrylamide monomers in air-equilibrated and argon-saturated solutions at (25 ± 1) °C, and O_2 quenching rate constants (k_q^{O2}).[a]

	MeCN			DCM			CH		
	τ_{air}/ns[b]	τ_{Ar}/ns[b]	$k_q^{O_2} \times 10^{-10}$ /$M^{-1}s^{-1}$ [c]	τ_{air}/ns[b]	τ_{Ar}/ns[b]	$k_q^{O_2} \times 10^{-10}$ /$M^{-1}s^{-1}$ [c]	τ_{air}/ns[b]	τ_{Ar}/ns[b]	$k_q^{O_2} \times 10^{-10}$ /$M^{-1}s^{-1}$ [c]
PA	11.7 (97%) 36 (3%)	14.5 (95%) 63 (5%)	0.92 (0.7)	8.6 (92%) 32 (8%)	10.9 (83%) 46 (17%)	1.2 (0.6)	6.8 (91%) 21 (9%)	9.4 (71%) 71 (29%)	1.8 (1.5)
PMA	8.1	14.7	3.1	9.7 (97%) 40 (3%)	11.5 (98%) 74 (2%)	0.78 (0.6)	8.0 (95%) 30 (5%)	10.2 (85%) 79 (15%)	1.2 (0.9)
PMeA	17.1	266	3.1	31.2 (98%) 58 (2%)	148 (90%) 235 (10%)	1.2 (0.6)	20.8	313	2.0
PMeMA	17.2	254	3.0	30.4	144	1.3	21.3	283	1.9

[a] Fluorophore concentration: 1.0–3.0 x 10^{-6} M; λ_{exc} = 343 nm (1-ns pulse LED at 500 KHz); λ_{em} = 400 nm; uncertainty of the lifetimes: ± 2% for single-exponential decays, ± 3% and ± 5% for the shorter-lived and longer-lived components of the double-exponential decays, respectively. Uncertainty of the rate constants: ± 10% for those obtained from single-exponential decays or from the shorter-lived component of the double-exponential decays; ± 30% for those obtained from the longer-lived component of the double-exponential decays. The dissolved O_2 concentrations at 760 Torr atmospheric pressure, 1.9 mM (MeCN), 2.2 mM (DCM) and 2.4 mM (CH), [38] have been corrected for the current atmospheric pressure at the altitude of our laboratory (658 m OSL) when each measurement under air was performed. In all cases, the corresponding fits were better than χ^2 1.1.

[b] In the case of 2-exp decay profiles, $I_F(t) = A + B_1\exp(-t/\tau_1) + B_2\exp(-t/\tau_2)$, the values in parenthesis accompanying the lifetime data represent the contribution to the overall fluorescence from each component: $\%_i = B_i\tau_i / \sum_i B_i\tau_i$

[c] Values in parenthesis correspond to the quenching rate constants calculated from the longer-lived component in the case of the 2-exp decays.

Consistently with the large differences in their fluorescence quantum yields due to the effect of the corresponding substituent, the emission lifetimes of PMeA and PMeMA in the absence of dissolved O_2 (266 and 254 ns, respectively) are much longer than those of PA and PMA (14.6 ns). The faster deactivation of the S_1 excited state of the PA and PMA monomers is caused by the more important contribution of the internal conversion deactivation pathway than in the pyrenylmethyl analogues due to the smaller S_1–S_0 distance in the former (λ_{em}^{max} of 389 nm vs. 378 nm), Table 4.1, together with the intramolecular charge-transfer character of the lowest excited state of PA and PMA by delocalization of the unshared electron pair of the *N*-amide nitrogen atom on the polycyclic aromatic system.

IV.5. Solvent effects on the absorption and fluorescence spectra of the pyrenyl(meth)acrylamide monomers

The spectral features of pyrene are extremely sensitive to the microenvironment around the probe: it displays an ensemble of absorption and emission peaks that report on the *polarity* of the *probe microenvironment* (particularly the fine structure of the fluorescence band), and an additional emission band at longer wavelengths (~ 470 nm), at and above mM concentrations (in cyclohexane), the appearance of which reflects the presence of another pyrene molecule in spatial *proximity* (< 0.5 nm, i.e., contact is required for the *excimer* formation) [41, 22]. Moreover, the high absorption coefficients of pyrene make it useful to investigate the microenvironment around the probe even at very low concentrations [42]. This would be the case when using pyrene-labelled *functional* monomers for preparing fluorescent MIPs to detect low concentrations of particular analytes.

In general, the vibrational components of the fine structure of a weak (i.e. *forbidden*) electronic transition are expected to show different intensities under the perturbation caused by different solvents [43]. However, this phenomenon can seldom be observed in the spectrum of electronically *allowed* transitions. Nevertheless, the vibrational structures of the fluorescence and absorption spectra of pyrene are significantly modified in various solvents, and this effect can be ascribed to the same well-known phenomenon called the "*Ham effect*" in benzene [44]. The latter consists in the appearance of a symmetry-forbidden 0-0 progression within the ${}^1A_{1g} \rightarrow {}^1B_{2u}$ band (i.e., the 260 nm or α band of benzene mentioned in section 4.4), influenced by dispersion forces between benzene and the solvent molecules, particularly the most polar ones. The effect also appears in PAHs such as naphthalene, phenanthrene and **pyrene**, among others, both within the lowest energy absorption band and in its mirror emission band [45]. Individual features in the *emission* band of pyrene change according to the polarity of its local medium. This polarity dependence is usually expressed in terms of the I(I)/I(III) **emission bands ratio**, where the I band corresponds actually to the $S_1^{(v=0)} \rightarrow S_0^{(v=0)}$ transition and is strongly sensitive to the solvent polarity, but the III band corresponding to the $S_1^{(v=0)} \rightarrow S_0^{(v=1)}$ transition is not. The relative band intensities in the pyrene fluorescence response to the solvent polarity are determined by the extent of vibronic coupling between the weakly allowed first excited singlet state and the strongly allowed second excited singlet state [28]. If vibronic coupling is the operative mechanism for the observed emission dependency on solvent polarity, then a PAH with a relatively forbidden $S_0 \rightarrow S_1$ transition and a strongly allowed $S_0 \rightarrow S_2$ transition, should exhibit a solvent polarity dependence, as it has also been found experimentally for benzene, coronene, pyrene

and benzo[e]pyrene, among other polycyclic hydrocarbons. The major contribution to the enhancement of the relevant vibronic band intensities arises from *specific* solute-solvent dipole-dipole couplings, although other effects due to π-orbital interactions between solute and solvent and the effect of the bulk dielectric constant of a solvent cannot be ruled out [46]. The fluorescence vibronic bands intensity ratio $I(\mathrm{I})/I(\mathrm{III})$ has even allowed to build an empirical *solvent polarity scale* (or "*py* scale") based on the pyrene probe [47].

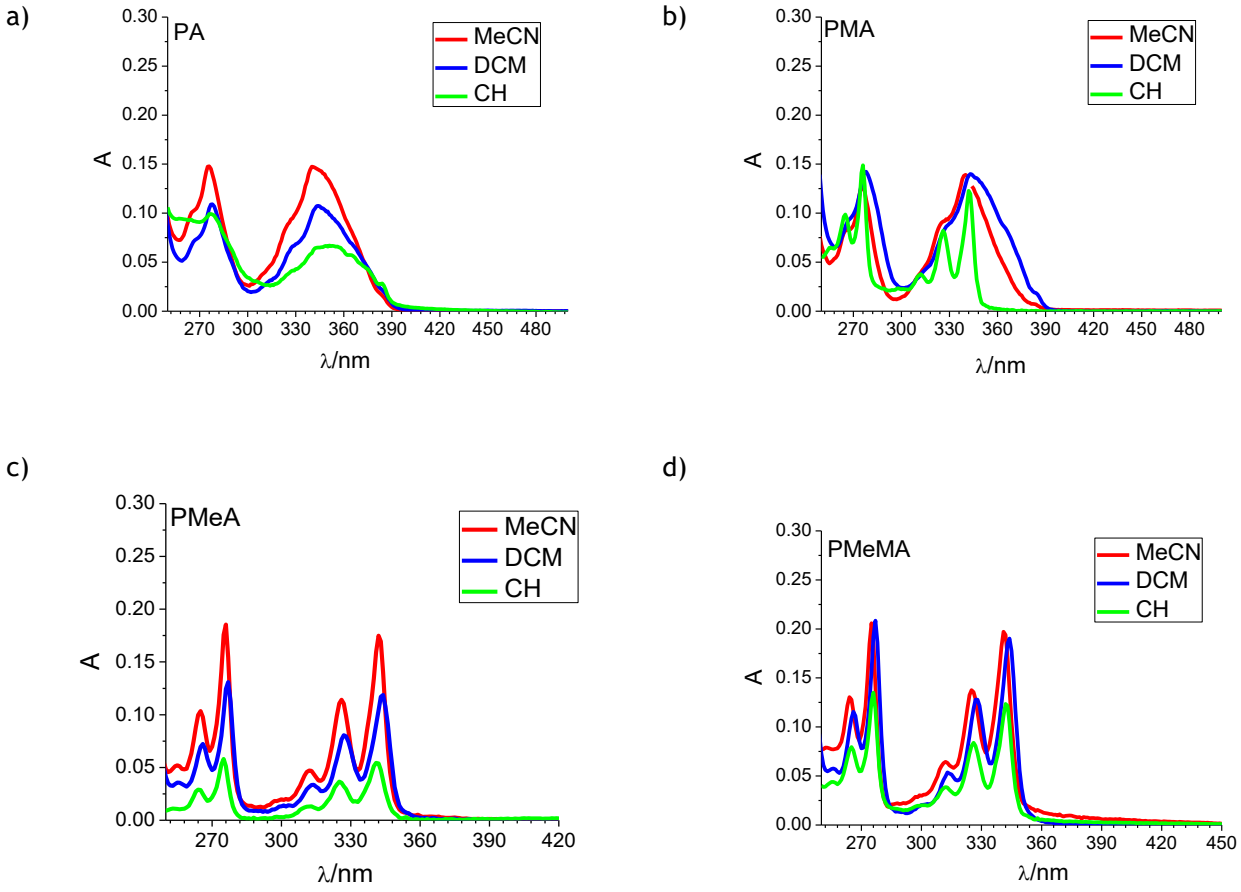

Figure 4.6: UV/vis absorption spectra of the pyrenyl-acrylamide monomers (10 µM) in acetonitrile (MeCN), dichloromethane (DCM) and cyclohexane (CH): a) PA; b) PMA; c) PMeA; d) PMeMA, at (25 ± 1) °C.

Fig. 4.6 depicts the absorption spectra of the pyrenyl-acrylamide monomers in acetonitrile (MeCN), dichloromethane (DCM) and cyclohexane (CH). The low solubility of PA in the three solvents, and of PMA and PMeA in DCM and CH, precludes resolution of the fine vibronic structure of their absorption bands due to aggregation of the pyrene moiety. At the same time, the aggregation phenomenon "breaks" the pyrene symmetry (see section 4.4), leading to a strong enhancement of the

very weak absorption α band above 350 nm in PA, PMA and PMeA. The much higher solubility of PMeMA determines its much similar electronic absorption features to those of the unsubstituted pyrene Fig. 4.3 [28], so that the α band remains hidden by the strong p band in all the investigated solvents.

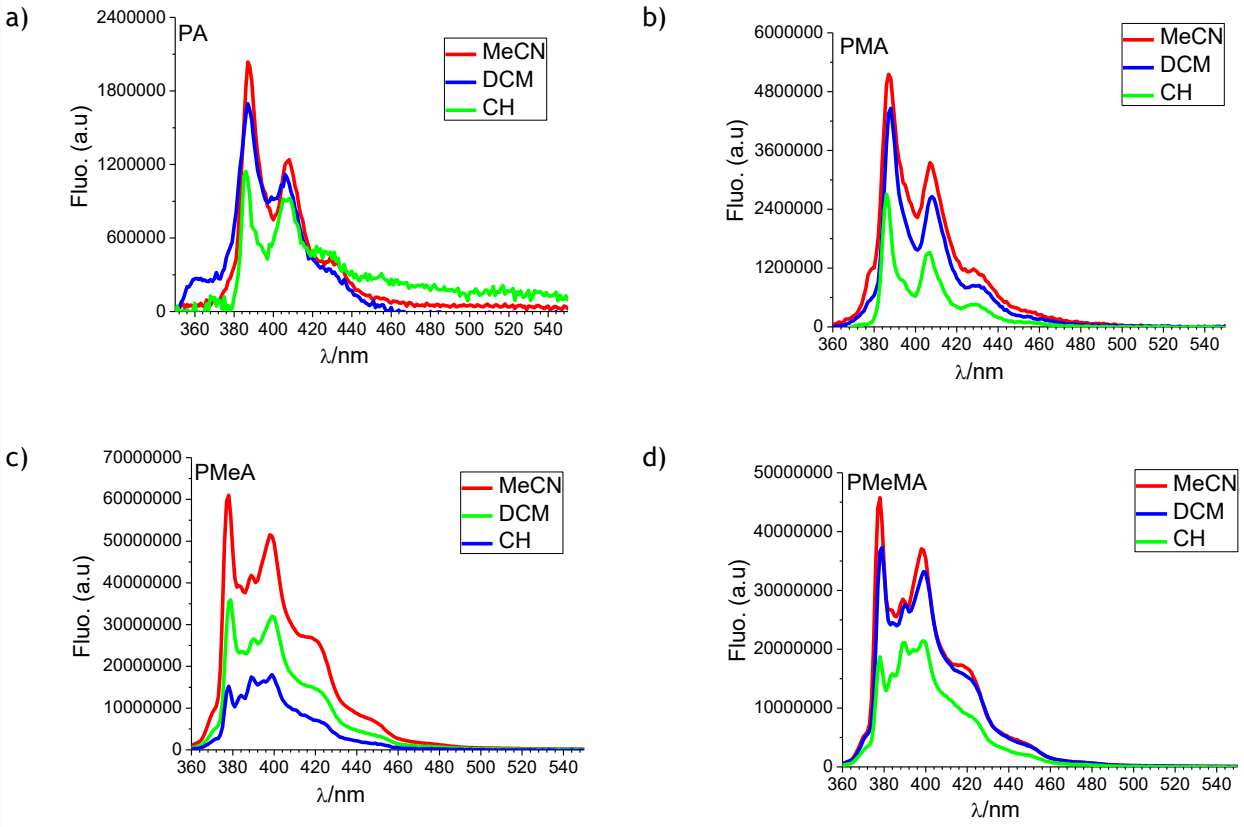

Figure 4.7: Fluorescence spectra of the pyrenyl-acrylamide monomers (10 µM) in acetonitrile (MeCN), dichloromethane (DCM) and cyclohexane (CH): a) PA and b) PMA with slits 1-1 nm; c) PMeA and d) PMeMA, with slits 2-2 nm; λ_{ex} = 340 nm, at (25 ± 1) °C.

The fluorescence spectra of the four pyrenyl-acrylamide monomers prepared in this work, in the three solvents of very different polarity (MeCN, DCM and CH), are shown in Fig. 4.7 and the relative intensities of the I and III bands of these spectra are collected in Table 4.4. The pyrene fluorescence I(I)/I(III) values in the same solvents under similar conditions have been taken from the literature for the sake of comparison [48]. The slits used to measure the fluorescence of PA and PMA are not the optimum to determine the exact I(I)/I(III) ratios [49]; unfortunately, their very low fluorescence

quantum yields prevent measurements with narrower slits without increasing the probe concentration up to levels beyond their solubility in those solvents.

The $I(\text{I})/I(\text{III})$ ratios for the PA and PMA monomers do not seem to follow any correlation with the solvent polarity either due to the strong electronic coupling of the *N*-amide substituent with the aromatic moiety and/or as a consequence of their low solubility in all the investigated solvents. The latter introduces a population of aggregated pyrene molecules with unknown composition but probing an environment very different from the bulk solvent. However, the PMeA and PMeMA monomers behave as excellent probes of the polarity of the microenvironment around them Table 4.4, yet with a slightly lower sensitivity than the unsubstituted pyrene. Therefore, *they might be used to investigate the polarity of the binding sites in a MIP* made with any of them as a functional monomer to recognize the target analyte. Such an approach has been reported in the literature to study the polarity of microheterogeneous media (micelles, vesicles, bilayers,…) [1, 50-52] and polymer materials [53, 42], and biopolymers [54-56].

Table 4.4: Vibronic bands intensity ratio ($I(\text{I})/I(\text{III})$) of the fluorescence of pyrene (**P**) and the pyrenyl-acrylamide monomers Fig. 4.6 (10 μM) in acetonitrile (MeCN), dichloromethane (DCM) and cyclohexane (CH) solution; λ_{ex}= 340 nm; PMeA and PMeMA with slits 2/2 nm; PA and PMA with slits 1/1 nm, at (25 ± 1) °C.[a]

	Peak intensities				
	P[b]	PA	PMA	PMeA	PMeMA
	$I(\text{I})/I(\text{III})$[a]				
MeCN	1.79	2.44	1.79	1.45	1.61
DCM	1.35	1.89	2.04	1.37	1.35
CH	0.58	2.13	3.03	0.87	0.88

[a] λ_{ex} = 340 nm; uncertainty: ± 5%
[b] λ_{ex} = 338 nm; slits 0.5/0.5 nm [57].

The fluorescence **lifetimes** of the four pyrenyl-acrylamide monomers investigated in this work, measured at 400 nm upon 1-ns wide LED excitation at 340 nm in the three selected solvents of very different polarity (MeCN, DCM and CH), are collected in Table 4.3. Representative emission decays are depicted in Figs. 4.8 and 4.9, both in the absence of O_2 and in the presence of dissolved air at ambient pressure. No scattering of the excitation uv light was observed for any of the samples. If the probe solubility in the solvent is enough (MeCN is the best solvent among the three selected ones), the decay profiles are strictly *exponential*, i.e., only one excited electronic state contributes to the observed steady-state emission spectrum; however, if the solubility of the pyrenyl-acryamide

monomer is limited (as inferred from the time it takes to dissolve and some control measurements performed at further dilution not shown), the fluorescence decays could only be successfully fitted to a double-exponential function Eq. 4.2. In these cases, the minor longer-lived component of the latter Table 4.3 must be assigned to the decay of pyrenyl-acrylamide aggregates. In the latter case, the pyrene moieties in the aggregates do not probe the polarity of the bulk solvent molecules of the solvation shell, but instead they are surrounded by a significant number of other pyrene molecules providing a more hydrophobic environment than the expected one.

$$I_F(t) = A + B_1\exp(-t/\tau_1) + B_2\exp(-t/\tau_2) \qquad (4.2)$$

Generally, the fluorescence lifetime of pyrene is longer in non-polar media (hydrocarbons) than in polar solvents (MeCN, dimethylformamide, dimethylsulfoxide) [28]. We have also observed the same result when comparing the emission lifetimes of PMeA and PMeMA in deoxygenated cyclohexane (ca. 300 ns), Table 4.3 to those measured in deoxygenated acetonitrile (ca. 260 ns), Table 4.3. Karpovich and Blanchard have shown that pyrene displays a strong (direct) correlation between the radiative decay constant ($k_r^{0\text{-}0}$) and the solvent polarity [28]. Therefore, the fluorescent excited state lifetime is expected to decrease with increasing solvent polarity, because the non-radiative decay constant does not display any dependence with the solvent polarity [28]. The reason behind such decrease of the emission lifetime with the solvent polarity is the increased efficiency of vibronic coupling between the closest lying electronic states (0-0) in polar solvents due to solvent dipole-solute induced dipole interactions. The dipolar nature of the solvent medium determines the extent to which the formation of an induced dipole moment is formed by vibrational distortion(s) of the nuclear coordinates of the pyrene moiety. Dichloromethane and other chlorinated solvents are an anomaly in the general behavior (we have measured a fluorescence lifetime of only 145 ns for PMeA and PMeMA under the same conditions) probably due to the very high refractive index of these solvents, in line with the observations of other authors [28].

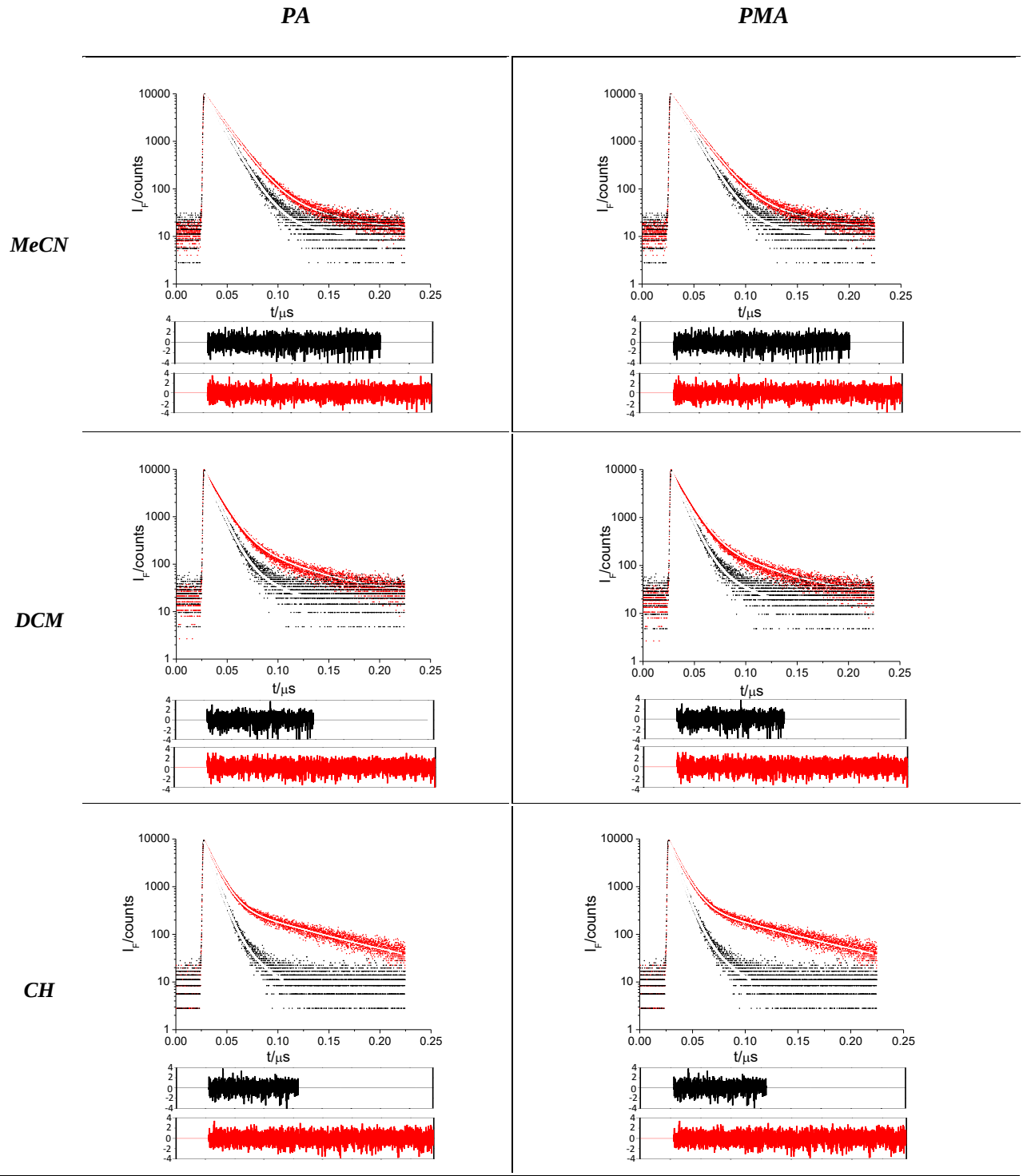

Figure 4.8: Fluorescence decays of PA and PMA in acetonitrile (MeCN), dichloromethane (DCM) and cyclohexane (CH) solution (black, air-equilibrated; red, Ar-saturated). The bottom curves represent the weighted residuals of the fit of the experimental points to a single- or bi-exponential decay function (white lines), λ_{ex} = 343 nm (Horiba NanoLED-340), λ_{em} = 400 nm, at room temperature.

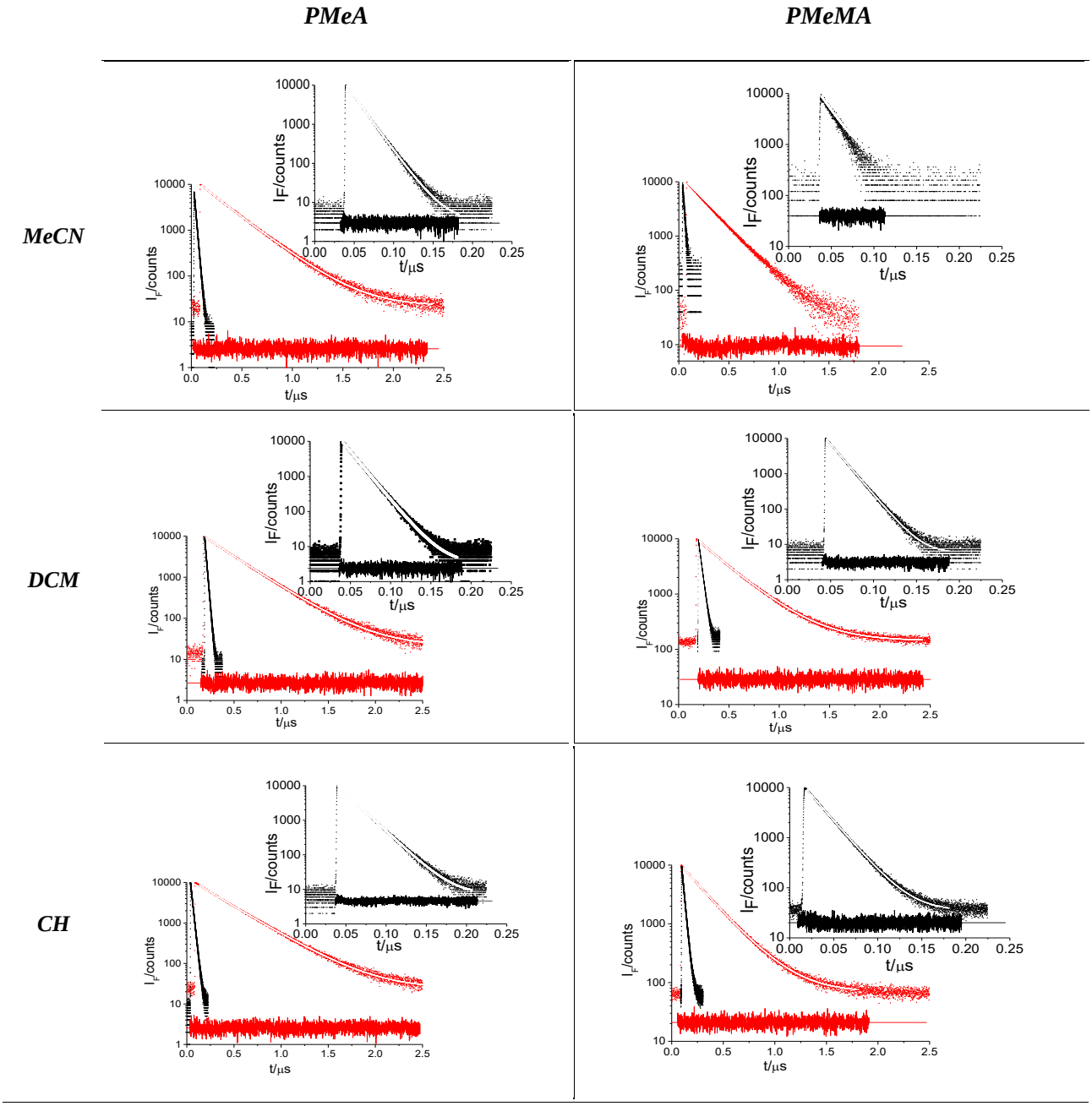

Figure 4.9: Fluorescence decays of PMeA and PMeMA in acetonitrile (MeCN), dichloromethane (DCM) and cyclohexane (CH) solution (black, air-equilibrated; red, Ar-saturated). The bottom curves represent the weighted residuals of the fit of the experimental points to a single- or bi-exponential decay function (white lines), λ_{ex} = 343 nm (Horiba NanoLED-340), λ_{em} = 400 nm, at room temperature.

The lifetimes of PA and PMA are exceptionally low in all solvents compared to those of PMeA and PMeMA under the same conditions Table 4.3, and do not follow the same variation with the solvent polarity than those of the pyrenemethyl(meth)acrylamides. The conjugation of the unshared electron pair of the amide N-atom with the pyrene moiety (*see section IV.4*) in PA and PMA enables a competing intramolecular charge-transfer (ICT) process in their fluorescent excited state which dramatically decreases the emission lifetime with respect to PMeA and PMeMA. This ICT process is favored in polar solvents because of the stabilization that these solvents impart to the charge-separated state. The latter is "decoupled" from the ground state of the molecule, so that it is known to be longer-lived than the vertical excited state [58]. Therefore, the fluorescence lifetime of the *N*-(pyrenyl)acrylamides is longer in acetonitrile (ca. 15 ns), Table 4.3 than in cyclohexane (ca. 10 ns), Table 4.3. The observed broadening of the emission spectra of PA and PMA, compared to those of PMeA and PMeMA Fig. 4.7, lends additional support to the ICT character of the excited state of the former.

IV.6. Effect of dissolved oxygen on the fluorescence features of the pyrenyl(meth)-acrylamide monomers in solution

As we have introduced above (see *section IV.4*), molecular oxygen is an excellent quencher of the lowest-lying electronic excited states or organic molecules. Both the fluorescence quantum yield Table 4.2 and lifetime Table 4.3 of the *N*-pyrenylamides are extremely sensitive to the presence of O_2 in all the solvents we have tested. The O_2 quenching rate constants, k_q^{O2}, calculated from the O_2 solubility in the different solvents at atmospheric pressure Table 4.3, the emission lifetimes in the absence of the quencher and under air (τ_{Ar} and τ_{air}, respectively), Table 4.3, and the Stern-Volmer Eq. 4.1 are dependent on the solvent, but *identical for all the pyrenyl(meth)acrylamides* in the same solvent: 3.0×10^{10} L mol^{-1} s^{-1} in acetonitrile (MeCN), 1.9×10^{10} L mol^{-1} s^{-1} in cyclohexane (CH), and 1.2×10^{10} L mol^{-1} s^{-1} in dichloromethane (DCM). This identity is a signature of diffusion-limited reactions [59]. The somewhat lower values found for PA in MeCN, PMA in DCM and PMA in CH Table 4.3 are due to the small variation the fluorescence lifetime of *N*-pyrenylamide monomers undergoes in the presence of O_2 because of their short values (9–14 ns in O_2-free solutions), together with the larger uncertainty of these lifetimes due to the need of using a bi-exponential function to fit their fluorescence decays (*see section IV.4*). Nevertheless, in spite of the larger uncertainty of the longer-lived components of the bi-exponential decays (i.e. those corresponding to the *aggregated*

pyrenylamides), the latter show a ca. 25–50% smaller O_2 quenching rate constant than the corresponding free fluorophores Table 4.3. The less efficient O_2 quenching is due to the protection that the aggregates impart to the inner-dwelling excited states. The O_2 quenching rate constants calculated from the fluorescence quantum yield data Table 4.2 are similar and follow the same trends than those calculated from the emission lifetimes, albeit with a larger uncertainty for PA and PMA due to their very low fluorescence quantum yields and the associated difficulty in obtaining accurate measurements from the (Parker & Reeves) relative method of comparison with a fluorescence quantum yield standard emitting in the same region (*see Experimental section V*) [60].

Due to the *diffusion-controlled* nature of the O_2 quenching reaction with the fluorescent excited state of the investigated pyrenylamides, their rate constants should be proportional to the diffusion coefficient of O_2 (D) in each particular solvent, the magnitude of which varies with the T/υ ratio, being T is the sample temperature and υ is the solvent kinematic viscosity Eq. 4.3, (Smoluchowski equation of the diffusion-limited rate constants; $\upsilon = \eta/\rho$, where η the solvent viscosity and ρ its density) [59, 1].

$$k = \frac{8RT}{3000\upsilon}\frac{pa}{b} \qquad (4.3)$$

In Eq. 3.4, R is the universal gas constant, p is the reaction probability per collision (usually assumed to be equal to unity), and a and b are the radii of the reaction partners.

The measured O_2 quenching rate constants in cyclohexane (1.9×10^{10} L mol^{-1} s^{-1}) and in acetonitrile (3.0×10^{10} L mol^{-1} s^{-1}), Table 4.3 scale indeed with the reciprocal of their corresponding kinematic viscosities (1.1482 and 0.4716 m^2 s^{-1}, respectively) [61]. Actually, the k_q^{O2} in acetonitrile is one of the largest achievable in solution due to the low kinematic viscosity of this solvent. However, the k_q^{O2} in dichloromethane is abnormally low for its kinematic viscosity (0.3121 m^2 s^{-1}) [61]. The fluorescence lifetimes of PMeA and PMeMA in this solvent are unusually low (145 ns *vs* ca. 300 ns in either MeCN or CH), Table 4.3, due to the "*heavy atom effect*" of the dichlorinated solvent that enhances the intersystem crossing (ISC) rate to the triplet state of these fluorophores. As the effect of O_2 on the lowest-lying (singlet) excited state of PMeA and PMeMA is to quench them by also enhancing ISC (*see section IV.4)*, the k_q^{O2} in dichloromethane must be significantly smaller than the expected one from the Smolouchowski equation for diffusion-limited rates.

Therefore, the use of the fluorescence quantum yield or lifetime of the pyrenemethyl-(meth)acrylamides probes incorporated into molecularly imprinted polymers as the analytical reporters is limited by the strong effect of O_2 on these two parameters. Variations in the accessibility of this gas to their emissive excited state will produce dramatic changes in the measured value. Only thorough degassing of the analyte solutions may render usable both features of the strong fluorescence of the probes.

IV.7. Fluorescence features of PMeMA in SDS micelles and alternariol surrogate S-2

With the aim of studying the photochemistry of the pyrenyl-acrylamide monomers in the presence of alternariol and test their usefulness as probes of the mycotoxin, several experiments were designed by using surfactant micelles as models of the probe environment when incorporated into MIP cavities. Moreover, the surfactant micelles facilitate dissolution of the hydrophobic pyrenyl-acrylamides and alternariol and its surrogates in water and foster their mutual interaction by incorporating both partners into the micelle interior.

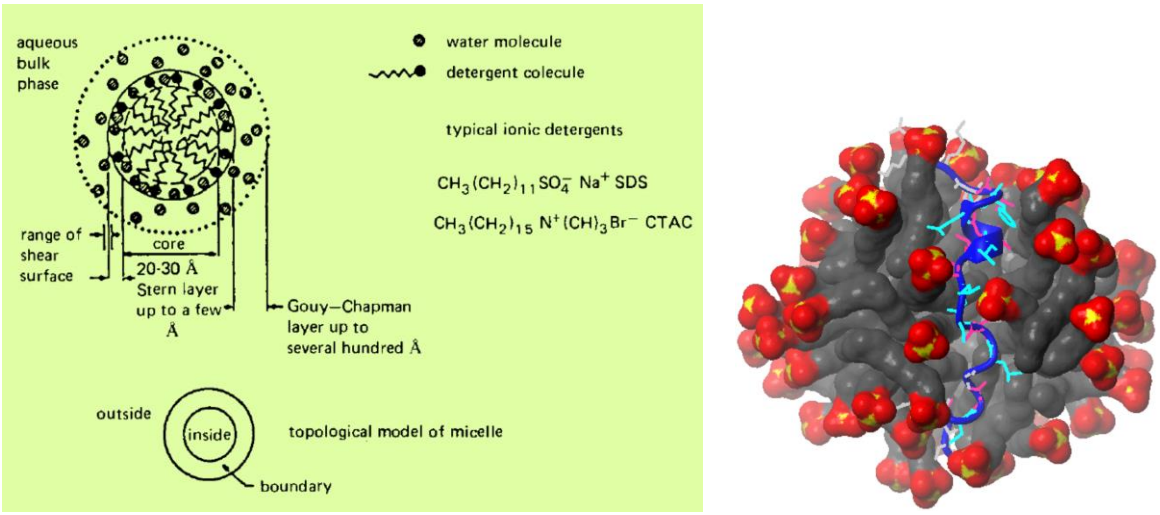

(a) (b)

Figure 4.10: (a) Schematic representation of a spherical ionic micelle such as those of SDS [1]. (b) Molecular dynamics simulation of an SDS micelle containing a peptide in its interior [62].

Micelles are organized molecular aggregates composed of surfactants; the latter are molecules with one or more long alkyl chains (with at least six methylene units) and a polar head group, positively or negatively charged, also called *amphipathic* or *amphiphilic* molecules due to their dual water-loving/water-hating character [1]. When dissolved in water at a defined temperature, and above a

particular concentration (called "critical micellar concentration" or cmc), surfactants form globular aggregates of colloidal dimensions called "micelles" in a way that the polar heads of the surfactant molecules in the aggregate are exposed to the water and the alkyl chains point out to the interior, with a variable degree of penetration of water molecules into the micelle Fig. 4.10. Hydrophobic solutes prefer to dissolve in the micelle interior rather than in the water bulk; this phenomenon is the basis of the mechanism of cloth cleaning using surfactant soaps so that they are also referred as "detergents". The name "surfactant" comes from the effect of these molecules on the surface tension of the water (they raise it). Sodium dodecyl sulfate ($CH_3(CH_2)_{11}OSO_3^-Na^+$ or SDS, also called lauryl sulfate) is one of the most typical anionic surfactants, with a cmc of 8.3 mM to form quasi-spherical micelles of ca. 3.5 nm diameter in water comprising 59 ± 5 molecules [63, 64].

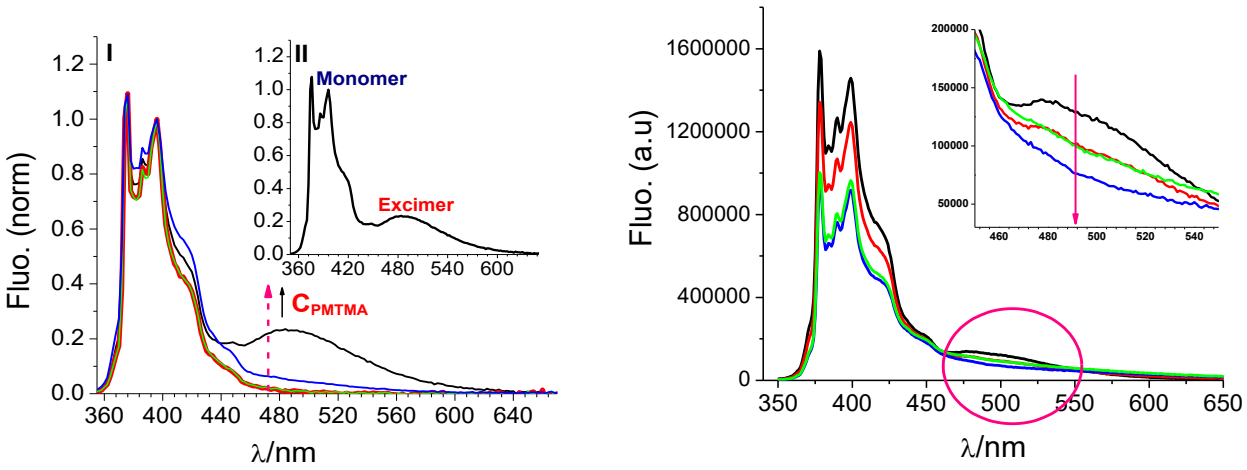

Figure 4.11: *(a)* Normalized fluorescence spectra of PMeMA (1–100 µM) in 20 mM SDS solution in water; *(b)* fluorescence titration of PMeMA (**100 µM**) in 20 mM SDS solution with increasing amounts of alternariol surrogate S-2 (**0.20**, **0.33** and **1.1** µM) (λ_{ex} = 341 nm, room temperature).

Although the PMeMA monomer is virtually insoluble in water, it can be solubilized therein at concentrations as high as 100 µM in the presence of SDS micelles. Fig. 4.11(a) depicts the fluorescence spectrum of PMeMA at various concentrations, in the presence of 20 mM SDS (equivalent to 340 µM of SDS micelles, taking into account the aggregation number mentioned above). The fluorescence spectrum of 100 µM PMeMA shows already the characteristic band of pyrene excimers at 490 nm (*see section IV.5*) due to the occupancy of some micelles by two PMeMA molecules according to the Poisson distribution (the fraction of micelles containing *i* molecules of

solute M_i is given by Eq. 4.4, where <*n*> is the average number of solutes per micelle and [*M*] is the concentration of micelles) [1] :

$$\frac{[M_i]}{[M]} = \left(< n >^i e^{-<n>}\right)/i! \qquad (4.4)$$

In our case, only 3% of SDS micelles are occupied by two PMeMA molecules, while 22% of them contain just a single PMeMA molecule. The *I*(I)/*I*(III) ratio for the vibronic bands of the PMeMA fluorescence reflects the incorporation of the pyrenyl moiety into a significantly hydrophobic environment Table 4.4.

Fig. 4.11(b) demonstrates that, in the presence of surrogate S-2 up to 1.1 μM concentration, the PMeMA fluorescence of both the monomer and its excimer are significantly quenched. The quenching mechanism is probably a *photoinduced electron transfer* from the electron-rich polyphenolic surrogate to the lowest-lying (half-occupied) π orbital of the photoexcited pyrene moiety of PMeMA. The Stern-Volmer plot for the emission intensity at 400 nm is depicted in Fig. 4.12. The Stern-Volmer plot is typical of static quenching: the F_0/F ratio strongly bends upwards until a point where all pyrene molecules dwelling into the SDS micelles are quenched by the incoming S-2 molecule(s), so that a further increase of the surrogate concentration does not produce any further quenching. Under this situation, only PMeMA molecules contained in SDS micelles where S-2 has not entered are able to display fluorescence.

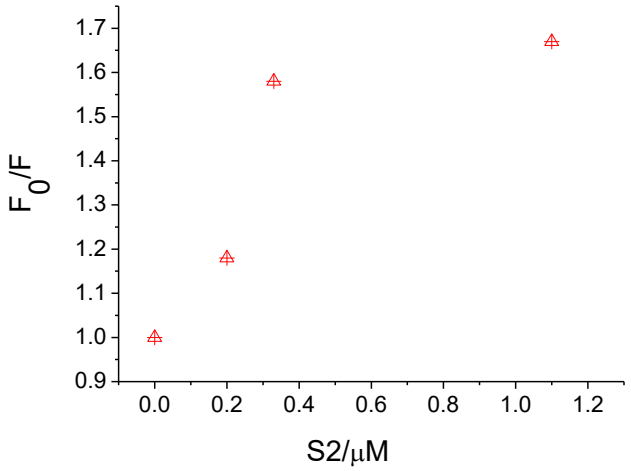

Figure 4.12: Stern-Volmer quenching plot of PMeMA (**100 μM**) by alternariol surrogate S-2 in 20 mM SDS aqueous solution (λ_{ex} = 341 nm; λ_{em} = 400 nm, room temperature).

The fluorescence lifetimes of PMeMA in the presence of SDS micelles and the S-2 surrogate Fig. 4.13 provide further support to the steady-state results discussed above. In the absence of quencher, the fluorescence decay of PMeMA in SDS micellar solution is biexponential, with a lifetime corresponding to the probe molecules contained into the singly-occupied micelles (94 ± 3 ns, 39%) and a shorter one corresponding to the PMeMA in doubly-occupied micelles (54 ± 2 ns, 61%). In the presence of the alternariol surrogate S-2, a very short lifetime of 0.7 ± 0.1 ns appears Fig. 4.13 due to the fluorescence of the surrogate Table 2.1 (in section II.2)[5]. However, the most interesting feature is the quenching that the photoexcited pyrene undergoes, showing lifetimes of 70 ± 4 ns and 27 ± 4 ns for the long and short components of the decay. The long-lived species, contributing 90 to 85% to the overall fluorescence from PMeMA, might be assigned to the quenched probe molecule into the SDS micelle, probably modulated by the entry and exit rates of the fluorophore from the micelles because we cannot assume that the decay of the photoexcited probe is much faster than the average residence time in the micelle taking into account the rather long fluorescence lifetimes of pyrene compared to typical ns-lived fluorophores. The short-lived species of the biexponential decays Fig. 4.13, without taking into account the fluorescence from S-2, contributing 10 to 15% to the overall fluorescence from PMeMA, would correspond to the surrogate-quenched PMeMA found into doubly-occupied SDS micelles.

Therefore, PMeA and PMeMA are expected to be good probes of alternariol when incorporated into the binding sites of the latter into tailored molecularly imprinted polymers. Both their fluorescence intensity and lifetime will decrease in the presence of the analyte due to efficient photochemical quenching. Further studies are being conducted in our Group to characterize the excited state quenching mechanism in more detail by laser kinetic spectrometry, as well as to develop MIPs for alternariol analysis based on pyrene-labeled functional monomers.

[5] The short fluorescence lifetime of S-2 (1.74 ns), Table 2.1 is impossible to be measured accurately in the wide time scale used in this experiments to be able to determine accurately the PMeMA emission lifetime.

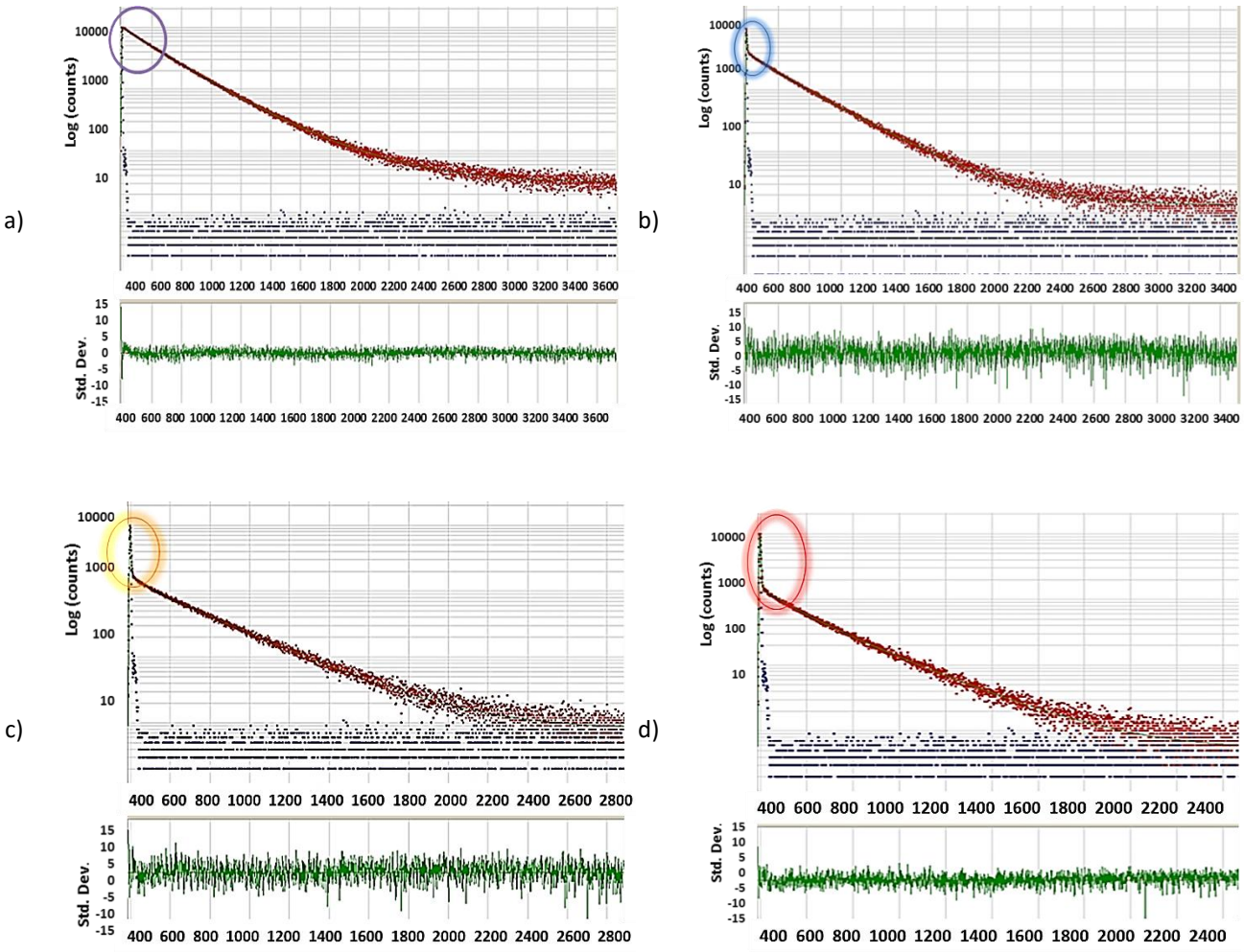

Figure 4.13: Fluorescence decays at 400 nm of photoexcited PMeMA (100 µM) in aerated 20 mM SDS aqueous solution, in the presence of increasing amounts of dissolved alternariol surrogate **S-2**. a) No S-2 added; b) 0.01 mM S-2 added; c) 0.05 mM S-2 added; d) 0.1 mM S-2 added (λ_{ex} = 343 nm, λ_{em} = 400 nm; room temperature). The bottom panels (green lines) show the distribution of the weighted residuals. The *x*-axis calibration is 0.22 ns/channel.

Bibliography

1. Kalyanasundaram, K., *Photochemistry in Microheterogeneous Systems*. Academic Press: London (UK), 1987.
2. Dunn, B.; Zink, J. I., Probes of Pore Environment and Molecule−Matrix Interactions in Sol−Gel Materials. *Chem. Mater.* **1997,** *9*, 2280-2291.
3. Duhamel, J., New insights in the study of pyrene excimer fluorescence to characterize macromolecules and their supramolecular assemblies in solution. *Langmuir* **2012,** *28*, 6527–6538.
4. Reichardt, C.; Welton, T., *Solvents and Solvent Effects in Organic Chemistry*. 4th ed ed.; Wiley-VCH: Weinheim (DE), 2011; Vol. 50, p 11289.
5. Chen, Z.; Álvarez-Pérez, M.; Navarro-Villoslada, F.; Moreno-Bondi, M. C.; Orellana, G., Fluorescent sensing of "quat" herbicides with a multifunctional pyrene-labeled monomer and molecular imprinting. *Sensors Actuators B: Chem.* **2014,** *191*, 137-142.
6. Hofkens, J.; Hotta, J.; Sasaki, K.; Masuhara, H., Molecular association by the radiation pressure of a focused laser beam: fluorescence characterization of pyrene-labeled PNIPAM. *J. Am. Chem. Soc.* **1997,** *119*, 2741-2742.
7. Hu, Y.; Horie, K.; Torii, T.; Ushiki, H.; Tang, X., Change in micro-environments in poly(acrylamide) gel with pyrenyl probe due to its volume phase transition induced by ph change. *Polym. J.* **1993,** *25*, 123-130.
8. J., G.; J., D.; M., Y.; J., C.; S., W.; L., J.; Lichao, W. Fluorescent chemosensor for rapidly and real-time detecting nitrofurantoin. 2009.
9. Takeuchi; Toshifumi Method for detecting target molecule in sample using molecular imprint microparticles. 2009.
10. Frahn, M. S.; Abellon, R. D.; Jager, W. F.; Luthjens, L. H.; Warman, J. M., Synthesis and characterization of a new fluorogenic probe molecule N-(1-pyrene)methacrylamide for monitoring radiation-induced polymerization. *NIMPR:B* **2001,** *185*, 241-247.
11. Antonio, S. S.; Ernesto, R. G.; Carmen Andriana, G. S.; Francisco Javier, I. M.; Jair Azael, E. G.; Yessica Selene, R. F. Fluorescent plastics used in black light illumination. 2014.
12. Yongtai Zheng, Y.; Akihito Hashidzume, A.; Takashima, Y.; Yamaguchi, H.; Harada, A., Switching of macroscopic molecular recognition selectivity using a mixed solvent system. *Nature Communications* **2012,** *3:831*, 1-4.
13. Akihito, H.; Yongtai, Z.; Akira, H., Interaction of cyclodextrins with pyrene-modified polyacrylamide in a mixed solvent of water and dimethyl sulfoxide as studied by steady-state fluorescence. *B.J.O.C.* **2012,** *8*, 1312-1317.
14. Laukkanen, A.; Winnik, F. M.; Tenhu, H., Pyrene-labeled graft copolymers of N-vinylcaprolactam: synthesis and solution properties in water. *Macromolecules* **2005,** *38*, 2439-2448.
15. Kanagalingam, S.; Ngan, C. F.; Duhamel, J., Effect of solvent quality on the level of association and encounter kinetics of hydrophobic pendants covalently attached onto a water-soluble polymer. *Macromolecules* **2002,** *35*, 8560-8570.
16. Bertrand, R.; Julien, W.; L., J. J.; David, W. W.; Erwin, R., A poly(cobaloxime)/carbon nanotube electrode: freestanding buckypaper with polymer-enhanced H2-evolution performance. *Angew. Chem. Int. Ed.* **2016,** *55*, 3952-3957.
17. Yotaro, M.; Michiko, S.; Yukio, T.; Mikiharu, K., Compartmentalization of chromophores in a molecular composite consisting of amphiphilic polyelectrolytesurfactant ion complexes. *J. Polym. Sci. A Polym. Chem.* **1992,** *30*, 2099-108.
18. Yotaro, M.; Kanji, K.; Michiko, S.; Osamu, A.; Kyoshi, U. Ionic complex useful for photochromic material. 1992.
19. Morishima, Y.; Tominaga, Y.; Kamachi, M.; Okada, T.; Hirata, Y.; Mataga, N., Photoinduced charge separation by chromophores encapsulated in the hydrophobic compartment of amphiphilic polyelectrolytes with various aliphatic hydrocarbons. *J. Phys. Chem.* **1991,** *95* 6027–6034.
20. Kolakkandy, S.; Pratihar, S.; Aquino, A. J. A.; Wang, H.; Hase, W. L., Properties of complexes formed by Na+, Mg2+, and Fe2+ binding with benzene molecules. *J. Phys. Chem. A,* **2014,** *118*, 9500–9511.

21. Amicangelo, J. C.; Armentrout, P. B., Absolute binding energies of alkali-metal cation complexes with benzene determined by threshold collision-induced dissociation experiments and ab initio theory. *J. Phys. Chem. A* **2000,** *104*, 11420–11432.
22. Malkin, J., *Photophysical and photochemical properties of aromatic compounds*. CRC Press: Boca Raton, Fla., USA, 1992.
23. Berlman, I. B., *Handbook of fluorescence spectra of aromatic molecules, 2nd ed*. Academic Press: New York,, 1971.
24. Rao, C. N. R., *Ultra-violet and visible spectroscopy*. Butterworth: London, 1967; p 210.
25. Birks, J. B., *Photophysics of aromatic molecules*. Wiley: London, 1970.
26. Nakajima, A., Intensity enhancement induced by solute-solvent interaction between pyrene and polar solvents. *Spectrochimica Acta A* **1982,** *38A*, 693–695.
27. Lianos, P.; Lux, **B.**; Gerard, D., Photophysical properties of pyrene and its derivatives of biophysical importance. *J. Chim. Phys. Phys.-Chim. Biol.* **1980,** *77*, 907-912.
28. Karpovich, D. S.; Blanchard, G. J., Relating the polarity-dependent fluorescence response of pyrene to vibronic coupling. Achieving a fundamental understanding of the py polarity scale. *J.P.C.* **1995,** *99*, 3951-3958.
29. Karpovich, D. S.; Blanchard, G. J., Relating the Polarity-Dependent Fluorescence Response of Qrene to Vibronic Coupling. Achieving a Fundamental Understanding of the Py. Polarity Scale. *J. Phys. Chem.* **1995,** *99*, 3951-3958.
30. Nijegorodov, N. I.; Downey, W. S., The Influence of Planarity and Rigidity on the Absorption and Fluorescence Parameters and Intersystem Crossing Rate-Constant in Aromatic-Molecules. *J Phys Chem-Us* **1994,** *98*, 5639-5643.
31. Birks, J. B.; Dyson, D. J., The relations between the fluorescence and absorption properties of organic molecules. *Proc. Royal Soc. A.* **1963,** *275*, 135-48.
32. Yao, C.; Kraatz, H. B.; Steer, R. P., Photophysics of pyrene-labelled compounds of biophysical interest. *Photochem. Photobiol. Sci.* **2005,** *4*, 191-199.
33. Wan, W.; Wagner, S.; Rurack, K., Fluorescent monomers: "bricks" that make a molecularly imprinted polymer "bright". *Anal. Bioanal. Chem.* **2016,** *408*, 1753–1771.
34. Wolfbeis, O. S., Optical technology until the year 2000. An historical overview. *Springer Series on Chemical Sensors and Biosensors* **2004,** *1*, 1-34.
35. Schweitzer, C.; Schmidt, R., Physical mechanisms of generation and deactivation of singlet oxygen. *Chem. Rev.* **2003,** *103*, 1685-1757.
36. Grellmann, K. H.; Hentzschel, P., Mechanism of the photochemical cis .dblharw. trans isomerization of thioindigo and 6,6'-diethoxythioindigo in solution. *Chem. Phys. Lett.* **1978,** *53*, 545-550.
37. Potashnik, R.; Goldschmidt, C. R.; Ottolenghi, M., Triplet state formation in the quenching of fluorescence by molecular oxygen. *Chem. Phys. Lett.* **1971,** *9*, 414-415.
38. Montalti, M.; Credi, A.; Prodi, L.; Gandolfi, M. T., *Handbook of Photochemistry*. CRC: Boca Raton, Fla. (USA), 2006.
39. Balzani, V.; Ceroni, P.; Juris, A., *Photochemistry and photophysics: concepts, research, applications*. Wiley-VCH: Weinheim (DE), 2014.
40. J., R. M. A., Quenching of fluorescence from pyrene in micellar solutions by cationic quenchers. *Chem. Phys. Lett.* **1978,** *53*, 165-169.
41. Birks, J. B., Excimer fluorescence of aromatic compounds. *Progress in Reaction Kinetics* **1970,** *5*, 181-272.
42. Duhamel, J., New Insights in the Study of Pyrene Excimer Fluorescence to Characterize Macromolecules and their Supramolecular Assemblies in Solution. *Langmuir* **2012,** *28*, 6527–6538.
43. Durocher, G.; Sandorfy, C., General occurrence of the Ham effect in the electronic spectra of aromatic hydrocarbons. *J. Mol. Spectrosc.* **1966,** *20*, 410-24.

44. Ham, J. S., A new electronic state in benzene. *J. Chem. Phys.* **1953,** *21*, 756-758.
45. Nakajima, A., Solvent effect on the vibrational structures of the fluorescence and absorption spectra of pyrene. *Bull. Chem. Soc. Jpn.* **1971,** *44*, 3272-3277.
46. Kalyanasundaram, K.; Thomas, J. K., Environmental effects on vibronic band intensities in pyrene monomer fluorescence and their application in studies of micellar systems. *J. Am. Chem. Soc.* **1977,** *99*, 2039-2044.
47. Dong, D. C.; Winnik, M. A., The Py scale of solvent polarities. Solvent effects on the vibronic fine structure of pyrene fluorescence and empirical correlations with ET and Y values. *Photochem. Photobiol.* **1982,** *35*, 17-21.
48. Dong, D. C.; Winnik, M. A., The Py scale of solvent polarities. solvent effects on the vibronic fine structure of pyrene fluorescence and empirical correlations with et and y values. *J. Photochem. Photobiol.* **1992,** *35*, 17-21.
49. Street, K. W.; Acree, W. E., Experimental artifacts and determination of accurate Py values. *Analyst* **1986,** *111*, 1197-1201.
50. Piñeiro, L.; Novo, M.; Al-Soufi, W., Fluorescence emission of pyrene in surfactant solutions. *Adv. Coll. Interf. Sci.* **2015,** *215*, 1-12.
51. Ray, G. B.; Chakraborty, I.; Moulik, S. P., Pyrene absorption can be a convenient method for probing critical micellar concentration (cmc) and indexing micellar polarity. *J. Coll. Interf. Sci.* **2006,** *294*, 248-254.
52. Winnik; M., F., Photophysics of preassociated pyrenes in aqueous polymer solutions and in other organized media. *Chem. Rev.* **1993,** *93*, 587-614.
53. Tedeschi, C.; Möhwald , H.; Kirstein, S., Polarity of Layer-by-Layer Deposited Polyelectrolyte Films As Determined by Pyrene Fluorescence. *J. Am. Chem. Soc.* **2001,** *123*, 954-960.
54. Bains, G.; Patel, A. B.; Narayanaswami, V., Pyrene: a probe to study protein conformation and conformational changes. *Molecules* **2011,** *16*, 7909-7935;.
55. Vasilescu, M.; Angelescu, D.; Almgren, M.; Valstar, A., Interactions of Globular Proteins with Surfactants Studied with Fluorescence Probe Methods. *Langmuir* **1999,** *15*, 2635-2643.
56. Lux, B.; Gerard, B., Reappraisal of the binding processes of N-(3-pyrene)maleimide as a fluorescent probe of proteins. *J. Biol. Chem.* **1981,** *256*, 1767-1771.
57. Kalyanasundaram, K.; Thomas, J. K., Environmental effects on vibronic band Intensities in pyrene monomer fluorescence and their application in studies of micellar systems. *JACS* **1977,** *99:7*, 2039-2044.
58. May, V.; Kühn, O., *Charge and Energy Transfer Dynamics in Molecular Systems* Wiley-VCH Weinheim, Germany, 2004.
59. Rice, S. A., Diffusion-Limited Reactions, Chemical Kinetics. Elsevier: Amsterdam, Netherlands, 1985; Vol. 25, pp 3-46.
60. Rurack, K., Standardization and Quality Assurance in Fluorescence Measurements I: Techniques, Resch-Genger, U. (Ed.). Springer: Berlin Heidelberg, Germany, 2008; pp 101-146.
61. Haynes, W. M.; Lide, D. R.; Bruno, T. J. E., *CRC Handbook of Chemistry and Physics, 97th ed.*; CRC Press: Boca Raton, Fla., USA, 2017.
62. Perdih, A.; Choudhury, A. R.; Župerl, Š.; Sikorska, E.; Zhukov, I.; Solmajer, T.; Novič, M., Structural analysis of a peptide fragment of transmembrane transporter protein bilitranslocase. *PLoS ONE* **2012,** *7*, e38967.
63. Thévenot, C.; Grassl, B.; Bastiat, G.; Binana, W., Aggregation number and critical micellar concentration of surfactant determined by time-dependent static light scattering (TDSLS) and conductivity. *Colloids and Surfaces A: Physicochem. Eng. Aspects* **2005,** *252*, 105–111.
64. Duplâtre, G.; Ferreira Marques, M. F.; Graça Miguel, M., Size of Sodium Dodecyl Sulfate Micelles in Aqueous Solutions as Studied by Positron Annihilation Lifetime Spectroscopy. *J. Phys. Chem.* **1996,** *100*, 16608-16612.

V-Experimental Section

INDEX

V.1. Materials and Instrumentation

V.1.1. Materials

Solvents: acetonitrile (>99.8%, dried over molecular sieves), methanol (HPLC >99.8%) and *m*-xylene (analytical standard,) were purchased from Fluka; toluene (≥99%), and chlorobenzene (>99.8%, dried over molecular sieves) were from Sigma-Aldrich; absolute ethanol was from Prolabo, chloroform (ISO-stabilized with methanol) and methanol (synthesis grade) were from Carlo Erba, tetrahydrofuran (THF, 99.5%, anhydrous), dimethyl sulfoxide (DMSO, 99.7%, anhydrous) and hexane were from Acros Organics; hydrochloric acid (37%), ethyl acetate, dichloromethane (extra pure, stabilized with 50 ppm amylene) were from Scharlau; trifluoroacetic acid (TFA, 99%) was from Alfa Aesar. All solutions for HPLC were filtered through a 0.45 μm nylon filter before use. Type I water was obtained from a Millipore Direct-Q 3UV purification system.

Reagents: alternariol (3,7,9-trihydroxy-1-methyl-6H-dibenzo[b,d]pyran-6-one) (96%), methacryloyl chloride (95%) and quinine sulphate dehydrate (+99%) were purchased from Acros Organics. Alternariol monomethyl ether (3,7-dihydroxy-9-methoxy-1-methyl-6H-dibenzo[b,d]pyran-6-one, ≤ 96%) was from Apollo Scientific; aluminum chloride (98%) and trifluoroacetic acid (TFA, 99.5%) were from Fluka; sodium hydroxide was from Scharlau; dibutyltin dilaurate (95%), dodecanethiol (99.8%, dried over molecular sieves), 2-bromo-4,5-dimethoxybenzoic acid (98%), 2-bromo-5-methoxybenzoic acid (97%), 3-methoxy-5-methylphenol (97%), 2,4-

dimethoxybenzoic acid (98%), resorcinol (97%), glutaric anhydride (95%), 2-isocyanatoethyl methacrylate (98%), tetrabutylammonium hydroxide (TBA^+OH^-), acryloyl chloride (97% with <210 ppm MEHQ as stabilizer), 1-aminopyrene (97%), sodium hydrogen carbonate, 1-pyrenemethylamine hydrochloride (95%), ethylchloroformate (97%), 2-cyano-2-propyl benzodithioate (CPDB, ≥ 97%), and (3-aminopropyl)triethoxysilane (APTES, 99%) were from Sigma-Aldrich; ammonium hydrogen fluoride (NH_4HF_2) was from Alfa Aesar.

Monomers and crosslinkers: ethylene glycol dimethacrylate (EDMA, 98%), divinylbenzene (DVB, mixture of *meta*- and *para*- isomers, technical grade, 80%), 4-vinyl-pyridine (4-VPy, 95%), methacrylic acid (MAA, 99%) were purchased from Sigma-Aldrich; 2-hydroxyethyl methacrylate (HEMA, 97%), 4-vinylbenzoicacid (4VBA, 96%) were from Acros Organics; methacrylamide (MAM, 98%) was from Fluka; 1-allylpiperazine (ALPP) was from Lancaster Synthesis; 2-aminoethyl methacrylate hydrochloride (EAMA, +95%) was from Polysciences; diethyl allylmalonate (DEAM, min. 95%) was from ABCR; allyl acetoacetate (AACA, min. 98%) was from Alfa.

Initiators: 2,2'-azobis(2,4-dimethyl)valeronitrile (ABDV, 97%) and 2,2'-azobis(2-methylpropionitrile) (AIBN, 98%) were purchased from Wako Pure Chemicals Ind.

Buffers: HEPES (2-[4-(2-hydroxyethyl)piperazin-l-yl]ethanesulfonic acid) (≥99.5%) and NaH_2PO4 (98-102%) were purchased from Sigma-Aldrich; Na_2HPO4 (99%) was from Acros Organics; ammonia/ammonium chloride (NH_4OH, 28%/NH_4Cl, 99%) were from Prolabo; Bogen Universal Indicator solution was from Carolina Biological Supply Co.

Other materials: porous spherical silica microparticles (SiliaSphere™ PC, 40-75 µm diameter, 500 Å pore size) were purchased from SiliCycle. Solid-phase extraction cartridges (1-2.5 mL) were from Varian, Palo Alto, CA, USA

Solvents for nuclear magnetic resonance (NMR) spectroscopy: desiccator-stored deuterated solvents (98.5 to >99% D-atom) acetonitrile (CD_3CN) and chloroform ($CDCl_3$) were purchased from Cambridge Isotopes Laboratories; dimethyl sulfoxide (DMSO-d_6, 99.9%) was from ACROS Organics.

Cleaning solutions: for cleaning sintered filters, a piranha solution (freshly prepared mixture of concentrated H_2SO_4 and 30% H_2O_2 in a 3:1, *v/v* ratio) was used; laboratory glass material was cleaned by immersing it for 24-48 h in a potassium hydroxide saturated isopropyl bath and further rinsing with deionized water; phosphate-free liquid lab detergent (PCC-P free) was purchased from Thermo Scientific.

V.1.2. Instrumentation

Synthesis setup: reactions were carried out inside ventilating fume hoods equipped with 99.995% argon (Praxair) and high vacuum (Edwards M8 dual stage pump) lines. For refrigeration purposes, Huber polystat CC1 circulators were used. The reaction mixture heating (< 310 °C) and stirring (< 1500 rpm) were carried out with IKA hotplates with magnetic stirrer (RCT BASIC), fitted with flask heat-on blocks/inserts (Radleys) and electronic contact thermometer (IKA, ETS-D5). When possible, the course of the reactions was followed by thin layer chromatography (TLC) analysis on silica gel (Silica gel 60 F_{254}, Merck) and UV lamp examination (254 and 365 nm). The pH of the buffer solutions and samples was adjusted with a CRISON GLP22 pH and Ion meter. The solid phase extraction experiments were performed using a Spetec Perimax 12 peristaltic pump (Gilson). The filtering system used for the 96-well plate was a Biotage VacMaster.

Evaporation: rotary evaporators from BÜCHI (R-215) and Heidolph (Hei-VAP Precision) were connected to either a BÜCHI V-700 vacuum pump equipped with BÜCHI V-850 vacuum pump controller, for evaporation of solvents up to 10 mbar, or a Telstar 2F-3 pump for difficult cases of solvent evaporation such as dimethyl sulfoxide. The latter was protected by a liquid nitrogen trap. The latter was also connected to a vacuum oven (Lab-line) to allow final drying of the products.

Preparation and cleaning: all reaction protocols were devised after careful study of Chemical Abstract Service (CAS) literature searches through its Scifinder engine tool. Two scales were used for weighing, namely a Denver Instruments TP-303 (± 1 mg) and a Mettler AT-260 (± 0.01 mg) for more precise measurements. Filtrations were performed through sintered glass plate funnels no. 4 or 5 (pore size range 1-15 µm). For promoting the dissolution of the chemicals, a sonicator bath (Fungilab) was used. The resulting solutions for NMR measurements were filtered with a glass/PTFE syringe (SGL) equipped with a 4–mm dia. 0.22 µm pore nylon filter (GE Osmonics).

Product purification: flash column chromatography was performed using Silica gel 60 (0.040-0.063 mm) (Merck).

V.1.3. Product characterization

Fourier transform infrared (FT-IR) spectra were recorded with a Bruker Alpha spectrophotometer with a DLaTGS detector in transmission mode, using either KBr pellets for solid samples or an ATR (attenuated total reflection) probe.

^{1}H NMR and ^{13}C NMR spectra were recorded on a Bruker Avance DPX at 300 MHz-BACS60 and Avance DPX500 spectrometer at 500MHz (UCM NMR Central Instrumentation Facilities, CIF). All the spectra were processed by the Bruker TOPSPIN (v2.1) software package and calibrated to meet the solvent shifts as reported by Gottlieb et al. [1]. The chemical shifts were assigned taking into consideration literature reports or with the aid of the prediction software ChemBioDraw Ultra (v11.0.1) [2,3].

ESI-MS spectra were obtained on an LTQ XL linear ion trap mass spectrometer fitted with an electrospray ionisation (ESI) sample inlet (UCM MS CIF).

Elemental analysis was performed on a Leco VTF-900/CHNS-932 elemental analyser (UCM Microanalytical CIF).

Electron microscopy. A scanning electron microscope (SEM) JEOL JSM 6355F Field Emission Gun (FEG) operating at 15 kV was used (UCM–Centro Nacional de Microscopía Electrónica, CNME). Before the measurements, samples were coated with a thin layer of gold by sputtering.

The liquid chromatography system consisted of an HP-1200 series high performance liquid chromatography (HPLC) from Agilent Technologies (Palo Alto, CA, USA) equipped with a binary pump, on-line degasser, autosampler, automatic injector, column thermostat, and diode-array detector (DAD).The samples were slurry-packed in the driving solvent into stainless steel HPLC columns (150 × 2.1 mm I.D.) for the chromatographic evaluation. The following conditions were used: 1.0 mL min^{-1} flow rate, 10 µL sample volume, 0.5 mM analyte concentration, at selected excitation/emission wavelengths for fluorescence detection.

Optical microscopy was performed on a HORIBA DynaMic fluorescence confocal microscope system equipped with a Lumenera Infinity 3-1UC refrigerated CCD color camera for obtaining images of the polymer samples with 1280×1024 pixels (gain 5.5 and pinhole 0.1 mm), producing microscopic images according to the used objective (10X, 20X or 40X).

V.1.4. Optical spectroscopy

UV-vis absorption spectra were recorded at 25 ºC in a Varian Cary 3-Bio spectrophotometer in double beam mode at a constant spectral bandwidth of 1.0 nm, incorporating a deuterium lamp for the UV region and a tungsten-halogen lamp for the visible region. 10×10 mm Suprasil QS-111.070 matched fluorescence cells from Hellma were used.

Fluorescence spectroscopy. A Horiba Fluoromax® 4-TCSPC spectrofluorometer equipped with a Xe arc lamp (150 W) as the excitation source and a Hamamatsu photomultiplier tube (R928P, 200-850 nm range) as the detector was used.

Fluorescence quantum yields (Φ_f) were measured at 25 ± 0.2 ºC. A solution of 9,10-diphenyl anthracene in cyclohexane (λ_{ex} = 340 nm) was used as a standard (Φ_f = 0.90) for the pyrene derivatives and the AOH and AME surrogates (spectral range of from 360 to 650 nm [4]). A correction for the solvent refractive index was applied according to reported equations [5,6].

Time-resolved emission measurements were carried out on a Horiba Fluoromax® 4-TCSPC spectrofluorometer equipped with a NanoLED-340 diode (343-nm, 1-ns pulses). Fluorescence decays were measured with a 200-ns to 5-µs window (4096 channels) after accumulating at least 10,000 counts in the peak channel. Emission lifetimes were extracted from the exponential curve fittings using the proprietary Horiba "grid-search" algorithm (with deconvolution of the instrumental response function). Any observed decay component equal to or below the laser pulse width was ignored.

Specific angle of rotation for optically active substances was recorded using an MCP 100 Polarimeter (Anton Paar), with a LED as the light source, using the Na wavelength at 589 nm and with an automatic Peltier temperature control at 20 or 25 °C.

Fluorescence polarization anisotropy (r) was measured using a Fluorolog® modular spectrofluorometer, with a 450-W xenon CW lamp and an L-format configuration. Several parameters were modified during the measurements namely temperature, pH, analyte concentration and excitation wavelength (for every different wavelength, the corresponding *G* factor was determined). The collected data was used to calculate the emission anisotropy (*r*) according to the Eq. 5.1 [7]:

$$r = \frac{I_{VV} - GI_{VH}}{I_{VV} + GI_{VH}} \quad (5.1)$$

where V and H refer to the vertical and horizontal orientation of the polarizer for intensity measurements, respectively. The *G* factor represents the ratio of the sensitivities of the detection system for the vertically and horizontally polarised light (λ_{em} dependent) calculated from Eq. 5.2:

$$G = \frac{I_{HV}}{I_{HH}} \quad (5.2)$$

Instantaneous emission anisotropy decay tests were measured by using a tuneable Ti:sapphire with ultra-short laser pulses [8]. The solvent of the sample was a H_2O-MeCN 70:30 mixture (*v/v*); λ_{ex} = 360 nm; λ_{em} = 392 nm and 12 nm slits.

Emission measurements in microtiter plates. A Clariostar microplate reader from BMG Labtech was used. This versatile instrument allows performing different types of measurements: polarization fluorescence anisotropy, steady state fluorescence, UV-vis absorption and time-resolved fluorescence for both, solid and liquid samples. For measurements with the solid samples, 96-well microtiter plates (Merck-Millipore MSRPN0410 Multiscreen Solvent Filter Plate, hydrophobic, PTFE, 0.45 µm, clear) were used. These plates are resistant to organic solvents such as acetonitrile or ethanol and possess a filter at the bottom of the wells that allows sample washing by filtration. In the case of liquid samples, 96-well microtiter transparent plates from Bioscience (650101, PS, U-bottom) were used for a UV-vis range of 250-500 nm.

V.2. Synthesis of alternariol and alternariol monomethyl ether surrogates for non-covalent imprinting of polymers

Alternariol surrogates S1-S6 Fig. 5.1 have been prepared by following straightforward synthetic routes with good reaction yields. The protocols followed are similar to those described in the literature for surrogates S1-S4 [9-12], and **s**urrogates S5 and S6 [13]. This allowed obtaining template molecules in suitable amounts (100 mg to > 1 g) for MIPs preparation. The molecular surrogates were chosen due to their similar structural and functional properties to the natural mycotoxins AOH and AME.

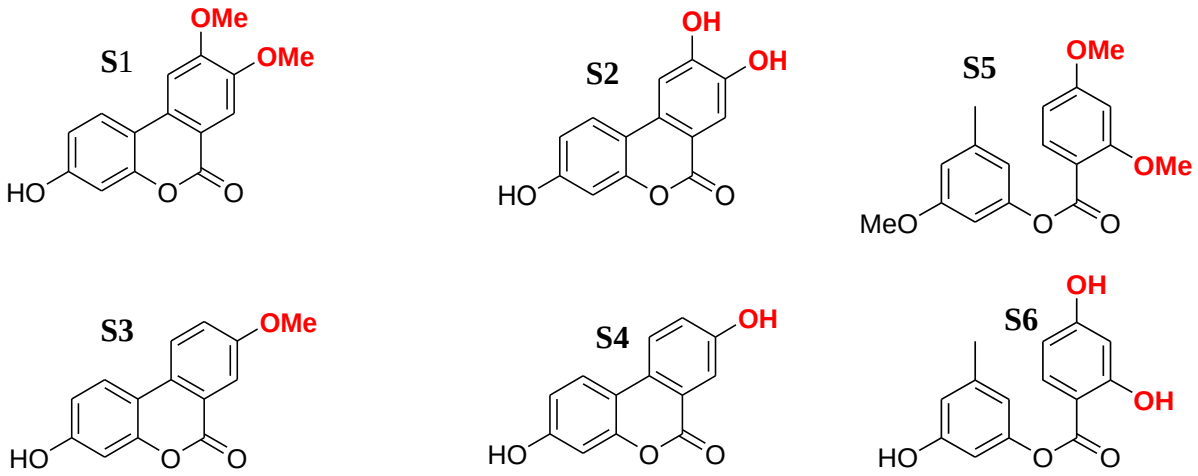

Figure 5.1: Surrogate molecules with similar structure and functional groups to the target AOH and AME mycotoxins: **S1-S4** as fluorescent, rigid molecules and, **S5** and **S6** as non-fluorescent analogues.

V.2.1. 3-Hydroxy-8,9-dimethoxy-6*H*-dibenzo[b,d]pyran-6-one (S1)

$C_{15}H_{12}O_5$ Mw: 272.25 g mol^{-1}

2-Bromo-4,5-dimethoxybenzoic acid (Br-DMBA, 0.95 g, 3.6 mmol) and resorcinol (0.93 g, 8.4 mmol) were dissolved in 4.25 mL of an aqueous solution of sodium hydroxide (0.339 g, 8.4 mmol), and heated at 80 ºC for 30 min. Then, a 5% (*w/v*) copper sulfate aqueous solution (1.45 mL) was added to the mixture, and a precipitate was formed after 10 min. The reaction mixture was neutralised by adding 0.9 mL of concentrated hydrochloric acid and filtered. After washing with 5 mL of water and 3 mL of methanol, the solid was suspended in 10 mL of methanol and heated at 50 ºC for 10 min. Once at room temperature, the solid was filtered out and washed with diethyl ether [14]. Yield: 71%.

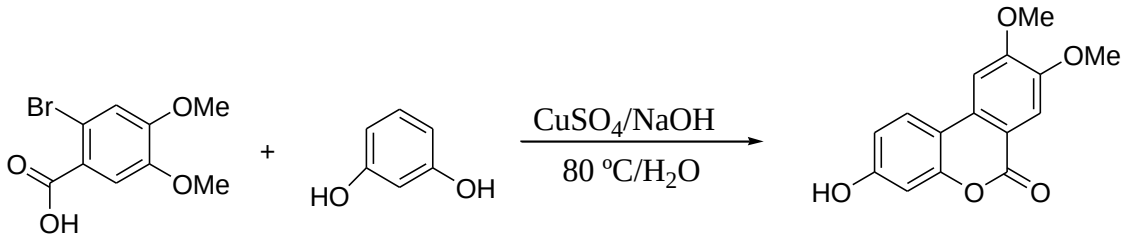

Br-DMBA **Resorcinol** **S1**

Reagent	Supplier	Volume/mL	Mass/g	Mol	Purity
Br-DMBA	Aldrich	---	0.95	3.6×10^{-3}	98%
Resorcinol	Aldrich	---	0.93	8.4×10^{-3}	98.5%
Cu_2SO_{4aq}, 5% (*w/v*)	Panreac	1.24	0.062	3.9×10^{-4}	99%
NaOH	Scharlau	4.25	0.339	8.4×10^{-3}	≥97.0%

Scheme 5.1: Synthesis of 3-hydroxy-8,9-dimethoxy-6H-dibenzo[b,d]pyran-6-one (adapted from Ito et al. [11]).

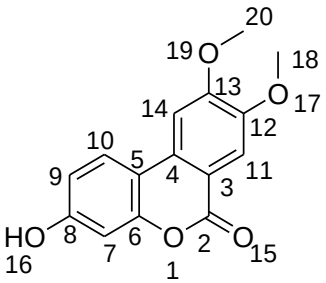

S1

TLC: CH_2Cl_2-MeOH (6:1, *v/v*) R_f = 0.42.

^{1}H NMR (300 MHz, DMSO-*d*$_6$) δ/ppm: 3.92 (s, 3H, -OCH_3), 4.05 (s, 3H, -OCH_3), 6.77 (d, *J* = 2.81 Hz, 1H, H_{Ar}), 6.88 (dd, J_1 = 8.69 Hz, J_2 = 2.33 Hz, 1H, H_{Ar}), 7.57 (s, 1H, $H11_{Ar}$), 7.72 (dd, 1H, H_{Ar}), 8.24 (d, *J* = 8.24 Hz, 1H, H_{Ar}), 10.58 (s, 1H, -OH).

^{13}C NMR (75 MHz, DMSO-*d*$_6$) δ/ppm: 57.4 (C20, -OCH_3), 58.0 (C18, -OCH_3), 104.8 (C7), 105.0 (C5), 111.4 (C3), 114.0 (C11), 114.9 (C4), 126.0 (C14), 133.0 (C9), 150.5 (C10), 153.7 (C13), 157.0 (C12, C-OCH_3), 160.9 (C6, C-O), 161.9 (C8, C-OH), 162.0 (C2, C=O).

FT-IR (ν/cm^{-1}): 3265 (γ OH), 2979, 2835, 1691, 1606, 1520, 1464, 1372, 1130, 1290, 1225, 1174, 1124, 1085.

MS-ESI (negative), *m/z*; calculated for $C_{15}H_{11}O_5$, $[M-H]^-$: 271.1; found: 270.7.

V.2.2. 3,8,9-Trihydroxy-6H-dibenzo[b,d]pyran-6-one (S2)

$C_{13}H_8O_5$ Mw: 244.22 g mol^{-1}

Anhydrous $AlCl_3$ (0.786 g, 5.8 mmol) was suspended in a mixture of dodecanethiol (0.5 mL) and chlorobenzene (8.5 mL) in an ice bath under argon. Then, S1 (0.337 g, 1.2 mmol) was added to the suspension and, after 30 min, the ice bath was removed, and the mixture was kept at room temperature for an additional period of 30 min. Finally, it was heated at 100 ºC. The reaction was monitored by TLC (silica, CH_2Cl_2-MeOH 20:1, *v/v*). After 5 h, the mixture was poured onto 15 mL of 3% aqueous HCl in an ice bath, and the precipitate was filtered off and washed with water and methanol. Yield: 72%.

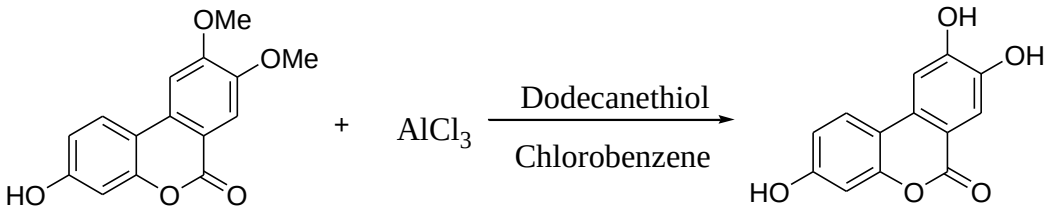

S1 **S2**

Reagent	Supplier	Volume/mL	Mass/g	Mol	Purity
$AlCl_3$	Aldrich	---	0.786	5.8×10^{-3}	99%
S1	GSOLFA	---	0.337	1.2×10^{-3}	---
Dodecanethiol	Aldrich	0.5	---	---	99.5%
Chlorobenzene	Aldrich	8.5	---	---	>99.8%

Scheme 5.2: Synthesis of 3,8,9-trihydroxy-6H-dibenzo[b,d]pyran-6-one.

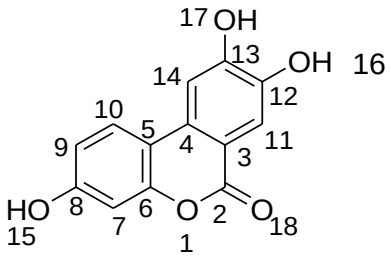

S2

TLC: CH_2Cl_2-MeOH (6:1, *v/v*) R_f =0.48.

^{1}H NMR (300 MHz, DMSO-d_6) δ/ppm: 6.72 (d, J = 2.34 Hz, 1H, H_{Ar}), 6.82 (dd, J_1 = 8.64 Hz, J_2 = 2.37 Hz, 1H, H_{Ar}), 7.47 (s, 1H, H_{Ar}), 7.53 (s, 1H, H_{Ar}), 7.88 (d, J = 8.82 Hz, 1H, H_{Ar}), 10.13 (s, 3H, -OH).

^{13}C NMR (75 MHz, DMSO-d_6) δ/ppm: 104.8 (C7), 108.8 (C14), 111.7 (C5), 112.9 (C3), 114.8 (C11), 116.1 (C9), 125.6 (C4), 131.0 (C10), 148.0 (C13, C-OH), 153.1 (C12, C-OH), 155.2 (C6, C-O), 160.3 (C8, C-OH), 162.1 (C2, C=O) ppm.

FT-IR (ν/cm^{-1}): 3363 (γ OH), 2924, 1762, 1619, 1460, 1383, 1326, 1283, 1212, 1127, 1065, 990, 883, 846, 805.

MS-ESI (negative), *m/z*; calculated for $C_{13}H_7O_5$, $[M-H]^-$: 243.0; found: 242.7.

Analysis (%): calculated C (63.94), H (3.30), N (0); found C (62.64), H (4.04), N (0.06)

Calculation of the p*Ka* of S2:

Universal Buffer

Solutions with a pH range from 2 to 12 could be obtained using a universal buffer recipe obtained from reference [15]. The recipe followed is shown below:

For 1 L of Universal Buffer:

0.1 M citric acid (21.01 g)

0.1 M potassium phosphate (13.61 g)

0.1 M sodium tetraborate (19.07 g)

0.1 M Tris (12.11 g)

0.1 M potassium chloride (7.46 g)

Since some of these ingredients were unavailable in the lab, the recipe was slightly modified. Instead of using citric acid and sodium tetraborate, citric acid·H_2O and sodium tetraborate·10 H_2O were used. With these substitutions, the modified recipe is as follows (1):

For 1 L of Universal Buffer:

0.1 M citric acid·H_2O (22.81 g)

0.1 M potassium phosphate (13.61 g)

0.1 M sodium tetraborate·10 H_2O (28.07 g)

0.1 M Tris (12.11 g)

0.1 M potassium chloride (7.46 g)

Each ingredient was weighed in a Mettler PB303 Electronic Balance on a weighing tray to minimise error (± 0.001 g). The ingredients were added to 900 mL of deionized water and mixed. Once all the solute was dissolved, the solution volume was modified with the addition of deionized water until a volume of 1 L was reached.

The universal buffer was used for the estimation of the p*K*a of S2. NaOH (5 M) was added to the universal buffer stock solution containing S2 (10 μM) that was constantly stirred in a 250 mL glass beaker. This addition was performed with a 10 μL pipette. For measuring the solution pH, a Fisher Scientific Accument 625 pH meter was used. At these incremental points, the actual pH values were recorded together with both fluorescence and absorption measurements. The p*K*a value was calculated with the IgorPro data analysis software.

V.2.3. 3-Hydroxy-9-methoxy-6H-dibenzo[b,d]pyran-6-one (S3)

$C_{14}H_{10}O_4$ Mw: 242.23 g mol^{-1}

2-Bromo-5-methoxy benzoic acid (Br-MBA, 2.0 g, 8.2 mmol) and resorcinol (2.0 g, 18 mmol) were dissolved in 9.1 mL of an aqueous solution of sodium hydroxide (0.727 g, 18.1 mmol), and heated at 80 ºC for 30 min. Then, a 5% (*w/v*) $CuSO_4$ aqueous solution (3.6 mL) was added and a precipitate separated after 10 min. The mixture was neutralised with 0.9 mL of concentrated aqueous HCl. After filtering and washing with 5 mL of water and 3 mL of methanol, the precipitate was further washed with 10 mL of hot methanol and finally diethyl ether. Yield: 59%.

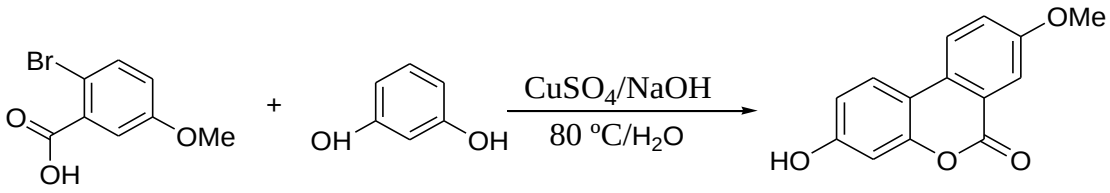

Br-MBA **Resorcinol** **S3**

Reagent	Supplier	Volume/mL	Mass/g	Mol	Purity
Br-MBA	Aldrich	---	2.0	8.6×10^{-3}	98%
Resorcinol	Aldrich	---	2.0	18×10^{-3}	98.5%
$Cu_2SO_{4\,aq}$, 5% (*w/v*)	Panreac	3.6	0.18	1.1×10^{-3}	99%
NaOH	Scharlau	9.1	0.727	18×10^{-3}	>97.0%

Scheme 5.3: Synthesis of 3-hydroxy-9-methoxy-6*H*-dibenzo[b,d]pyran-6-one.

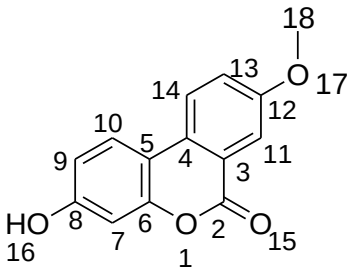

S3

TLC: CH_2Cl_2-MeOH (3:1, *v/v*) R_f = 0.37.

^{1}H NMR (300 MHz, DMSO-d_6) δ/ppm: 3.93 (s, 3H, -OCH_3), 6.79 (d, J = 2.25 Hz, 1H, H_{Ar}), 6.87 (dd, J_1 = 8.66 Hz, J_2 = 2.33 Hz, 1H, H_{Ar}), 7.54 (dd, J_1 = 8.87 Hz, J_2 = 2.78 Hz, 1H, H_{Ar}), 7.64 (d, J = 2.73 Hz, 1H, H_{Ar}), 8.14 (d, J = 8.73 Hz, 1H, H_{Ar}), 8.26 (d, J = 8.91 Hz, 1H, H_{Ar}), 10.27 (s, 1H, -*OH*).

^{13}C NMR (75 MHz, DMSO-d_6) δ/ppm: 57.5 (C18, -OCH_3), 104.7 (C7), 111.2 (C5), 112.8 (C11), 115.0 (C13), 121.9 (C9), 125.2 (C3), 125.8 (C10), 126.0 (C14), 130.3 (C4), 136.1 (C6), 153.0 (C8, C-OH), 160.1 (C12, C-OCH3), 162.0 (C12, C=O) ppm.

FT-IR (ν/cm^{-1}): 3635 (γ OH), 2988, 2839, 1768, 1693, 1497, 1460, 1324, 1289, 1173, 1126, 1069, 1032, 836, 811, 774, 730.

MS-ESI (negative), *m/z*: calculated for $C_{14}H_9O_4$, $[M-H]^-$: 241.1; found: 240.7.

V.2.4. 3,8-Dihydroxy-6H-dibenzo[b,d]pyran-6-one (S4)

$C_{13}H_8O_4$ Mw: 228.20 g mol^{-1}

Anhydrous $AlCl_3$ (0.700 g, 5.2 mmol) was suspended in a mixture of dodecanethiol (0.5 mL) and chlorobenzene (8.5 mL) and placed in an ice bath under argon. Then S3 (0.300 g, 1.2 mmol) was added, and after 30 min, the ice bath was removed, and the mixture was kept at room temperature for additional 30 min. Finally, it was heated at 100 ºC. The reaction was monitored by TLC (silica, CH_2Cl_2–MeOH 6:1, *v/v*). After 5 h, the mixture was poured onto 15 mL of 3% aqueous HCl in an ice bath, and the resulting precipitate was filtered and washed with water and a few millilitres of methanol. Yield: 70%.

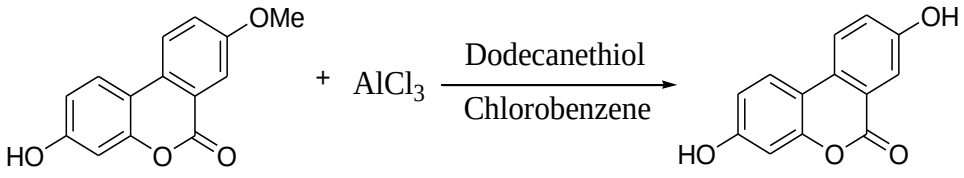

S3 **S4**

Reagent	Supplier	Volume/mL	Mass/g	Mol	Purity
$AlCl_3$	Aldrich	---	0.700	5.2×10^{-3}	99%
S3	GSOLFA	---	0.300	1.2×10^{-3}	---
Dodecanethiol	Aldrich	0.5	---	---	99.5%
Chlorobenzene	Aldrich	8.5	---	---	>99.8%

Scheme 5.4: Synthesis of 3, 8-dihydroxy-6*H*-dibenzo[b, d]pyran-6-one.

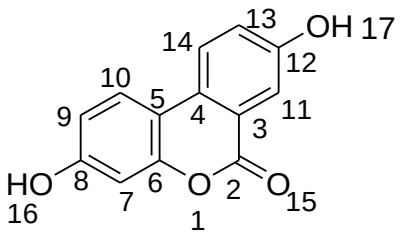

S4

TLC: CH_2Cl_2-MeOH (6:1, *v/v*) R_f = 0.45.

^{1}H NMR (300 MHz, DMSO-d_6) δ/ppm: 6.75 (d, J = 2.37 Hz, 1H, H_{Ar}), 6.83 (dd, J_1 = 8.67 Hz, J_2 = 2.37 Hz, 1H, H_{Ar}), 7.34 (dd, J_1 = 8.7 Hz, J_2 = 2.69 Hz, 1H, H_{Ar}), 7.53 (d, J = 2.64, 1H, H_{Ar}), 8.05 (d, J = 8.76 Hz, 1H, H_{Ar}), 8.14 (d, J = 8.85 Hz, 1H, H_{Ar}), 10.21 (s, 2H, -OH).

^{13}C NMR (75 MHz, DMSO-d_6) δ/ppm: 103.5 (C7), 107.0 (C5), 110.1 (C13), 111.0 (C11), 112.8 (C9), 114.8 (C3), 123.7 (C-14), 129.6 (C10), 146.5 (C4), 152.0 (C6), 153.8 (C12, C-OH), 158.5 (C8, C-OH), 160.9 (C2, C=O).

FT-IR (ν/cm^{-1}): 3321 (γ OH), 3196, 2924, 2854, 1773, 1700, 1615, 1462, 1317, 1272, 1126, 1080, 729.

MS-ESI (negative), *m/z*; calculated for $C_{13}H_7O_4$, $[M-H]^-$: 227.0; found: 226.7.

Analysis (%): calculated C (68.42), H (3.53), N (0); found C (66.64), H (4.03), N (0.07).

Additionally, surrogates S5 and S6 were prepared with the aim of having AOH and AME molecular analogues which are non-fluorescent. If employed for MIP synthesis, such templates would

not provide a fluorescent background signal if the molecule is not completely washed out. To this end, two molecules with a similar structure and functional groups as the mycotoxins were selected, with the difference, that, in this case, the molecules are not rigid, therefore, are weakly or non-fluorescent. For the synthesis of these two compounds, also dimethoxybenzoic acid and phenol were employed for the formation of the corresponding ester via a condensation reaction, as in the case of S1. However, in the case of S5, the DMBA molecule lacks the Br leaving the atom, since no intramolecular cyclisation is required. The surrogate S5 obtained in this way is afterwards demethylated in the presence of $AlCl_3$ and dodecanethiol to yield the compound S6.

V.2.5. 3-Methoxy-5-methylphenyl 2,4-dimethoxybenzoate (S5)

$C_{17}H_{18}O_5$ Mw: 302.30 g mol^{-1}

2,4-Dimethoxybenzoic acid (DMBA, 0.186 g, 1.02 mmol) and 3-methoxy-5-methylphenol (MMPhOH, 0.273 g, 1.98 mmol) were weighed into a two-neck round bottom flask and dissolved at room temperature in anhydrous toluene (4.0 mL). Then, trifluoroacetic anhydride (1 mL, 13.1 mmol) was added, and the solution was left stirring under argon overnight. The solvent was eliminated by rotavaporation, and the solid was purified by column chromatography (silica, CH_2Cl_2–MeOH 60:1, *v/v*). Yield: 69%.

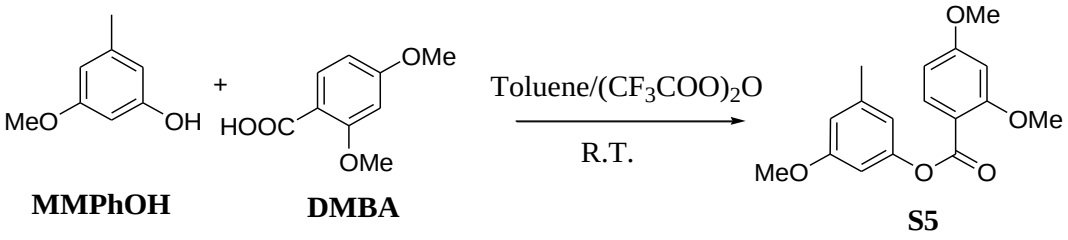

MMPhOH **DMBA** **S5**

Reagent	Supplier	Volume/mL	Mass/g	Mol	Purity
DMBA	Aldrich	---	0.186	1.02×10^{-3}	98%
MMPhOH	---	---	0.273	1.98×10^{-3}	97%
Toluene	Aldrich	4.00	---	---	99.8%
TFA anhyd.	Fluka	1.00	1.49	1.31×10^{-2}	>99.5%

Scheme 5.5: Synthesis of 3-methoxy-5-methylphenyl 2,4-dimethoxybenzoate (adapted from Kumar et al. [16]).

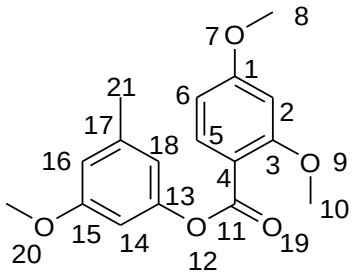

S5

TLC: CH_2Cl_2-MeOH (6:1, *v/v*) R_f = 0.40.

^{1}H-NMR (300 MHz, DMSO-d_6) δ/ppm: 3.7 (s, 3H, H21, CH_3), 3.90 (d, J_1 = 3.57 Hz, 6H, H8, H10, –OCH_3), 6.63 (s broad, 2H, H16$_{Ar}$), 6.74-6.68 (m, 6H, H18, 6, 2, 14 $_{Ar}$), 7.95 (d, J = 8.67 Hz, 2H, H5$_{Ar}$).

^{13}C-NMR (75 MHz, DMSO-d_6) δ/ppm: 22.3 (C21, -CH_3), 57.0 (C8, -OCH_3), 57.4 (C10, -OCH_3), 57.8 (C20, -OCH_3), 101.0 (C2), 106.9 (C14), 107.8 (C5), 112.0 (C6), 113.9 (C16), 116.7 (C4), 135.5 (C18), 140.3 (C5), 153.5 (C17), 161.8 (C15), 163.2 (C1), 164.9 (C3), 166.8 (C11, C=O).

MS-ESI (positive), *m/z*; calculated for $C_{17}H_{18}O_5Na$, $[M+Na]^+$: 325.1, found: 325.1.

V.2.6. 3-Hydroxy-5-methylphenyl 2,4-dihydroxybenzoate (S6)

$C_{14}H_{12}O_5$ Mw: 260.24 g mol^{-1}

Anhydrous $AlCl_3$ (0.758 g, 4.4 mmol) was suspended in a mixture of dodecanethiol (0.5 mL) and chlorobenzene (5.5 mL) and placed in an ice bath under argon. Then S5 (0.250 g, 8.3 mmol) was added, and after 30 min, the ice bath was removed, and the mixture was kept at room temperature for additional 30 min. Finally, it was heated at 100 ºC. The reaction was monitored by TLC (silica, CH_2Cl_2–MeOH 6:1, *v/v*). After 5 h, the mixture was poured onto 15 mL of 3% aqueous HCl in an ice bath, and the resulting precipitate was filtered and washed with water and a few millilitres of methanol. Yield: 65%.

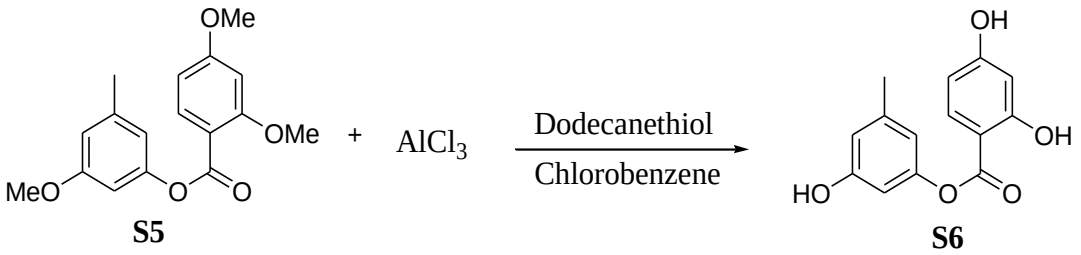

S5 **S6**

Reagent	Supplier	Volume/mL	Mass/g	Mol	Purity
$AlCl_3$	Aldrich	---	0.583	4.4×10^{-3}	99%
S5	GSOLFA	---	0.250	8.3×10^{-4}	---
Dodecanethiol	Aldrich	0.5	---	---	99.5%
Chlorobenzene	Aldrich	5.5	---	---	>99.8%

Scheme 5.6: Synthesis of 3-hydroxy-5-methylphenyl 2, 4-dihydroxybenzoate.

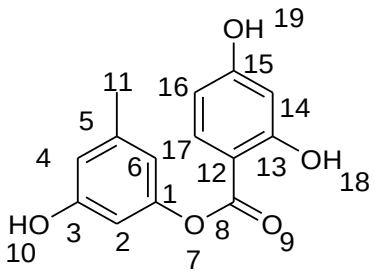

S6

TLC: CH_2Cl_2-MeOH (6:1, *v/v*) R_f = 0.40.

^{1}H-NMR (300 MHz, DMSO-d_6) δ/ppm: 3.7 (s, 3H, H11, CH_3), 6.4 (d, *J* = 2.28 Hz, 1H, $H4_{Ar}$), 6.47 (d, *J* = 2.2 Hz, 1H, $H14_{Ar}$), 6.49 (*m*, *J* = 2.3 Hz, 1H, $H16_{Ar}$), 6.51 (s, broad, 1H, $H6_{Ar}$), 6.56 (*d*, 1H, $H2_{Ar}$), 7.86 (d, *J* = 8.76 Hz, 1H, $H17_{Ar}$), 9.70 (s, 1H, -OH), 10.47 (s, 1H, -OH), 10.68 (s, 1H, -OH).

^{13}C NMR (75 MHz, DMSO-d_6) δ/ppm: 22.0 (C11, -CH_3), 104.3 (C14), 105.4 (C12), 108.0 (C2), 110.2 (C16), 114.8 (C4), 115.3 (C6), 134.0 ($C17_{Ar}$), 141.6 (C5), 152.7 (C1), 164.9 (C3, C13, C-OH), 166.4 (C15, C-OH), 169.0 (C8, C=O).

MS-ESI (negative), *m/z*; calculated for $C_{14}H_{11}O_5$, $[M-H]^-$: 259.1, found: 258.8.

Analysis (%): calculated C (64.61), H (4.65), N (0); found C (60.64), H (5.03), N (0.08).

V.3. Synthesis of an alternariol surrogate for covalent imprinting of polymers (S7).

As it has already been discussed in the Introduction section, there are two main methods for the imprinting of polymers, via *covalent* attachment of the template in the polymer matrix, or via a *non-covalent* immobilisation. The most frequently employed method, due to its simplicity in the synthesis and easy template extraction protocols, is the one based on the non-covalent interaction of the template molecule with the functional monomers. Covalent attachment of the surrogates, however, could yield to polymer cavities with better recognition properties, because in this way, functional groups are better oriented in the polymer for further re-binding of the target. An interesting strategy combines the advantages of both methods by employing a covalent imprinting via chemical bonds which are easily broken by clean and non-aggressive methods. A chemical group that meets these requirements is the urethane function Scheme 5.7. The urethane bond is formed between an isocyanate and alcohol or a phenol group, and can be easily broken simply by heating at T > 60 ºC. After the urethane decomposition, the template molecule is no longer linked to the polymer, and it can be easily washed out from the material [17,18].

Synthesis of diurethane S7

$C_{27}H_{26}N_2O_{10}$ Mw: 538.50 g mol^{-1}

2-Isocyanatoethyl 2-methylacrylate (0.20 g, 1 mmol) was added to a solution of S4 (0.050 g, 0.219 mmol) in dry pyridine (0.657 ml). The reaction mixture was stirred 40 h at room temperature, and the reaction was quenched with ice cold water (2 mL). The precipitated solid was filtered and dried under vaccum at 45 ºC to yield 2-{[({3-[({[2-(methacryloyloxy)ethyl]amino}carbonyl)oxy]-6-oxo-6*H*-benzo[*c*]chromen-8-yl}oxy)carbonyl]amino}ethyl 2-methylacrylate (S7). Yield: 75%.

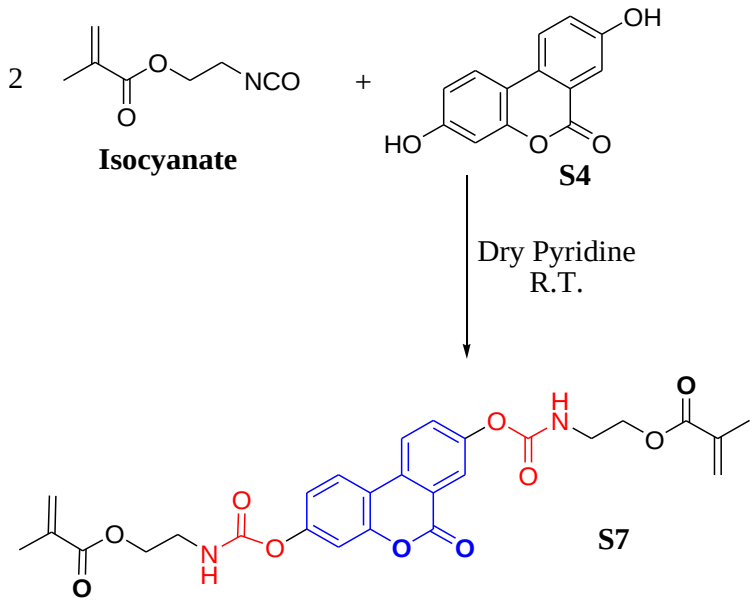
2
NCO
O
O
Isocyanate
+
OH
HO
O
O
S4
Dry Pyridine
R.T.
H
N
O
O
O

MS-ESI (positive), *m/z*; calculated for $C_{27}H_{26}N_2O_{10}Na$, $[M+Na^+]$: 561.1, found: 561.2.

FT-IR (ν/cm^{-1}): 3356 (γ NH), 2996, 2924, 2852, 1719, 1623, 1252, 1121, 1067, 777.

V.4. Synthesis of tenuazonic acid and its surrogate

V.4.1. Synthesis of the sodium salt of tenuazonic acid (*Na^+ rTeA$^-$*)

$C_{10}H_{15}NO_3$, Mw: 197.23 g mol^{-1}

Sodium 3-(1-hydroxyethylidene)-5-[(1*S*)-1-methylpropyl]pyrrolidine-2,4-dione, "synthetic" tenuazonic acid (Na^+ *r*TeA$^-$) was prepared as follows: (5.39 mmol) L-isoleucine methyl ester hydrochloride was dissolved in *m*-xylene (5.39 mL), and the calculated amount of Et_3N (5.39 mmol) was added to the mixture. After complete disolution, 2,2,6-trimethyl-4*H*-1,3-dioxin-4-one (30 mmol) was added dropwise during 30 min at room temperature; after 5 h reflux, the mixture was filtered when it was still hot and after cooling down, the solid was washed with diethyl ether; the solvent was evaporated giving an oily compound in 99% yield.

Sodium methoxide solution in methanol (58 mmol, 3.3 mL) was added to a solution of methyl *N*-acetoacetyl-L-iso-leucinate (5.8 g, 27.2 mmol) in 5–10 mL of dry methanol and refluxed with stirring for 4 h. Then the solvent was removed under reduced pressure, the residue was dissolved in 20 mL of water and washed with diethyl ether (3×20 mL). The aqueous layer was separated and acidified to pH 2–3 with 1 M HCl; a white solid and a browny oil appeared. The acidic solution was extracted with diethyl ether (3×20 mL) and ethyl acetate (20 mL). Finally, both organic layers were collected together and acidified to (pH 2–3) with 1 M HCl and washed with 20 mL of water. After drying over $MgSO_4$, the solvent was evaporated under reduced pressure to yield a crude sodium salt of acid tenuazonic acid as an orange-red oil. Yield: 3.74 g, 71%.

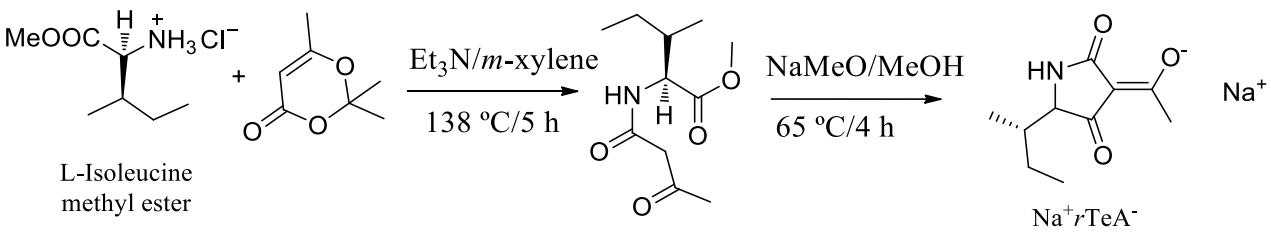

L-Isoleucine methyl ester

Na^+rTeA^-

Reagent	Supplier	Volume/mL	Mass/g	Mol	Purity
L-Isoleucine methyl ester HCl	Aldrich	---	1.00	5.39×10^{-3}	≥98%
Et_3N	Aldrich	0.747	0.542	5.35×10^{-3}	97%
Diketene	Acros	4.00	4.28	30.1×10^{-3}	95%
m-Xylene	Fluka	5.39	---	---	analytical
MeOH	Aldrich	30.2	---	---	99.0%
MeONa in MeOH	Aldrich	3.3	0.003	5.9×10^{-5}	95.0%

Scheme 5.8: Synthesis of 3-(1-hydroxyethylidene)-5-[(1*S*)-1-methylpropyl]pyrrolidine-2,4-dione, as its sodium salt (*Na^+rTeA$^-$*) [21].

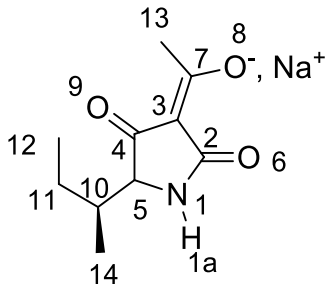

Na^+ rTeA$^-$

TLC: CH_2Cl_2-MeOH **(**9:1, *v/v*) R_f = 0.24(with potassium permanganate as TLC developer[1]).

^{1}H-NMR (300 MHz, $CDCl_3$) δ/ppm: 0.95 (*m*, *b*, 6H, *H12*, *H14*), 1.28 (*m*, 2H, *H11*), 1.97 (*m*, 1H, *H10*), 2.46 (*s*, 3H, *H13*), 3.80 and 3.92 (*d*, 1H, *H5*, *E- Z-*), 6.60 and 6.70 (*s b*, 1H, *H1a*).

^{13}C NMR (75 MHz, $CDCl_3$) δ/ppm: 12.0 (*C12*), 16.1 (*C14*), 20.0 (*C13*), 23.0 (*C11*), 37.3 (*C10*), 67.0 (*C5*), 102.8 (*C3*), 177.0 (*C7*), 184.9 (*C2*), 195.8 (*C4*). **DEPT 135** (75 MHz, $CDCl_3$) δ/ppm: 12.0 ($C_{pos.}$, *C12*, -CH_3), 16.1 ($C_{pos.}$, *C14*, -CH_3), 20.0 ($C_{pos.}$,*C13*, -CH_3), 22.7 ($C_{neg.}$, *C11*, -CH_2-), 37.3 ($C_{pos.}$, *C10*, -CH-), 67.0 ($C_{pos.}$, *C5*, -CH-).

MS-ESI (negative), *m/z*; calculated for $C_{10}H_{14}NO_3$, $[M-H]^-$: 196.1, found: 195.8.

FT-IR (ν/cm^{-1}): 3247(γ O-H stretching), 2963, 2932 (aliphatic C-H stretching), (C=O, keto group, cyclic) 1712, 1611, 1563, 1377, 1212.

[1] This particular stain is excellent for functional groups which are sensitive to oxidation. It was prepared with 1.5 g of $KMnO_4$, 10 g of K_2CO_3 and 1.25 mL of 10% NaOH in 200 mL H_2O. Its typical lifetime is approximately 3 months.

Absorption: UV-vis (MeOH): λ_{max} (nm): 240 and 279.

HPLC t_R (min) = 10.5 (MeOH with addition of zinc acetate, λ_{abs} = 280 nm).

Rotation $[\alpha]_{\lambda}^{T}$: λ_{abs} (280, 240 nm) MeOH (c_{TeA} = 1 g/100 mL): $[\alpha]_{578}^{21} = 50.5°$; $[\alpha]_{546}^{21} = 59.5°$; $[\alpha]_{546}^{25} = 45.4°$; $[\alpha]_{578}^{25} = 52.3°$; $[\alpha]_{546}^{25} = 51.2°$

Analysis (%): calculated C (60.90), H (7.67), N (7.10); found C (60.93), H (7.86), N (6.64).

V.4.2. Synthesis of tenuazonic acid surrogate (*Na^+sTeA^-*)

$C_{10}H_{15}NO_3$, Mw: 197.23 g mol^{-1}

L-leucine methyl ester hydrochloride (5.39 mmol) was dissolved in 5.39 mL of *m*-xylene, and the calculated amount of Et_3N (0.747 mL, 5.39 mmol) was added to the mixture. After complete dissolution, 2,2,6-trimethyl-4H-1,3-dioxin-4-one was added dropwise during 30 min at room temperature. After 5 h reflux, the mixture was filtered when it was still hot, and after cooling down, the solid was washed with diethyl ether; the solvent was evaporated giving an oily compound in a 99% reaction yield.

Sodium methoxide solution in methanol (3.3 mL, 58 mmol) was added to a solution of methyl *N*-acetoacetyl-L-leucinate (5.8 g, 27.2 mmol) in 10 mL of dry methanol and refluxed with stirring for 4 h. Then the solvent was removed under reduced pressure, the residue was dissolved in 20 mL of water and washed with diethyl ether (3×20 mL). The aqueous layer was separated and acidified to pH 2–3 with 1 M HCl; a white solid and a browny oil appeared. The acidic solution was extracted with diethyl ether (3×20 mL) and ethyl acetate (20 mL). Finally, both organic layers were collected together and acidified to pH 2–3 with 1 M HCl and washed with 20 mL of water. After drying over $MgSO_4$, the solvent was evaporated under reduced pressure to yield a crude sodium salt of the 3-(1-hydroxyethylidene)-5-[2-methylpropyl]pyrrolidine-2,4-dione (Na^+ $sTeA^-$) as an orange-red oil. Yield: 4.22 g, 80%.

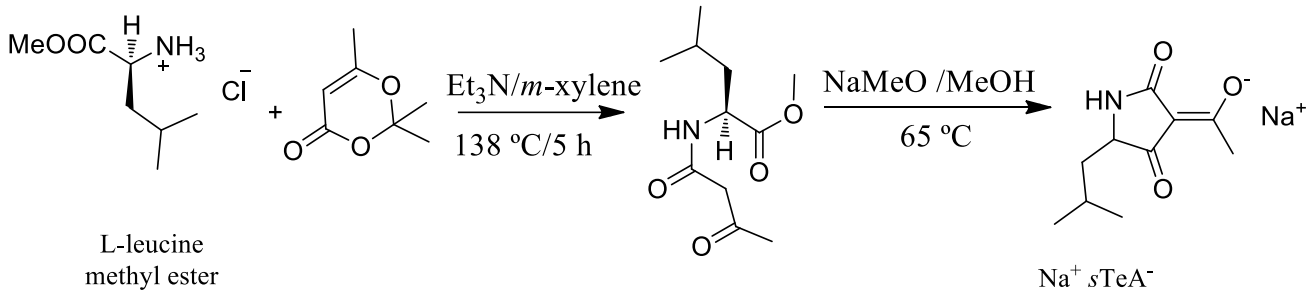

L-leucine methyl ester

Na^+ *s*TeA^-

Reagent	Supplier	Volume/mL	Mass/g	Mol	Purity
L-leucine methyl ester HCl	Aldrich	---	1.00	5.39×10^{-3}	≥98%
Et_3N	Aldrich	0.747	0.542	5.35×10^{-3}	97%
Diketene	Acros	4.00	4.28	30.1×10^{-3}	95%
m-xylene	Fluka	5.39	---	---	analytical
MeOH	Aldrich	30.2	---	---	99.0%
MeONa in MeOH	Aldrich	3.0	0.003	5.3×10^{-5}	≥97.0%

Scheme 5.9: Synthesis of 3-(1-hydroxyethylidene)-5-[2-methylpropyl]pyrrolidine-2,4-dione (*s*TeA) in the form of sodium salt.

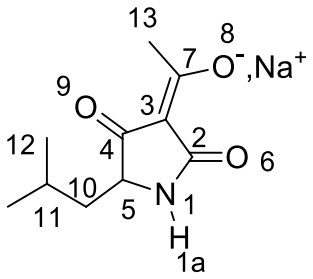

Na^+ *s*TeA

TLC: CH_2Cl_2-MeOH **(**9:1, *v/v*) R_f = 0.24 (with potassium permanganate as TLC developer).

^{1}H-NMR (300 MHz, $CDCl_3$) δ/ppm: 0.95 (*m*, 6H, *H12*, *H14*), 1.42 (*m*, 2H, *H11*), 1.72 (*m*, 1H, *H10*), 2.45 (*s*, 3H, *H13*), 3.82 and 3.85 and 4.10 (*dd*, 1H, *H5*, *E- Z-*), 6.69 and 6.83 (*s b*, 1H, *H1a*, -NH).

^{13}C NMR (75 MHz, $CDCl_3$) δ/ppm: 19.9 (*C14*), 21.8 (*C12*), 23.7 (*C11*), 25.8 (*C13*), 41.3 (*C10*), 61.2 (*C5*), 101.9 (*C3*), 176.0 (*C2*), 184.9 (*C7*), 198.1 (*C4*).

MS-ESI (negative), *m/z*; calculated for $C_{10}H_{14}NO_3$, $[M-H]^-$: 196.1, found: 195.8.

FT-IR (ν/cm^{-1}): 3247(γ OH stretching), 963, 2932 (aliphatic C-H stretching), 1712 (C=O, keto group, cyclic), 1611, 1563, 1377, 1212.

Analysis (%): calculated C (60.90), H (7.67), N (7.10); found C (60.85), H (7.75), N (6.62).

V.4.3. Complexation of tenuazonic acid with Cu(II)

In order to ensure the complete conversion of *r*TeA into the *r*TeA sodium salt, the synthetized tetramic acid was passed through a sodium cation exchanger resin. For this purpose, Amberlite® IR120 Na^+ (10 g) was kept in methanol for 2 h for swelling. After elimination of MeOH, the resin was transferred to a beaker containing a solution of tenuazonic acid (1.69 mmol) in methanol under and kept stirring at room temperature for 2 h. After that, the resin was packed in a glass column, and the tetramic acid was collected as Na^+rTeA^-. After elimination of methanol, a sticky oil was obtained (71.3% yield).

For the preparation of the copper(II) complex, Na^+rTeA^- (1.2 mmol) was mixed with 1.6 mmol of copper(II) acetate in water with gentle agitation at room temperature for 1 h. The tenuazonic acid copper salt was then extracted from the aqueous phase with chloroform (3×10 mL). After evaporation of chloroform, Cu(*r*TeA)$_2$ was obtained in a 75% yield.

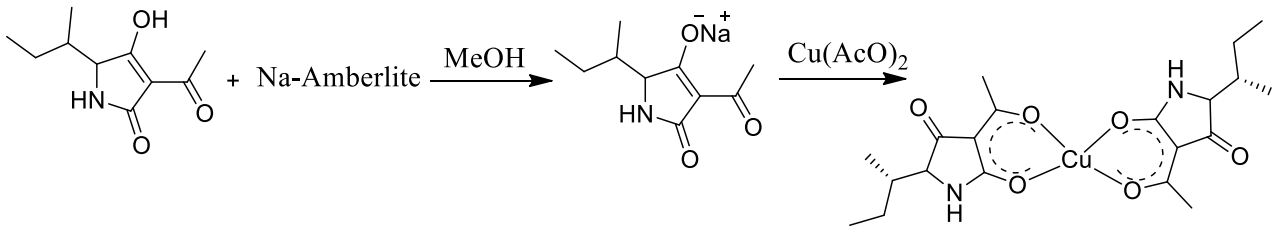

Figure 5.2: Synthesis of the tenuazonic acid-copper(II) complex, Cu(*r*TeA)$_2$ [22,23].

Absorption UV-vis (MeOH): λ_{max} (nm): 289.

HPLC t_R (min): 10.6 (with addition of zinc acetate in MeOH, λ_{abs} = 280 nm).

V.5. Synthesis of fluorescent pyrene monomers

V.5.1. *N*-pyren-1-ylacrylamide (PA)

$C_{19}H_{13}NO$ Mw: 271.28 g mol^{-1}

Acryloyl chloride (110 µL, 1.35 mmol) was slowly added to a cooled (0 ºC) solution of *1-aminopyrene* (148 mg, 0.66 mmol) in a mixture of acetonitrile (9.5 mL) and water (0.5 mL). The reaction mixture was stirred at room temperature for 3 h. The resulting suspended solid was filtered, washed with ice-cooled acetonitrile and dried. Yield: 62%. The compound was crystallised from *p*-xylene. M.P.: 233-234 ºC.

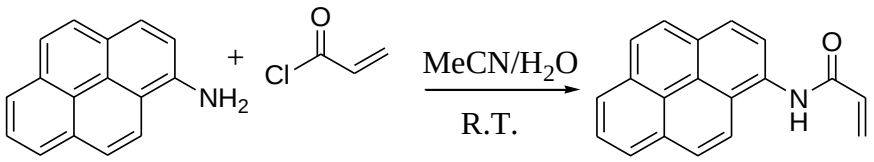

PA

Reagent	Supplier	Volume/mL	Mass/g	Mol	Purity
Acryloyl chloride	Aldrich	0.110	---	1.35×10^{-3}	97%
1-aminopyrene	Aldrich	---	0.1479	0.66×10^{-3}	97%
Acetonitrile	Aldrich	9.5	---	---	>99.8%

Scheme 5.10: Synthesis of *N*-pyren-1-ylacrylamide (PA). Adapted from Munkholm et al. [19]

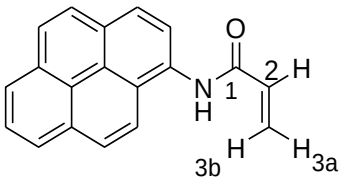

PA

TLC: Hexane-AcOEt (2:1, *v/v*) R_f = 0.32.

^{1}H-NMR (300 MHz, DMSO-d_6) δ/ppm: 5.88 (*dd*, J_1 = 10.8 Hz, J_2 = 1.5 Hz, 1H, H3a), 6.38 (*dd*, J_1 = 17.3 Hz, J_2 = 1.5 Hz, 1H, H3b), 6.80 (*dd*, J_1 = 17.6 Hz, J_2 = 10.87 Hz, 1H, H2), 8.3-8.0 (*m*, 9 H_{Ar}), 10.5 (*s*, 1H, NH).

^{13}C-NMR (75 MHz, DMSO-d_6) δ/ppm: 122 (C10b, C_{Ar}), 123 (C_{Ar}), 124 (C_{Ar}), 124 (C_{Ar}), 125 (C_{Ar}), 126 (C3, CH_2), 127 (C_{Ar}), 127 (C_{Ar}), 128 (C_{Ar}), 131 (C_{Ar}), 131 (C2), 132 (C3, C_{Ar}), 133 (C2, CH), 164 (C1, CO).

MS-ESI (positive), *m/z*; calculated for $C_{19}H_{15}NONa$, $[M+Na]^+$ ion: 294.3, found: 294.0.

FT-IR (ATR, ν/cm^{-1}): 3248, 3031, 2925, 1661, 1630, 1557, 1525, 842, 711.

V.5.2. *N*-pyren-1-ylmethacrylamide (PMA)

$C_{20}H_{19}NO$ Mw: 289.37 g mol^{-1}

Methacryloyl chloride (44 µL, 0.46 mmol) was slowly added to a cooled (0 ºC) solution of 1-aminopyrene (50 mg, 0.23 mmol) in acetonitrile (2 mL) and water (40 µL). The reaction mixture was stirred at room temperature for 3 h; then filtered. The filtrate was evaporated, and the solid dissolved in chloroform (10mL), washed with 10% aqueous $NaHCO_3$ (5 mL) and extracted with (2×5 mL) water. The organic phase was dried over $MgSO_4$ and evaporated to give a green oil that was purified by column chromatography (hexane: ethyl acetate 8:1 to 4:1, *v/v*) to furnish 35 mg. Yield: 59%, off-white solid compound.

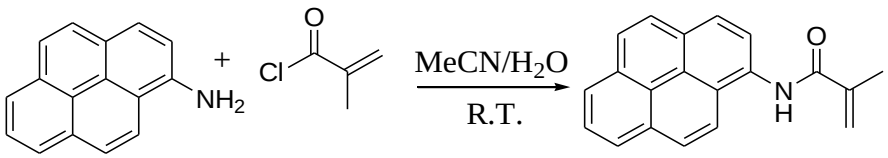

PMA

Reagent	Supplier	Volume/mL	Mass/g	Mol	Purity
MTAC	Acros	0.044	---	0.46×10^{-3}	95%
AMP	Aldrich	---	0.0499	0.23×10^{-3}	97%
Acetonitrile	Aldrich	9.5	---	---	>99.8%

Scheme 5.11: Synthesis of *N*-pyren-1-ylmethacrylamide (PMA).

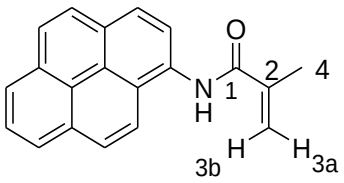

PMA

TLC: Hexane-EtOAC (2:1, *v/v*) R_f = 0.40.

^{1}H-NMR (300 MHz, DMSO-*d*$_6$) δ/ppm: 2.09 (3H, H4, CH_3), 5.46 (d, *J* = 3.89 Hz, 1H, H3b), 6.20 (*d*, *J* = 3.89 Hz, 1H, H3a, CH2), 8.3-8.0 (m, H_{Ar}), 10.33(*d*, *J* = 8.3, 1H, NH).

^{13}C-NMR (75 MHz, DMSO-*d*$_6$) δ/ppm: 19 (C4, CH_3), 120 (C3, CH_2), 123 (C_{Ar}), 124 (C_{Ar}), 124 (C_{Ar}), 125 (C_{Ar}), 125 (C_{Ar}), 126 (C_{Ar}), 126 (C_{Ar}), 129 (C_{Ar}), 131 (C_{Ar}), 132 (C_{Ar}), 140 (C2, CH=CH2), 167 (C1, C=O).

MS-ESI (positive), *m/z*; calculated for $C_{20}H_{15}NONa$, $[M+Na]^+$ ion: 308.3, found: 308.0.

FT-IR (ATR, ν/cm^{-1}): 3275, 1656, 1600, 1515, 846.

V.5.3. *N*-(pyren-1-ylmethyl)acrylamide (PMeA)

$C_{20}H_{15}NO$ Mw: 285.34 g mol^{-1}

Acryloyl chloride (25 µL, 0.3 mmol) and pyrenemethylamine hydrochloride (80 mg, 0.3 mmol) were refluxed in toluene (3 mL) for 3 h. The solvent was evaporated, the solid treated with chloroform (10 mL), washed with water (5 mL) and 10% aqueous $NaHCO_3$ (5 mL) till neutralisation and extracted with (3×5 mL) water. The organic phase was dried over $MgSO_4$ and evaporated, the residue was purified by column chromatography (hexane-ethyl acetate, 2:1 to 1:1, *v/v*) to furnish 75 mg. Yield: 87%, off-white solid compound. M.P.: 204-205 ºC in toluene.

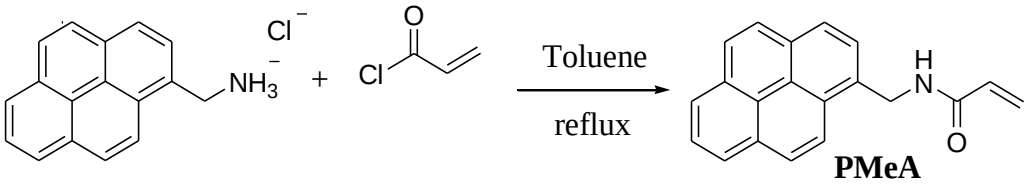

PMeA

Reagent	Supplier	Volume/mL	Mass/g	Mol	Purity
AC	Aldrich	0.025	---	0.3×10^{-3}	97%
1-Pyrenemethylamine hydrochloride	Aldrich	---	0.080	0.3×10^{-3}	95%
Toluene	Aldrich	3.0	---	---	>99%

Scheme 5.12: Synthesis of *N*-(pyren-1-ylmethyl) acrylamide. Adapted from Shama et al. [20]

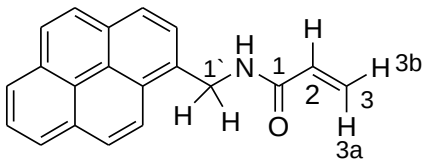

PMeA

TLC: CH_2Cl_2-MeOH (10:1, *v/v*) R_f = 0.45.

^{1}H-NMR (300 MHz, DMSO-d_6) δ/ppm: 5.15 (*d*, J = 5.4 Hz, 2H, H1´, NH-CH_2), 5.75 (*d*, J = 5.3 Hz, 1H, H2, CO-CH), 6.23 (*d*, J = 4.1 Hz, 1H, H3a), 6.39 (*d*, J = 4.3 Hz, 1H, H3b), 8.5-8.0 (*m*, H_{Ar}) 8.88 (*s*, 1H, NH).

^{13}C-NMR (75 MHz, DMSO-d_6) δ/ppm: 41 (C1, NH-CH_2), 123 (C3, CH_2), 124 (C_{Ar}), 125 (C_{Ar}), 125 (C_{Ar}), 126 (C_{Ar}), 126 (C_{Ar}), 127 (C_{Ar}), 127 (C_{Ar}), 128 (C_{Ar}), 128 (C_{Ar}), 129 (C_{Ar}), 130 (C_{Ar}), 131 (C_{Ar}), 133 (C2), 165 (C1, C=O).

MS-ESI (positive), *m/z*; calculated for $C_{20}H_{15}NONa$, $[M+Na]^+$ ion: 308.3, found: 308.0.

FT-IR (ATR, ν/cm^{-1}): 3280, 3043, 1653, 1617, 843, 1535, 843.

V.5.4. *N*-(pyren-1-ylmethyl)methacrylamide (PMeMA)

$C_{21}H_{17}NO$ Mw: 299.37 g mol^{-1}

Methacryloyl chloride (35 µL, 0.37 mmol) and pyrenemethylamine hydrochloride (0.31 mmol) were refluxed in toluene (3 mL) for 12 h till complete disappearance of starting material. The solvent was evaporated, the solid treated with chloroform (10 mL), washed with water (5 mL) and 10% aqueous

$NaHCO_3$ (10 mL) washed with water (2×10 mL) again till neutralisation and extracted with (3×5 mL) water. The organic phase was dried and evaporated, the residue was purified by column chromatography (hexane-ethyl acetate, 8:1 to 2:1, *v/v*) to furnish 78 mg. Yield: 85%, shiny light-white solid compound. M.P.:141-142 ºC in toluene.

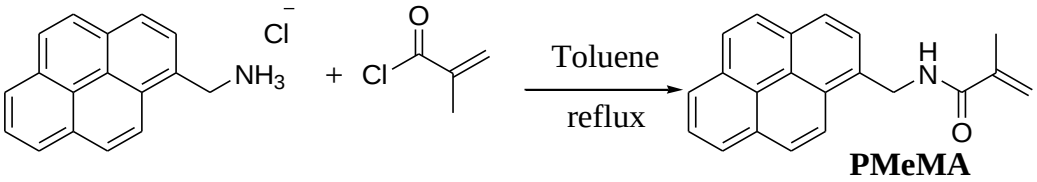

PMeMA

Reagent	Supplier	Volume/mL	Mass/g	Mol	Purity
MTAC	Acros	0.035	---	0.37×10^{-3}	95%
1-Pyrenemethylamine hydrochloride	Aldrich	---	0.080	0.31×10^{-3}	95%
Toluene	Aldrich	3.0	---	---	>99%

Scheme 5.13: Synthesis of *N*-(pyren-1-ylmethyl) methacrylamide.

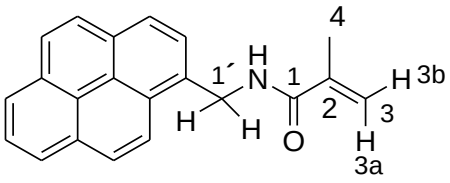

PMeMA

TLC: CH_2Cl_2-MeOH (10:1, *v/v*) R_f = 0.46.

^{1}H-NMR: (300 MHz, DMSO-d_6) δ/ppm: 1.90 (3H, H4, CH_3), 5.05 (*d*, *J* = 5.4 Hz, 2H, H1´, NH-CH_2), 5.40 (*d*, *J* = 4.1 Hz, 1H, H3a), 5.78 (*d*, *J* = 4.1 Hz, 1H, H3b), 8.50-8.00 (m, H_{Ar}), 8.78 (*d*, *J* = 8.3, 1H, NH).

^{13}C-NMR: (75 MHz, DMSO-d_6) δ/ppm: 19 (C4, CH_3), 41 (C1, NH-CH_2), 120 (C3, CH_2), 124 (C_{Ar}), 125 (C_{Ar}), 125 (C_{Ar}), 126 (C_{Ar}), 126 (C_{Ar}), 127 (C_{Ar}), 127 (C_{Ar}), 128 (C_{Ar}), 128 (C_{Ar}), 130 (C_{Ar}), 131 (C_{Ar}), 131 (C_{Ar}), 134 (C_{Ar}), 140 (C2), 168 (C1, C=O).

MS-ESI (positive), *m/z*; calculated for $C_{21}H_{19}NONa$, $[M+Na]^+$ ion: 322.4, found: 322.0.

FT-IR (ATR, ν/cm^{-1}): 3290, 3041, 2922, 2878, 1651, 1608, 842, 1531, 842.

V.6. Synthesis of a MIP for AOH and AME recognition

V.6.1. Synthesis of a MIP library for the selection of the best MIP composition for AOH and AME recognition

Since the possibilities for polymer synthesis –selection of an appropriate template, functional monomer, cross-linker, porogen, radical initiator, etc.) can be very diverse, for the preparation of MIPs selective for AOH and AME we decided to follow a combinatorial approach for obtaining, in a small synthetic scale, different MIPs. From this MIP and NIP series, the composition yielding to the MIP with the best recognition properties for the mycotoxins was selected for the preparation of MIPs on a greater scale or in a more appropriate format (such as porous microsphere particles). To this end, a selection of functional monomers (1-ALPP, MAM, HEMA, MAA, VBA, DAEM, VPY and EAMA, see Fig. 5.3, were tested in combination with different templates (S1 to S4) and two different cross-linkers (DVB and EDMA). In all cases, DMSO was used as the porogen and ABDV as radical initiator. The template (T):functional monomer (FM):cross-linker (CL) molar ratio was always kept at 1:32:160.

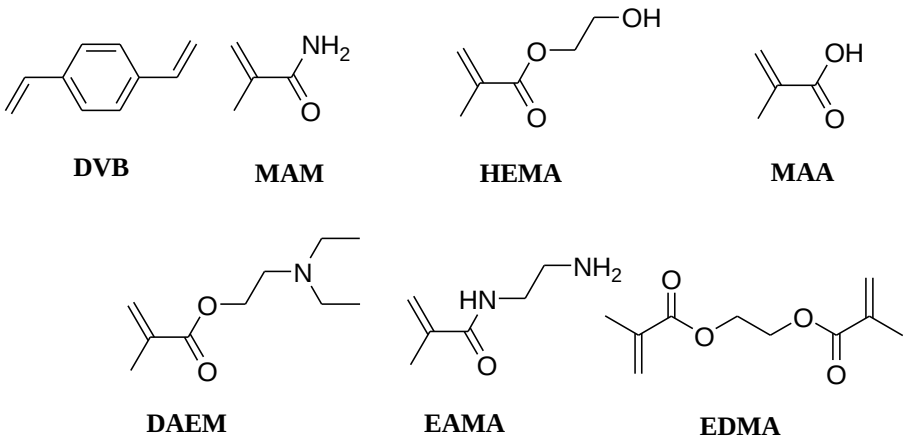

Figure 5.3: Functional monomers and cross-linkers employed for the combinatorial synthesis of MIPs and NIPs.

The volume of porogen (DMSO) was calculated in such a way that the ratio $V_{DMSO}/(V_{DMSO} + V_{total\ monomers})$ was kept at ~ 0.57. Non-imprinted polymers (NIPs) were prepared in the same way as the corresponding MIPs, but without adding the template to the monomer mixture. The polymerization

was performed in 96-well 2-mL/well polypropylene plates sealed with PTFE-coated lids (Radleys, UK), in a distribution that is shown in Table 5.1. All the solutions were purged previously with argon for 5 min. Stock solutions of the components (monomers, initiator, and template) were transferred into the wells. In the case of the imprinted polymers, each template (7 mg) was weighted and placed in a different well. Then, the corresponding functional monomer for each MIP/NIP pair was weighted and placed into a different 96-well plate. Monomers that were supplied as the hydrochloride salt were firstly neutralised by adding a stoichiometric amount of TBAOH. To this end, the solvent in the required amount of commercial 1 M solution of TBAOH in methanol was removed by rotavaporation, and the solid residue was dissolved in anhydrous DMSO purged with argon beforehand. Then, either neat DMSO or the DMSO-TBAOH mixture was added to the wells containing the functional monomers, in such a way that the total volume was either 300 µL for the polymer series based on DVB as cross-linker, or 475 µL if the cross-linker was EDMA (in order to keep the ratio $V_{DMSO}/(V_{DMSO} + V_{total\ monomers}) \sim 0.57$). Then, the selected template was added to each DMSO solution of monomers and left equilibrating for 15 min at room temperature to allow for the monomer-template interaction to occur. Finally, the ABDV radical initiator and the chosen cross-linker (EDMA or DVB) were added to each well. The 96-well plates were purged with nitrogen for 5 min and sealed with the PTFE-coated lids. Then, the plate was placed in an oven for one day at 50 °C and a second day at 70 °C. The bulk polymers obtained in this way were ground with an agate mortar, and the grains were transferred to another 2 mL/well 96-well plate containing a 10 µm polypropylene porous membrane per well. This membrane is used as a filter, allowing, once the reaction is finished, washing of the polymers in the same wells.

For extracting the template from the imprinted polymers, the latter were washed 3 times with 2 L of a solution of HCl 5% in MeOH and 500 mL of water. After each washing step, HPLC analysis of the supernatant was performed to determine whether the template was still present. Non-imprinted polymers (NIPs) were treated in the same way.

The washed polymers were employed to carry out binding experiments with our target analyte, AOH. Prior to incubation with the mycotoxin, the library was washed with water and conditioned with the buffer used for the tests. Then, 1000 µL of a solution of AOH (7.5 mg L^{-1}) in either HEPES (0.1 M, pH 7.5) or acetonitrile experiments (see Chapter II Table 2.2 and Table 2.3) was added to 20

mg of each polymer placed in each well and the microplate was left to equilibrate for 24 h. The 7.5 μg load of the toxin corresponds roughly to 10% of the maximum concentration of binding sites, taking into account the amount of template that was used during the MIP synthesis and assuming quantitative template removal. After filtration, the concentration of free AOH in the solution was determined by reverse-phase HPLC analysis. The amount of mycotoxin bound by the polymer particles was determined from Eq. 5.3:

$$B = \frac{(C_0 - F)}{C_0} \times 100 \qquad (5.3)$$

where B is the percentage of AOH bound to the polymer, C_0 (mM) is the initial AOH concentration, and F (mM) is the final mycotoxin concentration in the supernatant. After the first binding experiment, the plate was washed with MeOH-TFA (99:1, *v/v*), until the template could no longer be detected by reverse-phase HPLC in the washing solution. The plates were subsequently reused in the next binding experiment.

Table 5. 1: Monomers and templates distribution in the 96-well plate for the preparation of the MIP/NIP library for AOH/AME.

Reference (FM)	1	2	3	4	5	6	7	8	9	10
A (ALPP)	NIP	S2	S1	S3	S4	NIP	S2	S1	S3	S4
B (MAM)	NIP	S2	S1	S3	S4	NIP	S2	S1	S3	S4
C (HEMA)	NIP	S2	S1	S3	S4	NIP	S2	S1	S3	S4
D (MAA)	NIP	S2	S1	S3	S4	NIP	S2	S1	S3	S4
E (VBA)	NIP	S2	S1	S3	S4	NIP	S2	S1	S3	S4
F (DAEM)	NIP	S2	S1	S3	S4	NIP	S2	S1	S3	S4
G (VPY)	NIP	S2	S1	S3	S4	NIP	S2	S1	S3	S4
H (EAMA)	NIP	S2	S1	S3	S4	NIP	S2	S1	S3	S4
	EDMA					DVB				

V.6.2. Alternariol re-binding with the polymer library

The synthesised library of NIPs and MIPs was incubated for 24 h with a solution of AOH (7.5 mg L^{-1}) in HEPES (100 mM, pH 7.5) and, in a different experiment, with a solution of AOH in neat acetonitrile. Then, the concentration of free analyte was determined in the supernatants by HPLC, and this concentration was converted to the total amount of bound analyte per polymer. The recoveries values for AOH are represented in *Chapter II Table 2.2 and 2.3*. These results show that the combination of EAMA as functional monomer and EDMA as cross-linker render the strongest binding for AOH when S2 is used as the template molecule. This combination (S2 = T; EAMA = FM; EDMA = CL) was selected for the synthesis of the polymer beads.

V.6.3. Evaluation of EAMA-S2 interaction by NMR experiments

In order to characterise the functional monomer (EAMA)–template interaction (S2), an NMR titration in deuterated DMSO was carried out. In this titration, the template S2 concentration was maintained constant, while increasing amounts of EAMA were added to the mixture. To that end, 4.2 mg (0.0172 mmol) of alternariol surrogate S2 were dissolved in 0.7 mL of anhydrous DMSO-d_6 (24.5 mM final concentration) in a glass vial. A stock solution of EAMA (0.287 M in DMSO-d_6) was prepared by dissolving 51.88 mg of EAMA hydrochloride in 1.1 mL of anhydrous DMSO-d_6 and adding this solution to a stoichiometric amount of solid TBAOH (from a 1 M solution in MeOH, evaporated at reduced pressure). Increasing amounts of EAMA stock solution were added to the S2 solution to final S2/EAMA mole ratios of 10, 5.0, 3.3, 2.0, 1.43, 1.25, 1.00, 0.67, 0.50, 0.40, 0.33, 0.25, 0.20, 0.13, and 0.10, and their ^{1}H-NMR spectra were recorded. It was observed that protons H7 and H10 (see the chemical structure and numbering in Chapter II) were the ones undergoing the largest chemical shift changes thus were the ones taken for representing the Job plot and for performing the calculations for the estimation of the FM-S2 association constants.

V.6.4. Polymerization into silica beads. Synthesis of MP-ME1 (S2:EAMA:MAM:EDMA 1:2:2:20) and MP-ME2 (S2:EAMA:EDMA 1:4:20)

For the synthesis of MP-ME1 in the form of porous microbeads, silica microspheres were employed as a mold for the polymerization. The synthetic protocol was as described in Fig. 5.4: 1 mmol of the template (S2), 2 mmol of the functional monomer (EAMA, neutralised with TBAOH as described above), and 2 mmol of the co-monomer (MAM), were dissolved in a DMSO-MeCN mixture (180/415 μL). After complete dissolution, 20 mmol of the cross-linker (EDMA) and the radical initiator 2,2'-azobis-(2,4-dimethylvaleronitrile) (ABDV, 2% by total weight of monomers) were added. The MP-ME2 microspheres were prepared in the same way but using instead 4 mmol of the neutralized functional monomer EAMA, and omitting the addition of the co-monomer MAM.

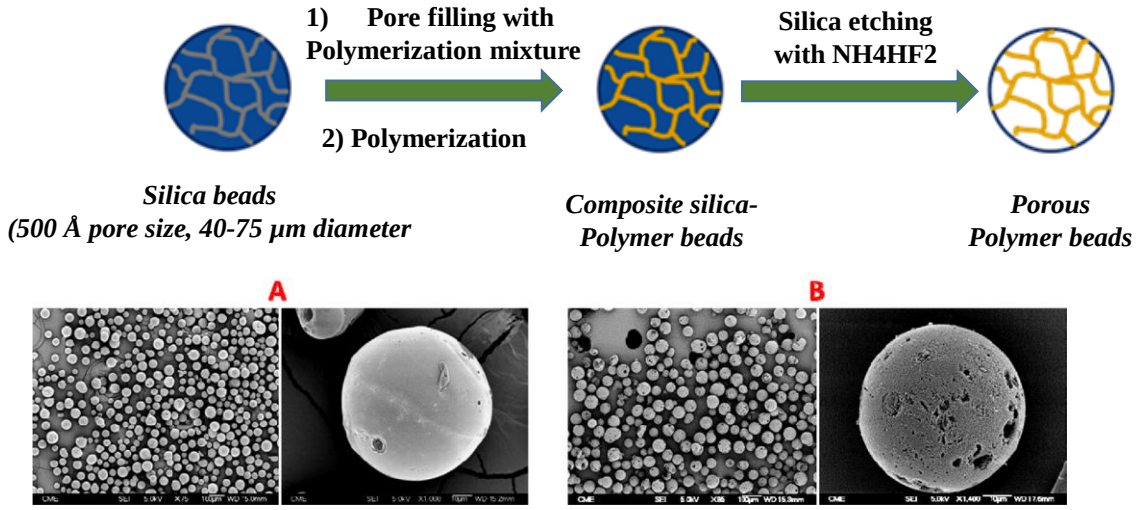

Figure 5.4: Preparation of MP-ME1 beads and NP-ME1 microspheres with a silica mould, and SEM images of the intermediate composite material (A) and the same beads after treatment with 3 M aqueous NH4HF2(B).

Then, 4.6 g of the silica microbeads were placed in a 100 mL glass vial and were mixed by stirring with the cocktail solution until the silica beads were freely flowing. The vial was sealed with a rubber septum, the system was purged with argon for 5 min, and the mixture was left in the oven for polymerization (60 °C, 24 h). Then, the silica was dissolved by adding 3×150 mL of an aqueous solution of ammonium hydrogen difluoride (3 M, Alfa Aesar) and shaking for 24 h after each addition. The final solid polymer obtained in this way was thoroughly washed with water (until pH ~

7), 1 L of MeOH-TFA (99:1, *v/v*) and, finally, 0.5 L of MeOH. The polymer beads were dried in a vacuum oven at 50 °C for 24 h before characterization and use. Then the powder was settled in water–MeOH (80:20, *v/v*) to remove fine particles. The corresponding non-imprinted polymers (NP-ME1 and NP-ME2) were prepared in the same way, but in the absence of the template molecule. The solvent volume to be used was determined using Eq. 5.4:

$$0.3 = \frac{V_{mL}}{(V + V_{tM})} \tag{5.4}$$

where V is the total volume in mL and V_{tM} is the total monomer volume. The total weight in g of silica microspheres was calculated from Eq. 5.5:

$$Si(g) = V_{tM} \times 2.5 \tag{5.5}$$

Reagent	Supplier	Volume/mL	Mass/g	Mol	Purity
S2	GSOLFA	---	0.488	2×10^{-3}	---
DMSO (anhydrous)	Acros	0.180	---	---	99.99%
EAMA·HCl	Polysciences	---	0.326	2×10^{-3}	99.5%
MeCN	Acros	0.415	---	---	>99.8%
MAM	Lancaster Synthesis	---	0.170	2×10^{-3}	98%
EDMA	Aldrich	3.77	3.96	20×10^{-3}	98%
ABDV	Wako Pure Chemicals	---	0.0107	2%	---
Silica	Silicycle	---	4.6	---	---

Scheme 5.14: Preparation of molecularly imprinted polymer in the form of spherical microparticles following the procedure of Titirici et al. [37].

Alternatively to the highly porous MP-ME microbeads, another format was considered for the preparation of MIPs with a good and rapid mass-transfer kinetics: core-shell nanoparticles, where the core is a silica nanoparticle which is coated by a thin, nanometric shell of MP-ME. The synthesis of this type of nanoparticles is described in the next section.

V.6.5. Synthesis of MIP-silica core-shell nanoparticles for AOH recognition (MP-CS/NP-CS nanoparticles)

Preparation of SiO_2 nanoparticles. SiO_2 nanoparticles were prepared in a round bottom flask using a mixture of 32% ammonia solution (823 mM), ethanol (16.25 mL) and water (24.75 mL). This mixture was stirred at 25 ºC at 1000 rpm and, subsequently, a solution of TEOS (0.02 mol) in ethanol (45.5 mL) was added. The reaction was further stirred at 500 rpm for 2 h at 25 ºC. The white solid obtained was separated by centrifugation washed by using distilled water and ethanol. Finally, after drying under vacuum overnight, 1.2 g of silica spheres of ca. 200 nm diameter (by electron microscopy) were obtained. The silica particles (1 g) were silanized with 1.7×10^{-2} mol of APTES in 60 mL of anhydrous toluene by refluxing 12 h under argon. The resulting -modified silica particles were separated by centrifugation, washed with toluene, and dried under vacuum [24].

Preparation of CPDB-coated SiO_2. Once the silica NPs were aminated, the RAFT (reversible addition-fragmentation chain-transfer) agent was immobilised on the NPs surface. For this, CPDB (4-cyano-4-(thiobenzoylthio) pentanoic acid, 0.822 g, 2.95 mmol), EtClForm (ethylchloroformate, 0.282 mL, 2.9 mmol) and triethylamine (0.402 mL, 2.9 mmol) were added into a three-necked round-bottom flask with 60 mL of anhydrous THF. The mixture was purged with Ar and cooled to –78 °C using a dry ice and acetone bath for 40 min. Then, 3.5 g of the modified SiO_2 nanoparticles were added at –10 °C (−10 °C can be achieved by adding a mixture 1:2.5 mixture of $CaCl_2$–ice) and the mixture was stirred at room temperature overnight. The particles were precipitated in 200 mL of hexane, washed with centrifugation using acetone and THF and dried under vacuum overnight.

Coating with a MIP layer of molar composition S2:EAMA:MAM:EDMA (1:2:2:20). The immobilized CPDB RAFT agent was then employed as the starting point for growing a MIP thin layer around the silica nanoparticles. To this end, CPDB-NPs (150 mg), S2 (20 mg, 81 mmol), MAM (14 mg, 0.162 mmol), EAMA (69 mg, 0.162 mmol), EDMA (305 µL, 1.62 mmol), and ABDV (40 mg) were suspended in a mixture of 19.8 mL MeCN-DMSO (70:30, *v/v*). The suspension was purged with Ar at –78 °C. Subsequently, the mixture was polymerized at 50 °C for 18 h and further aged for 2 h at 70 °C. The synthesised particles were washed with MeCN and dried under vacuum overnight. The non-imprinted polymer control particles (NP-CS) were synthesised under identical conditions

but without the template. The size and core/shell structure of the nanoparticles were determined by transmission electron microscopy (TEM) (section II.5 Fig. 2.23).

Table 5.2: Preparation of MP-CS and NP-CS nanoparticles using synthetic silica core particles.

Reagent	Supplier	Volume/mL	Mass/g	Mol	Purity
Ammonia	ABCR	9.00	2.88	0.08×10^{-4}	32%
H_2O	Millipore	24.75	---	---	Type I H_2O
TEOS	Aldrich	4.50	4.18	0.02	99.99%
Silica Core	GSOLFA	---	1.00	---	>99.8%
APTES	Aldrich	4.00	3.78	0.017	99%
TEA	Aldrich	0.402	0.293	2.9×10^{-3}	≥99%
CPDB	Aldrich	---	0.822	2.9×10^{-3}	>97%
EtClForm.	Aldrich	0.282	0.320	2.9×10^{-3}	97%
EtOH	Aldrich	61.75	---	---	≥99.8%
THF	Acros	0.180	---	---	99.99%
Toluene	Aldrich	60.00	---	---	≥99%
Hexane	Acros	200.00	---	---	HPLC

V.6.6. Optimisation of the MISPE procedure for AOH extraction. Studies with BMP1-BNP1.

General protocol for solid phase extraction (SPE) with the synthesised bulk polymers (BMP1 and BNP1). An SPE cartridge of 1 mL was filled with 25 mg of the corresponding BMP1 or BNP1 polymers. In order to prevent leaks of the polymer, frits of PTFE (20 µm pore size) were placed at the top and bottom of the cartridge paths. The cartridge was conditioned with 5 mL of HEPES buffer (0.1M, pH 7.5), and the same solvent was also used to load the sample. Then the cartridge was washed with 0.5 mL of a mixture of MeCN-H_2O (30:70, *v/v*), and AOH was percolated in the same solvent mixture to facilitate a selective retention of AOH in the polymer. Finally, the mycotoxin is eluted with 1 mL MeOH/trifluoroacetic acid (TFA) at 5% (*v/v*), and the composition of the sample was analysed by HPLC with fluorescence detection (FLD).

Breakthrough volume. The same cartridges and setup as for the solid phase extraction experiment were used in order to determine the breakthrough volume. Each cartridge was conditioned with 2 mL HEPES-MeCN 70:30 (*v/v*) prior to use. Afterwards, charges with the volume of 0.5, 1, 2, 5, 10, and 20 mL containing a 200 ppb solution of alternariol in HEPES-MeCN (70:30, *v/v*) were passed through the cartridge. A washing step with 500 µL HEPES-MeCN 70:30, (*v/v*) was employed after passing the charge. The analyte was eluted with 1 mL MeOH/TFA 5% (*v/v*) and analysed by HPLC.

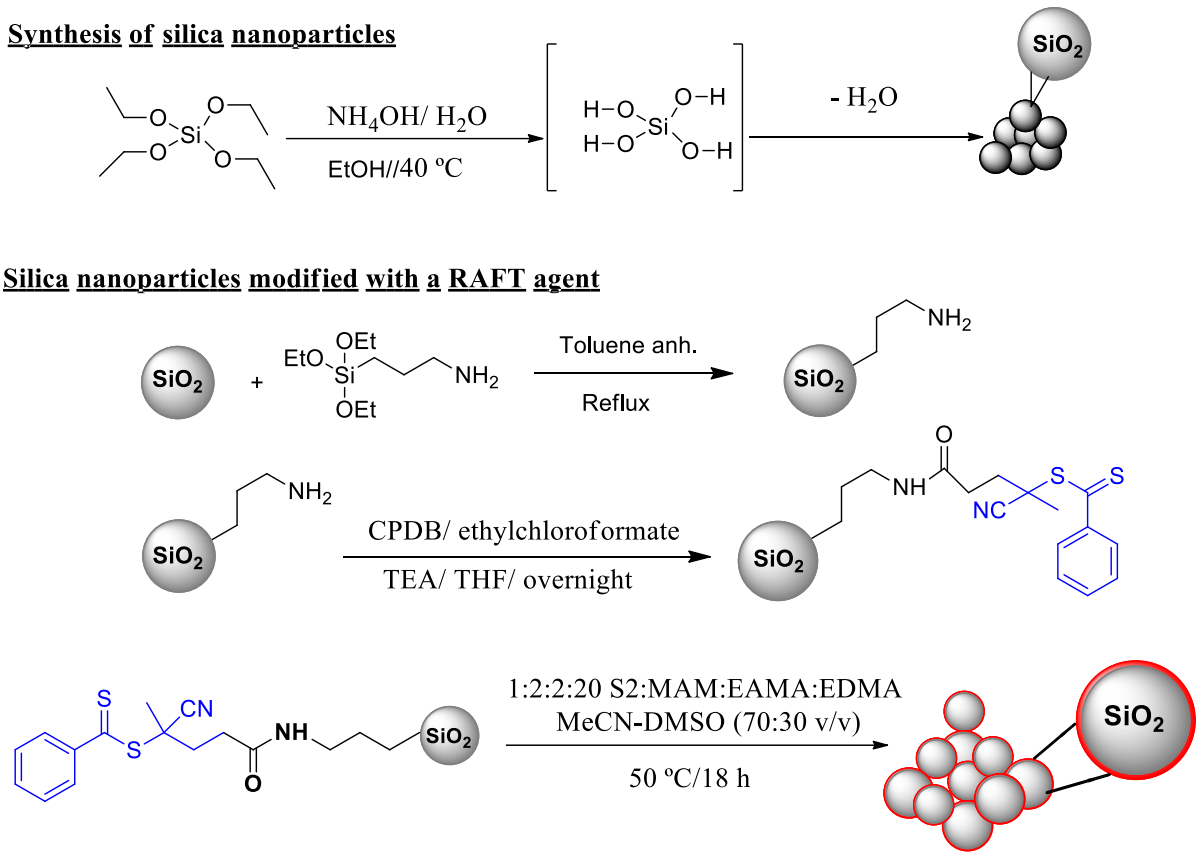

Figure 5.5: Preparation scheme of MP-CS and NP-CS nano-particles using synthetic silica core particles.

V.6.7. Chromatographic evaluation of the polymer microspheres MP-ME1 and NP-ME1

Imprinted and non-imprinted microspheres were slurry-packed in methanol into stainless steel HPLC columns (150 × 2.1 mm I.D.) using water-MeOH (80:20, *v/v*) as the driving solvent. For their chromatographic evaluation, the following conditions were used: 1.0 mL min^{-1} flow rate, 10 µL sample volume, 0.5 mM analyte concentration, excitation/emission at 258/440 nm for fluorescence detection. Each elution was repeated three times. Methanol was used as void volume marker. The retention factor (k) for each analyte was calculated as $k = (t_R - t_0)/t_0$, where t_R and t_0 are the retention times of the analyte and the void marker, respectively. The imprinting factor (IF) was calculated as $IF = k_{MP\text{-}ME1}/k_{NP\text{-}ME1}$, i.e., the ratio of the retention factor of each analyte in the MP-ME1 column to that in the NIP column. The selectivity of the polymer towards analogues of the template molecule

was evaluated using acetonitrile-water (20:80, *v/v*), as it allows elution of all the analytes within 30 min.

V.6.8. Equilibrium re-binding experiments with MP-ME1 and NP-ME1

Polymer microbeads (20 mg) were mixed with 2 mL of acetonitrile-water (20:80, *v/v*) mixture containing different amounts of AOH (0.005–0.750 mM) and the mixtures were incubated for 24 h at room temperature. After incubation, the supernatant was collected and injected into the HPLC as described above. The amount of guest species bound to the polymer (*B*) was calculated by subtracting the free amount of the former (*F*) from the initial mycotoxin concentration in the mixture. Binding experiments were carried out in duplicate.

V.6.9. Optimised extraction procedure of AOH in the MP-ME1 cartridge

To select the *composition of the elution solvent*, 10 mL samples of AOH (200 μg L^{-1}) dissolved in phosphate buffer (100 mM, pH 8.5) were percolated through the cartridges (containing 20 mg of polymer MP-ME1) and eluted with 1% TFA in MeOH. Quantitative mycotoxin recoveries (R = 102%, RSD 5%, *n* = 3) were achieved using 1 mL of 1% TFA in MeOH (*v/v*), a solvent that was selected for further experiments.

The effect of the *loading solution flow rate* on the recovery of AOH was studied with 10 mL samples of AOH (200 μg L^{-1}) dissolved in phosphate buffer (100 mM, pH 8.5) and loaded into the MP-ME1 cartridge. Recoveries close to 100% were obtained at flow rates ≤ 0.93 mL min^{-1}. A loading flow rate of 0.93 mL min^{-1} was selected as optimal for further experiments.

Several water-MeCN mixtures (100–50%, *v/v*) were evaluated as *washing solvents* for the MISPE procedure to minimise the non-specific interactions between the mycotoxin and the imprinted polymer. The retention of AOH in the MP-ME1 and in the NP-ME1 was higher at lower MeCN concentrations in the washing solvent. The largest differences between the MP-ME1 and NP-ME1 were obtained using water-MeCN (80:20, *v/v*) mixture. Under these conditions, AOH recoveries were 96% (RSD 2%, *n* = 3) for the MP-ME1, and lower than 1% in the NP-ME1. Therefore, this solvent composition was selected for the washing step.

In order to evaluate the *breakthrough volume*, the cartridges were loaded with increasing volumes (1–50 mL) of AOH (200 μg L^{-1}) in phosphate buffer (100 mM pH 8.5) and rinsed with 3 mL of water-MeCN (80:20, *v/v*); then, the analyte was eluted with 1 mL of 1% TFA in methanol and the eluates were analysed by HPLC-FLD. An increase from 20 to 100 mg in the amount of polymer per cartridge led to larger breakthrough volumes, and recoveries higher than 91% were obtained for sample volumes up to 50 mL. Recoveries in the NIP were below 10% in all cases.

V.6.10. Tomato sample analysis with a MP-ME1 cartridge

Fresh tomatoes, obtained from a local supermarket, were chopped in portions and stored at 4 °C in the dark. Samples were fortified (n = 6) with AOH at five concentration levels (0, 33, 50, 75 and 110 μg kg^{-1}) and let stand for 30 min in the dark before analysis. Aliquots of the fortified samples (2 g) were extracted with 20 mL of phosphate buffer (100 mM, pH 8.5) by sonication for 10 min (Ultrasons, Selecta). Then, the extracts were filtered through a double cellulose filter (10 μm) and 15 mL of the filtrate were loaded in the cartridges and analysed as described previously. For quantification purposes, non-fortified tomato extracts were pre-concentrated in the MP-ME1 cartridges, checked for the absence of the analyte at the method detection limits, and spiked with the mycotoxins stock solutions. Linear calibration graphs were obtained in the 0 – 500 μg L^{-1} range for AOH (r^2 > 0.990). All the experiments were run in triplicate.

V.6.11. Fluorescence lifetimes and fluorescence polarization studies of MP-MV (1:2:2:20 S2:MAA:VPY:EDMA) with AOH and its surrogate S2

- *Fluorescence lifetime measurements* were performed with a Horiba Jobin-Yvon Fluorolog fluorescence spectrophotometer (Kyoto, Japan) available at the Supramolecular and Molecular Photophysics and Photochemistry (PPSM) research group in Cachan (France; Prof. R. Pansu). Right-angle illumination was used for excitation of the sample. A 50 μM solution of S2 in H_2O-MeCN (3:7, *v/v*) and a suspension of MP-MV (2 mg mL^{-1}) were incubated for 1 h. The excitation light source used was a Horiba NanoLED pulsed diode with a peak wavelength at 340 nm and a pulse duration of 1.1 ns. The fluorescence emission wavelength was set at 420 nm, and excitation and emission

bandpass were set at 5 nm. The data were collected using the Horiba DataStation software, to 10000 counts in the peak, and the time calibration was 0.0549 ns per channel. The data were then analyzed using Igor Pro software and, for both samples, a double exponential fit was used as model. For the free S2 molecule, the data were analyzed from channel 390 to channel 1100, and for the sample of the suspension of MP-MV incubated with S2, the data were analyzed from channel 410 to channel 1200.

V.7. Luminescent molecularly imprinted polymers for TeA detection

V.7.1. Synthesis of luminescent polymers for TeA detection in bulk format (BMPEu/NP-Eu)

592 μL of diethyl allylmalonate (DEAM, 3.0 mmol) was dissolved in 20 mL of ethanol containing 1 mL of aqueous sodium hydroxide (c_{NaOH} = 2 M in water) in a two-neck round bottom flask. Then, 366 mg (1.0 mmol) of $EuCl_3 \cdot 6H_2O$ were added. After complete dissolution, 197 mg of Na^+rTeA^- (1.0 mmol) were added. The mixture was stirred at room temperature for two hours to allow the formation of the *r*TeA-DEAM-Eu(III) complex, and after that, the cross-linker EDMA (2.84 mL, 15.05 mmol) and the radical initiator ABDV (225 mg, 3% *w/w* monomers) were added Table. 5.3.The reaction mixture was refluxed for 4 h. The white precipitate was isolated by filtration, washed with water and methanol, and finally dried at 45 ºC under vacuum.

Once the polymer was synthetized, it was necessary to proceed with the extraction of the template molecule, *r*TeA. For this, the cross-linked polymer was washed four times by using a mixture of MeOH-HCl 9:1, *v/v* (2 h of shaking time for every washing step, at room temperature). The washing solvent was removed by centrifugation. The solid was finally collected and dried under vacuum at 45 ºC. Following this washing protocol, not only *r*TeA was being washed out, but also Eu(III) was partially removed. For this reason, and before proceeding with the analytical characterization of the polymer, it was necessary to reincorporate Eu(III) in the solid. For this, a mixture of the extracted polymer (200 mg) was suspended in 17 mL of ethanol. Then, a solution of $EuCl_3$ (46.1 mg, 12.5 mmol in 1.57 mL of ethanol) containing 0.33 mL of an aqueous solution of NaOH (c_{NaOH} = 2 M) was added to the polymer suspension. This reaction mixture was refluxed overnight. The white precipitate was isolated by filtration, washed with water and methanol, and finally, the polymer was dried in a vacuum oven at 45 ºC overnight.

The corresponding non-imprinted polymer was synthesised following the same protocol but in the absence of the tenuazonic acid template.

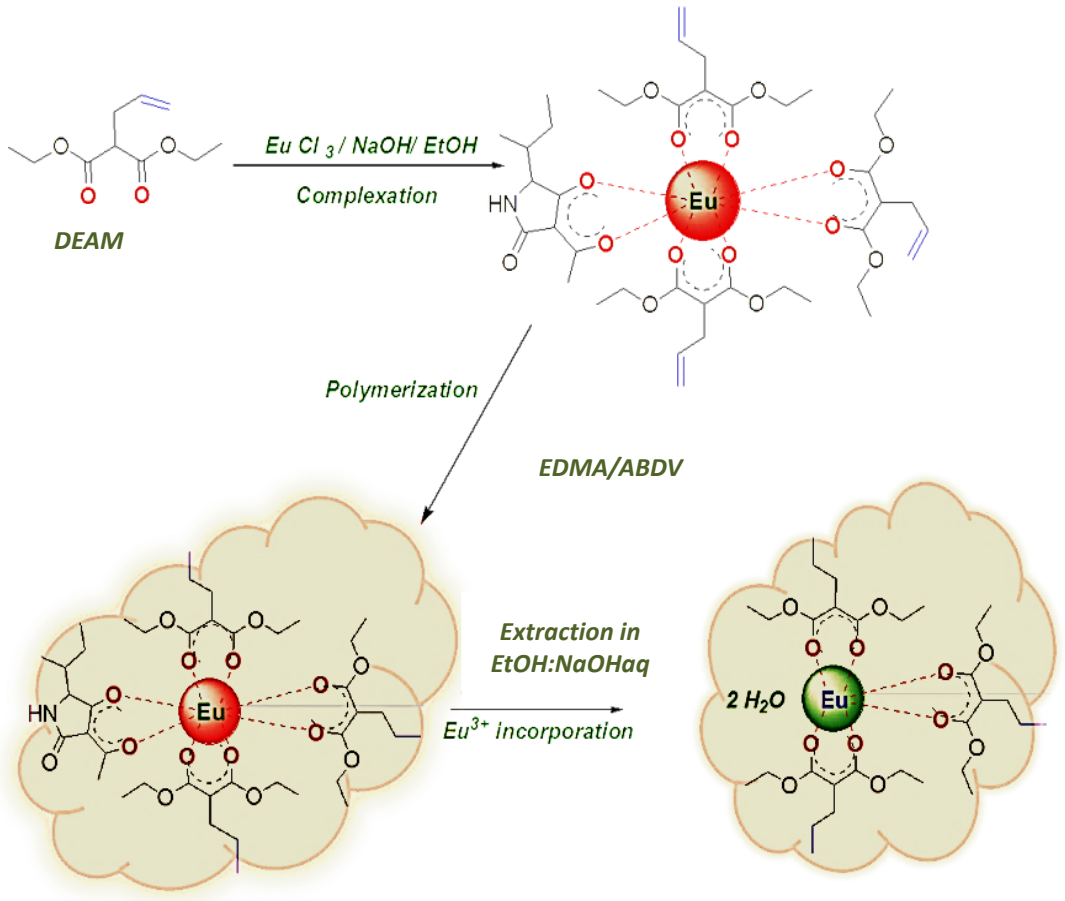

Figure 5.6: Preparation of MIP and NIP using Eu(III) as a chelating agent and DEAM as a functional monomer [25].

Table 5.3: Reagents employed in the synthesis of the rTeA BMP-Eu and BNP-Eu polymers in bulk format.

Reagent	Supplier	Volume/mL	Mass/g	Mol	Purity
DEAM	ABCR	0.592	0.600	3.00×10^{-3}	98%
*r*TeA	GSOLFA	---	0.197	1.00×10^{-3}	---
$EuCl_3{\cdot}6H_2O$	Aldrich	---	0.366	1.00×10^{-3}	99.9%
EDMA	Aldrich	2.84	2.98	15.05×10^{-3}	98%
EtOH	Aldrich	20.00	---	---	≥99.8%
2M NaOH	Scharlau	1.00	0.12	3.00×10^{-3}	---

V.7.2. Preparation of a library of imprinted and non-imprinted luminescent polymers for TeA recognition in bulk format (BMEu1/BNEu1 to BMEu12/BNEu12)

Two functional monomers, DEAM or AACA, were used to create BMEu and BNEu libraries. For this, different T:FM molar ratios were tested, namely 3:1, 2:2 and 1:3. The volume of porogen (EtOH-2 M NaOH 20:1, *v/v*) for each polymer synthesis was calculated in such a way that the ratio $V_{solvent}/(V_{solvent} + V_{total\ monomers})$ was kept at ~ 0.57. Non-imprinted polymers containing europium but prepared in the absence of *r*TeA (BNEus) were prepared in the same way, but without adding the template to the monomer mixture. Also, non-imprinted polymers (named as NIPs) were prepared, but in this case without adding neither the template *r*TeA nor the Eu(III) chloride salt.

All the solutions were purged previously with argon for 5 min. The polymers were synthesised in 2 mL 96-square well polypropylene plates (Radleys) following the pattern shown in Table 5.4. The 96-well plates were sealed with PTFE-coated lids (Radleys, UK). In the case of the imprinted polymers, the template Na^+rTeA^- was weighted in different wells in the amounts displayed on Table 5.4, depending on the polymer (BMEu1 to BMEu12). Then, the corresponding functional monomer (DEAM or AACA) was added in different amounts, followed by addition of a fixed amount (0.24 mg) of $EuCl_3 \cdot 6H_2O$ to each well. A mixture of EtOH:NaOH (20:1, *v/v*) was added as the porogen, and the volume was adjusted as shown on Table 5.4.

The mixture was left equilibrating for 15 min at room temperature to allow for the monomer-template interaction to occur. Finally, 11 mg of the corresponding radical initiator ABDV or AIBN and the chosen cross-linker EDMA (354 µL) were added to each well. Then, the plate was placed in an oven for one day at 50 °C and another day at 70 °C. The bulk polymers obtained in this way were ground with an agate mortar and the grains were transferred to another 2 mL 96-well plate containing a 10 µm polypropylene porous membrane per well for the washing procedure.

For the extraction of the, the polymer powders were washed 4 times with 2 L of a solution of MeOH-HCl (9:1, *v/v*) and 500 mL of water. After each washing step, the supernatant was collected, and its phosphorescence was recorded to determine whether the luminescent *r*TeA:Eu(III) complex was still present.

Non-imprinted polymers (BNEu1 to BNEu12) were prepared in the same way, but without addition of the template. Despite the template was not present in this case, the polymers were also treated with the MeOH-HCl (9:1, *v/v*) mixture and washed with water for comparison purposes.

Table 5.4. Amounts of template $Na^{+}rTeA^{-}$ and functional monomers (DEAM or AACA) used for the preparation of the Eu(III)-MIP library. The amount of $EuCl_3 \cdot 6H_2O$ (24.4 mg), cross-linker EDMA (354 µL) and radical initiator (11 mg) was kept constant for the whole series.

Polymer	$Na^{+}rTeA^{-}$ /mg	DEAM/µL	AACA/µL	EtOH:2 M NaOH (20:1)/µL	Radical initiator
BMEu1[a]	39.4	13	-	488	ABDV
BMEu2[b]	26.3	26	-	506	
BMEu3[c]	13.1	39	-	524	
BMEu4[a]	39.4	-	9	483	
BMEu5[b]	26.3	-	18	496	
BMEu6[c]	13.1	-	27	507	
BMEu7[a]	39.4	13	-	488	AIBN
BMEu8[b]	26.3	26	-	506	
BMEu9[c]	13.1	39	-	524	
BMEu10[a]	39.4	-	9	483	
BMEu11[b]	26.3	-	18	496	
BMEu12[c]	13.1	-	27	507	

[a]T:FM (3:1); [b]T:FM (2:2); [c]T:FM (1:3) molar ratios.

Reincorporation of Eu(III) to both, BMEu and BNEu polymers. 200 mg of each washed polymer was suspended in 0.8 mL of ethanol. Then, the calculated amount of 2 M NaOH was added according to the ratio of the functional monomer in the polymer. NaOH was added for deprotonation of the corresponding β-diketone. After that, 332 µL of a solution of $EuCl_3$ in ethanol (41.6 mg, C_{EuCl3} = 0.341 M) was added to each well. This mixture was shaked at 50 °C for 4 h. After 4 h, the solid was centrifuged and washed 4 times, first with water and then with methanol. Finally, the corresponding powder was dried under vacuum at 45 °C.

V.7.3. Polymerization into silica beads. Synthesis of MPE1, MPE2 and MPE3

Taking into account the best composition and template-to-functional monomer/cross linker ratios obtained with the MIP library for *r*TeA recognition in the previous section, three different types of MIPs (MPE1, MPE2, MPE3) and NIPs (NPE1, NPE2 and NPE3) were prepared in the form of highly porous spherical microparticles. These three types of polymers differ in the kind of functional monomer chosen (DEAM for MPE1 and MPE3 or AACA for MPE2) or in the molecule used as template (*r*TeA for MPE1 and MPE2, or the surrogate *s*TeA for MPE3). In all cases, EDMA was used as the cross linker and ABDV as the radical initiator. The molar ratio employed was0.75 mmol T:0.75 mmol $EuCl_3$:0.75 mmol FM:3.75 mmol CL (or T:Eu(III):FM:CL 1:1:3:15). ABDV was added in a 3% *w/w* ratio with respect to the total weight of monomers.

Synthesis of mesoporous molecularly imprinted microspheres. SilicaSphere™ PC, 40-75 µm diameter, 500-Å pore size microparticles were employed as a silica mold for the synthesis of the imprinted polymers in the form of porous microspheres (see part V.6.4). For this, a solution of the corresponding functional monomer (DEAM or AACA, 0.75 mmol) in a mixture of ethanol:2 M sodium hydroxide was added to 92 mg (0.25 mmol) of $EuCl_3$ in a two-neck round bottom flask. Table 5.5 shows the corresponding amounts of FM and porogen for the three different polymers MPE1 to MPE3. After complete dissolution, 49 mg (0.25 mmol) of the molecular template (*r*TeA or sTeA) were added. The mixture was stirred at room temperature for two hours to allow Eu(III) complex formation. After that, EDMA (707 µL, 3.75 mmol) and 27 mg of ABDV were added. Then 3.57 g of the silica microbeads were placed in a 25 mL glass vial and were mixed by stirring with the cocktail solution until the silica beads were freely flowing. Then, the vial was sealed with a rubber septum, the system was purged with argon for 5 min, and the mixture was left in the oven for polymerization at 70 °C for 24 h. After that, the silica was dissolved by adding 3 x 150 mL of an aqueous solution of ammonium hydrogen difluoride (3 M, Alfa Aesar) and shaking for 24 h after each addition. The final solid polymer obtained in this way was thoroughly washed with water (until pH ~ 7), 1 L of MeOH-TFA (99:1, *v/v*) and, finally, 0.5 L of MeOH. The polymer beads were dried in a vacuum oven at 50 °C for 24 h prior to characterization and use. Then the powder was settled in water:MeOH (80:20, *v/v*) to remove fine particles.

Table 5.5. Amounts of template (*Na⁺rTeA⁻* or *Na⁺sTeA⁻*), functional monomer (DEAM or AACA), cross-linker (EDMA) and porogen used for the preparation of the Eu(III)-MIP mesoporous microspheres. The amount silica template (3.57 g), $EuCl_3 \cdot 6H_2O$ (92 mg) and initiator (ABDV, 27 mg) was kept constant for the whole series.

Polymer	*Na⁺rTeA⁻*/mg	*Na⁺sTeA⁻*/mg	DEAM/μL	AACA/μL	EtOH: 2 M NaOH/(μL:μL)
MPE1	49	-	148	-	349:18
MPE2	49	-	-	103	331:17
MPE3	-	49	148	-	349:18

[a] Final T:Eu(III):FM:CL molar ratio was 1:1:3:15

Extraction of the Eu(III):template complex. The cross-linked polymer was washed four times (shaking at room temperature for 1 h each time) by using a mixture of MeOH-HCl 9:1 *v/v*, followed by centrifugation. The solid was finally dried in a vacuum oven at 45 ºC.

Reincorporation of the Eu(III) cation into the polymer matrix. A solution of $EuCl_3$ (125 mg, 34 mmol) in ethanol (1.72 mL) was added to a suspension of the extracted polymer (600 mg) in 50 mL of ethanol containing 1 mL of aqueous NaOH (41 mg, 1 mmol). The reaction mixture was incubated overnight at 70 °C with shaking. The polymer was isolated by centrifugation, washed with water and methanol, and the final polymer was obtained after drying under vacuum overnight at 45 ºC.

The corresponding non-imprinted NPE microspheres were prepared following the same steps but without the addition of the molecular template.

Bibliography

1. Gottlieb, H. E.; Kotlyar, V.; Nudelman, A., NMR chemical shifts of common laboratory solvents as trace impurities. *J. Org. Chem.* **1997,** *62*, 7512-7515.

2. Marker, A.; Canty, A. J.; Brownlee, R., Carbon-13 chemical shifts of some pyridines, 2,2'-bipyridyls and 1,10-phenanthrolines. *Aust. J. Chem.* **1978,** *31*, 1255-1263.

3. Orellana, G.; Ibarra, C. A.; J., S., H-1 and C-13 NMR coordination-induced shifts in a series of tris(a-diimine)ruthenium(II) complexes containing pyridine, pyrazine, and thiazole moieties. *Inorg. Chem.* **1988,** *27*, 1025-1030.

4. Morris, J. V.; Mahaney, M.; A.; Huber, J. R., Fluorescence quantum yield determinations. 9,l0-diphenylanthracene as a reference standard in different solvents. *J. Phys. Chem.* **1976,** *80*, 969-973.

5. Resch-Genger, U., Standardization and quality assurance in fluorescence measurements I. Techniques. In *Springer series on fluorescence*, Wolfbeis, O. S., Ed. Springer: Verlag Berlin Heidelberg, 2008; Vol. 5, p 493.

6. Crosby, G. A.; Demas, J. N., Quantum efficiencies of transition-metal complexes. I. d-d luminescence. *J. Am. Chem. Soc.* **1970,** *92*, 7262-7270.

7. Kusba, J.; Bogdanov, V.; Gryczynski, I.; Lakowicz, J. R., Theory of light quenching: effects on fluorescence polarization, intensity, and anisotropy decays. *Biophys. J.* **1994,** *67*, 2024-2040.

8. Moulton, P. F., Spectroscopic and laser characteristics of Ti:Al_2O_3. *J. Opt. Soc. Am. B.* **1986,** *3*, 125-133.

9. Chae, J., Practical demethylation of aryl methyl ethers using an odorless thiol reagent. *Arch. Pharm. Res.* **2008,** *31*, 305-309.

10. Ghosal, S.; Lal, J.; Singh, S. K.; Kumar, Y.; Soti, F., Chemistry of two bioactive benzopyrone metabolites. *J. Chem. Res. Synop.* **1989,** *11*, 350-351.

11. Ito, H.; Iguchi, A.; Hatano, T., Identification of urinary and intestinal bacterial metabolites of ellagitannin geraniin in rats. *J. Agric. Food Chem.* **2008,** *56*, 393-400.

12. Node, M.; Nishide, K.; Fuji, K.; Fujita, E., Hard acid and soft nucleophile system. 2. demethylation of methyl ethers of alcohol and phenol with an aluminum halide-thiol system. *J. Org. Chem.* **1980,** *45*, 4275- 4277.

13. Kumar, K. C. S.; Müller, K., Depsides as non-redox inhibitors of leukotriene B4 biosynthesis and HaCaT cell growth. 1. Novel analogues of barbatic and diffractaic acid. *Eur. J. Med. Chem.* **1999,** *34*, 1035-1042.

14. Bialonska, D.; Kasimsetty, S. G.; Khan, S. I.; Ferreira, D., Urolithins, intestinal microbial metabolites of pomegranate ellagitannins, exhibit potent antioxidant activity in a cell-based assay. *J. Agric. Food Chem.* **2009,** *57*, 10181-10186.

15. Perrin, D. D.; Dempsey, B., *Buffers for pH and metal ion control*. Chapman and Hall laboratory manuals in physical chemistry and biochemistry 1974; p 180.

16. Kumar, K. C. S.; Müller, K., Depsides as non-redox inhibitors of leukotriene B(4) biosynthesis and HaCaT cell growth, 2. Novel analogues of obtusatic acid. *Eur. J. Med. Chem.* **2000,** *35*, 405-411.

17. Jung, B. M.; Kim, M. S.; Kima, W. J.; Chang, J. Y., Molecularly imprinted mesoporous silica particles showing a rapid kinetic binding. *Chem. Commun.* **2010,** *46*, 3699-3701.

18. Lee, K.; Ki, C. D.; Kim, H.; Chang, J. Y., Selectivity control by chemical modification of the recognition sites in two-point binding molecularly imprinted polymer. *Macromolecules* **2004,** *37*, 5544-5549.

19. Munkholm, C.; Parkinson, D. R.; Walt, D. R., Intramolecular fluorescence self-quenching of fluoresceinamine. *J. Am. Chem. Soc.* **1990,** *112*, 2608-2612.

20. Shama, S. A.; Tran, T. L., Amides and hydrazides from amine and hydrazine hydrochlorides. *J. Chem. Edu.* **1978,** *55*, 816.

21. Carroll, M. F.; Bader, A. R., The reactions of diketene with ketones. *The research laboratories of A. Boake, Roberts & Co. Ltd.* **1953,** *75*, 5400-5402.

22. Lebrun, M. H.; Duvert, P.; Guademer, F.; Guademer, A.; Deballon, C.; Boucly, P., Complexation of the fungal metabolite tenuazonic acid with copper (II), iron (III), nickel (II), and magnesium (II) ions. *J. Inorg. Bioch.* **1985,** *24*, 167-181.

23. Lucas, A. D.; Valverde, J. L.; Romero, M. C.; Gómez, J.; Rodríguez, J. F., Ion exhange equilibria in nonaqueous and mixed solvents on the cationic exchanger amberlite IR-120. *J. Chem. Eng. Data.* **2001,** *46*, 73-78.

24. Wan, W.; Biyikal, M.; Wagner, R.; Sellergen, B.; Rurack, K., Fluorescent sensory microparticles that "light-up" consisting of a silica core and a molecularly imprinted polymer (MIP) shell. *Angew. Chem. Int. Ed. Engl.* **2013,** *52*, 7023-7027.

25. Kim, H.; Y., K.; Chang, J. Y., Preparation of a molecularly imprinted polymer containing europium(III) ions for luminescent sensing. *J. Poly. Sci. Part A: Poly. Chem.* **2012,** *50*, 4990-4994.

VI-Conclusions

INDEX

General Conclusions

This thesis has described innovative approaches for developing optical sensing methods based on molecularly imprinted polymers (MIPs) as artificial recognition elements in combination with luminescence for detection of the analyte binding to the polymer. The target analytes of this work have been three of the main mycotoxins produced by the *Alternaria* fungi namely, alternariol (AOH), alternariol monomethyl ether (AME) and tenuazonic acid (TeA). Luminescence detection has been performed either directly in the case of fluorescent analytes such as AOH or AME, or indirectly for non-fluorescent targets (TeA) by monitoring changes in the emission of a luminescently doped MIP upon the analyte binding. The main contributions of this Thesis include: i) the rational creation of MIPs by designing and synthesizing apt molecular surrogates of AOH and AME, preparation and characterization of polymer libraries for selecting the best functional monomers and co-monomers ratios, and demonstration of the recognition properties of the MIPs by solid phase extraction; ii) the use of diverse spectroscopic techniques for detection of the analyte binding to the MIPs (emission intensity, fluorescence anisotropy, time-resolved emission, or time-gated luminescence in the case of long-lived luminophores such as Eu(III)-doped MIPs for low-background detection). For optimization of the polymer composition, the MIPs have been firstly prepared in bulk format. Once the optimal composition has been established, the MIPs have been also synthesized in the form of highly porous micrometric particles for accelerating the mass-transfer kinetics in the template removal and analyte (re-)binding processes.

Molecularly imprinted polymers for alternariol recognition

- Novel fluorescent molecules have been designed and prepared as laboratory surrogates to the natural toxins AOH and AME for the synthesis of MIPs to selectively recognize and bind those toxins. The ability of the surrogates to mimic AOH and AME is due to the similarity of their chemical structure to the target analytes: all of them possess a 6-membered lactone ring bonded to two aromatic rings bearing –OH substituents in appropriate positions (one to three –OH substituents or, in the case of the AME analogues, the surrogates contain one or two –OMe groups). These surrogate templates have been obtained in only one (AME analogues) or two (AOH analogues) steps, with good reaction yields (60 to 70%), starting from cheap and easily available commercial precursors. This feature allows preparation of inexpensive MIPs for AOH and AME on a large scale, something that would not be feasible using the analyte themselves as the molecular templates.

- Four of the novel surrogates described in this thesis have shown to be significantly fluorescent in the violet-blue region (λ_{em} = 398 nm for S1 and S2, or 421 nm for S3 and S4, with $0.18 \geq \Phi_F \geq 0.26$) and decay very rapidly from their excited state (1-2 ns fluorescence lifetime) in MeCN solution. In comparison, the target analytes AOH and AME display a shorter excited state lifetime (< 1 ns) and have lower fluorescence quantum yields (Φ_f = 0.062 in both cases). These differences could be attributed to the occurrence of an excited state intramolecular proton transfer (ESIPT) process in the case of AOH and AME (two emission bands can be observed in this case: one at 390 nm and a new broad red-shifted band at *ca.* 470 nm) that accelerates deactivation of the excited state via non-radiative processes. This ESIPT process is absent in the case of the surrogates due to the relative position of the –OH group on C-7 of the aromatic skeleton and the C-6 carbonyl.

- An additional advantage of using surrogates for the templating process is to avoid false positives and to increase the sensitivity to the analyte in the chromatographic analysis of the target toxins due to leaching of non-thoroughly washed template. Moreover, handling of the *toxic* natural metabolites during the synthesis of the MIPs is avoided.

- *N*-(2-Aminoethyl)methacrylamide (EAMA) has shown to be particularly adequate as a functional monomer to prepare polymers for alternariol recognition. ^{1}H-NMR titrations have enabled a detailed characterization of the interaction between the surrogate template S2 and the

functional monomer EAMA that will lead in the future to the design of efficient novel MIPs for phenolic analytes (preservatives, fusarium toxins, flavonoids, bisphenol-A, neurotransmitters, antiseptics, flavorings and non-ionic detergents, among other relevant species).

- As the S2 surrogate can be obtained in multigram scale, a library of polymers with different compositions was prepared and evaluated by chromatographic methods to unveil the material with the best selective recognition of AOH. Among the different surrogates (S1 to S4), functional monomers (ALPP, MAM, EAMA, MAA, VBA, DAEM and VPY), and cross-linkers (DVB and EDMA) tested in our study, S2, EAMA and EDMA yielded the best polymers for AOH. Therefore, these components were chosen for preparing MIPs in the form of mesoporous microspheres by using silica gel microparticles as polymerization mould. Optimum microspheres were prepared with an S2:EAMA:MAA:EDMA 1:2:2:20 molar ratio ("MP-ME") and with an S2:VPY:MAA:EDMA 1:2:2:20 molar ratio ("MP-MV").

- The MP-ME microspheres were able to bind AOH in water-acetonitrile mixtures with an affinity constant of $(1.04 \pm 0.11) \times 10^5\ M^{-1}$and were successfully applied as the stationary phase in solid phase extraction of the toxin in tomato samples.

- Binding to the MIP cavities of the S2 surrogate could be confirmed by fluorescence anisotropy measurements. Equilibrium binding isotherms yielded a binding capacity of 25 µmol g^{-1} of S2 with the MP-VP polymer beads. Time-resolved fluorescence anisotropy measurements confirmed that the emission lifetimes increased when S2 was bound to the polymer.

- Non-luminescent alternariol surrogates (S5 and S6) have been prepared to eliminate the signal background of molecularly imprinted polymers intended for steady-state emission or fluorescence polarization measurements. Moreover, a novel alternariol surrogate (S7) containing thermally labile urethane bonds for covalent molecular imprinting, has also been synthesized.

Luminescent MIPs for tenuazonic acid recognition

- A streamlined preparation route for obtaining (racemic) tenuazonic acid sodium salt in 85% yield has been optimized. The synthesis overcomes the limitations of the high cost of tenuazonic acid and its commercial availability only as Cu(II) salt which does not show any template effect. Following the same route, it was also possible to obtain a molecular surrogate, *Tenuazonic acid sodium salt surrogate* with an 80% yield.

- Capitalizing on the ability of tenuazonic acid to form transition metal chelates due to its β-diketonate structure, luminescent Eu(III)-doped MIPs have been prepared to recognize and bind the analyte. Eu(III) chelates emit a very long-lived narrow luminescence at 615 nm when coordinated to antenna ligands that sensitize the lanthanide emission. We have demonstrated that tenuazonic acid can act as the antenna ligand upon binding to this species.

- A Eu(III)-doped MIP has been prepared by using diethyl allylmalonate (DEAM) as a functional monomer in a 1:3 (Eu^{3+}:DEAM) molar ratio. In this way, two coordination positions are available for coordinating the (bidentate) TeA ligand, which is added in a 1:1 molar ratio to Europium). Incorporating EDMA as cross-linker, and with a free radical polymerization initiated with ABDV, a bulk polymer (BMIP-Eu) was prepared and successfully detected tenuazonic acid, showing a 3-fold increase of its luminescence in the presence of the analyte in acetonitrile (water is a well know quencher of Eu(III) luminescence). The emission increase was higher than that observed for the corresponding non-imprinted polymer.

- A library of twelve Eu-doped MIPs has been obtained into a microtiter plate (bulk polymerization) for optimizing the functional monomer (diethyl allylmalonate, DEAM, or allyl acetoacetate, AACA). The performance of the corresponding polymers was studied by luminescence measurements after 24-h incubation with tenuazonic acid in MeCN. The polymers with the strongest increase of the analytical signal and largest different with the non-imprinted polymer response were those prepared with a 1:1:3 TeA:Eu(III):DEAM ratio.

- With the optimized TeA:Eu(III):DEAM (1:1:3) composition, spherical mesoporous MIP microparticles were synthesized (MPE1) using the sacrificial silica microbead molds. For the sake of comparison, similar beads (MPE2) were also prepared using AACA as functional monomer instead of DEAM or using the surrogate *s*TeA instead of TeA (MPE3). Analytical characterization of the MIP beads for TeA analysis yielded LODs of 5.2, 9.9 and 4 μM for MPE

1, MPE 2 and MPE 3, respectively, using suspensions of 0.67 mg mL^{-1} of each polymer in MeCN, enabling the determination of TeA up to 15, 29.9 and 14 μM, respectively. These values allow the use of the novel MIPs to analyze the mycotoxin in foods.

- Cross-reactivity studies for the three polymers (MPE1, MPE2 and MPE3) have shown a negligible response to other potential interferents that could also be present in a feed sample, such as the mycotoxins AOH or zearalenone, or other components of the sample like glucose or fructose. Only the surrogate *s*TeA, that elicited a similar response to TeA, and the structurally related cyclopiazonic acid mycotoxin, that gave a higher response than TeA due to its higher hydrophobicity, turned out to be interferents. These results indicate the necessity of a *β*-diketone group in the analyte for successful Eu(III) binding into the MIP cavities.

Pyrene-labeled acrylamide monomers

- Four fluorescent acrylamide monomers, namely *N*-pyren-1-ylacrylamide monomers (PA), *N*-pyren-1-ylmethacrylamide (PMA), *N*-(pyren-1-ylmethyl)acrylamide (PMeA), and *N*-(pyren-1-ylmethyl)methacrylamide (PMeMA), have been *prepared* and photophysically *characterized* by absorption, steady-state and time-resolved emission spectroscopy for their future use as both molecular probes of the MIP binding cavities, and polyfunctional monomers to recognize the alternariol and related toxins, with binding-reporting capability by fluorescence quenching.

- PMeA and PMeMA display a *strong fluorescence* in the violet-blue with vibronic structure (Φ_F > 0.63) and long emission lifetimes (144 to 313 ns in the absence of O_2, depending on the solvent), similar to those exhibited by the unsubstituted pyrene; however, the pyrenyl(meth)acrylamides (PA and PMA) show a significantly weaker fluorescence intensity and lifetime due to the mixing of the n-π* and π-π* transitions for the lowest excited state of the latter compared to the pure π-π* nature of the same excited state of pyrene and the alkyl-substituted pyrenes. The very high emission quantum yields of PMeA and PMeMA make these monomers very appropriate for fluorescent MIPs development provided we place them exclusively in the analyte-binding cavities, and undergo (static) quenching with the bound analyte.

- The fluorescence quantum yield of the synthesized pyrenemethyl(meth)acrylamides has been shown to be very sensitive to the presence of dissolved molecular oxygen in solution, with

quenching rate constants controlled by diffusion and, therefore, dependent of the solvent (kinematic) viscosity. Therefore, it is expected that they will be slow down once PMeA and PMeMA are immobilized into a molecularly imprinted polymer.

- Unlike PA and PMA, the vibronic bands of the pyrenemethyl(meth)acrylamides display a similar Ham effect to those of pyrene as a function of the perturbation caused by the solvent. This fact makes PMeA and PMeMA excellent candidates to use them as fluorescent *probes* of the polarity of the MIP binding site once they are incorporated into the binding cavities of the molecular recognition polymers. This feature would allow extending the empirical solvent polarity scale (or "*py* scale") based on the pyrene probe to polymer materials including MIPs to gain further insight into the host-guest interactions that take place in the latter.

- The fluorescence lifetime of PMeA and PmeMA has been found to decrease with increasing solvent polarity because of the higher efficiency of the vibronic coupling between the closest lying electronic states (0-0) in polar solvents due to solvent dipole-solute induced dipole interactions. Dichloromethane and other chlorinated solvents are an anomaly in this general behavior as it has also been reported by other authors for pyrene itself. The short lifetimes of PA and PMA, largely independent of the dissolved O_2 concentration, do not follow the same trend with the solvent polarity due to specific solvent-solute interactions.

- The photochemical quenching of PMeMA by the alternariol surrogate S-2 has been evaluated into sodium dodecyl sulfate micelles as a model of the pyrene-labelled MIP binding cavities for the toxin. An efficient static quenching by alternariol was evidenced, probably due to the formation of an exciplex between the alternariol surrogate and the photoexcited probe molecule. Further investigations are being carried out to elucidate the exact photochemical quenching mechanism. Given the similarity between S-2 and alternariol, it is expected that the toxin will produce a similar excited state quenching to the PMeMA probe.

Bibliography

i) Jung, B. M.; Kim, M. S.; Kim, W. J.; Chang, J. Y., Molecularly imprinted mesoporous silica particles showing a rapid kinetic binding. *Chem. Commun.* **2010,** *46*, 3699–3701.

ii) Lee, K.; Ki, C. D.; Kim, H.; Chang, J. Y., Selectivity control by chemical modification of the recognition sites in two-point binding molecularly imprinted polymer. *Macromolecules* **2004,** *37*, 5544-5549.

Annex

***Spectra*[1]……...**

[1] The assignment of ^{13}C-NMR spectra is temptative (ACD/Labs software).

V.2.1. 3-Hydroxy-8,9-dimethoxy-6H-dibenzo[b,d]pyran-6-one (S 1) or (8, 9-Di-O-methylurolithin C)

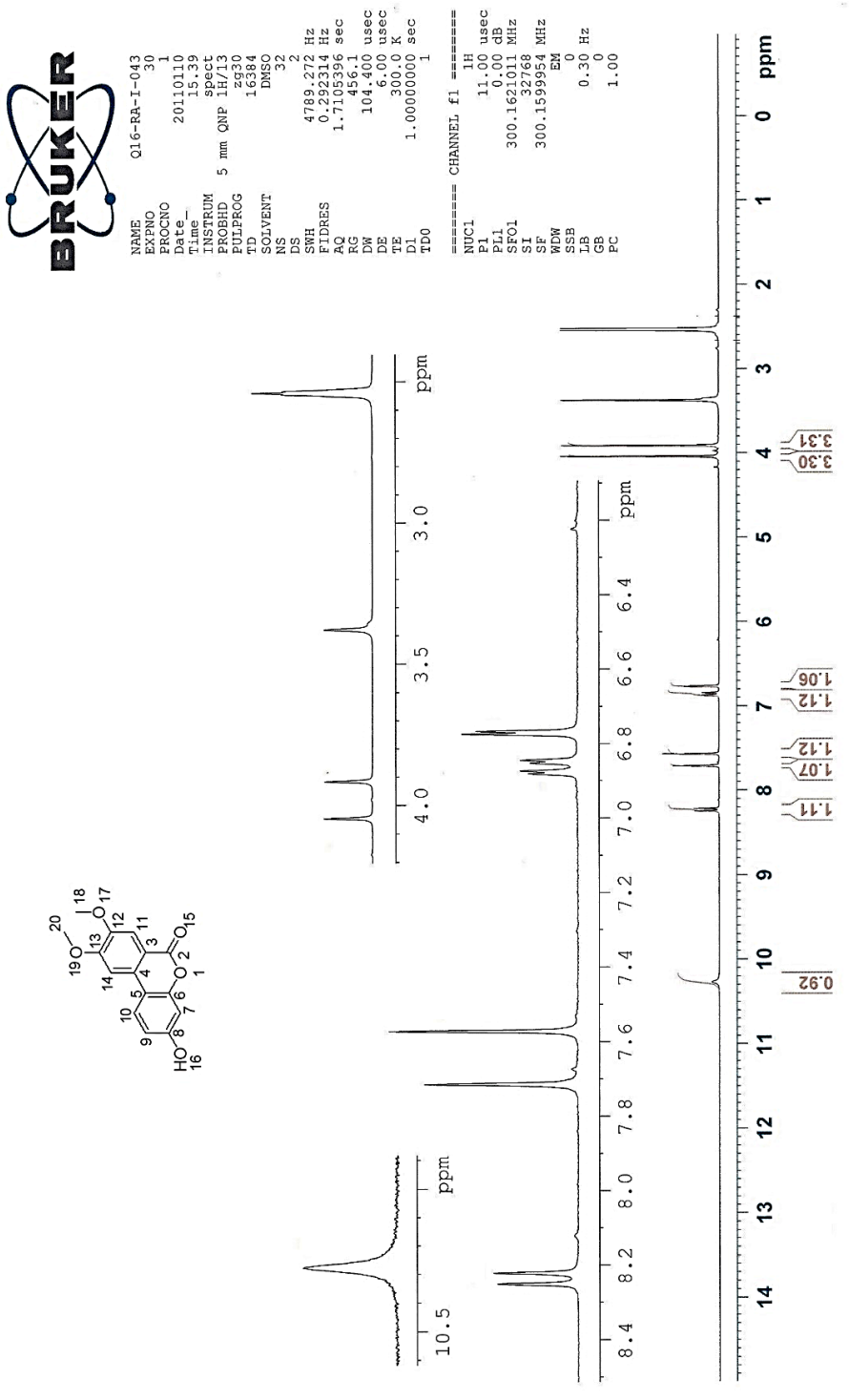

Figure A1. ^{1}H-NMR (DMSO-d_6) spectrum of **3-Hydroxy-8,9-dimethoxy-6H-dibenzo[b,d]pyran-6-one (surrogate 1)** . Preparation procedure described in section V.2.1.

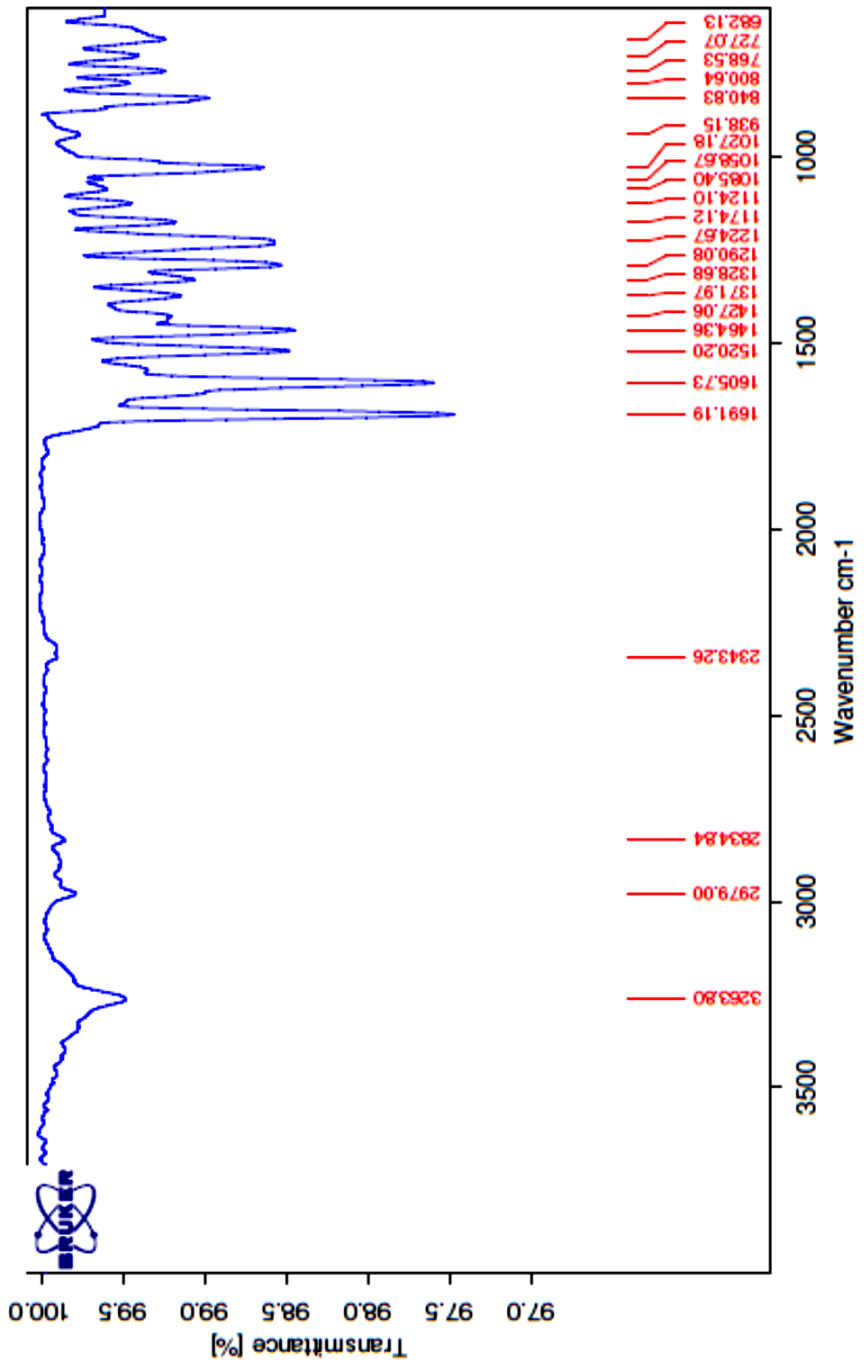

Figure A2: FT-IR (KBr disc) spectrum of **3-Hydroxy-8,9-dimethoxy-6H-dibenzo[b,d]pyran-6-one (surrogate 1)** . Preparation procedure described in section V.2.1.

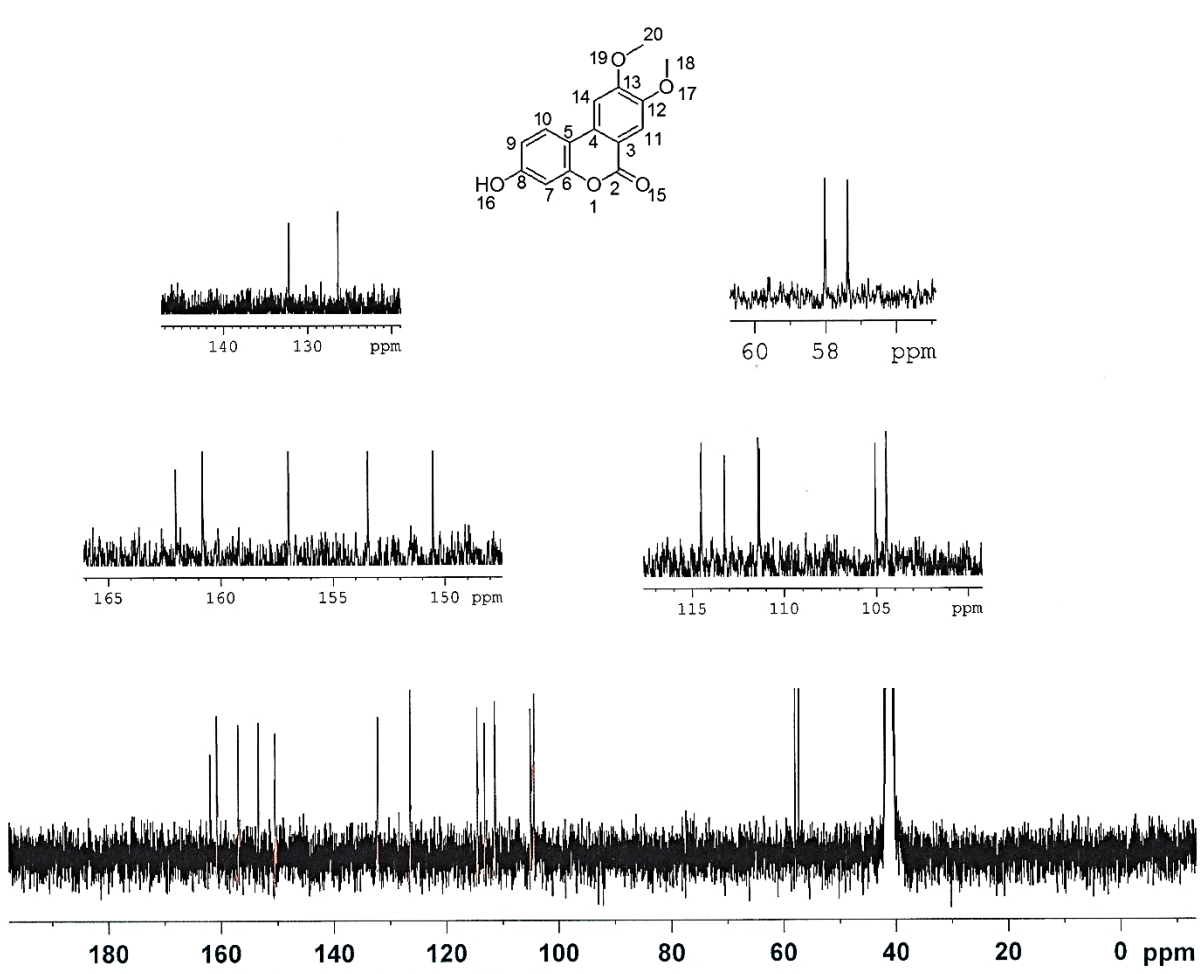

BRUKER

NAME	surrogtel-...
EXPNO	531
PROCNO	1
Date_	20121012
Time	21.23
INSTRUM	spect
PROBHD	5 mm QNP 1H/13
PULPROG	zgpg30
TD	65536
SOLVENT	DMSO
NS	800
DS	4
SWH	17985.611 Hz
FIDRES	0.274439 Hz
AQ	1.8219508 sec
RG	2048
DW	27.800 usec
DE	6.00 usec
TE	295.9 K
D1	2.00000000 sec
d11	0.03000000 sec
DELTA	1.89999998 sec
TD0	1
======== CHANNEL f1 ========	
NUC1	13C
P1	10.00 usec
PL1	-2.00 dB
SFO1	75.4828396 MHz
======== CHANNEL f2 ========	
CPDPRG2	waltz16
NUC2	1H
PCPD2	80.00 usec
PL2	0.00 dB
PL12	17.00 dB
PL13	17.00 dB
SFO2	300.1612006 MHz
SI	32768
SF	75.4752009 MHz
WDW	EM
SSB	0
LB	1.00 Hz
GB	0
PC	1.40

Figure A3: ^{13}C-NMR (DMSO-d_6) spectrum of **3-Hydroxy-8,9-dimethoxy-6H-dibenzo[b,d]pyran-6-one (surrogate 1) .** Preparation procedure described in section V.2.1.

Mass Spectrum List Report

Analysis Info

Analysis Name	RAI04300.d	Acquisition Date	01/21/11 13:56:13
Method	STOP1.M	Operator	Dr. Nour Kayali
Sample Name	RA-I-043	Instrument	Esquire-LC_00126
Comment	DIRECTO EN METANOL		

Acquisition Parameter

Ion Source Type	ESI	Ion Polarity	Negative	Alternating Ion Polarity	n/a
Mass Range Mode	Std/Normal	Scan Begin	100.00 m/z	Scan End	900.00 m/z
Capillary Exit	-60.7 Volt	Skim 1	-9.7 Volt	Trap Drive	40.0
Accumulation Time	100000 µs	Averages	11 Spectra	Auto MS/MS	Off

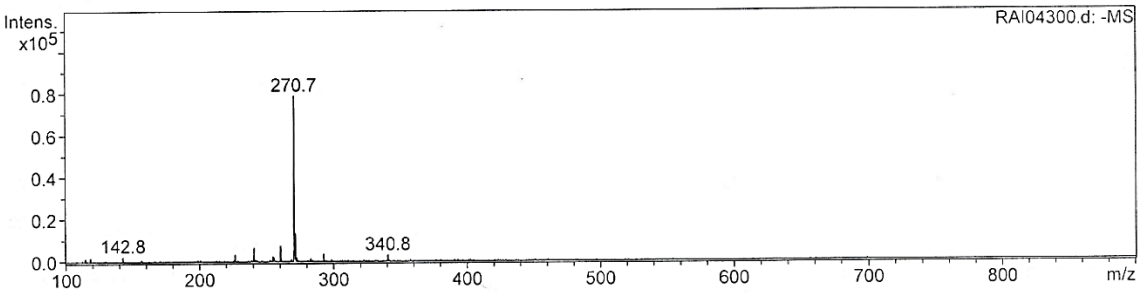

#	m/z	I	FWHM	S/N
1	114.8	1578	0.3	57.5
2	118.6	1742	0.4	63.5
3	142.8	2345	0.3	85.5
4	226.8	3417	0.4	124.5
5	240.8	6539	0.4	238.3
6	254.9	2454	0.4	89.4
7	255.9	1716	0.5	62.5
8	260.5	7368	0.3	268.5
9	270.7	78755	0.4	2870.0
10	271.7	13305	0.3	484.9
11	272.7	1842	0.4	67.1
12	292.9	3559	0.3	129.7
13	340.8	3005	0.4	109.5

Figure A4: MS-ESI (negative ion detection) spectrum of **3-Hydroxy-8,9-dimethoxy-6H-dibenzo[b,d]pyran-6-one (surrogate 1) .** Preparation procedure described in section V.2.1.

V.2.2. 3, 8, 9-Trihydroxy-6H-dibenzo[b,d]pyran-6-one (S 2) or (8, 9-Di-O-methylurolithin C)

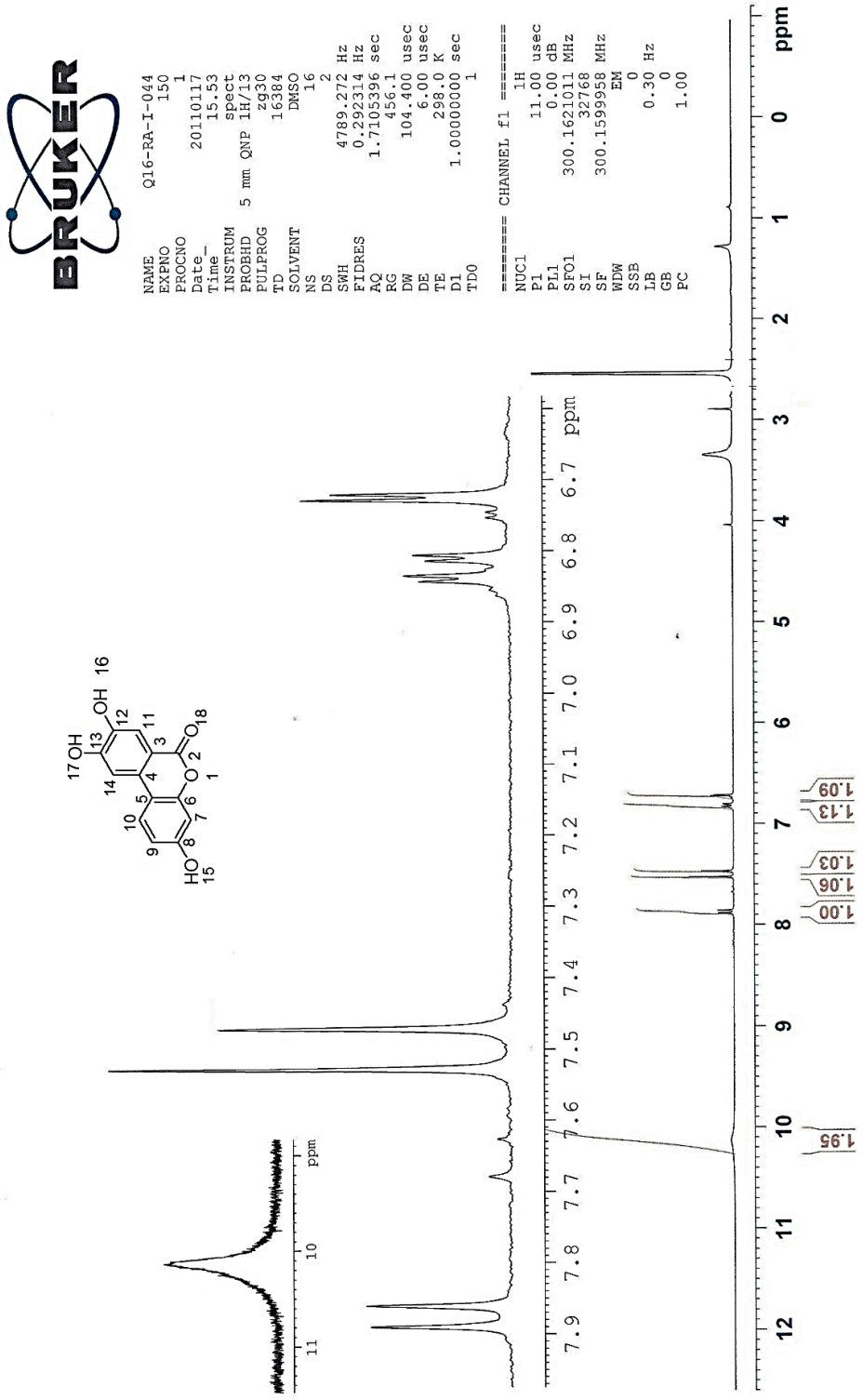

Figure A5:. ^{1}H-NMR (DMSO-d_6) spectrum of **3-Hydroxy-8,9-dimethoxy-6H-dibenzo[b,d]pyran-6-one (surrogate 2)** . Preparation procedure described in section V. 2. 2.

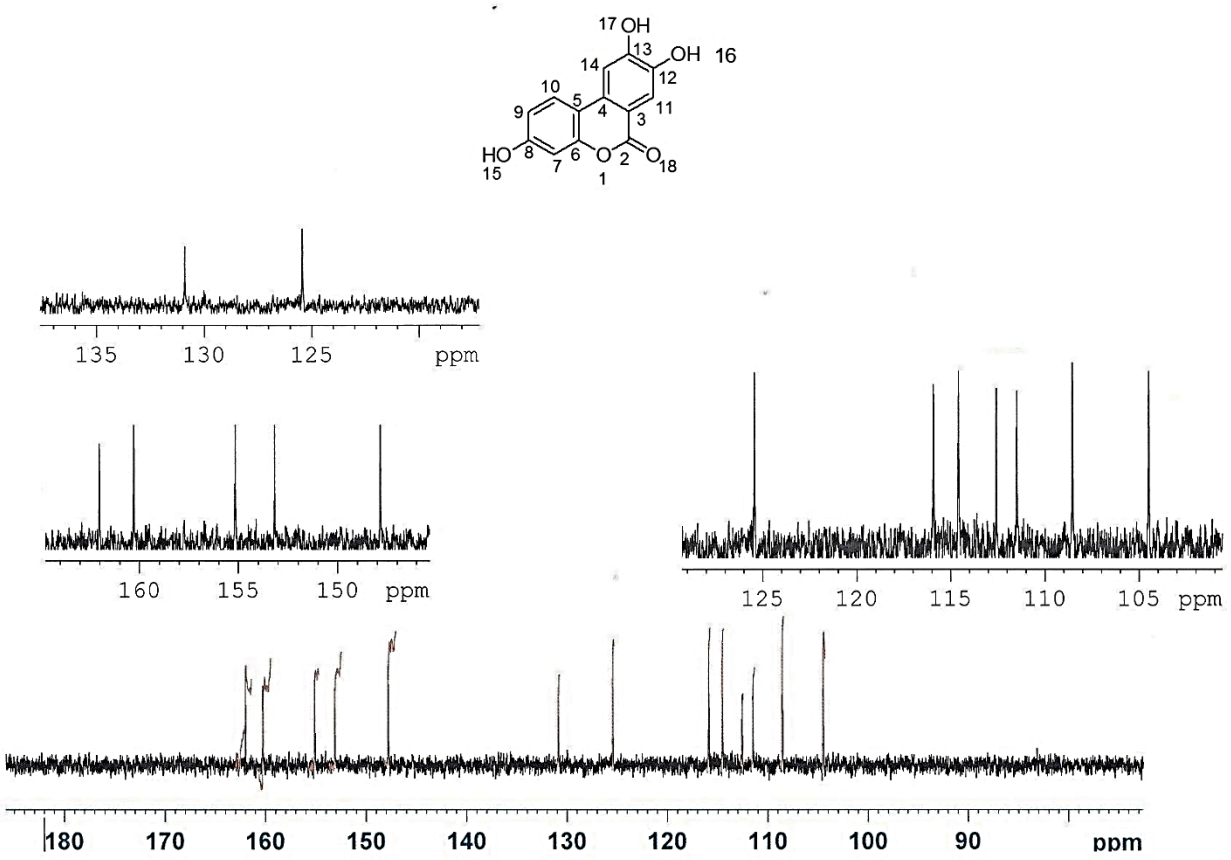

BRUKER

NAME	SURROGATE2-H,C
EXPNO	581
PROCNO	1
Date_	20121009
Time	1.50
INSTRUM	spect
PROBHD	5 mm QNP 1H/13
PULPROG	zgpg30
TD	65536
SOLVENT	DMSO
NS	800
DS	4
SWH	17985.611 Hz
FIDRES	0.274439 Hz
AQ	1.8219508 sec
RG	1824.6
DW	27.800 usec
DE	6.00 usec
TE	295.6 K
D1	2.00000000 sec
d11	0.03000000 sec
DELTA	1.89999998 sec
TD0	1
========	CHANNEL f1 ========
NUC1	13C
P1	10.00 usec
PL1	-2.00 dB
SFO1	75.4828396 MHz
========	CHANNEL f2 ========
CPDPRG2	waltz16
NUC2	1H
PCPD2	80.00 usec
PL2	0.00 dB
PL12	17.00 dB
PL13	17.00 dB
SFO2	300.1612006 MHz
SI	32768
SF	75.4751991 MHz
WDW	EM
SSB	0
LB	1.00 Hz
GB	0
PC	1.40

Figure A6: ^{13}C-NMR (DMSO-d_6) spectrum of **3-Hydroxy-8,9-dimethoxy-6H-dibenzo[b,d]pyran-6-one (surrogate 2) .** Preparation procedure described in section V. 2. 2.

UCM
CENTRO DE MICROANALISIS ELEMENTAL
Dpto. Q. Orgánica y Farmacéutica. F. Farmacia
Sotano sur. Edif. QA. F. CC. Químicas
UNIVERSIDAD COMPLUTENSE DE MADRID

INFORME DE ENSAYO SIMPLIFICADO

Código: PGC11-FR02.00
Fecha de edición: 30/11/10

TIPO DE ENSAYO: CHN ☑ CHNS ☐

CENTRO DE MICROANÁLISIS ELEMENTAL

UNIVERSIDAD COMPLUTENSE DE MADRID

Tlf.: 91 394 17 53 / 52 11. Fax: 91 394 52 11. Correo electrónico: microanalisis. elemental@farm.ucm.es

Código Cliente: GOM

Fecha de resultados: 17/02/2012

Equipo: *LECO CHNS 932.* ***Código:*** 3288

Contraseña Muestra CAI	***Contraseña Muestra***	***%C***	***%H***	***%N***	***Descripción de la muestra***	***Observaciones***	***Desviaciones del método***
Q02-12-092	RA-I-03 org	62,64	4,04	0,06	Sólido blanco		

C.A.I. MICROANÁLISIS ELEMENTAL

Responsable Técnico
José Carlos Menéndez Ramos

Fecha de emisión: 17/02/2012

Alcance Validado: %C: 0,50 - 94,70. %H: 0,50 - 7,60. %N: 0,50 - 23,00. %S: 0,50 - 30,60

Los resultados aquí expuestos no reflejan la información completa del ensayo, la cual se encuentra en el informe correspondiente
Los Informes de ensayo simplificados sin marca ENAC no están cubiertos por la acreditación

Figure A7: Elemental analysis assay (CHN) spectrum of **3-Hydroxy-8,9-dimethoxy-6H-dibenzo[b,d]pyran-6-one (surrogate 2) .** Preparation procedure described in section V. 2. 2.

Mass Spectrum List Report

Analysis Info

Analysis Name	RAI04401.d	Acquisition Date	01/21/11 13:28:05
Method	STOP1.M	Operator	Dr. Nour Kayali
Sample Name	RA-1-04[illegible]	Instrument	Esquire-LC_00126
Comment	DIRECTO EN METANOL		

Acquisition Parameter

Ion Source Type	ESI	Ion Polarity	Negative	Alternating Ion Polarity	n/a
Mass Range Mode	Std/Normal	Scan Begin	100.00 m/z	Scan End	900.00 m/z
Capillary Exit	-40.7 Volt	Skim 1	-9.7 Volt	Trap Drive	30.0
Accumulation Time	1258 µs	Averages	11 Spectra	Auto MS/MS	Off

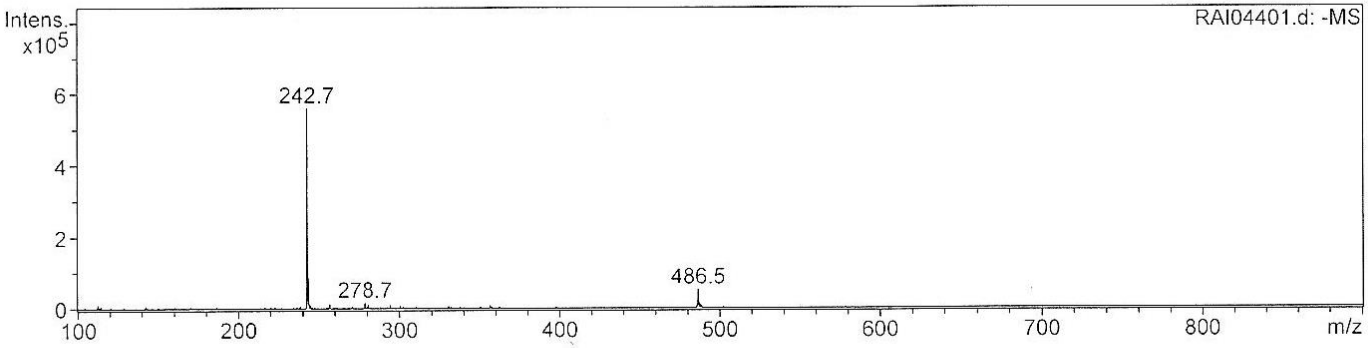

#	m/z	I	FWHM	S/N
1	242.7	558888	0.3	3315.2
2	243.7	85784	0.3	508.9
3	256.7	11909	0.4	70.6
4	278.7	15416	0.4	91.4
5	280.6	11255	0.3	66.8
6	486.5	51740	0.5	306.9
7	487.5	12137	0.5	72.0

Figure A8: MS-ESI (negative-ion detection) spectrum of **3-Hydroxy-8,9-dimethoxy-6H-dibenzo[b,d]pyran-6-one (surrogate 2) .** Preparation procedure described in section V. 2. 2.

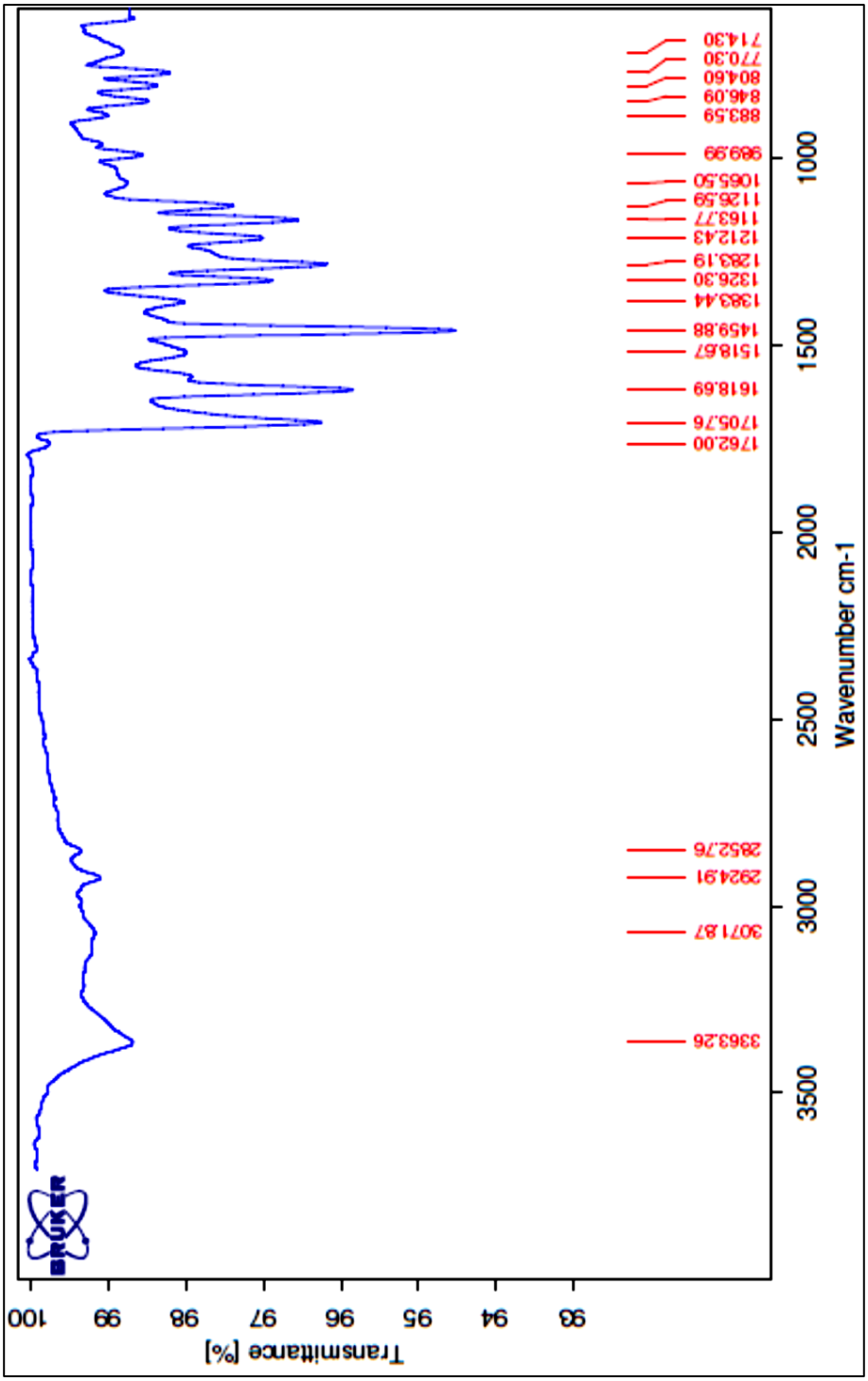

Figure A9: FT-IR (KBr disc) spectrum of **3-Hydroxy-8,9-dimethoxy-6H-dibenzo[b,d]pyran-6-one (surrogate 2)** . Preparation procedure described in section V. 2. 2.

V.2.3. 3-Hydroxy-9-methoxy-6H-dibenzo[b,d]pyran-6-one (S 3) or (8-O-methylurolithin A)

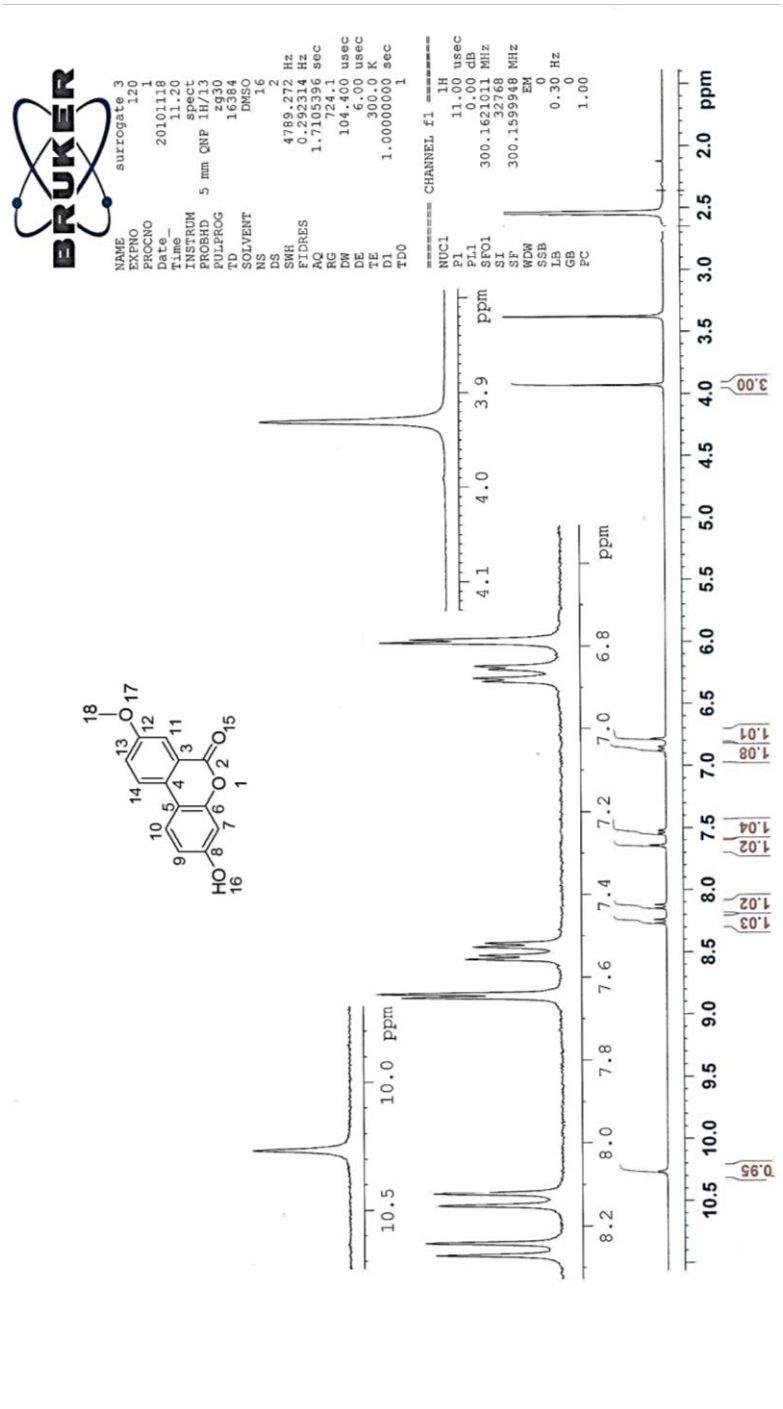

Figure A10: ^{1}H-NMR (DMSO-d_6) spectrum of **3-Hydroxy-9-methoxy-6H-dibenzo[b,d]pyran-6-one (surrogate 3).** Preparation procedure described in section V.2.3.

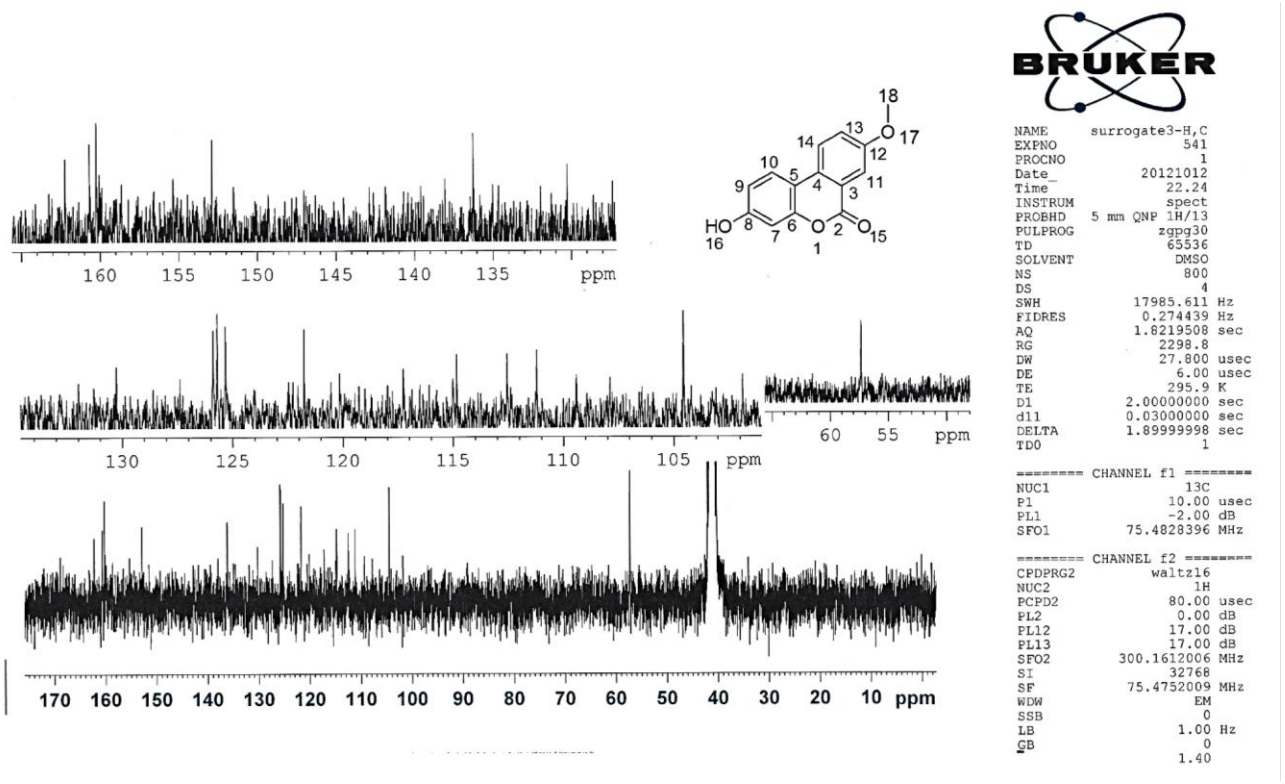

Figure A11: ^{13}C-NMR (DMSO-d_6) spectrum of **3-Hydroxy-9-methoxy-6H-dibenzo[b,d]pyran-6-one (surrogate 3).** Preparation procedure described in section V.2.3.

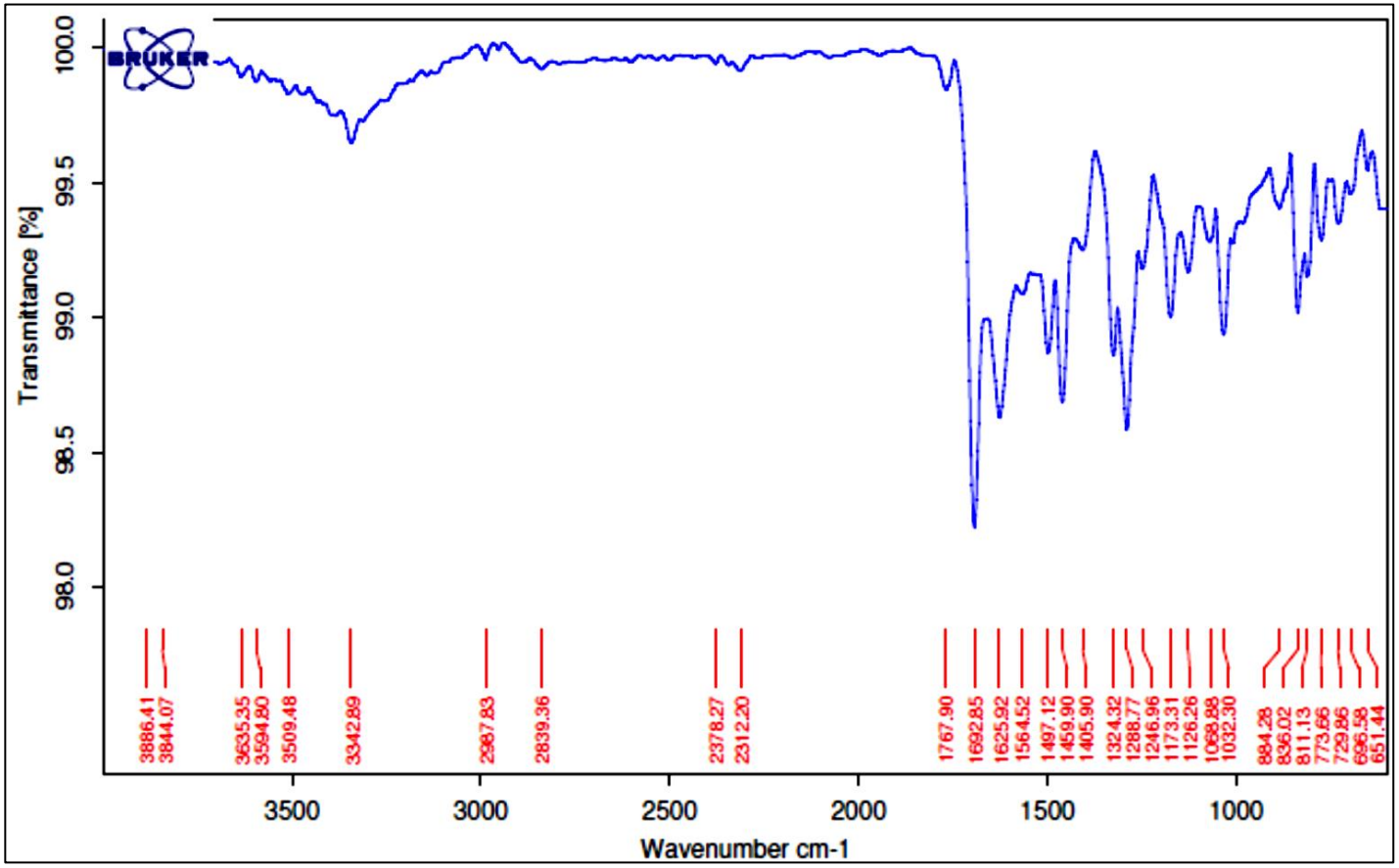

Figure A12: FT-IR (KBr disc) spectrum of **3-Hydroxy-9-methoxy-6H-dibenzo[b,d]pyran-6-one (surrogate 3).** Preparation procedure described in section V.2.3.

Mass Spectrum List Report

Analysis Info

Analysis Name	RAI03201.d	Acquisition Date	01/21/11 13:48:15
Method	STOP1.M	Operator	Dr. Nour Kayali
Sample Name	RA-I-032	Instrument	Esquire-LC_00126
Comment	DIRECTO EN METANOL		

Acquisition Parameter

Ion Source Type	ESI	Ion Polarity	Negative	Alternating Ion Polarity	n/a
Mass Range Mode	Std/Normal	Scan Begin	100.00 m/z	Scan End	900.00 m/z
Capillary Exit	-60.7 Volt	Skim 1	-9.7 Volt	Trap Drive	40.0
Accumulation Time	493 µs	Averages	11 Spectra	Auto MS/MS	Off

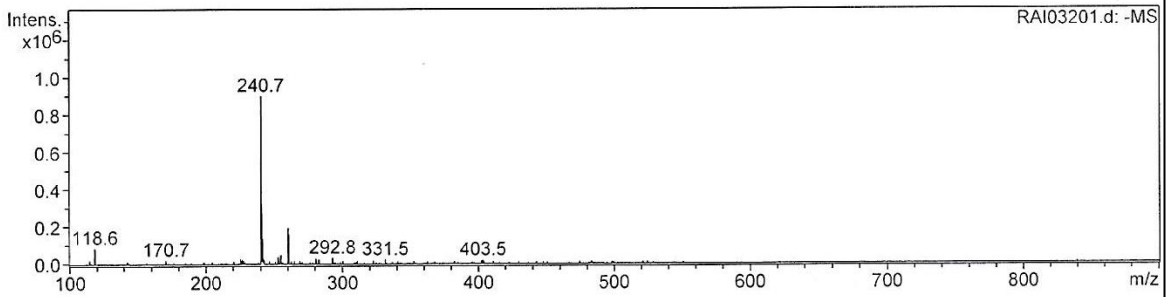

#	m/z	I	FWHM	S/N
1	114.8	21373	0.3	52.0
2	118.6	85807	0.3	208.8
3	170.7	20100	0.3	48.9
4	225.7	25972	0.3	63.2
5	226.9	24425	0.4	59.4
6	240.7	898356	0.4	2185.9
7	241.7	136194	0.4	331.4
8	242.7	23271	0.4	56.6
9	252.9	36654	0.4	89.2
10	254.9	48215	0.5	117.3
11	260.5	191490	0.4	465.9
12	280.9	27866	0.4	67.8
13	283.0	23465	0.3	57.1
14	292.8	31534	0.3	76.7
15	331.5	22176	0.3	54.0
16	403.5	20240	0.3	49.2

Figure A13: ESI-MS (negative ion detection) of**3-Hydroxy-9-methoxy-6H-dibenzo[b,d]pyran-6-one (surrogate 3).** Preparation procedure described in section V.2.3.

V.2.4. 3,8-Dihydroxy-6H-dibenzo[b,d]pyran-6-one (S 4) or (Urolithin A)

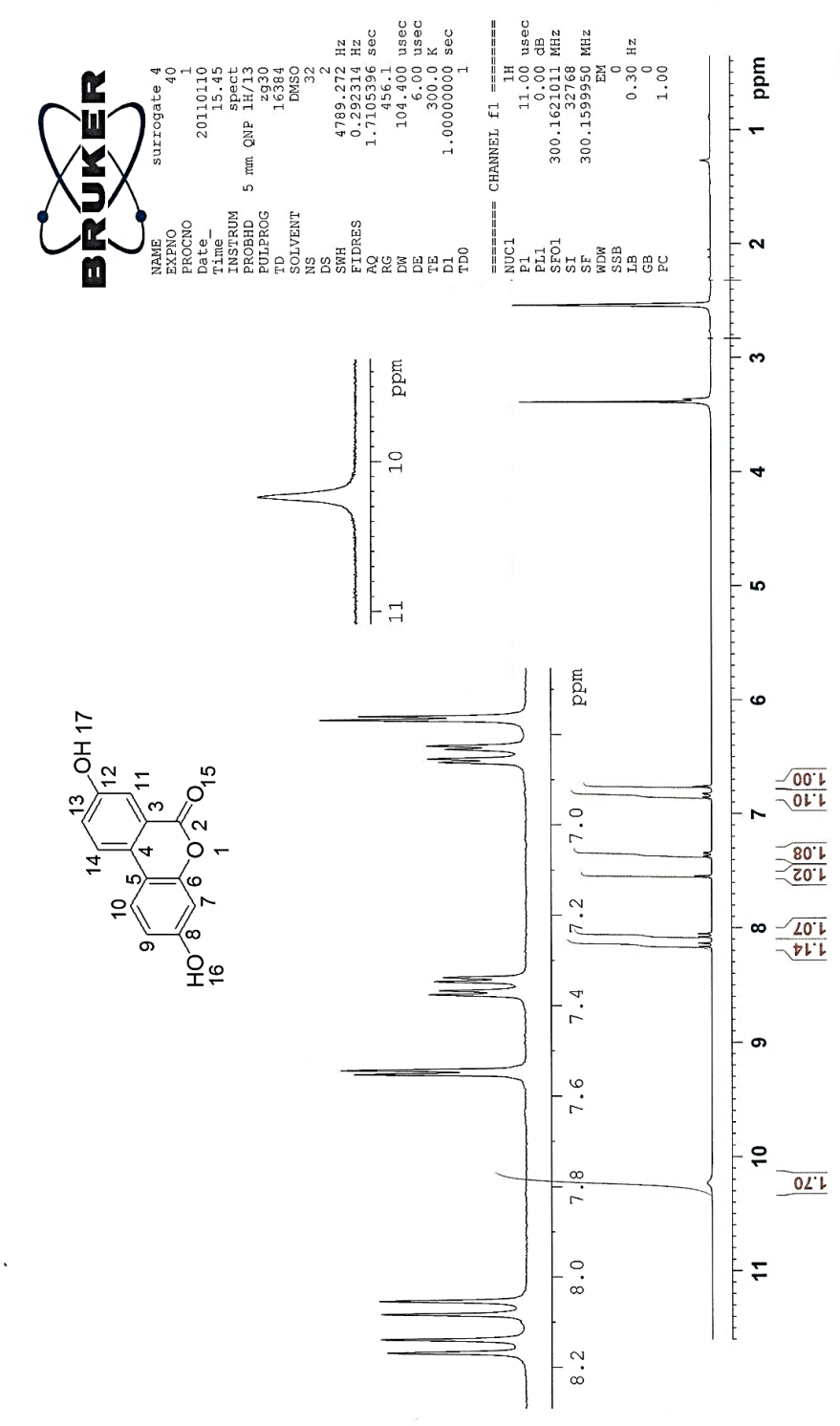

Figure A14:. ^{1}H-NMR (DMSO-d_6) spectrum of **3,8-Dihydroxy-6H-dibenzo[b,d]pyran-6-one (surrogate 4).** Preparation procedure described in section V.2.4.

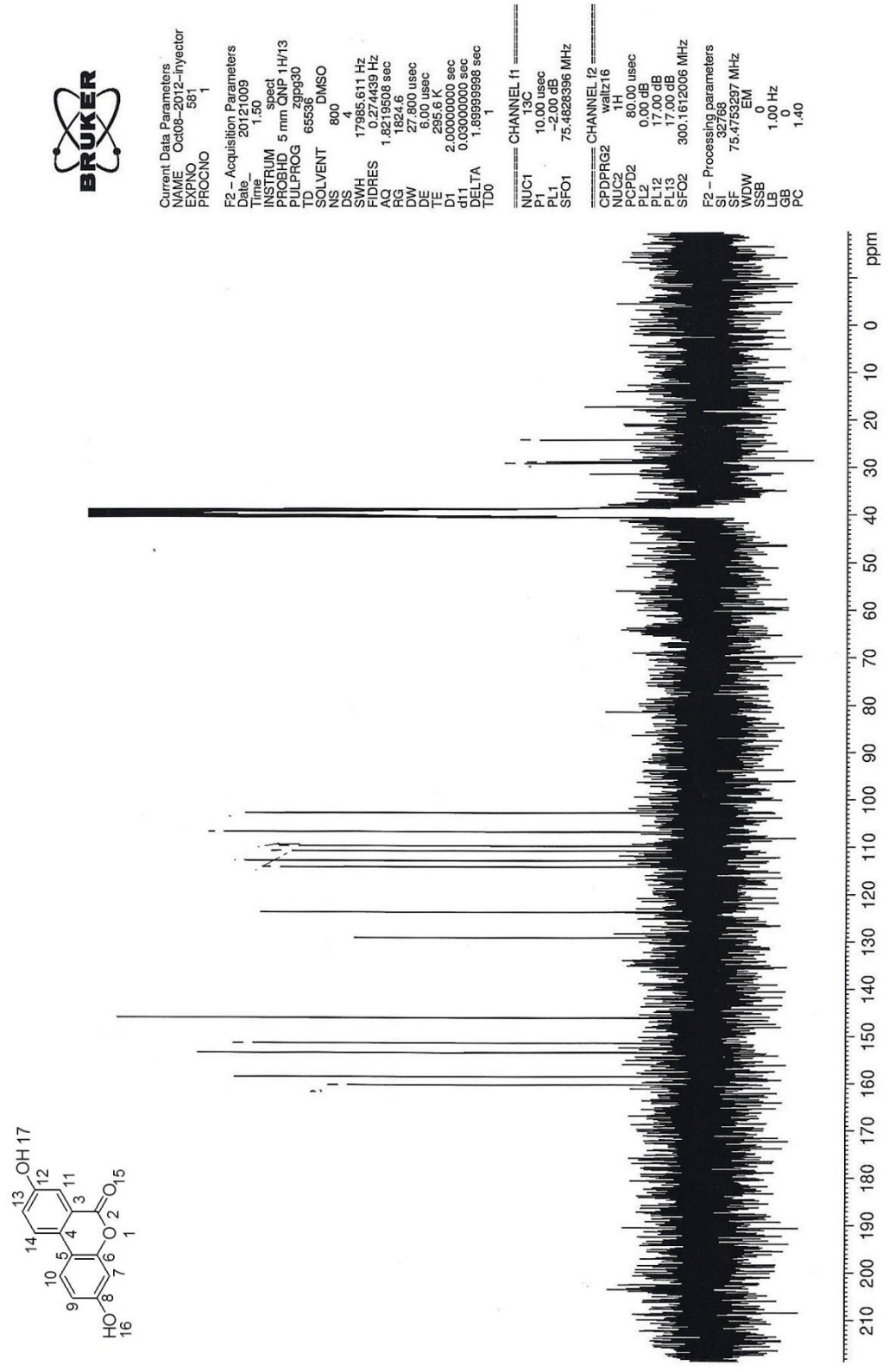

Figure A15:. ^{13}C-NMR (DMSO-d_6) spectrum of **3,8-Dihydroxy-6H-dibenzo[b,d]pyran-6-one (surrogate 4).** Preparation procedure described in section V.2.4.

UCM
CENTRO DE MICROANALISIS ELEMENTAL
Dpto. Q. Orgánica y Farmacéutica. F. Farmacia
Sotano sur. Edif. QA. F. CC. Químicas
UNIVERSIDAD COMPLUTENSE DE MADRID

INFORME DE ENSAYO SIMPLIFICADO

Código: PGC11-FR02.00
Fecha de edición: 30/11/10

TIPO DE ENSAYO: CHN ☑ CHNS ☐

CENTRO DE MICROANÁLISIS ELEMENTAL
UNIVERSIDAD COMPLUTENSE DE MADRID

Tlf.: 91 394 17 53 / 52 11. Fax: 91 394 52 11. Correo electrónico: microanalisis. elemental@farm.ucm.es

Código Cliente: GOM

Fecha de resultados: 12/04/2012

Equipo: *LECO CHNS 932.* ***Código:*** 3288

Contraseña Muestra CAI	*Contraseña Muestra*	*%C*	*%H*	*%N*	*Descripción de la muestra*	*Observaciones*	*Desviaciones del método*
Q03-12-358		66,33	4,03	0,07	Sólido beis		

Responsable Técnico
José Carlos Menéndez Ramos
Fecha de emisión: 12/04/2012

Alcance Validado: **%C: 0,50 - 94,70. %H: 0,50 - 7,60. %N: 0,50 - 23,00. %S: 0,50 - 30,60**

Los resultados aquí expuestos no reflejan la información completa del ensayo, la cual se encuentra en el informe correspondiente
Los Informes de ensayo simplificados sin marca ENAC no están cubiertos por la acreditación

Figure A16: Elemental analysis assay (CHN) spectrum of **3,8-Dihydroxy-6H-dibenzo[b,d]pyran-6-one (surrogate 4).** Preparation procedure described in section V.2.4.

Mass Spectrum List Report

Analysis Info

Analysis Name	RAI04001.d	Acquisition Date	01/21/11 13:33:46
Method	STOP1.M	Operator	Dr. Nour Kayali
Sample Name	RA-I-040	Instrument	Esquire-LC_00126
Comment	DIRECTO EN METANOL		

Acquisition Parameter

Ion Source Type	ESI	Ion Polarity	Negative	Alternating Ion Polarity	n/a
Mass Range Mode	Std/Normal	Scan Begin	100.00 m/z	Scan End	900.00 m/z
Capillary Exit	-90.7 Volt	Skim 1	-9.7 Volt	Trap Drive	25.0
Accumulation Time	2293 µs	Averages	11 Spectra	Auto MS/MS	Off

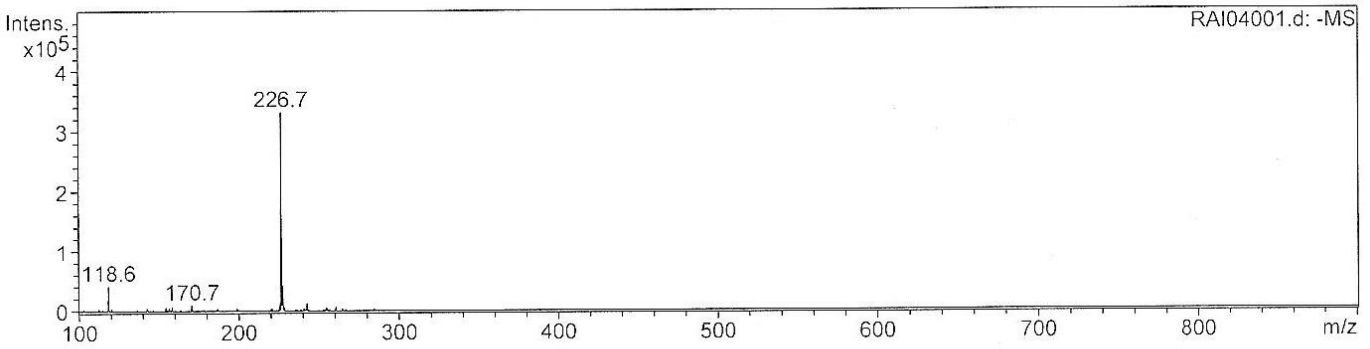

#	m/z	I	FWHM	S/N
1	118.6	41968	0.3	561.0
2	158.6	6755	0.3	90.3
3	170.7	9738	0.3	130.2
4	225.7	12128	0.3	162.1
5	226.7	331181	0.4	4426.8
6	227.7	42756	0.4	571.5
7	242.7	12415	0.3	165.9

Figure A17: MS-ESI (negative -ion detection) of **3,8-Dihydroxy-6H-dibenzo[b,d]pyran-6-one (surrogate 4).** Preparation procedure described in section V.2.4.

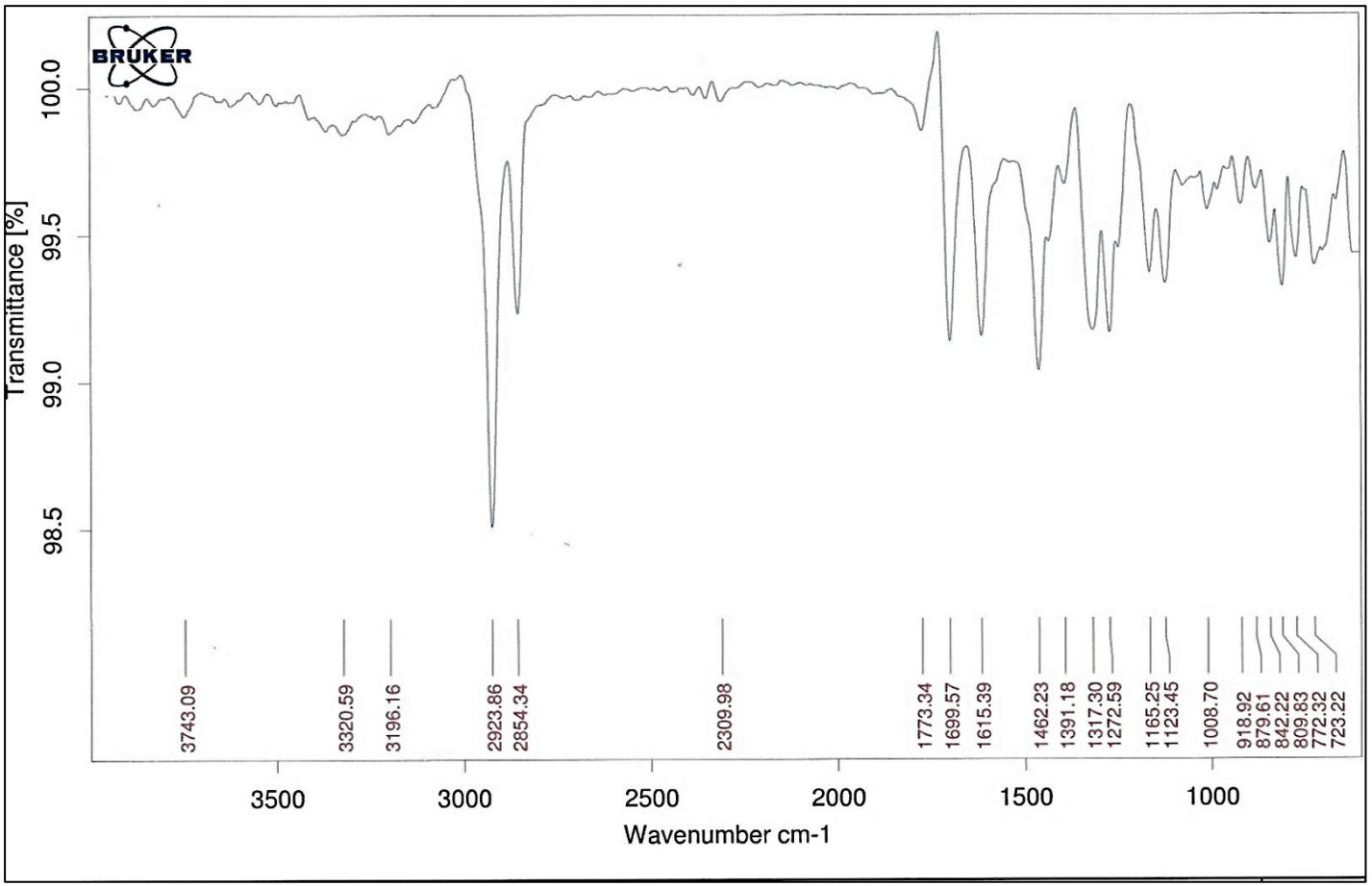

Figure A18: FT-IR (KBr disc) spectrum of**3,8-Dihydroxy-6H-dibenzo[b,d]pyran-6-one (surrogate 4).** Preparation procedure described in section V.2.4.

V.2.5. 3-Methoxy-5-methylphenyl 2,4-dimethoxybenzoate (S 5)

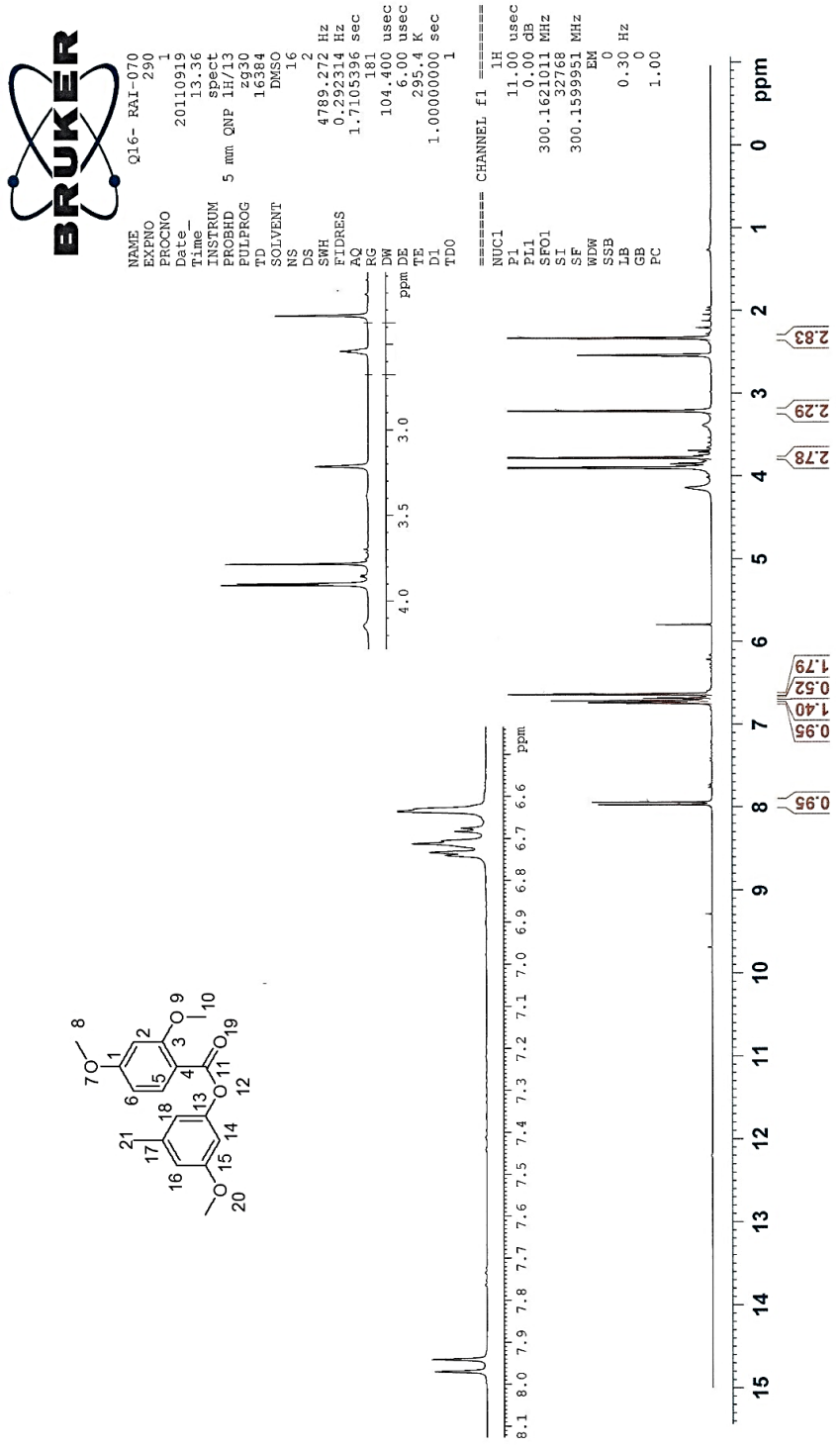

Figure A19: ^{1}H-NMR (DMSO-d_6) spectrum of **3-Methoxy-5-methylphenyl 2,4-dimethoxybenzoate (Surrogate 5).**.
Preparation procedure described in section V.2.5.

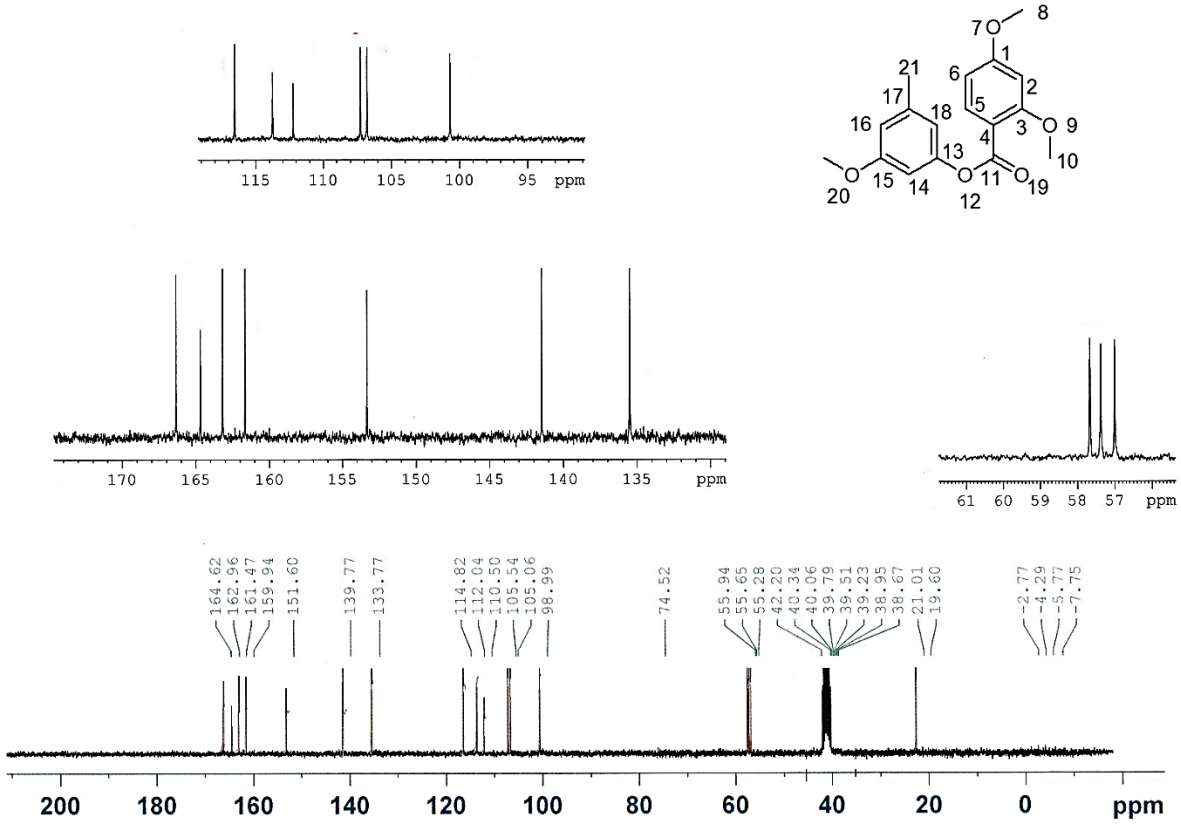

NAME	surrogate5-H;C	
EXPNO	511	
PROCNO	1	
Date_	20121012	
Time	19.20	
INSTRUM	spect	
PROBHD	5 mm QNP 1H/13	
PULPROG	zgpg30	
TD	65536	
SOLVENT	DMSO	
NS	800	
DS	4	
SWH	17985.611	Hz
FIDRES	0.274439	Hz
AQ	1.8219508	sec
RG	1824.6	
DW	27.800	usec
DE	6.00	usec
TE	296.0	K
D1	2.00000000	sec
d11	0.03000000	sec
DELTA	1.89999998	sec
TD0	1	
======== CHANNEL f1 ========		
NUC1	13C	
P1	10.00	usec
PL1	-2.00	dB
SFO1	75.4828396	MHz
======== CHANNEL f2 ========		
CPDPRG2	waltz16	
NUC2	1H	
PCPD2	80.00	usec
PL2	0.00	dB
PL12	17.00	dB
PL13	17.00	dB
SFO2	300.1612006	MHz
SI	32768	
SF	75.4751996	MHz
WDW	EM	
SSB	0	
LB	1.00	Hz
GB	0	
PC	1.40	

Figure A20: ^{13}C-NMR (DMSO-d_6) spectrum of **3-Methoxy-5-methylphenyl 2,4-dimethoxybenzoate (Surrogate 5).**.
Preparation procedure described in section V.2.5.

Mass Spectrum List Report

Analysis Info

Analysis Name	RAI06901.d	Acquisition Date	05/26/11 18:29:53
Method	carbenos.MS	Operator	Dr. Nour Kayali
Sample Name	RAI069	Instrument	Esquire-LC_00126
Comment	DIRECTO, EN MeOH		

Acquisition Parameter

Ion Source Type	ESI	Ion Polarity	Positive	Alternating Ion Polarity	n/a
Mass Range Mode	Std/Normal	Scan Begin	100.00 m/z	Scan End	500.00 m/z
Capillary Exit	72.2 Volt	Skim 1	6.5 Volt	Trap Drive	31.1
Accumulation Time	12096 µs	Averages	12 Spectra	Auto MS/MS	Off

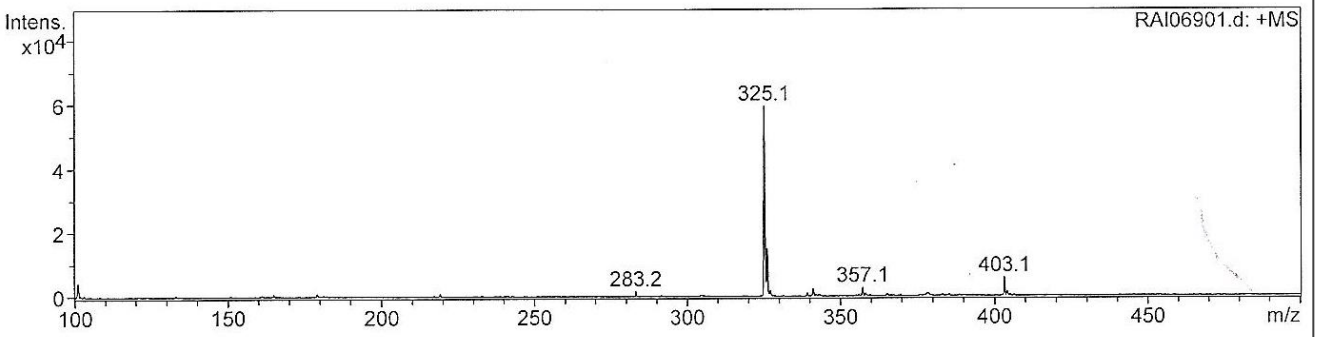

#	m/z	I	FWHM	S/N
1	101.1	4344	0.5	100.5
2	283.2	1581	0.3	36.6
3	325.1	59316	0.4	1372.9
4	326.0	14889	0.4	344.6
5	327.0	1783	0.3	41.3
6	341.0	2414	0.4	55.9
7	357.1	2649	0.4	61.3
8	403.1	5779	0.4	133.8
9	404.1	1416	0.4	32.8

Figure A20: MS-ESI (positive ion detection) of **3-Methoxy-5-methylphenyl 2,4-dimethoxybenzoate (Surrogate 5).**. Preparation procedure described in section V.2.5.

V.2.6. 3-Hydroxy-5-methylphenyl 2,4-dihydroxybenzoate (S 6)

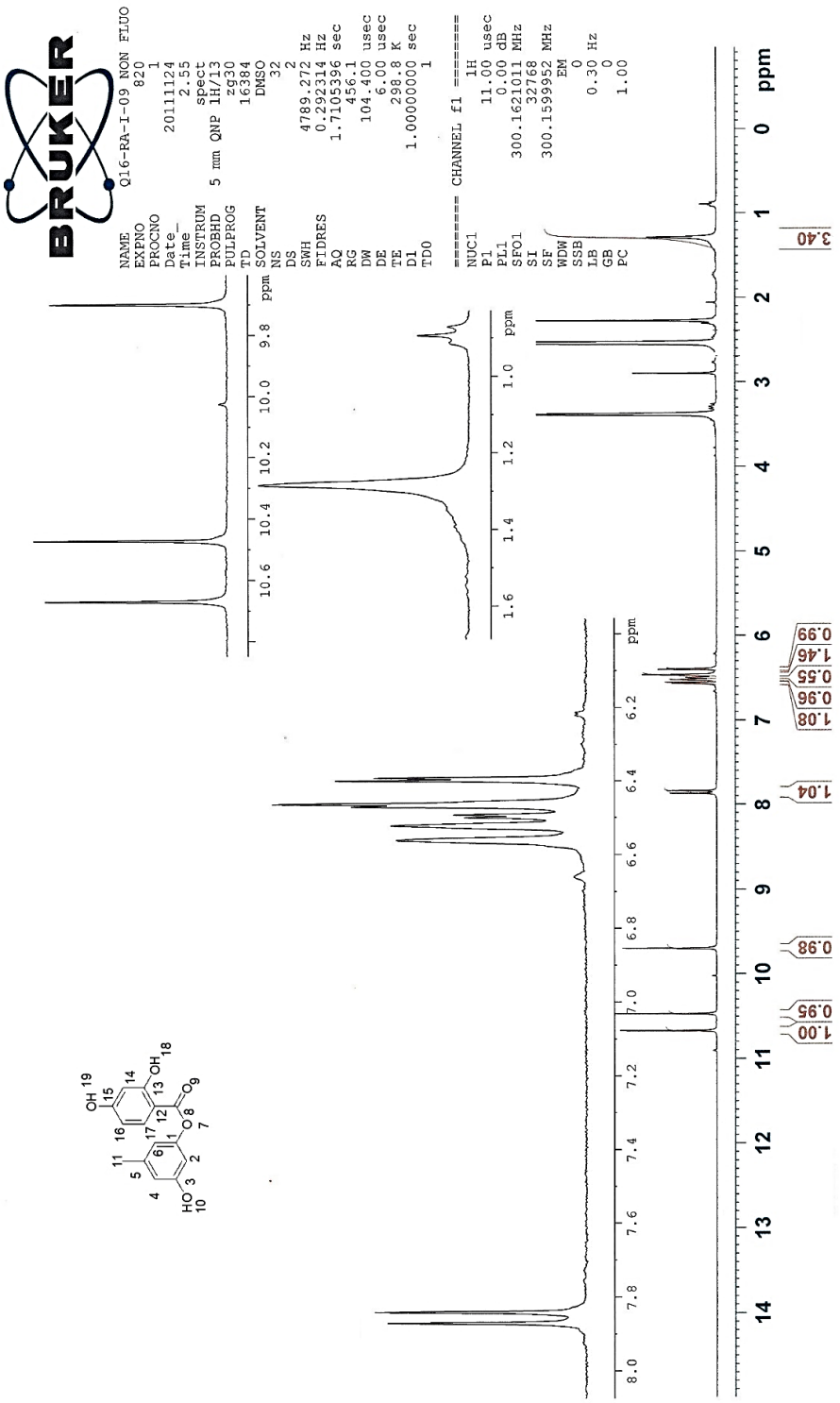

Figure A21: ^{1}H-NMR (DMSO-d_6) spectrum of **3-Hydroxy-5-methylphenyl 2,4-dihydroxybenzoate (surrogate 6).**
Preparation procedure described in section V.2.6.

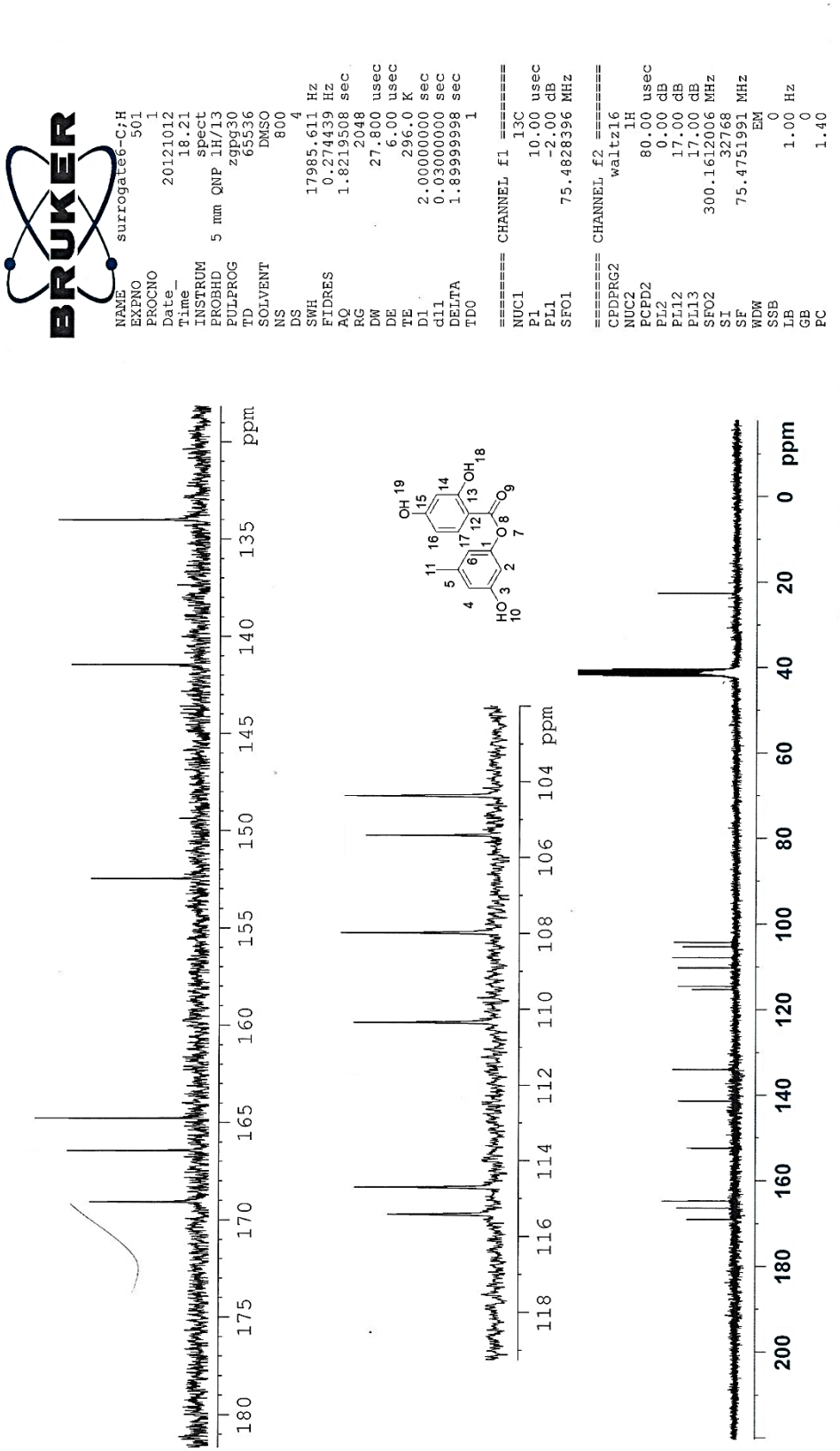

Figure A22: ^{13}C-NMR (DMSO-d_6) spectrum of **3-Hydroxy-5-methylphenyl 2,4-dihydroxybenzoate (surrogate 6).** Preparation procedure described in section V.2.6.

Mass Spectrum List Report

Analysis Info

Analysis Name	RA109000.d	Acquisition Date	12/02/11 11:46:34
Method	XQ Default.ms	Operator	Dr. Nour Kayali
Sample Name	RA109	Instrument	Esquire-LC_00126
Comment	DIRECTO, EN MeOH		

Acquisition Parameter

Ion Source Type	ESI	Ion Polarity	Negative	Alternating Ion Polarity	n/a
Mass Range Mode	Std/Normal	Scan Begin	50.00 m/z	Scan End	600.00 m/z
Capillary Exit	-16.4 Volt	Skim 1	-5.8 Volt	Trap Drive	25.0
Accumulation Time	28209 µs	Averages	20 Spectra	Auto MS/MS	Off

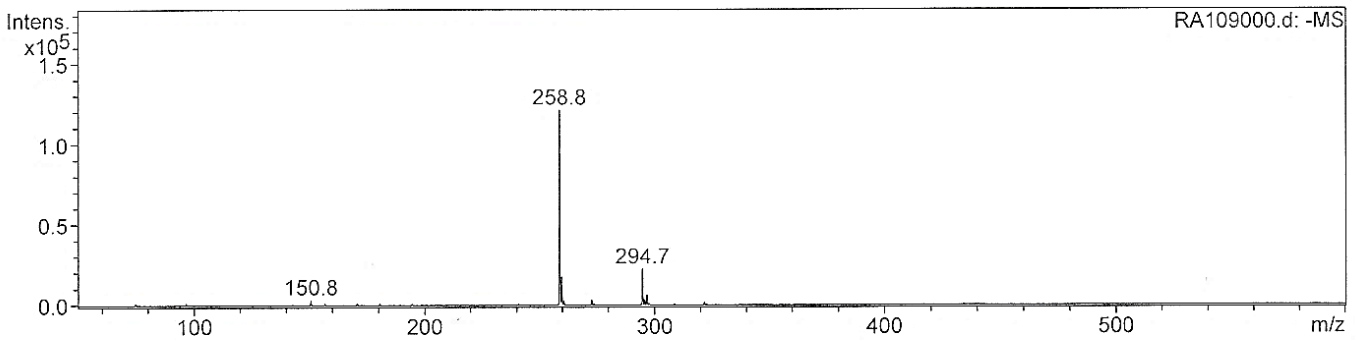

#	m/z	I	FWHM	S/N
1	150.8	3121	0.3	350.1
2	258.8	121133	0.3	13587.9
3	259.7	17548	0.4	1968.4
4	260.7	2657	0.4	298.0
5	272.7	3172	0.4	355.8
6	294.7	22536	0.4	2527.9
7	295.7	3524	0.3	395.3
8	296.7	6308	0.3	707.6

Figure A23: MS-ESI (negative ion detection) of **3-Hydroxy-5-methylphenyl 2,4-dihydroxybenzoate (surrogate 6).** Preparation procedure described in section V.2.6.

UCM
CENTRO DE MICROANALISIS ELEMENTAL
Dpto. Q. Orgánica y Farmacéutica. F. Farmacia
Sotano sur. Edif. QA. F. CC. Químicas
UNIVERSIDAD COMPLUTENSE DE MADRID

INFORME DE ENSAYO SIMPLIFICADO

Código: PGC11-FR02.00
Fecha de edición: 30/11/10

TIPO DE ENSAYO: CHN ☑ CHNS ☐

CENTRO DE MICROANÁLISIS ELEMENTAL
UNIVERSIDAD COMPLUTENSE DE MADRID

Tlf.: 91 394 17 53 / 52 11. Fax: 91 394 52 11. Correo electrónico: microanalisis. elemental@farm.ucm.es

Código Cliente: GOM

Fecha de resultados: 12/04/2012

Equipo: *LECO CHNS 932.* ***Código:*** 3288

Contraseña Muestra CAI	*Contraseña Muestra*	*%C*	*%H*	*%N*	*Descripción de la muestra*	*Observaciones*	*Desviaciones del método*
Q03-12-357	RA-I-09	46,83	5,94	0,08	Sólido beis		

Responsable Técnico
José Carlos Menéndez Ramos
Fecha de emisión: 12/04/2012

Alcance Validado: **%C: 0,50 - 94,70. %H: 0,50 - 7,60. %N: 0,50 - 23,00. %S: 0,50 - 30,60**

Los resultados aquí expuestos no reflejan la información completa del ensayo, la cual se encuentra en el informe correspondiente
Los Informes de ensayo simplificados sin marca ENAC no están cubiertos por la acreditación

Figure A24: Elemental analysis assay (CHN) spectrum of **3-Hydroxy-5-methylphenyl 2,4-dihydroxybenzoate (surrogate 6).** Preparation procedure described in section V.2.6.

V.3. Synthesis of Alternariol surrogates with urethane functionalities for covalent imprinting of polymers

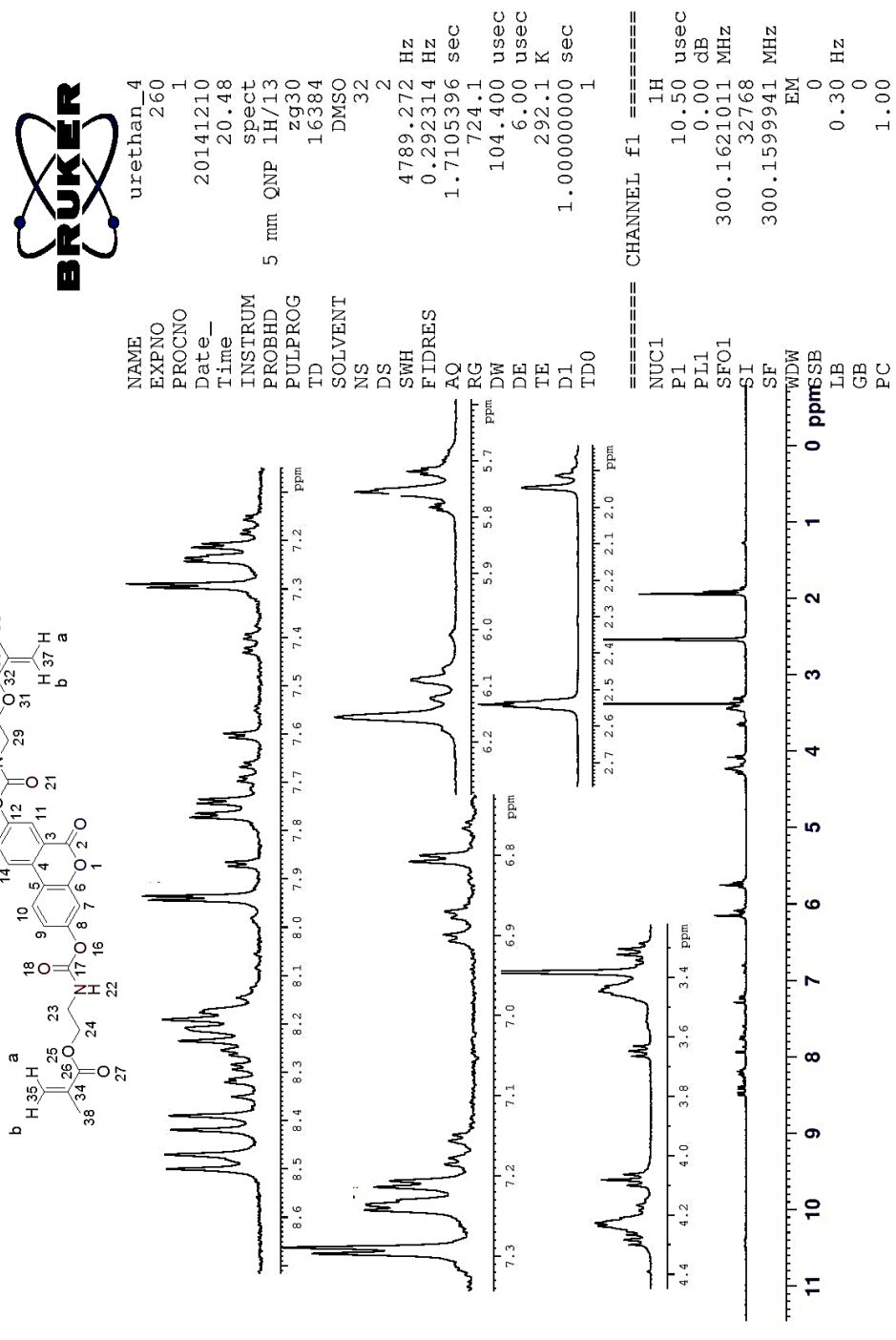

Figure A25: ^{1}H-NMR (DMSO-d_6) spectrum of **Alternariol surrogates with urethane functionalities for covalent imprinting of polymers.** Preparation procedure described in section V.3.

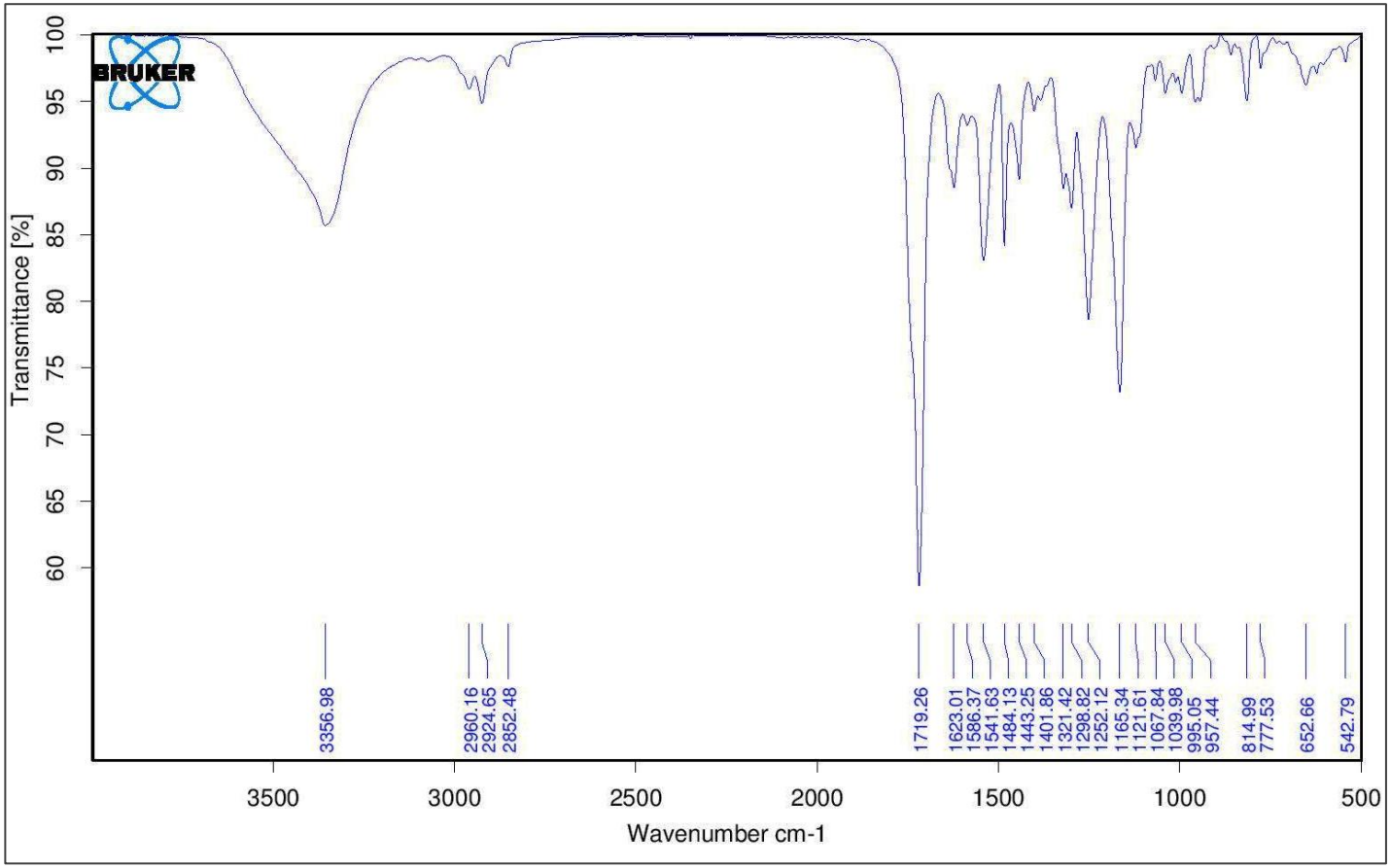

Figure A26: FT-IR (KBr disc) spectrum of **Alternariol surrogates with urethane functionalities for covalent imprinting of polymers.** Preparation procedure described in section V.3.

Mass Spectrum List Report

Analysis Info

Analysis Name	URE-PRY5.d	Acquisition Date	04/10/12 18:15:32
Method	XQ Default.ms	Operator	Dr. Nour Kayali
Sample Name	URE-PRY	Instrument	Esquire-LC_00126
Comment	DIRECTO, MeOH		

Acquisition Parameter

Ion Source Type	ESI	Ion Polarity	Positive	Alternating Ion Polarity	n/a
Mass Range Mode	Std/Normal	Scan Begin	150.00 m/z	Scan End	2200.00 m/z
Capillary Exit	148.1 Volt	Skim 1	60.4 Volt	Trap Drive	44.4
Accumulation Time	509 µs	Averages	11 Spectra	Auto MS/MS	Off

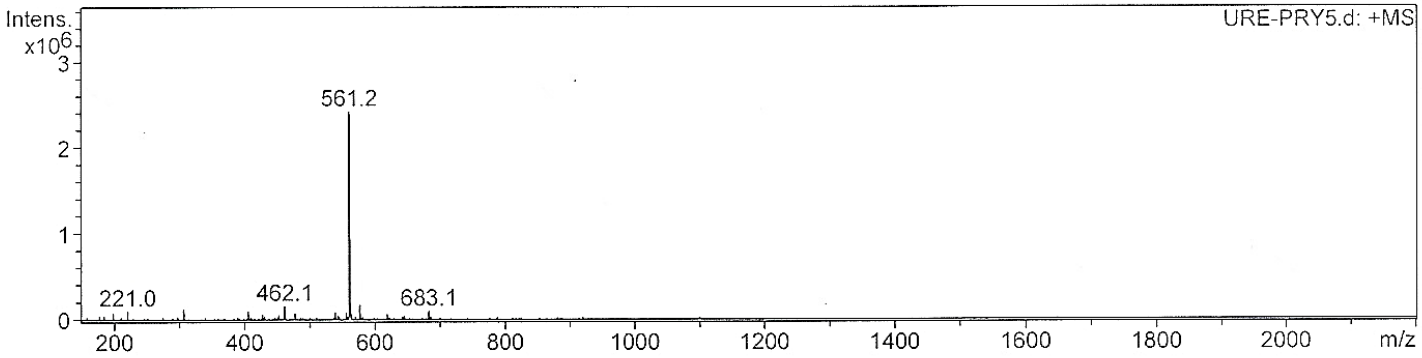

Figure A27: MS-ESI (negative ion detection) of **Alternariol surrogates with urethane functionalities for covalent imprinting of polymers.** Preparation procedure described in section V.3.

V.4.1 Sodium salt of Tenuazonic Acid *r*TeA

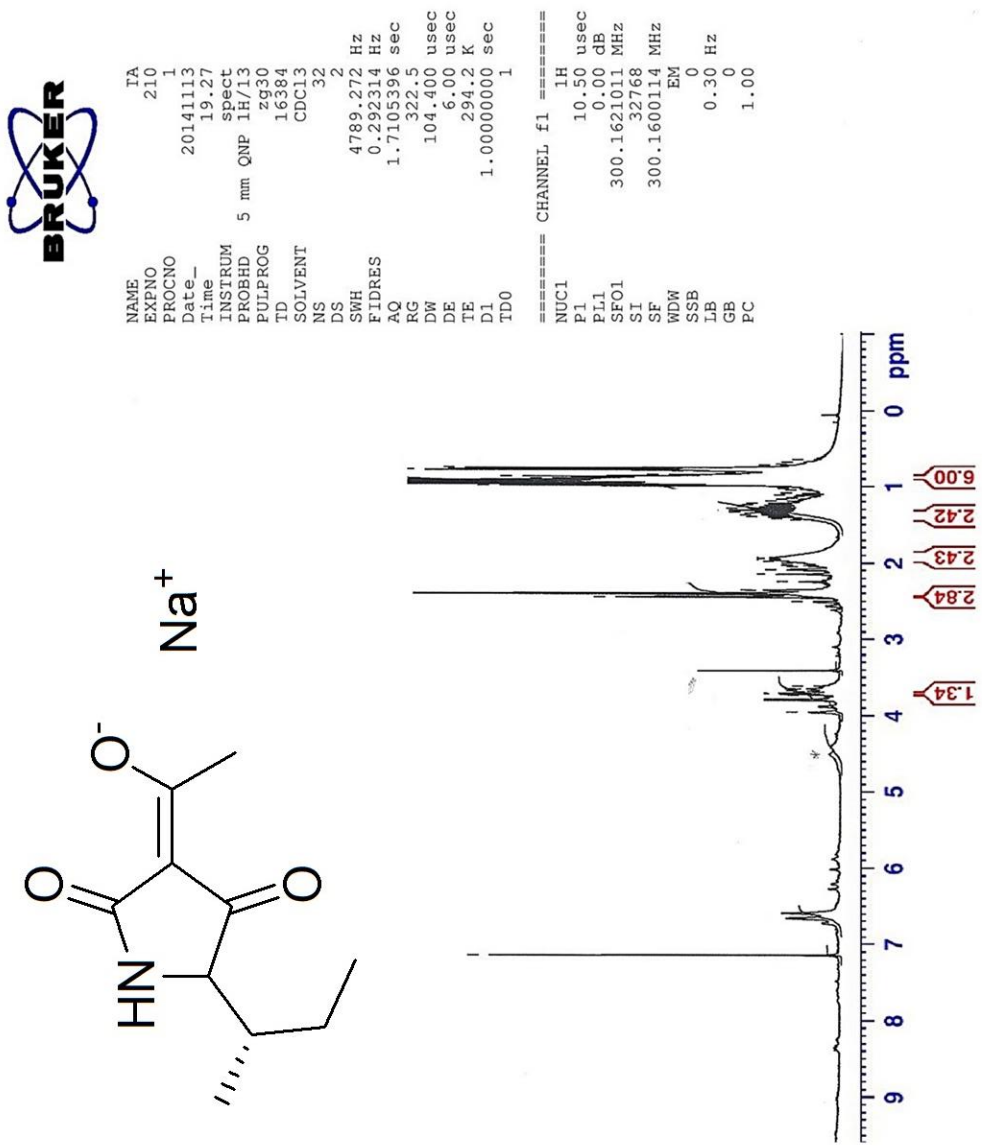

Figure A28: ^{1}H-NMR (CDCl3-d_1) spectrum of **Sodium salt of Tenuazonic Acid.**

Preparation procedure described in section V.4.1.

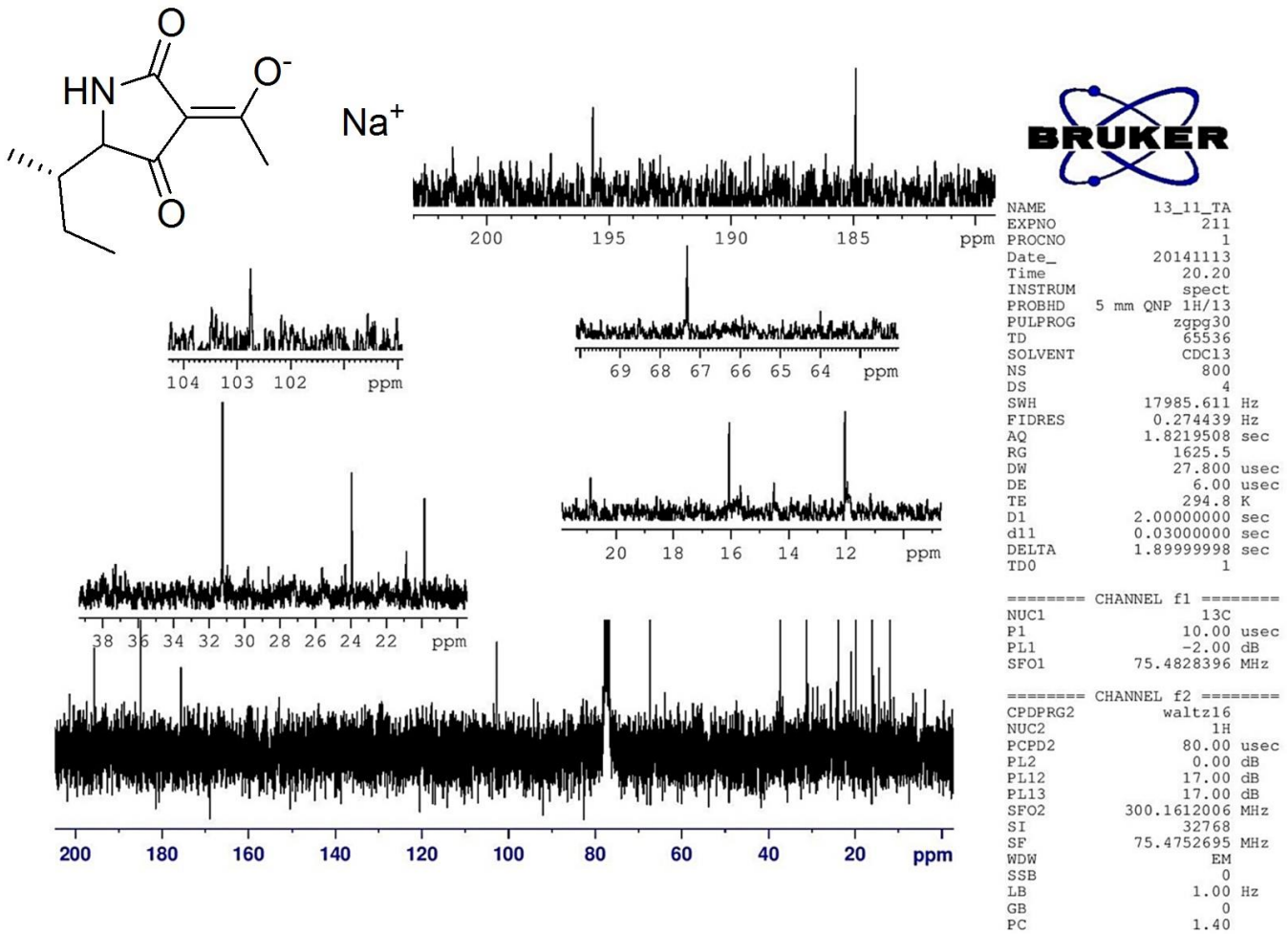

Figure A29: ^{13}C-NMR (CDCl3-d_1) spectrum of **Sodium salt of Tenuazonic Acid.** Preparation procedure described in section V.4.1.

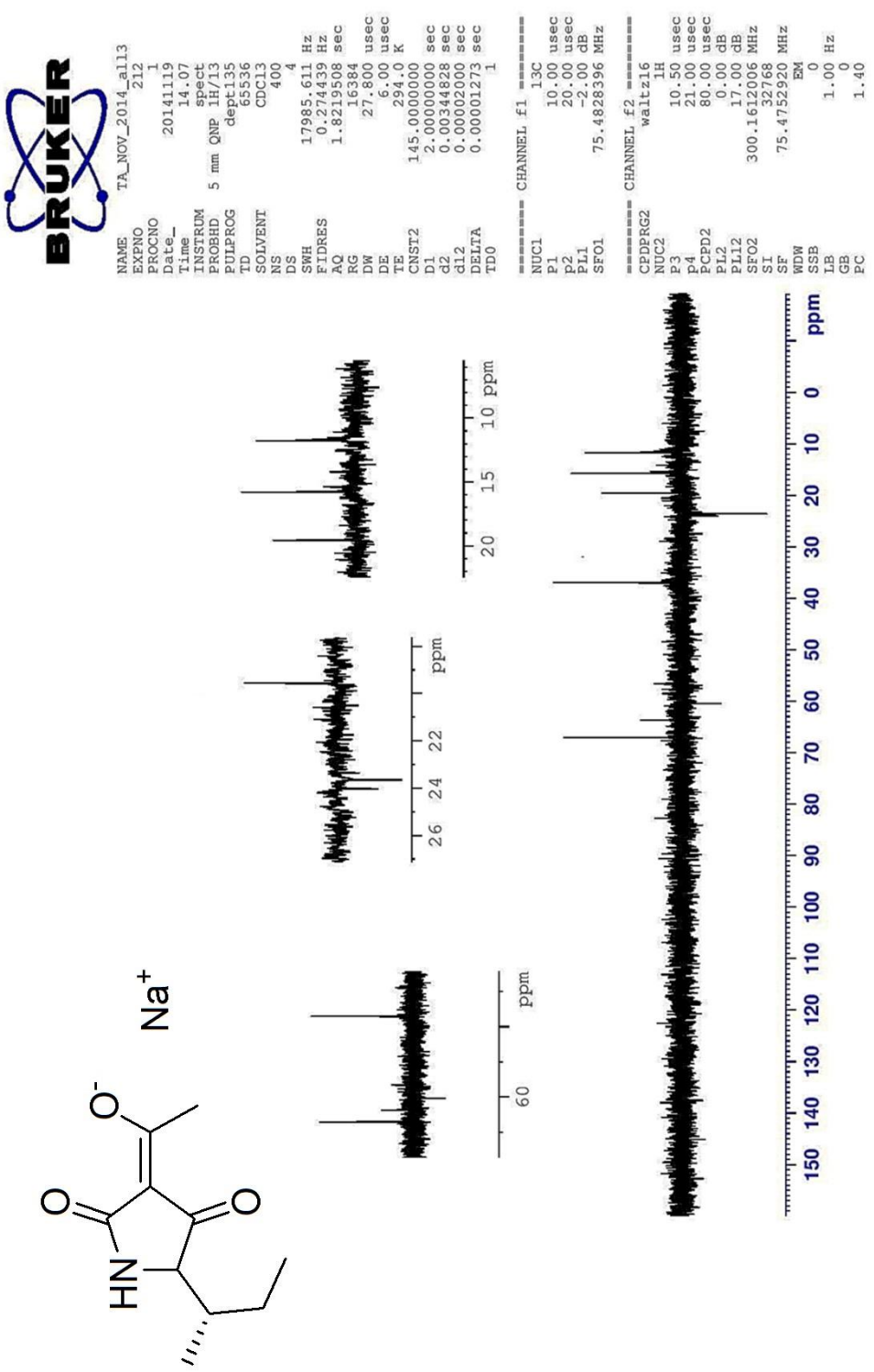

Figure A30: DEPT 135 ($CDCl_3$-d_1) spectrum of **Sodium salt of Tenuazonic Acid.** Preparation procedure described in section V.4.1.

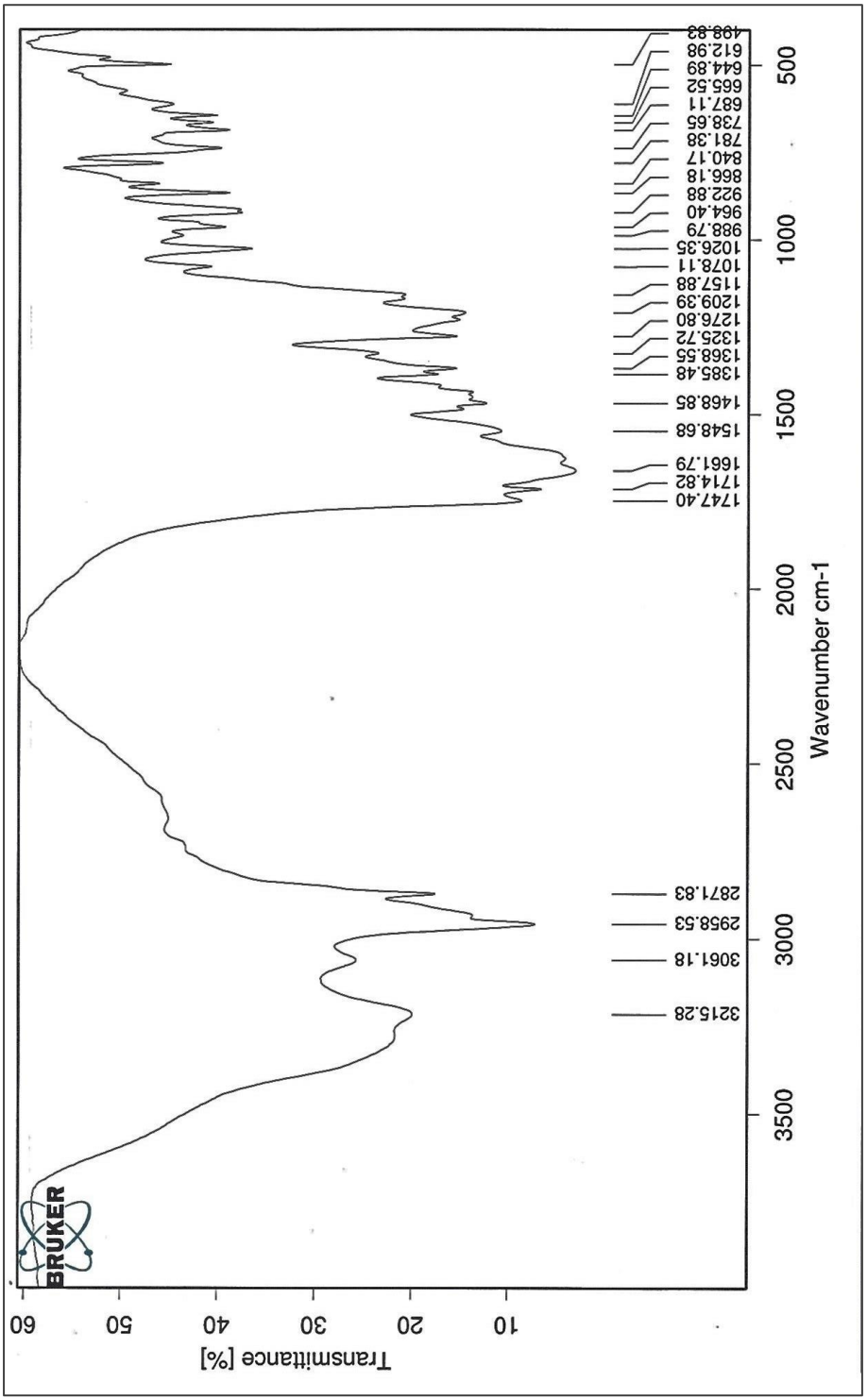

Figure A31: FT-IR (KBr disc) spectrum of **Sodium salt of Tenuazonic Acid.** Preparation procedure described in section V.4.1.

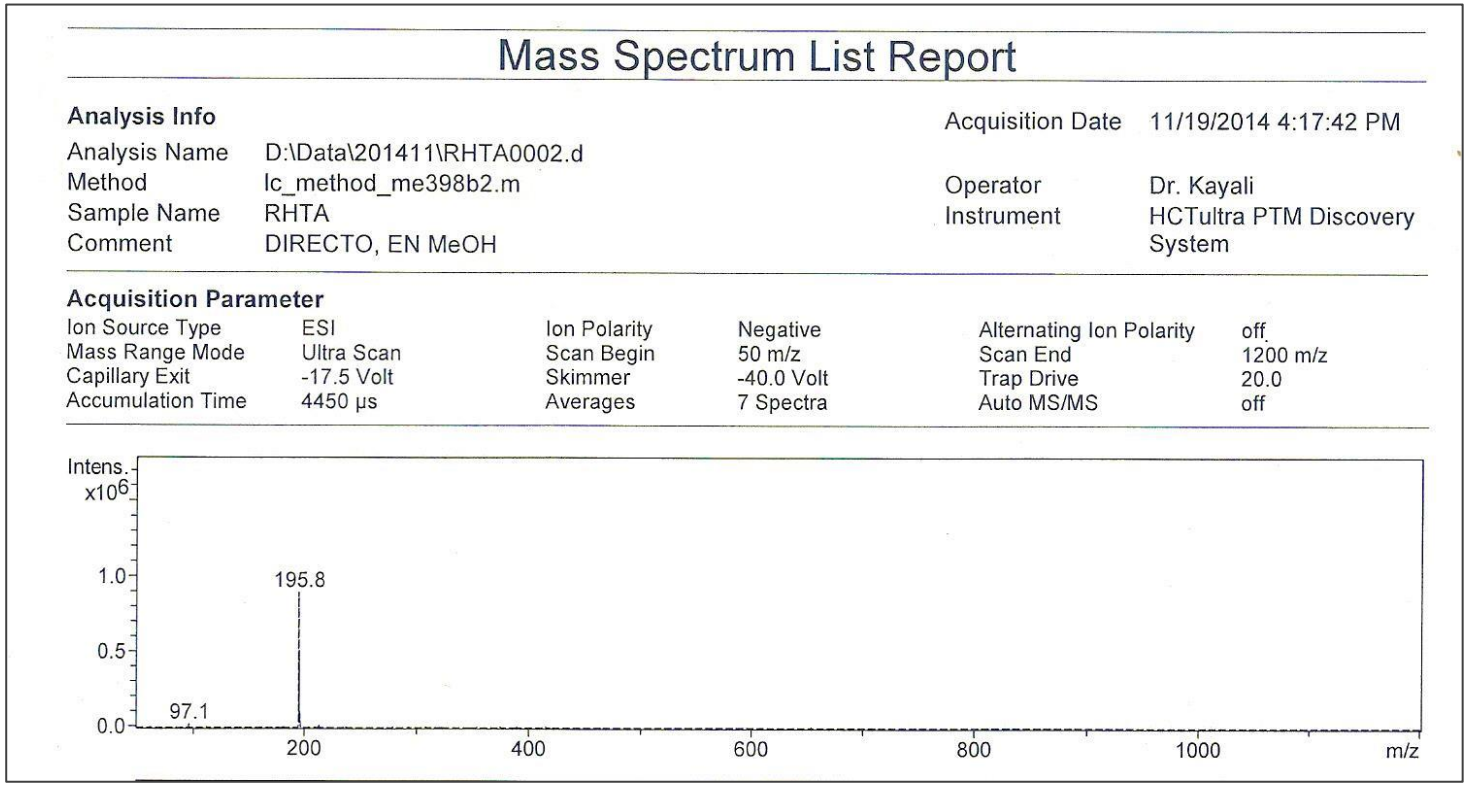

Mass Spectrum List Report

Analysis Info

Analysis Name	D:\Data\201411\RHTA0002.d	Acquisition Date	11/19/2014 4:17:42 PM
Method	lc_method_me398b2.m	Operator	Dr. Kayali
Sample Name	RHTA	Instrument	HCTultra PTM Discovery System
Comment	DIRECTO, EN MeOH		

Acquisition Parameter

Ion Source Type	ESI	Ion Polarity	Negative	Alternating Ion Polarity	off
Mass Range Mode	Ultra Scan	Scan Begin	50 m/z	Scan End	1200 m/z
Capillary Exit	-17.5 Volt	Skimmer	-40.0 Volt	Trap Drive	20.0
Accumulation Time	4450 µs	Averages	7 Spectra	Auto MS/MS	off

Figure A32: MS-ESI (negative ion detection) of **Sodium salt of Tenuazonic Acid.** Preparation procedure described in section V.4.1.

INFORME DE ENSAYO

Código: PGC11-FR01.11
Fecha de edición: 15/01/14
Los ensayos marcados no están amparados por la acreditación de ENAC
ENAC ENSAYOS Nº 371/LE769

C.A.I MICROANÁLISIS ELEMENTAL
Universidad Complutense.
Ciudad Universitaria s/n. 28040 Madrid
Telf. (91) 394 1753/5211. Fax (91) 394 18 22.
E-mail: microanalisis.elemental@farm.ucm.es

Nº Registro: 57

TIPO DE ENSAYO: CHN ☒, CHNS ☐

Informe de ensayo nº **Q11-14-046**

Usuario GUILLERMO ORELLANA MORALEDA Código Cliente GOM
Centro FACULTAD DE CC. QUÍMICAS. UNIVERSIDAD COMPLUTENSE
Departamento DPTO. Q. ORGÁNICA I
Dirección CIUDAD UNIVERSITARIA S/N. 28040 MADRID Tel 91.394.42.20. Lab
Fecha/Hora Entrada 13/11/14 11:00 Fecha/Hora Análisis 19/11/14 01:12
Descripción de la muestra Viscoso marrón
Observaciones
Método utilizado PNT01 Equipo LECO CHNS-932. Código 3288
Ubicación equipo Sótano sur. Edif. QA. Facultad de CC. Químicas

RESULTADO DEL ANÁLISIS:

Código CAI	C. Muestra	%C ± I	%H ± I	%N ± I
Q11-14-046	RA-TAJ	**60,93 ± 0,26**	**7,86 (>LS)**	**6,64 ± 0,25**

Figure A33: Elemental analysis assay (CHN) spectrum of **Sodium salt of Tenuazonic Acid.** Preparation procedure described in section V.4.1.

V.4.2 Tenuazonic Acid surrogate *s*TeA

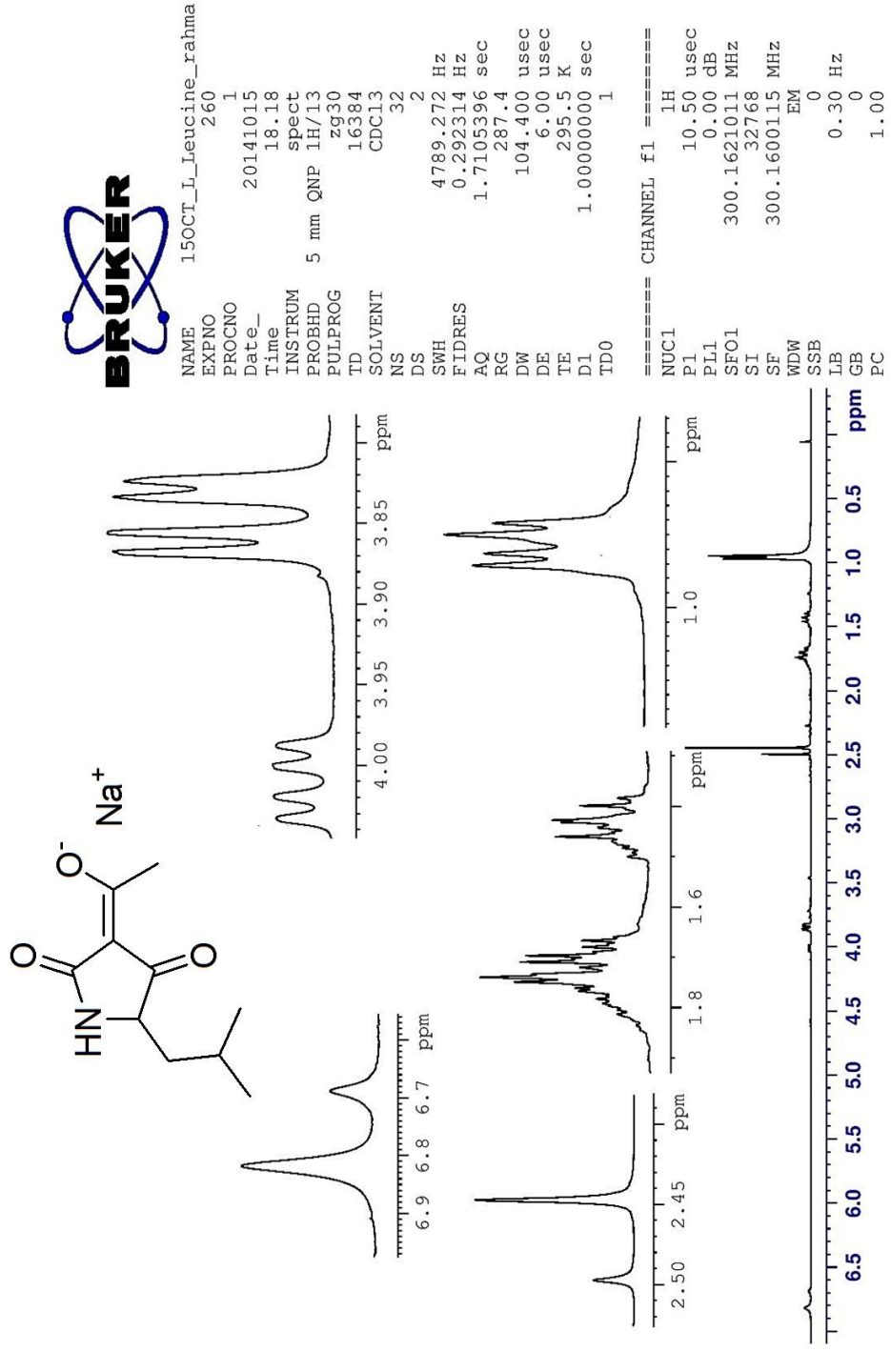

Figure A34: ^{1}H-NMR (CDCl3-d_1) spectrum of **Tenuazonic Acid surrogate.** Preparation procedure described in section V.4.2.

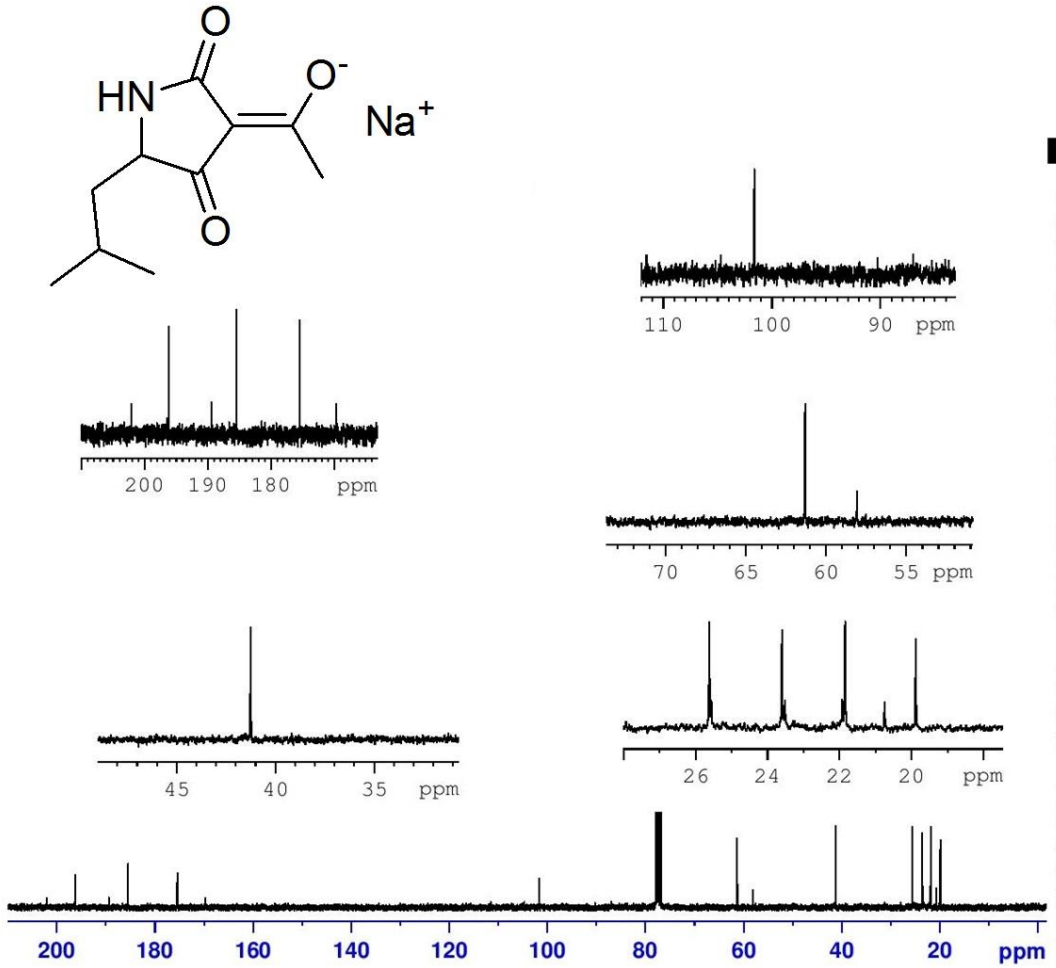

BRUKER

```
NAME          15OCT_L_Leucine_rahma
EXPNO                           261
PROCNO                            1
Date_                      20141015
Time                          19.11
INSTRUM                       spect
PROBHD    5 mm QNP 1H/13
PULPROG                     zgpg30
TD                           65536
SOLVENT                      CDCl3
NS                             800
DS                               4
SWH                    17985.611 Hz
FIDRES                  0.274439 Hz
AQ                     1.8219508 sec
RG                        2580.3
DW                       27.800 usec
DE                        6.00 usec
TE                        295.9 K
D1                    2.00000000 sec
d11                   0.03000000 sec
DELTA                 1.89999998 sec
TD0                               1

======== CHANNEL f1 ========
NUC1                          13C
P1                       10.00 usec
PL1                       -2.00 dB
SFO1                 75.4828396 MHz

======== CHANNEL f2 ========
CPDPRG2                   waltz16
NUC2                          1H
PCPD2                    80.00 usec
PL2                       0.00 dB
PL12                     17.00 dB
PL13                     17.00 dB
SFO2                300.1612006 MHz
SI                           32768
SF                   75.4752693 MHz
WDW                             EM
SSB                              0
LB                        1.00 Hz
GB                               0
PC                            1.40
```

Figure A35: ^{13}C-NMR (CDCl3-d_1) spectrum of **Tenuazonic Acid surrogate.** Preparation procedure described in section V.4.2.

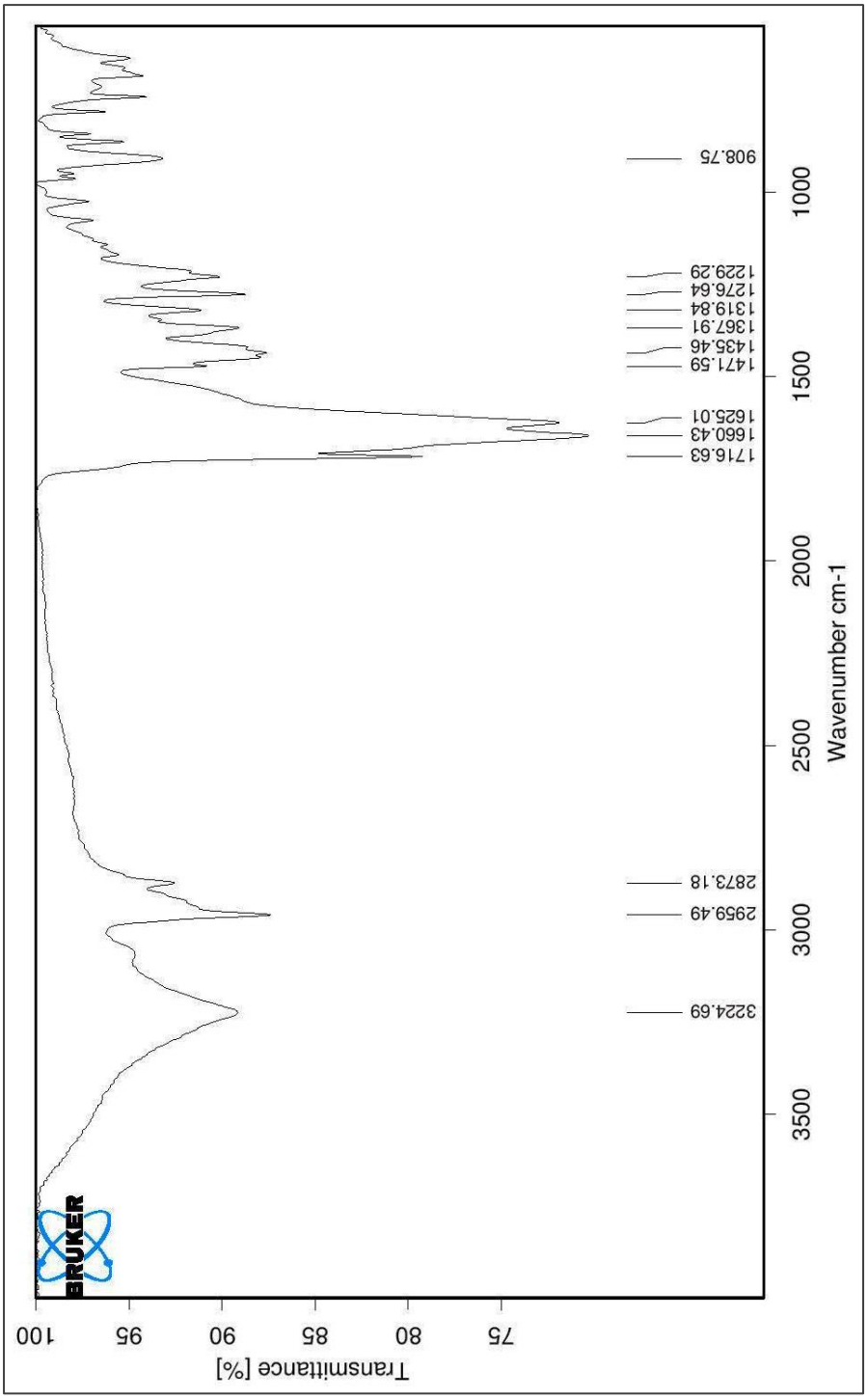

Figure A36: FT-IR (KBr disc) spectrum of **Tenuazonic Acid surrogate.** Preparation procedure described in section V.4.2.

Mass Spectrum List Report

Analysis Info

Analysis Name	D:\Data\201410\RAIVTAL0.d	Acquisition Date	10/23/2014 11:39:56 AM
Method	lc_method_me398b2.m	Operator	Dr. Kayali
Sample Name	RAIVTAL	Instrument	HCTultra PTM Discovery System
Comment	DIRECTO, EN MeOH		

Acquisition Parameter

Ion Source Type	ESI	Ion Polarity	Negative	Alternating Ion Polarity	off
Mass Range Mode	Ultra Scan	Scan Begin	50 m/z	Scan End	600 m/z
Capillary Exit	-29.8 Volt	Skimmer	-40.0 Volt	Trap Drive	22.0
Accumulation Time	1058 µs	Averages	14 Spectra	Auto MS/MS	off

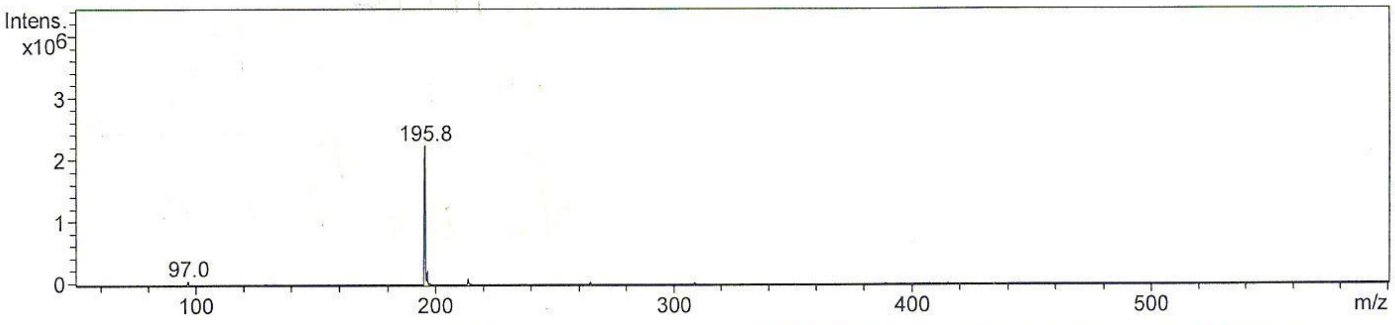

Figure A37: MS-ESI (negative ion detection) of **Tenuazonic Acid surrogate.** Preparation procedure described in section V.4.2.

UCM
CENTRO DE MICROANALISIS ELEMENTAL
Dpto. Q. Orgánica y Farmacéutica. F. Farmacia
Sotano sur. Edif. QA. F. CC. Químicas
UNIVERSIDAD COMPLUTENSE DE MADRID

INFORME DE ENSAYO SIMPLIFICADO

Código: PGC11-FR02.01

Fecha de edición: 21/05/12

TIPO DE ENSAYO: *CHN* ☑ *CHNS* ☐

CENTRO DE MICROANÁLISIS ELEMENTAL

UNIVERSIDAD COMPLUTENSE DE MADRID

Tlf.: 91 394 17 53 / 52 11. Fax: 91 394 52 11. Correo electrónico: microanalisis. elemental@farm.ucm.es

Código Cliente: GOM

Fecha de resultados: 24/01/2013

Equipo: *LECO CHNS 932.* ***Código:*** 3288

Contraseña Muestra CAI	*Contraseña Muestra*	*%C*	*%H*	*%N*	*Descripción de la muestra*	*Observaciones*	*Desviaciones del método*
Q12-12-203		60,85	7,75	6,62	Viscoso naranja		% H > LS

Figure A38: Elemental analysis assay (CHN) spectrum of **Tenuazonic Acid surrogate.** Preparation procedure described in section V.4.2.

Tenuazonic acid molecularly imprinted europium polymer (MPE1) before washing the template

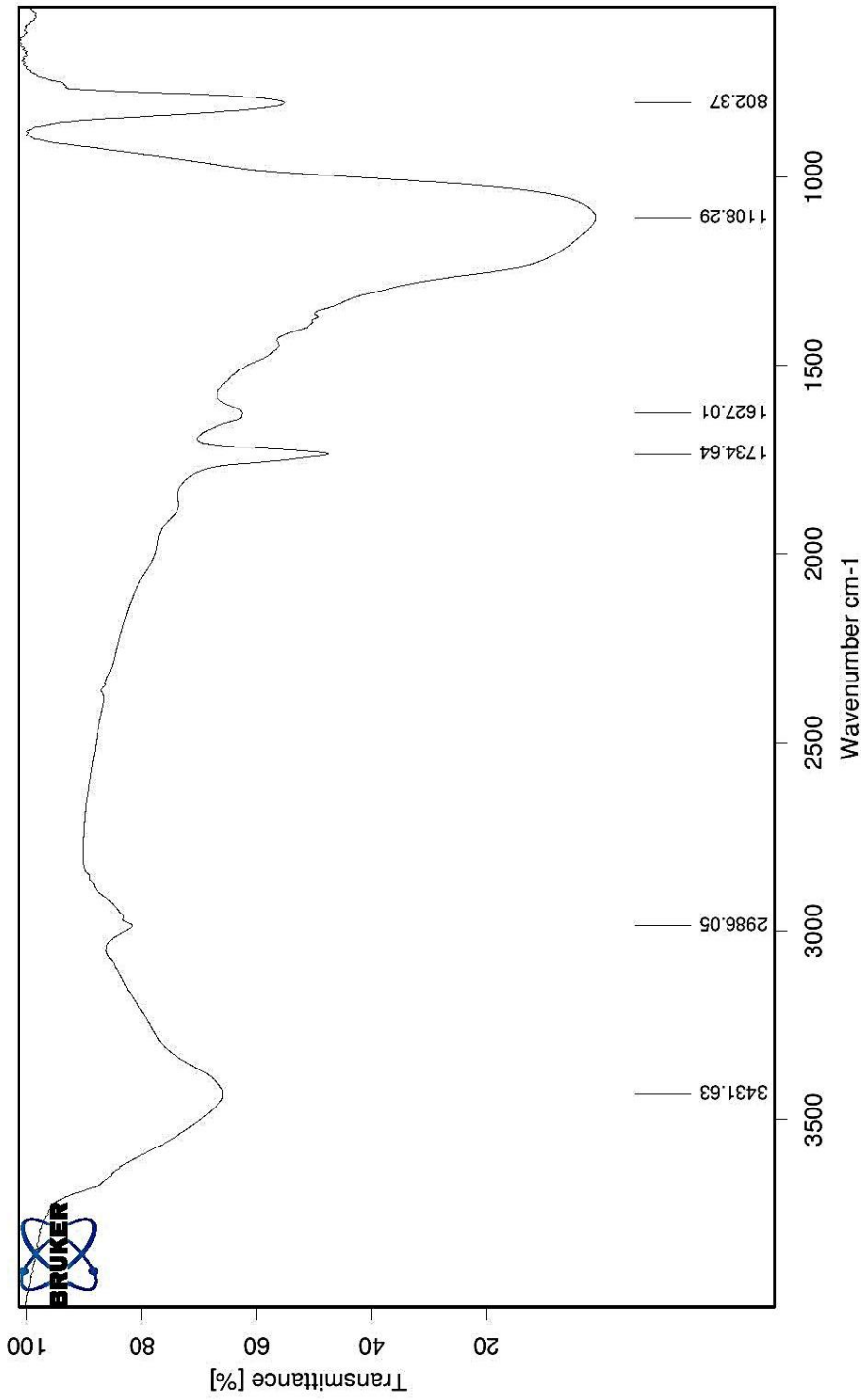

Figure A39: FT-IR (KBr disc) spectrum of **Tenuazonic acid molecularly imprinted europium polymer (MPE1) before washing the template**

Tenuazonic acid molecularly imprinted europium polymer (MPE1) after washing the template

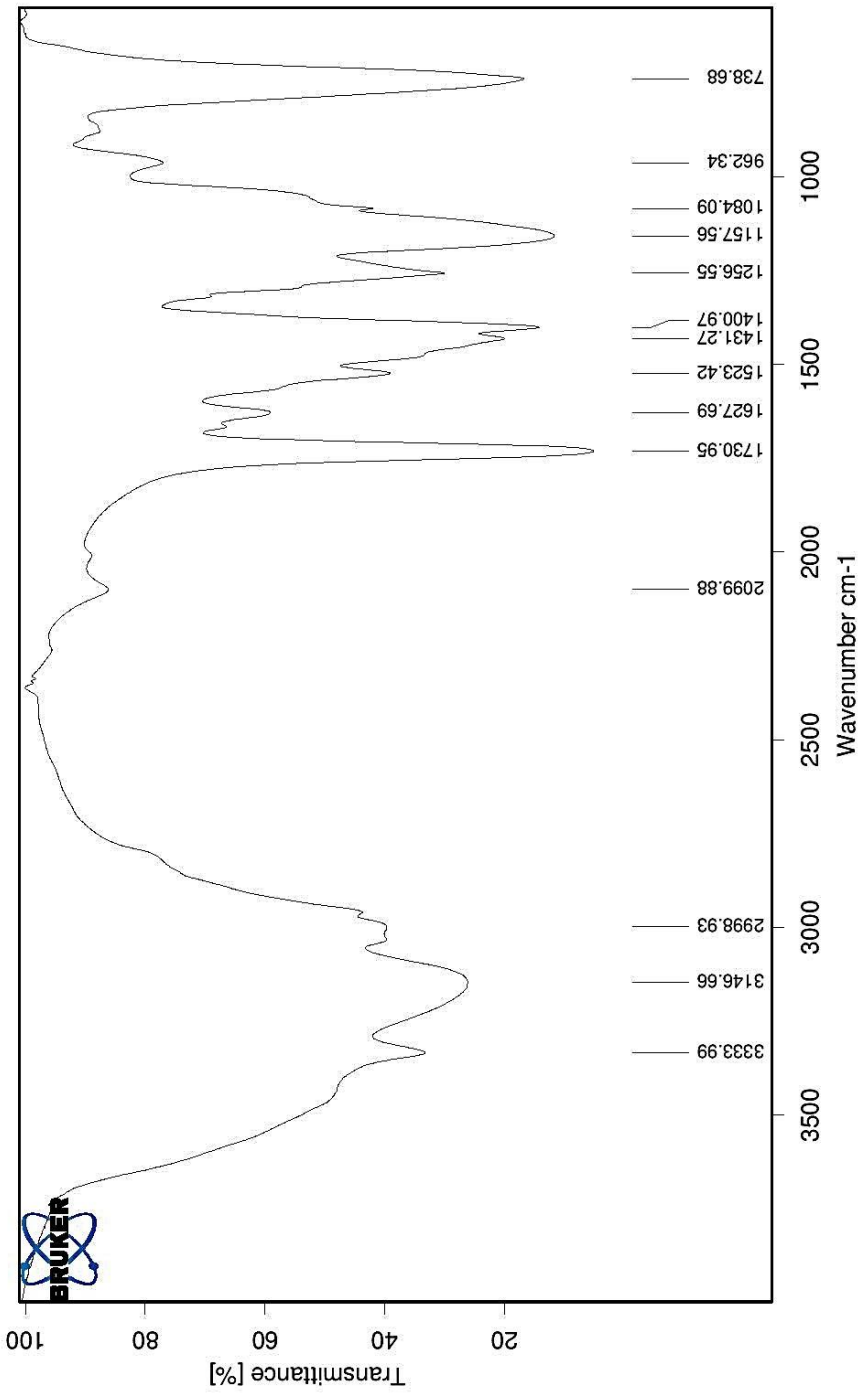

Figure A40: FT-IR (KBr disc) spectrum of **Tenuazonic acid molecularly imprinted europium polymer (MPE1) after washing the template**

Tenuazonic acid molecularly imprinted europium polymer (MPE2) before washing the template

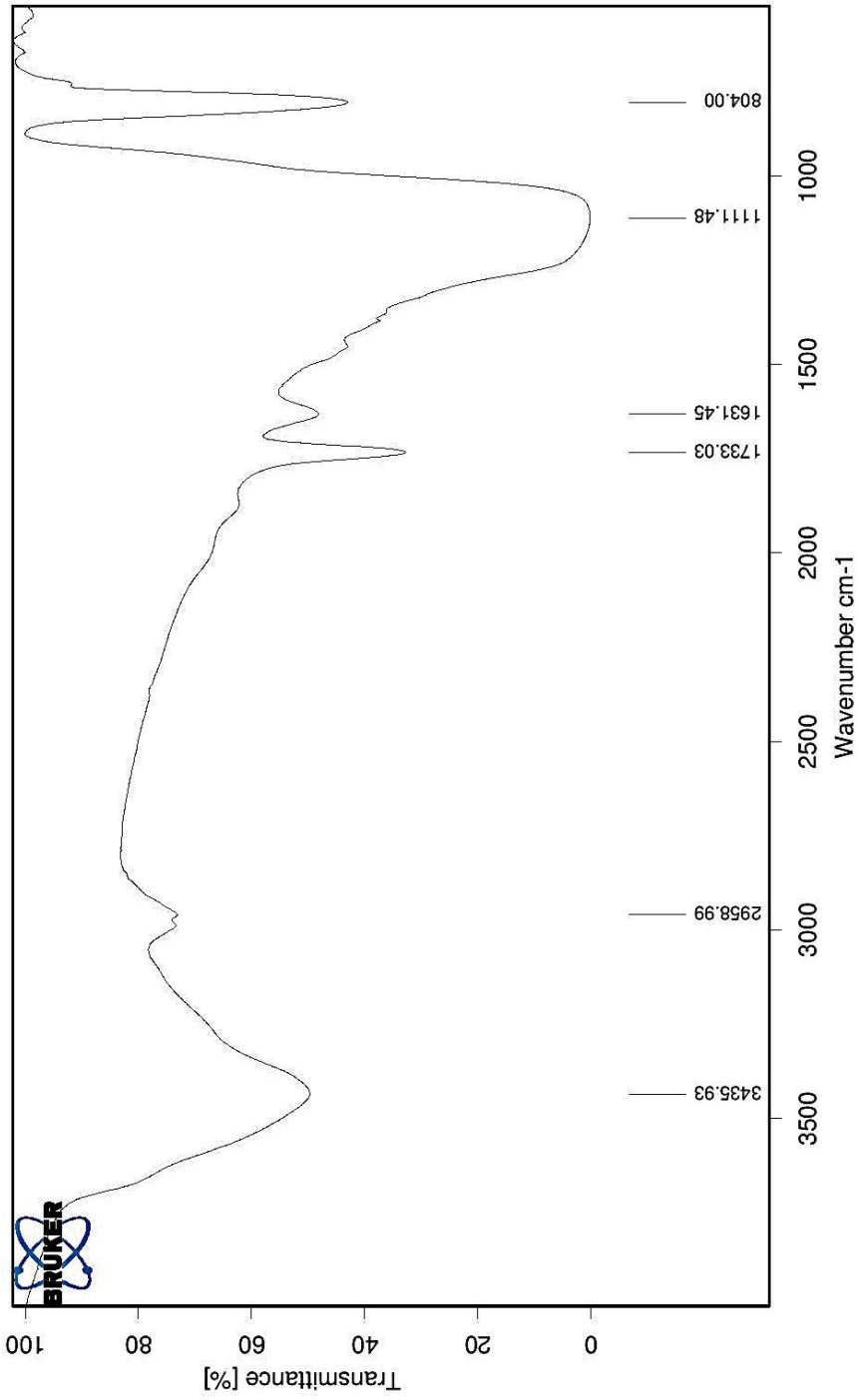

Figure A41: FT-IR (KBr disc) spectrum of **Tenuazonic acid molecularly imprinted europium polymer (MPE2) before washing the template**

Tenuazonic acid molecularly imprinted europium polymer (MPE2) after washing the template

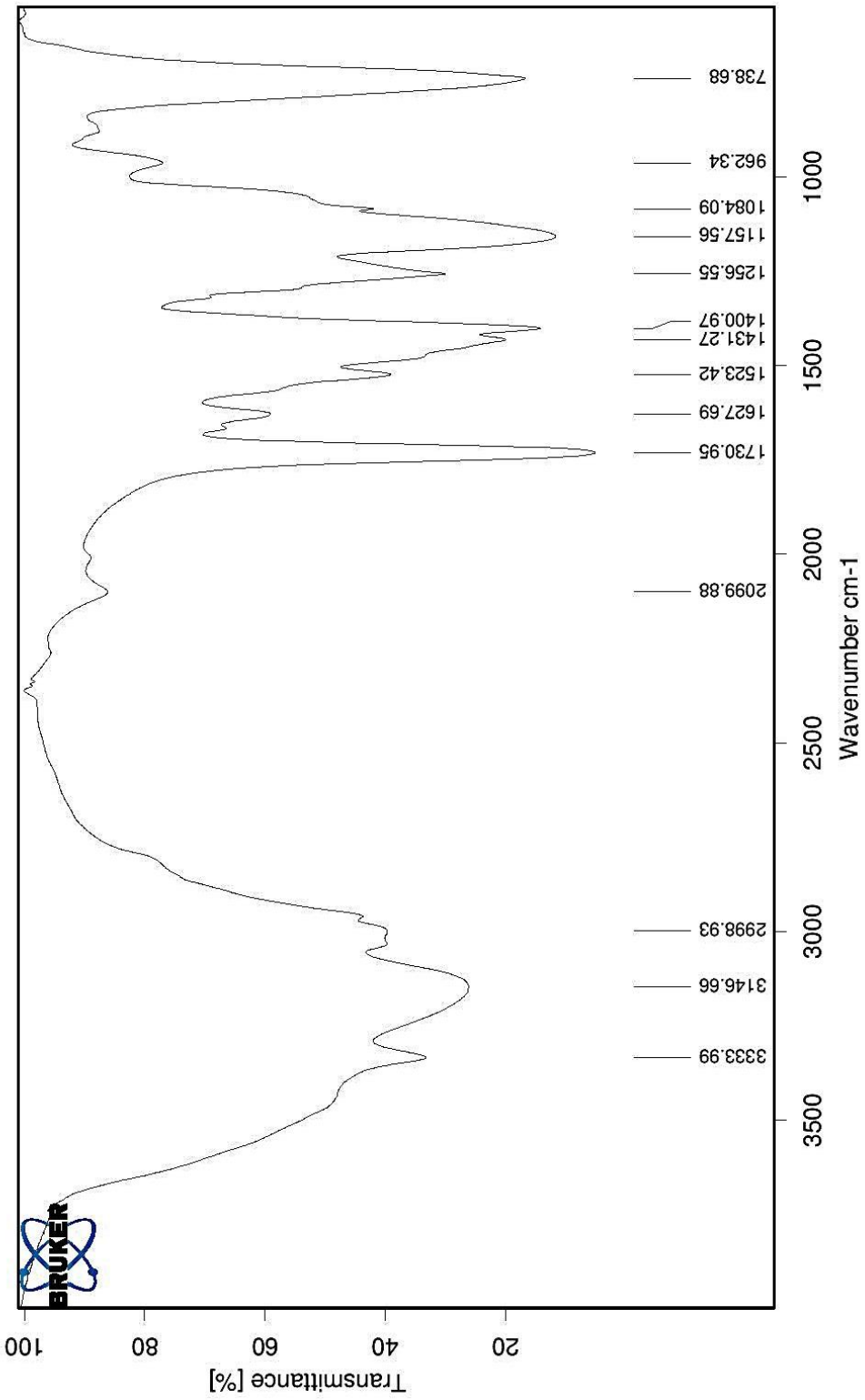

Figure A42: FT-IR (KBr disc) spectrum of **Tenuazonic acid molecularly imprinted europium polymer (MPE2) after washing the template.**

Tenuazonic acid non-imprinted europium polymer (NPE1) after washing

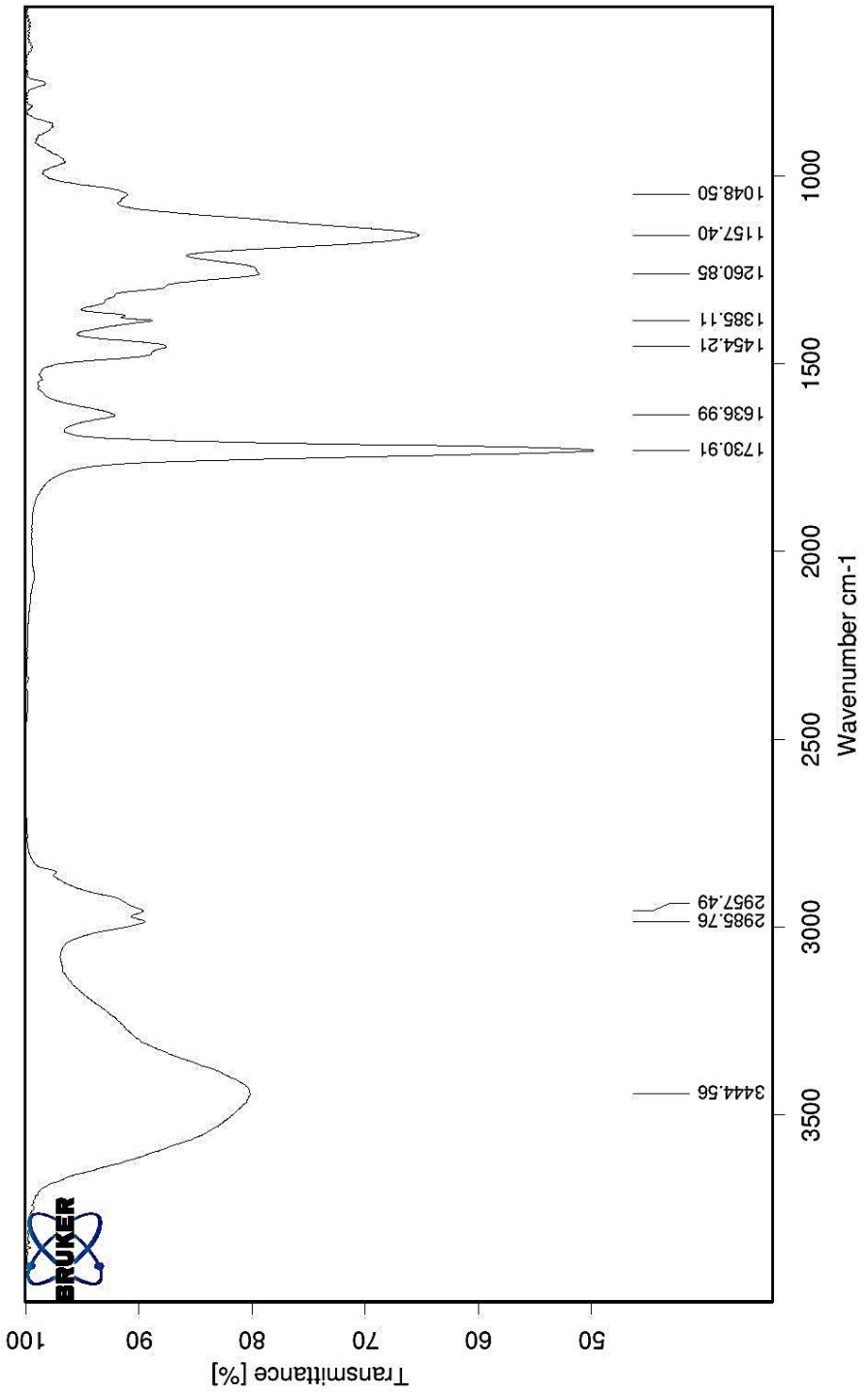

Figure A43: FT-IR (KBr disc) spectrum of **Tenuazonic acid non-imprinted europium polymer (NPE1) after washing**

Tenuazonic acid non-imprinted europium polymer (NPE2) after washing

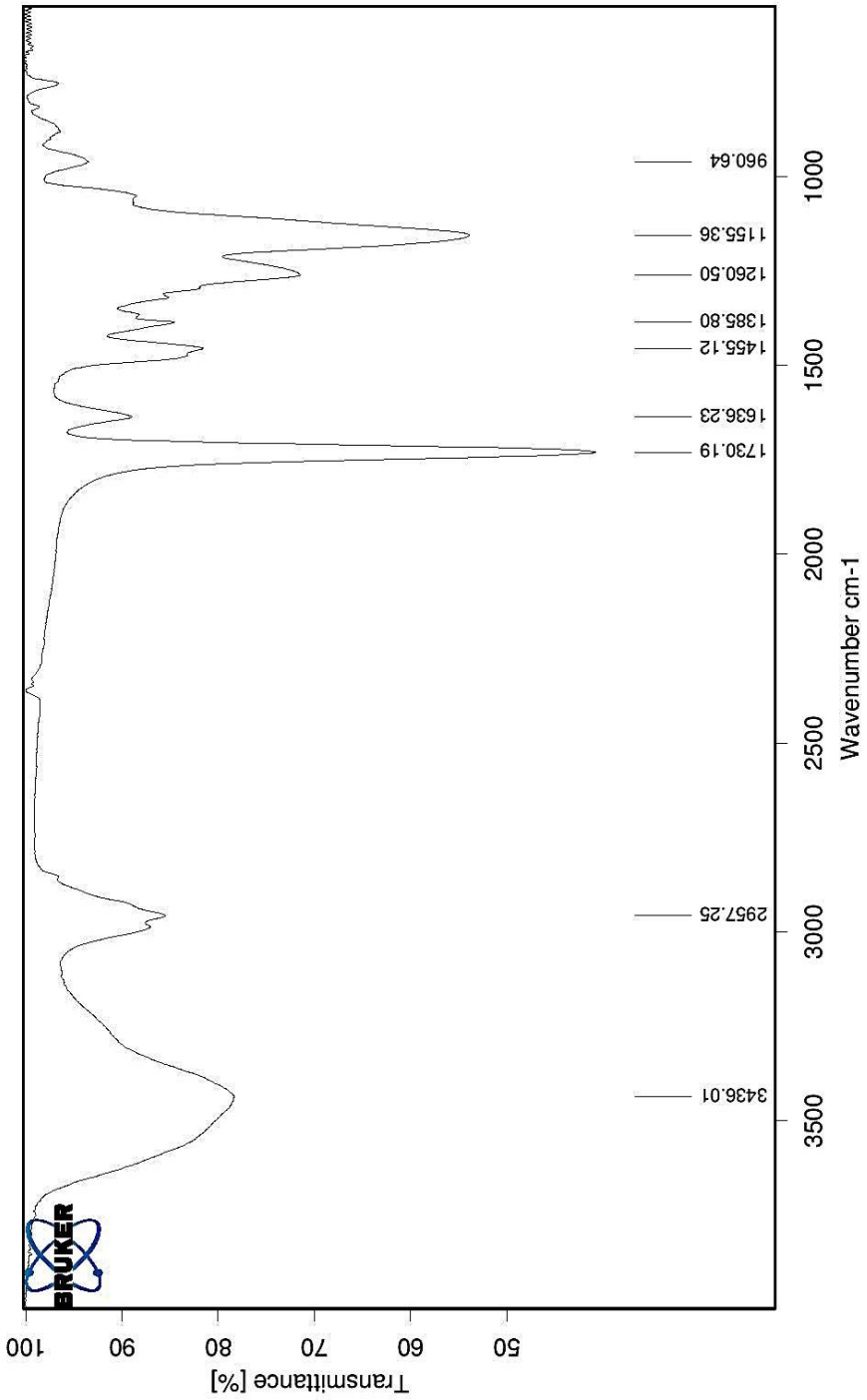

Figure A44: FT-IR (KBr disc) spectrum of ***Tenuazonic acid non-imprinted europium polymer (NPE2) after washing***

V.5.1 *N*-pyren-1-ylacrylamide (PA)

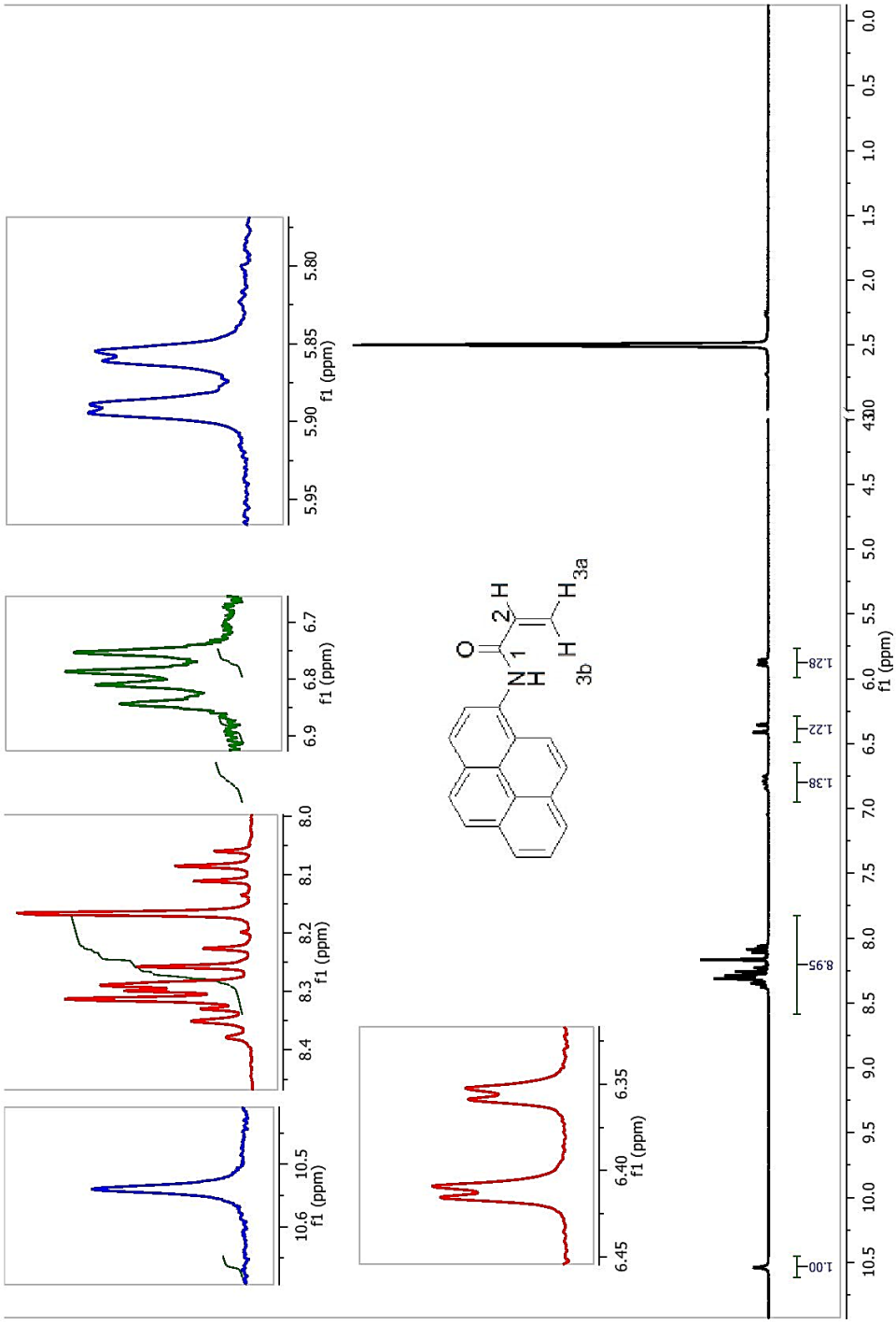

Figure A45: ^{1}H-NMR (DMSO-d_6) spectrum of **Pyreneacrylamide (PA).** Preparation procedure described in section V.5.1.

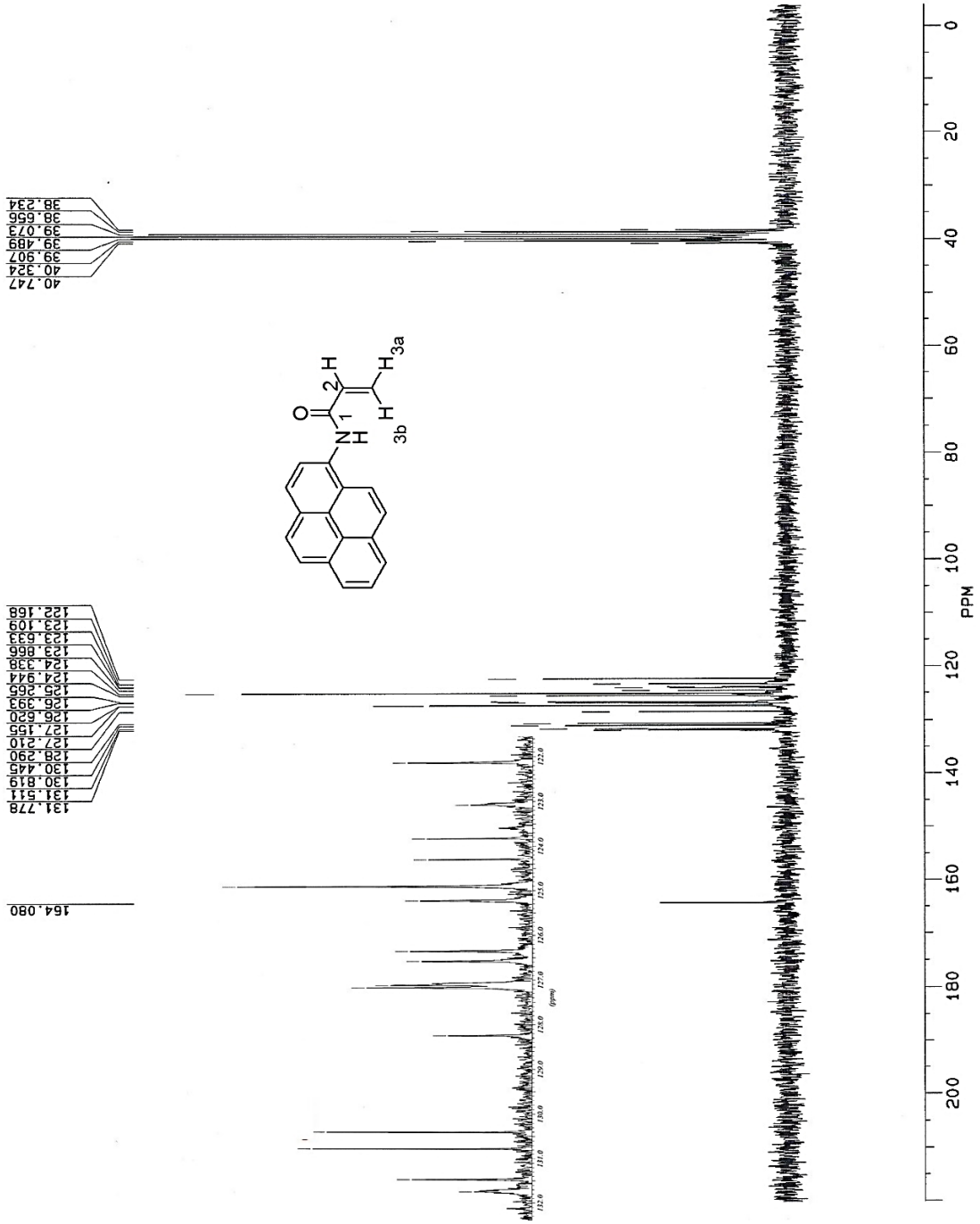

Figure A46: ^{13}C-NMR (DMSO-d_6) spectrum of ***N*-pyren-1-ylacrylamide (PA).** Preparation procedure described in section V.5.1.

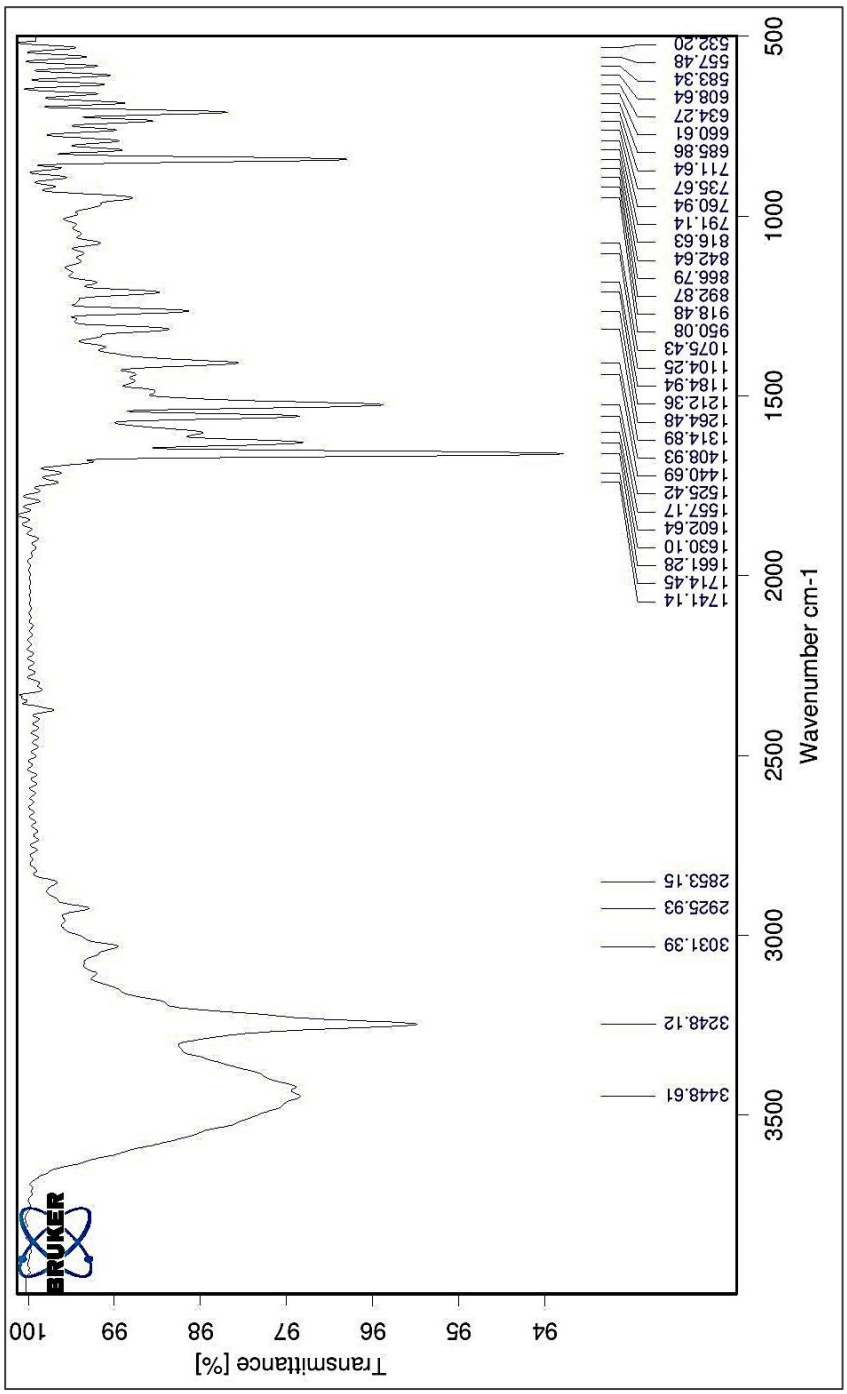

Figure A47: FT-IR (ATR) spectrum of **Pyreneacrylamide (PA).** Preparation procedure described in section V.5.1.

Mass Spectrum List Report

Analysis Info

Analysis Name	D:\Data\201501\PYRENE30.d	Acquisition Date	1/8/2015 12:03:34 PM
Method	lc_method_me398b2.m	Operator	Dr. Kayali
Sample Name	PYRENE3	Instrument	HCTultra PTM Discovery System
Comment	DIRECTO, EN MeOH		

Acquisition Parameter

Ion Source Type	ESI	Ion Polarity	Positive	Alternating Ion Polarity	off
Mass Range Mode	Ultra Scan	Scan Begin	50 m/z	Scan End	2300 m/z
Capillary Exit	97.5 Volt	Skimmer	40.0 Volt	Trap Drive	42.7
Accumulation Time	1078 µs	Averages	14 Spectra	Auto MS/MS	off

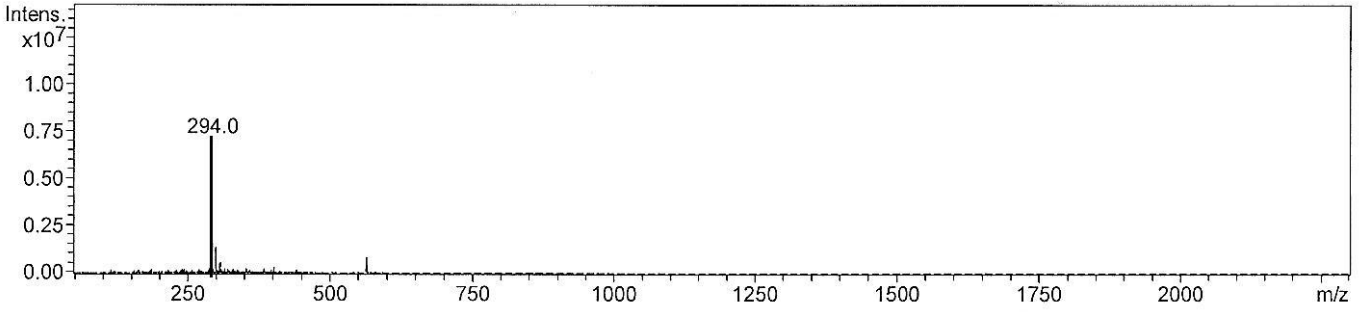

Figure A48: MS-ESI (negative ion detection) of **Pyreneacrylamide (PA).** Preparation procedure described in section V.5.1.

V.5.2 *N*-pyren-1-ylmethacrylamide (PMA)

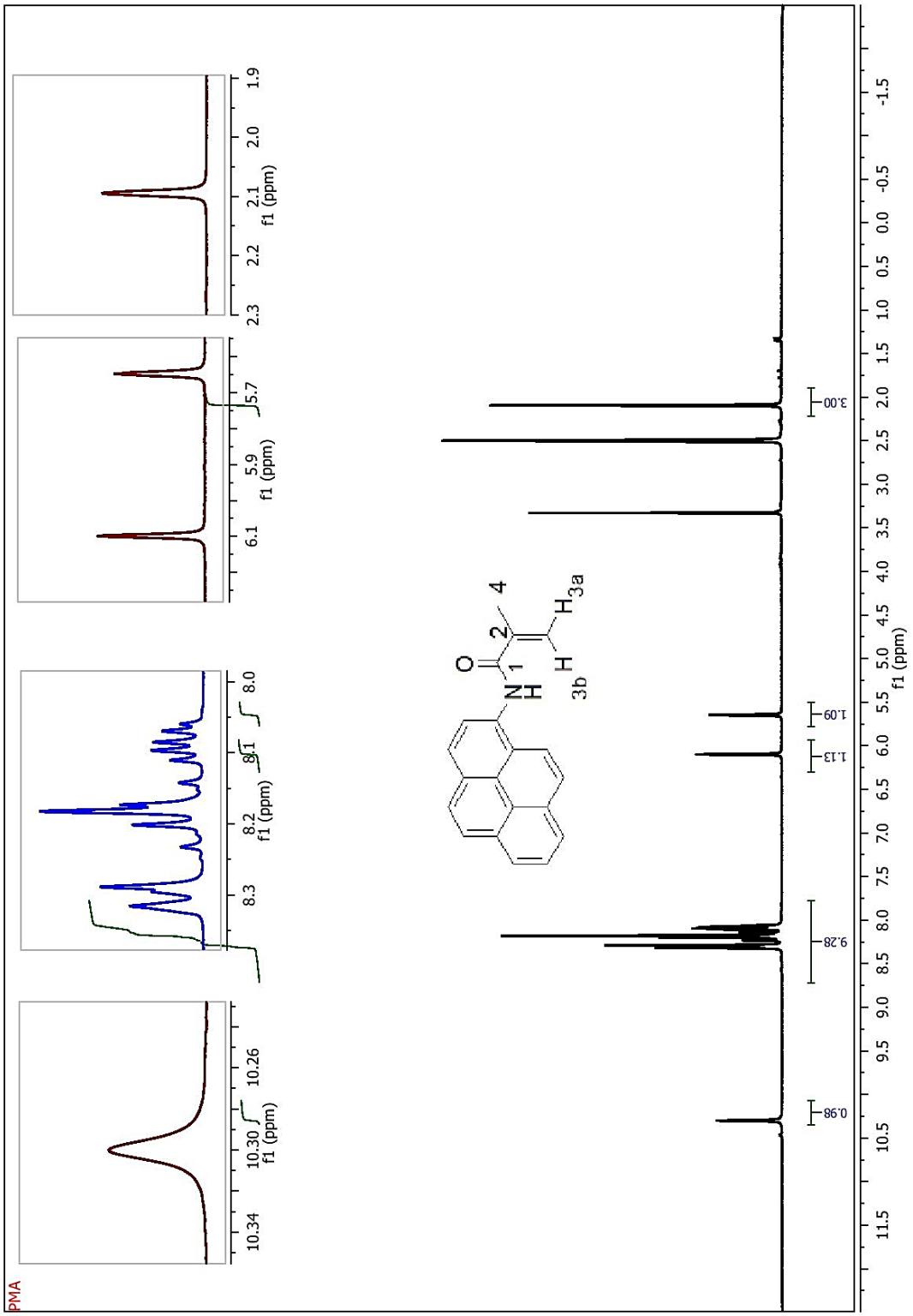

Figure A49: ^{1}H-NMR (DMSO-d_6) spectrum of ***N*-pyren-1-ylmethacrylamide (PMA).** Preparation procedure described in section V.5.2.

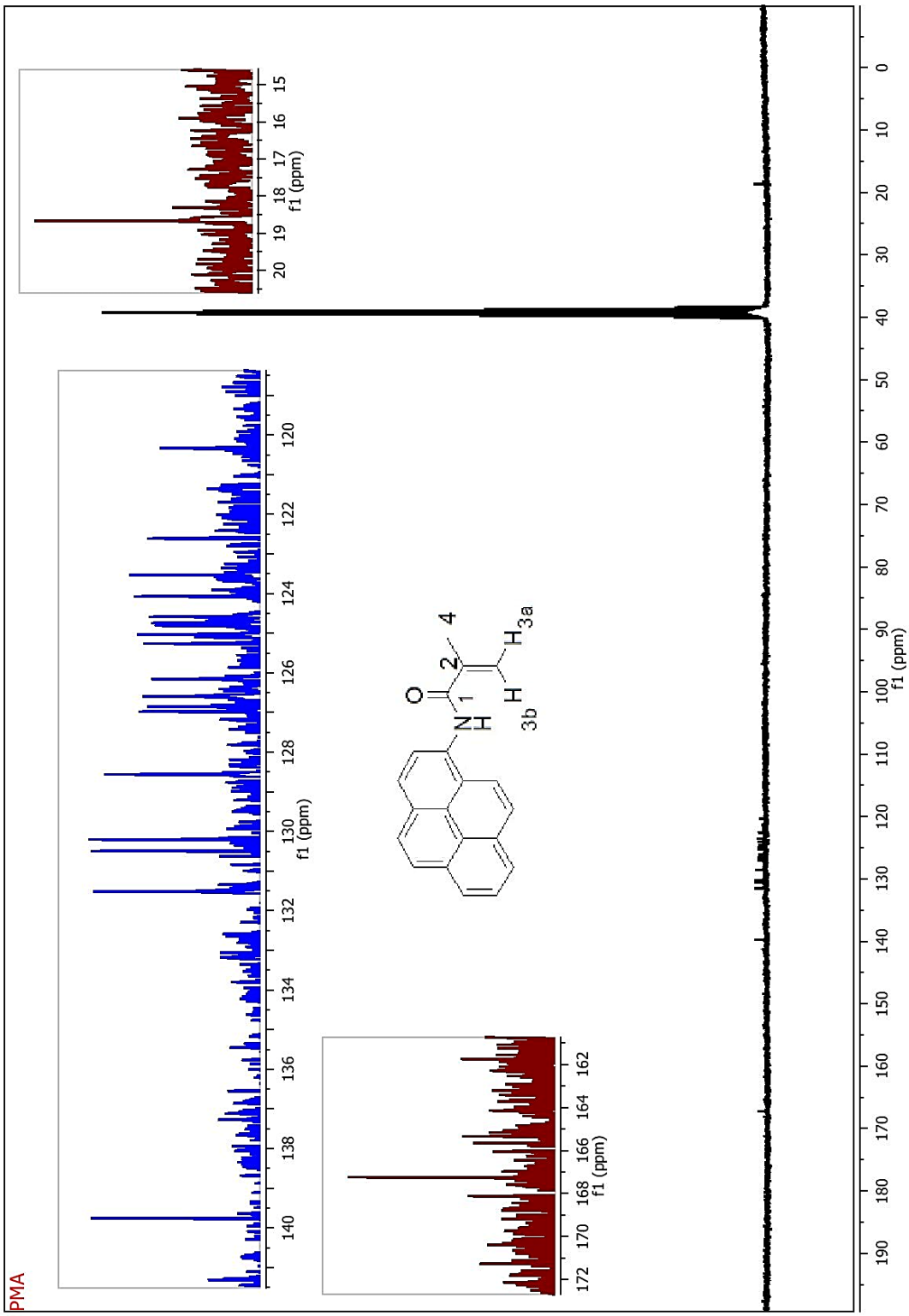

Figure A50: ^{13}C-NMR (DMSO-d_6) spectrum of ***N*-pyren-1-ylmethacrylamide (PMA).** Preparation procedure described in section V.5.2.

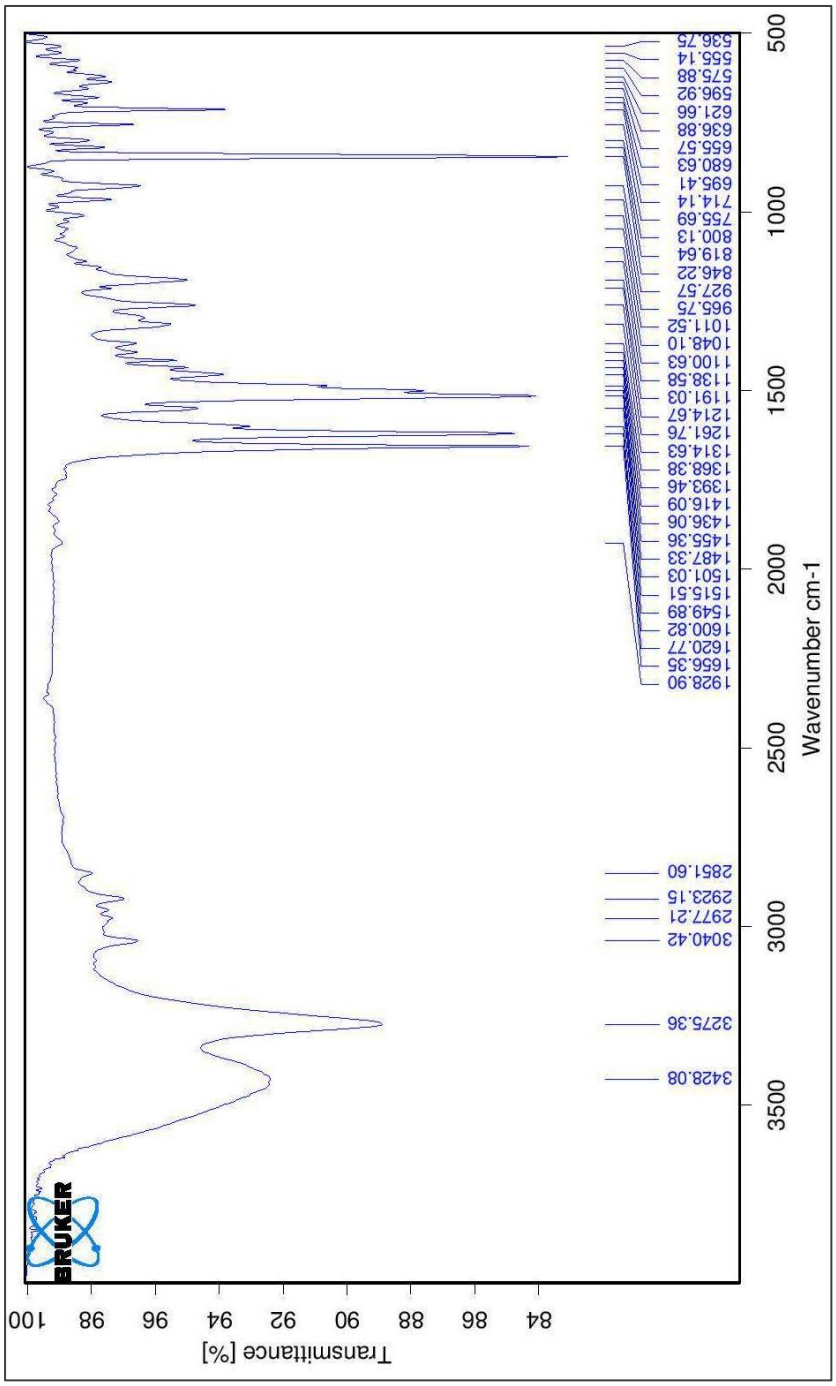

Figure A51: FT-IR (ATR) spectrum of ***N*-pyren-1-ylmethacrylamide (PMA).** Preparation procedure described in section V.5.2.

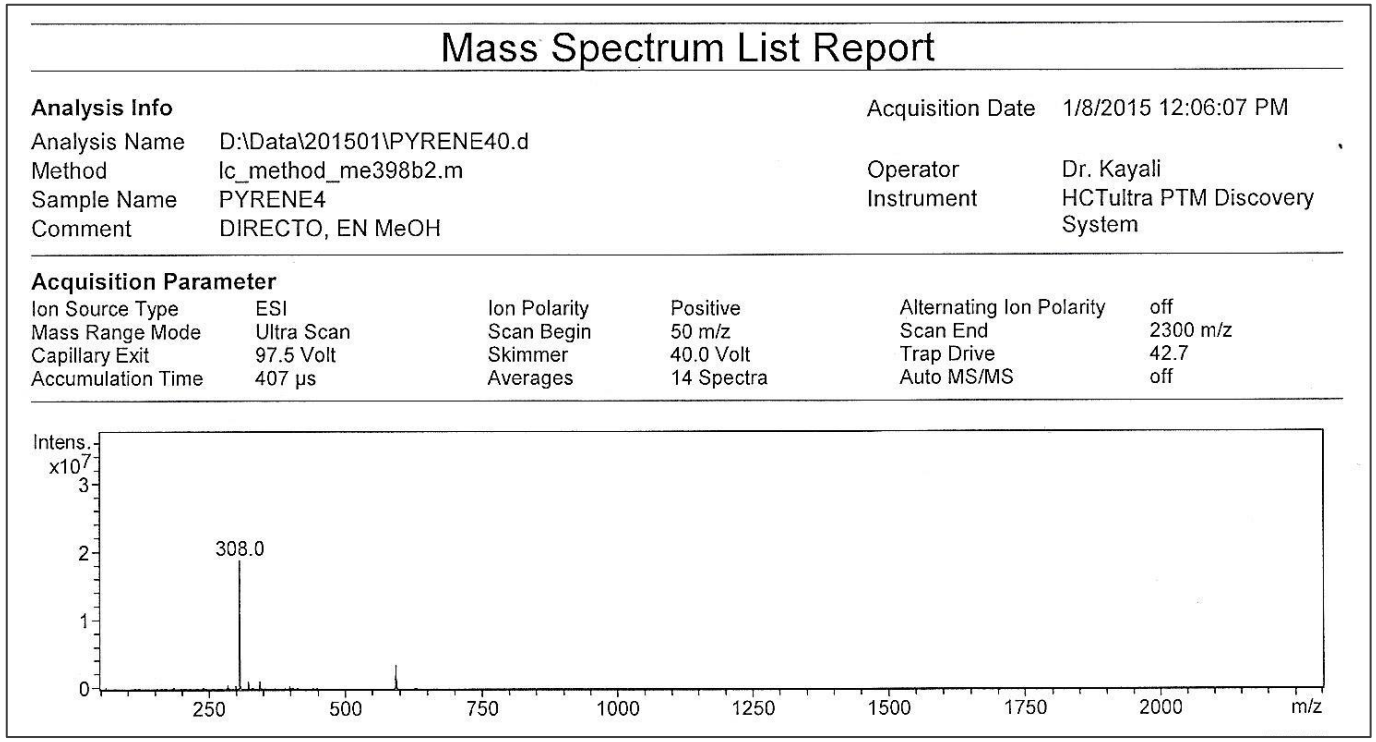

Mass Spectrum List Report

Analysis Info

Analysis Name	D:\Data\201501\PYRENE40.d	Acquisition Date	1/8/2015 12:06:07 PM
Method	lc_method_me398b2.m	Operator	Dr. Kayali
Sample Name	PYRENE4	Instrument	HCTultra PTM Discovery System
Comment	DIRECTO, EN MeOH		

Acquisition Parameter

Ion Source Type	ESI	Ion Polarity	Positive	Alternating Ion Polarity	off
Mass Range Mode	Ultra Scan	Scan Begin	50 m/z	Scan End	2300 m/z
Capillary Exit	97.5 Volt	Skimmer	40.0 Volt	Trap Drive	42.7
Accumulation Time	407 µs	Averages	14 Spectra	Auto MS/MS	off

Figure A52: MS-ESI (negative ion detection) of ***N*-pyren-1-ylmethacrylamide (PMA).** Preparation procedure described in section V.5.2.

V.5.3 *N*-(pyren-1-ylmethyl)acrylamide (PMeA)

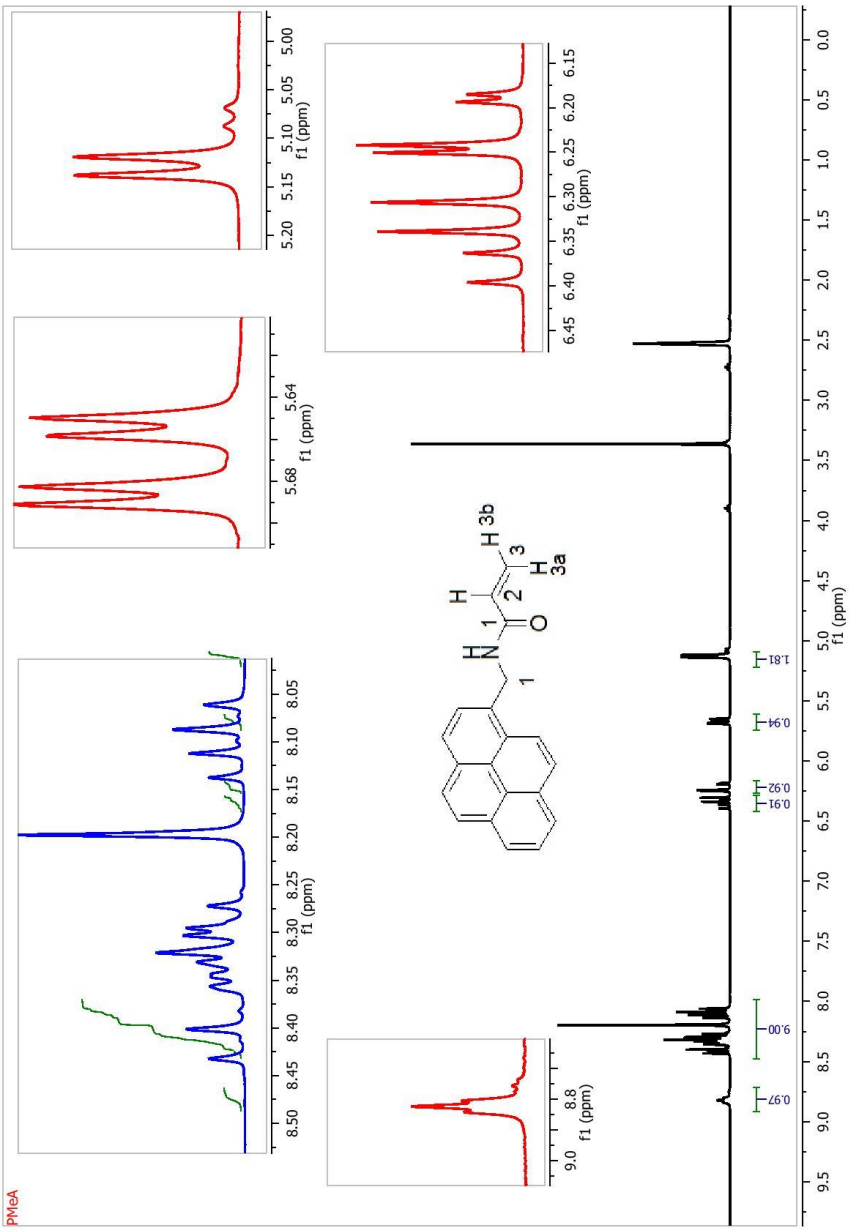

Figure A53: ^{1}H-NMR (DMSO-d_6) spectrum of ***N*-(pyren-1-ylmethyl)acrylamide (PMeA).**

Preparation procedure described in section V.5.3.

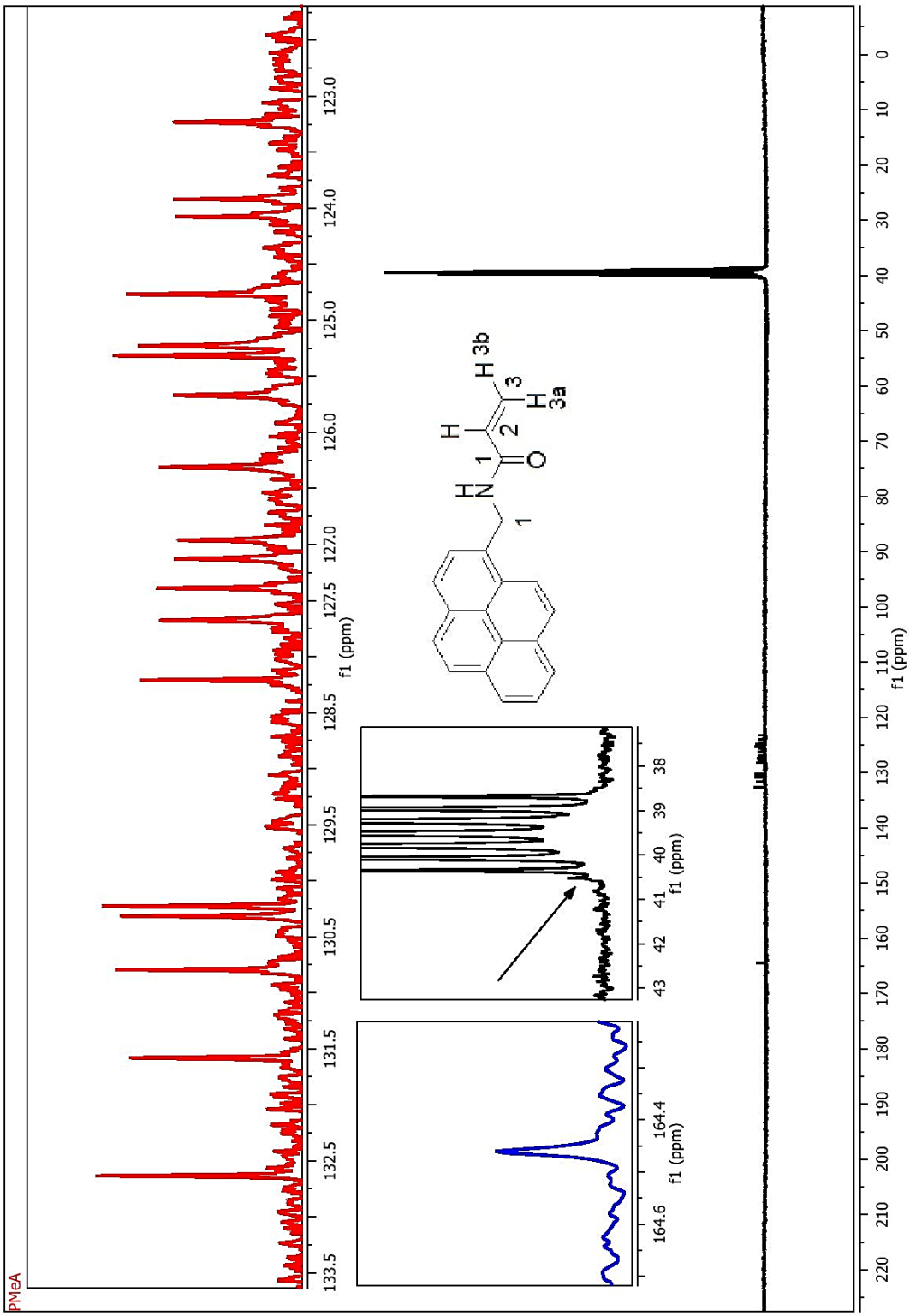

Figure A54: ^{13}C-NMR (DMSO-d_6) spectrum of ***N*-(pyren-1-ylmethyl)acrylamide (PMeA).** Preparation procedure described in section V.5.3.

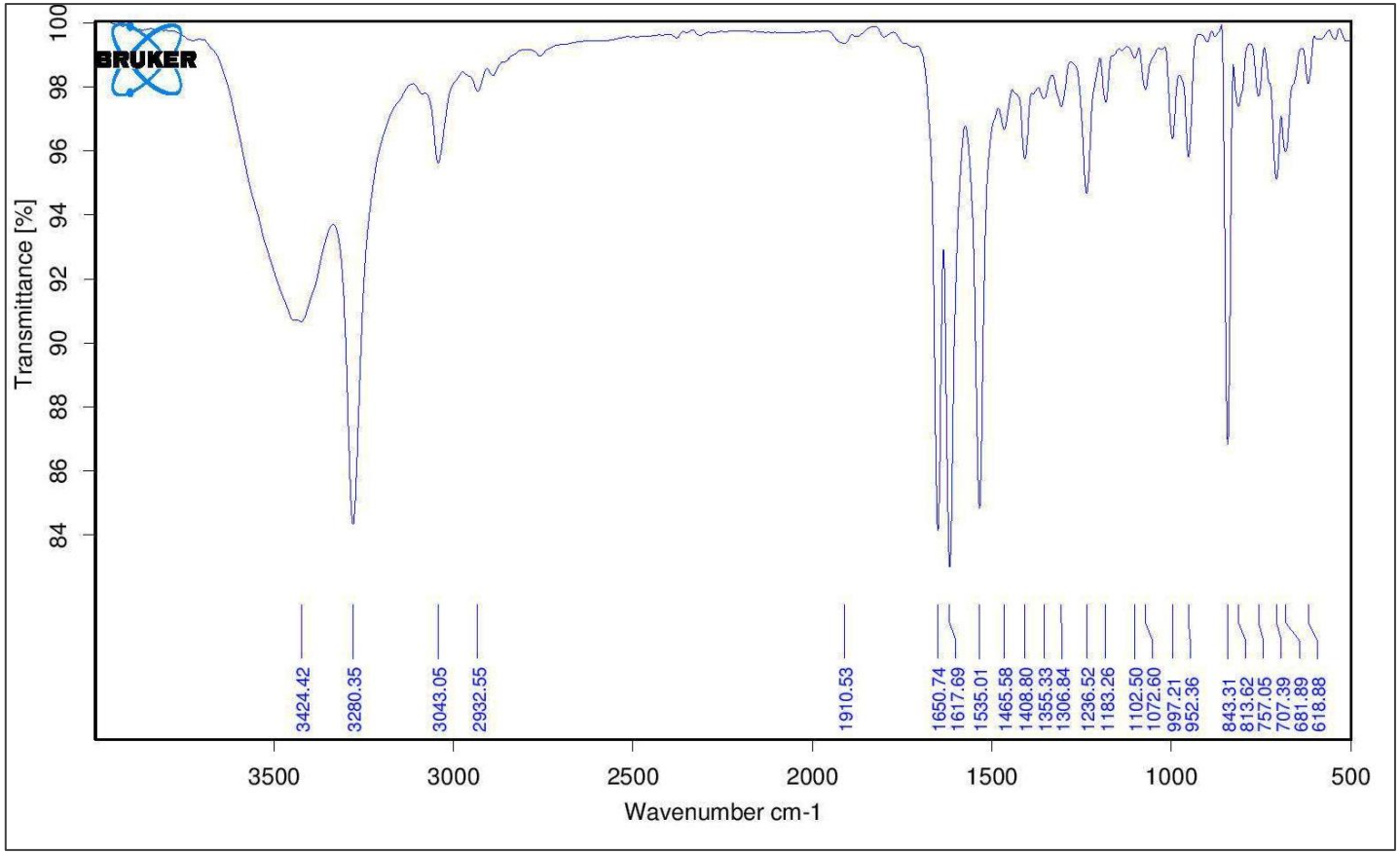

Figure A55: FT-IR (ATR) spectrum of ***N*-(pyren-1-ylmethyl)acrylamide (PMeA).** Preparation procedure described in section V.5.3.

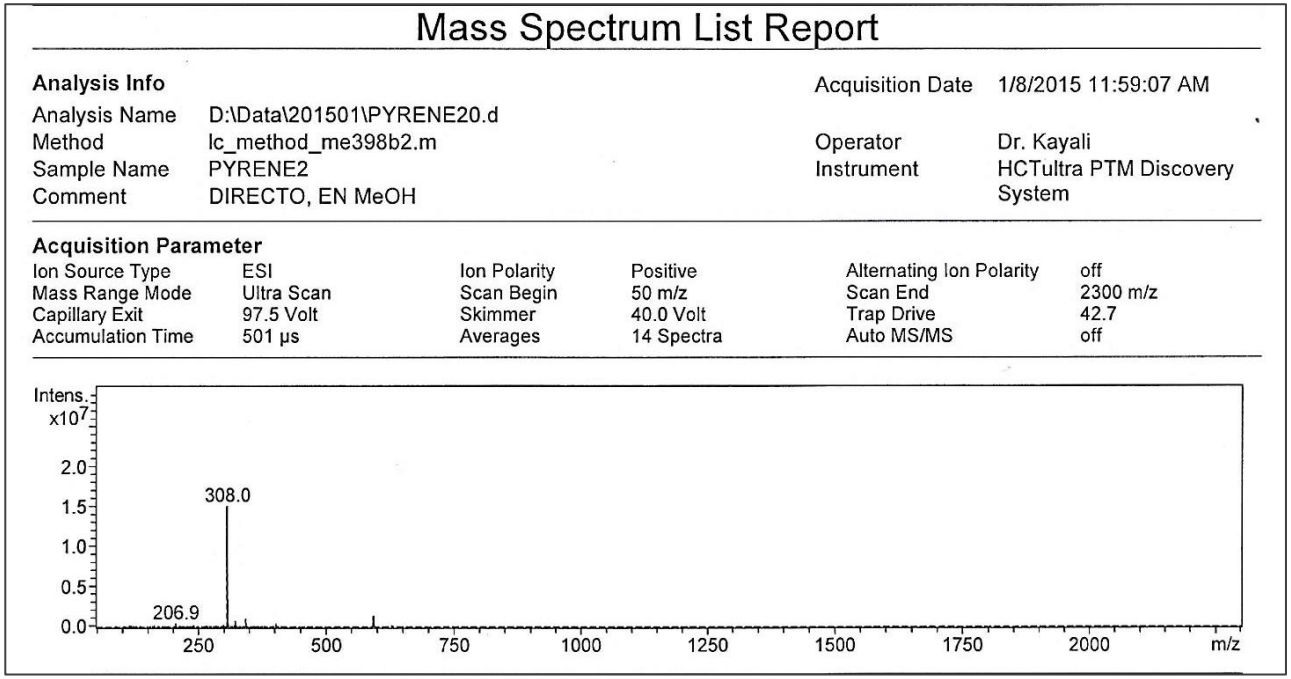

Figure A56: MS-ESI (negative ion detection) of ***N*-(pyren-1-ylmethyl)acrylamide (PMeA).** Preparation procedure described in section V.5.3.

V.5.4 *N*-(pyren-1-ylmethyl)methacrylamide (PMeMA)

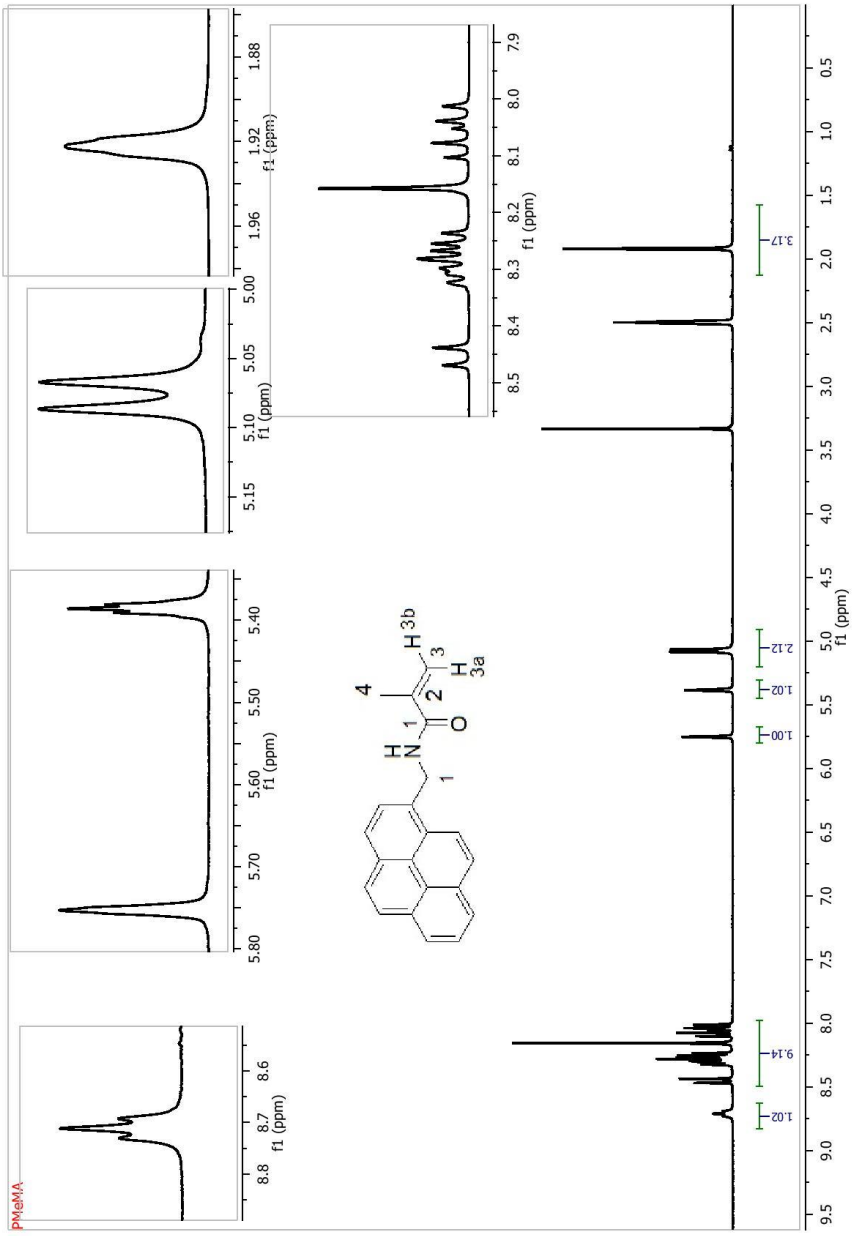

Figure A57: ^{1}H-NMR (DMSO-d_6) spectrum of ***N*-(pyren-1-ylmethyl)methacrylamide (PMeMA).**

Preparation procedure described in section V.5.4.

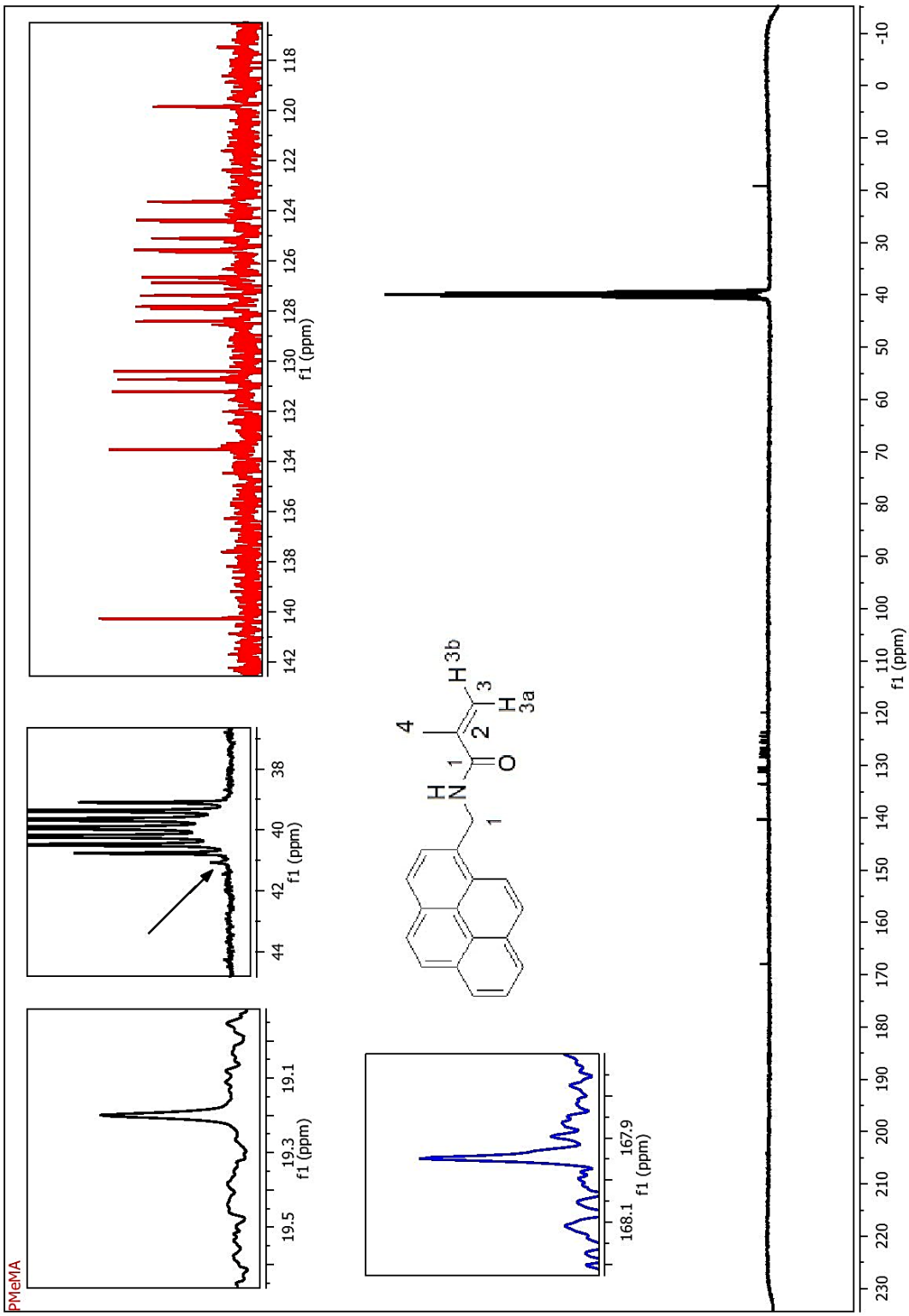

Figure A58: ^{13}C-NMR (DMSO-d_6) spectrum of ***N*-(pyren-1-ylmethyl)methacrylamide (PMeMA).** Preparation procedure described in section V.5.4.

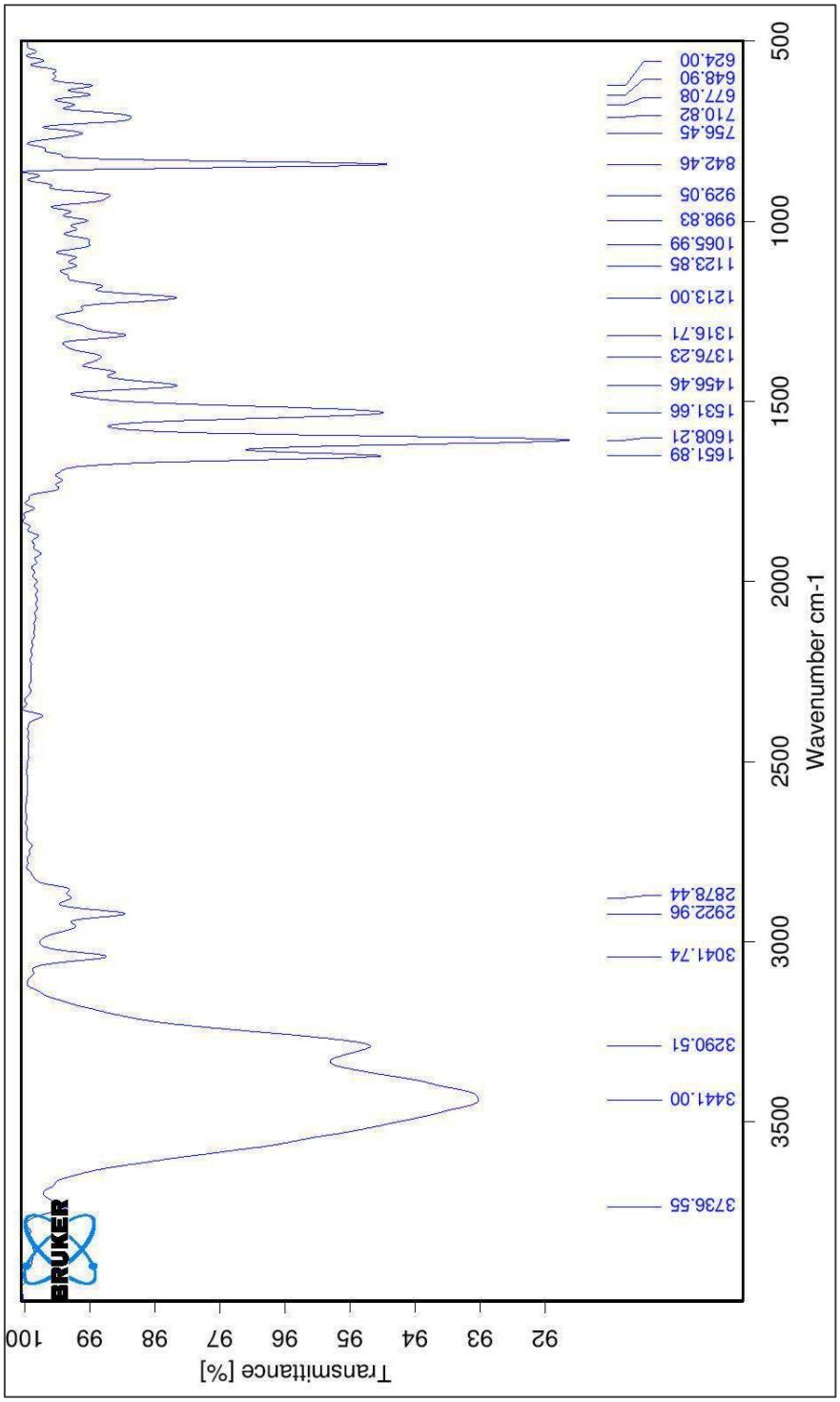

Figure A59: FT-IR (ATR) spectrum of ***N*-(pyren-1-ylmethyl)methacrylamide (PMeMA)**. Preparation procedure described in section V.5.4.

Mass Spectrum List Report

Analysis Info

Analysis Name	D:\Data\201501\PYRENE10.d	Acquisition Date	1/8/2015 11:54:15 AM
Method	lc_method_me398b2.m	Operator	Dr. Kayali
Sample Name	PYRENE1	Instrument	HCTultra PTM Discovery System
Comment	DIRECTO, EN MeOH		

Acquisition Parameter

Ion Source Type	ESI	Ion Polarity	Positive	Alternating Ion Polarity	off
Mass Range Mode	Ultra Scan	Scan Begin	50 m/z	Scan End	2300 m/z
Capillary Exit	97.5 Volt	Skimmer	40.0 Volt	Trap Drive	42.7
Accumulation Time	955 µs	Averages	14 Spectra	Auto MS/MS	off

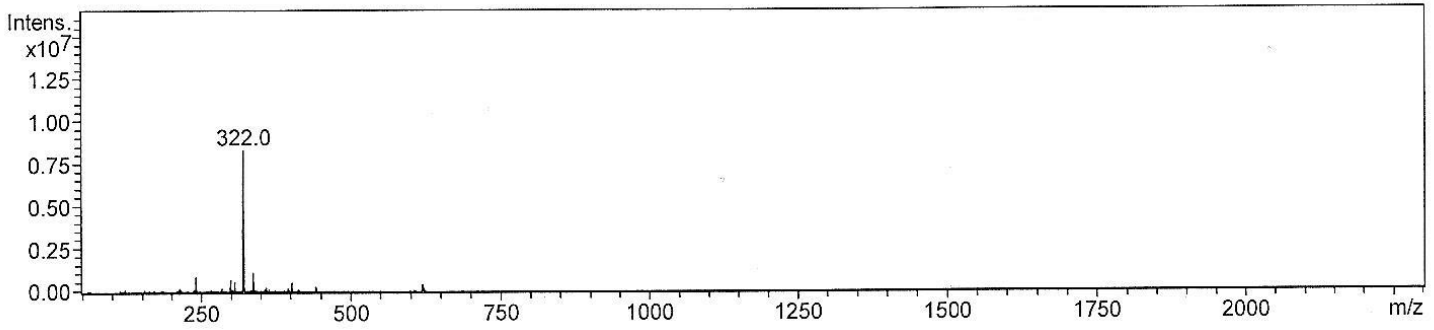

Figure A60: MS-ESI (negative ion detection) of ***N*-(pyren-1-ylmethyl)methacrylamide (PMeMA).** Preparation procedure described in section V.5.4.

Achievements

List of publications and conferences attended

Publications:

- *"Tailoring molecularly imprinted polymer beads for alternariol recognition and analysis by a screening with mycotoxin surrogates"*; **Rahma A.G. Abou-Hany**, J. L. Urraca, A.B. Descalzo, L.N. Gómez-Arribas, M.C. Moreno-Bondi, G. Orellana. *Journal of Chromatography A*, **2015**, *1425*, 231–239.

- *"Fluorescence sensing of Alternaria mycotoxins using biomimetic molecularly imprinted polymers"*; **Rahma A.G. Abou-Hany**, J.L. Urraca, A.B. Descalzo, M.C. Moreno-Bondi, and G. Orellana; ***EUROPT(R)ODE XI*** , Barcelona, Spain**,** *1-4 April*, **2012.**

- *"Fluorescence polarization sensing to report Alternariol mycotoxin binding to molecularly imprinted polymers"*; **Rahma A.G. Abou-Hany**, J.L. Urraca, A.B. Descalzo, M.C. Moreno-Bondi and G. Orellana; ***EUROPT(R)ODE XII*** , Athens, Greece, *13-16 April*, **2014**.

Manuscripts in preparation:

- *"Pyrene-Labeled Acrylamide Monomers as Fluorescent Probes".*

- *"Development of Luminescent MIPs for Tenuazonic Acid Detection".*

Patents:

"Materials for selective recognition of alternaria mycotoxins (alternariol and alternariol monomethyl ether)". G. Orellana, M.C. Moreno-Bondi, A.B. Descalzo, J. L. Urraca, **Rahma A.G. Abou-Hany**, **WO 2013144394**: Universidad Complutense de Madrid, Spain, **2013**.

Conferences attended:

- **EUROPT(R)ODE XI** conference on optical chemical sensors & biosensors, *1-4 April*, **2012,** Barcelona, Spain. (**Poster communication**).

- **EUROPT(R)ODE XII** conference on optical chemical sensors & biosensors, *13-16 April*, **2014**, Athens, Greece. (**Poster communication**)